Conference Proceedings

Nineteenth Annual Meeting of the American Society of Biomechanics

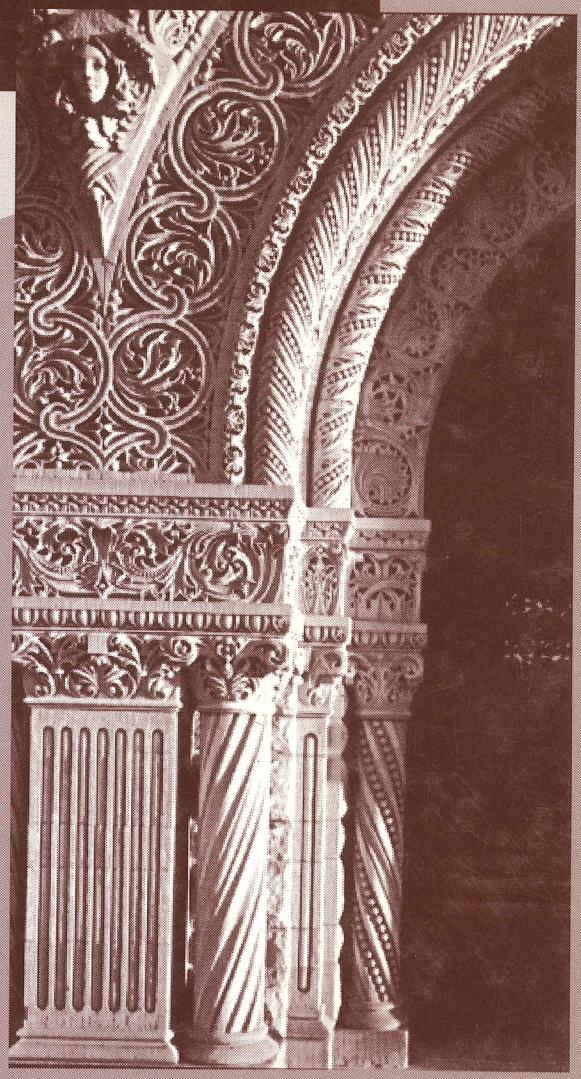

Stanford University
Stanford, California
24–26 August 1995

founded 1977
AMERICAN SOCIETY OF BIOMECHANICS

LELAND STANFORD JUNIOR UNIVERSITY
ORGANIZED 1891

NASA

DEPARTMENT OF VETERANS AFFAIRS
UNITED STATES OF AMERICA

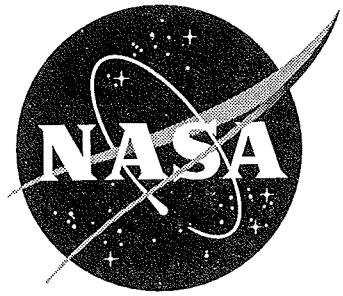

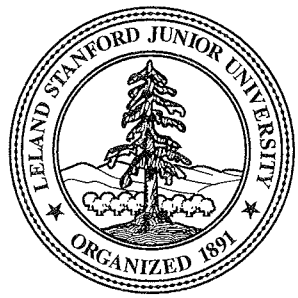

Conference Proceedings

AMERICAN SOCIETY OF BIOMECHANICS

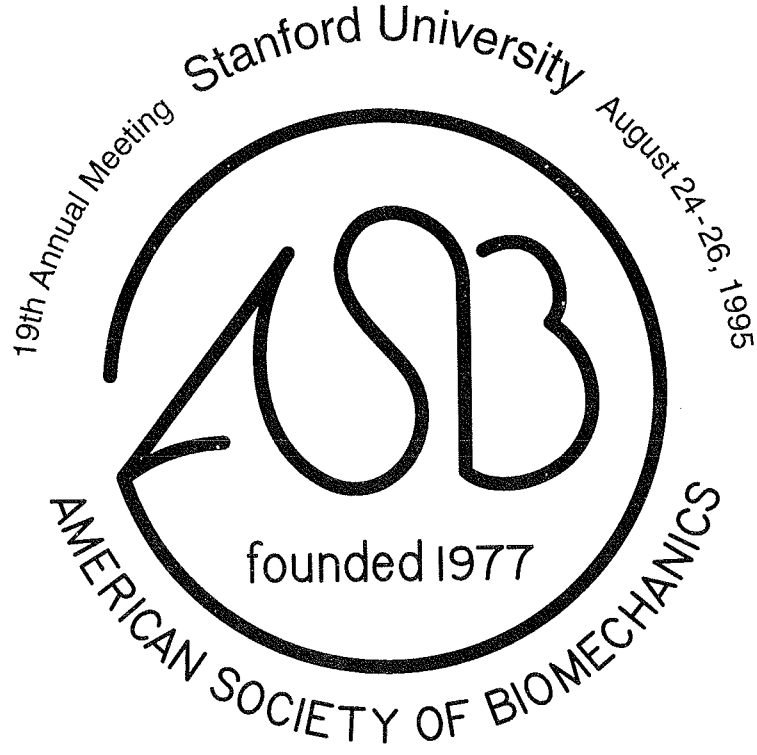

edited by
Keith R. Williams, Ph.D., The University of California, Davis

Local Organizing Committee

Gary S. Beaupré, Ph.D.
VA Palo Alto Health Care System
Stanford University
Dennis R. Carter, Ph.D.
Stanford University
VA Palo Alto Health Care System
Steve A. Kautz, Ph.D.
VA Palo Alto Health Care System
Stanford University
Marjolein C. H. van der Meulen, Ph.D.
VA Palo Alto Health Care System
Stanford University
Robert T. Whalen, Ph.D.
NASA Ames Research Center

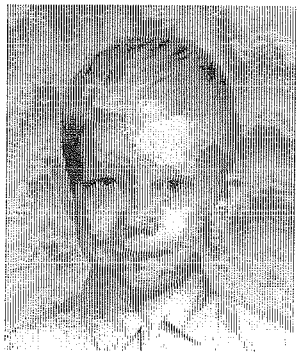
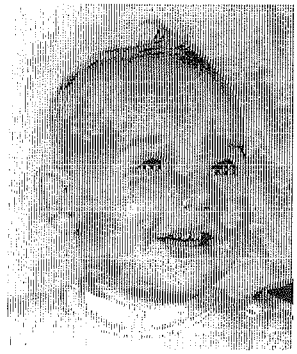
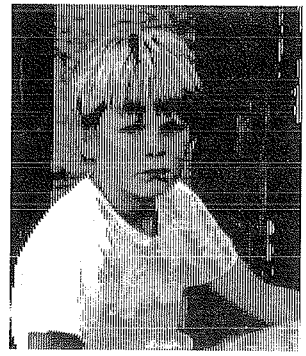

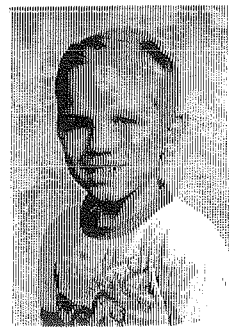

The organizers of the 19th Annual Meeting of the American Society of Biomechanics gratefully acknowledge ***The Whitaker Foundation*** for an educational grant, and the following organizations for their generous contribution of personnel and resources:

Stanford University

Department of Veterans Affairs Rehabilitation R&D Service

NASA Ames Research Center

This meeting was made possible by the generous underwriting provided by the following Corporate Sponsors:

Ace Medical Company
Los Angeles, California

Depuy, Inc.
Warsaw, Indiana

Digital Equipment Corporation
Maynard, Massachusetts

Endura-Tec Systems Corporation
Eden Prairie, Minnesota

Failure Analysis Associates, Inc.
Menlo Park, California

Howmedica, Inc.
Rutherford, New Jersey

Johnson & Johnson Professional
Raynham, Massachusetts

MTS Systems Corporation
Eden Prairie, Minnesota

Nike, Inc.
Beaverton, Oregon

Noraxon USA, Inc.
Scottsdale, Arizona

Norian Corporation
Cupertino, California

Osteonics Corporation
Allendale, New Jersey

Smith & Nephew Richards Inc.
Memphis, Tennessee

Symbolic Dynamics, Inc.
Mountain View, California

American Society of Biomechanics

The American Society of Biomechanics was formed in 1977. The purpose of the Society is to provide a forum for interaction among the diverse disciplines in biomechanics research and applications. Th term biomechanics in this context refers to the study of structure and function of biological systems using the methods of mechanics. The active membership of the Society includes scientists who conduct research in the biological sciences, engineering and applied sciences, ergonomics and human factors, exercise and sports sciences, and health sciences.

The principal activity of the Society is an annual scientific meeting. The meeting is held over a three-day period, and consists of keynote addresses, tutorial sessions, podium and poster presentations and student member functions. In keeping with the objectives of the Society, the papers address a wide range of topics and broad interests.

The Executive Board that has governed the Society during the past year is represented by the following individuals:

President:	Philip E. Martin, Arizona State University
Past President:	Thomas D. Brown, University of Iowa
President-Elect:	Kai-Nan An, Mayo Clinic
Secretary-Treasurer:	Mark D. Grabiner, The Cleveland Clinic Foundation
Meeting Chairperson:	Gary S. Beaupré, VA Palo Alto Health Care System
Program Chairperson:	Keith R. Williams, University of Calfornia, Davis
Program Chairperson-Elect:	David P. Fyhrie, Henry Ford Hospital
Membership Committee Chairperson:	M. Melissa Gross, University of Michigan
Education Committee Chairperson:	Jill McNitt-Gray, University of Southern California

Sustaining Members of the Society

The Society would like to thank the following organizations for their continuing support as Sustaining Members:

Aircast
DePuy, Inc.
Howmedica, Inc.
Kistler Instrument Corporation
Motion Analysis Corporation
MTS Systems Corporation
Noraxon USA, Inc.
Orthofix, S.R.L.
Peak Performance Technologies, Inc.

Program Committee

Keith R. Williams, Ph.D., Program Chair
University of California, Davis
David P. Fyhrie, Ph.D., Program Chair-Elect
Henry Ford Hospital
David Hawkins, Ph.D.
University of California, Davis
Rodger Kram, Ph.D.
University of California, Berkeley
Mark Latash, Ph.D.
Pennsylvania State University
R. Bruce Martin, Ph.D.
University of California, Davis
Rick N. Robertson, Ph.D.
University of Pittsburgh Medical Center
Mary M. Rodgers, Ph.D.
University of Maryland
Gerald Smith, Ph.D.
Oregon State University

Exhibitors at the 1995 Meeting

AMTI
Ariel Dynamics, Inc.
Benjamin/Cummings Publishing
Bertec Corporation
Cambridge University Press
Dynamic Spinal Analysis, Inc.
Elsevier Science Inc.
Instron Corporation
The Journal of Bone and Joint Surgery
Kistler Instrument Corporation
Motion Analysis Corporation
MTS Systems Corporation
Noraxon USA, Inc.
Northern Digital Inc.
Novel Electronics, Inc.
Peak Performance Technologies, Inc.
Qualisys Inc.
Skill Technologies, Inc.
Strawberry Tree Incorporated

Conference Schedule

Thursday, August 24

8:00 - 18:30	Registration, Elliot Program Center
9:00 - 12:15	NASA Tour, departs from Governor's Corner
10:00 - 12:15	VA RR&D Center Tour, departs from Governor's Corner
13:00 - 14:45	Tutorial #1, History Room 2
15:00 - 16:45	Tutorial #2, History Room 2
17:00 - 18:30	Opening Reception, Elliot Program Center
18:30 - 22:00	Executive Board Meeting, Elliot Program Center

Friday, August 25

7:00 - noon	Registration, Annenberg Plaza
7:00 - 8:00	Continental Breakfast, Annenberg Plaza
8:00 - 8:50	Keynote Presentation #1, Annenberg Auditorium
9:00 - 10:15	Parallel Sessions I, II
10:15 - 10:30	Refreshment Break, Annenberg Plaza
10:30 - 12:00	Parallel Sessions III, IV
12:00 - 13:30	Lunch on your own / Student Luncheon, Lagunita Dining Hall
13:30 - 14:50	Symposium, Annenberg Auditorium
15:00 - 16:30	Parallel Sessions V, VI
16:30 - 18:00	Wine and Cheese at Posters and Exhibits, Cummings Art
18:30 - 20:30	Banquet, Inner Quad
20:30 - 21:15	Organ Recital, Memorial Church

Saturday, August 26

7:00 - 9:00	Registration
7:00 - 8:00	Continental Breakfast, Annenberg Plaza
8:00 - 8:50	Keynote Presentation #2, Annenberg Auditorium
9:00 - 10:15	Parallel Sessions VII, VII
10:15 - 10:30	Refreshment Break, Annenberg Plaza
10:30 - 12:00	Parallel Sessions IX, X
12:00 - 13:30	Awards Luncheon, Lagunita Dining Hall
13:45 - 14:45	Borelli Lecture, Annenberg Auditorium
14:50 - 15:30	Business Meeting, Annenberg Auditorium
15:30 - 16:15	Refreshments at Posters and Exhibits, Cummings Art
16:15 - 17:30	Parallel Sessions XI, XII
18:00 - 22:00	Executive Board Meeting, Elliot Program Center

Session Schedule

Friday, 25 August 1995

Saturday, 26 August 1995

Conference Schedule

Tutorial #1

Thursday, 1:00 – 2:45 pm, History Room 2

Acceleration, Force and Pressure Distribution – Measurement Techniques and their Application in Biomechanics

Ewald Hennig — *Sportsmedizinisches Institut, Essen, Germany*

Tutorial #2

Thursday, 3:00 – 4:45 pm, History Room 2

Muscle Force Determination

Richard E. Hughes — *Mayo Clinic*

Kenton Kaufman — *San Diego Childrens Hospital*

Kai-Nan An — *Mayo Clinic*

Keynote Presentation #1

Friday, 8:00 – 8:50 am, Annenberg Auditorium

Running on Water

Thomas A. McMahon — *Harvard University*

James Glasheen — *Harvard University*

Symposium on Comparative Locomotion12

Friday, 1:30 – 2:50 pm, Annenberg Auditorium

Swimming Mechanics of Skipjack Tuna

Robert E. Shadwick — *Scripps Institution of Oceanography*

Muscles Inside a Skeleton: Isolated Muscle Function and Musculoskeletal Modeling of Running Insects

Robert J. Full — *University of California, Berkeley*

Using Animal Studies to Understand How Muscles Power Locomotion

Andrew A. Biewener — *University of Chicago*

Keynote Presentation #2

Saturday, 8:00 – 8:50 am, Annenberg Auditorium

Predictions for Neural Control Based on Limb Dynamics

Judith L. Smith — *University of California, Los Angeles*

Award Presentations

Borelli Award:

Wilson C. Hayes
Beth Israel Hospital and Harvard Medical School
An Update on the Movement of Animals: Falls among Elderly Humans

Post-Doctoral Young Scientist Award:

Boris I. Prilutsky
University of Calgary
Biomechanical Features of the Organization of Highly Skilled Locomotor Movements

Pre-Doctoral Young Scientist Award:

Christoph Reinschmidt
University of Calgary
Tibiofemoral and Calcaneus-Tibia Motion during Running: Skin vs. Bone Markers

Nominees for the Clinical Biomechanics Award:

Bing Yu, Mayo Clinic
Reproducibility of the Kinematics and Kinetics of the Lower Extremities in Stairclimbing

Kevin P. Granata, The Ohio State University
Influence of Back Belts on Dynamic Lifting Motions

Steve A. Kautz, VA Palo Alto Health Care System
Effects of Increased Exertion during Pedaling Exercise on Kinetic Measures of Motor Performance for Hemiplegic Persons

Stuart M. McGill, University of Waterloo
Indwelling EMG of Psoas: Clinical Implications for Low Back Injury and Rehabilitation

Geza F. Kogler, Southern Illinois University
The Biomechanics of Longitudinal Arch Support Mechanisms in Foot Orthoses and their Effect on Plantar Aponeurosis Strain

Friday, 25 August 1995

Session I – Joints — **History Room 2**

Session II – Gait — **Annenberg Auditorium**

Saturday, 26 August 1995

Session VII – Ergonomics **History Room 2**

Nominee for Clinical Biomechanics Award

Session VIII – Rehabilitation **Annenberg Auditorium**

Nominee for Clinical Biomechanics Award

Nominee for Clinical Biomechanics Award

Session XI – Spine **History Room 2**

Session XII – Musculoskeletal **Annenberg Auditorium**

Poster Session

ABSTRACTS

EXPERIMENTAL TECHNIQUE HAS AN EFFECT ON MEASURED CONTACT CHARACTERISTICS OF THE HUMAN HIP JOINT

B.K. Bay, S.A. Olson, A.J. Hamel
Orthopaedic Research Laboratories, University of California Davis, Sacramento, CA 95817

INTRODUCTION

Most laboratory investigations of hip joint contact characteristics have used cadaver acetabulae cut from the surrounding bone and potted in cement. The specimens were aligned with the proximal femur in a materials testing machine and compressed to simulate *in vivo* loading. This technique, although correctly simulating the resultant load on the hip, may predict a load distribution far different from *in vivo* conditions. To achieve a more physiologic loading environment, we have developed a methodology which uses intact pelves and simulates the action of the hip abductors to reproduce the joint reaction forces which occur during the single leg stance phase of gait. This study was undertaken to compare hip joint contact measurements for the two testing methodologies.

REVIEW AND THEORY

Previous investigations by Brown *et. al.* and Afoke *et al.* removed the acetabulum from the pelvis and applied an axial load, equivalent to about 3 times body weight, across the rearticulated joint. The resulting load distributions show concentration of load in the superior and anterosuperior portion of the acetabulum, respectively.

In these two studies, contact forces and pressures were measured using two different methods. Brown *et al.* used piezoresistive transducers mounted in the cartilage of the femoral head, while Afoke *et al.* used pressure sensitive Fuji Prescale film. Piezoresistive transducers do not introduce an extra thickness to the joint, but are limited in number (hence resolution) and may alter how the articulating surfaces interact. Fuji film introduces extra thickness which may alter joint mechanics, but gives better resolution of load distribution. In our study, we used Fuji film to measure the load distribution.

By removing the acetabulum and casting it rigidly in cement, the joints natural ability to react to an applied load may be lost. By using an intact pelvis and loading in a more physiologic manner, the surrounding bone is not constrained by cement and is able to deform in a manner more consistent with *in vivo* conditions. This study was undertaken to ascertain if our model resulted in different loading patterns. This would suggest that experimental technique has an effect on the measurement of contact pressures within the hip joint.

PROCEDURES

Each hip was first loaded using the simulated abductor mechanism and an intact pelvis, then potted and loaded using the methodologies described by Brown and Afoke.

Intact pelves were excised from fresh cadavers and cleaned of excess tissue, leaving the joint capsules intact. Pulleys were attached to the iliac crest and to the greater trochanter of the femur (Fig. 1). A single cable was strung through these pulleys and tightened to achieve axial load at the sacrum (mounted to a load cell in an Instron machine) equivalent to body weight. This resulted in a joint reaction force of about 3 times body weight.

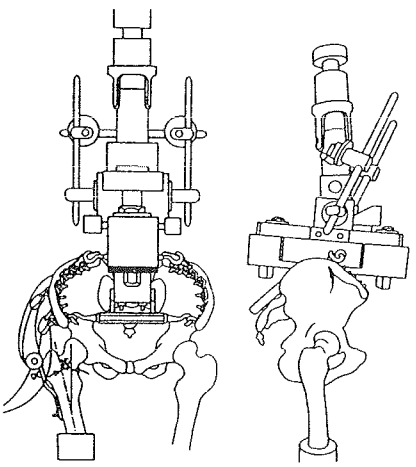

Figure 1: Loading apparatus using an intact pelvis.

In order to better classify the distribution of load, the acetabulum was marked with two small drill holes in the middle of the articular cartilage to delineate between posterior wall, superior dome and anterior wall. These were placed at points 30° anterior and posterior to a line formed by the superiormost portion of the acetabular rim and the center of the acetabulum.

Fuji film was placed on the femoral head and protected from moisture with latex barriers. The hip joint was rearticulated and loaded by tensioning the abductor cable. This process was repeated several times for both intact hips. The acetabulae were then cut from the pelvis and potted in polymethylmethacrylate (PMMA). The potted joint was placed in the Instron with Fuji film, and loaded to the same joint reaction force vector seen in the intact model. Fuji film patterns were digitized with a flatbed scanner and analyzed with Image software (W. Rasband, NIMH).

RESULTS

The Fuji film patterns in the intact model show a distributed load across the acetabulum with significant contact in the posterior and anterior walls (Fig. 2). In the potted model the load was highly concentrated in the dome or superior portion of the joint (Fig. 3), which is consistent with the piezoresistive transducer measurements of Brown.

Figure 2: Intact model load distribution pattern.

Figure 3: Potted mode load distribution pattern.

A repeated measures analysis of variance showed significant differences between the two models for both contact area and mean pressure. Specifically, the potted model showed a significant increase in contact area in the superior acetabulum and a decrease in contact area in the posterior wall (Fig. 4). The potted model also showed a significant increase in mean pressure in the superior acetabulum (Fig. 5).

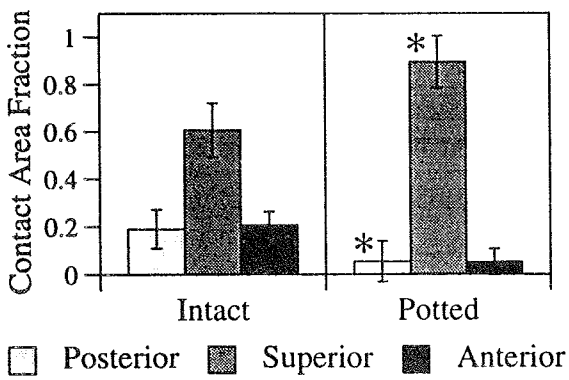

Figure 4: Contact area fraction in the three regions, with an asterisk denoting significance ($p < .05$).

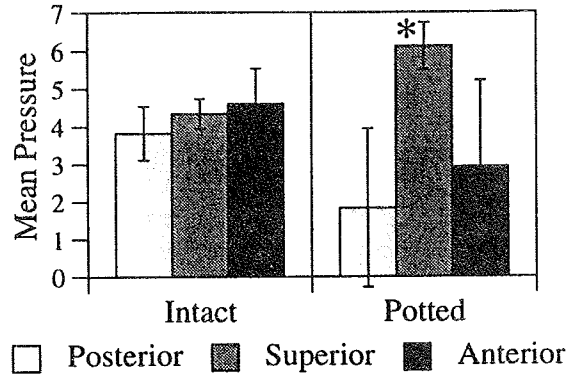

Figure 5: Mean pressure in the three regions, with an asterisk denoting significance ($p < .05$).

DISCUSSION

Previous studies which have utilized the potted model may have excessively altered the joint mechanics by removing it from the pelvis. The loading patterns seen might therefore contain artifact. Joint contact characteristics may be significantly influenced by elastic deformation of the iliac wing due to abductor action and support coming from the bridge formed by the intact pubic and ischial bones. Also, with the axial force of body weight transmitted through the sacroiliac joint, this load is applied at a physiologically correct position, not as an idealized axial force acting directly on the joint.

It has been argued that Fuji film, by increasing the diameter of the femoral head, artificially increases peripheral loading. However, Fuji film was used in both models to ascertain load distribution and significantly different patterns were seen. Therefore, the distributed load in the intact model is not due to a Fuji film artifact, since such an artifact would have been seen in both methods.

The most important result of this study is that the two methods give substantially different results for the same joint reaction load applied to the same hip. By simulating muscle activity and allowing the pelvis to deform, our method may better represent *in vivo* loading conditions in the hip joint.

REFERENCES

Brown, T. D., Shaw, D. T., *J. Biomechanics*, 16, 6, 373-384, 1983.

Afoke, N.Y.P., Byers, P.D., Hutton, W.C., *J. Bone Joint Surg*, 69-B, 4, 536-541, 1987.

THE EFFECTS OF ANTERIOR CRUCIATE LIGAMENT DEFICIENCY AND RECONSTRUCTION ON THE CONTACT CHARACTERISTICS OF THE PATELLOFEMORAL JOINT

Yeou-Fang Hsieh and Louis F. Draganich, Sherwin Ho, and Bruce Reider

Section of Orthopaedic Surgery and Rehabilitation Medicine
Department of Surgery
The University of Chicago
Chicago, Illinois

ABSTRACT

This study was performed to investigate the effects of deficiency of the anterior cruciate ligament (ACL) and intraarticular reconstruction (IAR) of the ACL on the contact characteristics (contact areas, resultant contact forces, three components of the resultant contact forces, contact pressure distributions, average contact pressures, peak contact pressures, and centers of pressure) of the patellofemoral joint in seven cadaveric knees. A bone-tendon-bone graft from the autogenous central one-third of the patellar tendon was used for the intraarticular reconstruction. Knee loading was produced by extending the knee with quadriceps forces based on one-third of reported maximum voluntary isometric extension moments. The position data of the patellofemoral and tibiofemoral joints were measured at 30°, 60°, and 90° of knee flexion with a six degree-of-freedom digitizing system. Fuji Prescale film was used to record patellofemoral contact pressure. Pressure intensity was digitized using a high resolution optical scanner. Digital image processing techniques in conjunction with kinematic transformations were applied to analyze the contact prints. Excision of the ACL caused significant decreases in total patellofemoral contact area, in anterior component of patellofemoral contact force, and in peak contact pressure on the medial facet of the patella. Intraarticular reconstruction of the ACL returned normal patellofemoral contact characteristics to the ACL-excised knee.

INTRODUCTION

The major forces acting on the patella consist of the patellofemoral contact force, quadriceps force, and patellar ligament force. Therefore, any imbalance in the extensor mechanism may lead to abnormal changes in patellofemoral contact areas, contact forces, and, hence, contact pressures, and to degeneration of the articular cartilage. Despite the fact that reconstruction of the anterior cruciate ligament (ACL) enhances the stability of the tibiofemoral joint, frequently, even with good stability, patients have complained of pain in the anterior aspect of the knee. One possibility is that patellar pain results from a malalignment between the patella and femur which leads to altered patellofemoral contact. To date, there have been no studies reporting on the effects of ACL deficiency on the contact characteristics of the patellofemoral joint. Furthermore, there have been no reports on the effects of ACL reconstruction on these contact characteristics. Thus, the objectives of this in vitro study were using Fuji Prescale film with digital image processing technique to determine the effects of removal and intraarticular reconstruction of the ACL on the patellofemoral contact characteristics for physiologic levels of quadriceps loads.

MATERIALS AND METHODS

Seven cadaveric knees from seven donors with a mean age of 51.4 years were studied. Tests were performed for three experimental states on each specimen, first on the intact knee, second following excision of the ACL, and finally following intraarticular reconstruction of the ACL for flexion angles at 30°, 60°, and 90°. An IAR was performed utilizing the autogenous central one-third of the bone-patellar tendon-bone graft. Patellofemoral contact areas and pressures were recorded using low-pressure Fuji Prescale film which was hermetically sealed in polyethylene sheets. Medial parapatellar incision was performed for insertion of film packets. Prior to testing, four reference holes, 1 mm in diameter, were drilled in an anteroposterior direction through the patella. These holes served as reference positions for the coordinate transformation between the pixel and patellar coordinate systems. Testing consisted of applying external flexion moments equivalent to 1/3 of values reported in the literature for maximum isometric quadriceps moments[1], equilibrating the knee with quadriceps forces at a particular flexion angle, measuring patellofemoral and tibiofemoral joint motions, and digitizing attachment sites of the quadriceps tendon and patellar ligament with a six degree-of-freedom digitizer. After the motion data were collected, the knee was disarticulated and bony landmarks of the femur, tibia, and patella were identified and digitized for construction of the anatomical coordinate systems.

The patellofemoral contact stain on the Fuji Prescale film was digitized with a high resolution (600 dpi X 600 dpi) scanner to obtain an image of size 640 X 480 pixels with an intensity (up to 256 levels) stored in each pixel. Before the contact stain could be analyzed, calibration for the scanning system and for the Fuji Prescale film was performed. Five scanning parameters (rotation, offset, and scaling parameters) were determined using the method of least-squares to establish a coordinate transformation between the pixel and patellar coordinate systems. A cubic polynomial for pressure calibration was used to characterize the relationship between the magnitudes of the pressure and the intensity of gray level. Patellofemoral contact pressure distribution maps were then

established. Contact area was defined as the locus of the contact pixels. Resultant contact force was obtained by integrating the pressure distribution over the entire contact area. Force and moment equilibrium of the patella under the actions of the quadriceps force, resultant contact force, and patellar ligament tension was performed to obtain the three components of the patellofemoral contact force and the center of pressure. Contact characteristics on the medial facet or lateral facet of the patella were defined according to the patellar coordinate system originating on the center of the patellar ridge. Paired t-tests were performed to determine significant differences in the patellofemoral contact characteristics between the intact and ACL-excised knees and between the intact and IAR knees. Based on a Bonferroni adjustment for two comparisons at three flexion angles, an α level of 0.008 was considered significant.

RESULTS

In the intact knee, patellofemoral contact area increased by 137%, the resultant contact force increased by 214%, the anterior component of contact force increased by 334%, average contact pressure increased by 38%, and peak contact pressure increased by 41% as the knee flexed from 30° to 90°. Removal of the ACL resulted in a significant reduction in contact area from that of the intact knee at 30° ($p<0.006$) and 90° ($p<0.002$) of knee flexion (Figure 1). Compared to the intact knee, removal of the ACL resulted in a significant reduction in the anterior component of contact force at 30° of knee flexion ($p<0.003$) (Figure 2). Removal of the ACL resulted in a significant reduction in peak contact pressure on the medial facet of the patella at 30° and 60° of knee flexion ($p<0.004$), when compared to that of the intact knee (Figure 3). The intraarticular reconstruction was found to return normal patellofemoral contact characteristics to the ACL-excised knee at all angles tested.

DISCUSSION

In agreement with those of previous studies[2,3,4,5,6,7], our results found for the intact knee demonstrated that the patellofemoral contact area, magnitude of the resultant contact force, average contact pressure, and peak contact pressure increased with knee flexion between 30° and 90° of knee flexion. Our results showed that excision of the ACL resulted in the smallest contact areas, anterior component of contact force, and medial peak contact pressure at all flexion angles tested among the three experimental states. It has been believed that loss of the ACL is associated with degeneration of the cartilage of the patella. Thus, the significant reduction in total contact area, the significant reduction in anterior component of contact force, the significant reduction in medial peak contact pressure, or all may be associated with degeneration of the patellar cartilage or patellar pain. Although we did not discover patellofemoral contact characteristics in the reconstructed knee to be significantly different from those of the intact knee, there were some differences which might become significant with a larger number of samples. However, the intraarticular reconstruction performed in this study was found to return normal tibiofemoral and patellofemoral kinematics to the ACL-excised knee. Thus, significant differences in patellofemoral contact would not be expected.

Figure 1. Patellofemoral Contact Area

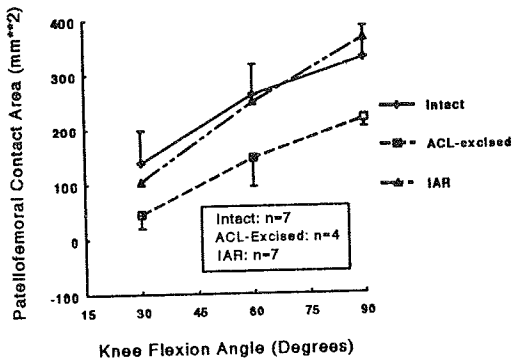

Figure 2. Anterior Component of contact Force

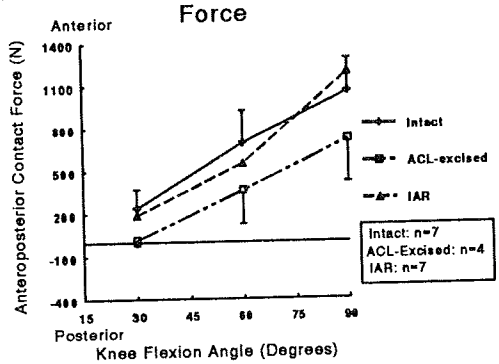

Figure 3. Medial Peak Contact Pressure

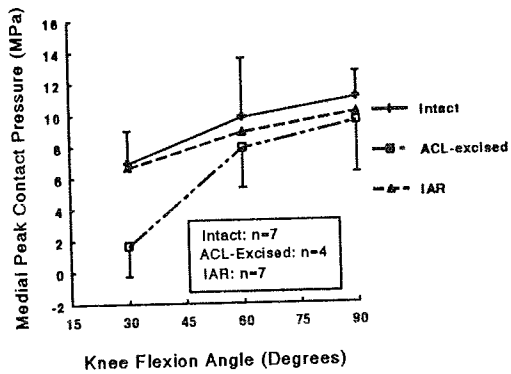

REFERENCES

1. Lieb et al: J Bone Joint Surg, 53A: 749-758, 1971.
2. Hefzy et al: J Biomedical Eng, 14: 329-343, 1992.
3. Hill et al: Arch Ortho Traum Surg, 104: 275-282, 1985.
4. Huberti et al: J Bone Joint Surg, 66A: 715-724, 1984.
5. Lewallen et al: J Ortho Res, 8: 856-862, 1990.
6. Seedhom et al: J Biomech, 10: 253-260, 1977.
7. Singerman et al: J Biomech 27: 233-238, 1994.

MUSCULAR FORCES AND EMGs BEFORE AND AFTER TRANSECTION OF THE ANTERIOR CRUCIATE LIGAMENT IN THE CAT HINDLIMB

E.M. Hasler, W. Herzog, T.R. Leonard
Human Performance Laboratory, The University of Calgary, Calgary, Canada

Introduction

Experimental joint injury models have produced osteoarthritis (OA) reliably. It is assumed that disruption of joint integrity will change joint mechanics and lead to alterations in joint structure and function. Transection of the anterior cruciate ligament (ACL) in the cat has recently been introduced as a model of OA (Herzog et al., 1993). Early changes in the cartilage of the ACL-deficient cat hindlimb were similar to those observed in the dog (Adams et al., 1991).

Biomechanical parameters representing joint mechanics such as muscular forces, EMGs, ground reaction forces (GRFs) and external kinematics were assessed during locomotion before and after ACL transection in the cat hindlimb. To our knowledge, this is the first time that muscular forces, which mainly determine the loading in the knee, have been measured in a joint injury model. This information may provide insight into the role of mechanical factors in joint degeneration.

Review and Theory

Changes in joint mechanics due to joint injuries are assumed to be initiating factors for OA (Moskowitz, 1977). In order to study the effects of changes in joint loading and joint kinematics on the articular cartilage, experimental models based on altering joint mechanics have been developed. A well established model that yields reproducible changes in the articular cartilage of the injured limb, is ACL transection in the dog (Adams et al., 1991; Brandt et al., 1991). Whereas morphological and biochemical changes in the articular cartilage of the unstable limb have been described extensively, corresponding studies on changes in joint loading are limited to measurements of external GRFs (O'Connor et al., 1992; Brandt et al., 1991). GRFs were taken as an indication of joint loading, however, external GRFs may not reflect the changes in joint loading that are associated with OA. Since joint loading is mainly governed by muscular forces (Morrison, 1968), a systematic in-vivo biomechanical study is needed to assess internal forces acting on the joint, and relate the changes in these forces to changes in the articular cartilage. The cat model was chosen to measure internal forces and joint kinematics because an extensive data base in terms of individual muscle force and EMG measurements and locomotor kinematics is available. The objective of this study was to assess muscular forces, EMGs, GRFs, and joint kinematics in the intact and ACL-deficient cat hindlimb during locomotion.

Procedures

External kinematics and GRFs were collected for one cat (4.9 kg) during normal locomotion on a treadmill and a walkway instrumented with two AMTI force plates in series. After data collection, both hindlimbs were instrumented with modified implantable force transducers (IFT) in the patellar tendon (Glos et al., 1993), buckle transducers in the gastrocnemius tendon, bipolar, indwelling EMGs in the semitendinosus (ST) and vastus lateralis (VL) muscles, and femoral nerve cuffs. Eight days after instrumentation, muscle forces, EMGs, external kinematics and GRFs were measured again during treadmill and walkway locomotion. Synchronization of force, EMG and video data was obtained using a series of LED pulses recorded on the video and on the computer. Following data collection, the ACL of the left hindlimb was transected. Data collection was repeated five and seven days after ACL transection.

In order to calibrate the IFTs in the intact knee joint, the hindlimb of the anaesthetized animal was fixed into a stereotaxic frame at various knee angles. Using an instrumented bar, the tibia was restrained from anterior movement. Knee extensor forces (using the instrumented bar) and IFT forces were measured simultaneously during isometric quadriceps contractions produced through electrical stimulation of the femoral nerve (100 Hz, 0.1 msec). Complete analysis of the calibration data is not available to date, but assuming a linear relation between IFT voltage output and force and independence of the IFT calibration with respect to knee angle (which is most likely not correct), absolute patellar tendon forces were estimated. The gastrocnemius force transducers were calibrated during a static in-situ procedure. After calibration, both hindlimbs were fixed in 90% buffered formalin in knee extension. In an additional experiment, the patellar tendon moment arm was derived from tendon travel recorded during passive knee flexion movements of the fixed hindlimb (Spoor et al., 1992). IFT forces are then calculated from the knee extensor moments measured by the tibial restraining bar and the moment arms of the system.

Although internal and external measurements were performed in both hindlimbs, results are only shown for the internal measurements of the experimental hindlimb before and seven days after ACL transection.

Results

Fig. 1 shows raw signals of gastrocnemius tendon forces, patellar tendon forces, ST EMG and VL EMG in the left hindlimb during level treadmill locomotion at a speed of approximately 0.4 m/s. Patellar tendon forces were less variable for consecutive steps than the corresponding gastrocnemius forces. The patellar tendon force peaks were maintained longer compared to the gastrocnemius force peaks.

Fig. 2 shows the raw signals from the same transducers under similar locomotor conditions but seven days after ACL transection. Both gastrocnemius and patellar tendon forces were decreased in amplitude.

Discussion

After ACL transection, the cat showed a distinct limp during locomotion but did not object to load the unstable limb during walking. The gastrocnemius and patellar tendon forces were decreased to about 50% seven days after ACL transection compared to before ACL transection. Similarly, EMG activity decreased from before to after ACL surgery. Gastrocnemius forces in the intact (right) hindlimb increased by almost 50% from before to after ACL transection indicating that the contralateral hindlimb compensates for the unloading of the injured limb, and therefore cannot be considered as a normal control. Unloading of the injured limb was also observed in the vertical GRFs after ACL transection compared to the preoperative values (not shown here). GRFs have been measured statically in cats (Herzog et al., 1993) and dynamically in dogs (O'Connor et al., 1992) before and one and two weeks after ACL transection, respectively. It was found in these studies that the ACL-deficient hindlimb was unloaded immediately after ACL transection, and it was assumed that decreased joint loads may initiate biochemical changes in the articular cartilage. However, muscular forces affecting the joint loading were not measured in these studies, and it is conceivable that muscular forces may actually be increased through co-contraction of agonist/antagonist muscles after ACL injury to protect the unstable limb. The preliminary data reported here, suggest that internal and external forces are decreased after ACL transection in the experimental hindlimb. Thus, early changes in the articular cartilage, as observed by Herzog et al. (1993), may be initiated by decreased joint loads. Monitoring internal and external forces in a joint injury model may provide insight into the loading history of an injured joint and may help to determine the role of mechanical factors in joint degeneration.

References

Adams, M.E. et al. *J. Rheumatol.*, 18, 428-35, 1991.
Brandt, K.D. et al. *J. Rheumatol.*, 18,436-446, 1991.
Glos, D.L. et al., *J. Biomech. Engng.*, 115, 335-343, 1993.
Herzog, W. et al. *Osteoarthritis and Cartilage*, 1, 243-251, 1993.
Morrison, J.B, *Bio-Medical Engng*, 4, 164-170, 1968.
Moskowitz, R.W., *Arthritis Rheum.*, 20, 5104-5108, 1977.
O'Connor, B.L. et al, *Trans. Orthop. Res. Soc.*, 478, 1992.
Spoor, C.W. et al., *J. Biomech.*, 25, 201-206,1992.

Acknowledgments

This work was supported by the Swiss Federal Sports Commission (ESK), the Arthritis Society of Canada, The Whitaker Foundation, and MRC of Canada. The help of A. Stano and H. Nguyen in the data collection was greatly appreciated.

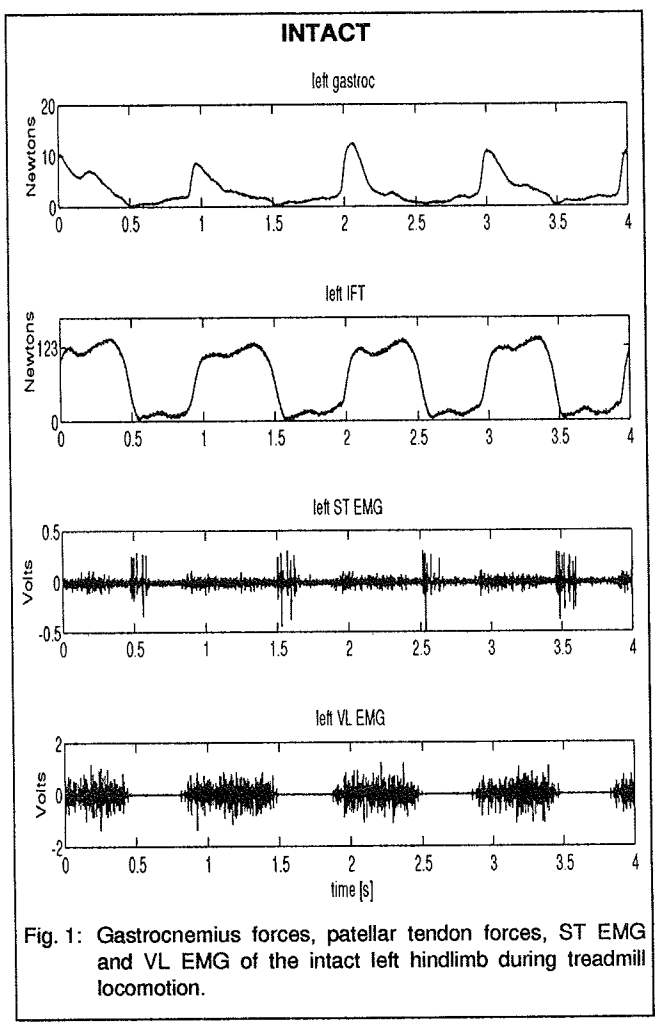

Fig. 1: Gastrocnemius forces, patellar tendon forces, ST EMG and VL EMG of the intact left hindlimb during treadmill locomotion.

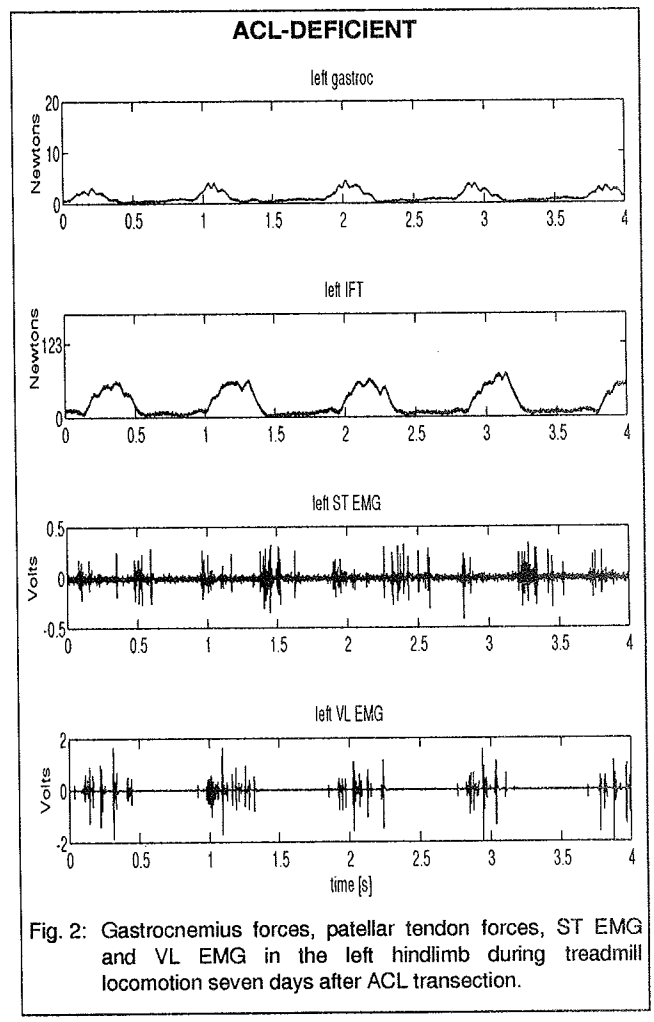

Fig. 2: Gastrocnemius forces, patellar tendon forces, ST EMG and VL EMG in the left hindlimb during treadmill locomotion seven days after ACL transection.

STRAIN IN THE ANTEROMEDIAL AND POSTEROLATERAL BUNDLES OF THE ACL OVER THE FULL RANGE OF FLEXION

J.M. Bach[1], M.L Hull[1], H.A. Patterson[2]
[1]Biomedical Engineering Graduate Group, University of California, Davis, CA 95616
[2]Department of Anatomy, University of California, San Francisco, CA

INTRODUCTION

This paper details experiments to characterize the reciprocating function of the two main anatomical bundles of the anterior cruciate ligament (ACL). This characterization is crucial to gaining a understanding of injury mechanisms so that improved injury prevention methodologies may be developed. Additionally this information may be useful for designing better surgical repair and replacement procedures.

Strain gages mounted on the anteromedial and posterolateral bundles (AMB and PLB, respectively) were used to record strain in the ACL as the knee was mobilized over the range of flexion from -8° (hyperextension) to 125°. The results of these experiments demonstrate that the strain in the PLB is significantly different from that of the AMB over the range of flexion angles examined. Furthermore, reciprocating behavior is exhibited by the two bundles.

REVIEW AND THEORY

No citations could be found which directly measured strain in the PLB over the full range of flexion. Several studies have examined the length changes in the AMB and PLB as the knee is flexed and extended (e.g. Amis & Dawkins, 1991, Fuss, 1991). Most of these studies have determined the length changes by measuring the distances between the femoral and tibial insertions of fibres as the knee is mobilized. Unfortunately the resulting straight line distance is an oversimplification which underestimates the true three dimensional behavior of the fibres. As a result the conclusions reached in these studies often contradict each other. Some authors report that the AMB is taught in flexion and the PLB is taught in extension (e.g. Amis and Dawkins, 1991) while others report exactly the opposite (e.g. Benninghoff, 1985 as cited in Fuss, 1991).

To better characterize the behavior of the AMB and PLB over the range of flexion, experiments were performed to test the following two hypotheses:

1) the strain in the PLB is significantly different from the strain in the AMB at the extremes of flexion and extension,
2) the two bundles reciprocate in function with the strain in the AMB increasing, and the strain in the PLB decreasing, with increasing flexion.

METHODS

A six degree of freedom, computer controlled, pneumatically actuated load application system (LAS) (Bach et. al., 1995) was used to perform the flexion-extension trials for these experiments. Ten specimens (mean age 49.8 years) with no visible signs of damage or disease were prepared for installation in the LAS. After initial dissection the specimens were installed in the apparatus and aligned using a functional alignment procedure (Berns et al., 1992). Following alignment the specimens were potted in the apparatus and then preconditioned for hyperextension, varus-valgus (V-V) rotation, and anterior-posterior (A-P) translation.

Liquid mercury strain gages (LMSGs) of approximately 0.625 mm diameter and 5 mm length were constructed for this application. A new technique, which did not effect the mechanics of the joint, was developed for mounting a strain gage on the PLB. An additional strain gage was installed on the AMB.

The protocol for investigating the passive flexion/extension (F/E) behavior of the ligaments involved flexing the knee from -8° of hyperextension to 125° of flexion and back to

hyperextension. Flexion/extension moment, 6 degree of freedom displacements, and strain from the two LMSGs were recorded continuously during the motion cycle.

A repeated measures analysis of variance (RANOVA) was performed on the data. The analysis included two within subject effects, flexion angle and strain measurement site. Flexion angle had 11 levels corresponding to eleven flexion angles analyzed (-8, -5, 0, 15, 30, 45, 60, 75, 90, 105, and 120 degrees). For the strain measurement site effect there were two levels corresponding to the AMB and PLB. Tukey's method of multiple comparisons was used to determine significant differences between the two strain sites at each flexion angle.

RESULTS

The means and standard errors for both bundles are plotted in Figure 1. The flexion angle effect was found to be significant ($p=0.004$) while the strain measurement site (bundle) was not ($p=0.270$). The interaction between these two effects (flexion angle * site) was highly significant ($p=0.0002$). The results of the Tukey's method of multiple comparisons procedure indicated that the strain in the PLB was significantly different ($\alpha=0.05$) from the strain in the AMB at flexion angles of -8, -5, 90, 105, and 120 degrees. The differences at the remaining flexion angles (0, 15, 30, 45, 60, 75) were not statistically significant at the $\alpha=0.05$ level.

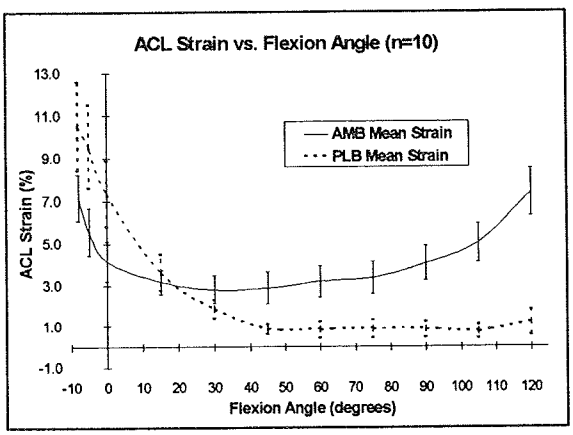

Figure 1 : Passive Flexion Results

DISCUSSION

The results of these experiments indicate that the strain in the AMB and PLB varies as the knee is mobilized through its range of flexion. Flexion angle has a statistically significant effect on the strain in both bundles. There is also a significant interaction between flexion angle and bundle such that in hyperextension and at full flexion, the strain in the two bundles is significantly different. When the knee is hyperextended, the strain in the PLB is significantly greater than the strain in the AMB. This situation is reversed when the knee is highly flexed (greater than 75 degrees), with the strain in the AMB being greater than that in the PLB.

The results of this study support those of Amis & Dawkins (1991) and others; the displacement-strain mechanics of the PLB are different from those of the AMB during passive flexion/extension. Since strain has been shown to be the variable which determines ligament failure (Woo, 1982), these results indicate that any future attempts to characterize and/or predict ACL failure mechanisms should account for the strain in both the anteromedial and posterolateral bundles of the ligament. These findings also have implications for ACL replacement techniques which must consider that the ligament does no behave as a single homogeneous structure.

REFERENCES

1) Amis, A.A. et al. *J. Bone Joint Surg.*, 73-B(2), 260-267, 1991
2) Bach, J.M. et al. to be published in *J. Biomech. Eng.*, 1995.
3) Benninghoff, A. 1985
4) Berns, G.S. et al. *J. Biomech. Eng.*, 102, 392-400, 1992.
5) Fuss, F.K. *Anat. Rec.*, 230, 283-289, 1991
6) Woo, S.L.Y., *Biorheology*, 19, 385-96, 1982

ACKNOWLEDGMENTS

The authors are grateful to the Tyrolia corporation of Vienna, Austria for continued support of our research program on skiing injury prevention.

SUBJECTS WITH ACL RECONSTRUCTION HAVE LARGER MUSCLE CONTRIBUTIONS TO THE SUPPORT OF VARUS KNEE MOMENTS

David G. Lloyd and Thomas S. Buchanan

Departments of Rehabilitation Medicine and Biomedical Engineering, Northwestern University, and Sensory Motor Performance Program, Rehabilitation Institute of Chicago, 345 East Superior Street, Chicago, IL, USA, 60611

INTRODUCTION

Normal and ACL reconstructed (ACLR) subjects performed a series of experiments where they generated various combinations of varus or valgus (VV) and flexion or extension (FE) moments at the knee. Using the EMG and external load data recorded during these tasks as inputs to a biomechanical model, the contributions of the muscles and soft tissues to the total external load were determined. The results showed there was increased muscle activation to support the varus and valgus loads in the ACLR subjects. The modeling results showed that, when compared to the normal subjects, the ACLR subjects relied upon their muscles more to support varus loads at the knee. However, the was no difference between the groups for the valgus knee loads.

REVIEW AND THEORY

Poor knee joint stability during varus-valgus loading has been implicated as a possible reason for development of osteoarthritis of the knee (Andriacchi, 1993; Noyes et al. 1992, Schipplein et al. 1991). Both ligaments and muscles contribute to varus-valgus knee stability. Loss of the ACL ligament can reduce the varus-valgus stability of the knee (Markolf *et al.*, 1984; Noyes *et al.*, 1992). Thus the problems caused by knee instability is of particular concern for people who have had ACL injuries (Andriacchi, 1993). Daniel *et al.* (1994) have shown that people with ACL reconstructions have an increased risk of developing osteoarthritis.

Co-contraction of knee muscles during walking and other activities can possibly enhance knee stability (Olmstead *et al.*, 1986). Andriacchi *et al.* (1984) have shown that muscles may be activated to support an externally applied varus or valgus load. However, in static isometric tasks Lloyd and Buchanan (1995) have shown that muscles only support up to about 15% of the external load in pure varus or valgus in a normal subject group. However, ACL impairment may increase reliance on muscles to support varus or valgus loads.

The purpose of this work was to see if subjects who have had an ACL reconstruction (ACLR) 1 to 2 years previous, depend on their muscles more to maintain knee joint stability when compared to a normal age matched control group.

PROCEDURES

There were 2 distinct stages to this study. First, each of the subjects performed a series of experiments where they generated various combinations of varus or valgus (VV) and flexion or extension (FE) moments at the knee. Second, using the data recorded during these tasks as inputs to a biomechanical model, the contributions of the muscles and soft tissues to the total external load were determined. The term *soft tissues* refers to the passive structures of the knee i.e., ligaments and capsule.

Experimental tasks

Seven normal subjects and 4 ACLR subjects performed the experiments. The EMGs from 10 muscles that cross the knee and all 6 components of the external knee joint loads were measured during the experimental tasks. Each subject was seated on a small platform with support under the ischial tuberosities such that the thighs were unsupported so the subject was free to abduct or adduct the hip. A cast was placed on the leg just proximal to the ankle which was then fixed to a six degree of freedom load cell.

For the experimental tasks the subjects were required to produce forces at the load cell in the transverse load plane while producing no axial (proximal to distal) forces on the tibia and no net hip internal-external rotation moment. The net hip internal-external rotation moment would register as moments about x-axis of the load cell which the subject had to keep equal to zero. The tibial axial force would be a force on the y-axis of the load cell which the subject also had to keep equal to zero. The forces in the transverse plane were various combinations of anteriorly or posteriorly directed forces and medially or laterally directed forces. Visual feedback of all these 4 force types was given to the subject and the data was only recorded during the period when the subject matched the required forces for 1 second.

The forces generated by the subjects' at the load cell were directed radially in transverse load plane with 15° or 20° increments between directions. These forces corresponded to combinations of flexion or extension (FE) and varus or valgus (VV) moments at the knee. A moment direction of 0° corresponded to a pure valgus knee moment, 90° a pure extension moment, 180° a pure varus moment, and 270° a pure flexion moment. The anterior, or extension, and posterior, or flexion, components of these forces were generated by extension and flexion moments at the knee respectively. The medial, or varus, and the lateral, or valgus, force components were generated by hip adduction and abduction moments respectively. The tasks were performed at 3 different knee flexion angles; 50°, 70° and 90°, and each subject's hip flexion angle was kept constant at 85°. To negate the affects of fatigue, the subjects had regular periods of rest and the order of knee flexion angles was randomly chosen.

Biomechanical Model

The data from these experiments were analyzed using a biomechanical model of the knee. Each subject's mean responses at each force direction and knee angle were used as inputs to the biomechanical model. These inputs consisted of the external loads just above the ankle, the joint angles of the hip, knee, and ankle and the average EMGs normalized to EMGs recorded during maximal contractions.

Following is a brief description of the biomechanical model used. It is described in detail in Lloyd and Buchanan 1995. The biomechanical model consisted of an anatomical model developed using SIMM™ (Musculographics Inc.) and EMG driven Hill type muscle models to estimate muscle forces.

The biomechanical model had two distinct processing stages. First, the contributions of the muscles to the external FE moments were determined. It was assumed that there were no ligament forces contributing to moments in this plane. To account for subject variability, each subject's muscle parameters were adjusted to ensure a good fit between experimental and model predictions of flexion and extension moments. The parameter adjustment was performed using a non-linear least squares method. Second, once the muscle parameters, and hence muscle forces, were established, the muscle and soft tissue contributions to

external VV moments were estimated. If the muscles were insufficient to support the external VV moment, condylar lift off would occur and the soft tissues would be required to support the remainder of the external moment. In this case the joint contact moments could not assist in preventing condylar lift off since the joint contact forces can only be compressive. When the muscle moments were more than sufficient to support the external moment, there would be no need for the soft tissue moments and there would be compression under both condyles.

The soft tissue moments were normalized to the total external moment giving the Soft Tissue Ratio (STR). For each subject at each knee angle, the STRs at the varus moment directions and the STRs at the valgus moment directions were averaged respectively. The EMGs of the muscles that supported valgus moments and EMGs of the muscles that supported varus moments were also averaged respectively. The differences between these average values from the normal and ACLR groups was tested using a 3 factor ANOVA. The 3 factors were knee angle, varus or valgus moment, and subject group.

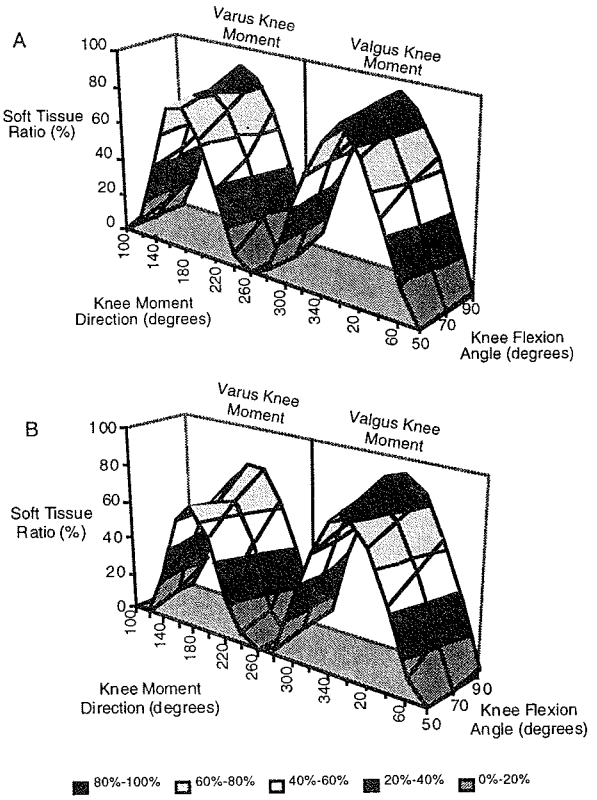

Figure 1. The soft tissue ratio for the different external moment directions and knee joint angles. A) is the average from the normal subjects, and B) is from the average from the ACLR subjects. Note the decrease in STR during varus moments for the ACLR subjects. This shows that under these conditions more of the load was supported by the muscles for ACLR subjects than for the normals.

RESULTS

In VV moment directions, the muscle contributions were insufficient to counter the external loads and, hence, soft tissue loading was required (figure 1). For all subjects (figure 1) the need for soft tissue loading forces increased as the external force direction moved further away from pure flexion (270° moment direction) or pure extension (90°) and peaked at pure valgus (0°) or pure varus (180°).

With a pure varus moment, the average STR, across all knee angles, was 83% for the normals and 70% for the ACLR subjects. The difference between the two groups was statistically significant ($p<0.01$). In pure valgus, the average STR was 92% in the normals and 87% for the ACLR, the difference not being significant.

	Soft Tissue Ratio (%)				*Average Muscle Activation*			
Knee	Normal		ACLR		Normal		ACLR	
Angle	varus	valgus	varus	valgus	varus	valgus	varus	valgus
50	34	44	27*	42	0.023	0.024	0.035*	0.050*
70	40	48	31*	47	0.030	0.035	0.045*	0.057*
90	49	56	40*	57	0.016	0.027	0.038*	0.043*

Table 1. Average Soft Tissue Ratios, and muscle activations for the varus and valgus moment directions. (*Significantly different to normal subjects, $p<0.01$)

The ACLR subject's had significantly smaller average varus STRs than the normal subjects ($p<0.01$) at all knee angles (Table 1). There was no significant difference between the average valgus STR moments from the two subject groups. The average activation of the muscles to support the varus and valgus moments was significantly different between the 2 subject groups.

DISCUSSION

Compared to the normal subjects the ACLR subjects had smaller soft tissue ratios during varus loading. They also had greater activation of the muscles supporting the varus moments. This means the ACLR subjects relied upon their muscles more to support the varus moments. This could be caused by reflexive alteration of the motor patterns due knee instability, or change of volitional control by training through the rehabilitation programs following surgery.

The ACLR subjects also had greater activation of muscles to support valgus moments compared to the normals. This, however, did not increase the muscular support of the valgus moments. This could have only occurred if there was a general increase in the activation of all muscles (muscles with varus and valgus moment arms) during valgus loading.

REFERENCES

Andriacchi, T.P. et al. *J. Orth. Res.*, 1:266-275, 1984.
Andriacchi, T.P. *J. Biomech. Eng.*, 115:575-581, 1993.
Daniel, D.M. et al. *Am. J. Sports Med.*, 22:632-644, 1994.
Lloyd, D.G. et al. *J. Biomech. Eng.*, (Accepted), 1995
Markolf, K.L. et al. *J. Bone Joint Surg.*, 66-A: 242-253, 1984.
Noyes, F.R. et al. *Amer. J. Sports Med.*, 20:707-716, 1992.
Olmstead, T.G. et al. *J Biomech.*, 19:565-577, 1986.
Schipplein, O.D. et al. *J. Orth. Res.*, 9:113-119, 1991.

ACKNOWLEDGMENTS

This work is supported, in part, by NIH Grant F05 TWO4864, the Dr. Ralph C. and Marion Falk Medical Research Trust and a grant from the Arthritis Foundation.

MINIMUM ENERGY TRAJECTORIES OF THE SWING ANKLE WHEN STEPPING OVER OBSTACLES OF DIFFERENT HEIGHTS

Li-Shan Chou, Louis F. Draganich, and Shin-Min Song*

Section of Orthopaedic Surgery and Rehabilitation Medicine, Department of Surgery
The University of Chicago, Chicago, Illinois 60637
*Department of Mechanical Engineering, The University of Illinois at Chicago, Chicago, Illinois 60680

ABSTRACT

The trajectories of the swing ankle during level walking and when stepping over obstacles of different heights were measured and predicted for eight healthy young adults. Unlike the measured trajectories, When stepping over obstacles the predicted trajectories of the swing ankle were just high enough for the swing toe to clear the obstacles. When stepping over obstacles the levels of work required to generate the measured trajectories were significantly ($p \leq 0.001$) larger than those required to produce the predicted trajectories. The results suggest that when crossing obstacles conservation of energy becomes a less dominant criterion than safety factor for governing the motion of the body.

INTRODUCTION

Recent experimental studies of gait when stepping over obstacles have demonstrated that the motion of the lower limbs resulted in a much larger clearance between the foot and obstacle than that found between the foot and ground during level walking (Chen et al., 1991; Patla et al., 1993). It was thought that this large clearance was produced to ensure safe crossing of the obstacle. In view of the results of our previous study which supported the hypothesis that gait is energy efficient during level walking (Chou et al., 1995), the question arose as to whether the strategy used for stepping over obstacles could be explained by the criterion of minimum energy consumption.

METHOD AND MODELING

Gait analysis was performed on eight healthy young adults (5 males, 3 females). The subjects had a mean age of 26 years (range, 18 to 33 years), an average height of 166 cm (range, 155 cm to 175 cm), and an average weight of 588.6 N (range, 435 N to 742 N). Subjects were instructed to walk barefoot along a 9.5 m walkway at a comfortable self-selected speed and step over an obstacle in their usual manner. Five experiments were performed: level walking and stepping over obstacles of 51, 102, 152, and 203 mm heights. Ground reaction forces were measured with a multicomponent force platform in the center of the walkway. Clusters of four infrared light-emitting diodes were rigidly attached to the feet, shanks, thighs, pelvis and the torso of the subject. The kinematics of the clusters were measured with an optoelectronic, 3-D digitizing system. The kinematic and force parameters were sampled at a rate of 100 Hz. The overall error of the system was less than 7 mm for a volume 2 m long, 1.5 m high, and 0.7 m wide.

During the single support phase of gait the lower extremities were modeled as a planar, five-link, open-chain (Fig. 1). A sixth link represented the head, arms and trunk (HAT) and was attached to the lower extremities at the position of the hip joint. A two-dimensional search space was defined, large enough to include that which might be traversed by the swing ankle from toe-off to heel-strike when stepping over an obstacle and excluded the space occupied by the obstacle. During swing, angular velocities and accelerations were predicted based on the assumption that the horizontal velocity and vertical acceleration of the swing ankle when traversing between two points in adjacent stages were constant. Then, using the predicted kinematic data for the swing limb and the experimentally obtained data for the stance limb, the recursive Newton-Euler method was used to compute the linear accelerations for all of the links and the forces and moments for all of the joints. A more detailed description of this methodology has been reported (Chou et al., 1995).

A multistage optimization method, dynamic programming (Bellman, 1957), was adopted to predict the optimum trajectory for the swing ankle (Chou et al., 1995). When searching for the optimum trajectory of the swing ankle there were two geometric constraints. First, the swing foot (heel-toe segment) was required to clear the ground, and second, it was required to clear the obstacle. The objective function selected was to minimize the mechanical work required by the joints of the lower extremities during the swing phase of gait.

Student's t-test was used to determine differences between the predicted and measured trajectories of the swing ankle and differences between the predicted and measured levels of total mechanical work during the swing period of obstacle-free level walking and during stepping over obstacles of four different heights. An α=0.0025 level of significance was used based on a Bonferroni adjustment for comparisons at 25 and 75 percent of the swing period and at the swing time of maximum height

of the swing foot for each of the obstacles. Linear regression analysis was performed to model the relationship between obstacle height and mechanical work generated during the swing period.

RESULTS

When stepping over the obstacle of 51 mm height, the predicted trajectory of the swing ankle was elevated just high enough for the toe to clear the obstacle and then the trajectory remained nearly horizontal until the toe crossed the obstacle (Fig. 2). When stepping over the obstacles of 102, 152, and 203 mm heights, the predicted trajectories of the swing ankle increased after toe-off until the toe crossed the obstacle. Just after the toe passed the obstacle, the predicted ankle trajectories for all four obstacle heights decreased rapidly to a height which was similar to the height of the ankle at heel-strike and then remained relatively constant to heel-strike. Except for the obstacles of 51 and 102 mm heights at 75% of the swing period, significant differences ($p \leq 0.002$) were found between the measured and predicted trajectories of the swing ankle.

Regression analysis demonstrated that the mechanical work, normalized by body weight, required to generate the measured and predicted trajectories of the swing ankle increased linearly ($p<0.02$, $r^2>0.92$) with obstacle height (Fig. 3). For the measured trajectories, there were significant increases in the mechanical work necessary for stepping over the obstacles of all four heights compared to level walking ($p<0.001$). Significant differences in the work required to generate the predicted trajectories were found between level walking and stepping over obstacles of 102, 152 and 203 mm heights ($p<0.05$). When stepping over obstacles the work required to generate the measured trajectories were significantly greater ($p \leq 0.001$) than those required to produce the predicted trajectories. However, during obstacle-free level walking a significant difference was not found in the work required for the measured and predicted trajectories of the swing ankle.

DISCUSSION

For the experimentally measured trajectory a significant larger amount of work was generated when crossing any of the obstacles compared to that generated for level walking. This larger amount of work was necessary not only to elevate the foot high enough to clear the obstacle, but apparently also to produce a large safety margin, more than 120 mm, between the toe and the obstacle. However, a similar increase in work was not observed for the predicted trajectories, presumably because a safety factor was not included in the model. When stepping over an obstacle significant differences were demonstrated in the trajectories of the swing ankle and in the amounts of mechanical work required between those experimentally measured and those predicted. This suggests that when stepping over an obstacle, a safe clearance over the obstacle may be more important than energy efficiency in order to avoid the cost of falling.

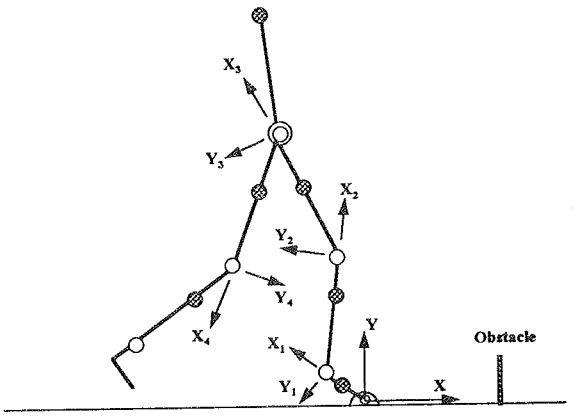

Figure 1. Planar linkage model for the swing phase of gait when stepping over an obstacle.

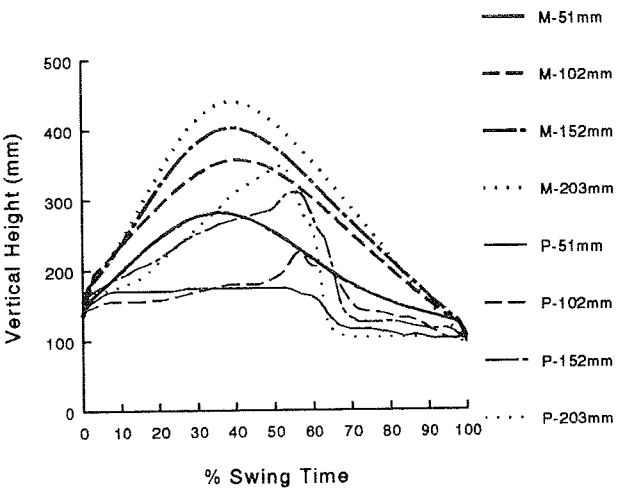

Figure 2. The measure (thick) and predicted (thin) trajectories of the swing ankle when stepping over obstacles of 51, 102, 152, and 203 mm heights.

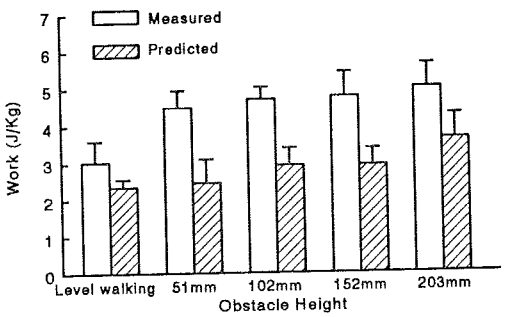

Figure 3. The average mechanical work computed from the measured and predicted trajectories of the swing ankle during level walking and stepping over obstacles of 51, 102, 152, and 203 mm heights.

REFERENCES

1 Bellman, *Dynamic Programming*, Princeton University Press, 1957.

2. Chen et al., *J Gerontology* 46, M196-203, 1991.

3. Chou et al., *J Biomechanics* 28: 377-385, 1995.

4. Patla et al., *Gait & Posture* 1, 45-60, 1993.

REPRODUCIBILITY OF THE KINEMATICS AND KINETICS OF THE LOWER EXTREMITIES IN STAIRCLIMBING

Bing Yu, Thomas Kienbacher, Eric S. Growney, Diana K, Hansen, Kai-Nai An
Orthopedic Biomechanics Laboratory, Mayo Clinic, Rochester, MN 55905

INTRODUCTION

The purpose of this study was to demonstrate and validate a newly established method for kinematics and kinetics of the lower extremities in stairclimbing. Three dimensional (3D) video and force plate data were collected for three trials for each subject during each of three conditions: ascending, descending, and level walking. The coefficient of multiple correlation (CMC) was used to determine the intra-subject reproducibility of joint angles and resultant moments. The results showed (a) that, generally, the kinematic and kinetic data of normal stairclimbing were reproducible, (b) that the sagittal plane data were more reproducible than those in the other two planes; and (c) that the kinetic data of the transition step from level walking to ascending or from descending to level walking are significantly less reproducible than those of the other steps, especially for the knee joint.

REVIEW AND THEORY

Stairclimbing (ascending and descending) is an important and common activity of daily living. Quantitative analysis of stair climbing has been suggested as an important evaluation procedure in the treatment of patients with different lower extremity disorders (Andriacchi, *et al.*, 1991). To apply quantitative analysis of stairclimbing as a clinical evaluation procedure, an understanding of the reproducibility of the kinematic and kinetic data in this activity is essential. McFadyen and Winter (1988) conducted the only study on intra-subject variance and inter-subject similarity of the kinematic and kinetic data in stairclimbing. In their study, the coefficient of variation (CV) was used to determine intra-subject variance in kinematic and kinetic data, and the Pearson product moment correlation coefficient was used to determine inter-subject reproducibility of the kinematic and kinetic data. The results of this study, to some degree, demonstrated that there are basic patterns in the kinematic and kinetic data of stairclimbing, especially for the knee. However, this study was basically two-dimensional in nature. Most of the results of this study were based on the data of three subjects, and the comparison of stairclimbing and level walking was actually based on the data of one subject on one step of stairclimbing. In addition, intra-subject reproducibility and the effect of walking condition on the reproducibility of the kinematic and kinetic data were not evaluated.

Due to the importance of joint angles and resultant moments in gait evaluation and limited knowledge on the reproducibility of these kinematic and kinetic data, the purposes of this study were: (a) to determine intra-subject reproducibility of the 3D joint angles and resultant moments of lower extremity in stairclimbing and (b) to examine the effects of walking condition on the reproducibility of these kinematic and kinetic data.

METHODS

Data Collection Six adults (3 males and 3 females) without any previous history of lower extremity disorders were recruited as the subjects for this study. Four video cameras and three force plates were used to record the subject's motion and ground reaction force at a sampling frequency of 60 Hz. A specially designed staircase was made which allows a four step staircase to be attached to two of the three force plates for measuring ground reaction forces during stairclimbing. Each step was 25.5 cm long and 80 cm wide. The rise between two consecutive steps was 18 cm.

Twenty one reflective markers were placed on the body of each subject as described by Kadaba *et al.* (1989). Each subject was asked to walk naturally at a self-determined speed during either level or stair walking. The video and force plate data were collected for the step immediately before ascending (Step A0) and the first two ascending steps (Steps A1 and A2) in ascending trials, the last two descending steps (Steps D2 and D1) and the step immediately after descending (Step D0) in descending trials, and two consecutive steps (Steps L and R) in level walking trials. Each subject had at least three trials in which he or she landed his or her feet on the force plates or stairs as required for each of ascending, descending, and level walking conditions.

Data Reduction The video records were tracked and 3D coordinates of the markers were calculated using the EV3D system (Motion Analysis Inc., Santa Rosa, CA). The 3D coordinates of the markers and force plate data were then used as the input to the OrthoTrak II System (Motion Analysis Inc., Santa Rosa, CA) to calculate joint angles and resultant moments at the ankles, knees, and hips.

Each gait cycle was divided into a stance phase and a swing phase and normalized to the full gait cycle. Joint resultant moments were normalized as the percentage of the product of subject's body weight (BW) and standing height (BH).

Determination of Intra-subject Reproducibility. The coefficient of multiple correlation (CMC) described by Kadaba *et al.* (1989) was used to determine the intra-subject reproducibility of each of the abduction/adduction (x), flexion/extension (y), and internal/external rotation (z) angles and moments at each of the ankle, knee, and hip joints.

Statistical Analysis. An analysis of variance with repeated measures was conducted to test the effect of walking condition on the CMC of each kinematic or kinetic variable. The 0.05 level of confidence was chosen to indicate statistical significance for each analysis of variance. The Bonferroni procedure was used in follow-up tests to guarantee the overall significance level for each analysis of variance.

RESULTS

It was found that the magnitudes of the CMCs for most of the joint angles were above 0.80, and that the magnitudes of the CMCs for the joint flexion/extension angles were generally above 0.95. Walking condition did not have a significant effect on the magnitude of CMCs for most of the joint angles except for the abduction/adduction angle of the hip joint. The

magnitude of the CMCs for the hip abduction/adduction angle during Steps A0 and D0 were significantly lower than those during the other steps ($p < 0.05$). The magnitudes of the CMCs for the hip abduction/adduction angle during different steps were presented in Figure 1.

It was also found that the magnitudes of the CMCs for most of the joint moments were about 0.90. Although, the magnitudes of the CMCs for most of the abduction/adduction and internal/external rotation moments are lower than that for the flexion/extension moment for the same joint, they are generally greater than the CMCs for the corresponding joint angles.

Walking conditions had significant effects on the magnitudes of CMCs of hip flexion/extension angle and knee flexion/extension and internal/external rotation moments. As shown in Figure 2, the magnitudes of CMCs of the knee flexion/extension and internal/external rotation moments during Step A1 and D1 were significantly lower than those during the other steps ($p < 0.05$)

The magnitudes of the CMCs for the joint angles and resultant moments during level walking matched those obtained in the study by Kadaba *et al.* (1989). There was no significant difference in the magnitudes of CMCs for any joint angle or resultant moment between Steps L and R.

DISCUSSION

The results of this study suggest that both joint angle and resultant moment data in stairclimbing are reproducible. However, it appears (a) that flexion/extension angles are more reproducible than abduction/adduction and internal/external rotation angles, (b) that flexion/extension moments are more reproducible than abduction/adduction and internal/external rotation moments, and (c) that the abduction/adduction and internal/external rotation moments are more reproducible than the corresponding joint angles. These results indicate the importance of kinetic data in the clinical evaluation of stairclimbing.

There are at least two possible explanations for the abduction/adduction and internal/external rotation angles and moments being less reproducible. First, it might be due to the error in the control exercised by the neuromuscular system (Kadaba *et al.*, 1989). Second, it might be due to the smaller peak-to-peak values of these variables. The data obtained in this study showed that the peak-to-peak values of the abduction/adduction and internal/external rotation angles and moments generally were smaller than those in the flexion/extension angles and moments, and that the standard deviations in the abduction/adduction and internal/external rotation angles and moments did not seem to be greater than those in the flexion/extension angles and moments. These results suggest that the second explanation is likely to be true.

The significant effects of walking condition on the magnitudes of the CMCs of hip abduction/adduction angle and knee flexion/extension and internal/external rotation moments suggest that these variables are less reproducible during the transition step from level walking to ascending or from descending to level walking than during the other steps. The peak-to-peak values of these variables during Steps A0 and D0 were very similar to those in the level walking (Steps L and R). No significant difference was found for these variables between level walking and the other steps in stairclimbing. These results combined together suggest that the lower reproducibility of these variables in Steps A0 and D0 were due to the adjustment or error in the control exercised by the neuromuscular system. During stairclimbing, step length was constrained by the dimension of the staircase. During Step A0, the neuromuscular system may need to make some adjustment to compensate for the error in foot placement relative to the first stair while during Step D0, the neuromuscular system may tolerate some extra error in the control because of the sudden loss of the constraint in the step length. These results indicate that the transition steps should be considered cautiously in the evaluation of stairclimbing.

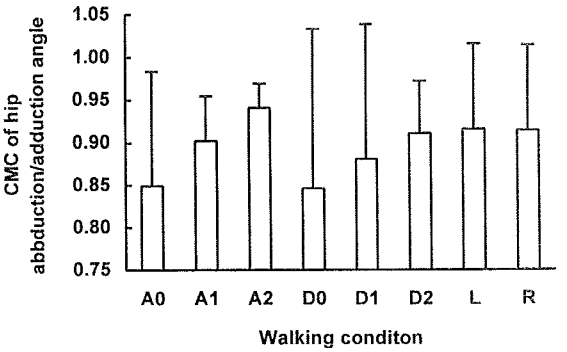

Figure 1. The effects of walking conditions on the reproducibility of hip abduction/adduction angle.

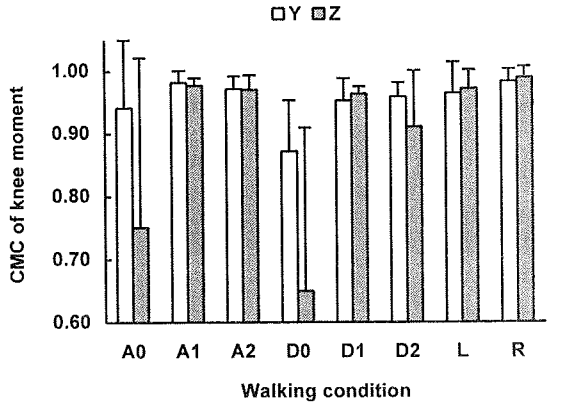

Figure 2. The effects of walking conditions on the reproducibility of knee flexion/extension (Y) and internal/external rotation (Z) moments.

REFERENCES

Andriacchi, T.P., *et al.*, 1991. **Basic Orthopaedic Biomechanics**, 51-92.

Kadaba, M. P., *et al.*, 1989. ***Journal of Orthopaedic Research***, **7**: 849-860.

McFadyen, B. F., *et* al., 1988. ***Journal of Biomechanics***, 21: 733-744.2

A BIOMECHANICAL STUDY OF THE EFFECTS OF SPEED AND EXPERIENCE ON STAIR CLIMBING MOVEMENT

J. Shih, T. Wang[#], M.H. Moeinzadeh[*], M.J. Adrian[#]

R. P. E. D. Department, University of Nevada, Reno, NV
[*]Department of General Engineering, [#]Department of Kinesiology
University of Illinois at Urbana-Champaign, Urbana, IL

INTRODUCTION

Since the 1980's, more and more people have become interested in the use of exercise devices for the improvement of health and fitness. The cycle ergometer, rowing machine, stair climbing machine, treadmill, and weight training equipment are among the most popular products used. Stair climbing is the fastest-growing form of aerobic exercise in the United States. Millions of people are working out on electromechanical stair climbing machines at home and in health clubs across the country. Although stair climbing machines provide for a flexible and convenient way to exercise, their appropriateness as an effective and biomechanically safe forms of exercise has not yet been investigated. No objective measures have been used to determine the impact forces and moment applied to each joint when people are walking on a stair climbing machine. Many questions remain unsolved.

When using a stair climbing machine, the exerciser is going up and down. From a biomechanical viewpoint , it is quite different from level walking and stair climbing (Andriacchi, 1980). The differences are reflected by changes in the range of motion in the different joints, and changes in the impact forces and moment applied on each joint in the lower extremities. In the study, we tested the hypotheses that speed and experience had no effect on kinematic and kinetic characteristics when people are walking on a stair climbing machine. Specifically, we tested the null hypotheses that there is no difference in biomechanical parameters a) with different speed of the stair climbing machine; b) between experienced and inexperienced people.

PROCEDURES

Subjects - Twelve healthy male stair climbing machine users recruited from the University of Illinois at Urbana-Champaign campus served as subjects for this study. Each subject was given written exercise history questionnaires. The answer to the first question "how often you use the stair climbing machine during a week" was evaluated for placement of the subject either in experienced or inexperienced category. Seven subjects were in experienced Group (EG) and five subjects were in inexperienced Group (IG).

Climbing Apparatus - A StairMaster 4000PT (StairMaster-Randal Sports/Medical Products, Inc. Kirkland, WA) was used as a stair climbing machine for this study. It was equipped with a pair of foot pedals and a microcomputer that monitored the climbing performance of the subject and displayed exercise time, climbing speed and distance. The four speed conditions were from 43 to 95 equivalent 8 inch steps per minute.

Data Collection - Elgons were used in this study to collect kinematic data. Five elgons were placed over the hip joint, knee joint, ankle joint, and both right and left pedal respectively. Output voltage signals are immediately converted into a computer. Thus the angle of hip, knee ankle joints and the right pedal were recorded by the computer. Two force transducers were placed on the pedals of StairMaster 4000PT, so the impact force being applied by each subject were recorded, thereby allowing the forces and moment in each joint to be calculated.

Data Analysis - Based on the data collected by elgons and force transducers, a sagittal plane rigid-body-linked segment analysis was used to determine joint kinetic parameters. This is commonly used to characterize gait (Winter, 1990). Maximum force applied on the pedal, maximum force applied on the handrails, maximum hip moment and maximum knee moment were normalized to the body mass as Fmax, FH, HM and KM respectively (Winter, 1987). A two-way ANOVA was used to test for significant effects among four speed conditions and between EG and IG.

RESULT AND DISCUSSION

The average value of Fmax in EG was 14.9% higher than that value in IG ($p<0.001$). The average value of FH in IG was 59.3% higher than that value in EG ($p<0.001$). Fmax was increased as the speed increased both in EG and IG, it ranged from 10.3 to 11.7 in EG and from 8.6 to 10.7 in IG (see Fig. 1)

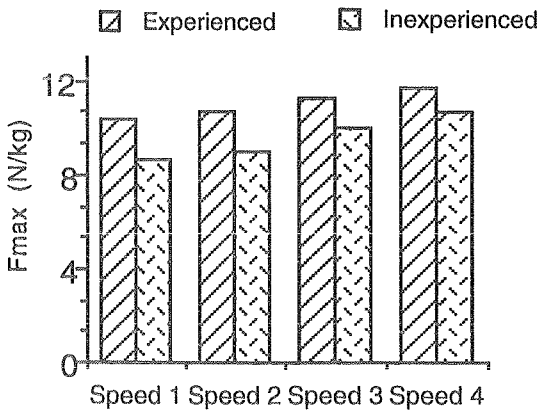

Figure 1. Fmax by main effect of subject and speed.

FH was decreased as the speed increased both in EG and IG, it ranged from 1.6 to 1.1 in IG and from 1.1 to 0.6 in EG (see Fig. 2).

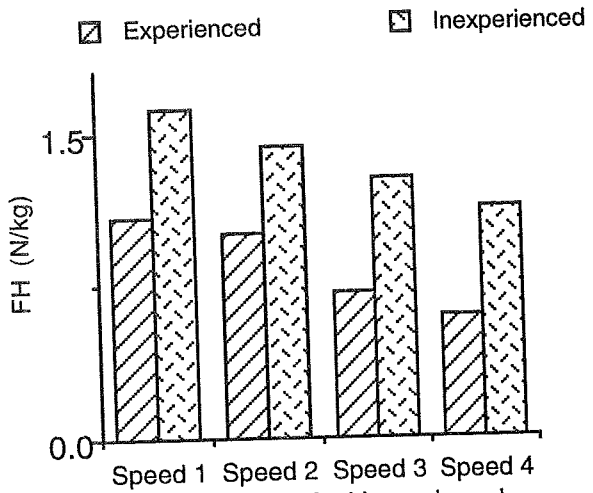

Figure 2. FH by main effect of subject and speed.

HM in IG was in a different trend in the higher speed condition than in EG. HM was decreased in IG and increased in EG with higher speed condition. The Average values of HM in IG was 31.1% higher than HM in EG. The average values KM in EG was 1.2; The average values of KM in IG was 1.0 (see Fig. 3 and 4).

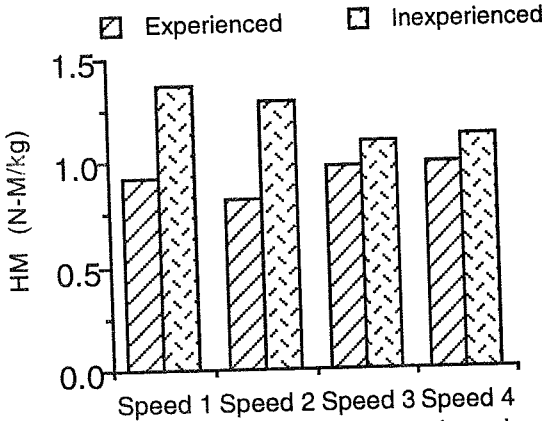

Figure 3. HM by main effect of subject and speed.

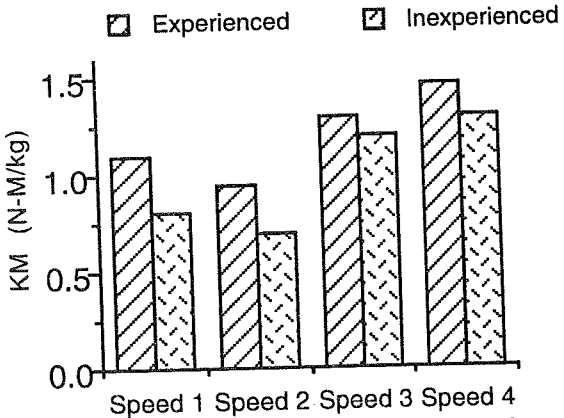

Figure 4. KM by main effect of subject and speed.

CONCLUSION

1) There are significant differences in Fmax, FH and HM crossing the four speed conditions and between experienced and inexperienced people; 2) Because inexperienced people tend to lean forward on the handrails, they have lower maximum force applied on the pedal but higher maximum force applied on the handrails than experienced people; 3) Walking on a stair climbing machine, people may have a lower risk of degenerative damage than jogging on a level surface because of the smaller magnitude of impact strides.

REFERENCES

Andriacchi, T.P., Andersson, G.B., Femier, R.W., Stern, D. & Galante, J.O. (1980). A study of lower-limb mechanics during stairclimbing. The Journal of Bone and Joints Surgery, 62 (5), 749-757

Voloshin, A., Wosk, J. & Brull, M. (1981). Force wave transmission though the human locomotor system. Journal of Biomechnical Engineering, 15, 21-27.

Winter, D., (1987). Biomechanics and Motor Control of Human Gait University of Waterloo Press.

Winter, D., (1990). Biomechanics and Motor Control of Human Movement. New York, New York. John Wiley & Sons Co.

ACKNOWLEDGMENTS

The study was supported by StairMaster-Randal Sports/medical Products, Inc. The authors thank the subjects for their cooperation.

BIOMECHANICS OF DESCENDING RAMPS IN YOUNG AND ELDERLY

M.S. Redfern[1,2] and J.J. DiPasquale[2]

Departments of Otolaryngology[1] and Industrial Engineering[2]
University of Pittsburgh, Pittsburgh, PA 15213

INTRODUCTION

The biomechanics of gait while descending ramps at varying angles was examined in a young and elderly population. Joint angles and moments were calculated for the lower extremities. Stride length decreased as ramp angle increased, while cadence slightly increased. Angle trajectories were affected by ramp angle, primarily at the knee between mid-stance and toe-off. Joint moments for the knee and hip changed as a function of ramp angle between heel contact and mid-stance. The elderly had significantly shorter stride lengths and increased cadence at all ramp angles compared to the young. The elderly also had significantly greater knee extension and lower knee moments at higher ramp angles. The results suggest that higher joint moments are generated at the knee and hip as ramp angle is increased in order to maintain relatively constant gait kinematics, and that the elderly reduce these moments by reducing step length and adjusting joint trajectories.

REVIEW AND THEORY

Falls account for 33 percent of hospitalized injured persons and 20 percent of those non-hospitalized. (Rice, et al., 1989). Falls are a particularly important problem in the elderly with the death rate due to falls among the elderly being 12 times greater than all other ages combined (Rice et al., 1989). Ramps present a falling hazard due to both slips and loss of balance, particularly when descending. The elderly may be at particular risk due to the motor control and strength requirements during gait during descent.

Shear forces at the feet increase as the ramp angle is increased, thus increasing the slip potential at the feet (McVay and Redfern, 1994; Buczek, et al.,1990;). Stride length, step period, and walking velocity while descending ramps in young subjects have been shown to decrease as ramp angle increased (Kawamura, et al.; 1991). Studies on treadmills report increased knee flexion during the end of stance phase and reduced hip flexion during swing phase with increased incline (Wall, et al., 1981). Joint moments as a function of ramp angle have not been reported in the literature. Moment generation will be directly related to strength and control requirements which may influence falls, particularly for the eiderly. The purpose of this study was to determine the effect of ramp angle on the kinematics and kinetics of descending ramps in young and elderly subjects.

PROCEDURE

Fifteen healthy young subjects (20-29 yrs) and 10 elderly subjects (> 65 yrs) participated. All subjects presented with no neurologic, orthopedic, or vestibular disease . Small reflective markers were placed on the left side of the subject, located at the lateral malleolus, lateral femoral epicondyle, greater trochantor, anterior superior illiac spine, radial styloid process, lateral humeral epicondyle, acromion and two markers on the head in line with the Frankfort plane.

A ramp (1.8 m length) which incorporated a force plate was used. A harness system with an overhead trolley was used to prevent injury from potential falls. Foot forces were recorded from the force plate on a 486 microcomputer via an analog-to-digital converter at a sampling rate of 240 Hz. Whole body movements in the sagittal plane were recorded using a standard Panasonic DV5100 video camera. Video recordings were digitized using the Peak Performance (Peak 5.0) motion analysis system. The kinematic data were combined with the foot force data to calculate joint moments at the ankle, knee and hip. Segmental masses and moments of inertia were used based upon Clauser et al. (1969).

The experimental protocol included five ramp angles (0, 5, 10, 15, and 20 degrees). A full factorial design was used with three replications per cell (5x3). Ramp angles were presented in random order, with all trials at that angle collected consecutively. Subjects were required to wear shoes with a standard 3/4 inch heel. They were instructed to walk at a comfortable pace during the experiment and were allowed practice at each ramp angle. During the trials, subjects walked to the top of the ramp, waited for approximately 30 s, then walked to the bottom of the ramp. Foot forces and video were recorded while walking down the rampway.

RESULTS

Mean walking speed in the young population (.58 (.12) m/s/stature) did not significantly change with ramp angle. Mean step length significantly decreased ($p<.05$) from .34 (.06) m/stature for level walking to .28 (.05) m/stature for 20 ^{o} ramp angle. Mean step period significantly decreased from .58 (.04) s to .53 (.05) s for a 20 ^{o} ramp angle. The elderly followed the same trend, but with significantly lower mean velocity (.43 (.05) m/s/stature) and step length (.26 (.03) m/stature at 0 ^{o} ramp angle), and increased step period (0.6 (.05) s at 0 ^{o} ramp angle).

Joint angle trajectories of the young varied as a function of ramp angle, primarily between mid-stance and toe-off. The most pronounced changes were found at the knee during the second half of the stance. (Table 1) Joint angle trajectories of the elderly were different from the young population as ramp angle was increased, particularly at the knee. Moments (normalized by body mass) generated at the ankle, knee and hip changed as a function of ramp angle, with the knee moment being most affected. (Figure 1) This was also true for both the young and elderly. Hip moments during the first 20 % of stance did not vary across ramp angles, but changed during the rest of stance from extension to slight flexion. Ankle moments had an increased dorsiflexion moment in the first 20 % of stance and a decreased plantar flexion moment occurring between 70 % and 80 % of stance phase. Differences between the young and elderly were most pronounced at the knee for higher ramp angles. In particular, the peak knee moments during the first half of stance showed differences between the young and elderly. (see Table 1)

Table 1: Key ramp angle effects on knee angles (@ 80 % stance) and knee moments (@ 25 % stance) for the young and elderly.

Ramp (deg)	Angle (deg)		Moment (Nm/Kg)	
	Young	Elderly	Young	Elderly
0	170	172	.30	.10
5	162	170	.75	.70
10	152	160	1.25	.80
15	140	150	1.50	1.20
20	128	145	1.70	1.25

DISCUSSION

The results of this study suggest that control of knee kinematics and moments is critical in walking down ramps. The body is lowered on the ramp primarily by increased knee flexion during the second half of stance. Higher knee extension moments for a longer duration are seen to accomplish this transfer on an inclined surface. Differences between the young and elderly were found in gait speed, cadence, angle trajectories and joint moments. The elderly subjects adjust gait kinematics during descent of ramps, resulting in a decrease in peak moments at the knee. While this study considered healthy elderly, the long duration of knee moments required during ramp descent may be increasingly difficult in elderly individuals with reduced function. Future work will investigate the biomechanics of gait on ramps for more functionally impaired or weak elderly.

REFERENCES

Buczek, et al. In *Slips, Stumbles and Falls*, ASTM STP 1103, ed. Gray, 1990, pp 39-54.

Clauser et al.AMRL-TR-69-70 (Ohio: A.M.R.L], 1969.

Kawamura, et al; *Acta Med Okayama*, 179-184, 1981.

McVay and Redfern, *J. AIHA*, , 626-634. 1994.

Wall, et al.*Ergonomics* , 807-816, 1981.

ACKNOWLEDGMENTS

Research was supported by CDC , R49/CCR308848

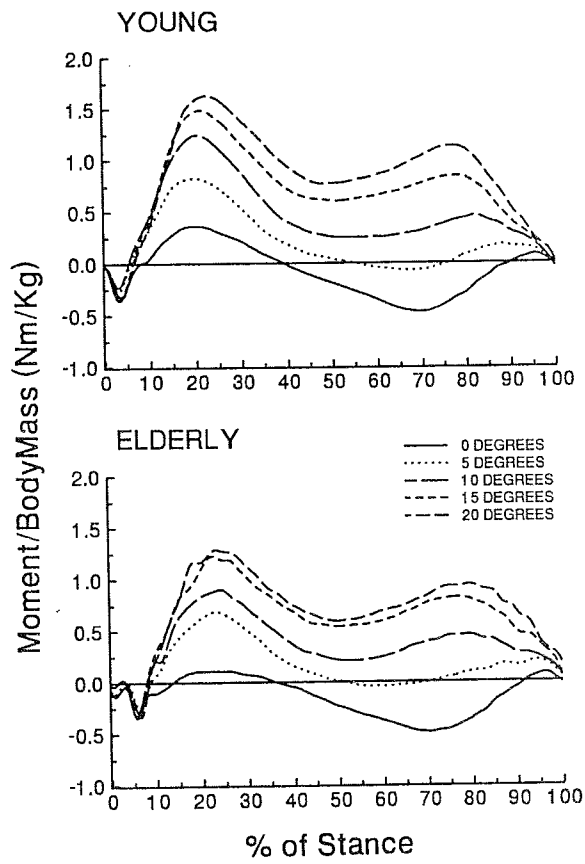

Figure 1. Moments generated at the knee as a function of ramp angle for young and elderly. (positive moment = extension)

EFFECT OF AN EXERCISE PROGRAM ON CHAIR-RISE BIOMECHANICS IN FRAIL ELDERLY

M. M. Gross[1§], N.B. Alexander[2§], M.R. Hofmeyer[2], W.L. Duren[1], and T. O'Bannon[3§]

[1]Department of Movement Science, [2]Department of Internal Medicine, [3]Department of Mechanical Engineering, and [§]Institute of Gerontology, The University of Michigan, Ann Arbor, MI 48109

INTRODUCTION

The ability to rise from a chair is an important activity of daily living that can be compromised with age, particularly in frail elderly (Schultz et al. 1992). The role of muscle strength decline in this problem is not known. In this study, we quantified chair-rise biomechanics in frail elderly before and after an exercise program to determine if chair-rise was improved with training.

REVIEW AND THEORY

Chair-rise challenges both strength and balance abilities. Schultz et al. (1992) suggested that many elderly may have sufficient strength to perform chair rise, and that factors such as balance may be important. Strength may be more of a limiting factor in the frail elderly, however, and chair-rise ability may improve with increases in muscle strength. The purpose of this study was to examine the biomechanics of frail elderly in a variety of chair-rise tasks designed to challenge both strength and balance, and to determine if chair-rise biomechanics improve following an exercise program in frail elderly.

PROCEDURES

30 subjects (mean age 84 yrs, range 69-93 yrs; 24 female) participated in the study. Subjects were residents of a local retirement community. Subjects were stratified by age, gender, and ADL status, and were assigned to training or control groups. Exercise subjects trained 3 times per week for 12 weeks on progressive resistance devices and practiced chair rise with a weighted vest. Control subjects participated 3 times per week for 12 weeks in group low-intensity flexibility exercises.

Biomechanics of chair rise were assessed for each subject at baseline (pretest), 6 weeks, and 12 weeks (posttest). Subjects rose from a chair with seat height adjusted to 3 different knee heights (140%, 100%, 60%), with and without use of hands. Subjects performed seven tasks: 140%, with hands (H140); 140%, no hands (NH140); 100%, with hands (H100); 100%, no hands (NH100); 100%, no hands, as fast as possible (F100); 60%, with hands (H60); and 100%, no hands, onto an 11 cm beam (B100).

Retroreflective markers were placed on each subject's left 5th metatarsal head, lateral malleolus, lateral femoral epicondyle, greater trochanter, acromion process, lateral humeral condyle, ulnar styloid process, and hand. Three 60 Hz video cameras were used with a Motion Analysis system to generate 3D coordinates of the joint markers. Reaction force data were obtained from force plates under each foot and in the chair seat. Hand forces were obtained from strain gauges attached to the chair arms.

Motion data were smoothed with a digital filter and differentiated to obtain joint kinematics. Joint torques were normalized by body height and weight. Linear momentum was normalized by body mass. Movement time was based on motion of the shoulder marker. Effect of training was detected using repeated measures analysis of variance with post hoc paired t-tests ($p<0.05$).

RESULTS

Movement times were shortest for F100 (2.01 ± 0.70 s) and NH100 (2.29 ± 0.56 s) tasks, and longest for H60 (4.57 ± 3.25 s) and B100 tasks (3.70 ± 0.85 s). Movement time decreased slightly from pretest to posttest for both groups; mean difference over tasks was 0.49 ± 0.24 s. However, the decrease was significant only for the exercise group in the H140 task. Relative ascent times were shortest for the H140 (60.7%) and NH140 (55.4%) tasks, and longest for the H60 (75.2%) and B100 tasks (74.7%). The relative amount of time spent in the ascent portion of the rise for each task was not affected by training.

The trunk angle at lift-off depended on both task and training. The trunk was most flexed in the H60, NH100, and B100 tasks, and was most upright in the H140 task (Fig. 1). Trunk angle increased significantly with training in the exercise group in five of the seven tasks (H140, NH140, H100, NH100, and B100) (Fig. 1). Knee and ankle angles at liftoff were not affected by training, except for a small but significant increase in the knee angle in the H100 task (83±4 and 86±5 deg, respectively).

Maximum normalized vertical momentum depended on task; it was greatest in the F100 (52.6±8.9 m/s) and NH100 (48.6±8.8 m/s) tasks, and least in the H140 task (19.0±6.6 m/s). Peak vertical momentum increased significantly with training only in the H140 task (20.1±7.3 to 24.1±6.8 m/s, $p<0.02$). Similarly, maximum horizontal momentum was greatest in the F100 (46.2±5.8 m/s) and NH100 (42.6±6.9 m/s) tasks, and least in the H140 task (23.3±5.7 m/s). Unlike vertical momentum, however, horizontal momentum was also large in the B100 task (46.6±6.6 m/s). There were no exercise effects on maximum horizontal momentum.

Maximum normalized joint torques depended on task but not on training. Peak hip and knee torques decreased when hands were used at both 140% (H=5.54 to 3.01; K=9.90 to 7.80) and 100% (H=8.11 to 4.40; K=11.8 to 9.65) chair heights. Hip and knee torques were greatest in the F100 and NH100 tasks, and lowest in the H140 task. Unlike the more proximal joints, ankle torques were greatest in the H60 (4.10) and B100 tasks (4.36).

Stability was assessed by the location of the center of pressure (COP) at liftoff in the hands free tasks, and by the time of hand release with respect to movement time in the other tasks. The COP tended to shift anteriorly with respect to the ankle from pretest to posttest (2.18±0.5 cm) for both groups, regardless of training. The time of hand release relative to total movement time did not change with training. Pretest mean hand-release time varied from 76.5% to124.7%.

DISCUSSION

Several tasks emerged which were particularly challenging to subjects' strength and balance abilities. The F100 and NH100 tasks had the shortest movement times and greatest vertical and horizontal momentum, requiring the greatest hip and knee torques. The H60 and B100 tasks had the longest movement times, longest relative ascent times, most flexed trunk at lift-off, and greatest ankle torques.

The primary effect of training was that subjects were more upright at the time of loss of contact with the chair, which is consistent with chair rise in young adults (Alexander et al. 1991). Although movement times during chair rise increase with age (Gross 1993; Alexander et al. 1991), movement time decreased significantly for only one task (H140) with training. The increase in vertical momentum with training for the task was consistent with this change.

The ability to control the trunk may be particularly important in performance of chair-rise. Although trunk control improved with our exercise intervention, stability measures were not changed and may be a limiting factor in some individuals. Interventions that include balance as well as strength training may further enhance the effectiveness of interventions designed to improve mobility in the elderly.

ACKNOWLEDGMENTS

We gratefully acknowledge the financial support of DVA grant E642 and a Predoctoral Fellowship from the Institute of Gerontology.

REFERENCES

Alexander N.B. et al. *J. Gerontol. Med. Sci.*, 46, M91-98, 1991.
Gross M.M. *Proc. XIV INt. Soc. Biomech. Cong.*, pp. 514-515, 1993.
Schultz A.B. et al. *J. Biomech.*, 25, 1383-1391, 1992.

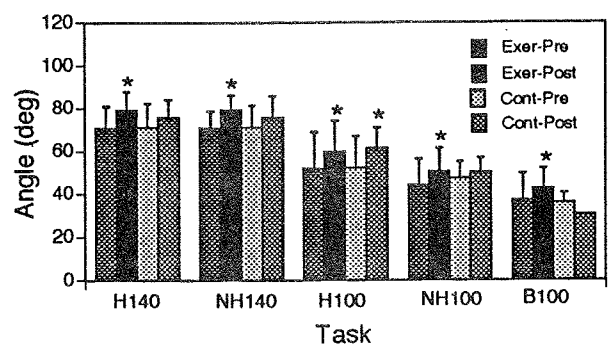

Fig. 1: Trunk angle at lift-off in chair rise tasks.

Trabecular Architecture in Relation to Functional Strain Patterns and Disuse

A. Biewener[1], N. Fazzalari[2], R. Baudinette[3], D. Konieczynski[1]

[1]Department of Organismal Biology & Anatomy, The University of Chicago, Chicago, IL 60637
[2]Department of Pathology, Royal Adelaide Hospital, Rundle Mall, Adelaide, S. Australia
[3]Department of Biological Sciences, Flinders University, Adelaide, S. Australia 5001

INTRODUCTION

The alignment of trabeculae within cancellous bone tissue has long been thought to arise and to be maintained in relation to the distribution of principal strain trajectories engendered through functional activity (1,2). Though commonly accepted and popularized as "Wolff's Law", the trajectorial theory of trabecular organization has been tested by few experimental data.

A goal of this study, therefore, is to attempt to correlate trabecular architecture with recorded patterns of functional *in vivo* strain within overlying cortical bone. We chose the calcaneus of the potoroo, a small Australian marsupial, as our bone model. A key advantage of the calcaneus is the simple and highly uniform cantilever-like loading that it experiences in transmitting Achilles tendon force to extend the ankle during gait. In addition, we also sought to examine how disuse would influence trabecular architecture; testing the hypothesis that, in the absence of functional strains, trabecular thickness and trabecular number would decrease, underlying an overall reduction in trabecular bone mass. We also hypothesized that the loss of elements would lead to a more random configuration of remaining trabeculae.

METHODS

Twelve adult male and female potoroos (0.87 to 1.35 kg) were used in the study and divided into two equal groups: Group A animals were trained to run on a treadmill, and then underwent surgery to attach a small rosette strain gauge (type FRA-1, Tokyo Sokki Kenkyujo) to the lateral aspect of the right calcaneus. Following recovery from surgery, the animals were exercised on the treadmill at speeds from 0.45 to 1.67 m/s and *in vivo* strains recorded. After these recordings were completed the animals were sacrificed, their calcaneii excised with the gauges intact, and the bones radiographed to determine gauge orientation.

Group B animals had a 5-8 mm length of their left Achilles tendon excised while under general anesthesia and were then allowed to recover. These animals were group housed for a period of 8 weeks, during which time their left calcaneus experienced little, if any, functional loading. The contralateral calcaneus served as the paired control in each animal.

After sacrifice, the calcaneii of Group A & B animals were vacuum embedded in plastic and sectioned to 8 to 10 μm. Two mid-sagittal sections of each bone specimen were then analyzed on an automated Quantimet 720 video image analysis system, which yielded the following stereological parameters: fractional trabecular bone volume (BV/TV), trabecular thickness (TbTh), trabecular spacing (TbSp), trabecular number (TbN) and trabecular anisotropy (TbAn).

RESULTS

In vivo and *in situ* recordings (produced by tensile forces applied to the Achilles tendon) indicated that principal compressive strains (ca. -600 to -1100 με) were directed at an angle of 159 ± 7° to the horizontal (longitudinal) axis of the calcaneus. Measurements of trabecular anisotropy correlated well with principal strain angle, showing maximal anisotropy (ie. alignment) close to 160° (Fig. 1; minimum TbAn at an angle of 70° corresponds to those trabeculae aligned in the principal tensile strain direction).

Measurements of tenotomized and contralateral control calcaneii revealed that following 8 weeks of disuse, trabeculae were 25% thinner and reduced by 16% in number (Fig. 2A). The decrease in TbTh and TbN corresponded to an overall 35% decrease in the trabecular bone volume fraction of tenotomized calcaneii

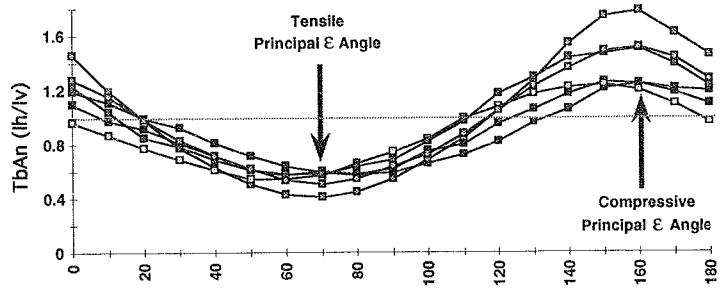

FIGURE 1.

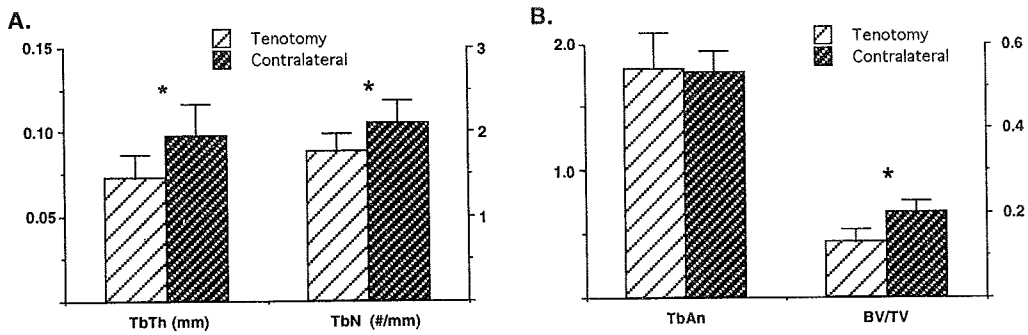

FIGURE 2.

(Fig.2B) and a 30% increase in trabecular spacing. Despite the thinning and loss of elements, however, no significant change in trabecular alignment (TbAn) was observed (Fig. 2B).

DISCUSSION

Our results are consistent with earlier studies of the sheep calcaneus, which indicated qualitative alignment of principal strains engendered during walking with underlying trabeculae (3) and generalized loss of bone mineral content following disuse (4). The present data show for the first time a direct correlation between measured *in vivo* principal strains and quantitated trabecular orientation. However, this correlation relies on the assumption that the orientation of surface cortical strains reflects the orientation of strains within the underlying trabecular network.

Our results support the hypothesis that disuse results in overall loss of trabecular bone by means of thinning and loss of trabecular elements. However, the fundamental structural alignment of the remaining trabeculae were not altered. This is similar to observations of trabecular alignment in the proximal tibia of rabbits with functional deficits induced by an osteoarthritis knee model (N. Fazzalari pers. obs.). It seems possible, then, that trabecular alignment develops with principal strain directions during growth and that the resulting alignment constrains realignment at maturity . To test this further, future studies could determine the response in trabecular alignment of growing bone to disuse, as the load-related signal guiding the active formation of trabeculae beneath the growth plate is altered.

REFERENCES

1. J Wolff (1982) *Des Gesetz Der Transformation der Knochen.* A. Hirschwald, Berlin.
2. WC Hayes & B Snyder (1981) *Trans. ASME* vol. 45: 43-57.
3. LE Lanyon (1974) *J. Bone Jt. Surg.* 56b:160-166.
4. CT Rubin, G Pratt, A Porter, LE Laynon & R Poss (1988). *Calc. Tiss. Int.* 42:309-312.

ACKNOWLEDGEMENTS

NIH AR-39828 to AAB

HIGH-RESOLUTION FINITE ELEMENT MODELS OF TRABECULAR BONE: THE DEPENDENCE OF TISSUE STRAINS AND APPARENT MODULUS ON IMAGING RESOLUTION

Oscar T. Chavez and Tony M. Keaveny
Orthopaedic Biomechanics Laboratory, Department of Mechanical Engineering
University of California, Berkeley, CA 94720-1740

INTRODUCTION

Knowledge of the stresses and strains in individual trabeculae ("tissue" values), and their relationship to whole specimen ("apparent") mechanical properties is of interest in a number of orthopaedic and biological areas, including osteoporosis, microgravity, and bone remodeling. Recent finite element studies have computed tissue stresses and strains and related them to apparent moduli using anatomically accurate "high-resolution" three-dimensional models of whole trabecular bone specimens [1–4]. Generation of the model geometry has been done by either serial sectioning [5] or micro-computed tomography [6]. The resulting three-dimensional images are digitized and converted into finite element models where each imaging voxel is mapped directly into a single eight-noded brick finite element, resulting in models with ≈ 500,000 elements [4]. Element sizes in these models have ranged from 20–50 microns on a side (thus the term "high resolution").

Due to the recent development of this powerful modeling technique, there remain a number of modeling issues that need to be addressed in order to ensure validity of the model predictions. One issue is the element size used in these models, and the dependence of model predictions, such as maximum tissue strain and apparent modulus, on this primary modeling parameter. To address this issue, we posed the following questions: 1) What is the sensitivity of the magnitudes of maximum tissue strain to element size? 2) Do locations of maximum tissue strain depend on element size? 3) What is the sensitivity of whole specimen properties such as apparent modulus and area fraction to element size? and 4) Are these trends dependent on trabecular architecture?

METHODS

Sagittal slices of three different bovine trabecular bone specimens, two tibial and one humeral, were used to create a series of two-dimensional finite element models of trabecular bone at different image resolutions and of different architectures (Figure 1). The dimensions of the slices were 7.67 mm x 8.06 mm, 7.78 mm x 8.14 mm, and 8.36 mm x 8.48 mm for the two bovine tibia and bovine humerus specimens, respectively. Each image was digitized at a pixel resolution of approximately 10 microns. These 10 micron pixels were consolidated into larger pixels to produce a series of images at lower resolutions, *i.e.* larger pixel sizes, ranging from 20 to 100 microns. The images were then converted into finite element models, where each pixel was transformed into a single eight-noded brick element (with a thickness equal to the pixel height). The finite element models ranged in size from 2,344 elements (bovine tibial #2, 100 micron resolution) to 51,619 elements (bovine humerus, 20 micron resolution).

Unconfined uniaxial compression tests in the vertical direction were then simulated with these finite element models, using a custom linear elastic finite element code running on a massively parallel super-computer (CM-5, Thinking Machines Corp. Cambridge, MA). The output parameters from these analyses were the tissue level strains in the vertical direction and the apparent modulus. To allow comparison with literature data, tissue level strains were expressed as percentages of the applied strain at the whole specimen level. Area fraction of bone was also calculated. Parameter studies were performed to determine the effects of element size (20–100 microns) on these output parameters, for all three specimens.

RESULTS

Maximum compressive tissue strains varied non-linearly with element size for the three specimens, indicating that element size had a substantial effect on maximum tissue strains (Figure 2); values in the vertical direction ranged from 3.78 (20 micron, bovine tibia #2 model) to 1.36 (100 micron, bovine humerus model) times the applied strain. With respect to the 20 micron model, percentage differences between the 100 and 20 micron models for these data were 42.9%, 35.4%, and 28.1% for the bovine humerus, bovine tibia #1 and #2 specimens, respectively. The location of maximum strain varied with element size for some cases.

The apparent modulus was also sensitive to element size, with percentage errors (with respect to the 20 micron model) ranging from 0.1–134%, depending on the element size and specimen architecture. Once again, the trends were non-linear. Area fraction increased linearly with increasing element size for all three models, with percentage errors of the 100 micron model (compared to the 20 micron model) ranging from 29-53%.

DISCUSSION

The demonstrated sensitivity of maximum tissue strain, apparent modulus, and area fraction to element size indicates the importance of element size when using high-resolution finite element models to study structure-function relationships and tissue level behavior for trabecular bone. One important finding was the sensitivity of errors to the architecture of the bone specimen under analysis. Thus, element sizes that are acceptable for one type of trabecular bone may not be acceptable for bone of a different architecture. Knowledge of these limitations will enhance interpretation of results from high-resolution finite element analyses of trabecular bone, and thus may lead to improved understanding of issues such as tissue level properties, failure mechanisms, and remodeling stimuli.

Our study is unique in that we examined as output parameters various measures of tissue level strain as well as apparent properties, and did so for specimens that exhibited different trabecular architectures. Our trends are consistent with those reported for fully three-dimensional models of a single specimen [4], providing support for our use of two-dimensional trabecular geometries in this analysis. Any limitations with the study relate primarily to the accuracy and generality of our findings. We do not know the "correct" values of tissue level strains. Toward this end, further studies are planned using smaller element sizes. However, the important issue here is that we have demonstrated that element size can be important, and that errors due to an inappropriate choice of this modeling parameter may be sensitive to the architecture of the bone. Since human trabecular bone is generally less dense with thinner trabeculae than the bone analyzed here, we expect similar or accentuated effects for human bone.

REFERENCES

1. Fyhrie and Hamid, Trans ORS, 175, 1993.
2. Hollister *et al.*, J Biomech 27, 433-44, 1994.
3. Edidin *et al.*, Trans ORS, 589, 1993.
4. van Rietbergen *et al.*, J Biomech 28, 69-81, 1995.
5. Odgaard *et al.*, J Microsc 159, 335-42, 1990.
6. Feldkamp *et al.*, J Bone Miner Res 4, 3-11, 1989.

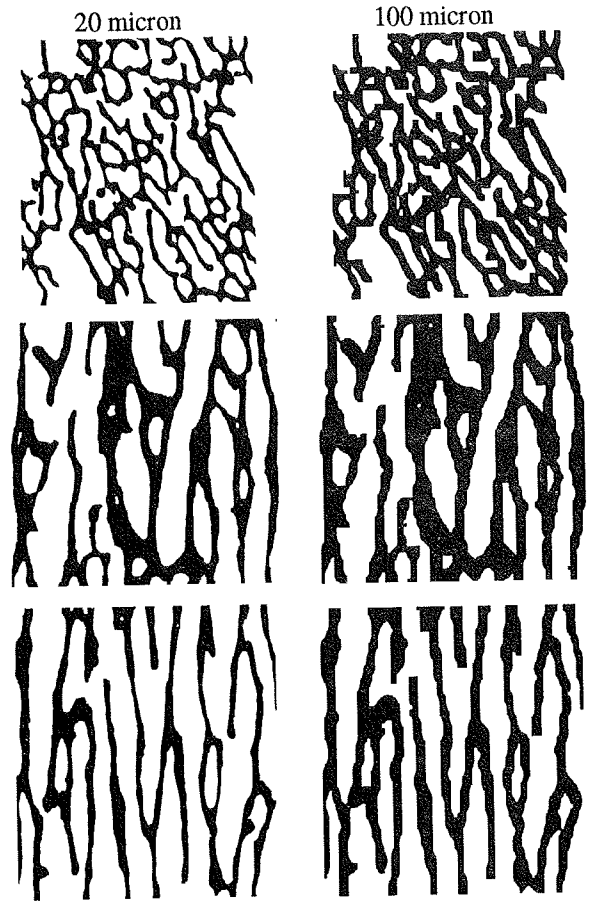

Figure 1: 2D models at high (left) and low (right) resolution of bovine humeral (top) and tibial (middle, #1, and bottom, #2) sections of trabecular bone. All models were loaded vertically in compression.

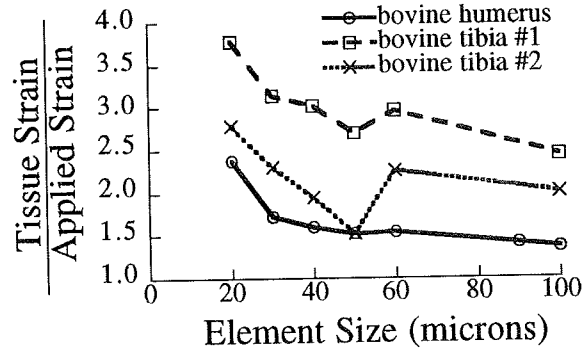

Figure 2: Maximum compressive tissue strain in the vertical direction vs. element size.

ACKNOWLEDGMENTS

Kapil K. Mathur for providing the finite element code; Dept. EECS at UC Berkeley and NSF CDA-8722788 for use of the CM-5; Whitaker Foundation and NIH R29 AR41481 for financial support; Jon Beck, James Chiu, and Denise Ching for technical assistance.

FINITE ELEMENT MODELING OF CANCELLOUS BONE DAMAGE: REDUCTION IN BONE STRENGTH AND STIFFNESS

D.P. Fyhrie, F.J. Hou, S.M. Lang

Breech Research Laboratory, Bone and Joint Center
Henry Ford Hospital, Detroit, Michigan 48202 U.S.A.

INTRODUCTION

Reduction in the ultimate strength of cancellous bone with age is partly responsible for the observed increase in vertebral fracture rate with age. However, in addition to a simple reduction in strength, it is possible that the trabecular organization of vertebral cancellous bone changes with age in such a way that older bone is less damage tolerant than younger bone. If this occurs, older bone will suffer a greater loss in strength and stiffness than younger bone for a given amount of damage (*e.g.*, micro-cracking), causing it to be more likely to fracture. This abstract reports on a nonlinear finite element analysis of human vertebral cancellous bone. Although no final conclusion can be made, the results indicate that younger tissue may be much more damage tolerant than older tissue.

PROCEDURES

Three vertebral cancellous bone cubes taken from different donors were scanned using microCT (Fyhrie et al, 1993). The first bone cube (Figure 1) had a 5mm edge length and a 5.18% hard tissue (bone) volume fraction (BV/TV). The second (Figure 2) and third bone cubes had 3.5mm edge lengths and values of BV/TV of 15.83% and 12.66% respectively. Special purpose programs were used to generate finite element models with 50 μm 8-noded hexahedral elements. The cancellous bone hard tissue was assumed to be elastic-perfectly plastic with a Young's modulus of 13 GPa and a yield stress of 67.5 MPa, approximately half the ultimate stress of haversian cortical bone (Mow and Hayes, 1991). Applied displacements equivalent to 2% strain were applied in the infero-superior (IS) direction through sliding interfaces with all other faces unconstrained. The finite element program NIKE3D was run on a SUN Sparcstation 20 workstation to perform the analyses.

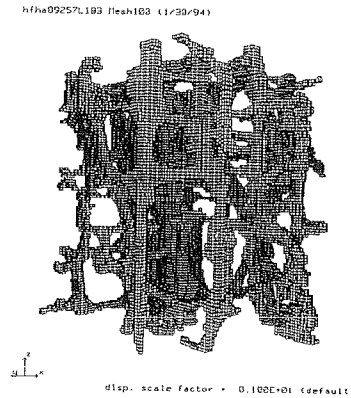

Figure 1: Low volume fraction model (5.18%).

The reaction force on the inferior face of the model was used to calculate apparent stresses at each increment of applied apparent strain. Secant modulus at each strain increment was determined and normalized by dividing by the initial modulus (E/E_0). At each strain increment, the percentage of the hard tissue that had become damaged (plastic volume fraction; Pl.V/BV) was calculated as the percentage of elements with non-zero effective plastic strain.

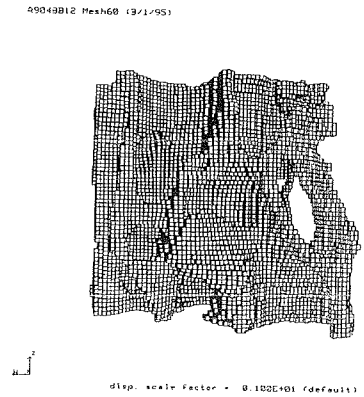

Figure 2: High volume fraction (15.83%).

RESULTS

The amount of plastic damage (Pl.V/BV) in the hard tissue was not a monotonic function of applied strain (Figure 3). For the three models currently completed, it was observed that lower BV/TV was associated with a decreased damage sensitivity to applied strain. For damage (Pl.V/BV) predicted by applied stress, a more intuitive result was found with lower volume fraction tissue associated with a more rapid increase in damage with applied stress (Figure 4). The sensitivity of cancellous bone stiffness to damage was estimated by plotting the secant modulus versus plastic damage (Figure 5). For the current model set, cancellous bone of lesser volume fraction loses stiffness more rapidly with damage than does higher volume fraction tissue.

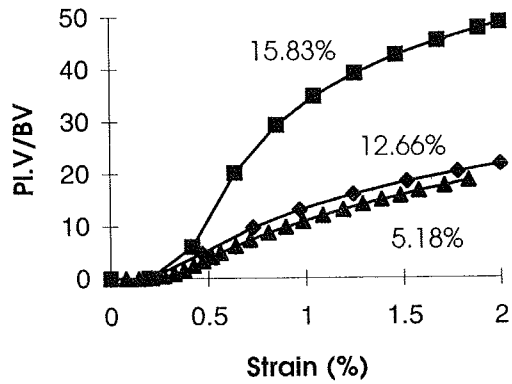

Figure 3: Pl.V/BV as a function of applied strain.

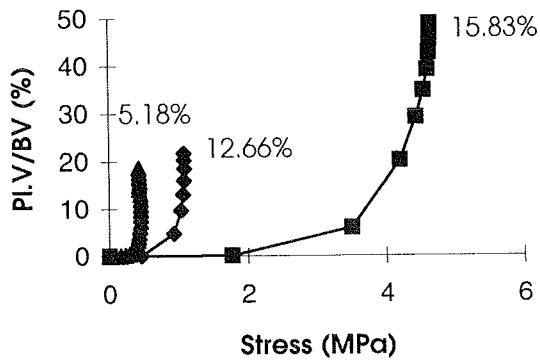

Figure 4: Pl.V/BV as a function of applied stress.

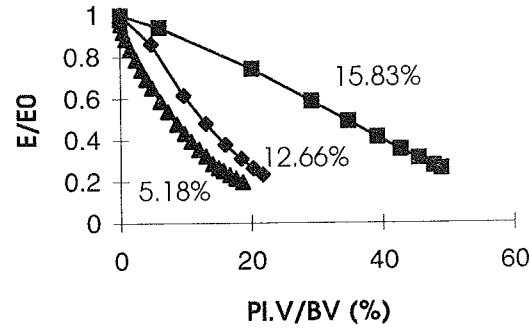

Figure 5: Residual stiffness (secant modulus) as a function of damage fraction (Pl.V/BV).

DISCUSSION

For the current model set, the sensitivity of the residual modulus to tissue damage, as estimated by secant modulus and Pl.V/BV, respectively, is negatively related to bone volume fraction (BV/TV). It is well known that BV/TV declines universally with aging, leading to the tentative conclusion that *old, low volume fraction bone is more damage sensitive than young, high volume fraction bone.*

We are currently investigating whether age related increases in damage sensitivity will result in an unstable "positive feedback" situation where small amounts of initial damage reduce bone stiffness sufficiently that the damage process continues in an unstable manner during normal activities of daily living.

REFERENCES

Fyhrie, D.P. et al. *J. Biomechanics*, 26(8), pp.955-967, 1993.
Mow, V.C. and Hayes, W.C., *Basic Orthopaedic Biomechanics*, Chap. 3, Raven Press, 1991.

ACKNOWLEDGMENTS

Dr. Brad Maker, Lawrence Livermore National Laboratory and NIH AR40776.

DETERMINANTS OF BONE MASS AND STRUCTURE DURING ADOLESCENT GROWTH

M. Moro [1], M.C.H. van der Meulen[1,3], B.J. Kiratli [4], L.K. Bachrach [2], D.R. Carter [1,3]
[1]Biomechanical Engineering, [2]Department of Pediatrics, Stanford University, Stanford, CA 94309
[3]Rehabilitation R&D Center, [4]Spinal Cord Injury Center, VA Medical Center, Palo Alto CA 94304

INTRODUCTION

Despite its importance in determining bone mass in later life, much remains unknown about bone mineralization in adolescence and the factors that influence it. We therefore measured bone mineral and cross-sectional properties of the femur in healthy Caucasian, African-American, Asian-American and Latino adolescents using DXA to study the determinants of bone mass and structure during adolescent growth and to evaluate gender- and ethnic-specific differences in bone accretion.

REVIEW AND THEORY

Bone mass and bone density in later life depend on both the rate of bone loss and the maximum bone mass achieved at skeletal maturity (Sambrook *et al.*, 1993). Because adolescence is a critical time in skeletal development, an understanding of the factors that determine bone acquisition in this stage of life is essential to maximizing peak bone mass and preventing osteoporosis.

Gender and ethnicity may play a significant role in the acquisition and loss of bone mass. Men have a lower incidence of osteoporosis than women, and African-American women have a lower prevalence of osteoporotic fractures than Caucasian women. However, few data are available on bone mineralization in males and non-Caucasians. In addition, body mass, age, hormonal status, physical activity and diet may influence bone acquisition in adolescence.

The purpose of this cross-sectional study was to 1) assess femoral mid-diaphyseal geometry and structural parameters in Caucasian, African-American, Asian-American and Latino adolescents and young adults, and 2) to determine the relative influences of age, body mass, gender, pubertal stage, and ethnicity on bone mass and structure during adolescent growth.

PROCEDURES

Healthy subjects between the ages of 9 and 26 were recruited in four ethnic categories: 98 African-American (57 females, 41 males), 97 Asian-American (48 females, 49 males), 101 Caucasian (53 females, 48 males) and 69 Latino subjects (43 females, 26 males). (African-American and Caucasian data were previously reported by van der Meulen *et al.*, 1994). DXA whole body scans were obtained using a Hologic QDR 1000/W Densitometer. The human subjects protocol was approved by the Stanford University Institutional Review Board, and written consent was obtained from each subject.

Body mass (BM), height, and pubertal stage (PS) based on Tanner classifications (Katzman *et al.*, 1991) were determined for each subject. The whole body scans were then analyzed using subregional software to determine diaphyseal length (L, cm) and mid-diaphyseal periosteal diameter (D, cm) of the left femur. L was measured along the longitudinal axis from the greater trochanter to the distal epiphysis, and D was calculated by dividing the projected area by the subregion length, making appropriate geometric corrections to account for the bone alignment angle in each scan. Bone mineral content (BMC, g/cm) was determined for a 6 cm section of the mid-diaphysis. Using the method of Martin and Burr (1984), these parameters were used to calculate bone mineral density (BMD, g/cm^2), cross-sectional moment of inertia (I, cm^4), section modulus (Z, cm^3) and whole bone strength index (S_b, cm^2).

Simple linear regression analyses were performed to determine the correlation between the bone measurements and age, pubertal stage, body mass and height. In addition, multiple linear regressions were performed on age, pubertal stage and body mass with ethnicity and gender as factors. Finally, a saturated model was used to regress body mass, age, ethnicity, gender and pubertal stage on all bone measures. The statistical results were analyzed for predictive power, and the effects of ethnicity and gender were tested by comparing regression slopes and intercepts. Differences were considered significant for $p < 0.05$.

RESULTS

Age-related increases in the structural parameters of all groups were observed during adolescence as expected. All femoral measures (L, BMC, BMD, D, I, Z, S_b) correlated more strongly with body mass than with age or pubertal stage. With the exception of bone length and BMD, the correlations between femoral measures and body mass were stronger than those with body height (Table 1).

While accounting for race and gender resulted in statistically different models, these factors provided little additional predictive value to the simple regressions of body mass on femoral measures. The saturated model explained only an additional 1 - 3% of the variance in BMC, D, I, Z and S_b compared to a model with body mass as the only predictor (Table 2).

Table 1: Coefficients of determination (adjusted r^2) for simple regressions

	Age	PS	Height	BM
L	0.28	0.36	0.83	0.48
BMC	0.41	0.46	0.66	0.86
BMD	049	0.50	0.68	0.65
D	0.24	0.33	0.47	0.77
I	0.15	0.21	0.32	0.70
Z	0.24	0.30	0.45	0.82
S_b	0.21	0.28	0.35	0.76

Table 2: Coefficients of determination (adjusted R^2) for multiple regressions

	2 Factor ANCOVA with Ethnicity and Gender			Age, PS, BM, Ethnicity, Gender
	Age	PS	BM	
L	0.46	0.51	0.54	0.60
BMC	0.50	0.56	0.87	0.88
BMD	0.54	0.59	0.71	0.76
D	0.35	0.43	0.79	0.79
I	0.26	0.32	0.75	0.73
Z	0.36	0.42	0.84	0.83
S_b	0.30	0.37	0.79	0.78

Gender had a significant effect on the relation between age and all bone parameters, with the male values generally greater at any given age. Ethnicity, however, did not affect the relation between age and the bone measurements. Adding gender to the age regression increased the predictive value of the model, but it was still less than that of body mass alone. For all bone parameters, the correlations with pubertal stage were greater than those with age, but still weaker than the correlations with body mass. Both gender and ethnicity had significant influences on the relations of pubertal stage and body mass with the bone measurements.

A comparison of the regression behavior of the 8 groups studied (Caucasian, African-American, Asian-American and Latino males and females) revealed that all groups had similar associations between body mass and bone measurements except for black females. In this group, there were slightly different regressions between body mass and L, BMD, I, Z, and S_b (but not BMC and D) (Figures 1 & 2). Despite these differences, accounting for ethnicity and gender added little, if any, information to the regressions with body mass alone.

DISCUSSION

Body mass is the best predictor of femoral bone mass and structural properties in all four ethnic groups and both genders studied. The stronger relation between all cross-sectional femoral parameters (except BMD) and body mass rather than height suggests that diaphyseal structure reflects a response to mechanical loading of the bone and not merely bone size. BMD may be an exception because it is an areal density which is influenced by bone size and is therefore influenced by body height (Katzman *et al.*, 1991). Furthermore, our results indicate that ethnicity does not influence the manner in which the measured femoral parameters change with age, while it does affect the relation between the femoral measures and pubertal stage or body mass. In summary, despite the influence of gender and ethnicity, differences in femoral cross-sectional properties are primarily related to differences in body mass.

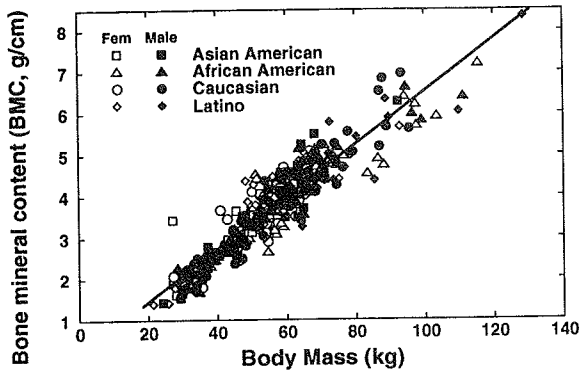

Figure 1: Correlation between BMC and body mass

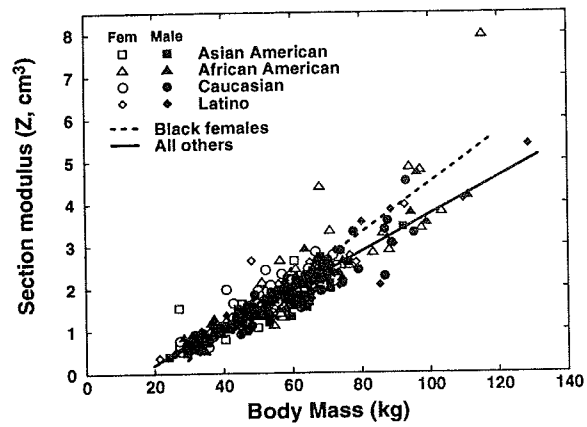

Figure 2: Correlation between Z and body mass

REFERENCES

Katzman et al. *J Clin Endocrinol Metab.*, 73, 1332-1339, 1991; Martin and Burr. *J Biomech.*, 17, 195-201, 1984; Sambrook et al., *Balliere's Clin Rheumatol,* 7(3), 445-457, 1993; van der Meulen et al. *Trans ORS*, 20, 1995.

ACKNOWLEDGEMENTS

This study was supported by NIH Grant DK45226, an NIH Minority Investigator supplement to M. Moro, and the Department of Veterans Affairs.

POTENTIAL INSTABILITIES IN BONE REMODELING

R.B. Martin
Orthopaedic Research Laboratories
UC Davis Medical Center, Sacramento, CA 95817

INTRODUCTION

Nonlinear dynamics has developed rapidly in the past decade. Phenomena which have historically been viewed as random and hopelessly unpredictable can often be shown to be chaotic states of rather simple systems which, under other conditions, behave predictably. This paper explores the possibility that certain bone conditions may represent chaotic states of the remodeling system, or perhaps pre-chaotic situations in which the system jumps continually between several states instead of maintaining an appropriate equilibrium.

THEORY

The discussion will be for cortical bone, although the same principles could apply to cancellous bone. Consider a region R containing a few cubic millimeters of cortical bone (e.g., in the femoral diaphysis). The remodeling variables defined hereafter correspond to those measured in two-dimensional cross-sections of R. We will be primarily concerned with interactions between mechanical stresses and remodeling, assuming biochemical variables constant. Remodeling is conceptualized in the form of Frost's Basic Multicellular Units (BMUs) inside the region R.

More recently, Frost (1987) introduced the "mechanostat" theory. This theory holds - in part - that diminished loading stimulates remodeling (to remove bone mass) and increased loading inhibits remodeling (to conserve bone mass). It is difficult for remodeling to add cortical bone since each BMU contains a resorption cavity (the "remodeling space") and each new osteon adds a Haversian canal, increasing porosity. Considerable experimental evidence exists supporting the mechanostat theory (Jee et al., 1990; Li et al., 1990). On the other hand, fatigue experiments have shown that remodeling is elevated by increased as well as diminished loading (Burr et al., 1989), consistent with its role in repairing fatigue damage.Therefore, remodeling is assumed here to be increased *both* when loading is too low, and when it is too high, as shown by the solid curve in Fig. 1. This is called the *Biological Curve* (BC) because it shows how strain affects remodeling.

Through the elastic modulus, strain is governed by bone's porosity. The dashed curve shows the mechanical effects of porosity on bone strain, as opposed to the remodeling effects of strain on porosity. This curve is therefore called the *Mechanical Curve* (MC) because it depends only on the bone's structure and composition. The BC and MC interact to regulate the mechanical aspects of internal cortical bone remodeling by BMUs.

The BC depends on the relationships between strain and remodeling rate and between activation frequency and porosity. There is convincing evidence that activation frequency increases both in disuse states (Schaffler, 1990) and when fatigue damage is substantial (Mori and Burr, 1993). Lacking quantitative data, a sigmoidal relationship is assumed for the left and right ends of the BC:

$$f_a = f_{a0} + \frac{(f_{am} - f_{a0})}{1 + \exp[D + A(f_{am} - f_{a0})(\varepsilon_0 - \varepsilon)]}$$

Here, ε_0 is an "set point" strain, f_a is activation frequency, and f_{a0} and f_{am} are its minimal and maximal values. A controls the rate at which f_a increases and D controls how much the strain has to change before the activation frequency is substantially affected ("dead zone"). To approximate the relationship between f_a and porosity, an equation of the form

$$P = f_a(\tau,\xi) + P_C$$

was derived, where τ represents the periods of each remodeling phase and ξ the mean osteonal cavity size for each. P_C is the Haversian canal porosity.

To define the MC, the relationship

$$\varepsilon = \sigma/E_0 (1 - P)^3$$

was used, where σ is the applied stress (assumed fixed), P is porosity and E_0 = 25 GPa.

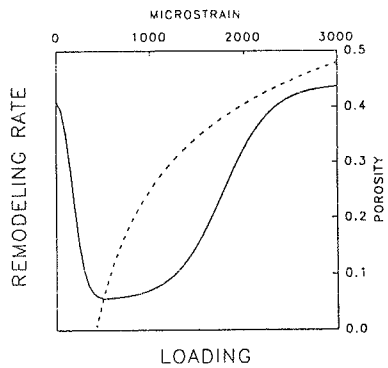

Figure 1

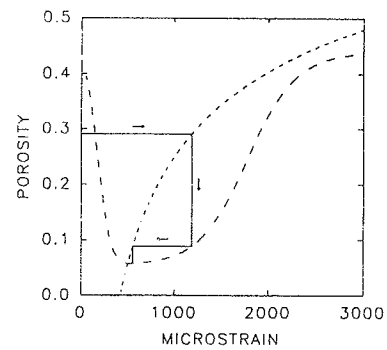

Figure 2

RESULTS

The behavior of the model is usually stable. If a local anomaly increases P above the equilibrium value (Fig. 2), E is reduced and ε increased. Through the BC, the new strain adjusts f_a such that porosity is reduced. Further corrections bring both P and ε back to the equilibrium point at the intersection of the

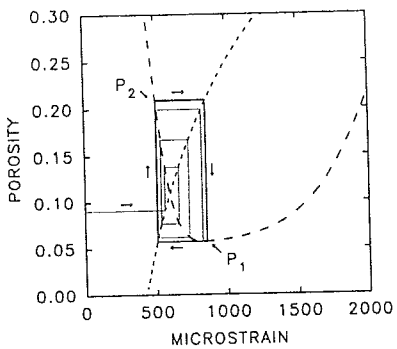

Figure 3

two curves. On the other hand, changes in the shapes of BC or MC can change the behavior of the system. Two illustrative situations, previously suggested by Frost (1987) as the basis for metabolic bone diseases, assume new interpretations in the context of this model. It has been postulated that some osteoporoses are caused by errors in the "set point" for adaptive bone remodeling. Here, this involves shifting the BC to the right, keeping its shape and the MC the same. After the optimal strain has increased about 50%, the system bifurcates and a limit cycle is produced with an attractor of period 2 (Fig. 3). P and ε shift endlessly between two values. (The remodeling rates associated with these two states, one abnormally high, the other essentially normal, mimic high and low turnover osteoporosis patients.) Increasing ε_0 further produces more bifurcations, until the system becomes chaotic (Fig. 4). The chaotic domain includes almost the entire range of possible remodeling rates.

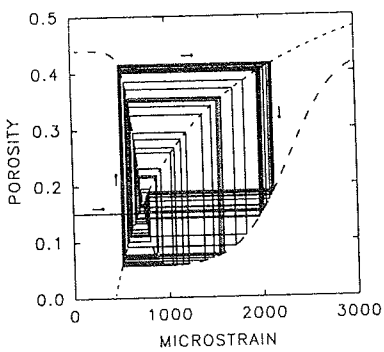

Figure 4

As a second example, consider the disease osteogenesis imperfecta (OI), caused by a genetic defect in Type I collagen synthesis. This may effect both the BC and MC. It is reasonable to postulate E_0 for OI bone is low; if so, strain will be increased at every porosity. In addition, the OI bone may

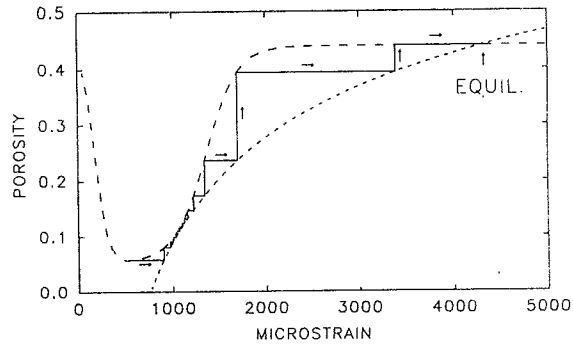

Figure 5

be more susceptible to fatigue damage, so that high strain side of the BC will rise more steeply than normal. If the two curves are thus modified, the system's equilibrium point can be at very high strain and remodeling values. Fig. 5 shows how such a system would move from the original equilibrium P and ε values to an new, pathologic equilibrium point if the MC and BC changes were great enough. This could account for the severe osteopenia and high remodeling rates, as well as the great fragility, of OI skeletons.

DISCUSSION

It must be emphasized that the correct shapes of the Biological and Mechanical Curves are not known. They could be quite different from those derived here. Even if they are, however, the theoretical basis of this paper, and its clinical implications, would not necessarily be undermined. This is because the existence of the instabilities which have been discussed is not critically dependent on the precise shapes of the two curves. What is important is that the Biological Curve is trough-shaped (provides two values of strain for each porosity), and that the Mechanical Curve is monotonic and intersects it at some point. The latter conditions are required for equilibrium under normal conditions, and double-valuedness is bound to obtain if both disuse and fatigue responses increase remodeling. Feigenbaum (1980) has shown that the progression from stability, through a series of limit cycles of increasing order, to chaos, is a *universal* behavior for systems of this type, *independent of the precise shapes of the curves.* This argues strongly in favor of the usefulness of the present model as a tool for understanding bone remodeling, Wolff's Law, stress fracture dynamics, and metabolic bone diseases.

REFERENCES

1. Frost, Anat. Rec 219, 1-9, 1987
2. Jee & Li, Anat Rec, 227, 418-426, 1990
3. Li et al., Anat Rec, 227, 12-24, 1990
4. Burr et al., Bone, 10, 215-221, 1989
5. Schaffler, Trans ORS, 15, 187, 1990
6.Mori & Burr, Bone, 14, 103-109, 1993

BONE BLOOD FLOW IS ELEVATED PRIOR TO OSTEOCLASTIC ACTIVITY INITIATED BY DISUSE OSTEOPENIA

Ted S. Gross, Ariff A. Damji, Robert C. Bray, and Ronald F. Zernicke

McCaig Centre for Joint Injury and Arthritis, Department of Surgery
University of Calgary, Calgary, Alberta, Canada T4N 2N1

INTRODUCTION

Bone is sensitive to a wide range of biophysical stimuli, but the pathway by which the loss of mechanical stimuli is translated into cellular recruitment is poorly understood. One physiologic process associated with remodeling in a wide range of tissues is increased tissue blood flow (1). Our study assessed whether the bone blood flow alterations initiated by disuse osteopenia precede the recruitment and differentiation of osteoclasts ultimately responsible for bone loss. Should these changes precede osteoclastic activity, we propose that blood flow, potentially via endothelial cells, may actively participate in the initiation of bone resorption.

REVIEW AND THEORY

Description of bone's vascular supply as an active mediator of tissue adaptation (as opposed to an entirely passive mechanism of cellular and nutrient transport) was reported in the early 1800's (2). More recently, endothelial cells have been shown to respond to altered fluid flow by adapting their morphology and expressing a number of factors that enhance osteoclastic differentiation or act as paracrine regulators of bone cell activity (3,4). In a preliminary *in vivo* study, we assessed bone blood flow following 4 wk of disuse, and found that cortical bone blood flow was elevated (5). However, as osteoclastic resorption had already begun, it was unclear whether these flow alterations were involved in initiating the resorptive process or were the byproduct of elevated cellular activity. Previous work with the functionally isolated avian ulna model identified 10 days as the time period necessary for disuse osteopenia to be transduced into the differentiation and recruitment of osteoclasts to bone surfaces (6). By examining flow alterations following 7 days of disuse, the current study examined the hypothesis that elevated bone blood flow precedes osteoclastic recruitment initiated by disuse.

PROCEDURES

Twelve adult white Leghorn roosters (1 yr) were randomly assigned to three groups of four animals each (1 wk disuse, 1 wk sham surgery, zero-time controls). The left ulna of each animal within the disuse group was isolated from mechanical stimuli via parallel metaphyseal osteotomies (7). Small bone wafers (2 mm thick) were removed at both metaphyses, and the exposed diaphyseal bone ends were covered with methacrylate filled delrin caps. The right ulnae served as intact, contralateral controls. The animals ambulated freely in group housing for 1 wk, while the left ulnae remained unloaded due to the osteotomies. Animals in the sham surgery group underwent an identical surgical procedure to that used for the disuse group. All feathers were removed from the wing, and the metaphyseal bone ends were exposed via 2 cm incisions. Partial osteotomies were then performed through 1/3 of the cortex at both metaphyses. This procedure disrupted the marrow and bone blood supply at these sites, but maintained the structural integrity of the left ulnae. The right ulnae of these animals were left undisturbed, and the animals were allowed free ambulation in group housing. Zero-time control animals were untouched prior to the microsphere procedure. For blood flow measurements, the animals were anesthetized and the aortic root cannulated retrograde from the right carotid artery. Colored microspheres in mixed suspension with saline (6 million, 15.5 μm dia.) were vortexed for 1 min and then injected into the base of the aorta over a 30 s period. Starting 10 s prior to the injection, a reference blood sample was drawn for 1 minute at 3 ml/min from a second catheter placed in the anterior tibial artery. After sacrifice, kidney, lung, and reference blood samples were removed and digested in 4M KOH. Using a diamond wafer saw, a 5 mm long cross-section was cut from the mid-diaphysis of each experimental and control ulna. The sections

were cleansed of marrow, decalcified, and then digested. Microspheres within the bone samples were isolated by filtering the digested tissues through a 7 μm polyester filter, and then directly counted with an epi-fluorescent microscope. Spheres within the reference blood sample, kidney, and lungs were assessed by eluting the dye from the trapped spheres with DMF and applying spectrophotometer readings to manufacturer calibration curves. Standardized blood flow (ml/min/100g) was determined by relating the sphere count of a tissue sample to the reference blood sample and normalizing to the mass of the tissue sample. Non-parametric Mann-Whitney tests ($p=0.05$) were used to (a) identify any differences between blood flow in the left (exp) and right (control) ulnae of each group, and (b) to determine if blood flow within the left ulnae differed between groups.

RESULTS

Mean (± S.E.) blood flow values were within 10% for the left and right kidneys and lungs. Mean blood flow was equivalent in the left and right ulnas in the zero-time group (2.8 ± 1.4 vs 2.1 ± 1.0 ml/min/100g). Sham surgery did not alter blood bone blood flow at 7 days post-surgery (2.3 ± 0.5 vs 3.7 ± 1.4). However, 7 days of disuse stimulated a 520% increase of blood within the experimental ulnae compared to intact contralateral controls (14.5 ± 5.5 vs 2.8 ± 1.3). Blood flow in the disuse ulnae was significantly greater than blood flow measured in the left ulnae of the zero-time and sham surgery groups (Fig 1).

DISCUSSION

The left/right symmetry of kidney, lung, and bone blood flows in the zero-time group indicated that the injected microspheres were adequately mixed and evenly distributed throughout the animal. There were no contralateral blood flow alterations in the model, nor did the sham surgery induce flow alterations in the ulna midshaft at 7 days post surgery. Thus, the 5-fold elevation in blood flow observed in the disuse bones was not due to surgical influences. Importantly, the flow elevation occurred prior to the onset of osteoclastic resorption. Using a simplified model to estimate shear stress due to flow in small vessels (8), we estimate that these flow elevations are sufficient to induce local shear stresses of 20 to 30 dynes/cm^2. Recognizing the extreme sensitivity of endothelial cells to local flow fluctuations (9), this stimulus would be sufficient to induce expression of vasoactive substances by endothelial cells (e.g., prostaglandins, endothelins, and nitric oxide). As these substances are known to initiate osteoclastic differentiation or act as paracrine regulators of bone cell activity, our data suggest that tissue blood flow may actively participate in the initiation of bone resorption.

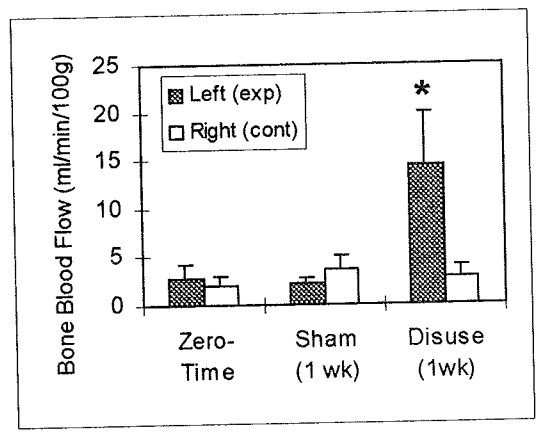

Fig. 1. Mean standardized blood flow (+S.E.) in the left and right ulnae. Blood flow in the ulnae exposed to 7 days of disuse was significantly elevated when compared with contralateral controls, and the left ulnae of the zero-time control and sham surgery groups ($p<0.05$).

REFERENCES

1. Hansen, et al., *Am J Phys,* H38-H46, 1992.
2. Jaffe, *Arch Surg,* 20(3): 355-385, 1930.
3. Alam, et al., *Endocrin,* 130:3617-3624, 1992.
4. Fiorelli, et al., *J.B.M.R.,* 9(3): 329-337, 1994.
5. Gross, et al., *A. Soc. Bio.,* 19:165-166, 1994.
6. Bain, et al., *J.B.M.R.,* 5(S2):S217, 1990.
7. Rubin, et al., *J.B.J.S.,* 66A: 397-402, 1984.
8. Arden, et al., *Neuropeptides,* 27:39-51, 1994.
9. Hecker, et al., *Am J Phys,* H828-H833, 1993.

ACKNOWLEDGMENTS

This work was supported by The Arthritis Society, Medical Research Council, Alberta Heritage Foundation for Medical Research, and the Natural Sciences and Engineering Research Council.

FORCES APPLIED BY ELITE AND SUB-ELITE SPRINT KAYAK PADDLERS

R.J. Neal and D.A. Aitken

Department of Human Movement Studies, The University of Queensland
Brisbane, AUSTRALIA

INTRODUCTION

In response to the need to measure the forces applied to the paddle, Aitken and Neal[1] developed a system that utilises strain gauges attached to the shaft of the paddle to measure the forces applied by the kayaker whilst paddling on the water. These data as well as the boat's velocity relative to the water were collected as subjects paddled over a 500 m course. The purpose of this study was to use the system of Aitken and Neal to investigate differences in technique between elite and sub-elite paddlers.

PROCEDURES

Subjects

Ten male subjects aged between 18 and 30 years, with varied paddling backgrounds, formed the experimental group. The subjects were assigned to one of two groups based on their performance at the 1992 Australian Sprint Kayak Championships). The elite group (N=5) were those paddlers who reached the final of either the K1 1000 m or 500 m races while the sub-elite was comprised of sprint kayak paddlers who competed at the Australian championships but did not reach the final in either the K1 500 m or 1000 m events.

Measurement procedures

All testing was performed on a non-tidal 500 m marked course. Each subject completed a 500 m time trial using the instrumented paddle, with the pitch of the blade and the length of the paddle adjusted so as to duplicate the dimensions of his regular paddle. The subjects were able to choose between a Cleaver-X or Hungarian boat (the two most commonly used boats in Australia). The seat position and foot bar were positioned so as to mimic the athlete's regular boat. The paddlers were also given 30 min. before the time trial to familiarise themselves with the test boat and paddle.

The boat and paddler were modelled as a single system to which the following forces are applied. Vertical and lateral accelerations were considered negligible thus the buoyant (F_b) and weight (mg) forces were considered equal. The inertia force ($m\dot{v}$) of the boat could be obtained by differentiating the velocity-time trace and the propulsive force on the blade (F_p) was measured using the strain gauged paddle.

The strain gauges were arranged so that they could detect the shear force applied by the water to the blade. Thus, the propulsive force was assumed to equal this shear force. (Note: Pilot testing using video cameras indicated that the effect of paddle angle was less than 10% and that this error occurred at the beginning and end of the strokes when the force was small anyway). Pairs of gauges, one undergoing compression and the other experiencing tension, were placed at two positions at each end of the paddle, between the hand and the blade. The sets of gauges were placed perpendicularly to the direction of the force applied to the blade. This setup was duplicated at the other end of the paddle so that the forces applied at the right and left hand ends of the paddle could be measured.

Data on the forces applied to the paddle and the boat's velocity were collected continuously on a 7 track Teac data recorder and subsequently digitised using an A/D board and software at 200 Hz. The following variables were calculated and each group's results were averaged for every 10 single sided strokes throughout the entire time trial.

1. Peak force (F_{max})
2. Work ($\int F\,ds$)
3. Power (dW/dt)
4. Time to peak force
5. Time paddle was in the water

Statistics

To determine differences between the two groups the dependent measures were submitted to a two way analysis of variance with factors of group (elite vs sub-elite) and time in the race (strokes 1-10, 11-20, 21-30, etc.). The mean values of each set of 10 strokes were used in this analysis. Descriptive statistics and coefficients of variation were used to describe the shape of individuals' force time curves and measures of their inter-stroke consistency respectively.

RESULTS

No significant differences were found between the groups on a number of anthropometric measures indicating that differences in performance and technique are not likely to be due to size differences of the athletes. The elite group completed the time trial in a significantly ($p < .01$) shorter time (X_e = 102.5 s) than the sub-elite group (X_s = 118 s) and with fewer strokes ($p < .001$).

Figures 1 and 2 show typical force-time curve (± 1 SD) for an elite and sub-elite paddler respectively, at the middle of the time trial. These graphs represent the average of 10 strokes. These figures show that the elite paddlers have a predominantly uni-modal profile whereas a bi-modal pattern is typical of the sub-elite paddlers. Additionally, the elite paddlers' inter-stroke variation is much smaller than the sub-elite paddlers, as evidenced by their smaller standard deviations.

Significant differences ($p < .01$) were also found for stroke distance (X_e = 1.67 m vs X_s = 1.45 m), time the paddle was in the water (X_e = 0.39 s vs X_s = 0.34 s) and coefficient of variation (X_e = 7 % vs X_s = 17%). No significant main effects were found for peak force, work, power, and impulse although a number of significant interactions were returned.

One important difference noted in the interactions was that over the last 30 strokes, the sub-elite group's performance dropped off compared to the elite paddlers whose remained virtually constant. This pattern was evident for stroke distance, impulse and work, three variables that are critical to performance.

DISCUSSION

Mann and Kearney[2] and Plagenhoef[3] reported that for their subjects, the paddle was in contact with the water for

similar results for both groups in our study but noted that the elite paddlers kept the paddle in contact with the water for a significantly longer period of time than the sub-elite paddlers.

Peak force was reached by the sub-elite paddlers in a significantly shorter period of time than the elite paddlers. The optimal force time curve has been described as one where peak force is as large as possible, reached in the shortest possible time, maintained at this level, and then reduced to zero as quickly as possible at the end of the stroke.

On the surface of our results, it appears that the sub-elite paddlers have an advantage in their technique because they reach peak force early. This apparent advantage may however be due to poor balance, requiring them to place the blade in the water to maintain boat stability. The tendency of *hurrying* and *slapping* the paddle into the water to maintain balance and causing an early time to peak force is consistent with the national coaching director's view on a poor paddling style.

The elite paddlers had a significantly longer stroke distance than the sub-elite group. As a result of this longer stroke it was expected that if the force was applied over a greater distance then greater work would be done by the elite athletes compared to the other group. This hypothesis was not confirmed and although the mean amounts of work done by the two groups were in the expected direction (X_e = 198 J vs X_s = 159 J) they were not significantly different. The failure to reach significance was probably due to small group numbers and high variance measures (σ^2_e = 2809 J vs σ^2_s = 1024 J).

Three of the five sub-elite paddlers exhibited a bi-modal force time cure. It was expected that there would be a significant difference between groups on the impulses applied to the paddles. Despite the elite paddlers having a 27% greater area under the force time curve than the sub-elite group, no significant difference was found. Once again, the small sample size and relatively large variance scores probably accounted for this finding.

A highly important finding from the practical perspective was that the elite paddlers showed significantly lower coefficients of variation compared to the sub-elite subjects indicating that the sub-elite were far less consistent in their actions than the elite group. A possible reason for this difference could be that the elite paddlers maintain a constant paddle and blade angle in the water thereby not allowing the paddle to *slip* through the water. The national coaching director also suggested that the bi-modal shaped curve of the sub-elite paddlers could be caused by the top hand pushing too much and therefore causing a change in the angle of the blade with respect to the water. This change could, in turn, cause the measured force to be reduced. Without the use of a system that quantitatively measures forces under race-like conditions on the water, small technial flaws such as the one suggested above, could not readily be detected. The regular use of this type of system allows the coach to continuously monitor technique and evaluate how coaching interventions influence motion of the boat and forces applied to the paddle.

CONCLUSIONS

No significant differences were found between the two groups on the variables of force, power, work and impulse indicating that these variables alone may not be the ones that discriminate between performance at the elite and sub-elite levels of sprint kayaking. Those measures that did show statistically significant differences between the groups were stroke distance, the time taken to reach peak force, the time that the paddle is in contact with the water, and the degree of inter-stroke variation.

REFERENCES

1. Aitken, D.A., & Neal, R.J. (1992). IJSB, 8,165-173.
2. Mann, R., & Kearney, J. (1980). MSSE, 12,183-188.
3. Plagenhoef, S. (1980). Res Quart, 50,43-49.

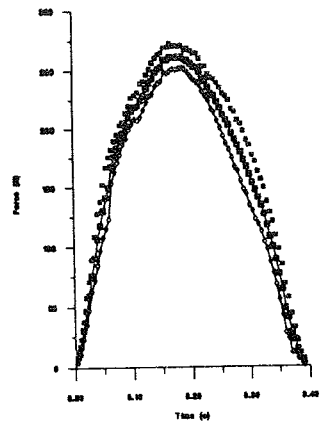

Figure 1. Average force-time graph of an elite paddler.

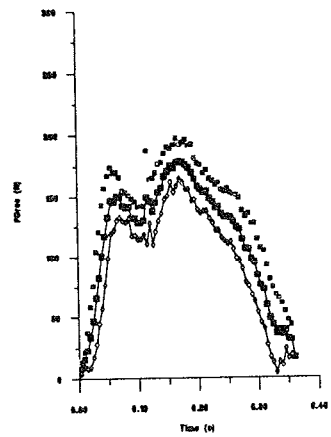

Figure 2. Typical bi-modal pattern displayed by three of the five sub-elite paddlers.

THE TWIST ROTATION IN HIGH JUMPING

J. Dapena

Department of Kinesiology, Indiana University, Bloomington, IN 47405.

INTRODUCTION

During the high jump takeoff the athlete makes forces on the ground which determine the height of the parabola and the angular momentum of the body. Once in the air, the high jumper makes a twisting somersault rotation which leads to a supine layout position over the bar (Fig. 1a). Problems in the twist rotation can produce a tilted position, with one hip lower than the other (Fig. 1b); the lower hip limits the result of the jump. An undertwisted position with the hip of the lead leg lower than the hip of the takeoff leg at the peak of the jump is the most common problem. This research project studied the mechanisms that produce the twist rotation in high jumping, and the possible causes for an undertwisted orientation of the hips at the peak of the jump.

METHODS

Twenty high jumps were studied: five normal trials by men, and five by women; five markedly undertwisted trials by men, and five by women. Body landmark locations during the jumps were calculated using standard three-dimensional (3D) film analysis. The body was modeled as a 16-segment mechanical system (Zatsiorsky and Seluyanov, 1983; Zatsiorsky *et al.*, 1990a, 1990b; parameter adjustments by de Leva, 1995). Center of mass location and angular momentum were calculated following a method based on Dapena (1978). The orientation of the longitudinal principal axis (minimum moment of inertia) was calculated following Hinrichs (1978).

The longitudinal principal axis of the body and the locations of the hips established a body reference frame defined by axes X_B, Y_B and Z_B. Z_B coincided with the longitudinal principal axis; X_B was mediolateral; Y_B was anteroposterior.

The angle between the bar and a line normal to the vertical plane containing both hips at the end of the takeoff was computed. Positive values were assigned to this initial hip orientation angle η_{TO} when the hips faced away (counterclockwise) from the landing pit. At the peak of the jump, the projection of a vertical vector on the plane normal to the longitudinal axis defined the neutral ("face-up") twist orientation. The actual hip twist angle at the peak (τ_{PK}) was based on the angle between this neutral twist orientation vector and axis Y_B. (The value $\tau = 90°$ was arbitrarily assigned to the neutral twist orientation at the peak; in undertwisted jumps, $\tau_{PK}<90°$.) Rotation from one frame to the next was determined by the Cardan angles (α, β, γ) of the three successive rotations about the X_B, Y_B and Z_B axes of the first frame that produced the orientations of the axes in the next frame. The third angle (γ) defined the twist rotation between the frames. The γ angles in all the frame intervals between takeoff and the peak were added to compute the cumulative twist rotation $\Delta\tau$ between takeoff and the peak. $\Delta\tau$ was subtracted from τ_{PK} to compute the hip twist angle at takeoff, τ_{TO}. (The values of τ_{TO} and η_{TO} generally are not the same. This is because the twist rotation needed to reach a face-up position at the peak of the jump depends not only on the hip orientation at takeoff, but also on the 3D path followed by the longitudinal axis in its somersault rotation between takeoff and the peak.)

In each frame, the angular momentum vector $\mathbf{H}$ was projected on the longitudinal axis, Z_B, to compute the twisting component of angular momentum, H_T. A positive sign was given to H_T if the vector pointed toward the head. The angular velocity of twisting associated with H_T in each interval between frames was calculated as $\omega_T = H_T / I_L$, where I_L was the moment of inertia about the longitudinal axis. The product of ω_T and the interval duration yielded the amount of twist

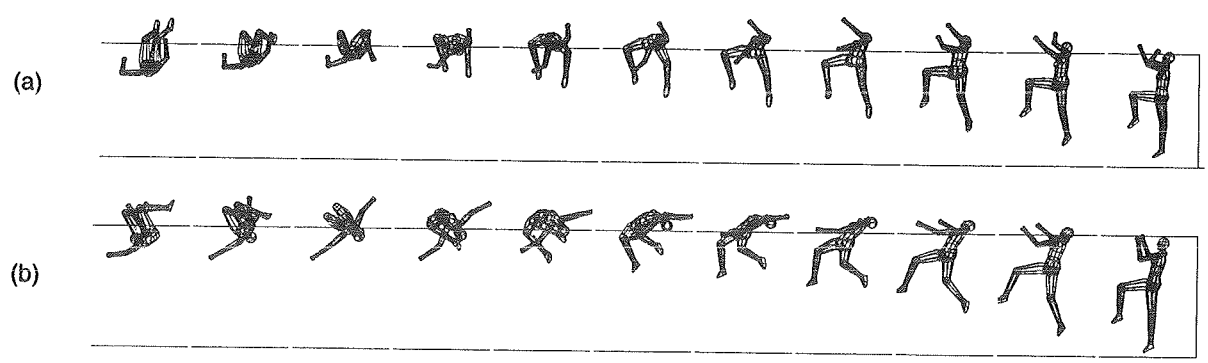

Figure 1: Normal high jump (a); high jump with problems in the twist rotation (b).

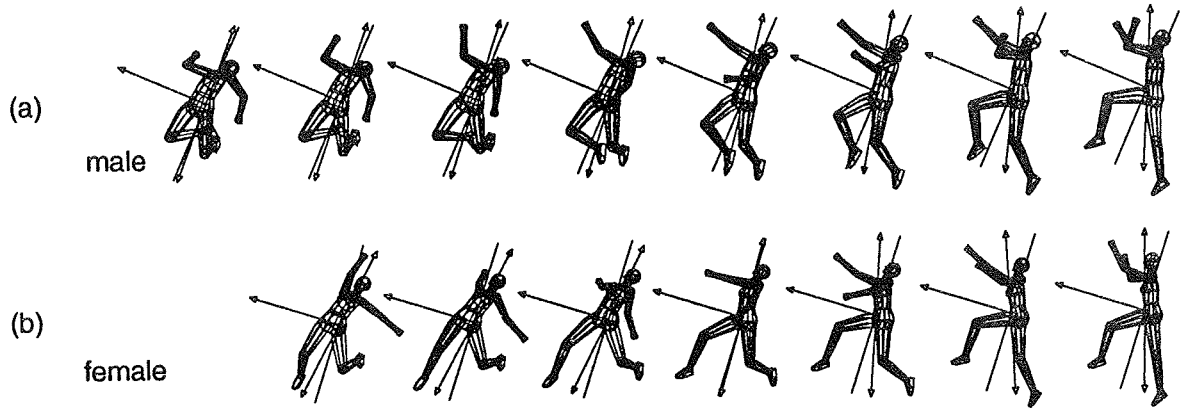

Figure 2: Typical jumpers, viewed normal to the plane containing the angular momentum vector and the longitudinal axis.

rotation produced by H_T during the interval. The amount of twist rotation produced by the twisting component of angular momentum between takeoff and the peak ($\Delta\tau_H$) was calculated as the sum of the twist rotations produced by H_T in the intervals between takeoff and the peak. The contribution of action and reaction rotations ("catting") to the twist rotation, $\Delta\tau_C$, was calculated as the difference between $\Delta\tau$ and $\Delta\tau_H$.

RESULTS AND DISCUSSION

The hip orientation relative to the bar at takeoff was similar in the normally-twisted men and women [$\eta_{TO} = 29 \pm 10°$ (men); $28 \pm 4°$ (women)]. The average hip twist angle of the women at takeoff was somewhat larger than that of the men, although there was overlap between the two groups [$\tau_{TO} = 34 \pm 5°$ (men); $41 \pm 7°$ (women)]. Between takeoff and the peak the women went through a slightly smaller twist rotation than the men, although there was overlap again [$\Delta\tau = 55 \pm 4°$ (men); $49 \pm 7°$ (women)]. The larger twist rotation of the men compensated for their smaller initial twist angle; the twist angle at the peak was essentially the same for both normally-twisted groups [$\tau_{PK} = 89 \pm 4°$ (men); $90 \pm 3°$ (women)]. (Of course, this had to be so, since a τ_{PK} value near 90° was the selection criterion for inclusion in these groups.) The men achieved more of their twist rotation through the twisting component of angular momentum than the women [$\Delta\tau_H = 33 \pm 7°$ (men); $14 \pm 8°$ (women)], while the women twisted more through catting [$\Delta\tau_C = 22 \pm 6°$ (men); $34 \pm 5°$ (women)]. This was a clear difference between the two normally-twisted group samples. The most surprising finding was the large contribution made by catting to the twist rotation: Considering both groups pooled together, catting produced more than half of the total twist rotation.

Fig. 2 shows two typical normally-twisted jumps. Each image is seen from a direction normal to the plane formed by the resultant angular momentum vector and the longitudinal axis at that time. (The direction of the view changed with each successive image, keeping pace with the somersault of the longitudinal axis.) The single-headed and double-headed arrows represent the total angular momentum vector and the principal longitudinal axis, respectively; the line is the plane normal to the angular momentum vector. After takeoff the longitudinal principal axis tilted toward the plane in all subjects. The tilt (a clockwise rotation in Fig. 2) seemed to be due mainly to the counterclockwise rotations implicit in the lowering of the lead leg and the lifting of the trailing leg behind the body. The change in the orientation of the longitudinal axis reduced the twisting component of angular momentum. In the men, the longitudinal axis almost never reached the plane (Fig. 2a). But it did in almost all the women, and actually crossed to the other side (Fig. 2b). This reversed the sign of the twisting component of angular momentum, which made a negative contribution to the twist rotation from there on. The smaller twist rotation achieved by the women through angular momentum ($\Delta\tau_H$) was due mainly to their smaller average twisting angular momentum between takeoff and the peak [$H_{T(AVG)} = 15.8 \pm 3.7 \cdot 10^{-3}$ s^{-1} (men); $8.0 \pm 5.0 \cdot 10^{-3}$ s^{-1} (women)]. The women compensated for this with more effective catting than the men.

The differences between the normally-twisted and undertwisted jumpers were not due to differences in the twist angle of the hips at takeoff, but to the subsequent rotation in the air. In the men, undertwisting was usually due mainly to a smaller amount of catting; in the women, to a smaller twisting component of angular momentum, ultimately traced to an excessive backward lean of the longitudinal axis at takeoff.

REFERENCES

Dapena, J. *J. Biomech.* 11:251-256, 1978.

De Leva, P. (Submitted for publication.)

Hinrichs, R. *Principal axes and moments of inertia of the human body: an investigation of the stability of rotary motions.* M.A. Thesis, University of Iowa, 1978.

Zatsiorsky, V.M. and V.N. Seluyanov. *Biomechanics VIII-B* (pp. 1152-1159). Human Kinetics, 1983.

Zatsiorsky, V.M. et al. *Biomechanics of Human Movement: Applications in Rehabilitation, Sports and Ergonomics* (pp. 186-202). Bertec Corp., 1990a.

Zatsiorsky, V.M et al. *Contemporary Problems of Biomechanics* (pp. 272-291). CRC, 1990b.

ACKNOWLEDGEMENTS

This project was funded by grants from the U. S. Olympic Committee and U.S.A. Track & Field.

Indirect Static and Dynamic Measurement of the Center of Buoyancy in Competitive Swimmers

S. McLean[1], R. Hinrichs[2]
[1]Department of Health and Human Performance, Iowa State University, Ames, IA 50011
[2]Department of Exercise Science and Phys. Ed., Arizona State University, Tempe, AZ 85287

INTRODUCTION

To date, the only measurements of the buoyant force (B) and the center of buoyancy (CB) have been static. This measurement has limited applicability to swimming. Therefore an indirect method of locating CB was developed and compared to direct measurements from an underwater reaction board. The direct trials were videotaped and the CB was located indirectly from digitized images for 8 competitive swimmers based on a segmental, volumetric model. The correlation between the direct and indirect methods was 0.87 for completely submerged static trials and 0.77 for partially submerged static trials. The mean absolute deviation from the direct measurement was 3.1 cm and 3.5 cm for the submerged and partially submerged static trials, respectively. The correlation of the direct and indirect measurements of the buoyant force was 0.98 for both submerged and partially submerged static trials. The indirect method was applied to a single hand propulsive phase of freestyle for 3 subjects. The CB moved up to 20 cm in a cranial-caudal direction and up to 10 cm in the anterior-posterior direction during this phase.

REVIEW AND THEORY

Buoyancy has often been proposed to offer females an advantage in swimming performance (Chatard *et al.*, 1991, Toussaint *et al.*, 1988, and Montpetit *et al.*, 1983). However, from the literature that discusses the nature of the buoyant force and its effect on swimming, only two studies have identified buoyancy characteristics applicable to competitive swimming (Gagnon and Montpetit, 1981, and McLean and Hinrichs, 1993). More importantly, all speculation of the contribution of buoyancy to performance has been based on static measurements of B and CB. It is apparent from the literature that buoyancy is affected by body position. However, this variable changes when swimming thus limiting the applicability of static measurements. A dynamic measurement of B and CB will help improve the understanding of the kinetics involved in swimming. To date swimming kinetics is limited to the study of hand propulsive forces (Schleihauf, 1986) and estimates of the resistive force encountered by a swimmer (Hollander, 1986). Thus there exists a need for an indirect method to locate the CB and the magnitude of the buoyant force during a dynamic situation.

The purposes of this study were:
(1) To develop a procedure to indirectly locate the CB and determine the magnitude of the buoyant force in a swimmer for a static, horizontal, streamline position while completely and partially submerged. (2) To validate the indirect method with direct measurements. (3) To apply this indirect method to locate the CB and estimate the magnitude of the buoyant force of a swimmer dynamically during a single hand propulsive phase in freestyle swimming.

METHODS

Individual segmental, volumetric models of eight subjects were created from measurements taken from sagittal and frontal videotaped views. The body was divided into 15 segments defined to avoid drastic or odd contour changes. The videotapes were digitized using an Ariel Performance Analysis System. The shape of each segment in both views was traced using up to 18 digitized points for each side of the segment. Cubic spline functions were fit to these points using a segmental reference frame whose origin was at the proximal joint center. These spline functions were interpolated at 1% increments of the segment length to provide medial, lateral, anterior, and posterior surface points.

Each segment was modeled as a series of 100 elliptical cylinders whose major axes were defined as half the distance between the medial and lateral surface points, and minor axes were defined as half the distance between the anterior and posterior surface points. The submerged segmental volume was computed by summing the individual submerged cylinder volumes. The y (A-P) and z (long axis) coordinates of the segmental CB were calculated in a manner similar to a segmental determination of the center of mass. The segmental CB was equal to the sum of the submerged volume moment about its respective axis divided by the total submerged segmental volume.

The subject's CB was measured directly for two levels of submersion (fully submerged and floating at the surface) using an underwater reaction board (McLean and Hinrichs, 1993). These trials were videotaped using an an underwater camera. The subjects were then videotaped while performing a 25 m freestyle sprint swim.

RESULTS

Table 1: Comparison of Direct and Indirect Methods of Measuring the Buoyant Force and Locating the CB.

	Submerged		Surface	
	AbsDev	r	AbsDev	r
B	2.77% (2.76%)	0.98	4.18% (3.13%)	0.98
CB	3.10 (3.25)	0.87	3.53 (2.46)	0.77

Note: AbsDev = Mean absolute deviation from the direct measurement. (Standard deviations).

There was good correlation between the indirect and direct methods of measuring the buoyant force. The correlation between methods for determining the location of the CB was slightly lower but was still considered strong. The mean absolute deviation represented an estimate of the measurement accuracy. The prediction of the buoyant force was within approximately 4% of the directly measured value. The prediction of the location of the CB was within approximately 3 cm.

Dynamic CB and buoyant force data for one subject is presented. The movement of the CB during the dynamic trial was characterized by three phases. The first phase lasted for approximately 30% of the propulsive phase. The CB moved cranially during this phase as the lead arm entered the water and the trailing arm exited the water. The second phase lasted for approximately 40% of the propulsive phase.

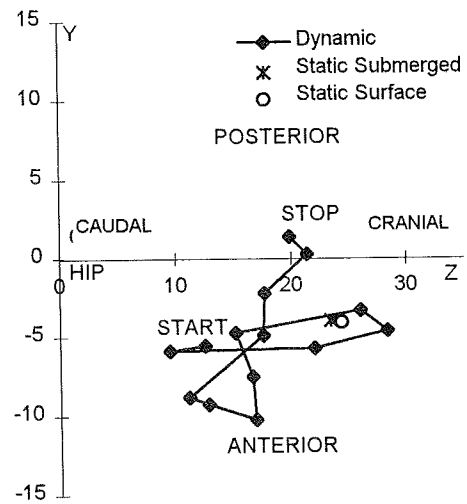

Figure 1 - Y-Z plot of the coordinates of the CB expressed relative to the hip (0,0). Comparison points for the static, indirect measurements are included. Data points are separated by 0.067 s.

The CB moved caudally and anteriorly during this phase as the lead arm began the pull back towards the hips. The final phase lasted for approximately 30% of the propulsive phase. The CB moved primarily in a posterior direction with a small amount of cranial movement as the lead arm completed the propulsive phase and the trailing arm entered the water cranial to the head.

DISCUSSION

The indirect method of locating the CB provided good estimates of the actual CB location. The increased variability in the indirect surface measurements of the CB were due in part to errors associated with locating the water surface relative to the body for these trials. This was done by modeling the surface as a line by locating two points along the surface. This procedure is susceptible to small errors in digitizing these points. Further work should be conducted to improve the ability to more accurately represent the water surface relative to the swimmers' body.

The measurement of the CB during a freestyle stroke represents the first reported dynamic values of this point. These data suggest that this method may provide an additional piece of information for the study of swimming kinetics.

REFERENCES

Chatard, J.C. *et al.* (1991). *Eur. J. Appl Physiol.* 63, 12-16

Gagnon, M. & Montpetit, R. (1981). *J. Biomechanics* 14, 235-241.

Hollander, A.P. *et al.* (1986). *J. Sport Sciences* 4, 21-30.

McLean, S.P. and Hinrichs, R.N. (1993). NCAA Final Report.

Montpetit, R.R. *et al.* (1983). Biomech. and Med. in Swimming, Human Kinetics

Schleihauf, R.E. (1986). *J. Swimming Res.* 2, 1-20.

Toussaint, H.M. *et al.* (1990). *MSSE*, 22 402-408.

A New Approach for Designing the Man-Machine Interface for Rowing

B. Sih[1], M. Hubbard[2,1], D. Hawkins[3,1]
[1]Biomedical Engineering Graduate Group, University of California, Davis CA 95616
[2]Department of Mechanical & Aeronautical Engineering, University of California, Davis CA 95616
[3]Department of Exercise Science, University of California, Davis CA 95616

INTRODUCTION

At the Olympic level, rowing is an extremely physical activity utilizing all the major muscle groups. However, based on the physiological processes involved in rowing, the useful power that can be delivered by the human body to an external source such as the oar and boat is dependent on the person's strength, anthropometrics, and limb kinematics as well as the external load. Despite this understanding of human muscle function, very little work has been done to design man-oar-boat systems which optimize specific features of the human machine. The computer simulation discussed in this paper incorporates some of the fundamental characteristics of the boat, oar and human in an attempt to gain further insight into the man-oar-boat system. The results indicate that it is possible to calculate the joint torques necessary to cause the motion and also to identify those torque bounds which limit performance. In addition, the model may be used to identify novel rowing motions and oar designs which maximize or minimize an oarsman's unique strengths and weaknesses.

REVIEW AND THEORY

The rowing motion used today has been developed mostly through trial and error rather than as a result of design based on an understanding of the potential and limitations of the human body. As the differences between winning and losing become smaller, it becomes increasingly more important to identify new areas where either the boat/oar design or human performance can be improved. One approach that can be used to increase boat velocity is to improve the impedance matching between the human and the boat. Proper impedance matching allows the human to generate his/her greatest power through proper design of the boat/oar hardware interface. The purpose of this study was to develop a realistic model that can be used to study the rowing motion in order to identify specific improvements in either the motion or in boat/oar hardware.

METHODS

The model for the rowing simulation consisted of a boat, a six rigid-link planar human and a rigid oar (Fig. 1).

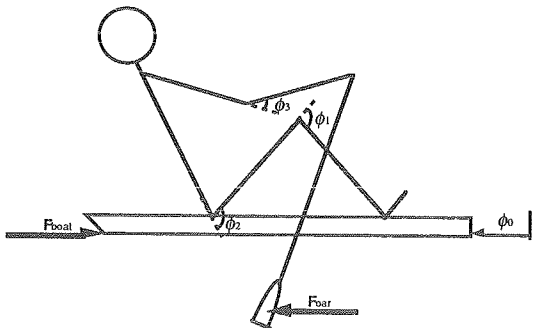

Figure 1: Man-oar-boat system

Appropriate drag forces proportional to the boat and oar velocities were implemented (Zatsiorsky and Yakunin, 1991). Constraints to the paths of the boat, seat, hand, and oar, reduced the system to the following four degrees of freedom: boat position, knee angle, hip angle, and elbow angle. The system was driven by applying five torques at the ankle, knee, hip, shoulder, and elbow. The upper bounds were established based on experimentally determined maximum isometric joint torques and a Hill-type force-velocity relationship.

The equations of motion, derived using Kane's Method (Kane and Levinson, 1985) and AUTOLEV© (a PC-based dynamic system analyzer) can be written in the following generalized form:

$$[\mathbf{C}_{4x4}]\begin{bmatrix}\ddot{\phi}_0\\ \ddot{\phi}_1\\ \ddot{\phi}_2\\ \ddot{\phi}_3\end{bmatrix}=\begin{bmatrix}0 & 0 & 0 & 0 & 0\\ A_{21} & 1 & 0 & A_{24} & 0\\ 0 & 0 & 1 & A_{34} & 0\\ 0 & 0 & 0 & A_{44} & -1\end{bmatrix}\begin{bmatrix}T_{ankle}\\ T_{knee}\\ T_{hip}\\ T_{shoulder}\\ T_{elbow}\end{bmatrix}+[\mathbf{F}_{4x1}] \quad (1)$$

where

- $\mathbf{C}_{4x4}$ contains the coefficients of accelerations of the four generalized coordinates
- $\ddot{\phi}_0, \ddot{\phi}_1, \ddot{\phi}_2, \ddot{\phi}_3$ are the accelerations of the four generalized coordinates (boat, knee, hip, and elbow, respectively)
- A_{ij} are the sensitivities of the left hand sides to the joint torques
- $\mathbf{T}^j$ is the matrix of joint torques
- $\mathbf{F}_{4x1}$ contains the contributions to the accelerations not dependent on the torques, i.e. boat and oar drag forces and Coriolis and centripetal accelerations of the rigid links.

Even if the motion of the three body configuration generalized coordinates were specified, (1) cannot be used in an inverse dynamic way to calculate the torques required because there are five joint torques in (1) and the motion is specified with only three generalized active forces. However, inspection of the right hand side of (1) reveals that the first row of $\mathbf{A}$ is identically zero. Thus, the joint torques directly affect only the three accelerations, $\ddot{\phi}_1, \ddot{\phi}_2$, and $\ddot{\phi}_3$. Therefore at any instant in time, three "effective" torques, $\mathbf{T}^e$ can be written as a linear combination of the five joint torques. Hence, (1) becomes:

$$[\mathbf{C}_{4x4}]\begin{bmatrix}\ddot{\phi}_0\\ \ddot{\phi}_1\\ \ddot{\phi}_2\\ \ddot{\phi}_3\end{bmatrix}=\begin{bmatrix}0 & 0 & 0\\ 1 & 0 & 0\\ 0 & 1 & 0\\ 0 & 0 & 1\end{bmatrix}[\mathbf{T}^e_{3x1}]+[\mathbf{F}_{4x1}] \quad (2)$$

where

$$\begin{bmatrix}T^e_1\\ T^e_2\\ T^e_3\end{bmatrix}=\begin{bmatrix}A_{21}T_{ankle}+T_{knee}+A_{24}T_{shoulder}\\ T_{hip}+A_{34}T_{shoulder}\\ A_{44}T_{shoulder}-T_{elbow}\end{bmatrix} \quad (3)$$

Rearranging (2) also demonstrates that it is possible to solve for both the acceleration of the boat, $\ddot{\phi}_0$, and the required $\mathbf{T}^e$ if the three accelerations $\ddot{\phi}_1$, $\ddot{\phi}_2$, and $\ddot{\phi}_3$ are specified, i.e. if the three angles ϕ_1, ϕ_2, and ϕ_3 (the kinematic profile) and the cadence are known.

$$\ddot{\phi}_0 = \left[-\left(C_{12}\ddot{\phi}_1 + C_{13}\ddot{\phi}_2 + C_{14}\ddot{\phi}_3\right) + F_1\right] / C_{11} \quad (4)$$

$$\left[\mathbf{T}^e\right] = \begin{bmatrix} 1 & 0 & 0 \\ 0 & 1 & 0 \\ 0 & 0 & 1 \end{bmatrix}^{-1} \left(\begin{bmatrix} C_{21} & C_{22} & C_{23} & C_{24} \\ C_{31} & C_{32} & C_{33} & C_{32} \\ C_{41} & C_{42} & C_{43} & C_{44} \end{bmatrix} \begin{bmatrix} \ddot{\phi}_0 \\ \ddot{\phi}_1 \\ \ddot{\phi}_2 \\ \ddot{\phi}_3 \end{bmatrix} - \begin{bmatrix} F_2 \\ F_3 \\ F_4 \end{bmatrix} \right) \quad (5)$$

Although any kinematic profile can be specified, a low order Fourier decomposition of ϕ_1, ϕ_2, and ϕ_3 was used whose amplitudes, frequencies and phases most closely approximated the shape of an actual rowing motion. The advantage of this approach is that accelerations for a given shape can be calculated analytically and the cadence (strokes per second) can be controlled by changing the fundamental frequency. Thus, cadence can be used as an independent control variable to maximize boat speed, subject only to restrictions on the ability of the human to generate the joint torques required.

In order to determine if $\mathbf{T}^e$ is physiologically possible for a given kinematic profile, it is desirable to calculate the bounds for $\mathbf{T}^e$. Because the linear relationship between $\mathbf{T}^e$ and $\mathbf{T}^j$ is known through (3), it is possible to calculate bounds for $\mathbf{T}^e$ knowing bounds for $\mathbf{T}^j$. However, (3) also indicates that, according to the signs of the entries of A_{ij}, $T_{shoulder}$ increases one element of $\mathbf{T}^e$ while simultaneously decreasing another. A method based on the linearity of (3) was derived to determine the value of $T_{shoulder}$ that would keep all elements of $\mathbf{T}^e$ within their bounds. Thus, adjusting the shoulder torque delays, until the highest possible cadence, the inability of the joints to supply the required torques. The maximum possible cadence for a given rowing motion shape was then calculated by increasing the cadence gradually until one or more of the elements of $\mathbf{T}^e$ reached their bounds. The resulting torque profiles and their corresponding bounds may then be evaluated to determine if either the rowing motion or boat/oar hardware could be modified to increase boat velocity.

RESULTS

Illustrated in Fig. 2 and 3 is T^e for the knee and hip, respectively, and the corresponding bounds for a single rowing stroke optimized by cadence. Typical boat and oar parameters as well as human anthropometric and maximal torque values were used. Torque bounds were reached at 12% of the rowing cycle for both T^e_{knee} and T^e_{hip} at a stroke rate of 42.25 strokes/min. T^e_{elbow} was within its bounds and was not a limiting factor in this rowing profile. The effective joint torque profiles do not track those of the maximum effective joint torque profiles. This suggests that there is considerable opportunity for improving the impedance matching of the man-machine interface in rowing.

DISCUSSION

This computer simulation provides a unique tool for studying the effects that both human and boat/oar parameters have on rowing performance. It can be used to design oars and to predict optimal cadence. For example, from Fig. 2, it is apparent that the effective torque profile of the knee through much of the stroke may be greatly modified to increase cadence, possibly through changes in oar length, paddle size, etc. Additional utility may come from the development of novel kinematic profiles that would maximize the power generating potential of the human. Oar and boat parameter optimization for the current rowing motion and individual's torque generating capabilities is also possible.

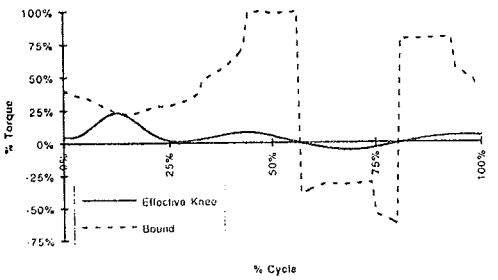

Figure 2: T^e_{knee} vs. % Rowing Cycle

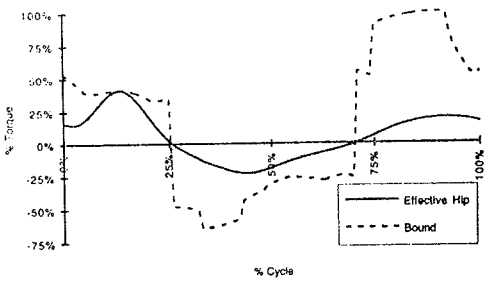

Figure 3: T^e_{hip} vs. % Rowing Cycle

The approach presented here represents a first approximation toward modeling the complex physiological/mechanical aspects of the man-boat-oar system. Improvements may attempt to impose more realistic constraints on the path of the hand (a spherical motion centered on the oarlock) and torque bound calculation which accounts for fatigue.

REFERENCES

Kane, T.R. and Levinson, D.A. *Dynamics: Theory and Applications*, McGraw-Hill Publishing Co., 1985.

Zatsiorsky, V.M. and Yakunin, N. *Intl. J. Sport Biomech.*, 7, 229-281, 1991.

TIBIOFEMORAL AND CALCANEUS-TIBIA MOTION DURING RUNNING: SKIN VS. BONE MARKERS

C. Reinschmidt[1], A.J. van den Bogert[1], A. Lundberg[2], N. Murphy[2], B.M. Nigg[1]
[1]Human Performance Laboratory, The University of Calgary, Calgary, Canada
[2]Karolinska Institute, Dept. of Orthopaedics, University Hospital, Huddinge, Sweden

Introduction

In biomechanical analyses of human movement, skin markers are typically used to represent the spatial positions of segments. Skin markers, however, may move considerably with respect to the underlying bone, especially during fast movements, such as running. Thus, large errors (skin movement artefact) may be introduced as a result of this relative movement between skin and underlying bone. The purpose of this paper was to investigate the difference between skin and bone based segmental kinematics during running.

Review and Theory

The skin movement artefact is a major source of error in routine motion analysis studies, and this error can be expected to be much larger than the system error of todays motion analysis systems. For example, Cappozzo et al. (1993) found that, at the thigh and shank, the relative movement between skin markers and underlying bone can be expected to be in the order of 1-2 cm during walking.
The number of studies investigating the skin movement artefact is limited. Previous publications were either confined to 2-d analyses (e.g. Lafortune et al., 1993) or slow movements (e.g. Holden et al., 1994). In particular, there are no investigations available that assessed the skin movement artefact during a highly dynamic movement such as running.

Procedures

Five male subjects (age 28.6 ± 4.3 yrs) participated in the study. Prior to the running trials, Hoffmann bone pins (2.5mm Ø) were inserted under local anesthesia into the lateral femoral and tibial condyles, and into the lateral aspect of the calcaneus of the subject's right leg. Light weight aluminum triads each with three reflective markers (appr. 6 cm apart) were attached to the intracortical pins of the femur, tibia and calcaneus.
Six reflective skin markers were each attached to the thigh and to the shank, while three markers were glued directly to the lateral aspect of the subject's shoe. The skin markers were glued to small strips of fabric which were fixed to the skin by double sided tape, and additionally, the ends of the strips were secured with tape. The thigh and shank markers were placed at standardized locations determined by the subject's anatomical landmarks. The first 3 thigh markers were placed at 0, 40, and 80% of the distance between the greater trochanter and the distal end of the lateral femoral condyle. Similarly, the 3 other thigh markers were placed at 45, 70, 95% of the distance between the anterior superior iliac spine and the proximal end of the patella. The 6 shank markers were also arranged in two rays. The first 3 shank markers were fixed at 20, 60 and 100% of the distance between the proximal end of the lateral tibial condyle and the lateral malleolus. The other three shank markers were attached at 0, 40, and 80% of the distance between the mid tibial plateau and the distal end of the tibia.
In order to accommodate the calcaneus pin, the running shoes (Adidas equipment cushioning) were slightly altered by removing the lateral part of the "Achilles tendon protector", and also by removing a half-circular (r = 1.2 cm) piece of the heel cap at the lateral part of the right shoe.
Five running trials (2.9 ± 0.2 m/s) and one standing trial ("neutral" position) were collected for each subject. The motion recordings (stance phase) were performed with 3 high-speed film cameras (LOCAM) each operating at a nominal frequency of 200 Hz. The cameras were synchronized with the use of a threshold detector connected to the force plate which the subject were asked to hit with their right feet. The threshold detector triggered small infrared lights mounted in front of the cameras. The lights were active during the entire stance phase, and determined the duration of stance phase in each film. Differences and fluctuations in camera speed were corrected with the use of internal LED (200 Hz) lights.
A high precision calibration frame was used to determine the 11 DLT (Direct Linear Transformation) coefficients for each camera. Additionally to the frames determining stance phase, five frames before touch-down and five frames after take-off were digitized. The coordinates of all markers in all three cameras were then normalized with respect to stance phase. The coordinates of all markers in the 3 cameras together with the DLT coefficients allowed the determination of the 3-dimensional coordinates of the skin and bone markers during the running trials as well as during the standing trial.
During the standing trial, it was arbitrarily assumed that the segmental coordinate systems were aligned with the global coordinate system. Generally, a similar procedure as described in Lafortune et al. (1992) was employed to calculate the attitude matrix between two adjacent (anatomical) segment coordinate systems. The use of a singular value decomposition method (Söderkvist et al., 1993) allowed to use 3 or more markers per segment to obtain the coordinate transformation between a set of markers in two different coordinate systems. For the thigh and shank, all 6 skin markers were used for these calculations.
Cardanic angles were used to represent the intersegmental motions for the tibiofemoral and calcaneus-tibia motion (Grood et al., 1983; Cole et., 1994), based on bone, skin, or shoe markers. The Cardanic angles were filtered with a bi-directional low-pass Butterworth filter with a cut-off frequency of 12 Hz.

Results

Qualitatively, the running style of the subjects appeared to be normal. In other words, psychological effects and effects due to the local anesthesia did not appear to influence the running style. During the experiments, the femur pin (loosening of the pin) had to be removed in one subject. It was suspected that the slit cut into the iliotibial band through which the femur pin was inserted may have been too small in this subjects. Hence, the data for the femur and thigh cannot be used for this particular subjects.
To date, the data of one subject are available. In Fig. 1, the tibiofemoral as well as the calcaneus-tibia motions are displayed based on skin and bone markers. Generally, the skin and bone based curves were very repeatable across the five trials. However, it appeared that the skin based motions showed more variability for the different running trials (Fig.1).

Tibiofemoral Motion. The ad/abduction at the knee joint was substantially different for the skin and bone markers. The skin markers indicated an adduction movement of 10° whereas the "true" adduction was in all trials less then 3°. The shape of the skin and bone marker based curves for ext/internal tibial rotation were very similar. However, the skin based curves of the five running trials were much more variable than the bone based knee rotation curves. Knee flexion and extension curves for the skin and bone markers were again very similar in shape. The difference between the two average curves was highest at around 15% and 50% of stance phase, and was in the order of 8°.

Calcaneus-Tibia Motion. The skin marker based in/eversion movements at the ankle-joint-complex (AJC) overestimated the eversion movement by more than 10°. This is a considerable difference considering the magnitude of the maximal eversion movement. The ad/abduction movement of the AJC was rather small for this subject and only small differences between the skin and bone marker based kinematics were found. The flexion/extension curves were similar, however, the skin marker based curves showed generally higher amplitudes. The highest differences in the order of 6° were found at around 15% and 60% of stance phase.

Discussion

Generally, the shape of the skin and bone based curves were similar, and it appeared that movements based on the skin markers typically exceeded the "true" movements. For both the tibiofemoral and calcaneus-tibia motion, the largest differences were found in the rotations around the anterior-posterior axes, i.e. ad/abduction at the tibiofemoral joint and in/eversion at the ankle joint complex. Unexpectedly, the difference in rotations along the proximal-distal axes (knee rotation, ab/adduction at the AJC) between skin and bone marker based kinematics was relatively small. However, the skin marker based curves of the single trials showed more variability. Based on the results of this subject, it may be speculated that a relative good estimate of rotation at the knee and abduction at the AJC may be obtained with skin markers when averaging over several trials.

In the present study, six skin markers were used for the thigh as well as for the shank. The difference between skin and bone marker based kinematics may be different when using different skin markers or skin marker combinations. In order to find out which thigh and shank marker placements/ arrangements are expected to give the best estimate of femur and tibia movements, it is planned to calculate tibiofemoral and calcaneus-tibia motion based on different marker combinations.

The analyses of the other subjects will show if the skin movement artefact is similar across subjects. If the differences between the skin and bone marker based kinematics were systematic across subjects, correction algorithms may be a powerful tool to get a better estimate of the bone movements through the use of skin markers.

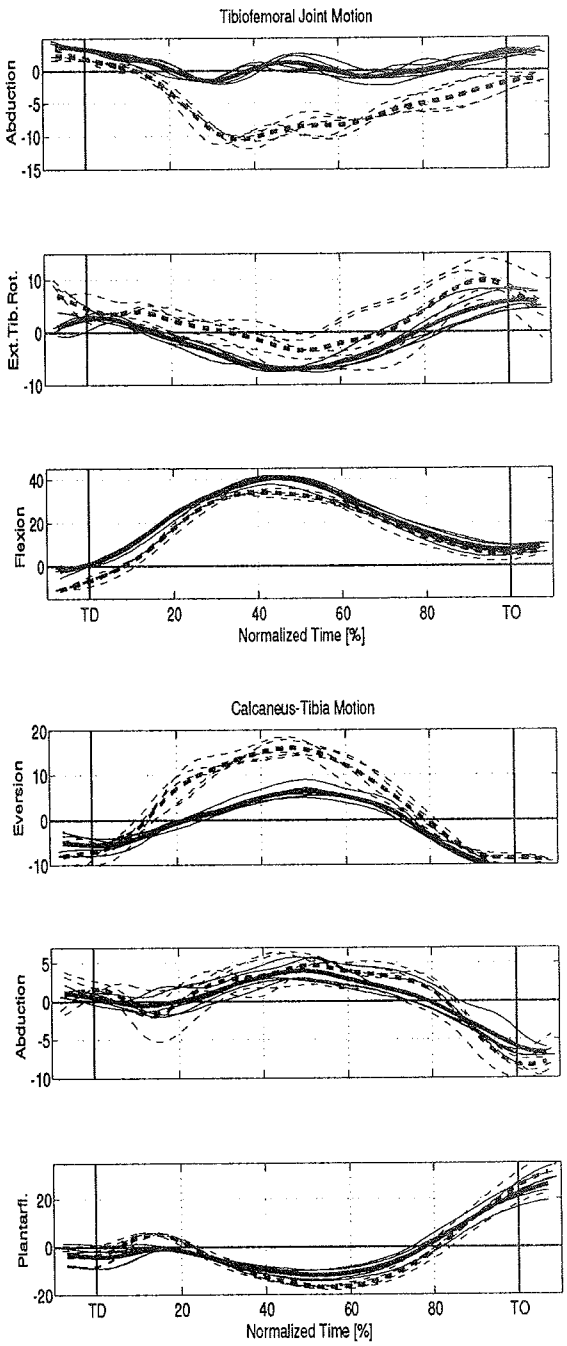

Figure 1: Tibiofemoral and calcaneus-tibia motion of subject #1 based on bone (—) and skin markers (--) displayed from touch-down (TD) to take-off (TO). Thick lines represent averages of 5 trials. Movements labeled on the y-axes indicate rotational movements in the positive direction of the y-axis.

References

Cappozzo, A. et al. *XIV ISB Congress*, 238-239, 1993
Cole, G.K. et al. *J. Biomech. Eng.*, 115, 344-349, 1993
Grood, E.S. et al. *J. Biomech. Eng.*, 105, 136-144, 1983
Holden, J.P. et al. *S. Biomed. Eng. Conf.*, 1035-1036, 1994
Lafortune, M.A. et. al. *NACOB II*, 101-102, 1992
Lafortune, M.A. et al., *J. Biomechanics*, 25, 347-357, 1992
Söderkvist, I. et al. *J. Biomechanics*, 26, 1473-77, 1993

Acknowledgments

This work has been supported by the Swiss Federal Sports Commission (ESK), adidas America, Going Global '92 Fund, the Swedish Defense Materials Administration, and the Olympic Oval Endowment Fund. The help of A.Stacoff, A.Stano and A.Josephson at various stages of the project was greatly appreciated.

BIOMECHANICAL PROFILES OF NEW AGAINST USED RUNNING SHOES

Ewald M. Hennig, Thomas L. Milani / Universität-GH Essen, Germany

During running a deterioration of footwear material occurs when shoes are exposed to many repetitive impacts with high mechanical loads. The protective functions of footwear such as the restriction of rearfoot motion and shock attenuation will change with the number of miles, run with the shoe. It should be expected that a good running shoe provides adequate protection for at least 1000 km of running. The purpose of the present study was to investigate the changes in biomechanical variables after wearing running shoes for a relatively short distance of 220 km.

METHODS

Two identical pairs of 19 different models of running shoes were available for this study. While one pair of all shoe models remained unused, 22 subjects with the same foot size ran in the second pair a distance of 10 km. To guarantee identical wear, each of the subjects ran in all available running shoe models along the same course on flat and hilly terrain. Using this rotation scheme, each of the shoes was worn by all subjects on different days for a total distance of 220 km. In the subsequent biomechanical test 12 subjects ran in the 38 pairs of new and used shoes in a single experimental session. The sequence of footwear selection was randomized. Five trials of rearfoot strike running across a "Kistler 9281 B" force platform were performed at a speed of 3.3 m/s in each of the footwear conditions. All shoes were high quality running footwear from internationally renowned manufacturers. An impacter assembly served to characterize the midsole properties of the rearfoot constructions. A pressure distribution unit PD-16 (Halm Inc.) with eight discrete piezoceramic transducers was used to record in-shoe pressures. The measuring elements were 4 by 4 mm with a thickness of less than 2 mm. Using adhesive tape, the transducers were positioned at specific anatomical locations underneath the foot: medial and lateral heel and midfoot, the metatarsal heads I, III and V, and the hallux. Simultaneously with the recording of the ground reaction force (GRF), acceleration along the tibial axis was measured with a low weight Entran accelerometer (Type EGAX-F-25). The accelerometer was embedded in a small piece of balsa wood. It was fastened to the skin above the medial aspect of the tibia, at half the distance between medial malleolus and the medial tibial condyle. Rearfoot motion was measured with an electrogoniometer. A light weight half circular metal construction with a potentiometer was fixed at the heel counter with its axis of rotation at the approximate height of the subtalar joint. The movable part of the goniometer was fixed at the lower leg in parallel to the achilles tendon orientation. For reference, the goniometer output of the achilles tendon neutral position was determined before the trials for all subjects in the different shoe conditions. Data collection occurred in pretrigger mode at a rate of 1 kHz per channel. A threshold of 5 N in the vertical GRF component was set to identify foot strike. Following an ANOVA post-hoc comparisons were made, and significance was accepted at $p<0.05$.

RESULTS AND DISCUSSION

In the table below, the averaged values across all new and used shoes are given for the impacter score (IMP-AC), the peak tibial acceleration (PACC), the maximum achilles tendon angle vs. neutral (PRON), and the peak pressures in the lateral heel (PP-LH), the lateral midfoot (PP-LM), and under the first metatarsal head (PP-I) (* $p<0.05$, ** $p<0.01$). Although the values for the impacter scores are about the same for the new and used shoes the higher peak tibial accelerations and the higher peak pressure values indicate a loss of cushioning in the used shoes.

	IMP-AC (g)	PACC (g)	PRON (°)	PP-LH kPa)	PP-LM (kPa)	PP-I (kPa)
New	13.0	6.4	10.1	794	392	775
Used	12.7 ns	7.0 **	11.9 **	857 **	406 **	837 **

Peak tibial acceleration was significantly higher in 10 footwear constructions with a mean increase of 16.6 %. A maximum value of 27.2% was found for one specific shoe model. From the 19 shoe models 15 showed significantly higher maximum pronation values. Across these 15 models the increase was 27.3 % with a highest value of almost 70% for one type of footwear. For this shoe construction the achilles tendon angle was enlarged from 10.7 degrees in the new to 17.7 degrees in the used shoe. Maximum pronation velocity for the used shoes was significantly higher in 8 footwear models and significantly reduced in 2 models. The highest increase in pronation velocity was 29.8% for one type of footwear and the largest reduction 21.4% in another shoe model. The reduction of 21.4% for the maximum pronation velocity in a used shoe appears surprising. However, for this particular shoe construction the peak tibial acceleration increased by 27% and the heel pressures by more than 20%. The loss of cushioning seems to have resulted in a reduction of rearfoot motion velocity.

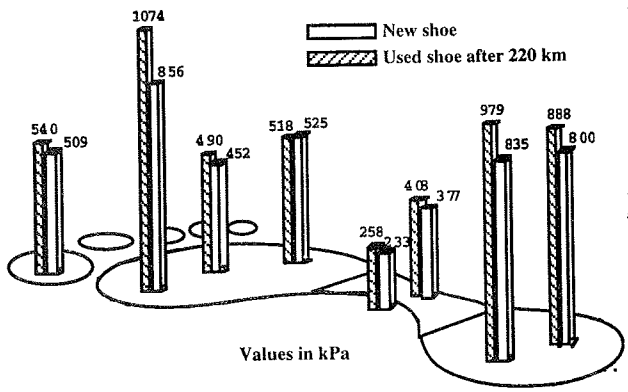

Visual inspection of the shoe demonstrated that the midsole height in the rearfoot region was lower for the used shoe, thus reducing pronation (Nigg & Bahlsen, 1988). Across all shoes, the peak plantar pressures for the eight anatomical locations were approximately 8% higher in the used shoes. Generally, foot areas which are exposed to more loading (heel and forefoot) demonstrated higher elevations in peak pressures for the used shoes. The figure below shows for a selected type of footwear a loss of shoe cushioning that is particularly high under the heel and under the first metatarsal head.

CONCLUSION

A relatively short running distance of 220 km resulted in substantial changes of footwear properties for some shoe models. Shock attenuation is reduced, plantar in-shoe pressures become higher, and rearfoot motion increases. For 15 out of 19 shoe constructions an average increase of rearfoot motion by almost 30% was determined in this study. Because excessive rearfoot motion has been linked to a variety of lower extremity complaints, this deterioration of protective function in high quality running shoes is not acceptable.

Literature

Nigg, B. M., & Bahlsen, H. A. (1988). Influence of heel flare and midsole construction on pronation, supination, and impact force for heel - toe running. Int. Journ. of Sport Biomechanics, 4, 205-219.

Finite Element Modeling of Surgical Procedures for Refractive Correction in Human Eyes

Peter M. Pinsky, Deepak V. Datye, Shou-sung Chang
Department of Civil Engineering, Stanford University, Stanford, CA 94305-4020

INTRODUCTION

There are a variety of refractive surgical procedures for the human cornea which alter its shape to correct refractive errors. These procedures include the implantation of intrastromal devices, incising of the cornea as in keratotomy (the most well-known being radial keratotomy), and the ablation of corneal tissue as in photorefractive keratectomy. Mechanical modeling of such surgical procedures requires tissue constitutive modeling that is based on the ultrastructure features and properties of the tissue constituents, along with objective estimates of *in vivo* corneal mechanical properties. In this paper we describe a constitutive model for the corneal tissue, and a nonlinear finite element implementation of this model suitable for simulating refractive surgical procedures. We also describe an experimental set-up for obtaining the *in vivo* values of the constitutive parameters for individual corneas. The tissue properties obtained are, to our knowledge, the first reported values for *in vivo* corneal tissue.

REVIEW AND THEORY

The human cornea is about 0.5 mm thick, and is divided into five layers. Ninety percent of the corneal thickness is accounted for by the stromal layer, which consists of thousands of collageneous ribbon-like lamellae placed one on top of the other and running continuously from limbus to limbus. The stroma is the principal load carrying layer of the human cornea which resists external forces principally through the development of tension in the collagen within individual lamella. Accordingly, the mechanical response of the cornea is governed by the nonlinear load-deformation behavior of the individual lamella. The angular distribution of these lamellae is more or less random. Each lamella is composed of collagen fibrils embedded in a jelly-like ground substance, whose shear modulus is several orders of magnitude smaller than the longitudinal modulus of the collagen fibrils.

In keratotomy surgical procedures very deep cuts, up to 95% of the corneal thickness, are introduced. Such procedures change the epithelial corneal contours by inducing an anisotropy in the corneal membrane rigidity which in turn results in a profound stress redistribution within the stroma. In an earlier work, Pinsky and Datye [1,2] developed a membrane model for keratotomy based on the premise that cut lamellae may slide relative to adjacent uncut lamellae until they achieve a stress-free configuration. The cut lamellae in this model were hence unable to contribute towards the corneal membrane rigidity. Based on geometric arguments, a quantitative representation for the induced anisotropy and inhomogeneity in the corneal membrane rigidity was obtained. This constitutive model was then employed in a geometrically nonlinear finite element membrane formulation.

In this paper, we describe a new nonlinear three-dimensional finite element formulation which is an extension of the membrane model by Pinsky and Datye [1,2] having wide applicability. We illustrate the model with applications to radial keratotomy and for simulating the effects of implanting intrastromal devices, such as rings. The constitutive model is based on the assumption that the corneal lamellae are orthotropic with a free energy density function of the general form,

$$W = K(e^{\mathbf{E}:\mathbf{D}:\mathbf{E}} - 1) \tag{1}$$

where $\mathbf{E}$ is the Green Lagrange strain, and $\mathbf{D}$ is a fourth order elasticity tensor satisfying certain isotropy conditions. The constitutive model for the stroma is constructed from the lamella constitutive model using a microstructurally-based averaging technique that takes into account the effects of load transfer between adjacent lamellae through the shear stiffness of the ground substance. The resulting model is incompressible and has high membrane and low transverse shear stiffness. Potential locking effects in the finite element model are avoided through the use of a mixed variational formulation.

A number of investigators have attempted to determine *in vitro* tissue property parameters, e.g. [3]. Reported values vary over a large range and have been obtained by performing experiments on isolated corneal tissues, or by conducting experiments on enucleated eye-balls inflated to non-physiological intraocular pressures. Hence these properties probably do not reflect the true mechanical properties of *in vivo* human corneas and therefore may not be reliable for modeling purposes. We have developed an experimental procedure for obtaining *in vivo* corneal mechanical properties relevant to the constitutive model in Eqn. 1. This pro-

cedure, described in the next Section, is based on obtaining load-contour histories for apical indentation of the cornea in conjunction with inverse estimation using finite element techniques. Hitherto, there have been no measurements of the mechanical properties if the *in vivo* corneal tissue.

PROCEDURE

We have developed an optomechanical testing device which can measure the contour of a cornea deformed *in situ* by a mechanical probe. The computer-controlled instrument built to perform the indentation is capable of three dimensional positioning, and is comprised of a mechanical probe, a load cell, a CCD camera, and light sources. After applying topical anesthetic on the subject's eye, the spherical end of the probe is pushed against the apex of the cornea in steps, and at each step, the corneal contour is captured by the CCD camera, and the force exerted is measured. The geometry of the undeformed cornea and the intraocular pressure are measured right before the experiment, and are used for constructing a finite element model of the individual cornea. In the axisymmetric nonlinear finite element model, the cornea is assumed to be fixed at the limbus, and loaded on the bottom surface by the intraocular pressure.

The conditions of incompressibility and transverse isotropy result in the need to determine three independent mechanical parameters. In this preliminary model, we choose two of the three to be independent, and these correspond, in the small strain limit, to the in-plane Youngs modulus, E, and the transverse shear modulus, G. These *in vivo* properties are obtained by inverse estimation. An objective function of E, and G is first defined to measure the discrepancy between the experimental data and the numerical simulation of the experiment. The simulation is performed over a selected range of parameters values and those values of E and G which minimize the objective function are taken to be best estimates of these parameters.

RESULTS AND DISCUSSION

Constitutive Parameters The indenting procedures were repeated at least twice on each human subject. The inverse estimation provided unique values for the parameters. Figure 1 shows a typical result from the inverse estimation. Results for the in-plane Youngs modulus ranged over 1 to 5 MPa, and the transverse shear modulus ranged over 10 to 30 KPa, with reproducibility within 15%. It is important to note that the shear modulus is determined *independently* from the Young's modulus. *In vivo* measurement of the mechanical properties of the cornea opens the possibility of characterizing the cornea of individual patients and of allowing for variations of the properties in planning a surgical procedure.

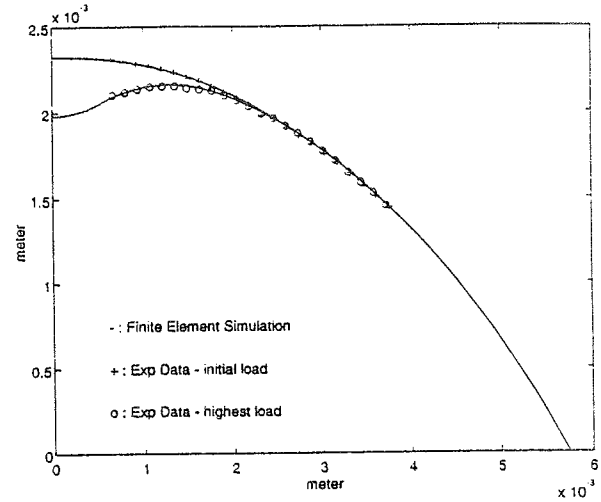

Figure 1:

Simulation of Refractive Surgery The finite element model was used to simulate radial keratotomy and has provided useful data on the effects of critical parameters, including number of incisions, incision depth and length, intraocular pressure, etc. Good correspondence was obtained between clinical findings and the numerical values predicted by the model. The model has also been employed in investigating the effects of implanting an intrastromal ring. Figure 2 shows the deformed mesh. Results compare well with parameters measured in the clinic.

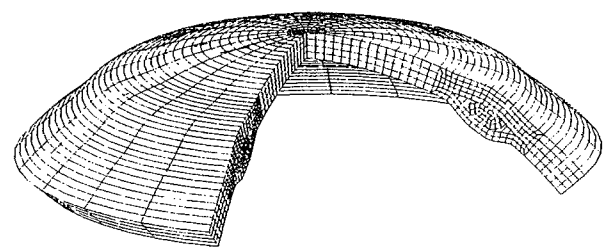

Figure 2:

REFERENCES

1. Pinsky P.M., Datye D.V. (1991) A Microstructurally-Based Finite Element Model of the Incised Human Cornea, *J.Biomechanics*, **24**, 907-922.
2. Pinsky P.M., Datye D.V. (1992) Numerical Modelling of Radial, Astigmatic and Hexagonal Keratotomy, *Refractive and Corneal Surgery*, **8**, 164-172.
3. Woo S.L., Kobayashi A.S., Schlegel W.A., Lawrence C. (1972) Non-Linear Material Properties of Intact Cornea and Sclera, *Experimental Eye Research*, **14**, 29-39.

AN ANALYTIC MODEL TO PREDICT THE STRENGTH OF TENDON REPAIRS

J.C. Lotz, PhD, J.S. Hariharan, MD, E. Diao, MD, O. Soejima, MD
Department of Orthopedic Surgery, University of California San Francisco,
San Francisco, CA 93143-0514

INTRODUCTION

The goal of this project was to develop a simple model for the behavior of the multi-component suture repair of flexor tendons, which could predict suture load sharing and thus serve as a basis for the design of stronger suture techniques. We experimentally tested the stiffness and strength of the individual components of the tendon repair (core and epitendinous suture) as well as that of the total repair. We collected data and evaluated the proposed model for two repair techniques: core suture plus epitendinous suture with shallow penetration (SES); and core suture plus epitendinous suture with deep penetration (DES).

REVIEW AND THEORY

Recent studies have demonstrated that early active mobilization following primary tendon repair improves tendon gliding and function[1-2]. However, currently popular repair techniques do not provide sufficient tensile strength to withstand the forces that would be associated with early active mobilization[3]. While many suture techniques have been evaluated experimentally in attempts to achieve greater tensile strength, no analytic model has been presented which could serve as a basis for the development of improved methods. In tendon repairs with both core and epitendinous suture components, the ultimate load of the repair will equal the sum of the load in the core stitch plus the load in the epitendinous stitch at failure. The strongest repair will result when both the individual core and epitendinous sutures reach their maximum load simultaneously. However, stiffness imbalances inherent in current suture techniques result in less than optimal load distribution between the two sutures, causing one suture to fail before the companion stitch has achieved its potential maximum load.

PROCEDURES

The tendon repair was modeled as two springs in parallel, representing the core and epitendinous sutures. These springs were in series with a spring representing the tendon itself (Figure).

Therefore, the effective stiffness of the tendon repair, K_{tot}, was represented as-

$$K_{tot} = \frac{1}{\left\{ \frac{1}{K1} + \left[\frac{1}{K2+K3} \right] \right\}}$$

where K1 is the tendon stiffness, K2 is the epitendinous stitch stiffness, and K3 is the core stitch stiffness. This spring model was used in conjunction with our experimental data (described below) to predict the stiffness and strength for the complete suture constructs (K_{tot}). To determine values for the stiffness K1, K2, and K3, we isolated 36 flexor digitorum superficialis tendons from 18 fresh frozen human hands over a length of 12 cm. The distal and proximal portions of each tendon were separated (resulting in 72 specimens) and placed into one of six groups. The six test groups were: 1) tendon alone (n=12); 2) severed tendon repaired with core stitch only (4-0 Dermalon using the modified Kessler technique; n=12); 3) severed tendon repaired with superficial epitendinous suture placement only (SES) (6-0 Surgilene; n=10); 4) severed tendon repaired with deep epitendinous suture placement only (DES) (6-0 Surgilene penetrating to half the distance to the center of the tendon; n=10); 5) severed tendon repaired with core plus SES (n=12); and 6) severed tendon repaired with core plus DES (n=12). We controlled for the length and diameter of the tendon, the site of the repair, the distance of the applied force from the repair, the length and tension of the core stitch, and the number and depth of bites of the epitendinous suture. Further details of the SES and DES techniques are described elsewhere[4]. All specimens were distracted to failure at a rate of 0.33 mm/sec., while submerged in physiologic saline. The specimen stiffness was calculated as the slope of the most linear region of the resulting load-deflection curve.

RESULTS

The predicted stiffness and strength of the total repair for both the SES and DES groups were statistically equivalent to those determined experimentally (5.9 N/mm & 22.3 N versus 6.8

N/mm & 21.7 N for the SES group and 10.33 N/mm & 37.2 N versus 12.9 N/mm & 38.9 N for the DES group;Table 1). For the SES technique, the model predicts that 65% of the total repair failure load was carried by the epitendinous suture, as compared to 83% for the DES technique. The model also suggests that the for both SES and DES, the total repair fails when the epitendinous suture reaches its maximum load, while the core suture is only at 50% of its capacity.

DISCUSSION

The simple analytic formulation derived using a spring analogy accurately predicted the behavior of both the SES and DES tendon repairs. Our model demonstrated that for both constructs, the epitendinous suture is stiffer and stronger than the core suture and reaches its maximum load at the point of construct failure. The model also demonstrates that the core suture achieves only 50% of its potential maximum load at the point of construct failure. These results suggest load sharing between parallel suture constructs may not be optimal, and that the strength of both the DES and SES constructs could be further improved by increasing the stiffness of the core suture such that it reaches its maximum load capacity concurrent with the epitendinous suture. Our results also demonstrate that a model based on a simple spring analogy can accurately represent the interaction between suture constructs loaded "in parallel". This model can thus provide an objective basis for developing predictable improvements to current tendon repair techniques.

Table 1: Stiffness (N/mm) and Strength (N) Results

	Tendon (K1)	Core (K3)	SES (K2)	DES (K2)	Full repair experiment		Full repair model	
Stiffness	32.8 ±10.1	2.5 ±0.7	4.7 ±2.2	12.6 ±3.6	SES	6.8* ±2.0	SES	5.9
					DES	12.9* ±3.3	DES	10.3
Strength		12.1 ±2.7	14.5 ±0.9	31.1 ±3.2	SES	21.7† ±3.6	SES	22.3
					DES	38.9† ±13.9	DES	37.2

* p>0.10 by one-way t-test to model results

† p>0.60 by one-way t-test to model results

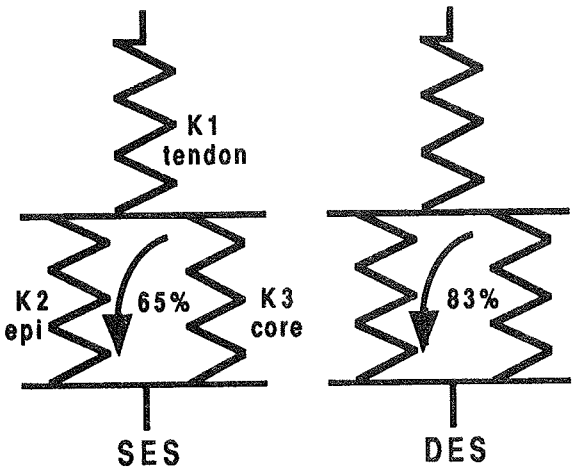

Figure: Spring Model

REFERENCES

1) Gelberman et al., Tendon surgery in the Hand. CV Mosby Co. 1987

2) Seyfer AE, and Bolger WE, Plast Reconstr Surg 83: pp. 122-8, 1989

3) Tsuge et al., J. Hand Surg 2: pp. 436-440, 1977

4) Diao et al., 2nd World Congress of Biomech. (2):229, 1994.

COLLAGEN CROSS-LINKING IN THE SKIN OF NORMAL AND DIABETIC FEET: INDIRECT MEASUREMENTS USING LASER-INDUCED TISSUE FLUORESCENCE.

B. L. Davis, R.M. Cothren, J.T. Arendt, J.E. Perry
Department of Biomedical Engineering, Research Institute,
The Cleveland Clinic Foundation, Cleveland, OH 44195.

INTRODUCTION

In the case of diabetic patients it is generally agreed that non-mechanical factors such as peripheral neuropathy, dry skin and/or vascular problems are often major contributing causes of skin ulceration. However, current opinion is divided as to the principal mechanical factors leading to ulcer formation--tissue changes, repetitive loads, shear and pressure have been cited as being potentially detrimental. Irrespective of the cause, foot ulceration is a diabetic complication that has been estimated to result in $800,000,000 worth of medical expenses per year in the United States alone (Davis, 1993).

REVIEW AND THEORY

There is evidence that in the presence of hyperglycemia some proteins, such as collagen-- a structural protein in the skin--can undergo nonenzymatic glycosylation (Brownlee et al. 1984, Monnier et al. 1984). This process causes glucose to attach to the protein and leads to increased cross-linking, thereby altering the protein's structure. Increased cross-linking is believed to contribute to increased mechanical stiffness of collagen containing tissues (Reiser 1991) and to be a major contributor to many of the complications of diabetes (Kennedy and Baynes 1984). In addition to highly cross-linked tissues being more rigid, they are more resistant to enzymatic digestion by collagenase (Reiser, 1991). This can result in greater callus buildup which also increases the risk of ulceration. Spectroscopic fluorescence techniques can be used to detect the presence of cross-linked proteins (Brownlee et al. 1984) and studies utilizing these methods have shown that diabetic skin tissue has increased fluorescence relative to non-diabetic tissue (Monnier et al. 1984). In all of these studies, results were based on the analyses of tissue acquired from cadavers or from skin biopsies.

PROCEDURES

Tissue autofluorescence techniques have been primarily used to detect cancer, dysplasia or atherosclerosis. In this study these techniques were adapted to study differences in the fluorescence spectra of three groups of subjects: 7 non-diabetic (i.e., control), 9 neuropathic diabetic (NP) and 9 non-neuropathic diabetic (NNP) patients.

The skin on the plantar surface of the foot and on the forearm was excited (to a depth of about 300μm) with weak ultraviolet light from a nitrogen-pumped dye laser. The autofluorescence spectra were obtained using an optical multichannel analyzer and quantified with a 12-bit A/D board that was interfaced with an IBM-compatible computer. The primary variable of interest was the area under the spectrum. This is related to the total fluorescence energy, and therefore the extent (or amount) of cross-linking.

RESULTS

The area under the fluorescence spectrum was significantly greater for neuropathic diabetic patients ($p < 0.01$) compared to control or non-neuropathic patients (Figure 1). Actual mean scores for the three groups were in the proportion 99 : 140 : 108 for controls, NP and NNP, respectively.

In addition to patient category, skin region also significantly affected the area under the fluorescence spectrum. The metatarsal head region had significantly higher total fluorescence than the arch of the foot, which in turn had a significantly greater "area" measurement than the skin of the forearm ($p < 0.001$). There were no significant differences between the skin's total fluorescence at the hallux and metatarsal head regions (Figure 2).

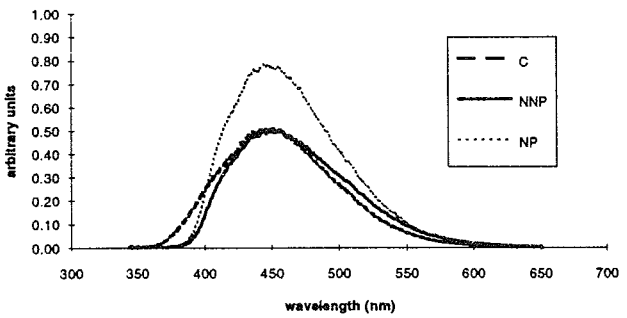

Figure 1. Fluorescence spectra for three groups of patients: Control (C), Non-neuropathic (NNP) and Neuropathic (NP) diabetic patients.

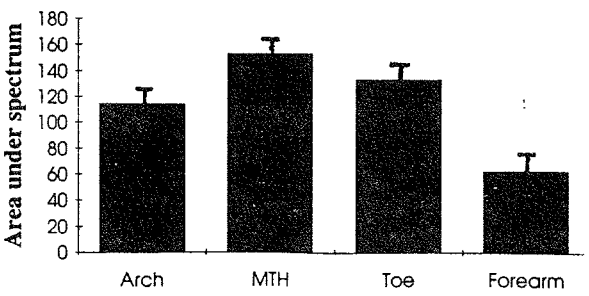

Figure 2. Area under fluorescence spectra for four regions of the body (averaged across patient groups).

DISCUSSION

While these data suggest that diabetes affects weightbearing skin differently than non-weightbearing skin in terms of total fluorescence, the finding of greatest importance is that neuropathic diabetic skin has a greater area under the fluorescence spectrum. This implies that neuropathic skin is almost certainly stiffer than skin from either non-neuropathic or control patients.

It is conceivable that patients with a stiffer epidermis on the plantar surface of the foot could experience deleterious stresses at the interface between the stiff outer layer and the relatively "softer" inner connective tissue. For instance, it is known that delamination can occur in polyethylene knee implants that have been surface hardened (Schmotzer, 1992). It is also known that certain diabetic ulcers initiate a few millimeters beneath the plantar skin surface (Delbridge et al., 1985). While the link between tissue stiffness gradients and foot ulceration needs further investigation, the conclusion of the present study is that laser-induced tissue fluorescence is a non-invasive, quick and painless method for assessing collagen cross-linking in the epidermis of diabetic patients.

REFERENCES

Brownlee, M. et al. *Ann. Int. Med.*, 101, 527-537, 1984.
Davis, B.L. *Medical Hypotheses*, 40, 44-47, 1993.
Delbridge, L. et al. *Br. J. Surg.*, 72, 1-6, 1985.
Kennedy, L. et al. *Diabetologia*, 26, 93-98, 1984.
Monnier, V.M. et al. *Proc. Natl. Acad. Sci.*, 81, 583-587, 1984.
Reiser, K.M. *Proc. Soc. Exper. Biol. Med.*, 196, 17-29, 1991.
Schmotzer, H. et al. *Proc. 8th Mtg. Eur. Soc. Biomechanics*, 114, 1992.

ACKNOWLEDGMENTS

The authors would like to acknowledge funding from the Juvenile Diabetes Foundation International.

THE MECHANICAL BEHAVIOR OF HUMAN LUMBAR DISCS WITH NUCLEUS VOLUME VARIATIONS

Y. Michael Lu, William C. Hutton*, and Vasanti M. Gharpuray
Department of Bioengineering, Clemson University, Clemson, SC 29634
* Emory Spine Center, Emory University, Atlanta, GA

INTRODUCTION

The intervertebral disc shows a loss of nucleus volume after a day's activity, with disc degeneration or herniation and after certain clinical treatments such as discectomy and chemonucleolysis. This nucleus volume loss will initiate changes in the mechanical behavior, and may influence the normal functioning of the intervertebral disc. To add insight to this problem, we developed a 3D finite element model of the L2-L3 lumbar intervertebral disc, both intact and with a nucleus volume loss, to determine the roles of the disc components in its mechanical behavior. We propose that a loss of nucleus volume may significantly affect the mechanical behavior of the disc and cause stress redistribution in disc components.

REVIEW AND THEORY

A loss in nucleus volume due to fluid flow during diurnal activities causes a decrease in disc height and affects disc stiffnesses (Botsford et al. 1994; Adams et al. 1990). The loss of disc materials caused by clinical treatments such as chemonucleolysis and discectomy may also significantly decrease the disc height and intradiscal pressure (Brinckmann et al. 1991; Konings et al. 1984) and influence the mechanical properties of disc (Goel et al. 1986). Shirazi-Adl (1992) simulated the gains and losses in nucleus content using a 3D finite element model and showed that volume change had a significant effect on the forces of facets and anular fibers. However, the simulated volume loss (12%) was small as compared to the daily volume change of 21% (Botsford et al. 1994) and the change in disc bulging behavior was not emphasized. Therefore, the purpose of this study was to study the changes in the load transfer mechanism and disc bulging behavior of the lumbar intervertebral disc after a loss in nucleus fluid content or in disc material.

PROCEDURES

A 3D finite element model of human lumbar motion segment L2-L3 with posterior elements (ligaments and facet joints) was developed from Computer Tomography (CT) scans of a fresh cadaveric lumbar spine. The FE code PATRAN was used for reconstructing the geometry and generating the FE mesh, and ABAQUS v.5.3 was used for processing and post-processing. The details of the model have been presented in a previous article (Lu, et al. 1995). In brief, the disc height was 8 mm. The cross sectional area was 13 cm^2 and 38% of it was the nucleus pulposus. The anulus fibrosus was simulated as a composite material of homogenous ground substance reinforced by collagen fibers (modeled by cable elements) with fiber volume fraction ranging from 5% in the innermost layer to 23% in the outermost layer. The endplates were 1 mm thick. The nucleus pulposus was simulated by 3D hydrostatic fluid elements. Loss of nucleus volume was simulated by applying an outward flux to the nucleus cavity in increments. Two procedures were employed: 1) a constant axial force of 1000 N was applied to the top surface of L2 to simulate the force acting on the lumbar disc in erect standing. Then, 22% of the total nucleus volume (900 mm^3) was removed in six increments. This procedure simulates diurnal volume change in the disc; 2) to simulate a loss of nucleus volume due to clinical treatments, 20% of the total nucleus was first removed. Then an axial compressive displacement up to 3.2 mm was gradually applied to the top surface of L2.

RESULTS

Intradiscal pressure and disc height were found to decrease significantly as a result of the nucleus volume loss. With a decrease in nucleus volume under a constant axial force of 1000 N, the radial disc bulge at posterolateral and posterior anulus sites became smaller, but increased slightly at the peripheral anterior and lateral sites. At the innermost anulus layer, the radial bulge decrease linearly and eventually bulged inwards (Figure 1). Compared with the intact disc, the disc with a volume loss of 20% did not show significant increase in radial disc bulge (less than 0.3 mm) (Figure 2). Nucleus volume loss also resulted in changes in the tensile stress in anulus fibers under a constant axial force of 1000 N (Figure 3). The tensile stresses increased moderately in both anterior and lateral peripheral fibers but dropped sharply in posterolateral and posterior fibers. The increase in tensile stress correlated well with the increase in radial disc bulge at the corresponding sites. After a loss of nucleus volume, the force transmitted through the outer region of the inferior endplate (corresponding to the area under the anulus fibrosus) increased while the force through central region (the area under the nucleus pulposus) decreased due to the drop in intradiscal pressure (Figure 4).

DISCUSSION

In a normal disc, the nucleus pulposus of lumbar discs carries a substantial portion of the applied load by generating an intradiscal pressure, which in turn, stretches the surrounding anular fibers to resist radial disc bulge (Shirazi-Adl 1992). With a loss in nucleus volume, the load-transfer capacity of the nucleus is compromised. Therefore, the question that arises is: is the anulus able to compensate for the load-transfer capacity loss and maintain a functioning disc?

The results from this study show that at a loss of 20% of nucleus volume, the lumbar intervertebral disc can still carry an axial force up to 4500 N without significant increase in radial disc bulge at anterior, lateral, posterolateral and posterior anulus periphery as compared to the intact disc (Figure 2). The stress

redistribution between nucleus pulposus, anulus, and anular fibers occur due to the reduced or diminished intradiscal pressure after a loss of nucleus volume. As the load transmitted through nucleus decreases, the anulus wall will take the applied compressive load by itself but at a mild increase in radial bulge on the disc periphery. This seems to occur mainly at the thicker anulus portion i.e. anterior and lateral parts in the current model because the thinner anulus wall tends to be more compliant in compression (Figure 4). Collagen fibers no longer play a role in resisting axial compression. But the peripheral anular fibers still sustain tensile stress due to the mild increase in radial disc bulge. Even when the compressive load supported by the anulus increases significantly, no instability of anulus wall was seen at a loss of nucleus volume up to 22%. Thus, the anulus is able to effectively resist compression after the load-bearing capacity of nucleus is damaged. These results are supported by an experimental observation (Markolf et al. 1974) that the anular wall after complete removal of all of the nucleus exhibited near-normal compressive stiffness.

Radial disc bulge following a nucleus volume loss increased at all sites in the periphery except in the posterior periphery when the applied axial force was below 2000 N (Figure 2). This agrees with a mild increase in radial disc bulge following chemonucleolysis confirmed from CT scans by Konings et al. (1984). This tends to suggest that the reduction in nerve root compression as a result of chymopapain injection may not come from a decrease in posterior disc bulge (as suggested by Kim et al. 1988) but may be more likely to come from the direct softening or dissolution of the extruded disc material (Krempen et al. 1975) or from localized disc bulge reduction at an injured region where a small section of the protruded anular wall compresses a nerve root.

In summary, the anulus was able to maintain a near-normal mechanical behavior intervertebral disc under compression by transmitting a high compressive load without significant increase in radial bulge following a loss of nucleus volume up to 20%.

REFERENCES

Adams, MA et al. *J Bone Joint Surg* 72B,266-70, 1990.
Botsford, DJ et al. *Spine* 19, 935-40, 1994.
Brinckmann, P et al. *Spine* 16, 641-46, 1991.
Goel, VK et al. *Spine* 11, 1008-11, 1986.
Kim, YE et al. *The Winter Annual Meeting of the ASME.* 461-71, 1988.
Krempen, JF et al. *Clin Orthop* 106, 336-49, 1975.
Konings, JG et al. *J Bone Joint Surg* 66B,417-21, 1984.
Lu, YM et al. submitted, *Spine*, 1995.
Markolf, KL et al. *J Bone Joint Surg* 56A,675-87, 1974.
Shirazi-Adl, SA. *Spine* 17, 206-12, 1992.

ACKNOWLEDGMENTS

The support provided by the National Center for Supercomputing Applications (NCSA) (Grant No. BCS950002N) is gratefully acknowledged.

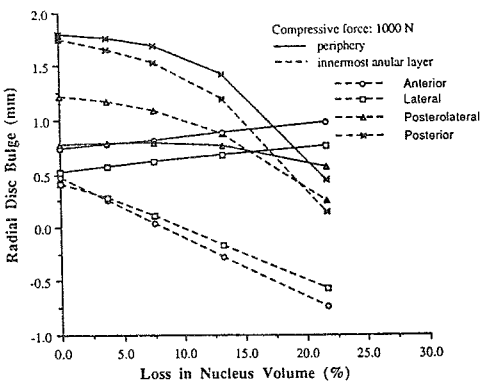

Figure 1

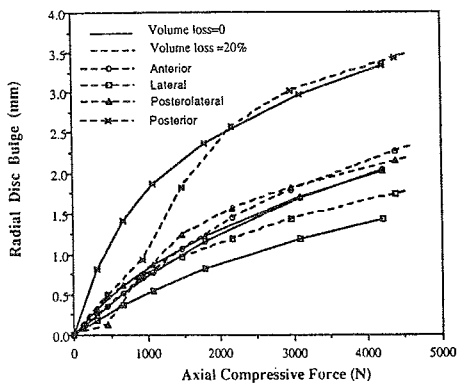

Figure 2

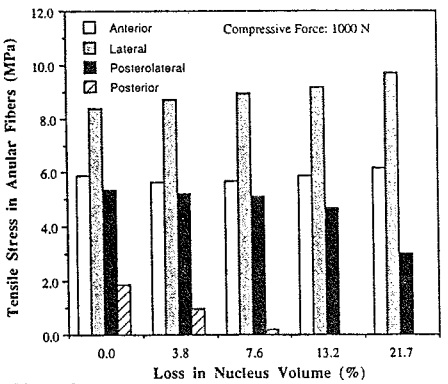

Figure 3

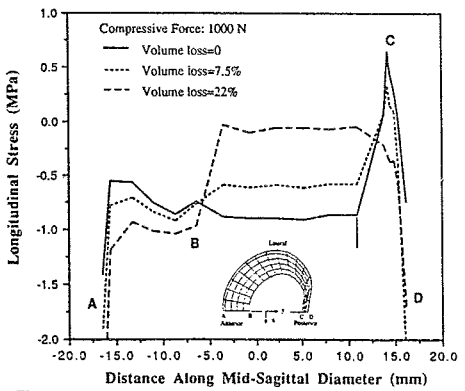

Figure 4

CHANGES IN CIRCUMFERENTIAL STRAIN GRADIENTS DURING LOCOMOTION

Stefan Judex, Ted S.Gross, Ronald F. Zernicke
Joint Injury and Arthritis Research Group, Departments of Surgery and Mechanical Engineering,
University of Calgary, T2N 4N1, Calgary, Alberta, Canada

INTRODUCTION

In vivo strains were recorded from the tarsometatarsus bone (TMT) in mature roosters during treadmill locomotion. The distribution of longitudinal normal strains acting on the midshaft cross-section and the circumferential strain gradients generated by this environment were determined using beam theory. In this study, we attempt to identify changes in these parameters induced by elevated locomotion speed. As bone is extremely sensitive to its mechanical environment, we anticipate that alterations in these mechanical stimuli will allow us to predict sites of adaptation engendered by an exercise regimen.

REVIEW AND THEORY

Bone is a highly dynamic tissue, and it is commonly accepted that the addition or deletion of mechanical stimuli induces rapid and substantial changes in its morphology. Nevertheless, the specific parameter responsible for controlling adaptation has not been identified. Numerous mechanical parameters have been proposed, including, but not limited to, strain magnitude (Rubin *et al.*, 1985), frequency (McLeod *et al.*, in press), rate (Goldstein *et al.*, 1991), and history (Carter, 1987). Recently, Gross and colleagues (1994) applied exogenous loads to isolated turkey radii and found that the sites of new bone formation correlated highly with the circumferential strain gradient of longitudinal normal strain. As this parameter was validated by its ability to predict adaptation under alternate loading conditions, the authors proposed that it was related to the process by which cells sense their mechanical environment. Although the hypothesis of circumferential strain gradients promoting bone formation is contrary to the premise that new bone is laid down primarily at sites subjected to the largest strains, strain gradients are proportional to fluid flow within the bone, and may therefore induce a number of physiologically relevant processes such as fluid shear and streaming potentials. Here, we determine the gradients induced during normal locomotion, and identify any alterations in these stimuli induced by elevated locomotion speed.

PROCEDURES

Three miniature triple rosette strain gages were attached with cyanoacrylate to the medial, anterior, and lateral aspects of the left diaphyseal TMT-midshaft in three mature White Leghorn roosters (40 wk old). After a 24-hour post-operative recovery period, strains were recorded while the roosters "walked" (0.51 m/s) and "ran" (1.66 m/s) on a treadmill. Data were sampled at 200 Hz for 10 s. Using linear beam theory, the distribution of longitudinal normal strain acting on the midshaft cross-section was determined. The cortex was then divided into 12 equal angle pie sectors with the cross-sectional center of mass as an origin (see inset **Fig.2**). The circumferential strain gradient within each sector was calculated as the difference between the normal strains on the periosteal surface of either border of each sector normalized to the linear distance between these points.

RESULTS

The position and orientation of the neutral axis varied little during the stance phase of each gait, and was similar across animals (< 20°).

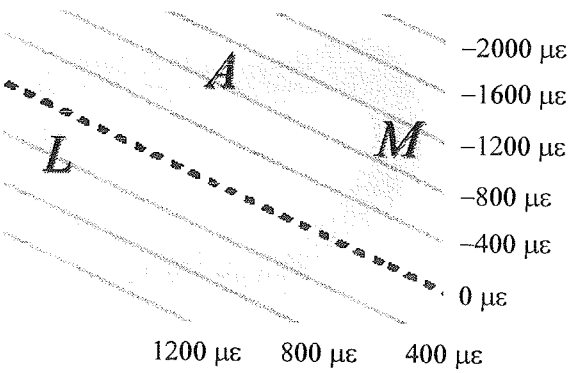

Figure 1. Distribution of peak longitudinal normal strain across the mid-diaphyseal TMT cross-section in a representative rooster walking at a speed of 0.51 m/s. The neutral axis is dashed with strain isopleths parallel to it. Compressive strains are negative, and tensile strains are positive.

The neutral axis spanned the medial/posterior and anterio/lateral cortices (**Fig.1**). In addition, the magnitude of the peak compressive strain was similar

across speeds (0.51 m/s: -1466±133 με; 1.6 m/s: -1566±33 με). Peak tensile strains were also consistent across speeds (0.51 m/s: 1033±16.7 με; 1.6 m/s: 1050±29 με).

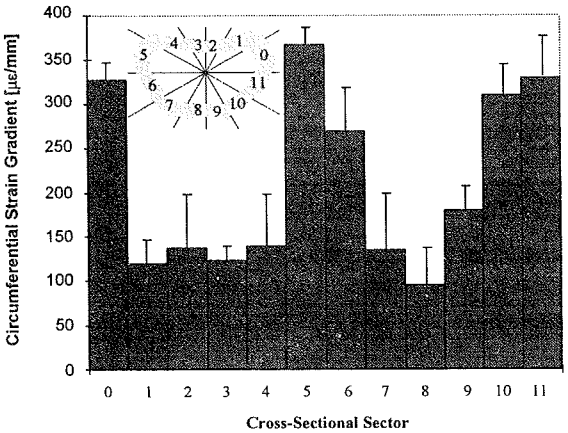

Figure 2. Circumferential strain gradient distribution of longitudinal normal strain (mean±S.E.) across a mid-diaphyseal transverse section (0.51 m/s). Sector numbers correspond to the cross-sectional sectors in the inset. Sectors with high strain gradients are located near the neutral axis.

Strain gradient distributions generated during stance-phase were similar between treadmill speeds, with largest gradients found on the medial and lateral cortices **(Fig.2)**. However, when strain gradients generated during the swing phase were taken into account (*i.e.*, maximum range of gradients during the entire gait cycle), increased treadmill speed was found to significantly elevate strain gradients in those sectors already demonstrating large magnitude gradients. **(Fig.3)**

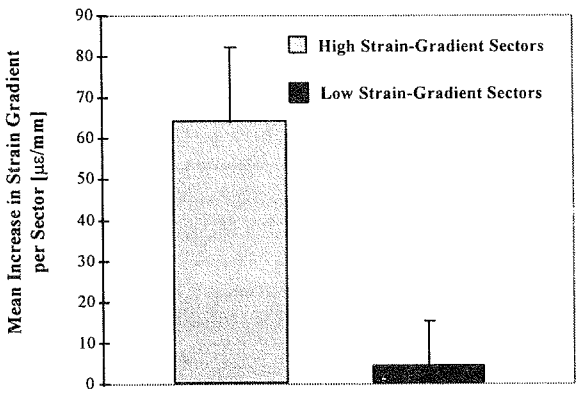

Figure 3. The mean increase ±S.E. in total circumferential strain gradients between a low (0.51 m/s) and a higher speed (1.66 m/s). The six sectors with the highest strain gradients (*e.g.*, sector 0,5,6,9-11; Fig.2) were grouped as "high strain-gradient sectors," while the remaining six were grouped as "low strain-gradient sectors." Strain gradients within the high strain gradient sectors were significantly ($P \leq 0.05$) increased by locomotion speed.

DISCUSSION

We found that despite a three-fold increase in locomotor speed, peak normal strains and the location of the neutral axis did not vary. Since normal strain distributions were determined across the midshaft cross-section, sites of peak strain were calculated without assumptions of the manner in which the bone was loaded. These observations are, therefore, not limited to the sites of strain gage attachment. *In vivo* circumferential strain gradients were found to be non-uniform and similar in distribution across locomotor speeds (*i.e.*, locations of the largest gradients were maintained across speeds). This extremely stable strain environment may be one explanation for the minimal adaptation demonstrated in previous exercise studies (Loitz *et al.* 1992).

As increased speed elevated the range of strain gradients at specific sites, we would predict that, if these stimuli are of sufficient physiologic magnitude, sites of new bone formation induced by exercise would be focused here. Currently, we are investigating whether modified exercise regimens (*e.g.*, uphill running) more substantially elevate these gradients and thus provide a larger stimulus for adaptation.

REFERENCES

Carter, D.R. *J Biomech*,**20**,1095-1109,1987.
Goldstein, S.A. *et al. J Biomech*,**24**,135-150,1991.
Gross, T.S. *et al. Trans Orth Res Soc*,**278**,1994.
Loitz, B.J. *et al.* J exp Biol,**170**,1-18,1992.
McLeod, K.J. *et al. J Biomech*,(in press).
Rubin, C.T. *et al.Calcif Tissue Int,* **37**,411-417,1985.

ACKNOWLEDGMENTS

This investigation was funded in part by the Natural Sciences and Engineering Research Council of Canada and the Alberta Heritage Foundation for Medical Research.

Nonlinear Radial Tensile Properties of the Lumbar Annulus Fibrosus: Effect of Site and Disc Degeneration

Yoshi Fujita, Neil A. Duncan and Jeffrey C. Lotz

Orthopaedic Bioengineering Laboratory
Department of Orthopaedic Surgery
University of California, San Francisco, San Francisco CA 94143-0514

INTRODUCTION

Disc disruption has historically been attributed to acute traumatic loads of a magnitude sufficient to produce sudden tensile failure of the collagen fibers of the annulus. Yet, the observation that the annulus often displays circumferential clefts suggests that disruption of the annulus may be the result of failure of the matrix between lamella rather than the collagen fibers.[1] In support of this, significant radial stresses have been predicted within the annulus during flexion and subsequent to a reduction of nuclear pressure.[2]

REVIEW AND THEORY

We previously reported the ultimate stress, elastic modulus and ultimate strain of radially oriented annular specimens as a function of radial and circumferential location.[3] The elastic modulus that we reported was calculated from the linear region of the stress strain curve. However, the predicted annular radial strain in-situ is near 50%, where the radial stress-strain relationship is nonlinear.[2]

The purpose of this study is to determine the nonlinear tensile behavior of radially oriented annular specimens to provide the needed data for accurate modeling of this tissue. In addition, the effect of site and degree of degeneration on the tensile properties is also investigated.

PROCEDURES

Tensile test: Eight intervertebral discs were harvested from fresh-frozen human lumbar spines. All discs were examined macroscopically and the degree of degeneration was assessed according to the Thompson grading scheme.[4] We prepared 145 rectangular specimens from the following six annular regions -- Anterior Outer: AO (23); Anterior Middle: AM (27); Anterior Inner: AI (27); Postero-lateral outer: PO (20); Postero-lateral Middle: PM (29); Postero-lateral Inner: PI (19). These specimens were cut parallel to the anatomic horizontal plane into 1 mm thick slices using a vibratome (Micro-Cut, H1200). Subsequently, the specimens were cut to a width of 3.2 mm using a precision die. The long dimension of the rectangular specimens was oriented in the anatomic radial direction, perpendicular to the annular lamina. The ends of each rectangular specimen were attached to a sandpaper frame using cyanoacrylate adhesive to facilitate easy transfer to the materials testing grips. The testing protocol consisted of submersion in 0.15M NaCl at room temperature, preconditioning with five cycles of tension to 0.5 N at 0.4 Hz, and distraction to failure at a rate of 1.2 mm/min. (0.4% strain/sec.). The applied load was measured using a precision force transducer (Sensotec, Model 31), and the specimen deformation was measured as the grip travel using the testing system LVDT. Stress and strain were calculated based on the initial undeformed dimensions.

Curve fitting: Typical stress-strain curves demonstrated an initial nonlinear (toe) region followed by a linear region. Therefore, the exponential function

$$\sigma = A(\exp(B\varepsilon) - 1),$$

was chosen to fit the stress-strain data.[5] The slope of this function was

$$d\sigma/d\varepsilon = B\sigma + AB.$$

and hence parameter B represented the rate of change of the elastic modulus with respect to stress, and the parameter AB represented the initial modulus. The elastic modulus was calculated as the slope of the stress-strain curve at 70% of the failure strain.

Mean values of these parameters for each specimen group were compared statistically by 3-way analysis of variance.

RESULTS

For all parameters, there were no significant differences between anterior and postero-lateral regions(Table1). However, statistically significant differences were noted between some parameters at different radial positions.

The initial modulus(AB) is similar at all 3 sites, however, in the middle specimens, the parameter, B, was significantly greater than inner and outer specimens. Consequently, the elastic modulus of outer specimens was significantly smaller than that of the other groups (Table 2). In addition, significant differences were noted between Grade 1 and Grade 2 specimens. While the elastic modulii were similar, the initial modulus(AB) was significantly smaller and the rate of change of the modulus(B) was significantly greater for the Grade 1 specimens compared to those of Grade 2 (Table 3, Fig.1).

Table 1. Region specific radial tensile properties of annulus

	Region		
Mean±S.E.	**Mean**	**Anterior**	**Postero-lateral**
Modulus (MPa)	0.47±0.02	0.50±0.04	0.43±0.03
AB(MPa)	0.21±0.02	0.22±0.03	0.19±0.02
B	2.36±0.12	2.50±0.18	2.19±0.15

Table 2. Site specific radial tensile properties of annulus

	Site		
Mean±S.E.	**Outer**	**Middle**	**Inner**
Modulus (MPa)*	0.35±0.04	0.52±0.04	0.44±0.04
AB(MPa)	0.19±0.02	0.23±0.03	0.20±0.02
B**	1.76±0.16	2.97±0.23	2.17±0.14

*Inner>Outer, Middle>Outer, p=0.009
**Inner>Outer, Middle>Outer, p=0.03

Table3. Grade specific radial tensile properties of annulus

Mean±S.E.	**Grade 1**	**Grade 2**
Modulus (MPa)	0.46±0.03	0.47±0.04
AB(MPa)***	0.16±0.01	0.28±0.03
B******	2.67±0.17	1.94±0.14

***Grade 1< Grade 2, p=0.0001
****Grade 1> Grade 2, p=0.01

DISCUSSION

The results of our study suggest differences in the nonlinear radial properties of the annulus that are dependent on both radial position and degree of degeneration. Though both Grade 1 and Grade 2 discs were of similar stiffness in the linear region, Grade 2 discs were significantly stiffer at lower strains which resulted in higher stresses at higher strains.

Disc degeneration causes significant biochemical and biomechanical changes. For example, Thompson et al. reported a threefold decrease in proteoglycan concentration occurred between Grade 1 and Grade 2 discs in the nucleus pulposus.[6] In addition, Uemura et al. reported that the capacity to retain water in the nucleus pulposus was reduced as the degree of disc degeneration advanced.[7] Despite these nuclear biochemical and biomechanical findings, there has been little data reported for the effect of disc grade on the biomechanical properties of annular tissue. Further work is needed to establish whether the nonlinear tensile properties of radially oriented specimens we report here are correlated with tissue biochemistry.

Our results suggest that the mechanical properties of the annulus fibrosus start to change at an early stage of disc degeneration. These findings have important implications toward understanding the pathomechanics of disc disruption and the development of circumferential clefts in the degenerated disc.

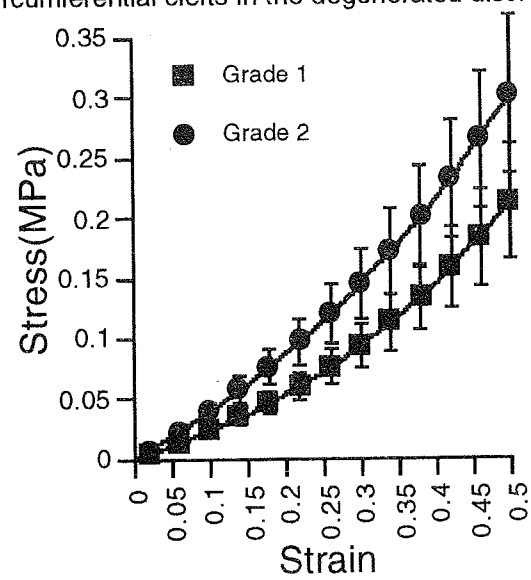

Fig.1. Average stress-strain curves (mean±SEM) for radially oriented annular specimens.

REFERENCES

1.Yasuma T et al., JBJS 72A:220-229,1986. 2. Shirazi-Adli A et al., J Biomechanics 19:331-50,1986 3. Fujita Y et al., Trans Orthop Res Soc 1995; 673 4.Thompson JP et al., Spine 15-5, 411-415, 1990 5. Danto MI, J Orthop Res 11:58-67,1993 6. Thompson JB., Trans Orthop Res Soc 1988; 13:276 7. Uemura et al. Trans Orthop Res Soc 1995 ; 674

THE MOTOR CONTROL OF STEPPING RESPONSES TO POSTURAL PERTURBATIONS

M.R. Carhart and G.T. Yamaguchi

Whitaker Center for Neuromechanical Control
and Department of Chemical, Bio and Materials Engineering
Arizona State University, Tempe, AZ 85287-6006

INTRODUCTION

In this study, perturbation induced stepping responses are examined for the characteristic kinetic, kinematic, and muscle activation patterns that have been reported previously for voluntary gait initiation. The motivation for this study is to determine how normals, subjected to large and unexpected perturbations, effect a step to maintain equilibrium. These responses will provide insight into the feasibility of providing paraplegics, standing via functional neuromuscular stimulation (FNS), with the ability react to perturbations.

REVIEW AND THEORY

While a number of studies have examined postural responses of man to small perturbations of standing, the process of equilibrium maintenance when "ankle" or "hip" strategies are insufficient is not clearly understood. It has been suggested that stepping responses to large postural perturbations consist of an initial unsuccessful ankle sway strategy followed by the initiation of a step or steps (Horak *et al.*, 1986; Maki *et al.*, 1993). However, such a superposition of the response strategies has yet to be demonstrated. Considerable data exist concerning anticipatory postural adjustments and temporal and synergistic behavior of the prime movers during gait initiation (Breniere *et al.*, 1987; Crenna *et al.*, 1991; Herman *et al.*, 1973). However, whether these patterns are evident in stepping responses to postural perturbations has not been investigated. Accordingly, the goal of this study is to examine stepping responses to postural perturbations for: (i) the anticipatory postural adjustments commonly observed in gait initiation (specifically, a shift in center of pressure toward the initial swing limb), and (ii) evidence of synergistic patterns of muscle activations driving the stepping motions.

PROCEDURES

Seven healthy adult male subjects participated in this study. Subjects stood in the center of the force sensing area, with their feet comfortably spaced and one foot on each of two Bertec (40x80 cm) six-component force platforms. Tracings of the feet were made to ensure consistent initial stance position across trials. Variable amplitude anterior waist-level perturbations were applied via an electro-pneumatic perturbation system. This system, illustrated in Figure 1, consisted of: (i) a belt secured over the subject's anterior superior iliac spines, (ii) an adjustable length cable and pulley system that connected to the belt anteriorly, (iii) a remotely controlled pneumatic actuator, and (iv) a tensile loadcell to measure the perturbation force. Five distinct levels of perturbation amplitude, ranging from 'small' to 'large', were administered without precue information by randomly fixing the stroke length of the pneumatic cylinder at one of five levels: 1.2", 2.4", 3.6", 4.8", or 6". The magnitude of the 'large' perturbation was selected, based on a pilot study, to represent a significant postural challenge (i.e., one that required a stepping response to prevent falling). Subjects were instructed that they would be pulled randomly and should simply avoid falling. Each subject was perturbed three times at each of the five perturbation amplitudes for a total 15 trials per subject.

Bilateral surface EMG was collected from the medial gastrocnemius, tibialis anterior, vastus lateralis, rectus femoris, and biceps femoris. Raw signals were digitally recorded at 1000 Hz and stored for off line analysis. Burst parameters were determined as follows: (i) 'on' and 'off' times were determined through visual inspection, (ii) intensity was calculated as the area under the channel linear envelope over the 'on/off' period, and (iii) centroid was calculated as the time corresponding to 1/2 of the burst intensity. Three-dimensional body segment kinematics were measured using spherical reflective markers (three per rigid-body-segment) and a four camera, 60Hz Motion Analysis system. Force plate and perturbation force data were digitally sampled at 180 Hz and stored for off line analysis.

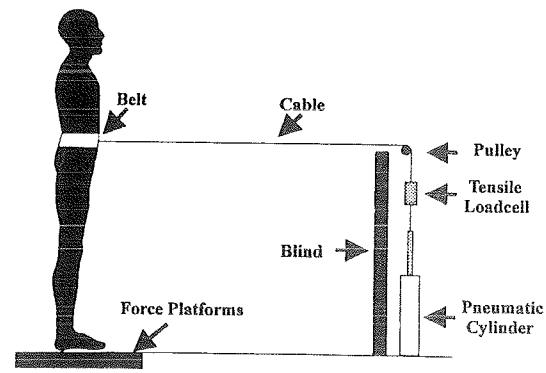

Figure 1: Illustration of the experimental apparatus.

RESULTS

Perturbation induced stepping was observed in 60% of the trials. As indicated in Table 1, subjects responded primarily with a "feet-in-place" response strategy when pulled at *small* perturbation amplitudes and adopted a stepping strategy when subjected to the larger perturbation amplitudes.

For the step trials, step onset time (defined as the time from perturbation onset to toe off) was 573 ± 173 ms. Additionally, a lateral shift of the center of pressure toward the initial swing limb (exceeding 10 percent of the base of support width) was observed in 94% of these trials. This lateral shift had an onset time of 204 ± 56 ms after perturbation onset and a maximum value of 3.0 ± 1.7 cm. For the non-step trials, a similar lateral shift of the center of pressure toward the preferred swing limb was observed in 86% of trials, occurring at 228 ± 82 ms.

Table 1: Occurrence of Stepping Response.

Perturbation Amplitude	# of "No Step" Responses	# of "Step" Responses
1.2"	19	2
2.4"	16	5
3.6"	7	14
4.8"	0	21
6.0"	0	21

For the step trials, normalized swing limb heel velocity profiles exhibited striking similarity within and across subjects, and a near zero foot velocity at heel contact (see Figure 2). Likewise, similar temporal patterns of activation of the swing side gastrocnemius, tibialis anterior, and rectus femoris muscles were observed within and across subjects. Burst onset, centroid, and off times for each of these muscles were strongly correlated with toe off time (see Table 2).

Table 2. Pearson's correlation coefficients between toe off time and muscle onset, centroid, and off times.

	Onset	Centroid	Off
Gastroc.	0.86	0.94	0.95
Tib. Ant.	0.97	0.97	0.93
Rec. Fem.	0.96	0.98	0.97

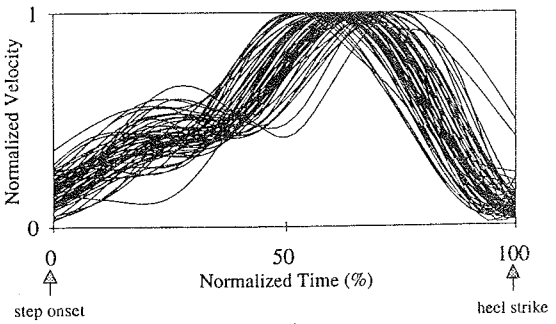

Figure 2: Normalized heel velocity profiles for all 63 stepping trials. Time normalization is over the period from step onset (defined as onset of swing limb hip and knee flexion) to heel contact; velocity is normalized by peak value.

DISCUSSION

The center of pressure results for the both the step and non-step trials indicate a similar low-latency lateral shift in center of pressure toward the preferred swing leg. This shift, commonly observed in the initiation of gait, is believed to represent preparation for stepping in that it generates necessary postural and dynamic conditions for the lateral progression of the center of mass toward the stance leg (Breniere *et al.*, 1987; Maki *et al.*, 1993). Taken together, the short latency of this shift and its presence in both the step and non-step responses suggest that preparation for stepping is embedded in (or is executed in parallel with) the early "automatic" postural response.

While the absolute timing of the step responses observed in this study was highly variable, relative timing of the swing limb muscle activations and foot trajectory profiles were consistent within and across subjects. These results suggest that the swing limb dynamics are governed by an underlying synergy of muscle activations that can be scaled to accommodate the speed and amplitude of the stepping movement (i.e., a *motor program*).

REFERENCES

Breniere *Y. et al. Jour. Motor Behav.*, **19**, 62-76, 1987.

Crenna *P. et al. Jour. Physiol.*, **437**, 635-653, 1991.

Herman *R. et al.* In *Control of Posture and Motion*, (pp. 363-388), Plenum, 1973.

Horak, F.B. *et al. Jour. Neurophys.*, **55**, 1369-1381, 1986.

Maki, B.E. *et al. Neurosci. Let.*, **149**, 87-90, 1993.

ACKNOWLEDGEMENTS

The authors wish to thank the National Science Foundation (BCS-9257395-01, BCS-9110658) and the Whitaker Foundation for their support of this research.

MOTOR ACTION AND PREDICTABILITY OF PERTURBATION IN ANTICIPATORY POSTURAL ADJUSTMENTS

Alexander S. Aruin[1] and Mark L. Latash[2]

[1] Department of Physical Medicine and Rehabilitation,
Rush-Presbyterian St.Luke's Medical Center, Chicago, IL 60612
[2] Department of Exercise and Sport Science, Pennsylvania State University, University Park, PA 16802

INTRODUCTION

We studied how anticipatory postural adjustments (ADA) changed with respect to predictability of postural perturbations and the magnitude of a motor action by the subject that induced the perturbation. Subjects stood on a platform and hold a balloon with a load in extended arms. The unloading was induced either by bilateral shoulder abduction movement, or by popping the balloon with a tack attached to the subject's middle finger, or by popping the balloon by the experimenter. ADA were observed during all self-triggered perturbations. They were larger in series with shoulder movements. We conclude that a voluntary motor act is a necessary and sufficient factor for ADA while, in unusual conditions, ADA magnitude may scale with respect to the magnitude of the motor act rather than of the expected perturbation.

REVIEW AND THEORY

When a task to perform a fast, focal voluntary movement coexists with a task to maintain equilibrium in the field of gravity or posture of a limb, feed-forward adjustments in the activity of apparently postural muscles are used to counteract the expected perturbing forces (ADA; for a review see Massion, 1992). Several studies used non-graded postural perturbations triggered by a voluntary movement. These experiments involved a postural task performed by one arm and an action by the other arm that could bring about a postural perturbation (Dufosse et al., 1985; Paulignan et al., 1989; Struppler et al., 1994). In particular, these studies raised a basic question related to the relative importance of predictability of a perturbation and a major motor action used to trigger the perturbation. Their preliminary conclusion was that only major movements, involving proximal muscles, are associated with ADA. We have decided to use the smallest possible finger movement to trigger postural perturbations in standing subjects, to quantify anticipatory changes in the muscle activity and displacements of the center of pressure, and to answer the basic question: Is predictability of a self-inflicted perturbation in a standing subject sufficient for ADA?

PROCEDURES

Subjects (n = 7) stood on a force platform and hold a 2.2 kg load or a balloon with the load suspended on a short, rigid cord in extended arms. In different series, they were required to release the load either by a low-amplitude, quick bilateral shoulder abduction or by touching the balloon with a tack taped to their right middle finger. In another series, the balloon was popped by the experimenter either unexpectedly for the subject or while the subject watched how the experimenter did it. Electromyograms of rectus abdominis (RA), erector spinae (ES), rectus femoris (RF), biceps femoris (BF), tibialis anterior (TA), and soleus (SOL) were recorded. An accelerometer was taped to the left palm and used for trial alignment. Displacements of the center of pressure (ΔCP) and EMG integrals within certain time intervals were calculated using averaged records.

RESULTS

ADA were seen in all three series when the unloading was induced by the subject. They represented a forward displacement of the center of pressure (ΔCP), an inhibition of the background EMG activity in ES, BF, and SOL, and an increase in the activity of RA, RF, and TA (Fig. 1). These effects were smaller in the series when the subjects popped the balloon with the tack as compared to the series with bilateral shoulder abduction movements. ADA were not seen in series when the balloon was popped by the experimenter, both when the subject's eyes were closed and when the subject watched how the experimenter touched the balloon with the tack.

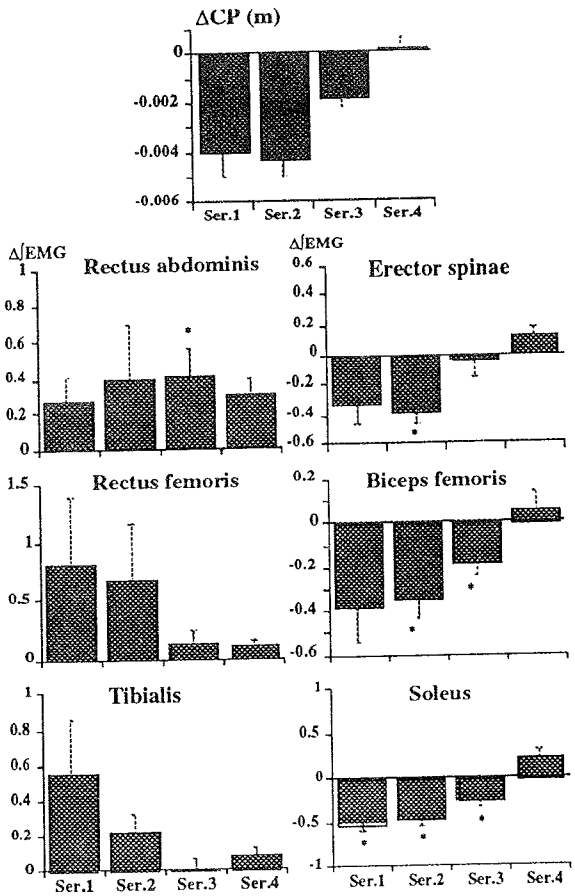

Figure 1

Anticipatory shifts of the center of pressure (ΔCP) and changes in the background EMG activity of postural muscles in experimental series with dropping the load with shoulder movement (Ser.1), dropping the balloon (Ser.2), popping the balloon by the subject (Ser.3), and popping the balloon by the experimenter (Ser.4). Statistically significant changes are shown by *.

DISCUSSION

Our findings let us formulate the following two major hypotheses related to the generation of anticipatory postural adjustments:
1). Self-initiation of a postural perturbation by a motor action is necessary and sufficient for the generation of an anticipatory postural reaction; and
2). The magnitude of an anticipatory postural adjustment is, to a large extent, determined by the magnitude of the voluntary motor action used to bring about the perturbation.

We suggest that postural adjustments may constitute an inherent part of a motor command generated by a hypothetical controller which is later transformed giving rise to commands to individual joints, $j_i(t)$. Classification of the joints into "focal" and "postural" may be done by the experimenters but not by the central nervous system. According to this scheme, one may expect commands to apparently postural joints to be closely tied to commands to apparently focal joints. Thus, anticipatory postural adjustments are not an addition to a "voluntary motor command" but an inherent component of this command. This scheme suggests the possibility of a close relation between the magnitude of anticipatory postural adjustments and the magnitude of a motor action that triggers a postural perturbation, if the same transformation process is used. Note that the actions by the subjects, by themselves, did not endanger equilibrium. Postural perturbations resulted from a contextual interaction of the focal voluntary movements with the load. Dropping a load is apparently a rather common action and, as such, it did not present a tough task for the subject's central nervous system. Popping the balloon is apparently an action that is rather uncommon. Its effects may be compared to the rebound experienced during rifle shooting. In such cases, apparently, the central nervous system does not have in stock an appropriate transformation of $x(t)$ into $j_i(t)$, and scales the adjustments with respect to the characteristics of the voluntary movement using an available, albeit inadequate transformation. We may only speculate that prolonged practice would have probably brought about an increase in the magnitude of postural adjustments to an appropriate level, just as it happens in experienced marksmen who do not show major postural perturbation during shooting (cf. Belenkiy et al., 1967).

REFERENCES

Belenkiy V.Y. et al. Biofizika 10, 135-141, 1967.
Dufosse M. et al. Exp Brain Res 60: 330-334, 1985
Massion J. Prog Neurobiol 38, 35-56, 1992.
Paulignan Y. et al. Exp Brain Res 77, 337-348, 1989.
Struppler A. et al. Neurosci Lett, 159, 115-118, 1993.

ACKNOWLEDGMENTS

This study was in part supported by a grant HD30128 from the National Center for Medical Rehabilitation Research, NIH.

ANALYSIS OF STABILITY OF HUMAN POSTURE STRATEGIES

A. D. Kuo
Dept. of Mechanical Engineering & Applied Mechanics, University of Michigan, Ann Arbor, MI 48109-2125

INTRODUCTION

Investigators have identified two distinct strategies, termed ankle and hip strategies, used in human posture. Testing and rehabilitation programs have been developed, based on these findings, to train patients with poor balance. Unfortunately, little is known about how training should be directed for specific diseases or deficits. Though specific conditions are known to trigger particular strategies when responding to a postural disturbance, these findings do not describe the relative stability of these strategies. However, the field of control theory offers numerous methods for assessing performance and stability. Application of these methods to study of posture control may help describe the relative merits of the two strategies, and result in improved postural rehabilitation programs. This abstract compares the two strategies with respect to avoidance of stepping, speed of stabilization, and tolerance to time delays such as neural conduction time.

REVIEW AND THEORY

Standing human subjects, when perturbed by backwards translation of the support surface, tend to respond with one or a combination of two strategies (Horak & Nashner, 1986). Small disturbances typically result in movement predominantly about the ankles (the ankle strategy), keeping the other joints nearly motionless. Larger disturbances tend to result in combined motion about the ankles and hips in opposite directions (the hip strategy), keeping the knees nearly motionless. An analysis of the mechanics of the ankle and hip strategies predicted that the hip strategy is more effective at stabilizing the body against large disturbances if the feet are to remain flat on the ground (Kuo & Zajac, 1993). Moreover, the hip strategy can produce far larger accelerations of the center of mass, making it particularly effective for countering large disturbances. These larger accelerations may also make the hip strategy a faster means of bringing the body to the upright position. To test this possibility, it is necessary to construct a model of feedback control of balance.

PROCEDURES

Optimal control techniques were used to develop a simple full-state feedback control model of human balance (Kuo, 1995). The feedback gains were parametrized by two values. The first parameter describes response magnitude, and scales the overall gains. This parameter is also proportional to the maximum acceleration of the center of mass. It is presumed that the human can scale a postural response based on either desired response quickness, or to counter disturbances of different magnitudes. The second parameter selects the proportion of ankle and hip strategies, and models the ability of humans to use combinations of the two. The system was designed so that these two parameters could describe responses to a variety of disturbances.

The model was tested against previously-collected experimental data of humans responding to initial-position disturbances. For a variety of initial positions, the model was able to capture the general characteristics of the human motion, as shown in Fig. 1.

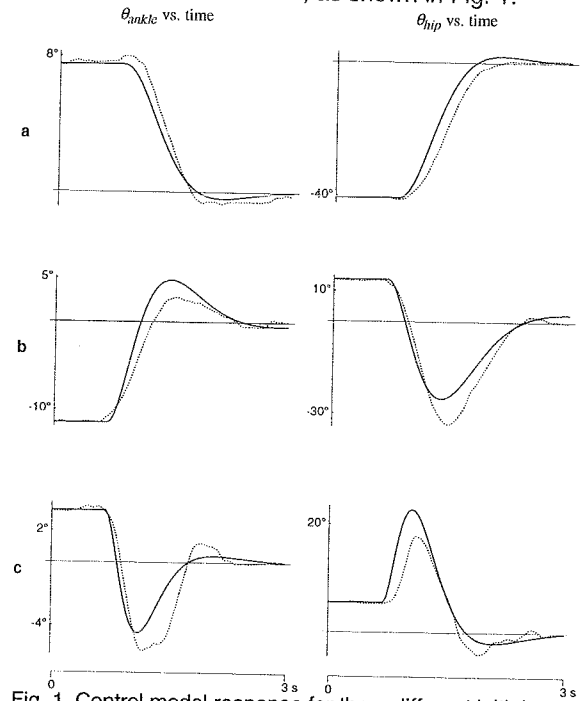

Fig. 1. Control model response for three different initial conditions. Solid line shows model response, dotted line shows experimental response. Left column shows ankle angle vs. time, right column shows hip angle vs. time.

Three characteristics of the ankle and hip strategies were studied. A "step index" is proportional to the ground reaction force under the heels. A large step index will cause the heels to lift off the ground, and may necessitate stepping to avoid falling. The settling time index describes the amount of time required not only to bring the center of mass to a stable position, but also to return to an upright stationary position. The tolerance to time delays describes the maximum amount of additional transmission delay that can be added to the system without making it unstable.

RESULTS

The model was used to assess three aspects of postural responses using the ankle and hip strategies. The first aspect, the step index, shows that for a given response index, that use of the ankle strategy has greater potential than the hip strategy in causing the heels to lift off the ground after a backwards disturbance (Fig. 2a). This relative difference increases with

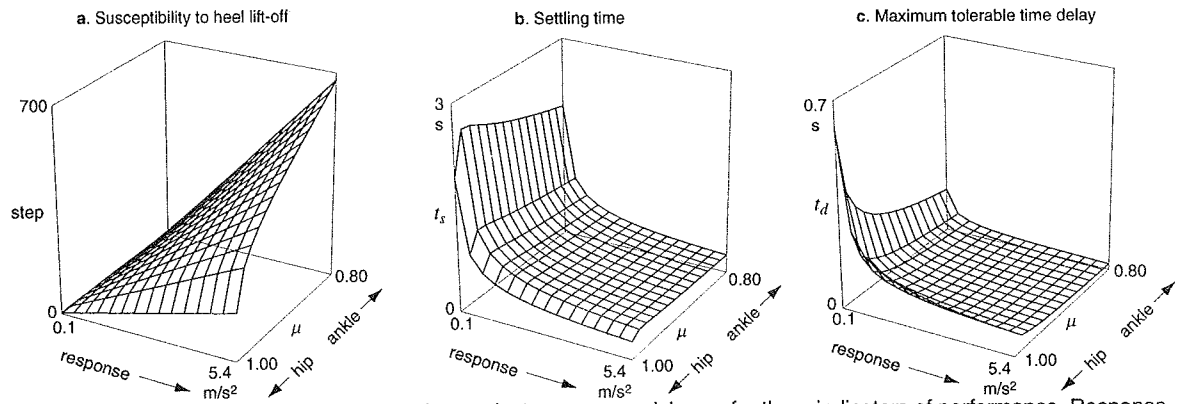

Fig. 2. Comparison of ankle and hip strategies against response quickness for three indicators of performance. Response quickness is proportional to maximum acceleration of the center of mass. Hip/ankle strategy describes the proportion of the two strategies. a. Step index describes the susceptibility of lifting the heels off the ground, thereby inducing a step. b. Settling time describes time to reach within 1% of equilibrium position. c. Maximum time delay tolerance describes maximum delay possible in stable feedback.

the response index, implying that for larger disturbances, the hip strategy is more effective, if it is desired to avoid stepping. The second index, settling time, shows that the ankle and hip strategies are approximately equivalent for a given response index (Fig. 2b). Note that smaller response indexes, which imply slow responses, have long settling times. Finally, the maximum tolerable time delay is identical for fast responses using either strategy (Fig. 2c). However, as the response index decreases, the maximum delay increases significantly for the hip strategy, while the ankle strategy changes very little.

DISCUSSION

The control model verifies the predictions made based on analysis of the mechanics of posture. As expected, if the subject wishes to avoid stepping, the hip strategy is more effective than the ankle strategy, especially for large disturbances. This also confirms observations that a shortened support surface forces subjects to use the hip strategy (Horak & Nashner, 1986), because such a condition effectively places an upper bound on the step index. The results also show that if a subject desires to return to upright quiet stance quickly, neither strategy is particularly advantageous. Though the hip strategy can result in faster accelerations of the center of mass, this advantage is offset by the additional motions necessary to return to the upright position. Analysis of the time delay results predicts that if neural conduction delays are excessive, the subject will be limited in the size of disturbances that can be stabilized, and also that the hip strategy will be more effective than the ankle strategy. This suggests that for some patients, for example those suffering from peripheral neuropathy, that posture rehabilitation may benefit from training for the hip strategy.

The control model describes the relative differences between the ankle and hip strategies with regard to stability. The criteria by which humans select strategies may be related to these and other characteristics. In particular, joint mobility and the performance of sensors may impinge on choice of postural responses. More complex models are needed to address these issues.

REFERENCES

Horak, F. B. & L. M. N ashner. *J. Neurophys*, 55: 1369-1381, 1986.
Kuo, A. D. *IEEE Trans. BME*, 42: 87-101, 1995.
Kuo, A. D., & F. E. Zajac. *J. Biomech.* 26 (suppl 1): 137-150, 1993.

ACKNOWLEDGEMENTS

This work was supported in part by NIH grants NS178662 and P60DC02072, and by a grant from the Whitaker Foundation.

TRAINING-RELATED CHANGES IN THE CONTRACTILE PROPERTIES OF SINGLE MOTOR UNITS IN ELDERLY SUBJECTS

D. A. Keen, G. H. Yue, and R. M. Enoka

Department of Biomedical Engineering
The Cleveland Clinic Foundation
Cleveland, OH, 44195.

INTRODUCTION

After elderly subjects performed a 12-wk strength training program, there was an improvement in their ability to sustain steady submaximal forces (Keen et al., 1994). This improvement was unrelated to changes in the distribution of motor unit forces. Because the degree of fusion in tetanic force is influenced by the time course of motor unit twitches and because both contraction time and half-relaxation time can be altered by training, the purpose was to determine the association between changes in steadiness and the time course of motor unit twitches. The data indicated that the training-related improvement in steadiness was unrelated to changes in the contraction time and half-relaxation time of spike-triggered averages of motor unit force.

REVIEW AND THEORY

One of the consequences of strength training for elderly persons is an improvement in their ability to exert steady submaximal forces. This adaptation could be caused by a change in the activation pattern of the motor neurons or in the twitch properties (time course and amplitude) of the activated motor units. We have found previously that differences in motor unit force due to age cannot account for the improvement in motor performance (Keen et al., 1994). Alternatively, the improved steadiness (decreased force fluctuations) could be caused by an increase in the degree of fusion of the twitch forces, due either to an altered activation pattern or a prolonged twitch time course. The time course of a motor unit twitch can be altered with training (Hainaut et al. 1981). The purpose of this study was to determine the association between the training-related decline in normalized force fluctuations (coefficient of variation) during a constant force task and changes in the time course of the twitch force from single motor units following a strength training program.

PROCEDURES

Twenty healthy subjects were assigned to one of two age groups, an elderly group with an average age of 65 yrs (range = 59-74) and a young group with an average age of 23 yrs (range = 18-27). All subjects were right-hand dominant and had no known neuromuscular disorders.

Each subject participated in a 12 wk strength training program. The exercise involved concentric and eccentric contractions of the first dorsal interosseous muscle of the left hand. The subjects performed 3 training sessions every week, each involving 6 sets of 10 repetitions of the exercise. The index finger was displaced through a 0.5-rad range of motion in the exercise. The training load was set and maintained at 80% of the maximum load that the index finger could lift.

Each subject participated in 4 experiments (at 0, 4, 8, and 12 wks). In these experiments, the subjects were required to perform an isometric MVC, constant-force contractions, and a recruitment-threshold task in which single motor units were recorded. For the constant-force task, a target force was displayed on the oscilloscope and the subject was encouraged to exert a steady abduction force with the index finger for 20 s to match the target force as closely as possible. Based on the MVC force of the subject for that session, target forces of 2.5, 5, 20, and 50% MVC force were calculated. The standard deviation (SD) and the coef-

ficient of variation (SD / mean x 100) of the force fluctuations about the target force were calculated. For the threshold task, a single motor unit was recorded with a bipolar intramuscular electrode while it discharged at a minimal rate for 3 minutes. An average of 8.4 motor units were recorded during each of the experimental sessions. The spike-triggered average of the force yielded twitch force, contraction time and half-relaxation time for each unit. The contraction time was measured from the action potential to peak force. All events less than 145 ms apart were not included in the average; this minimized the fusion between motor unit twitch forces.

RESULTS

The training program caused a reduction in the coefficient of variation of the force fluctuations for the elderly subjects at the lower target forces of 2.5, 5, and 20% MVC force by -29.3, -20.5, and -11.6%, respectively. The young subjects showed no significant changes with training. The majority of the improvement observed in the elderly subjects occurred in the first 4 wks of training. The elderly subjects had significantly longer contraction times (64.0 ± 1.4 vs 59.5 ± 1.2 ms) and half relaxation times (75.8 ± 2.3 vs. 69.2 ± 1.6 ms) than the young subjects. The improvement in the coefficient of variation, however, was unrelated to changes in the distribution of any of the motor unit contractile properties (Figure 1).

DISCUSSION

The main finding of this training study was that the improved ability of the elderly subjects to maintain a steady submaximal force was not associated with changes in the time course of motor unit twitch force. This improvement occurred in the first 4 wks of training, and was not associated with a consistent change in any of the contractile properties of the motor units. When combined with our previous findings, it is evident that the improved steadiness is not due to changes in the amplitude or time course of motor unit twitch forces. This leaves the possibility that the elderly subjects improved their performance by changing the activation of the muscle, such as the pattern of activation of the agonist and antagonist muscles (Vallbo & Wessberg, 1993) or the modulation of motor unit discharge rate. The latter could involve, for example, raising the minimum discharge rate so that there is greater fusion of motor unit force.

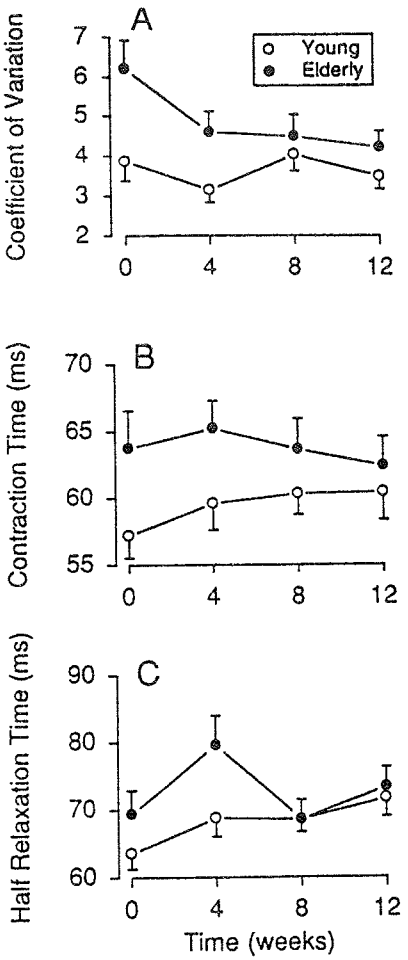

Figure 1. Changes in the normalized force fluctuations (A), the contraction time (B), and the half relaxation time of single motor units (C) over the 12-wk training program.

REFERENCES

Hainaut K et al. *Prog Clin Neurophysiol* 9: 241-249, 1981.

Keen DA et al. *J Appl Physiol* 77: 2648-2658, 1994.

Vallbo ÅB, Wessberg J. *J Physiol (Lond)* 469: 673-691, 1993.

Supported by NIH grant AG 09000 to RME.

MUSCLE COORDINATION IN ELBOW JOINT COMPLEX MOVEMENTS

Roger V. Gonzalez[1,4], Lawrence D. Abraham[2,3], Ronald E. Barr[1,3], and Thomas S. Buchanan[4]

[1]Departments of Mechanical Engineering and [2]Kinesiology & Health Education and the [3]Biomedical Engineering Program The University of Texas at Austin, Austin, TX 78712, and [4]Departments of Rehabilitation Medicine and Biomedical Engineering, Northwestern University, 345 East Superior St., Chicago, IL 60611

INTRODUCTION

The elbow joint complex (EJC) refers to the articulations responsible for the combined movements of elbow flexion-extension (f/e), forearm pronation-supination (p/s), and abduction-adduction (passive motion). Based on previous isometric and dynamic EJC studies, we hypothesized that muscles that cross the EJC are affected by *both* the *orientation* of the elbow and forearm and by the *task* performed. We further hypothesized that these effects could be represented by a 3-D musculotendinoskeletal computer model that mathematically represents the musculoskeletal geometry and the joint's motions for various ballistic movement tasks.

REVIEW AND THEORY

Although isometric muscle interactions at various elbow and forearm positions have been studied (Buchanan et al., 1989; Jamison et al., 1993), little research has been conducted towards fully understanding how the muscles contribute to dynamic elbow and forearm movements. Previous studies of ballistic movements for the elbow (Brown et al., 1981; Meinck et al., 1984) have not thoroughly analyzed how the elbow and forearm *orientation* and its *task* affect the actuators crossing this joint. Yet they have shown that the EMG patterns of both the agonist and antagonist muscles have a tri-phasic behavior (ABC; A = Activation, B = Braking, C = Clamping; Hannaford et al., 1985) in ballistic movements.

PROCEDURES

Computational Modeling

Development the biomechanical model of the EJC required the quantitative description in which the general components were skeletal, muscular, and neural. The muscles included in the model were: Biceps brachii (BIC), triceps brachii (TRI), brachialis (BRA), brachioradialis (BRD), pronator teres (PRT), pronator quadratus (PRQ), supinator (SUP), and anconeus (ANC). A complete description of the EJC musculotendinoskeletal model can be found in Gonzalez et al. (1995).

Optimal control was used in determining the individual musculotendon activations that best minimized the performance index (movement time) while maintaining a set of constraints. A numerical optimal control method (Pandy et al., 1992) was used to converge on minimum time suboptimal solutions of isolated and combined ballistic EJC movements starting from rest and ending at rest (i.e. zero velocity and zero acceleration) at the final experimental position. The initial controls (muscle activations and final movement time) were based on inspection of the EMG and movement data.

Experimental

A specially designed electrogoniometer (Chao et al., 1980) was used to gather the kinematic data. Surface and intramuscular electrodes were used to measure muscle activity and subjects were asked to move through a loosely defined angular range of motion *as quickly as possible*, with speed emphasized over accuracy of movement, and to hold the final position. EJC movements were performed which incorporated isolated ballistic movements of elbow flexions and extensions, and combinations of elbow flexion or extension with forearm pronation or supination. The raw EMG signal was digitally filtered by creating a zero mean, band-passing (50-200 Hz), rectifying, and low-passing (10 Hz). Both signals were normalized to 70% of a dynamic maximum EMG value for each individual muscle determined from all the protocols measured.

To determine the strength of the tri-phasic bursts, the values of the processed EMG signal and predicted activations were averaged per normalized time intervals. The movement time intervals used to determine muscle bursts strengths were: A burst - 0->43%; B burst - 43->86%; and C burst - 86->100% of movement time. These intervals were determined based on Brown et al., 1991, visual inspection of the EMG's, and on the interval between the model's activation nodes (14%).

RESULTS

Ballistic elbow flexions were performed at forearm orientations of full supination (F@S), neutral (F@N), and full pronation (F@P) to investigate how forearm orientation affected the activation of the BIC, BRA, BRD and PRT muscles during a ballistic flexion (likewise, isolated extensions for TRI and ANC). Combined movements were also performed to investigate the dynamic interactions of two *dfs* (f/e and p/s). Four 2-*df* movements were experimentally performed and modeled. These protocols were an elbow flexion with forearm pronation (FAP), with forearm supination (FAS), and an elbow extension with forearm pronation (EAP), and with forearm supination (EAS).

Strength of Tri-phasic Bursts

The intensity of the ABC bursts in the subject and model is shown for the BIC (Figure 1). In general, the model always had higher average intensities for the B and C bursts. The A burst in the model and subject agreed for the BIC muscle. This is especially evident in the large averages in F@N, F@S, FAS and median averages in E@S, EAS, F@P, and FAP given by the model. The average BIC activation being larger with forearm supination and yet smaller with forearm pronation orientation or task was represented well in the model data. The main difference was the larger average in the A burst of the BIC muscle in the F@N protocol of the model. The model selected to recruit the pronator muscles to counter the additional superimposed supination moment caused by the higher BIC activity. The BIC's B bursts for the model were much larger but appeared to occur at the protocols where the subject had some activity. Clearly in the E@S and EAS protocols, the BIC was braking the movement, and the lower BIC activities of the other extension protocols are representative of the final f/e velocity constraint going unmet. While the BIC's C bursts were very small in the subject, the model was selective in the amount of activity it produced depending on the task.

Sequencing of A Bursts

Acceleration bursts for 4 muscles, which indicate the tasks in which the muscle was active and its relative magnitude, are shown in Figure 2. This figure indicates how the optimal controller altered the given A burst to minimize the final movement time. The BIC activity for the subject and model displayed a very similar activity envelope except that the model's BIC magnitude was twice as large for the F@N. The excess supination moment produced by the model's BIC was

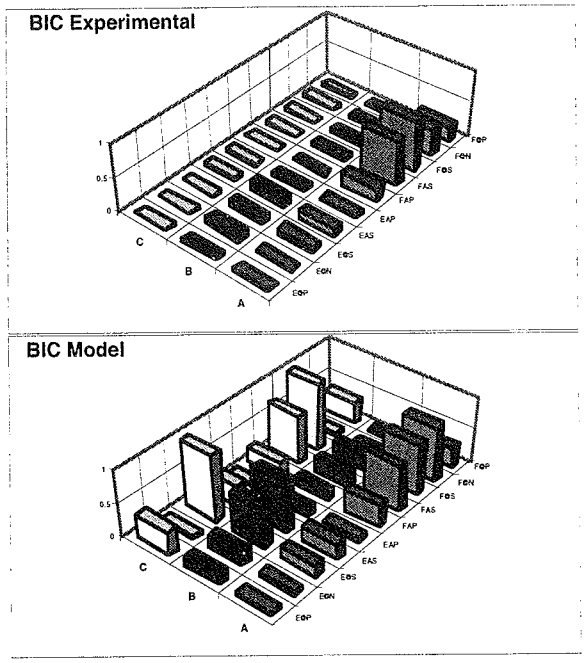

Figure 1: Strength of the tri-phasic muscle activations for the Biceps Brachii (BIC) for all ten tasks. The experimental averages (top) and model averages (bottom) are shown based the selected normalized time intervals.

countered by increased PRT activity. Lower BIC activity for pronation activities or when the forearm was in a pronated position, as seen in both the subject and model, has also been observed (Buchanan et al., 1989; Jamison et al., 1993). The general BRA activity patterns were also similar yet the EMG magnitudes were lower (except for F@P). The increase in the model's BRA magnitude in FAP was used to increase flexion moment and therefore reduce the movement time. The subject probably could not increase the activity of the BRA without affecting the BIC activity. In the model, the magnitude of the BRA A burst in F@N was lower than in the other flexion tasks due to the initial conditions taken from the EMG. Why the subject only partially activated the BRA, a one *df* muscle, in the forearm neutral position is not clear (subject two also displayed a decrease in BRA activity with respect to the other isolated flexions). BRD patterns were very similar but larger in the model. BRD activity in F@N was lower in the subject because of the lower BIC activity in the subject and these two muscles activations were independent in the model. BRD activity in F@S was larger in the model because the model was able to oppose the secondary supination moment of the BRD with PRT and PRQ activity (similarly for FAS). The envelopes of TRI muscle activity were also very similar yet, in contrast to the other muscles, the EMG magnitudes were slightly larger. This figure indicates that the subject had small amounts of co-contraction during flexion tasks while the model minimized TRI activity, as TRI moment would be counter productive to the performance criteria. Lastly, PRT activity patterns were all directed toward flexions where the model shows a large PRT magnitude in FAS. This is not observed in the subject data. Since the PRT is a flexor, in order to minimize the movement time, the model created a larger acceleration flexion moment by activating the PRT and countering the secondary pronation moment with increased SUP activity.

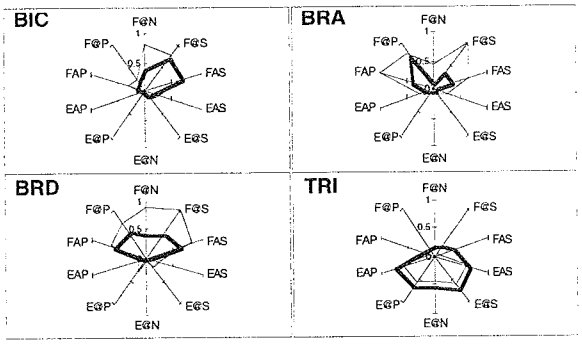

Figure 2: Agonist muscle activation (A) used to accelerate the forearm toward its destination in both model (bold) and subject (light) are shown for 4 muscles in all ten protocols. BIC is top left, BRA is top right, BRD is bottom left, and TRI is bottom right.

DISCUSSION

This model elucidated how muscles that cross the elbow joint complex are activated based on the *orientation* of the joint and on the *task* involved and not on any particular synergistic rule (Buchanan et al., 1989; Jamison et al., 1993). Findings presented here, which are supported by the literature, are that muscle synergies at the elbow joint are rather uncommon and that the activation of these muscles is situation dependent. This is due to the necessary coupling of joint torques proceed by the multi-joint muscles such as the BIC, BRD, and PRT, which sometimes produce secondary torques countered by other muscles. No fixed synergies were observed as the activation of individual flexor muscles crossing the elbow joint during elbow flexion and extension tasks was affected by the position of the forearm. Lastly, protocols F@P, FAS, and EAS showed how non-contributory or antagonist muscles can reduce movement times in ballistic movements by allowing other multi-*df* muscles to be more fully activated. Whether subjects can be trained to replicate the patterns of muscle activations deemed by the model as "more appropriate" for movements performed "as quickly as possible" remains to be seen.

REFERENCES

Brown J. M. et al. Eur. *J. Appl. Physiol.* 63, 381-386; 1991.
Brown S. H. et al. *J. Physiol.* 316, 107; 1981.
Buchanan T. S. et al. *J. Neurophysiol.* 62, 1201-1212; 1989.
Chao E. Y. et al. *J. Biomech. Engng.* 102, 301-310; 1980.
Gonzalez R. V. et al. *J. Biomech. Engng.* (accepted).
Hannaford B. et al. *Exp. Neurology.* 90, 619-634; 1985.
Jamison J. C. et al. *J. Neurophysiol.* 70, 947-960; 1993.
Meinck H. et al. *Exp. Brain Res.* 55, 127-133; 1984.
Pandy M.G. et. al. *J. Biomech. Engng.* 114, 450-460, 1992.

ACKNOWLEDGMENTS

This research was supported in part by NASA/JSC, Grants NGT-70252, NAG9-588, and NIH R29-AR40408.

SIMULATED CHANGES IN CONTROL STRATEGY DURING ALTERED GRAVITY PEDALING

B.J. Fregly[1] and R.T. Whalen[2]
[1]Rasna Corporation, 2590 North First Street, Suite 200, San Jose, CA 95131
[2]NASA Ames Research Center, Life Science Division, Moffett Field, CA 94035

INTRODUCTION

Treadmill locomotion is the primary exercise used to maintain muscle and bone mass in space. The gravity loading needed to perform the exercise can be approximated by applying an external downward force equal to the astronaut's 1-g body weight to the body's center of mass (CoM). If this force is created by tethering the astronaut to the treadmill with elastic chords, only about 0.6-g body weight can be achieved (Davis and Cavanagh, 1993). For this reason, an alternate methodology has also been proposed. By enclosing the upper body in a positive pressure air chamber, larger downward forces equal to the pressure differential times waist cross sectional area can be applied to the approximate CoM (Whalen *et al.*, 1994).

While this second approach may be able to emulate gravity loading on the body's CoM, it does not account for gravity loading on the individual lower extremity limb segments. Thus, an altered control strategy may be required in space in order to produce an Earth-equivalent motion. The purpose of this investigation was to determine the extent to which gravity forces acting on the limb segments affect the control of locomotion. Computer simulations of seated ergometer pedaling under 0-g and 2-g conditions were used for the investigation, since the control strategy necessary to produce the motion is not affected by gravity's influence on the body's CoM (assuming the rider remains fixed to the seat).

REVIEW AND THEORY

The influence of gravity on the control of pedaling has not been widely investigated. Recently, however, a state-space analysis of mechanical energy flow during seated ergometer pedaling revealed that gravity forces acting on the limb segments play an important energy transfer role (Fregly and Zajac, 1995). For roughly the first half of the crank cycle (i.e., the downstroke), because the weight of the limb presses down on the pedal, ipsilateral gravity forces transfer energy from the limb to the crank, thereby assisting in crank propulsion. In contrast, during the second half of the cycle (i.e., the upstroke), because the weight of the limb still presses down on the pedal, gravity forces transfer energy from the crank back to the limb, thereby assisting in limb recovery.

Interestingly enough, the analysis also revealed that the net ankle joint torque functions in a similar fashion. Because the ankle joint remains essentially fixed throughout the crank cycle, the net ankle joint torque primarily transfers (as opposed to generates or absorbs) mechanical energy, with the direction of energy transfer (i.e., from the limb to the crank or vice versa) being the same as that produced by ipsilateral gravity forces in each half of the crank cycle.

PROCEDURES

Two dynamic optimizations were performed to predict the pedal force and net muscle joint torque control strategies needed to produce a 1-g pedaling motion in 0-g and 2-g environments. The optimizations utilized a three degree-of-freedom, two-legged cyclist model which included the bicycle ergometer as well as the limb segmental dynamics (Fig. 1). Each leg of the rider was modeled as part of a planar five-bar linkage, where the crank angle θ_1 and the two foot segment angles θ_2 and θ_3 defined the three generalized coordinates. All lower extremity joints were assumed to be frictionless and revolute, and both hips were assumed to remain stationary. Including both legs in the model permitted the investigation of both intralimb and interlimb control issues.

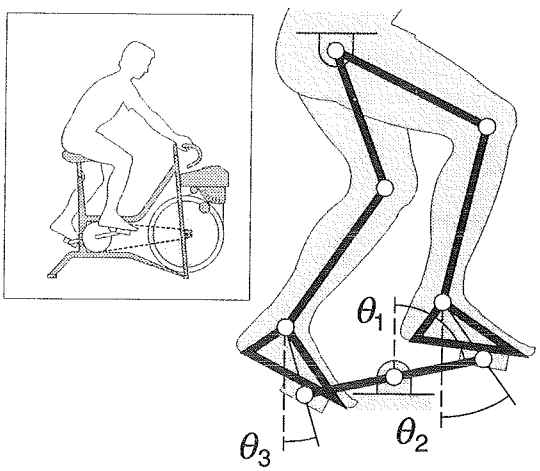

Figure 1: *Three degree-of-freedom two-legged cyclist model used in the dynamic optimizations.*

The starting point for both optimizations was experimental 1-g ergometer pedaling data collected at a 75 rpm cadence and 225 W workload (Fregly and Zajac, 1995). A parameter optimization approach (Pandy *et al.*, 1992) was used to reproduce the 1-g kinematics under 0-g and 2-g conditions. The cost function minimized rms changes in the 1-g net muscle joint torques, while control symmetry and terminal constraints were used to obtain a symmetric motion.

RESULTS

Large changes in driving pedal force (calculated using Kane's method) were required to reproduce the 1-g pedaling kinematics under altered gravity conditions

(Fig. 2). Increasing gravity from 0-g to 2-g resulted in more driving pedal force in the downstroke (e.g., near 90°), more retarding pedal force in the upstroke (e.g., near 270°), and an increase in overall force range.

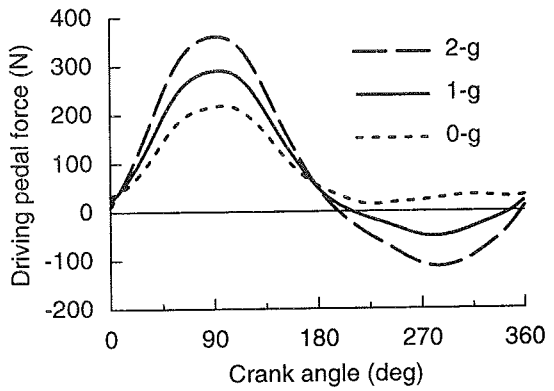

Figure 2: *Simulated 0-g and 2-g driving (i.e., torque generating) pedal force relative to 1-g experimental data. Positive force advances the crank.*

These pedal force changes were caused primarily by the net ankle joint torque (Fig. 2). While the net hip and knee joint torques changed little with increased gravity (Fig. 2a and b, respectively), the entire net ankle joint torque curve shifted upward by 6 N-m for each 1-g increase in gravity (Fig. 2c). Large changes in only one net muscle joint torque were somewhat surprising given that the cost function penalized changes in all three net muscle joint torques equally.

DISCUSSION

The predicted changes in pedaling control strategy can be explained by understanding how mechanical energy flows to the crank. The net ankle joint torque is the only net muscle joint torque whose primary function is to transfer mechanical energy (Fregly and Zajac, 1995). Since ipsilateral gravity forces transfer mechanical energy in a similar manner, as discussed above, the simplest way to compensate for changes in gravity is to change only the net ankle joint torque.

There are two ways this compensation could occur, assuming an overall balance of mechanical energy flow must be maintained. First, the net ankle joint torque could compensate for gravity forces acting on the *same* leg, meaning that increased gravity would necessitate decreased *ipsilateral* net ankle joint torque. Second, the net ankle joint torque could compensate for gravity forces acting on the *opposite* leg, meaning that increased gravity would necessitate increased *contralateral* net ankle joint torque. Due to bilateral symmetry, this would result in increased driving pedal force in the downstroke and increased retarding pedal force in the upstroke (Fig. 2). This second possibility apparently results in the smallest changes in net muscle joint torques, since this is the result found by the optimization.

The above results suggest that the body must adjust its control strategy to produce a 1-g pedaling motion

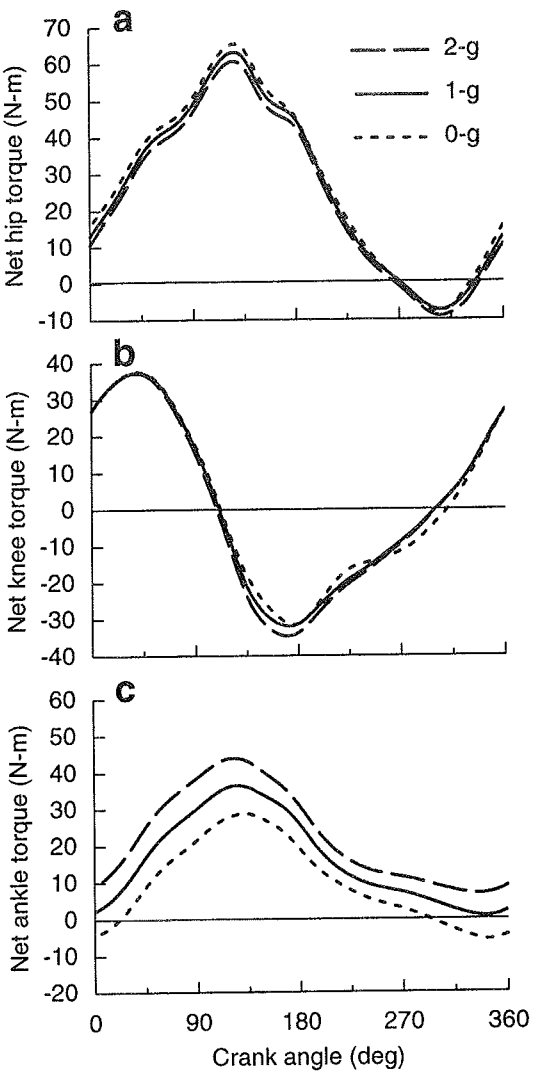

Figure 3: *Simulated 0-g and 2-g net muscles joint torques relative to 1-g experimental data. (a) Net hip torque. (b) Net knee torque. (c) Net ankle torque. Extensor and plantarflexor torque are positive.*

in an altered gravity environment. We would therefore expect to find measurable changes in control strategy during 0-g treadmill locomotion as well, although the extent of these changes remains unclear.

REFERENCES

Davis, B.L. and Cavanagh, P.R., *Aviat. Space Environ. Med.*, 64, 557-566, 1993.

Fregly, B.J. and Zajac, F.E., *J. Biomechanics*, in press, 1995.

Pandy, M.G., Anderson, F.C., and Hull, D.G., *J. Biomech. Eng.*, 114, 450-460, 1992.

Whalen R.T., Breit, G.A., and Schwandt, D.F., *Proc. 18th Meeting ASB*, 209-210, 1994.

ACKNOWLEDGMENTS

The authors wish to thank the Palo Alto VA Medical Center for providing computer resources for this work.

INFLUENCE OF BACK BELTS ON DYNAMIC LIFTING MOTIONS

K.P. Granata, W.S. Marras and K.G. Davis
Biodynamics Laboratory
The Ohio State University

INTRODUCTION

Back belts have become a topic of significant interest in the industrial, rehabilitation and ergonomics communities, but very little research has been performed to examine the biomechanics associated with back belts. The influence of back belts upon lifting dynamics was examined to document the biomechanical relation between back belts and trunk motions. Dynamic lifting exertions were performed while trunk and pelvic motion parameters were recorded. Although total flexion angle was not influence by the back belts, a significant trade-off was demonstrated between the trunk and pelvis. Reduced trunk flexions, velocities and accelerations were observed from belted lifting exertions while pelvic motions increased. Although back belts influenced kinematic parameters associated with dynamic spinal loads, biomechanical analyses of muscle coactivity and spinal loads must be performed before conclusions can be reached regarding back belts and spinal loads during lifting exertions.

REVIEW AND THEORY

Previous studies of back belt have failed to reach a consensus as to their effectiveness. Clinical trials have hinted that injured subjects may benefit from back belts, but there are indications back belt use by healthy subjects may increase the risk of low-back pain (Reddell et.al., 1992). Biomechanical analyses have demonstrated increased intra-abdominal pressure (IAP) with back belts. Although some argue that biomechanical support from IAP may reduce compressive loads on the spine, others (Nachemson et.al., 1986) have measured increased spinal loads with IAP, most likely due to associated muscle coactivity (McGill and Norman, 1987).

Trunk angle, velocity and acceleration have been linked to spinal loads via their influence upon muscle co-contraction and dynamic loading (Granata and Marras, 1995). Kinematic analyses have indicated twisting and lateral range of motions are reduced with a back belt, but flexion was not influenced (Lavender et.al., 1994). Trunk stiffness and load support from lifting belts have been examined by assessing the acceptable lifted weight. Some have indicated the acceptable load increases with lifting belts (McCoy et.al. 1988) whereas others suggest back belts offered no significant increases in lifting strength (Kenyeri and Lavender, 1993), and may reduce endurance (Helmstrom and Moritz, 1992).

There have been no conclusive biomechanical analyses which have attempted to examine biomechanical loads as a function of back belts during dynamic lifting exertions. The objective of this study was to examine the influence of back belts on the dynamic motion parameters associated with spinal loads.

PROCEDURES

Nine male subjects lifted boxes weighing 14 and 23 kg from a platform set to knee elevation, 25 cm. above knee elevation, and at a horizontal distance of 45 cm. from of the center of stance. Asymmetric exertions were performed from a platform located 60^{o} from sagittal at an elevation of 70 cm. Dynamic trunk motions were monitored by a Lumbar Motion Monitor and pelvis motions recorded from an electro-mechanical goniometer fixed to the pelvis. Applied kinetic data and ground reaction dynamics were measured from a force plate (Bertec 4060A).

Subjects performed lifting exertions without a back belt (No Belt) and identical exertions while wearing each of three styles of back belts. The belts included an elastic belt and suspenders (Stretch Belt), a cloth belt with rigid posterior support (Rigid Belt), and a leather weight-lifting belt (Weight Belt). All belts were commercially available, were applied as per the manufactures specifications and tensioned to 4.5 kg.

RESULTS AND DISCUSSION

Although spinal loads were not directly measured, the dynamic lifting parameters associated with those loads have been documented in relation to back belt use. Trunk flexion angle has been associated with increased loads on the spine due to increased moment arm distances and increased muscle coactivity (Mirka and Marras, 1992). Peak trunk flexion angle,velocity and acceleration were significantly ($p<.01$) influenced by lifting height, and back belt. Post-hoc analyses demonstrate the unbelted exertions generated significantly greater trunk flexion than when wearing than when wearing the weight belt. Although all of the belted conditions were characterized by reduced peak trunk flexion,

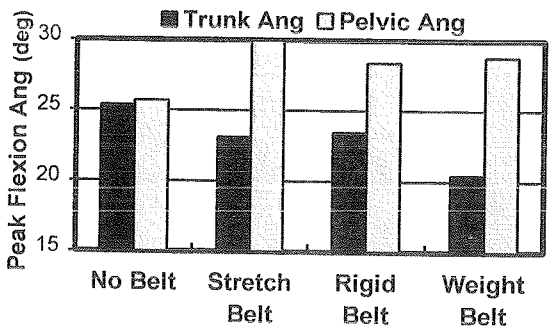

Figure 1. Peak flexion angles of the trunk decreased with back belts. Pelvic angles increased to compensate.

there were no statistically significant differences between the peak trunk flexion angle of the other two belts and the no-belt or weight belt conditions. However, subjects were able to bend and reach the origin heights with reduced trunk flexion through greater pelvic flexion during the belted conditions. Post-hoc analyses demonstrated all of the belted conditions were associated with increased peak pelvic flexion, but only the no-belt and stretch belt values were significantly different. Task asymmetry did not influence sagittal trunk or pelvic motions and no significant interactions were evident.

Biomechanical analyses examining isokinetic lifting exertions have demonstrated spinal load increases with lifting velocity (Granata and Marras, 1995). These trends agree with epidemiologic assessment (Marras et. al., 1993) that show high risk jobs in industry were associated with significantly greater trunk velocities. Peak trunk and pelvic extension velocities were significantly influenced by origin height, box weight and back belts. Each of the back belts significantly reduced trunk velocities compared to the no-belt condition. Reduced trunk velocities were compensated by pelvic velocities, which increased in the belted conditions. The stretch belt and rigid belt were associated with peak velocities significantly greater than the unbelted condition.

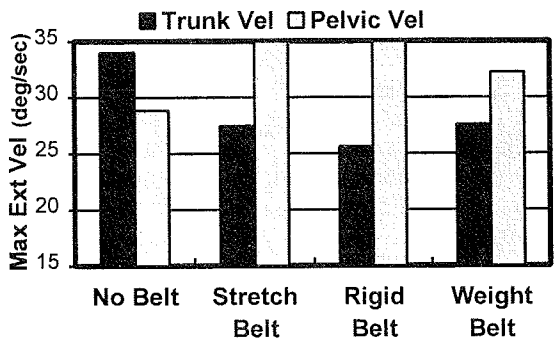

Figure 2. Peak extension velocity of the trunk decreased and pelvic velocity increased with back belts.

Acceleration of the trunk generated inertial forces and moments which contribute to the loads on the spine. Research indicates spinal compression during dynamic lifting conditions may be as much as 45% greater than static lifts. All of the tested back belts significantly reduced the peak trunk extension acceleration compared to the unbelted condition. Although the pelvic acceleration increased with the use of lifting belts, post-hoc analyses demonstrated there were no significant differences between the belted or unbelted conditions. There were no statistical differences in trunk or pelvic angle, velocity or acceleration between the belt styles.

Since back belts influenced dynamic lifting motions, peak lifting moments were examined to discern whether or not the modified kinematics influenced the

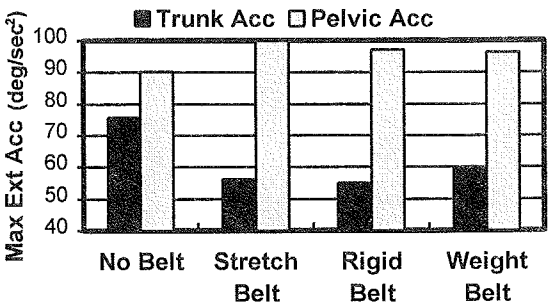

Figure 3. Peak extension accelertion of the trunk decreased and pelvic acceleration increased with back belts.

the external loads. Analyses revealed there was no change in the peak lifting moment with any of the belted or unbelted conditions.

Although the dynamic motion parameters associated with spinal loads were influenced by back belts, we have not demonstrated a change in spinal load. The results indicate a mechanism by which those loads may be influenced by back belts, but other factors must also be considered. Dynamic motion parameters influence spinal loads via their influence upon muscle coactivity (Granata and Marras, 1995). Reduced trunk velocity may be associated with reduced muscle coactivity and concomitantly lower spinal loads. Conversely, back belts may influence the relationship between dynamic motion parameters and muscle coactivity. Therefore, one can not logically conclude that back belts influence spinal loads one way or the other. Results of this study demonstrate that dynamic motion parameters of lifting exertions are partially transferred from the trunk to the pelvis when wearing one of a variety of back belts. Future analyses should be conducted to examine the twisting and lateral motion parameters and biomechanical loads on the spine.

REFERENCES

Granata KP. and WS.Marras *Spine,* in press, 1995.

Holmstrom E. and U. Moritz *J. Spine Disorders*, 5 (3) 260-266, 1992.

Kenyeri R. and Lavender SA. *Proc. Human Factors Ergon Soc.*, 1993

Lavender SA. et.al. *Proc. Am. Soc. Biomech.*, 9-10, 1994.

Marras WS. et. al. *Spine*, 18 (5), 617-628, 1993

McCoy MA. et.al. *Intl. J. Ind. Ergon.*, 2, 259-266, 1988.

McGill SM. and RW. Norman *Ergonomics,* 30 (11), 1565-1588, 1987.

McGill SM. et.al. *Spine*, 19 (6), 696-704, 1994.

Mirka GA. and WS. Marras *Spine*, 17 (3), 318-326, 1992.

Nachemson AL. et.al. *Spine*, 11(5) 476-479, 1986.

Reddell CR. et.al. *Appl. Ergonomics*, 23 (5), 319-329, 1992.

ACKNOWLEDGMENT

Funding was provided by the Ohio Bureau of Worker's Compensation, Division of Safety and Hygiene.

THE RELATIONSHIP OF MUSCLE ACTIVITY TO THE INTERACTION OF SPINE FLEXION AND PELVIS ROTATION DURING DYNAMIC LIFTING TASKS

D.C.Ursulak and J.R. Potvin
School of Human Biology, University of Guelph, Ontario, Canada, H1G 2W1

INTRODUCTION

In a previous study conducted by Ursulak & Potvin (1994), different relative contributions of spine flexion and pelvic rotation were observed between the genders. Females had higher pelvic rotation, while males had higher spine flexion for the same lifts.

Extensor muscular involvement can greatly influence strains placed on the posterior ligaments, and shear forces created at the L4/5 disc. Dolans et al.(1994) found there were effects of load on flexion angles. They also found that females used less passive lumbar extensor moment than the males. Differences in EMG activity and kinetics between the genders may greatly influence the stresses and strains placed on the passive tissues including the intervertebral discs and posterior ligaments. This current study was designed to further investigate the previously found kinematic relationships in the hopes that there may be a functional muscular relationship to the gender differences observed.

METHODS

Five female subjects (age 23±3.3 yr, height 1.63±0.045 m, weight 65±15.0) and five male subjects (age 29±8.3 yr, height 1.79±0.027 m, weight 80±11.0), volunteered to participate in the study after informed written consent. Subjects were screened for low back traumas or recurrent pain.

Subjects performed three types of lifts in the saggital plane: 1) bending predominantly at the knee, called a "squat" lift, 2) bending predominantly with the trunk , called a "stoop" lift, 3) subjects were allowed to lift in whatever manner they were either most comfortable with or did on a regular basis, called a "freestyle" lift.

Subjects performed the above lifts with three loads (female: 7, 13, 20 kg., male: 9, 18, 27 kg.), with three repetitions of each. The highest loads for males and females was determined from maximal acceptable loads recommended by Mital et al. (1993). The total number of lifts equaled 27, with lifting techniques and loads presented in random order. The various techniques were chosen to ensure that all ranges of trunk inclination would be observed. There were no limitations as to the speed of the lift nor the time allowed between lifts.

Each subject was instrumented with five unilateral pairs of surface electrodes (thoracic erector spinae (ES), lumbar erector spinae (LS), rectus femoris or quadriceps (Q), biceps femoris (BF), and gluteus maximus (G)), all on the right side of the body. Maximal voluntary contractions (MVC) of the five muscle groups were obtained immediately prior to performing the lifts. EMG data was sampled at 30 Hz, full-wave rectified, low pass filtered at 3 Hz, and non-linearly normalized using the MVC values as 100% .

Lifts were performed using a load pan with handles approximately shoulder width apart, 15 cm from the floor and parallel to the saggital plane. Subjects were allowed ten warm up lifts with the medium load to help avoid injury and to facilitate a prediction of the exertion required.

Reflective markers were affixed to the lateral malleolus, lateral epicondyle, greater trochanter, L4L5, C7T1, with sacral and thoracic triangular frames cemented to the sacrum and T12L1 respectively. Videography was recorded at 60 Hz, with digitizing completed on a Peak5 system at 30 Hz. Erect standing biases were used to determine the zero reference point for normal lordosis and pelvic rotation. Pelvic rotation was monitored with the rotation of the sacrum triangle. Spine rotation was defined as the T12L1 minus the sacrum triangle rotations.

For the third lift in each condition, maximum spine flexion, pelvic rotation and knee flexion were recorded. EMG data were recorded for each lift and means (MVC standardized) were compared across muscle groups, techniques of lift, loads and gender with a repeated measures ANOVA on the data from the lifting phase of the lift/lower cycle.

RESULTS

The observed gender differences for the means of peak spine flexion and pelvic rotation were consistent with the previous study of Ursulak & Potvin (1994). Since the previous kinetic measurements were collected under identical conditions, the two data sets were combined to yield 12 females and 12 males in the final kinematic analysis. However, EMG was collected only for the 5 male and 5 female subjects described in this paper.

With the kinematic variables, males were observed to have higher mean peak spine flexion (M 55° vs F 48°) and knee flexions (M 102° vs F 96°) , while females had high peak pelvic rotations (M 15° vs F 25°) ($P<0.05$).

Significant differences in EMG existed between the genders in mean activation levels for various muscle groups (Fig. 1)($P<0.01$). Differences were consistent across the different lifting techniques. Increasing load was found to increase EMG levels in the thoracic ES, lumbar ES, gluteus and biceps femoris (Fig. 2)($P<0.01$). This load effect was consistent between the genders.

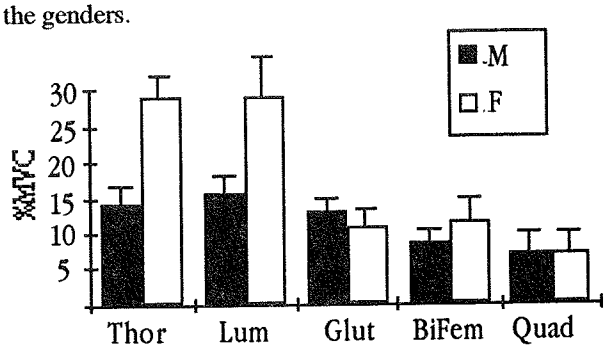

Fig. 1 Mean muscle group EMG for each gender pooled across loads and techniques.

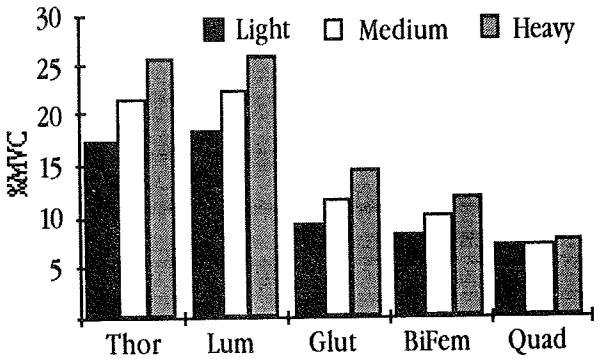

Fig.2 Effect of load on mean muscle group EMG pooled across techniques and genders.

Discussion

The data are consistent with a previous study that indicates that a kinematic difference between males and females in spine flexion and pelvic rotation during lifting. Incorporation of EMG data for the five major muscle groups with the kinematic data has offered insight into the controlling aspects of lifting mechanics.

When compared to males, females will rotate about the hips more and flex the spine less. An EMG analysis showed that females had significantly higher erector group activity, suggesting that this activity might be serving to limit spine flexion. The converse was true for the males, who exhibited higher gluteus activity. This may suggest that the pelvis flexion is being arrested by the gluteus, necessitating a continuation of spine flexion .

There was a significant increase in EMG as load increased. This would confirm a previous suspicion that muscles, and not ligaments, are primarily responsible for meeting the demands of increased loads. This has been demonstrated previously (Potvin et al. 1991). However, differences observed between male and female recruitment levels might suggest that this is not accomplished equally between the genders. The observation that males flex the spine further than females, may indicate that they utilize the passive extensor tissues more than females. This is consistent with the findings of Dolan et al. (1994) who demonstrated higher 'passive' extensor moments in males during lifting.

When compared to females, males performed the lifts with less biceps femoris and more gluteus activity. This may be related to the higher knee flexion angles observed in the males, especially with the squat and freestyle techniques. With lower amounts of forward pelvis rotation, males seem to resort to more spine and knee flexion during lifts from the floor. Conversely females utilize more pelvic rotation and less spine and knee flexion to perform their lifts. The paradox that exits with the two joint musculature of the biceps femoris and rectus femoris of the thigh may explain the interaction of knee flexion and pelvic rotation. Rectus femoris activity was found to be consistent between genders. Therefore, it might be suggested that biceps femoris activity must be increased to control the pelvic rotations through the larger angle seen in females.

In conclusion, it appears that males and females perform lifting movements with different relative contributions from spine and pelvis rotations when lifts are performed from the floor. EMG data has been presented in an effort to explain the neural control mechanisms that result in these observed differences. Females appear to have higher erector spinae activity to control the degree of spine flexion. Differences in pelvic rotations result from a complex interaction of the one and two joint muscles controlling movements about the hips and knee.

References

Dolan et. al. *J. Biomech.* 27(8):1077-1085 (1994)
Mital et al. *A Guide to Manual Materials Handling* (1993)
Potvin, J.R. *Spine.* 16(9): 1099-1107 (1991)
Ursulak & Potvin. *Conference Proceedings of the 18th Meeting of the ASB.* 189, 1994

A COMPARISON BETWEEN THE STOOP, SQUAT AND FREE STYLE LIFTING TECHNIQUES

S. Sadek, PhD, T. Khalil, PhD, PE, E. Abdel-Moty, PhD
University of Miami, Comprehensive Pain and Rehab Center - 600 Alton Road, Miami Beach, FL 33139

INTRODUCTION

The aim of this study was to compare the squat, stoop and free style lifting techniques based on EMG activity of the erector spinae and the rectus femoris muscles and the peak kinetic and kinematic variables of the ankle and knee joints and trunk; and to utilize these parameters to determine the preference of one technique over the other for two conditions of load weight and two positions.

REVIEW AND THEORY

Available scientific studies and commercial literature present conflicting explanations of the mechanism of lifting, which has led to controversy regarding the use of the "proper" or "safe" lifting technique. There are basically two main lifting techniques: straight legs-bent back (stoop) and straight back-bent legs (squat); and many others that could be considered "derivatives" or hybrids of those two.

Supporters of the stoop lift report that most people have weak leg muscles and very strong, broad and extensive back muscles which are powerful which when used correctly, usually protect the spine (The Back Book, 1988 and The Back Pain Monitor, 1992). Park and Chaffin (1974) reported that lifting of objects that cannot pass between the legs should be done with the traditional stooped-over torso posture. Giat and Pike (1992) concluded that humans may naturally prefer the stoop lifting method to the squat lifting because of the greater demand the squat lift imposes on the knee extensors.

Sullivan (1989) reported that using the squat lift shortens the horizontal distance between the load and the body thus reducing the compressive forces in the invertebral discs. Sullivan also reported that the lower center of gravity in the squat lift improves balance and the ability to redirect force rapidly if needed. Another reason for preferring the squat method over the stoop method is that the hamstring muscles operate closer to their resting length, which could improve their efficiency as stabilizers of the pelvis (Gossman, et al. 1982).

Anderson (1970) reports that the method of instruction of workers is "harmful". Workers are being taught to acquire "a kind of drill" in which they constantly have to think about bending their knees and keeping their back straight and to consciously position their head, hands and feet while performing their tasks. He reports that trying to consciously regulate different parts of the body at the same time will produce unnecessary muscular tension which will consequently lead to an increase in the risk of injury. He believes that it is safer to "*allow workers to use their own common sense and muscle sense than to teach them new drills*".

PROCEDURES

Subjects:
Nine male subjects whose ages ranged from 20 to 31 years ($\bar{x}$ =25.89, sd=4.20) volunteered for this study. The subjects had no reported history of musculoskeletal disorders.

Variables:
Independent Variables:
a. Lifting technique - The back, squat lift and the free style techniques were studied.
b. Weight of load - The loads selected were: 10 and 50 lbs.
c. Load distance - The box containing the weights was placed at the subject's tip toes and double-tip-toes distances.

Dependent Variables:
a. EMG activity - EMG activity of the erector spinae (lumbar paraspinals), and rectus femoris (quadriceps) muscles was recorded throughout the activity. The measure of EMG was the integrated rectified signal/time.
b. Kinetic and kinematic parameters - Peak displacements of ankle, knee and trunk; and torque at the L5/S1 level and knee joint were calculated from the motion analysis of videographic recordings of activity.
c. Sway - Sway was measured throughout the lift and the "sway rectangle" was calculated. The sway rectangle is a rectangle drawn as an envelope of the center of gravity of the body (*plus the box*) during the lift.
d. Duration of activity - The duration of the lift was calculated based on the number of frames that were digitized.

Controlled Variables:
a. The load was placed in a 12" x 12" x 12" box.
b. The lift was performed from floor to 30" table height.

Equipment:
a. For motion analysis, Ariel Performance Analysis System (APAS).
b. The Kistler force platform (Piezo-Instrumentation Kistler, Nr 6.9287, Type 9287) connected to the APAS was used for sway measurements.
c. EMG was recorded using the Grass EMG system (Grass, Model 12, Neuroacquisition System for signal recording and the APAS for signal analysis).

Experimental procedure:
1. Initially, there was a basic set-up of the system.
2. The subject was informed of the procedure and was asked to read and sign a "consent form".
3. Reflective markers were placed at the ankles, knees, hips, shoulders, elbows, wrists, midway between shoulders, midway between hips, and forehead. Two markers were also placed on the box. EMG surface electrodes were placed at the L3-L4 level approximately 0.5 inches from the spine and on the rectus femoris.
4. To standardize instructions, the subject was shown a video tape narrated by an occupational therapist explaining the different common lifting techniques.

5. A box containing the test weights (either 10lbs or 50lbs) was placed in front of the subject on a wooden platform at the same elevation as the balance platform and at the predetermined distance from the subject (either at tip toes or at double tip toes).
6. The subject was asked to lift the box using his preferred technique. Video recording took place continuously.
7. A rest period of 1 min was allowed before the following treatment was performed. The order of the load/positions was randomly assigned.
8. During each lift, motion was videotaped, EMG was collected, and area of sway was measured.
9. The subject was then shown another video on the squat and stoop lifting techniques. He received as much practice as he requested on those two techniques.
10. Steps 5-8 were repeated for the back & squat techniques.
11. Analysis of the lifts was done as follows: for the stoop and squat, 2D, unilateral analysis was performed. For the free style trials 3D, bilateral analysis was performed.

RESULTS

Twelve treatments were administered to nine subjects. The results presented in Table I are based on a significance level of $\alpha < 0.05$. They are based on the adjusted degrees of freedom, if the assumption of sphericity was violated. A repeated measures design was adopted using the MANOVA command of the SPSS/PC+.

Table 1 Percentages of the peak values of the dependent variables

	Back				Squat				Free			
	10T	10D	50T	50D	10T	10D	50T	50D	10T	10D	50T	50D
AnkDisp	40	29	23	23	75	56	44	42	M	M	M	M
	Back*Squat*Free											
KnDisp	8	9	4	8	M	M	93	M	87	88	M	98
	Back*Squat,Free											
TrkDisp	M	M	98	93	7	10	11	14	M	99	M	M
	Squat*Back,Free											
TrqL5S1	83	75	91	81	24	33	73	88	M	M	M	M
	10lbs: Squat*Back*Free			20lbs: no diff			TT: Squat*Back,Free			DT: no diff		
TrqKnee	63	60	M	M	69	75	17	39	M	M	76	62
	10lbs: Back*Free				20lbs: Squat*Free*Back							
ParaEMG	86	91	M	M	50	75	66	76	M	M	95	85
	Squat*Back,Free											
QuaEMG	27	38	26	48	99	M	91	80	M	97	M	M
	Back*Squat,Free											
Time	94	M	69	82	M	97	M	M	73	67	93	96
	Free*Back,Squat											
Sway	24	57	37	84	M	M	M	M	N	N	N	N
	Back*Squat											

AnkDisp = Displacement of the ankle
KnDisp = Displacement of the knee
TrkDisp= Displacement of the trunk
TrqL5S1 =Torque at the L5/S1 level
TrqKnee= Torque on the knee
ParaEMG= EMG of the lumbar paraspinals
QuaEMG= EMG of the quadriceps
Time= Duration of activity
Sway = Area of sway
TT= Tip Toes
DT = Double Tip Toes
M = Maximum (100%)
N = Not Applicable

For the free style, the results are based on the higher of both sides. Results are displayed as percentages of the maximum values attained *(eg. for the 10lbs double tip toes lift, quadriceps EMG was: 38% of max for the back lift, the max for the squat lift and 97% of the max for the free style)*. The lower row shows the significance or lack of between the different independent variables *(eg. for the torque at the knee, there was a significant difference between the back lift and the squat lift for the 10lbs weight and a significant difference between the three techniques for the 50lbs weight)*. This table can be used as a selection tool to select the technique of lift based on weight characteristics.

Results show that there are significant differences between the three lifting techniques that were studied. Each lift minimizes on some variables and not the others. Weight of the load and position of the load also appear to have a significant effect on several of the variables under study for each lifting technique.

CONCLUSIONS

Findings suggest that no one technique minimizes on all of the dependent variables on all the body parts simultaneously. Selecting a technique that will produce lower values of a particular variable of interest (for a specific weight and position) is possible; however, selecting a technique that is considered a "safe lifting technique" or a "perfect lift" in order to train ALL people to use regardless of their personal characteristics, pain or prior injury, or the characteristics of the load to be lifted is not fully justified. Instead, basic guidelines should be followed in order to achieve a "safer" lift. An understanding of individual characteristics and limitations including joint and muscle strength appears also important in recommending the least stressful lifting style for that individual.

REFERENCES

Anderson, T (cited in Snook and Ciriello, 1972), *Human kinetics in strain prevention*, British Journal of Occupational Safety, v.8, no.93, 1970.

Giat and Pike, *Mechanical and electromyographic comparison between the stoop and squat lifting methods*. J of Safety Research, vol. 23, 1992.

Gossman, M, et al. (cited in Sullivan, 1989), *Review of length-associated changes in muscle: Experimental evidence and clinical implications*. Phys Ther, 62:1799-1808, 1982.

Park, K and Chaffin, D, *A Biomechanical evaluation of Two Methods of Manual Load Lifting*. AIIE Transaction, 6:2, pp 105-113, 1974.

Sullivan, M, *Back Support Mechanisms During Manual Lifting*. Physical Therapy, 69:1,38-45, 1989.

The Back Book, The American Back School, FPR Publisher, KY, 1986.

The Back Pain Monitor, Vol 10, no 4, 1992.

ACKNOWLEDGEMENTS

This study was performed at the University of Miami, Comprehensive Pain and Rehabilitation Center. The authors acknowledge the help of Drs. S. Asfour, S. Czaja and R. Morgan of the University of Miami.

A DYNAMIC ANALYSIS OF LUMBOSACRAL LOADS IN BEDMAKING

P.D. Milburn[1], R.S. Barrett[2]

[1]Division of Health Sciences, University of Otago, New Zealand

[2]School of Exercise Science, Griffith University, Queensland, Australia

INTRODUCTION

The initiative to investigate the stresses associated with occupational bedmaking arose as a result of a trend towards the use of larger and heavier beds in the hospitality industry and the perception amongst linen maids that this was related to an apparent increase in the incidence and severity of low back injury. It was hypothesised that these increased loads, coupled with extreme forward flexed lifting postures, confined working spaces and the high repetition lifting over intense work periods, may increase the physical stress on the employee to a potentially hazardous level.

REVIEW AND THEORY

The stresses imposed on the musculoskeletal system during bedmaking were initially investigated using a static planar model (Barrett et al., 1991). Observational techniques were used to determine the predominant movement patterns assumed to be associated with the greatest potential for excessive lumbar stress and were subsequently defined as (i) bedding on, (ii) bedding off, (iii) lifting the corner of the mattress, (iv) pushing the bed, and (v) pulling the bed. Results indicated that some aspects of the bedmaking task may exceed safe lifting limits. However, estimates of lumbar loads using static models have been shown to underestimate the stresses associated with dynamic loading by up to 40% (Frievalds et al., 1984, McGill et al., 1985). In order to properly account for the effect of inertial forces on lumbar spinal loads, it was necessary to conduct a full dynamic analysis of each simulated bedmaking task.

Therefore, the purpose of this study was to assess the effect of bedmaking task and bed size on the dependent measures of dynamic lumbosacral (L5/S1) compression and statically determined L5/S1 shear forces.

PROCEDURES

Fifteen paid female linen-maids employed in the hospitality industry volunteered to participate in the study. The mean age, height, weight and work experience were 33.5 years, 161.0 cm, 57.7 kg and 4.8 years respectively. The bedmaking tasks selected for analysis were the same as those used by Barrett et al. (1991) with the addition of one extra task determined from further analysis of standard work practices (Fig 1).

Abbreviated task definitions were as follows:

Bedding on: The symmetrical planar action used to apply a blanket to a bed.

Bedding off: The symmetrical planar action used to remove a tucked sheet from a bed.

Lift corner: The planar action used to raise the corner of the mattress 200mm with one hand for the purpose of fixing the sheet in place.

Lift middle: The planar action used to raise the centre of the mattress 200mm with one hand for the purpose of fixing the sheet in place.

Push bed: The symmetrical planar action used to push the bed 400mm away from subject.

Pull bed: The symmetrical planar action used to pull the bed 400mm toward subject.

Subjects performed all tasks while standing on a Kistler 600x400mm force platform positioned so that the plate coincided with the midline of the long axis of the bed with the exception of the "Lift corner" task for which the bed was moved so that the corner was positioned adjacent to the force plate.

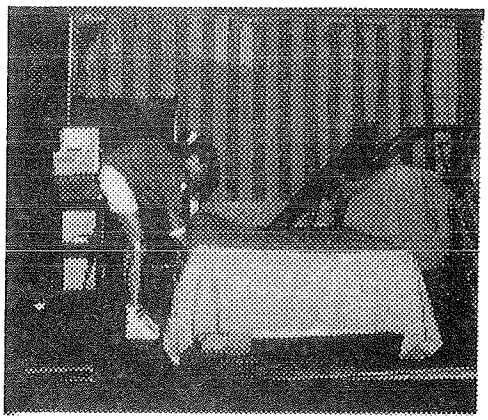

Figure 1. Subject performing the Lift middle task. This task was not analysed in the original study but was added to the present study for completeness.

Following completion of a medical screening questionnaire and informed consent procedures, all subjects performed one trial of the six simulated bedmaking tasks for the three bed size conditions. The mass characteristics of the beds and bedding are shown in Table 1.

Table 1. Mass characteristics of beds and bedding

Bed size	Bed mass (kg)	Bedding mass (kg)	Total mass (kg)
Single	47.8	2.7	50.5
Double	59.7	4.0	63.7
King	100.2	5.2	105.2

The two dimensional dynamic strength prediction program (LiftTrak version 2.1, 1992) was used to assess average dynamic L5/S1 compression and static shear forces for each test condition. The model required input defining the (i) load at the hands, (ii) subject anthropometry, and (iii) a distance scaling factor for the computation of segmental accelerations.

The load at the hands was measured directly using a ± 1kN load cell (Lebow model 3167). Three trials of each task on each bed size were performed by one subject and the calculated averages were assumed to be representative of the load at the hands for all subjects. Video film (60Hz) was automatically digitised by the LiftTrak system following identification of joint markers. The height and weight of each subject were used by the model to scale segment lengths and masses for the computation of joint forces and moments. The distance scaling factor employed was the actual distance between the hip and the knee markers (upper leg length).

A two factor (6 x 3) multiple analysis of variance (MANOVA) was used to test the effect of bedmaking task and bed size on the dependent measures of L5/S1 compression and shear force.

RESULTS

The estimated forces acting at the hand for each task x bed size condition are displayed in Table 2. Results indicated that the estimated hand loads for the double and king size bed conditions were similar and that the "push" and "pull bed" tasks were associated with the greatest load.

Table 2. Forces at the hand for each bed condition

Task	Bed size		
	Single (N)	Double (N)	King (N)
Bedding on	20	32	37
Bedding off	65	73	74
Lift corner	51	79	79
Lift middle	82	113	109
Push bed	110	188	232
Pull bed	155	180	255

Both task and bed size had a significant main effect on average dynamic L5/S1 compression ($p<0.0001$). A task x size interaction effect was also determined ($p<0.0004$).

Average dynamic L5/S1 compression forces exceeded the NIOSH Back Compression Design Limit (BCDL) of 3427N for the tasks of "bedding on", "lift corner", "lift middle" and "pull bed" at the double and king size bed conditions and for "bedding off" at all bed sizes (Fig 2). Loads in excess of this limit are considered to place the worker at increased risk of musculoskeletal injury and warrant ergonomic and/or administrative intervention. The task x size interactions occurred for "bedding off" where the maximum average L5/S1 compression was recorded for the single bed condition and for the "lift middle" task where the average dynamic L5/S1 compressive force was greatest for the double bed condition.

Average dynamic L5/S1 compression forces were between 54% and 67% greater than average L5/S1 compressive force estimates, with the greatest differences associated with the tasks performed more rapidly ("bedding on" and "bedding off").

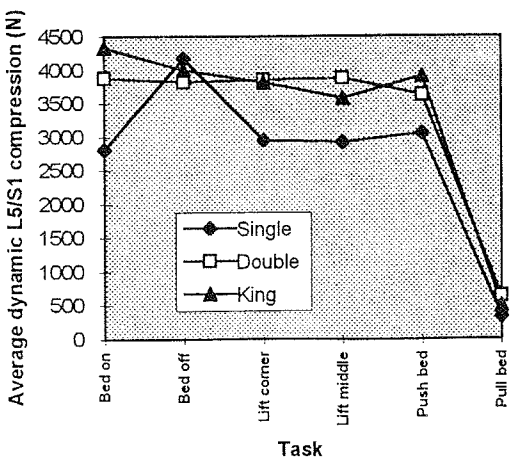

Figure 2. The effect of task and bed size on average dynamic L5/S1 compression force.

Task and bed size also had significant main and interaction effects on average static L5/S1 shear forces at the 0.0001 level (Fig 3). The lowest shear forces were measured in the "push bed" task where the average L5/S1 compressive force had been correspondingly high. Similarly, average static L5/S1 shear forces were relatively high for the "pull bed" task where the average dynamic L5/S1 compression had been low. The greatest average static L5/S1 shear forces were associated with the "lift" and "pull" tasks. Average static L5/S1 shear decreased with increased bed size in the "push bed" task but increased with increased bed size in the "pull bed" task. Bed size had relatively little effect on average static L5/S1 shear in "bedding on" and "bedding off".

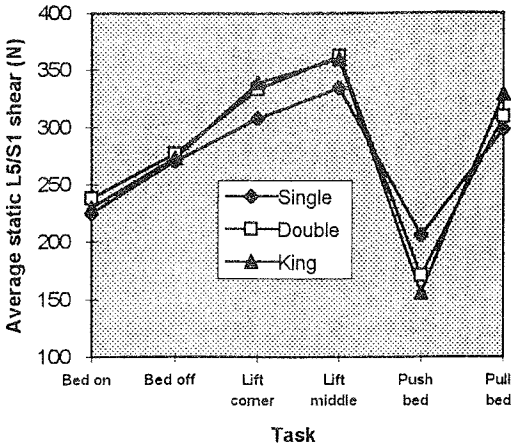

Figure 3. The effect of task and bed size on average static L5/S1 shear force.

DISCUSSION

The results of this study indicate:

1. the extent to which static estimations of average dynamic L5/S1 compressive force underestimate the loads on the body for inertial lifting conditions;
2. that increased hand load was generally associated with increased L5/S1 load;
3. that the greatest hand loads were not associated with the greatest L5/S1 loads due to differences in the way each task was performed;
4. that lumbosacral loads produced in bedmaking may exceed safe lifting limits for certain task-size combinations; and
5. the trend toward the use of larger and heavier beds in the hospitality industry imposes increased load on the lumbar spine.

The investigation of alternative work practices designed to minimise loads on the lumbar spine is recommended.

REFERENCES

Barrett, R.S. et al. Proceedings XIIIth Int. Cong. Biomechanics, 210-211, 1991.
Frievalds et al. J. Biomechanics, 17, 251-262, 1984.
McGill et al. J. Biomechanics, 18, 877-885, 1985.

ACKNOWLEDGMENTS

This study was supported by a Worksafe Australia grant.

A NETWORK-BASED MODEL OF LUMBAR MUSCLE COORDINATION DURING STATIC ASYMMETRIC TRUNK LOADING

M.A. Nussbaum[1], D.B. Chaffin[1], B.J. Martin[1], and S.A.. Lavender[2]
[1]Center for Ergonomics, The University of Michigan, Ann Arbor, MI, 48109-2117
[2]Rush Presbyterian-St. Luke's Medical Center, Chicago, IL 60612-3864

INTRODUCTION

The mechanisms by which complex patterns of muscle recruitment are planned and coordinated are of great interest to both biomechanists and motor control investigators. A model that can predict these motor patterns would provide useful insight regarding central control of the redundant physical system and allow for determination of mechanical loading of at-risk tissues during physical exertions. The development of such a model, based on a modification of a common artificial neural network (ANN) architecture, is described here for the lumbar musculature. The model is based on simple assumptions regarding muscle physiology, geometry, and interactions. The model is shown to generate realistic patterns of muscle activity through comparisons with existing EMG data, and its behavior is further examined to offer hypotheses regarding the mechanism of central control and the existence of antagonism.

REVIEW AND THEORY

Contemporary approaches to muscle activity prediction have traditionally employed two approaches: optimization and EMG measurement. Both techniques have associated advantages and drawbacks. Some recent work has created a hybrid between the two (Cholewicki et al., 1995). While these methodologies can generate reasonably valid predictions, none has offered convincing evidence that an underlying control process is being simulated. Most of the objective functions proposed for optimization-based models have not been given a physiological basis, and often have failed to predict realistic levels of antagonism. The EMG-driven models, while providing estimates of muscle force with a high degree of veracity, offer no explanation for how or why these patterns of force occur, nor can they be employed outside an experimental setting.

ANN models provide a third alternative. Previously, an ANN model was presented which could generalize from a subset of 'teaching' patterns of muscle activity (Nussbaum, 1992). The model was able to extract regularities in the muscle recruitment patterns and estimate accurate levels of activity for novel moment loading situations. This model was limited, though, in its dependence on a 'training' set of moment-EMG patterns. To overcome this dependency, several modifications were undertaken to create a model that relieves some of the dependency on experimental data and which can be given a stronger physiologic justification.

PROCEDURES

The model is intended to mimic muscle recruitment during static asymmetric moment loading of the lumbar spine at L3/L4. The architecture is that of a feed-forward ANN (Figure 1). The model is composed of several layers of simple processing units. Each unit receives input through weighted connections from units in the previous layer. An activation level is associated with each unit, and is computed as a non-linear function of the sum of inputs multiplied by corresponding connection weights. An input layer of units receives the magnitudes of externally applied triaxial moments. A first hidden layer contains a variable number of units (4 used to generate results below) and is used to develop an internal representation of the moment loading. A second hidden layer, the muscle layer, contains 10 units corresponding to the major bilateral torso muscles (ES, RA, EO, IO, and LD). The activation levels of muscle layer units are the model predictions of muscle activity. Output units correspond to the model estimates of triaxial reactive moments.

The network is a variant of the basic backpropagation neural network (Rumelhart et al., 1986). The differences occur in the muscle and output layers. Connections between muscle units and output units are interpreted as the moment generating potential of a given muscle about a particular axis. A second difference involves interconnections within the muscle layer (Figure 2). Each muscle unit sends an inhibitory signal to itself (S) and to all other muscle units (I). These inhibitory connections serve to limit the activation of a unit and allow an active unit to limit the activation of other units. The inhibitory connections were intended to mimic feedback signals from such sources as Golgi tendon organs and Renshaw cells. Development of the model required three steps. First, the connection strengths between muscle layer units and output units were determined using a geometric model of the torso musculature. Second, suitable magnitudes of the S and I inhibitory connection weights were found through a trial-and-error process wherein predicted patterns of muscle activity were compared with experimental normalized EMG (NEMG) data (Lavender et al., 1992a). Third, a learning process was needed to allow the model to achieve moment equilibrium. The standard backpropagation algorithm was employed to iteratively update all other weights within the model until moment equilibrium could be reached within $\pm$ 5%. Behavior of the model was empirically evaluated by statistical comparison of predicted muscle activity levels with additional experimental EMG data.

RESULTS

Upon testing the model with a distributed set of triaxial moments of moderate levels (0-60 Nm), the static moments were closely equilibrated (r^2=0.99; s.e.=1.66Nm). Predicted patterns of muscle activity, in response to moments applied from several orientations, were smooth and continuous (Figure 3). These predicted recruitment patterns closely matched the subject averaged NEMG data of Lavender et al. (1992b), a distinct data set from that used during training and while determining the I and S parameter values. Comparisons using linear regression confirmed the veracity of model predictions (average r^2=0.79).

The patterns of predicted muscle recruitment could be systematically altered by varying the inhibition parameters. Decreasing S resulted in an increase in the overall muscular activity level. Increasing I yielded higher competition between active muscles. As an example, with a combined flexion and

right lateral bending moment, the activity of the left ES increased when I increased. The associated increase in inter-muscular inhibition caused a subsequent decrease in right ES activity. In general, the qualitative behavior of the various muscles was altered as a function of the magnitude of I.

DISCUSSION

An ANN model was developed, as an abstract representation of the human motor control system, to provide predictions of lumbar muscle activity over a range of static external loads. In contrast to existing EMG-based methods, the present model, once trained, is applicable to novel situations in the absence of EMG measures. In contrast to several optimization-based approaches, the model may more easily be given a physiological justification or interpretation. The present model may be considered as an analogy for the 'central pattern generator,' which is hypothesized to act without significant feedback (Schmidt, 1988). The training methods employed here offer a possible mechanism whereby such a pattern generator could emerge in the absence of specific training examples. Fully animated, dynamic responses would involve the open-loop operation of the generator within the larger framework involving higher levels of control and proprioceptive input.

Only static loads in a single posture were examined to maintain simplicity. Asymmetric postures can be implemented by modifying the connections between muscle and output units. Since each of these connections specifies the moment generating potential of a muscle, changes in capacity due to length and geometry must be incorporated.

The results may help in understanding the presence of antagonistic muscle co-contraction. The model predicted realistic levels of antagonism (e.g., Figure 3) for all the included muscles with the exception of the LD. Though not presented here, predicted levels of antagonism (e.g., during torsional efforts) could be varied by changing the inhibition parameters (I and S). Individuals may thus have similar recruitment plans, and variations in observed antagonism could be a consequence of differences in muscular interactions and competition. That varying patterns of antagonisms could be simulated in this way, suggests this may be a mechanism by which the nervous system can achieve goals other than moment equilibrium. Further, it implies that elevated levels of co-contraction should exist at an early state in motor learning, before the inhibition mechanisms have fully developed. Perhaps the focus on antagonistic co-contraction, rather than explaining why it occurs, might more profitably consider why it does *not* occur.

REFERENCES

Cholewicki, J. et al. *J Biomech*, 28, 321-331, 1995.

Lavender, S.A. et al. *J Orth Res*, 10, 691-700, 1992a.

Lavender, S.A. et al. *Hum Fact*, 34, 239-247, 1992b.

Nussbaum, M.A. *Proc. NACOB II*, 475-476, 1992.

Rumelhart, D. et al. *Parallel Distributed Processing*, MIT Press, 1986.

Schmidt, R.A. *Motor Control and Learning (pp. 202-205)*, Human Kinetics, 1988.

ACKNOWLEDGMENTS

This work was supported by NIH Grant 1R01-AR39599 in cooperation with Dr. Gunnar B.J. Andersson of Rush Presbyterian, Chicago.

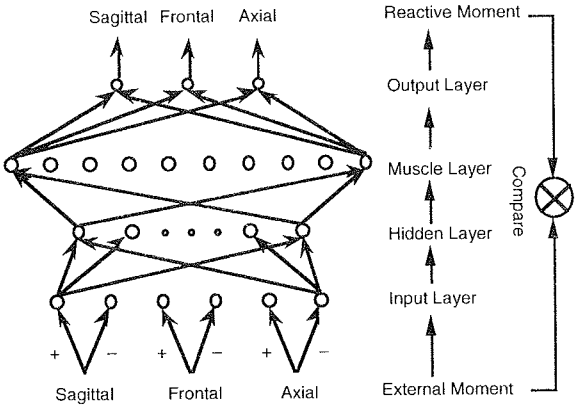

Figure 1. Architecture of the feed-forward neural network. Details within the muscle layer are shown in Figure 2.

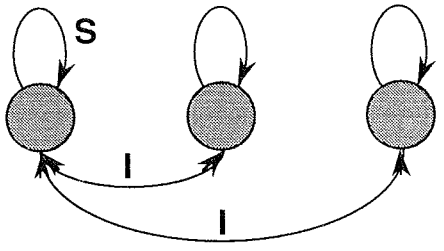

Figure 2. Interconnections within the muscle layer units. Inhibition is transferred via self-inhibition (**S**) and intermuscular-inhibition (**I**). Only three of the 10 units are shown for clarity.

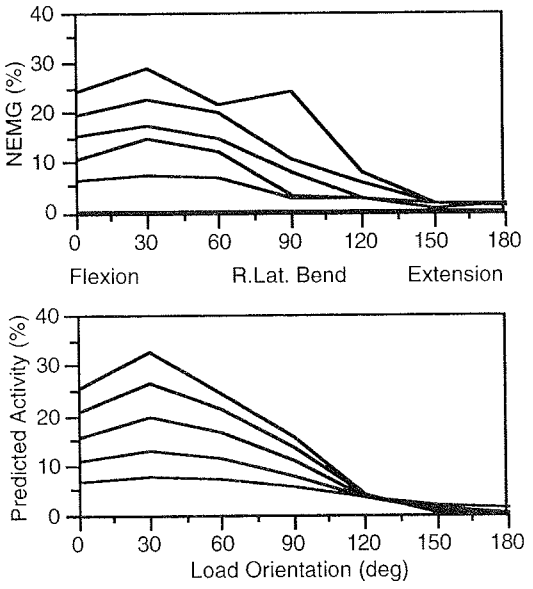

Figure 3. Response patterns of the left ES for static moment loads (10, 20, 30, 40, and 50 Nm) applied at L3/L4 from a range of orientations. Subject-averaged NEMG data from Lavender et al. (1992a) are shown at the top figure, and ANN model predictions for the same moment loads are shown at the bottom.

Direct Intra-operative Passive Muscle Tension Measurement System

M. E. Pannunzio, M.D., J. P. Romano, B.S.[1], D. L. Damiano, PhD. P.T., C. L. Vaughan, PhD., M.F. Abel, M.D.

Department of Orthopaedic Surgery, University of Virginia Health Sciences Center, Charlottesville, Virginia 22903
[1]Department of Biomedical Engineering, University of Virginia, Charlottesville, Virginia 22903

Introduction

Cerebral Palsy (CP) is the most prevalent physical disability originating in childhood with an incidence of 2-3 per 1000 live births. Caused by a static injury to the motor centers of the brain, it results in muscle spasticity and difficulties with selective muscle control. Musculo-tendinous lengthening surgery is frequently performed to relieve joint contractures resulting from muscle tightness in CP. By lengthening the muscle-tendon unit, passive tension at any given joint angle is decreased, and joint range of motion may thereby be increased. It has been observed however, that overlengthening of a tendon decreases the force-generating capacity of the muscle, and leads to weakness about the joint across which a muscle acts. At the present time, precise guidelines for the extent of lengthening do not exist, nor does the surgeon have at his disposal a method for quantifying tendon tension in the operating theater. A tension measuring device (TMD) which could be applied to an intact tendon *in vivo* during the course of a surgical procedure was designed and constructed. Initially tested on cadaveric specimens and later applied in the operating theater, this device is currently being utilized in research protocols designed to evaluate the length-tension curve for muscles affected by CP.

Review and Theory

The TMD described above is based on the buckle transducer originally conceived by Salmons et al. in 1969. It functions to translate a longitudinal tension in an intact tendon into a force in the transverse direction which is then measured using a standard force transducer. Several types of transducers have been described in the literature (Salmons et al., 1969; Barnes and Pinder, 1974; Lewis and Frasier, 1979; Barry and Ahmed, 1986; An et al., 1990). These systems have used some type of buckle frame and strain gauges deforming under load. These designs were temperature sensitive, difficult and expensive to construct, and required that the strain gauges be meticulously insulated to provide electrical isolation from surrounding tissues. Over time, with repeated use and sterilization of the frames, the insulation would degrade and require attention. The buckle frames were also quite sensitive to specimen size and several were needed to accommodate a study population. The TMD is innovative in that it utilizes a combined force transducer, power supply and display which is attached to, but not integral with, the tissue interface, thereby eliminating temperature sensitivity and enhancing durability. The force transducer has a digital output port to simplify data recording and is battery powered. The tendon interface is of stainless steel and may be autoclave-sterilized. In addition, the TMD is adjustable to accommodate a wider range of specimen sizes. The goal is to validate the TMD as a tool which can be used to intra-operatively measure tension in a muscle-tendon unit.

Procedures

The tendon interface consists of two concave rollers separated by a fixed distance, which cup the tendon. The roller assembly inserts to an adjustable-depth fixture mounted on the force transducer. A hook is threaded behind the tendon and attached to the strain gauge of the force transducer. The rollers are advanced to deflect the tendon creating the offset in Fig. 1. This offset determines the geometry of the TMD, and is a variable in Equation 1. Increasing the offset yields greater sensitivity, but this shortens the specimen, and forces it to flex at a more acute angle. This increase in sensitivity with increasing offset was also seen in the buckle-type transducer described by An et al., (1990).

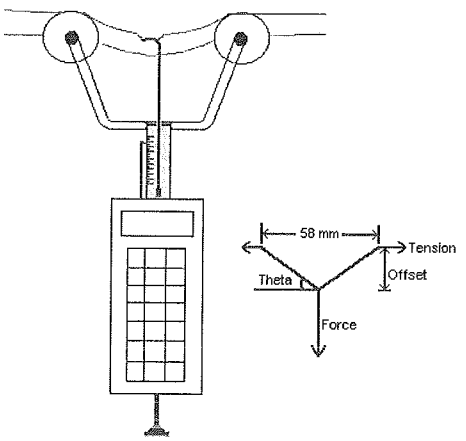

Figure 1

$$\theta = \mathrm{ATAN}\,\frac{\mathrm{offset}}{29} \qquad \mathrm{tension} = \frac{\mathrm{force}}{2\,(\sin\theta)}$$

Equation 1

The device underwent six test cycles using four embalmed, cadaveric hamstring muscle-tendon specimens in our materials testing laboratory. The specimens were clamped into holding fixtures and stretched at 150N

several times to remove any slack in the system, and to test for slippage or tearing of the specimen through this range. The device was then applied to the tendon using a 15mm offset, in an area where the tendonous aponeurosis envelopes the muscle belly (this is typically where a surgical lengthening would be performed). The MTS was programmed to apply a constant displacement of 0.25mm/sec, and readings were taken from the device at four second intervals.

When used to measure tendon tension in hamstring muscles intra-operatively, the device is applied as described above. The desired offset is generated, and the leg extended. Using a goniometer, incremental measurements are made at varying angles of knee flexion. The hook of the TMD remains in place while the surgeon performs the tendon lengthening, and a second set of measurements is then made.

Results

Results from the calibration trials show that, like the MTS, the TMD is a valid indicator of passive muscle tension as demonstrated by near perfect correlation in all trials (Pearson r $\geq$ 0.99). At higher loads there was progressive error in the absolute values, with the MTS consistently reading higher tensions than the TMD (Fig. 3). The difference between the slope of the curves is higher at low offsets and smaller at high offsets. We have found that when working at the muscle-tendon interface, the specimen is progressively flattened at high loads by both the rollers and the hook thus reducing the actual offset in Equation 1. When employing a mathematical correction factor, the absolute values of the TMD more closely approximate those from the MTS.

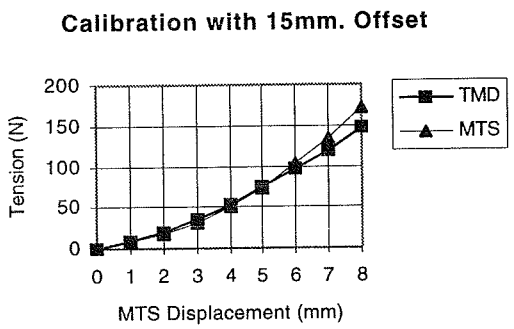

Figure 2

The pre and post-lengthening results for one patient-leg are plotted in Figure 3. The reduction in tension produced by lengthening of the spastic muscle-tendon unit is clearly demonstrated by the TMD, and is seen throughout the range of motion. In this patient-leg, passive range of motion, measured under anaesthesia, was increased approximately 25 degrees through lengthening of the semi-membranosis muscle.

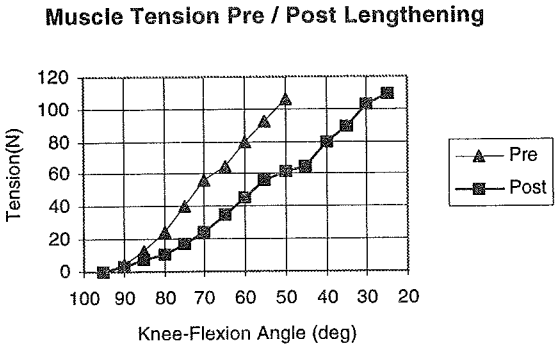

Figure 3

Discussion

Currently there is much research underway examining theeffects of various treatment modalities on muscle strength in CP. The TMD was conceived out of a need for a portable, durable, and easy to use device that could be applied to the intact muscle-tendon unit within the operative field. Results of calibration trials with the MTS have validated the TMD as a means for measuring tension during musculo-tendinous surgery. Intra-operative experience is being gathered, and the data collected suggest that the TMD could be used as a clinical guide to suggest the amount of length that need be added to a tendon in order to achieve the desired range of joint motion. In cases where more than one tendon crosses a single joint, the TMD could be used to determine the relative restriction to joint motion offered by these, and hence, the amount of length that need be added to each. Further, if after a degree of lengthening the desired range of motion is not achieved, the TMD could be used to suggest whether the operated tendon continues to be the restrictive factor, or if another spastic muscle-tendon unit, a tight joint capsule, or intra-articular pathology might be involved. Ultimately, the goal of the design and testing of the TMD is to provide a clinical tool for use by orthopaedic surgeons and researchers endeavoring to improve the outcome of musculo-tendinous surgery in cerebral palsy.

References

An, K.N. et al., J. Biomechanics, 23(12), 1269-71, 1990.

Barnes, G. R. G., and Pinder, D. N., J. Biomechanics, 7, 35-42, 1974.

Barry, D., and Ahmed, A.M., J. Biomech. Engin., 108, 149-52, 1986.

Lewis, J.L., and Frasier, G., Proceed. 1979 ASME Biomech. Symp., 71-74, 1979.

Salmons, S., Biomed. Engineering, 4, 467-74, 1969.

Acknowledgments

Joe Hale, PhD., for assistance with MTS calibration, and the support of the National Institute on Disability and Rehabilitation Research.

FUNCTIONAL AND BIOMECHANICAL EFFECTS OF HAMSTRING LENGTHENING ON THE KNEE JOINT IN SPASTIC CEREBRAL PALSY

J.P. Romano BS[1], M. Pannunzio MD[2], M. Abel MD[2], D. Damiano PhD[2]
[1] Department of Biomedical Engineering, University of Virginia, Charlottesville VA 22908
[2] Department of Orthopaedic Surgery, University of Virginia Health Sciences Center, Charlottesville VA 22903

INTRODUCTION

Cerebral Palsy (CP) is a prevalent neurological disorder originating in childhood. A common orthopedic problem in spastic CP is "crouch gait" which is characterized by excessive knee flexion during walking. As a result, high knee joint moments occur at the knee during stance phase. Surgical lengthening of the hamstrings tendon is often performed to reduce the degree of crouch. The procedure allows a more erect posture, at the expense of reducing the effective strength of the hamstrings due to the shift in the muscle length-tension curve. The goal of this study is to analyze the biomechanical effects of the hamstring lengthening procedure, focusing on strength and moments at the knee.

REVIEW AND THEORY

Relatively few studies have been published which consider gait effects of hamstring lengthening in cerebral palsy. Thometz et al. (1989) studied crouch gait kinematic patterns in the sagittal plane pre- and post-operatively, as well as time and distance parameters. Total arc of motion at the knee did not change appreciably, but range of motion was shifted towards extension. Unfortunately, kinetics were not studied. Gage (1991) reported a case study of the kinematic and kinetic effects of a bilateral hamstring lengthening, in which post-operative internal knee moments during gait were reduced. In agreement with Gage (1991), we hypothesize that extension moments at the knee will be reduced post-operatively.

The surgically elongated tendon should allow greater passive and active knee extension. Overall passive joint excursion increases, although active excursion may not necessarily increase. The hamstrings are effectively "weaker" due to a shift in the length-tension curve, and the quadriceps/hamstrings strength ratios are also altered. We postulate that these angle-dependent strengths and ratios directly affect gait patterns.

PROCEDURES

A total of four subjects (eight sides) with CP underwent tendon elongation procedures performed by the same surgeon. All subjects had bilateral gastrocnemius lengthenings (GL). In addition, one subject had bilateral hamstring lengthenings (HL) (two sides) and two of the subjects had unilateral HL (two sides). One subject underwent GL only. The four GL sides were included as a comparison group to the four HL + GL sides. Gait analyses and voluntary strength measurements were done pre-operatively and 6-month post-operatively at the Motion Analysis Lab at the University of Virginia. Kinematic and force plate data were collected to analyze joint angles and moments. Maximum voluntary contractions of the quadriceps and hamstrings muscle groups were measured isometrically with a hand-held dynamometer. Hamstring strength was measured in a seated position at 90° knee flexion. Quadriceps strength was measured with the subject seated and the knee alternately at 30° and 90° of flexion.

RESULTS

The sides undergoing hamstring surgery experienced the greatest effects at the knee in the sagittal plane and are illustrated below. (Table 1, Figures 1-3). Pre-operative, post-operative, and typical normal curves are overlaid. Post-operatively, knee extension increased throughout the entire gait cycle as expected (Figure 1). Knee extension moment (normalized to % body mass) was reduced for most of stance phase (Figure 2) while the vertical GRF pattern also changed (Figure 3). The first vertical peak force was reduced, and the second peak force was restored since prior to surgery no second peak was evident. Strength is illustrated in Figure 4, showing a decrease in hamstrings strength and an increase in quadriceps strength at 30° of knee flexion. Except for a reduction in knee excursion and stride length, minimal changes in kinematics, kinetics, and strength were found in the comparison group.

Table 1. Knee parameters

	HL Group		GL Group	
Parameter	Pre	Post	Pre	Post
total excursion (deg.)	32	41	46	37
max. ext. moment (Nm/kg)	1.07	0.54	0.47	0.52
hamstrings strength (N)	88.8	60.9	80.0	83.0
quadriceps strength (N)	75	102	106	104
stride length (m)	0.80	0.85	0.73	0.67

DISCUSSION

Post-operative knee kinematic patterns in the HL group appear much closer to the normal patterns, and the subjects are in a more erect posture, in agreement with Thometz et al. (1989) and Gage (1991). Overall excursion of the knee joint increased post-operatively, in contrast to Thometz et al. This may be partially attributable to the gastrocnemius lengthening (Rose et al., 1993), however based on the comparison group data, this point is arguable.

Knee extension moment was reduced post-operatively for most of stance with a shift towards flexion. During late stance, the vertical GRF has increased, yielding a second peak. The GRF vectors in the sagittal plane have similar directions before and after surgery, but the magnitude has increased post-operatively. This apparent inconsistency with the moment data can be explained by the reduction in the moment arm at the knee due to the more upright position post-operatively. An illustration of one of the HL subjects while on the force plate before and after surgery at late stance is provided in Figure 5.

As expected, hamstrings strength is reduced post-operatively in the HL group. Meanwhile, quadriceps strength at 30° has increased post-operatively. There are two possible explanations for this trend. Since restraint by the hamstrings is reduced, quadriceps are functioning more effectively, and therefore exhibit an increase in strength. Second, the increase in hamstring length promotes function of the quadriceps in the more extended portion of the range. Thus, it is interesting to see that the quadriceps strength increases post-operatively, although their activity during level walking does not increase the knee extension torque.

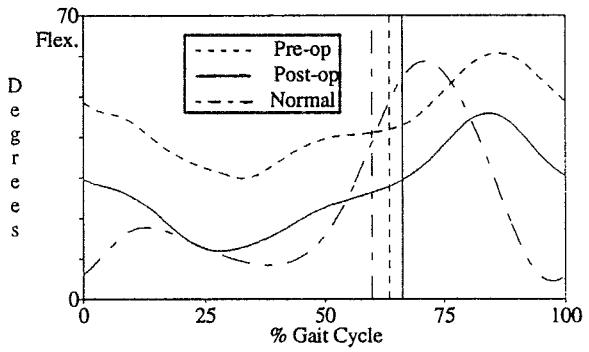

Figure 1. Knee Flexion/Extension Angle

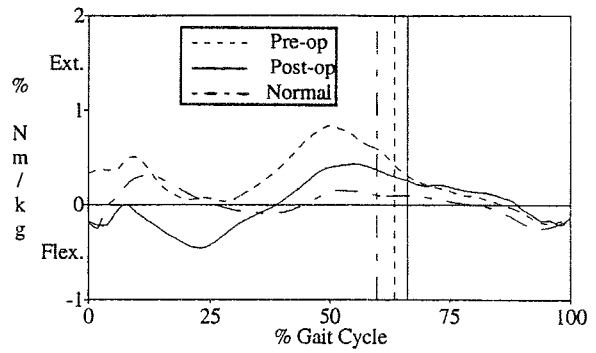

Figure 2. Knee Flexion/Extension Moment

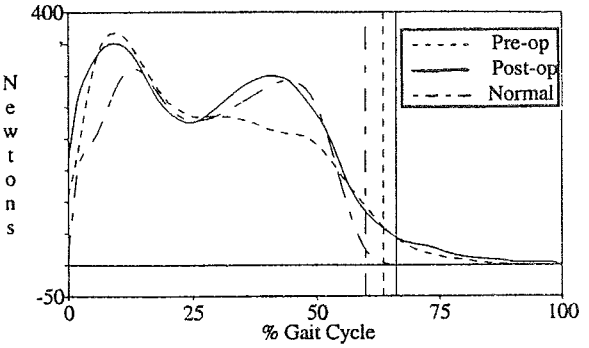

Figure 3. Vertical Ground Reaction Force

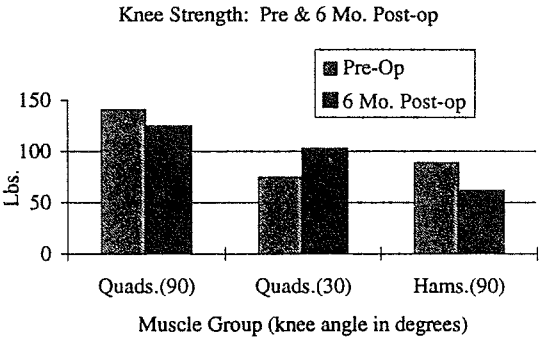

Figure 4. Knee Strength

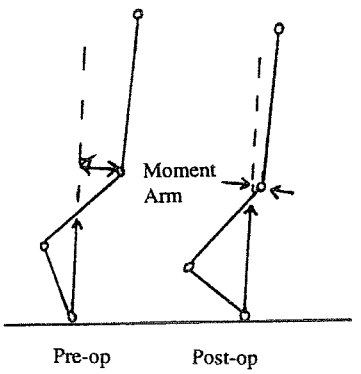

Figure 5. Sagittal View

REFERENCES

Gage JR. ***Gait Analysis in Cerebral Palsy***. Mac Keith Press, 184-200, 1991.

Rose SA et al. ***J. Ped. Orth.***, 13:727-732, 1993.

Thometz J et al. ***JBJS.***, 71-A (3):345-353, 1989.

ACKNOWLEDGEMENTS

I would like to thank Dr. C.L. Vaughan for his help in preparing this manuscript.

EFFECTS OF INCREASED EXERTION DURING PEDALING EXERCISE ON KINETIC MEASURES OF MOTOR PERFORMANCE FOR HEMIPLEGIC PERSONS

S.A. Kautz, D.A. Brown, C.A. Dairaghi

Rehabilitation R&D Center, VA Medical Center (153), Palo Alto, CA 94304

INTRODUCTION

While a neurologically normal individual can exercise against high workloads at high movement speeds, a hemiplegic stroke patient has limited ability to perform under these exertional conditions. Controversy exists as to whether the hemiplegic person should avoid exertion during exercise since it may exacerbate his or her already impaired motor performance . We have previously shown that hemiplegic persons have significantly reduced work output for their plegic leg, as compared to their non-plegic leg, during pedaling exercise at moderate workloads and speeds (Brown et al, 1994). Will increased exertion (workload and/or movement speed) further impair force production by the affected leg, thereby compromising motor performance, and by implication reduce the potential rehabilitative benefits? This study examines kinetic measures of motor performance during pedaling in a neurologically normal and a hemiplegic population as exertion is increased to provide a clinical rationale for prescribing the exertional level for exercise in hemiplegic stroke patients.

REVIEW AND THEORY

Hemiplegic stroke patients with unilateral lower limb dysfunction constitute a sizable portion of the rehabilitation patient population. The impaired function observed in plegic limbs is partially due to decreased muscular strength and poor timing of muscular activation, both of which should potentially benefit from exercise. However, exertional effort by hemplegic persons has been discouraged: "excessive effort is worse than useless in spastic conditions, for it reinforces the abnormal patterns of posture and movement and increases spasticity (Bobath, 1978)." This view is somewhat controversial and whether exertion exacerbates impaired motor performance and, therefore, should be avoided during exercise, remains an open question.

We are investigating pedaling because it is a common clinical exercise for addressing problems associated with hemiplegic lower limb dysfunction, and it allows standardized control of workload and movement speed (cadence). Pedaling is complex enough to provide a functionally relevant test for motor performance since it demands multi-segmental coordination of a bilateral, reciprocal movement.

This study investigates both increased workload and speed to differentiate their effects and study their interactions. Voluntary movement deficits have been linked to ineffective muscular contractions which reduce muscle force output (Bourbonnais et al., 1989) and delayed termination of agonist activity at the end of movement (Sahrmann et al., 1977). Increased speed may be especially detrimental to motor performance if significant effects from delayed termination of agonist activity exist during reversal periods in this cyclical movement. We hypothesize that the measured motor performance of the plegic limb during pedaling is related to the level of exertion associated with both workload and cadence.

PROCEDURES

A standard Monarch ergometer was modified to include a backboard seating mechanism with shoulder and lap harnesses to stabilize subjects. Reaction forces oriented normal and fore-aft to both pedal surfaces were measured by instrumented pedals. Angular rotation of the crank and pedals were measured using optical encoders. To more precisely define pedaling kinematics, 3D coordinates of both anterior superior iliac spines (ASIS) were recorded using a two-camera 3D video system.

Experiments were conducted on nine healthy elderly subjects (5 male, 4 female) of age 72.9 ± 4.5 years (mean ± std. dev.) and 5 hemplegic stroke patients (3 male, 2 female) of age 64.4 ± 7.4 years (4 right and 1 left CVA, with no associated cognitive or sensory deficits). All subjects were instructed to pedal (while given visual cadence feedback) at each of three cadences (25, 40 or 55 rpm) and four workloads (45, 90, 135 and 180 J) for 20 seconds. The 3 x 4 presentation of cadences and workloads was randomized (with adequate rest allowed between trials to prevent fatigue) and the extrinsic cadence feedback presented the difference from the goal without reference to the absolute cadence.

Motor performance measures were then calculated from the experimental data. First, filtered pedal-system data were converted to radial and tangential forces (with respect to the crank arm) and the external work done was calculated. Second, sagital plane hip joint center coordinates were located by assuming fixed locations relative to the video data of ASIS positions. Third, the pedal-system data, anthropometric measures and hip joint center data were used to calculate the kinematics and joint torques of the legs using a five-bar linkage model (Hull et al, 1985). Fourth, the absolute sum of the negative work done by the net joint torques were calculated by integrating the individual joint powers while allowing intercompensation between joints spanned by biarticular muscles (Kautz et al., 1994).

To test for differences with changes in cadence and workload, the experimental model was a randomized complete block design. Mean values of external work

done and the negative work done by the net joint torques were calculated for each subject-cadence-workload combination. The results were blocked by subject, and a two-way ANOVA tested for significant differences due to cadence and workload allowing for interactions ($p<0.05$). When significant differences were evident, Duncan's multiple range test was used to determine which means differed.

RESULTS AND DISCUSSION

Kinetic measures of motor performance indicate that increased workload does not exacerbate the impaired motor performance of hemiplegic persons during pedaling exercise. The amount of work done by the plegic limb was significantly affected by workload ($p<0.001$, Figure 1) with posthoc tests revealing an

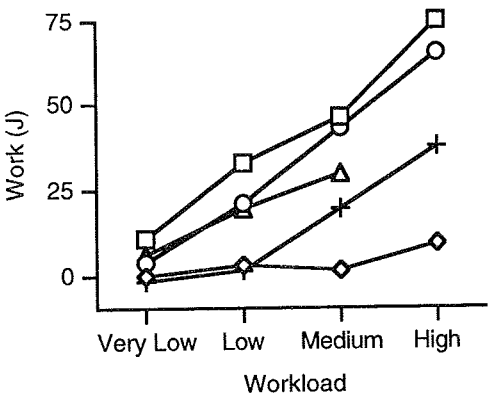

Figure 1: Increased workload results in increased work output of the plegic limb (symbol types represent different subjects).

ordered effect with all means different. Neither cadence nor interaction effects were significant ($p>0.05$). The work done by the plegic limb is a meaningful measure of motor performance because it represents the functional output of the limb. This

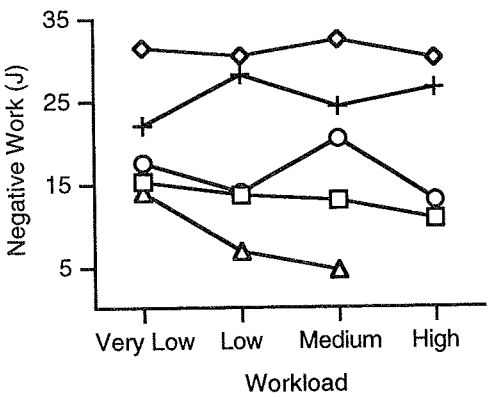

Figure 2: Negative work done by the joint torques was not associated with increased output of the plegic limb (symbol types represent different subjects).

increased output did not reduce the quality of the movement since the negative work performed by the net joint torques of the plegic limb was unchanged or lower at higher workloads ($p>0.05$, Figure 2).

Analysis of the negative work done by the net joint torques for the hemiplegic subjects implied that the calculated values were a sensitive measure of motor performance. A paired t-test revealed the average magnitude of the negative work across all conditions for the plegic limb (19.7 ± 10.0 J) was significant greater ($p<0.0001$) than for the non-plegic limb (11.0 ± 8.8 J). Also, the magnitude of negative work for the non-plegic limb was of comparable value to the average magnitude of the control subjects (8.9 ± 8.6 J). Since negative work provides a measure of motor performance that is able to differentiate between the plegic and non-plegic limbs, the lack of change in the negative work with workload argues strongly that the already impaired motor performance was not further degraded by increased exertion. While our calculations allow intercompensation of net joint torques by biarticular muscles, future research will include electromyographic measures to assess motor performance at the individual muscle level.

The results of this study provide evidence for encouraging high levels of exertion during pedaling exercise in persons with post-stroke hemiplegia. However, these results do not address whether training at higher levels of exertion will result in better transfer of motor performance to daily tasks such as walking. Also, high levels of exertion should be approached with caution in patients with a history of cardiac and/or orthopedic problems. Additionally, the results of this study demonstrate that there may be differences between exertion due to increases in speed versus workload. Workload challenges resulted in enhanced force production, whereas no significant effects on motor performance with respect to increased movement speed were detected.

Therefore, this study can be used a model for developing an exercise protocol. By monitoring quantitative measures of motor performance at different cadences and workload, the appropriate exertional level for exercise can be determined. Future studies will investigate the training effects of pedaling at optimally determined speeds and workloads, with special emphasis on functional measures.

REFERENCES

Bobath, B. *Adult Hemiplegia.* Heinemann, 1978.
Bourbonnais, D. et al. *Brain* , 112, 85-102, 1989.
Brown, D.A. et al. *Vestibular Front* , Elsevier, 1994.
Hull, M.L. et al. *J Biomech* ,18, 631-644, 1985.
Kautz, S.A. et al. *J Biomech* 27,1459-1467.
Sahrmann, S.A. et al. *Ann Neurol* , 2, 460-465, 1977.

ACKNOWLEDGMENTS

This work was supported in part by a grant from the Foundation for Physical Therapy, Inc.

LOWER EXTREMITY CYCLING MECHANICS IN SUBJECTS WITH UNILATERAL CEREBROVASCULAR ACCIDENT

K. Perell[1], R Gregor[2], A.M. Erika Scremin[1]
[1]Physical Medicine & Rehabilitation Service, West Los Angeles VA Medical Center, Los Angeles, CA 90073
[2]Department of Health & Performance Sciences, The Georgia Institute of Technology, Atlanta, GA 30332

INTRODUCTION

While the kinematics and crank mechanics have been described for subjects with cerebrovascular accident (CVA) (Rosecrance & Giuliani, 1991, Benecke *et al.*, 1983, Brown *et al.*, 1992), the cycling mechanics of the lower leg have not been explored. Particularly as the bicycle has many advantages as a training tool for symmetry, it has potential benefits for increased loading of the involved leg. The purpose of this study was to examine the cycling mechanics of the lower leg in subjects with CVAs to address the asymmetrical relationship between the involved (IN) and noninvolved (NI) legs.

REVIEW & THEORY

Hemiplegia caused by CVA is the most common neurologic impairment accounting for approximately 25% of all severely disabled persons. Physical therapy programs utilize strengthening, range of motion exercises, in addition to gait training, to facilitate independent walking. In addition, the bicycle ergometer has been used in the treatment of hemiparesis.

The asymmetrical nature of hemiplegic posture and gait results from abnormal muscular activity, abnormal postural mechanisms, and sensory deficit. Treatment for improving posture and gait focuses on increased loading of the involved leg. The bicycle can serve as a tool for enhancing rehabilitation of patients with CVAs. Bicycling provides an opportunity for to evaluate bilateral reciprocal patterns of the lower leg without the weight bearing demands that locomotion requires. Cycling is similar to gait in that it requires reciprocal use of both legs, fosters symmetry of movement, can have a rate similar to normal walking, is a pre-CVA learned task, is rich in proprioceptive and timing cues, and provides alternating muscle activation of antagonists (Brown & DeBacher, 1987).

PROCEDURES

Eight male subjects with unilateral CVAs, at least six months post stroke were evaluated. All subjects were outpatients of the West Los Angeles Veterans' Administration Medical Center (WLA VAMC). All subjects were right hand dominant. Each subject was able to locomote independently with the use of a single-point or four-point (quad) cane.

The bicycle apparatus was a recumbent bicycle (ProTech Sports PTS Turbo 1000) with the seat adjusted for each subject's leg length. Attached to each crank were custom built pedals capable of measuring normal (F_N) and tangential (F_T) components of the applied load. Pedal forces were collected (200 Hz) during the final 15 seconds of the one-minute trial.

Joint markers were placed on the subject's greater trochanter, knee joint center, lateral malleolus, and 5th metatarsal-phalangeal (MP) joint bilaterally. Markers were also placed on the anterior and posterior portions of the pedal, on the pedal spindle, and on the portion of the crank attached to the bicycle for purpose of measuring pedal and crank angle. Trials were filmed at 50 frames per second. Subjects were instructed to cycle at a comfortable speed for one minute. Film data for each leg were collected during separate trials.

Kinematic and kinetic data describing two consecutive pedal revolutions were isolated for analysis. Coordinate data were obtained by digitizing serial film images (Numonics digitizer - IBM XT computer). Cutoff frequencies were determined using a power spectrum analysis program. The cutoff frequency for each coordinate was selected at the point where 97% of the signal energy was maintained. Data were smoothed using a 4th order, zero-lag Butterworth filter. The lower extremity was modeled as a planar, three-segment rigid body system with an external reaction force located at the pedal spindle. Equations of motion for the three segments were formulated using conventional Newtonian mechanics.

RESULTS & DISCUSSION

Exemplar data from one subject is shown in Fig. 1 for the ankle, knee, and hip generalized muscle moments (GMMs) bilaterally. As presented in Fig. 1A the IN leg lacked an ankle dorsiflexor GMM during the first 90^o of the pedaling cycle found in the NI leg. This dorsiflexor GMM in the NI leg aids in pulling the NI leg up through 0^o when the leg is most flexed in the recumbent configuration. The ankle GMM pattern, however, was quite variable between subjects depending on the amount of ankle control the subject had. A lack of knee extensor GMM (Fig. 1B) was evident in the IN leg during the power phase (0-180^o). At the hip, two patterns emerged. In three subjects, the IN leg showed no hip flexor GMM during the recovery phase (180-360^o) whereas the NI leg transitioned from an extensor GMM to a flexor GMM midcycle (Fig. 1C). The other five subjects demonstrated a hip flexor GMM throughout the cycle. This second pattern limited the power generation of the IN hip to the recovery phase, consequently the NI hip was required to produce power throughout the entire cycle.

The average $\pm$ SD percent contribution of each joint to the total positive muscle work across subjects is shown in Table 1. The hip joint overwhelmingly contributed the greatest percentage in the IN leg while a more even distribution between the knee and hip was seen in the NI leg. Power production during the power phase of the IN leg was quite limited in all subjects except those with the hip extensor GMM during the power phase, while all three joints contributed to power production during the power phase of the NI leg.

FIGURE 1

1A: NI vs IN ANKLE GMM

1B: NI vs IN KNEE GMM

1C: NI vs IN HIP GMM

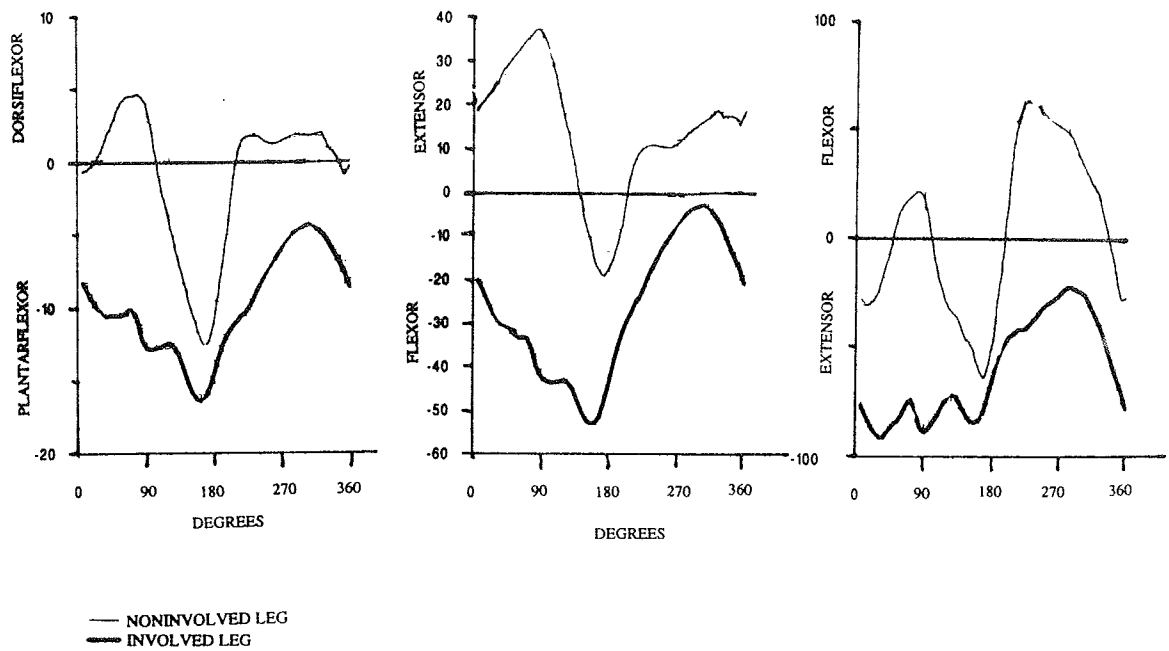

TABLE 1: PERCENT CONTRIBUTION OF EACH JOINT TO THE TOTAL POSITIVE MUSCLE WORK ACROSS SUBJECTS

	NONINVOLVED LEG	INVOLVED LEG
ANKLE	3.74 ± 2.45	1.09 ± 0.60
KNEE	39.34 ±13.08	22.00 ±19.97
HIP	56.81 ±11.79	78.60 ±17.05

Patterns of muscle torques showed similarities between normal data reported by Gregor *et al.*, (1985) from recreational cyclists on an upright bicycle and the noninvolved leg of the subjects with CVAs on the recumbent bicycle in this study. The resulting muscle power patterns were similar in all joints for the noninvolved leg to those patterns reported by van Ingen Schenau *et al.*, (1990) except that power absorption was more apparent in the ankle and knee of the noninvolved leg of subjects with CVAs. This is partly explained by slower pedaling rates.

REFERENCES

Benecke *et al* (1983) Motor Control Mechanisms in Health and Disease, ed. JE Desmedt, Raven Press; 1035-1046.

Brown & DeBacher (1987) Physical Therapy, 11:1715-1719.

Brown *et al* (1992) Forum on Physical Therapy Issues Related to Cerebrovascular Accident, 1992 Combined Sections Meeting Proceedings, 8-15.

Gregor *et al* (1985) J. Biomechanics, 18:307-316.

Ingen Schenau, van *et al* (1990) European J Applied Physiology, 61:11-19.

Rosecrance & Giuliani (1991) Physical Therapy, 71:334-343.

ACKNOWLEDGMENTS

The authors wish to acknowledge the data collection and analysis assistance of Kari Matsumoto, technical assistance of John Franco, Dr. Oscar Scremin, and Dr. William Whiting.

INDWELLING EMG OF PSOAS:
CLINICAL IMPLICATIONS FOR LOW BACK INJURY AND REHABILITATION

Stuart M. McGill[1], Daniel Juker[2], Peter Kropf[3]

[1]Occupational Biomechanics and Safety Laboratories, Department of Kinesiology, University of Waterloo, Waterloo, Ontario, N2L 3G1, [2]Institute of Sports Science, Federal School of Sports, Magglingen, Switzerland, [3]Institute for Computer Science and Applied Mathematics, University of Bern, Bern, Switzerland

Introduction

Very little is known about the activation levels of psoas, due to the inaccessibility with surface EMG electrodes. Past work reporting the activation levels of this deeper muscle, has been sparse, and the data has been qualitative in nature. The objective of this work was to obtain normalized activation amplitudes from psoas to understand its role in spine mechanics - and more specifically, for use in rehabilitation and investigations into the injury process. The specific purpose of this paper was to report the normalized and scaled EMG activation profiles of psoas over a wide variety of tasks. Furthermore, simultaneous collection of several surface muscle EMG's facilitated analysis of whether surface electrodes can be used to predict psoas activity.

Specific hypotheses to be tested were as follows: H1) psoas is predominantly a hip flexor; H2) the psoas is activated at low levels during challenging barbell lifting, at least lower than the back extensors; H3) psoas activity is higher during upright sitting than during slouched unsupported sitting and standing; H4) psoas is less active during bent knee situps than straight leg situps; H5) during situps, psoas is inhibited by pressing the heels down and activating the hamstrings; H6) psoas is least active during curlups compared to all other abdominal exercises; H7) psoas is equally active during internal and external hip rotation; H8) during symmetric bucket holding, psoas will increase its activity with increasing load in the hands; H9) a single surface electrode may be used as an EMG surogate to represent psoas in all activities.

Methods

Five men and three women were recruited from a student population. Also these were healthy and had never experienced disabling low back pain. Experimental protocol was approved by the ethics committee, the Faculty of Medicine, University of Bern.

Both surface and intra muscular wire electrodes were used: psoas - two pairs of wire electrodes inserted posterio-laterally at the L3 level using a 12 cm hypodermic needle under the visual guidance of ultrasound imaging; quadratus lumborum - same pathway was used as with psoas; external oblique, internal oblique and transverse abdominis - midway between the linea semi lunarus and the midline laterally and at the transverse level of the umbilicus; surface electrodes were placed over rectus abdominus 3 cm lateral to the umbilicus; external oblique approx. 15 cm lateral to the umbilicus and at the transverse level of the umbilicus, internal oblique below the external oblique electrodes just superior to the inguinal ligament. All raw myoelectric signals were preamplified, filtered (10-500 Hz) and amplified to produce signals of approx. ± 5V. The sagittal plane of the subjects was also filmed on video tape and scaled so the joint coordinates could be obtained for input into a biomechanical link segment model to calculate moments about the lumbar spine and hips.

Two sets of tasks were performed in this study. The first set consisted of a series of maximal effort isometric exertions intended to produce the largest possible amplitude of myoelectric activity to provide a basis for EMG normalization. In a second set of tasks, a wide variety of tasks were selected to test the hypotheses stated earlier. The tasks were grouped into subsections: those primarily used for examining the mechanics of torso flexion (including bent leg and straight let situps and leg raises, curlups, pushups), lateral bend (standing lateral bends, side supports, twisting, standing and seated) extension (and lifting loads up to 70 kg) and hip internal/external rotation (seated and standing).

Results and Discussion

The EMG activity from the muscles monitored from indwelling electrodes are listed in Table 1 together with a few surface muscles listed for reference and to further document the demands of each task. In addressing the specific hypotheses listed earlier: H1) the quantitative activation data of this study agrees with the clinical conclusions from several qualitative studies (e.g., Basmajian, 1958; Nachemson, 1966) that the psoas activity is most closely linked with the generation of hip flexion moment. Further, the activation data is consistent with the morphology and geometry of psoas reported by Bogduk et al, (1992) and Santaguida & McGill, (1995) demonstrating that its mechanical advantage gives highest priority to flex the hip; H2) the hypothesis is accepted as the psoas is activated at levels of 16% MVC or less even during the lifting of barbells up to 70 kg. The fairly high demands of this task are exemplified by erector spinae activation of 62% MVC on average; H3) the hypothesis is accepted as both sitting postures required higher activation levels than during standing (less than 1% MVC). Furthermore, sitting upright caused activation in the psoas to reach as high as 12% MVC while sitting slouched was never higher than 4% MVC; H4) hypothesis is rejected as both the psoas and abdominal musculature have higher levels of activity during bent knee style of situps. However, although the neural drive to psoas may be larger, the muscle is shorter during the bent knee position and force production is likely modulated (i.e., reduced) by the force-length relationship; H5) hypothesis is rejected as our data does not support the clinical notion that psoas activity can be somewhat inhibited by activating hamstrings in the manner described; H6) hypothesis is accepted as certainly curlups activate psoas (less than 10% MVC) less than any style of situp where psoas is active between 15 and 34% MVC; H7) this hypothesis was rejected, the psoas activity was higher during external rotation in both seated and standing postures than during internal rotation. However, while psoas activity is biased towards external hip rotation, the co-contraction would suggest that the psoas is not a prime mover in either of these hip rotation movements; H8) while there was a trend, the variability in psoas activation precluded any solid conclusions regarding the role of psoas as a lumbar stabilizer during externally applied compressive load; H9) the hypothesis is rejected as psoas activity is best represented by rectus femoris (surface) for flexor tasks ($R^2 = 0.45$, RMS diff 12% MVC), twisting tasks ($R^2 = 0.55$, RMS diff 10% MVC), hip rotation tasks ($R^2 = 0.45$, RMS diff 10% MVC) and extensor tasks ($R^2 = 0.37$, RMS diff 7% MVC). During lateral bending internal oblique (surface) is the best EMG surogate ($R^2 = 0.35$, RMS diff 9% MVC).

Major clinical implications can be summarized. The best abdominal flexion exercise to minimize psoas activation level is the curlup. It appears that any type of situp activates psoas to levels in the range of 15-34% MVC and the clinically relevant issue is not what type of situp should be considered - but, should situps be considered at all? The issue as to whether psoas is an internal or external rotator of the hip appear to be a clinical non-issue since psoas activity is not heavily modified by performing any one of these activities. Several have suggested that the psoas stabilizes the lumbar spine (e.g., Nachemson, 1966). From the data of this study we question the importance of psoas in this role since its activation level was not greatly modulated with increasing compressive load on the spine, and its relatively low activity during very demanding tasks such as heavy barbell lifting. We are currently in the process of examining quadratus lumborum given its geometric advantages to laterally stabilize with multi segmental attachment and greater moment arm than the psoas.

References
Basmajian, J.V. (1958) Anat. Rec. 132: 127-132.
Bogduk, N., Pearcy, M., Hadfield, G. (1992) Clin. Biomech. 7: 109-115.
Nachemson, A. (1966) Acta. Orthop. Scand. 39: 47-57.
Santaguida, L. and McGill, S.M. (1995) J. Biomech. 28(3): 339-345.

Table 1. EMG activation normalized to 100% MVC - subject mean and (standard deviation). Note Psoas channels (1 and 2), External Oblique, Internal Oblique, and Transverse Abdominis are intramuscular electrodes while Rectus Abdominis, Rectus Femoris, Erector Spinae are surface electrodes. Activation levels are reported for the most strenuous part of the task. All electrodes are on the left side of the body.

TASK	Psoas 1	Psoas 2	Ext. Oblique	Int. Oblique	Trans. Abdominis	Rect. Ab. (S)	Rect. Fem. (S)	Erect. Spin. (S)
Straight-leg situps	15(12)	24(7)	44(9)	15(15)	11(9)	48(18)	16(10)	4(3)
Bent-knee situps	17(10)	28(7)	43(12)	16(14)	10(7)	55(16)	14(7)	6(9)
Press-heel situps	28(23)	34(18)	51(14)	22(14)	20(13)	51(20)	15(12)	4(3)
Bent-knee curlup	7(8)	10(14)	19(14)	14(10)	12(9)	62(22)	8(12)	6(10)
Bent-knee leg raise	24(15)	25(8)	22(7)	8(9)	7(6)	32(20)	8(5)	6(8)
Straight leg raise	35(20)	33(8)	26(9)	9(8)	6(4)	37(24)	23(12)	7(11)
Isom. hand-to-knee								
left hand-right knee	16(16)	16(8)	68(14)	30(28)	28(19)	69(18)	8(7)	6(4)
right hand-right knee	56(28)	58(16)	53(12)	48(23)	44(18)	74(25)	42(29)	5(4)
Cross curlup Rshoulder→across	5(3)	4(4)	23(20)	24(14)	20(11)	57(22)	10(19)	5(8)
LShoulder→across	5(3)	5(5)	24(17)	21(16)	15(13)	58(24)	12(24)	5(8)
Isom. side support	21(17)	12(8)	43(13)	36(29)	39(24)	22(13)	11(11)	24(15)
Dyn. side support	26(18)	13(5)	44(16)	42(24)	44(33)	41(20)	9(7)	29(17)
Pushup from feet	24(19)	12(5)	29(12)	10(14)	9(9)	29(10)	10(7)	3(4)
Pushup from knees	14(11)	10(7)	19(10)	7(9)	8(8)	19(11)	5(3)	3(4)
Lift light load (20 kg)	9(10)	3(4)	3(3)	6(7)	6(5)	14(21)	6(5)	37(13)
Lift heavy load (up to 70 kg)	16(18)	5(6)	5(4)	10(11)	10(9)	17(23)	6(5)	62(12)
Symmetric bucket hold, 0kg	1(2)	0(1)	2(1)	2(2)	2(1)	10(9)	2(1)	2(1)
20kg	2(4)	1(1)	7(4)	5(3)	5(1)	10(7)	3(3)	3(6)
30kg	3(4)	1(1)	9(5)	6(4)	6(1)	10(8)	3(3)	4(7)
40kg	3(5)	1(1)	10(6)	8(6)	6(2)	10(8)	3(3)	3(2)
Seated Isom. twist CCW	30(20)	17(15)	18(8)	43(25)	49(35)	17(22)	7(4)	14(6)
Seated Isom. twist CW	23(20)	11(8)	52(13)	15(11)	18(19)	13(10)	9(10)	13(8)
Standing hip internal rotation	21(18)	10(9)	18(12)	24(23)	33(20)	13(9)	9(7)	18(6)
Standing hip external rotation	27(20)	22(19)	17(13)	21(19)	31(17)	13(8)	19(11)	17(9)
Sitting hip internal rotation	19(15)	21(18)	36(31)	30(30)	31(29)	18(8)	20(19)	12(8)
Sitting hip external rotation	32(25)	25(20)	11(9)	15(17)	16(13)	15(9)	16(13)	8(8)
Sitting upright	12(7)	7(5)	3(6)	3(3)	4(2)	17(9)	4(2)	5(8)
Sitting slouched/relaxed	4(4)	3(3)	2(5)	2(2)	4(3)	17(11)	3(2)	5(8)
Standing lateral bend								
bending left	9(10)	1(2)	11(8)	18(14)	12(7)	13(7)	3(2)	11(13)
bending right	6(5)	1(2)	19(18)	18(14)	25(20)	14(9)	3(1)	8(8)

FOREFOOT PLANTAR PRESSURE MEASUREMENTS MAY BE USEFUL IN PREDICTING INTERNAL SKELETAL LOADING

N. Sharkey, L. Ferris, T. Smith, D. Matthews

Orthopaedic Research Laboratories, University of California, Davis, CA

INTRODUCTION

Studies of plantar pressure have been used clinically to identify sites of high pressure that may be sources of pain or that may signify regions at risk for soft tissue breakdown, and to evaluate the effects of interventions, such as the use of orthotic devices or surgery on pressure redistribution under the foot (Patel et al., 1994). We hypothesis that such measurements might also be used to predict abnormal loading in the metatarsals of the foot; bones frequently affected by stress reaction and fracture during intense military or athletic training. This study was undertaken to determine if distinct characteristics of forefoot contact could be correlated with second metatarsal strain and loading.

REVIEW AND THEORY

Proper loading and efficient function of the foot during gait is dependent on the simultaneous and coordinated contraction of the controlling musculature. During stance phase gait, active deceleration of dorsiflexion and then plantar flexion at heel-rise depends on the coordinated contraction of the triceps surae (TS), flexor hallucis longus (FHL), flexor digitorum longus (FDL), peroneus brevis and longus (PB/PL), and tibialis posterior (TP) (Perry et al., 1992). Dysfunction of any of these muscles as a result of tendon rupture, neuromuscular disorder, or physiologic fatigue may result in abnormal gait and foot deformity despite normal skeletal structures.

Recently, we presented data which suggests that physiologic muscle fatigue may precipitate metatarsal stress fracture (Sharkey et al., 1995). We found that reduced tension in the FHL and FDL during simulated plantar flexion of cadaver feet caused significant increases in metatarsal strain and bending. Because compromised muscle function will also influence plantar pressure, in principle, one might use the pattern of plantar pressure to infer the loading environment of the metatarsals. Such a procedure might be used to identify individuals at increased risk for metatarsal stress fracture due to muscle dysfunction or physiologic fatigue.

PROCEDURES

Three strain gauges were applied circumferentially to the second metatarsal of nine fresh cadaver feet and the feet were mounted in a custom loading apparatus designed to simulate the action of the triceps surae, tibialis posterior, peroneus longus and brevis, flexor digitorum longus, and flexor hallucis longus. Specimens were rigidly fixed in the heel-rise position with the tibial shaft angled fifteen degrees forward in the sagittal plane and the ankle in 0-5 degrees of dorsiflexion. The forefoot rested on a pressure measurement platform (Pedobarograph, BTE, Hanover, MD) with the heel elevated 5-10 mm (Fig 1). A load cell placed in series with the pedobarograph enabled simultaneous measurement of ground reaction force (GRF) and pressure distributions under the forefoot.

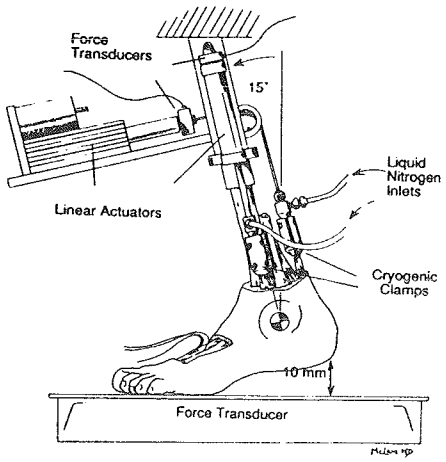

Figure 1: The foot loading apparatus.

Specimens were loaded to 750N GRF by simulated contraction of the various plantar flexors. Repetitive tests were run on each specimen using the following combinations of

simulated active muscle conditions: 1) TS, PB/PL, TP, FDL, and FHL; 2) same as group 1 except no FHL; 3) same as group 1 except no FHL or FDL; 4) TS and PB/PL; 5) TS and TP; and 6) TS only. Strain in the three metatarsal gages and pressure distribution images were captured at 750N GRF. *In-situ* bending moments and loads on the second metatarsals were calculated from strain data. Digital pressure map files obtained from each muscle condition were translated and imported into IMAGE software (W. Rasband, NIMH) for analysis. Contact area, mean pressure, peak pressure, and force were determined for the entire forefoot, the metatarsal region of the forefoot excluding the toes, the great toe, the second toe, and the three lesser toes. Peak pressures under the first and second metatarsal heads were also measured.

Simple correlations were performed to isolate any associations between the plantar pressure parameters and second metatarsal strain and loading. Stepwise multiple linear regressions were then used to develop predictive equations for second metatarsal loading. Statistical tests yielding $p < 0.05$ were considered significant.

RESULTS

Correlations between foot contact parameters and second metatarsal strains were weak. Second toe contact area correlated inversely with dorsal strain ($r = -0.356$; $p < 0.006$), peak pressure under the first metatarsal head correlated inversely with lateral strain ($r = -0.402$; $p < 0.001$), and peak pressure under the second metatarsal head correlated positively with medial strain ($r = 0.349$; $p = 0.005$).

The greatest positive correlation was found between peak pressure under the second metatarsal head and plantar-to-dorsal bending moment in the second metatarsal ($r = 0.801$). Correlation analyses between mean pressure under the first toe or peak pressure under the second metatarsal head and axial loading of the second metatarsal yielded coefficients greater than 0.50. Contact area, peak pressure, and mean pressure under the entire forefoot including the toes, and peak pressure under the metatarsal region of the forefoot, all correlated significantly with the second metatarsal plantar-to-dorsal bending moment (r between 0.477 and 0.492; $p < 0.000$).

Using stepwise multiple regression and plantar pressure distribution parameters, the equation which most closely estimated dorsal strain yielded an r-value equal to 0.691 ($r^2 = 0.477$; $p < 0.001$) and a standard error of 710 microstrain.

The equation which most closely estimated the actual plantar-to-dorsal bending moments in the second metatarsal was more accurate and had an r-value equal to 0.897 ($r^2 = 0.805$; $p < 0.001$; Fig 2). The standard error of the estimate was 1.306 Nm. The regression formula was:

$$PDM\ (Nm) = [2.92 \times PP_{MTH2}\ (MPa)] - [1.70 \times PP_{T2}\ (MPa)] - [2.64 \times W\ (cm)] + 25.6\ (Nm)$$

Where: PDM = plantar-to-dorsal bending moment; PP_{MTH2} = peak pressure under the second metatarsal head; PP_{T2} = peak pressure under the second toe, and W = foot width (as measured at the widest point of the forefoot).

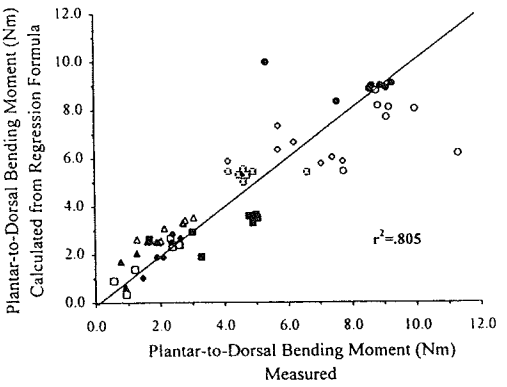

FIGURE 2: Plot comparing experimentally determined and calculated second metatarsal bending moments.

DISCUSSION

Plantar-to-dorsal bending moment in the second metatarsal was highly correlated to plantar pressure under the second ray and width of the foot indicating the potential use of plantar pressure measurements in diagnosing metatarsalgia and stress reactions.

REFERENCES

Patel, V.G. et al. Am J Surg, 167:297-301, 1994.
Perry, J. et al. Gait Analysis, Slack Inc, 1992
Sharkey et al. Trans Orthop Res Soc, 704, 1995

THE BIOMECHANICS OF LONGITUDINAL ARCH SUPPORT MECHANISMS IN FOOT ORTHOSES AND THEIR EFFECT ON PLANTAR APONEUROSIS STRAIN

G.F. Kogler†, S.E. Solomonidis§, J.P. Paul§

† Orthopaedic Bioengineering Research Laboratory,
Southern Illinois University School of Medicine, Springfield, IL, USA 62794-9230.
§ Bioengineering Unit, University of Strathclyde, Glasgow, Scotland, UK.

INTRODUCTION

In this investigation, several types of foot orthoses were evaluated on cadaveric donor limbs to determine the efficacy of their respective longitudinal arch support mechanisms. Strain in the plantar aponeurosis was employed as a performance measure to quantify the integrity of the foot's arch. Orthoses which produced a statistically significant decrease in plantar aponeurosis strain compared to the barefoot control were considered effective as an arch support. Three of the five orthoses studied had efficient longitudinal arch support mechanisms. Two of the orthoses and the test shoe exhibited no arch support properties. The time-to- load data showed statistically significant differences among the various test conditions indicating the relative cushioning properties of the shoe/orthosis systems.

REVIEW AND THEORY

One of the primary mechanisms of a foot orthosis is the longitudinal arch support, hence the origin of its earlier descriptive term 'arch support'. Despite its wide use for the treatment of various foot pathologies, few scientific studies have documented its biomechanical influence on foot function and its effectiveness as a structural support. The diversity of orthotic techniques and designs associated with foot orthoses has led to a degree of uncertainty as to magnitude of control they will provide to the foot.

Morphologically the foot has an arciform appearance when viewed in the sagittal plane. Structurally it is not a true arch since it relies on adjacent soft tissues to maintain its curved posture. The plantar fascia is of fundamental importance to the biomechanics of foot function (Sarrafian, 1987). Much of the load transmitted by the foot is experienced by the plantar fascia (Hicks, 1955). When subjected to a load (body weight) the foot's arch elongates producing a tensile force in the plantar fascia (Wright et al., 1964). Repeated loading of the foot and excessive tension of the plantar fascia has been implicated to be a causal factor for the condition plantar fasciitis, which results in symptomatic heel pain and inflammation (Campbell et al., 1974). The objective of orthotic intervention is to resist depression of the foot's arch during weight bearing through skeletal support, thereby decreasing tension in the plantar aponeurosis. We hypothesized that if strain is alleviated with the longitudinal arch support mechanism of a foot orthosis, a quantifiable reduction in tension of the plantar aponeurosis should be seen via fixation of a strain transducer. The aims of this study were (1) to quantify the longitudinal arch support properties of various foot orthoses, and (2) to explain the fundamental biomechanics of longitudinal arch support mechanisms and the features of their design in terms of their orthotic attributes for skeletal foot control.

PROCEDURES

Seven fresh frozen cadaveric limbs disarticulated at the knee were used in the study. A differential variable reluctance transducer (DVRT) (The Microstrain Co., Burlington, VT.) was surgically implanted into the plantar aponeurosis of cadaveric lower limb feet, through which strain was calculated in each condition. The experiment consisted of seven different conditions: specimen barefoot (t #1), specimen with shoe (t #2), and five tests combining specimen with shoe and foot orthosis; a prefabricated orthosis (t #3), a soft orthosis (t #4), a semi- rigid orthosis (t #5), a rigid orthosis (t #6); and a UC-BL foot orthosis (t #7). The barefoot condition (t #1) was used as a control. Each specimen was instrumented and mounted to a Scott electro-mechanical test machine Model CRE/500 (GCA Precision Scientific, Chicago, IL.). Specimens were preconditioned just prior to testing by cyclical loading. Ten cycles were performed at the selected parameters which consisted of a loading rate of 508 mm/min. and a load application from 0-900 N. Following specimen preconditioning the reference length and 'zero' position of the strain transducer were determined. Initial length was established by positioning the limb in an upright position and using the respective limb mass to produce slight tension in the plantar aponeurosis. This permitted a proportional load for each specimen calibration. Five test runs were conducted with each condition bringing the total number of test runs performed on each specimen to 35. All specimens were subjected to the seven conditions in a varied order utilizing a "Latin testing sequence square." A shoe alignment plate and a mounting fixture assured that limb placement and position would be unchanged as a specimen was prepared for each treatment condition. The voltage output from the transducer and load cell were transferred via amplifier/signal conditioner to a data acquisition board for analog to digital conversion sampled at 750 Hz for a 1.5 second test. As data was sampled it was simultaneously stored on a micro-computer. Time, load, and strain data were collected and analyzed at four load levels (225, 450, 675, 900 N). In addition the measurements and test design were evaluated for reliability.

RESULTS AND DISCUSSION

Three orthoses exhibited exceptional longitudinal arch support properties, the semi-rigid orthosis (t #5), the soft accommodative orthosis (t #4) and the University of California Biomechanics Laboratory (UC-BL) foot orthosis (t #7). Similar results were reported in a pilot study by the authors (Kogler et al., 1995). The findings favor the orthotic principles espoused by Campbell and Inman (1974) which emphasized decreased tension in the plantar aponeurosis for the treatment of plantar fasciitis. In addition to being

statistically significant ($p < 0.05$) from all other tests conducted, they typically generated negative strain values (Figure 1, Table 1). This occurrence exemplifies the resistive properties of the longitudinal arch support mechanisms of these devices, since the measured strains remained lower than the designated zero position of the strain transducer even at the highest load of 900 N. This has important clinical implications when plantar aponeurosis strain reduction is the desired treatment objective. Time-load histories showed that certain orthoses were more effective than others at cushioning the foot during loading (Table 2). This is of interest since delayed loading has also been suggested as a form of treatment for plantar fasciitis by cushioning the foot during weight-bearing (Helal et al., 1988).

The distinguishing features of the orthoses which decreased plantar aponeurosis strain were: surface contours of medial and central regions, the magnitude of their longitudinal curvatures, medial trimline delineation, and negative impression methods. In general, the effective longitudinal arch support mechanisms possessed higher medial profiles and the angles related to their arch shapes were more acute. Trimline delineation complimented this trait by encompassing a greater portion of the foots medial aspect which proportionally increased the surface area of the orthosis. In contrast, the two orthoses which demonstrated poor longitudinal arch support capabilities, the stock orthosis (t #3) and the rigid orthosis (t #6), had relatively planar surface contours with longitudinal curvatures nominal in height and acuteness as compared to their more supportive counterparts (t #4; t #5; t #7). Medial trimline extensions were also less encompassing.

We theorize that to decrease the arch-flattening moment of the foot, the longitudinal arch support mechanism of an orthosis must support the apical bony structures of the foot's arch: the proximal shafts of the metatarsals, cuneiforms, and talus via the navicular and sustentaculum tali of the calcaneus. Orthotic restraint in this region encourages plantar flexion of the metatarsals and calcaneal inversion which together limit and control arch depression. In contrast a longitudinal arch support mechanism that confines support to only distal structures, the distal shaft of the metatarsals and distal portion of the calcaneus, will produce a dorsiflexion moment at the tarsal-metatarsal joint which translates to an arch-flattening effect. This may explain why shallow longitudinal arch support mechanisms did not show any arch support properties and in fact often increased the strain in the plantar aponeurosis relative to the barefoot tests. It is unclear if this occurrence was the result of a 'bowstring' effect to the plantar aponeurosis described by Campbell and Inman (1974) or an arch lengthening response. The presupposition of many clinicians, that an orthosis with a relatively low arch is capable of providing some support to the foot's skeletal structure is refutable with respect to our findings.

REFERENCES

Campbell, J.W. et al. Clin. Orthop., 103,57-62, 1974.
Helal, B. et al. The Foot, 1004, Churchill, Livingstone, 1988.
Hicks, J.H. Acta. Anat., 25:34-45, 1955.
Kogler, G.F. et al. J. Clin. Biomech., in press, 1995.
Sarrafian, S.K. Foot Ankle., 8, 4-18, 1987.
Wright, D.G. et al. J Bone Jt Surg., 46A: 482-492, 1964.

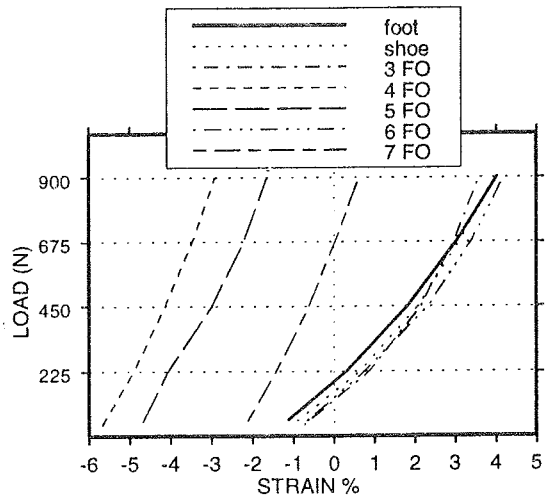

Figure 1. Representative load-strain curves of the plantar aponeurosis of a donor specimen.

Table 1. **STRAIN %**

test	225 N	450 N	675 N	900 N
#3 (FO)	2.88 (2.01)	3.98 (2.18)	4.71 (2.30)	5.29 (2.41)
shoe	2.50 (1.78)	3.66 (1.83)	4.50 (1.89)	5.20 (1.95)
#6 (FO)	2.31 (1.78)	3.51 (1.89)	4.35 (1.98)	5.03 (2.05)
barefoot	1.31 (1.46)	2.62 (1.78)	3.54 (2.02)	4.29 (2.20)
#7 (FO)	-2.64 (2.88)	-2.13 (3.15)	-1.62 (3.34)	-1.16 (3.51)
#4 (FO)	-2.76 (3.53)	-1.56 (3.17)	-0.74 (3.02)	-0.66 (2.96)
#5 (FO)	-3.58 (3.39)	-2.39 (3.28)	-1.59 (3.25)	-0.98 (3.24)

Mean values and (SD) for percent strain. (n=7)
Shaded area indicates foot orthoses (FO) that had efficient longitudinal arch support mechanisms. Their values were statistically different from all other tests ($p<0.05$)

Table 2. **TIME (s)**

test	225 N	450 N	675 N	900 N
foot	0.32 (0.15) d	0.47 (0.17) e	0.55 (0.19) e	0.61 (0.21)e
#7	0.31 (0.11) d	0.49 (0.12)d, e	0.60 (0.13)d	0.69 (0.14)d
shoe	0.33 (0.13) c,d	0.52 (0.15)d	0.63 (0.17)d	0.72 (0.18)d
#3	0.36 (0.15) b, c	0.56 (0.17) c	0.69 (0.19) c	0.80 (0.21)c
#6	0.36 (0.13) b, c	0.58 (0.15) b, c	0.71 (0.18) b, c	0.82 (0.19) b, c
#5	0.40 (0.14) b	0.61 (0.16) b	0.75 (0.18) b	0.87 (0.20)b
#4	0.43 (0.14) a	0.67 (0.16) a	0.82 (0.18)a	0.94 (0.19)a

Mean values and (SD) for time-to-load. (n-7)
Results of Duncan's multiple range test. All grouped values (a,b,c,d,e) were statistically significant from each another ($p<0.05$).

ACKNOWLEDGMENTS

This work was supported by a Central Research Committee Award from Southern Illinois University School of Medicine and by a grant from the Pedorthic Footwear Association Research Foundation.

EFFECT ON TISSUE RESPONSE TO SIZE OF POLYETHYLENE PARTICLES ADJACENT TO UNSTABLE IMPLANTS

J.E. Bechtold[1], K. Søballe[2], J.L. Lewis[3], R.B. Gustilo[1]

[1] HCMC Orthopaedic Biomechanics Laboratory, Minneapolis, MN 55415
[2] Orthopaedic Hospital, University of Aarhus, Aarhus, Denmark
[3] Bioengineering Laboratory, University of Minnesota, Minneapolis, MN 55455

INTRODUCTION

Total joint arthroplasty has improved the function and quality of life for millions of individuals. In the United States alone, over 200,000 hip replacements and 200,000 knee replacements are performed annually (Praemer et al., 1992). Although the success rate for primary joint replacement is good (averaging 95% survival at 10 year follow up), with an increased number of implanted joints, the number of revision joint replacements is also increasing. Twenty thousand revision hip replacements are performed annually in the United States (Pellicci, 1990), and have poorer function than primary surgeries. The 1994 NIH Consensus Development Conference on Total Hip Replacement noted that "outcomes of revision hip surgery are less reliable and satisfactory than those of primary procedures" (NIH Consensus Conference, 1994).

REVIEW AND THEORY

Several comprehensive schema for the initiation and progression of prosthesis loosening have been proposed (Figure 1). An initially stable implant can destabilize as a result of trabecular fracture or due to local bone destruction caused by particulate wear debris. If it does not stabilize, an unstable implant (unstable from the time of surgery, or initially stable but subsequently unstable) will, through bone resorption and fibrous repair, for a bursa. Motion (which can also generate particulate debris and metal ions) then stimulates the bursa to produce bone resorbing factors such as cytokines. This cycle can repeat itself, causing further bone resorption, loosening and pain. Clinical studies have yielded findings that corroborate this view of implant instability and the confounding factor of particulate debris as mechanical initiators of prosthetic loosening.

The term "mechanical instability" refers to relative motion between the implant and the bone. This instability contributes to implant loosening in two ways; through the direct effect of motion on cells, and through its role in increasing production of particulate debris.

Particulate debris may be the direct initiator of the biochemical bone response. Particle size, material, quantity and shape are all important factors in the character of the response. The present study focuses on the effect of particle *size*. Debris smaller than 10-15 μm can be phagocytosed by macrophages, thereby potentiating the release of cytokines. In clinical retrieval studies, larger particles are usually walled off by fibrous tissue or foreign body giant cells.

Retrieved particles from membranes surrounding failed joint replacement implants have shown variable size, ranging from 0.1 μm to 250 μm, with approximately 75% to 90% being less than 1.0 μm (Shanbhag, 1994).

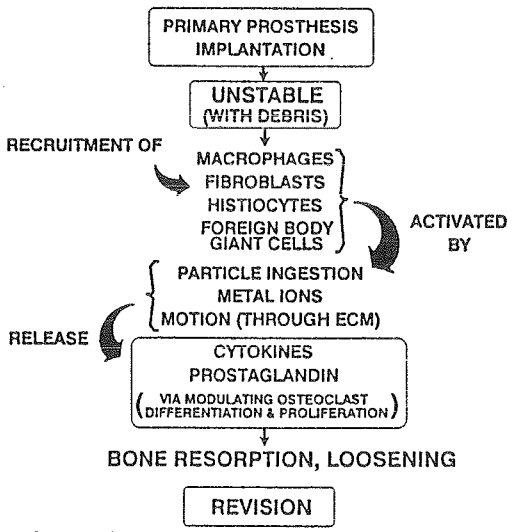

Figure 1: Events leading to aseptic loosening of joint replacement implant

The **hypotheses** examined in this study are: the density of macrophages, histiocytes, synovial-like cells, and foreign body giant cells in the membrane and bone surrounding an unstable implant depend on (1) the presence of, and (2) the size of polyethylene particles.

PROCEDURES

An unstable Søballe implant (Figure 2, Søballe, 1993) was used to represent a loosened human implant. It is a 6.0 mm diameter cylinder which pistons 500 μm in the medial femoral condyle of a dog during each gait cycle. The magnitude and axial direction of motion during weight bearing is carefully controlled via a centralizing bearing. A polyethylene cap on the distal end protrudes above the articular cartilage, and is axially depressed during weight bearing. A loose cemented implant was modeled as a molded

polymethylmethacrylate (PMMA) cylinder threaded on the unstable implant's core.

Figure 2: Unstable implant with controlled motion

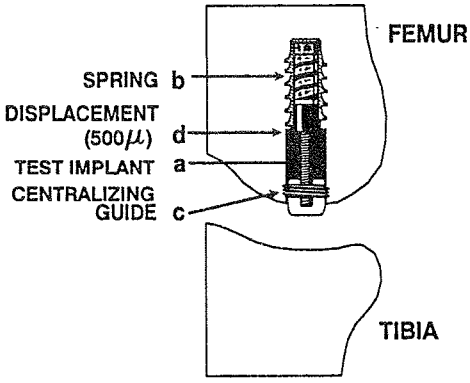

UNSTABLE IMPLANT	HISTIOCYTES/ MACROPHAGES	SYNOVIAL-LIKE LINING	DENSE/LOOSE FIBROUS TISSUE	FOREIGN BODY GIANT CELLS
No Debris	NO	NO	LOOSE	NO
Type A PE Debris	YES	YES	DENSE	NO
Type B PE Debris	YES	YES	DENSE	NO

Table 1: Summary of histologic findings

Twelve mature mongrel dogs were randomized to three treatment groups, all with unstable implants having: (a) no debris, (b) particulate high density polyethylene (PE) (Type A: 4.7 μm mean (.5-12 μm)) and, (c) PE: (Type B: 0.5 - 50 μm; 50% < 1.0 μm; 85% < 10 μm). Eight implants were evaluated per group. The particulate was ultrasonically and manually mixed with hyaluronic acid (LifeCore Biomedical, Chaska, MN) and injected in the implant cavity at a concentration of 0.5×10^8 particles /implant (Lalor et al., 1994). Animals were allowed unlimited cage activity, and were euthanized eight weeks following implantation. The above protocol was approved by our institution's Animal Care Committee prior to commencing the experiments.

RESULTS

Effect of implant motion alone All implants were surrounded by fibrous tissue. Under histologic examination, there was a reparative response with no inflammation. There was no neutrophilic, macrophage/histiocytic or lymphocytic response. New cartilage formation and abundant vascularity was observed. Fibroblasts were mature spindle shaped cells, characteristic of a reparative response.

Effect of implant motion and Type A debris (0.5 - 12 μm): All implants were surrounded by fibrous tissue. Sheets of macrophages and histiocytes were present, often with intracellular PE particles. The membrane had synovial-like cells at the surface interfacing with the implant, and was composed of spindle shaped fibroblasts. PE particles were identified with polarized light and Oil Red O staining, and were seen to remain in the membrane surrounding the implant. PE was also seen in the adjacent bone. No foreign body giant cells were seen. Rare lymphocytes and cartilage formation, and rare osteoclasts were seen.

Effect of implant motion and Type B debris (0.5 - 50 μm): Histologic examination of the interface membrane reveals a very similar picture to that seen with the smaller Type A debris; i.e. dense fibrous tissue with synovial-like cells, and macrophages with intra- and inter-cellular PE. The expected finding of foreign body giant cells in response to larger debris was not seen in the interface membrane, although 15% of the particles were >10μm. Foreign body giant cells were seen in the synovial tissue.

DISCUSSION

The results in this model of a cement-coated implant pistoning 500 μm for eight weeks suggest that motion by itself did not generate an aggressive membrane characteristic of that retrieved from human revisions (Athanasou et al., 1992, Goldring, 1986). The addition of both Types A and B particulate polyethylene to the unstable implant recruited macrophages, histiocytes, synovial cells and osteoclasts. Foreign body giant cells were not seen in the membrane. These results suggest, that in this model of an unstable implant, particulate debris is necessary to generate an aggressive membrane as seen in clinical loosening (in agreement with Hypothesis 1), but within the size range and concentration studied, there is not a size dependent difference in the periprosthetic tissue response (not in agreement with Hypothesis 2). Other factors not studied here, including concentration of particulate, time frame, and shape may play a role in modulating the tissue response.

REFERENCES

Athanasou, N.A. et al., *JBJS* 74(B)1:57,1992.
Goldring, S.R., Arthritis & Rheumat. 29(7):836,1986.
Lalor P.A. et al., *Trans. 40th ORS,* 19:845, 1994.
NIH Consensus Development Conference on Total Hip Replacement, Bethesda, MD, September 1994.
Pellicci P.M. *Surgery of the Musculoskeletal System* (p 383), Churchill Livingstone, 1990.
Praemer, M.A. et al.: *Musculoskeletal Conditions in the United States*, American Academy of Orthopaedic Surgeons, 1992. Shanbhag A.S. et al., *JBJS* 76B(1):60, 1994.
Søballe, K. *Acta. Orthop. Scand.* 64 (Supplement 225), 1993.

ACKNOWLEDGEMENTS

Aided by grants from the Orthopaedic Research and Education Foundation, and the Biomedical Interfacial Engineering Program of the NSF Center for Interfacial Engineering at the University of Minnesota.

IN VITRO STABILITY OF THE HIP AFTER SIMULATED TRANSVERSE ACETABULAR FRACTURES

Mark S. Vrahas, Kevin A. Thomas, John W. Noble, J. Spence Reid,
Christopher M. Bearden, and Miguel Guzman,
Louisiana State University Medical Center, Department of Orthopaedic Surgery,
2025 Gravier Street, Suite 400, New Orleans LA 70112

INTRODUCTION

One of the primary considerations in determining whether an acetabular fracture should be managed operatively or non-operatively is the relationship of the fracture to the weight-bearing portion of the acetabulum. To address this problem, a method was developed to measure hip stability after simulated transverse acetabular fractures.

REVIEW AND THEORY

Unreduced fractures involving the weight-bearing portion of the acetabulum lead to post-traumatic arthritis, while fractures outside this area portend a better prognosis. Little previous work has carefully examined hip joint stability following either actual or simulated acetabular fractures. None of the numerous clinical studies examining hip fracture dislocations clearly define what is meant by stability or quantify the amount of acetabulum necessary to maintain stability.

The purpose of this study was to distinguish fractures that require operative reduction from those that can be treated with traction and those which require even less aggressive measures to prevent post-traumatic arthritis.

PROCEDURES

An *in vitro* model simulating transverse acetabular fractures was developed utilizing cadaveric pelves and proximal femora. Nine human cadaveric pelves were harvested, radiographically examined and stripped of all soft tissues prior to testing. There were no significant abnormalities noted by radiographic or visual inspection of the specimens. A full complement of data was obtained from nine specimens (consisting of an acetabulum and proximal femur).

For testing each specimen was mounted in a servo-hydraulic mechanical testing machine. Each femur was potted in a cylindrical fixture, mounted onto an instrumented x-y displacement table, and secured to the load cell of a mechanical testing machine (858 Bionix, MTS, Minneapolis MN). Each acetabulum was potted and mounted to the test machine actuator using an articulated fixture which allowed accurate positioning of the specimens to simulate various degrees of hip flexion, extension, abduction, and adduction.

Prior to potting two Steinmann pins were inserted into the acetabulum to provide a standard reference to the sagittal, coronal and transverse planes. During all preparation and tests the articular cartilage was kept moist by frequent misting with physiologic saline.

Each specimen was first evaluated with the acetabulum intact. The specimen was loaded in multiple positions simulating hip flexion from 0° to 80° with either 0°, 10°, or -10° of adduction. After application of a 50 N preload, the specimens were loaded in compression to 800 N (at 200 N/sec in load control for three cycles). Simultaneous recordings were made of the load, displacement, and x-y translation of the femur. The specimen was then loaded a fourth time at each position with pressure sensitive film inserted to evaluate intra-articular stresses.

A custom guide was then used to make an osteotomy simulating a transverse acetabular fracture at a roof arc angle of 90°. The loadings were repeated at all positions, with displacements carefully monitored to determine if the osteotomy had made the hip unstable. The entire process was repeated with simulated fractures at roof arc angles of 60°, 30° and 0°.

For statistical analysis a score was computed weighting the stability by the angle of flexion:

Stability Score = flexion weight X stability

where *flexion weight* = 1 for 0° flexion, 2 for 20°, 4 for 40°, 6 for 60°, and 8 for 80°, and *stability* = 1 for a stable hip, 0 for an unstable hip. The stability scores were computed separately for each specimen at each roof-arc angle and each ab/adduction angle. The scores were analyzed using the Wilcoxon rank sum test.

RESULTS

In all test positions, the specimens were consistently observed to be either stable or unstable during loading. Peak loads for the unstable conditions were generally less than 400 N.

The results are summarized in the graph below, which shows the range of flexion over which the specimen remained stable. With the acetabula intact the specimens remained stable when loaded with the hip flexed from 0° to 60°, but dislocated when the hip was flexed to 80°. For simulated fractures with a 90° roof arc angle the specimens were again stable with the hip flexed 0° to 60°, but dislocated when the hip was flexed to 80°. With 60° roof arc fractures the specimens were stable only at hip flexion of 0° to 40°. For the 30° roof arc fractures the specimens were stable with the hip flexed from 0° to 40° degrees, but dislocated at very low loads for flexion beyond this. For the 0° roof arc fractures the specimens were unstable at all position of flexion/adduction.

Analysis of the stability scores demonstrated that stability was not affected by ab/adduction angle alone, but was significantly affected by the roof-arc angle, and by the interaction of roof-arc angle and ab/adduction angle (Wilcoxon rank sum test, $p < 0.05$)

DISCUSSION

Our results suggest that transverse fractures with a roof arc angle of 90° do not affect the weight bearing portion of the acetabulum. However, fractures with a roof arc angle of 60° begin to infringe on the weight bearing area, and fractures with roof arc angles less than 30° are clearly in the weight-bearing region.

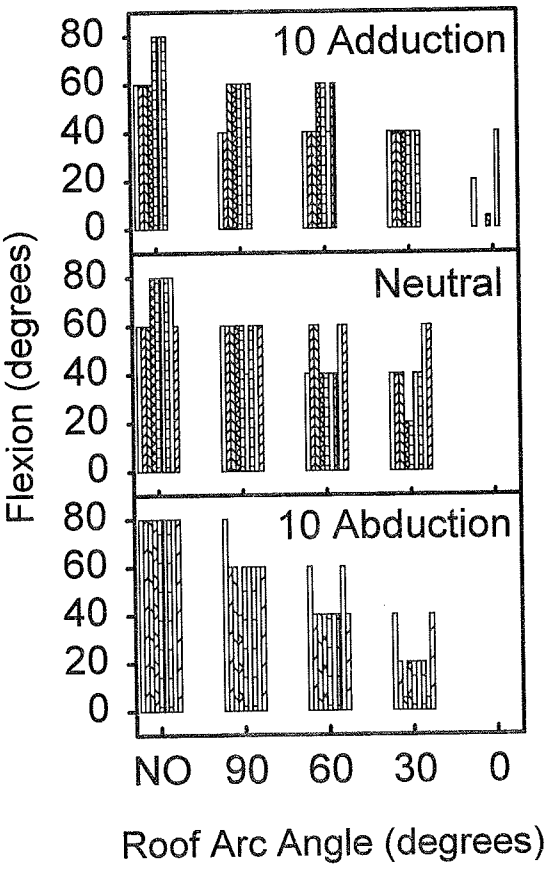

Plot showing the range of stability after simulated transverse acetabular fractures. NO = intact acetabulum; n=9 specimens.

THE INFLUENCE OF POST-OPERATIVE FOLLOW-UP TIME ON "EARLY" PREDICTION OF LONG-TERM WEAR RATE IN TOTAL HIP ARTHROPLASTY

S.M. Shaver, T.D. Brown, J.J. Callaghan

Department of Orthopaedic Surgery, The University of Iowa, Iowa City, IA 52242

INTRODUCTION

Polyethylene wear is a major factor affecting the longevity of total hip arthroplasty [4]. The ability to accurately make early wear measurements and then confidently predict long-term wear, based on these measurements, would give early insight into long-term behavior. Inaccuracies of most techniques effectively prohibit application to early or small wear cases [1-3], and therefore, a digital edge detection computer algorithm was developed to estimate early polyethylene wear in total hip arthroplasty. In comparison to previous wear methods, the automated technique substantially reduces observer subjectivity by evaluating intensity gradients in digitized radiographic images and objectively inferring the components' margins. Application of the new measurement method was demonstrated by measuring wear in a series of 18 patients and then constructing regression models between follow-up and long-term wear rates. Results show follow-up wear rates generally predict long-term rates, with the models becoming more precise at later follow-up times.

REVIEW AND THEORY

Since only anteroposterior films exist for most long-term patient series, techniques relying on more advanced modalities (e.g., computed tomography scans, Roentgen stereophotogrammetric analysis) cannot be used in a retrospective manner. In addition, it is not common practice to use these time and labor intensive techniques prospectively on large cohorts of patients. For these reasons, we developed and a new digital image analysis method [5] to measure wear in archived radiographs. Using a numerical method gradient operator, the technique estimates the elliptical shadows of the femoral head and cup backing on digitized images, and computes the separation distance between the ellipses. (Ellipses - rather than circles - are fitted since the spherical components cast elliptical shadows whenever the beam source lies in the mid-sagittal plane.) Changes in the ellipse separation distance on each follow-up image, as compared to the post-operative image, represent the linear wear. Linear wear rates are calculated by dividing each linear wear measurement by the follow-up time. The technique was validated by proving capable of estimating both small and large magnitudes of polyethylene wear [5]. With this reliable tool, the predictability of long-term wear is evaluated, based on corresponding follow-up wear measurements.

PROCEDURES

Eighteen patients were selected for wear evaluation, each having components consisting of a Ti-BAC (titanium backed, cemented) acetabular system, articulating with a 28 mm diameter chrome cobalt femoral head (Iowa total hip system, Zimmer, Inc., Warsaw, IN). An antero-posterior pelvic post-operative radiograph and periodic follow-up films were available for each patient, all having been obtained in the same suite, with the same radiographic machine, and with a standardized pelvic positioning procedure. The post-operative film and serial radiographs closest to 2-(short-term), 6-(intermediate-term), and 10-(long-term) years follow-up were digitized as two-dimensional gray scale arrays of 8-bit (256 gray levels) integers using a QCS-1260 flatbed imaging scanner (Imapro Corp., Ottawa, Canada). The images were rendered on a CRT screen of a 4000-60 VAXStation workstation (Digital Equip. Corp., Maynard, MA).

A linear regression model was constructed between the linear wear rate measured on each patient's earliest follow-up film (~2yrs) and the linear wear rate measured on each patient's most recent film (~10yrs). The coefficient of determination (R^2) and regression confidence intervals (95%) also were calculated. Three additional models were developed with the constraint that the follow-up time must exceed a varying threshold. For those patients whose earliest follow-up film existed prior to this time threshold, the follow-up data points were substituted by follow-up data points from a succeeding film (~6yrs). The thresholds were chosen such that the first regression model contained only 2 yr data (no substitutions) and the last regression model contained only 6 yr data (all substitutions).

RESULTS AND DISCUSSION

The short-term follow-up period ranged from 17 to 37 months (mean, 25 months), the intermediate-term follow-up period ranged from 46 to 115 months (mean, 76 months), and the long-term follow-up period ranged from 110 to 139 months (mean, 122 months).

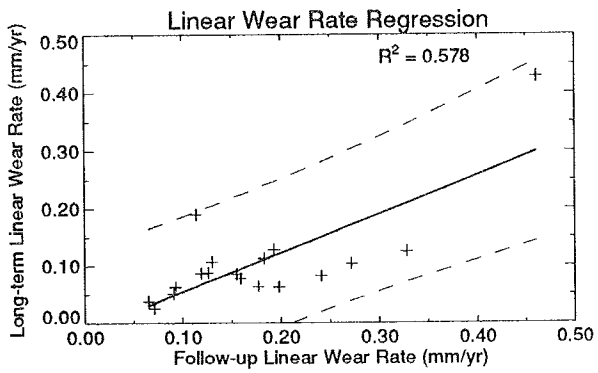

a) minimum follow-up, 17 months
average follow-up, 25.8 months

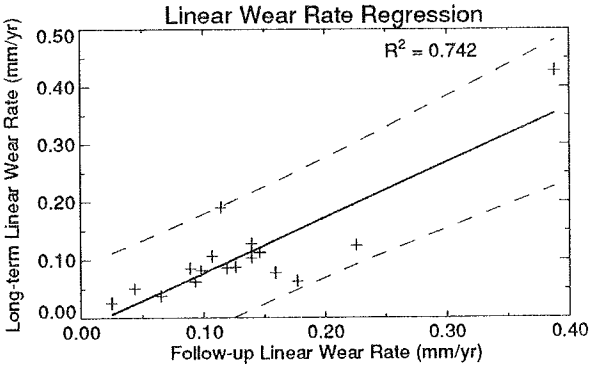

b) minimum follow-up, 25 months
average follow-up, 59.2 months

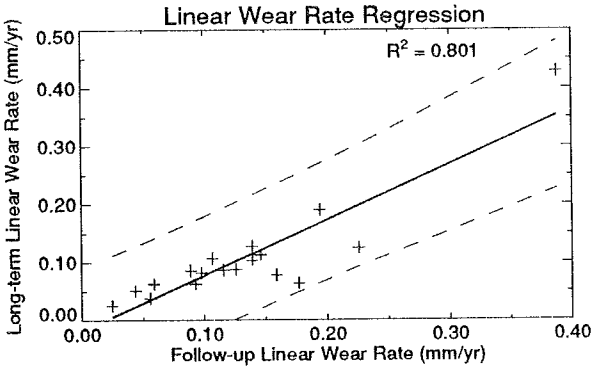

c) minimum follow-up, 35 months
average follow-up, 70.0 months

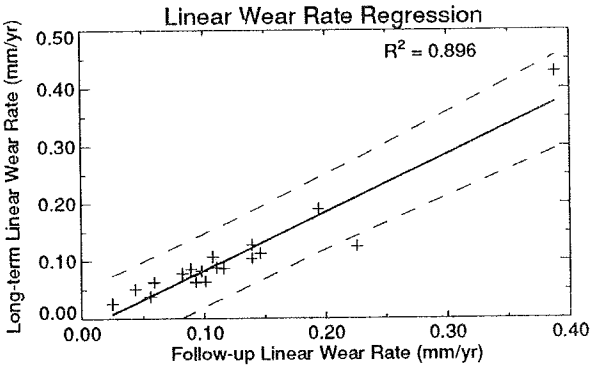

d) minimum follow-up, 46 months
average follow-up, 75.6 months

Figure 1a-d: Regression models for early wear rates at various follow-up times versus corresponding long-term wear rates. Sample regression lines (—) and 95% confidence intervals (---) are shown for each model.

The short-term linear wear rate averaged 0.170 mm/yr (range, 0.065 to 0.461 mm; standard deviation, 0.094 mm), the intermediate-term linear wear rate averaged 0.123 mm/yr (range, 0.025 to 0.388 mm; standard deviation, 0.083 mm), and the long-term linear wear rate averaged 0.103 mm/yr (range, 0.014 to 0.428 mm; standard deviation, 0.083 mm).

The four linear regression models are shown in Figure 1a-d. The (+) symbols represent corresponding follow-up and long-term linear wear rates, the solid line is the sample regression line, and the dashed lines are the confidence intervals. The coefficients of determination increase as the average follow-up measurement times approach the average long-term measurement time, indicating that wear data taken closer in time to the long-term wear data greater predict those long-term values. The confidence intervals generally decrease in width with increasing R^2 values, and exhibit a characteristic minimum width at the average follow-up wear rate.

In general, long-term wear rates can be predicted on the basis of earlier follow-up wear rates. Long-term predictability might have increased by using non-linear regression, or by multi-variable regression to simultaneously incorporate both follow-up wear measurements. These results obviously are influenced by the non-uniform distribution of the follow-up wear rates and the small sample size, as occasional outlier data points greatly influence the precision of the confidence intervals. Yet, early identification of high wear rate outliers are of primary interest, as precautions may be taken to reduce the long-term rate of polyethylene wear in such cases.

REFERENCES

1. Charnley, J. et al., Clin. Ortho., 95:9-26, 1973.
2. Devane, P.A. et al., M.S. Thesis, U. of W. Ontario
3. Livermore, J. et al., JBJS, 72A(4):518-528, 1990.
4. Schmalzried, T.P. et al. Clin. Ortho., 274:60-78, 1992.
5. Shaver, S.M., M.S. Thesis, U. of Iowa

ACKNOWLEDGMENTS

Financial assistance provided by De Puy, Inc., and by NIH Grant #AR43314.

FEMORAL SURFACE STRAIN ANALYSIS: A COMPARISON BETWEEN A CUP ARTHROPLASTY AND CONVENTIONAL LONG-STEM PROSTHESES

S.J. Hazelwood, J.J. Rodrigo, N.A. Sharkey, K. Raiszadeh
Orthopaedic Research Laboratory
University of California, Davis

INTRODUCTION

The destructive effects of stress shielding in the proximal femur following hip replacement surgery have been the subject of much research in recent years. It is desirable to predict how much stress shielding occurs for certain types of implants to determine which will produce the least amount. This was accomplished in this study by a strain gage analysis, which was used to determine the femoral surface strain distribution on normal, intact femurs and those implanted with a surface arthroplasty or conventional long-stem prostheses. A statistical analysis was then performed to determine which femur-implant configuration produced a strain distribution more similar to the intact femur.

REVIEW AND THEORY

It is recognized that the transmission of load from the implant to the bone is one of the most important factors in determining the longevity of femoral prostheses (Huiskes, 1990). Bone resorption of the proximal femur, believed to be the normal remodeling response due to the shielding of bone from stress by the femoral component, has been attributed as the major cause of several long-term failures of the implant and surrounding bone (Bobyn et al., 1992). This is particularly a problem for younger hip implant recipients, who tend to be more active and need an implant which lasts longer than normal. With the recent increase in the number of young patients receiving hip implants, an interest has been rekindled among several orthopaedists to return to the femoral "cup" type of arthroplasty, whose design is such that bone resorption due to stress shielding may be prevented. Specifically, the design simulates the actual femur head size and preserves a majority of the original bone stock, which will theoretically approximate the normal transmission of stresses to the bone. To quantitatively determine which femur-implant construct produces a more natural strain distribution of the femur, a femoral surface strain analysis was performed comparing a cup arthroplasty with both a cemented and a cementless conventional long-stem prosthesis.

PROCEDURES

Freshly harvested human cadaveric femurs (donor age range: 35-70 years) were stored at -4°C until use. The distal ends of each were removed and their shafts were potted in a polymethylmethacrylate base for fixation into an Instron 1122 universal material testing machine. Axial strain gages were bonded longitudinally to each femur surface at five locations: medially on the neck, medially and laterally on the proximal femur shaft in the trochanteric region (P/M and P/L respectively), and medially and laterally on the distal femur shaft (D/M and D/L respectively). The femurs were mounted into the Instron in a 10° varus position, simulating the single leg stance phase of gait. Compressive loads were exerted on the head of the femur (at a load rate of 2mm/min) to 2000N, and strains were recorded at 10N increments.

Strain levels of the intact femurs were measured to provide baseline values. Strain measurements were again performed after resurfacing the head of the femurs with TARA trial prostheses implanted both with (n=24) and without the stem (n=23). Finally, long-stem prostheses were either cemented (n=10) or press-fit (n=10) into place, and the strain levels were again recorded. Implanting the long-stem prostheses necessitated elimination of the neck strain gage. A comparison was then made between each configuration at each gage location using analysis of variance

($p<0.05$ significant). When significant, a follow-up *t*-test determined which variable was statistically different.

RESULTS

Figure 1 provides mean strain results at each gage location for each configuration tested at a load of 2000N. Strains are presented as a percent of the intact femoral strain for purposes of clarity. Error bars were determined from one standard deviation. For the three proximal gage locations (neck, P/M, and P/L) there were no significant differences in strain measurements made with the intact femurs or either cup configuration. Intact strain results, which provided the baseline values, are represented on the graph by the line at 100%. The strain gage measurements

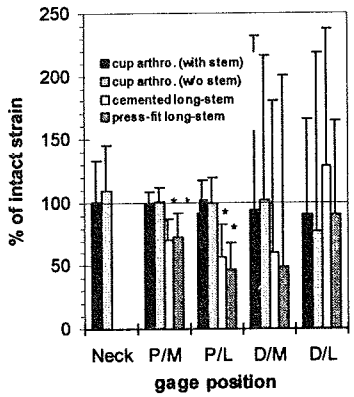

Figure 1. Axial strain distribution on femur surface for 2000N load

made with the conventional long-stem implants, on the other hand, decreased significantly at both the P/M (cemented: 70.9% ± 17.1%, $p=0.0001$; press-fit: 72.6% ± 19.1%, $p=0.0032$) and P/L (cemented: 57.7% ± 24.8%, $p<0.0001$; press-fit: 47.4% ± 20.6%, $p<0.0001$) locations.

The strain measurements at the D/M and D/L gage locations were statistically similar for all configurations tested, primarily due to the rather large variation in values. This was thought to be a result of the relatively small distal strain measurements (up to 20 times smaller than corresponding proximal strains); causing these values to be more sensitive to the testing procedure.

Statistically similar results were also obtained for the strain measurements of a given implant as a function of load, thus this graph is representative of the results for the other loads at which data were collected.

DISCUSSION

The trial femoral prosthesis of the cup arthroplasty procedure, with or without the stem, provided a strain distribution more similar to the intact femur than either conventional long-stem prosthesis. This was particularly true at the proximal femur, where strain values for the long-stem prostheses were significantly below the intact results. Though cup arthroplasties cannot be used in all situations (bone of good quality must remain after the femoral head has been resurfaced for the implants to be supported), this study shows that they should be considered a viable option in certain cases for younger patients because they preserve more bone stock at the time of surgery and, by providing more natural loading to the femur, may be expected to prevent bone loss as a result of stress shielding.

REFERENCES

Huiskes, R. *Clin Orthop.*, 261: 27-38, 1990.
Bobyn, J.D. et al. *Clin Orthop.*, 274: 79-96, 1992.

BIOMECHANICAL FEATURES OF THE ORGANIZATION OF HIGHLY SKILLED LOCOMOTOR MOVEMENTS

B. I. Prilutsky
Biomechanics Laboratory, Central Institute of Physical Culture, Moscow, Russia 105483
Current address: Human Performance Laboratory, Faculty of Physical Education, The University of Calgary, Alberta, Canada T2N1N4

INTRODUCTION

Assuming after Bernstein (1947) that highly skilled movements are performed with the minimum necessary muscle activity, biomechanical features of the organization of highly skilled movements were derived from the formulation of an optimization problem and optimization criteria typically used in the literature to predict muscle forces. These features were: 1) activity of antagonistic muscles are the minimal necessary to provide a given movement; 2) the phases of movements where a high net moment at a joint should be produced are characterized by longer muscle moment arms about this joint; 3) the phases of movements where high muscle forces should be produced are characterized by high instantaneous contractile conditions of the muscles; 4) the external and passive joint forces are used (i) to move segments of the body in the desired direction without muscle activity, where possible, and/or (ii) to increase muscle force and power per unit of muscle activity; 5) activity of multi-joint muscles is organized in such a way that the total muscle force (and, possibly, activity) is decreased. In this study, the above features of the movement organization were experimentally sought and found in human walking, running, and jumping.

REVIEW AND THEORY

The principles underlying the organization of highly skilled multi-joint movements are not well understood. In particular, it is not clear why certain patterns of joint angles and muscle forces are chosen by the central nervous system (CNS) from an unlimited number of possible patterns to perform a given motor task. Bernstein (1947) suggested that completely acquired motor skills are performed with the minimum necessary muscle activity. This hypothesis may explain why skilled movements are performed in the certain way. The results of muscle force predictions in human skilled movements using the minimization of the total muscle force, muscle stress, or mechanical work done by the muscles support Bernstein's hypothesis. The predicted optimal muscle forces are typically in a qualitative agreement with activity patterns of the corresponding muscles (Davy and Audu, 1987; Prilutsky and Raitsin, 1993). Assume that the patterns of muscle forces satisfy one of the above optimization criteria; that is, the muscle forces are approximately the minimum necessary to provide a given skilled movement. Then the organization of this movement should have certain features which can be derived from the analysis of the optimization problem formulation, the optimization criterion, and the design and properties of the musculoskeletal system. These features can be sought experimentally in highly skilled movements in order to support or reject Bernstein's hypothesis that completely acquired skills are characterized by the minimum necessary muscle activity. The aim of this study was to analyze how skilled locomotor movements are organized mechanically, or which (and how) features of these movements may provide economy of muscle activity.

PROCEDURES

Five features of the organization of highly skilled movements were derived from the analysis of the optimization problem formulation (Prilutsky and Raitsin, 1993), the optimization criterion (the minimum sum of muscle forces), and the design and properties of the musculoskeletal system. These features are listed in INTRODUCTION. In order to check if these features occur in human locomotion, a series of experiments was conducted.

Recording of the electrical muscle activity. Ten subjects took part in the experiments. Electrical muscle activity was recorded by surface bipolar silver electrodes 8 mm in diameter at a sampling frequency of 2000 Hz. Eight muscles of the right lower limb were studied. The electrical activity was recorded during walking and running on a treadmill operated at different constant speeds. The EMGs were rectified and integrated every 40 ms. Discrete IEMG values were connected by an interpolation spline function from which IEMG values for each percent of the walking cycle were determined. The IEMG amplitude of each muscle was normalized to its maximum level in a single cycle of locomotion. For each percent of the cycle, the average IEMG and its standard deviation over all cycles available for all subjects were calculated. A total of 20 walking and running cycles were processed.

Determination of mechanical characteristics of locomotion. A total of five subjects participated in the second series of experiments. Three of them walked and ran at different constant speeds on a special wooden rostrum 40 m in length. In the middle of this rostrum, two force platforms were embedded. Two subjects, high-performance athletes, performed their maximal running long jumps (up to 7.0 m). A built-in force platform was fixed within the area of take-off. The force platforms were used to record the three components of the resultant vector of the ground reaction forces, and coordinates of its point of application. The bilateral stereophotogrammetric filming was used for the registration of kinematics (for details see Prilutsky and Zatsiorsky 1994). Twenty one reflective markers attached to the main joints of the subject's body were flashed by stroboscopes operated at 100-150 Hz. Traces of the markers were exposed onto photoplates of four photogrammetric cameras. Coordinates of the body markers were digitized with a precision of 1 μm using a stereocomparator. A 16-link, 3D model of the human musculoskeletal system and the software HUMMOT (Prilutsky, 1993) were used for computation of kinematic, dynamic, and energetic characteristics of locomotion. The model allows for estimation of individual muscle forces from the net moments at joints using two different approaches: an elimination of redundancy approach (Prilutsky and Zatsiorsky, 1994), and an optimization approach (Prilutsky and Raitsin, 1993). Mass and moments of inertia of the subjects' body segments necessary for calculations were obtained from anthropometric measurements of the subjects using the empirical regression equations (Zatsiorsky and Seluyanov, 1985). Muscle moment arms and changes in muscle lengths were calculated from the joint angles using the empirical regression equations (Aruin et al. 1988). Cross-sectional areas of the muscles were estimated from Pierrynowski (1982).

RESULTS AND DISCUSSION

Activity of antagonistic muscles. Fig. 1 shows the averaged IEMG and its standard deviation for two pairs of antagonistic muscles -- hamstrings and rectus femoris, and soleus and tibialis anterior -- during a walking cycle. It can be seen that the antagonistic muscles are typically not active simultaneously. A low activity of the antagonists allows the agonists to produce the desired joint moments with less activity.

The use of muscle moment arms. Fig. 2 shows the net moment at the knee joint of the support leg and the moment arms of m. quadriceps at the knee joint of the support and swing legs, respectively, during the support phase of the running long jump. During the support

phase where the large extensor moment occurred, the moment arm of the knee extensor muscles was typically longer in the support leg than in the swing leg. Similar results were obtained in walking and running. The larger moment arms allow the muscles to produce the desired moments with less activity.

The use of muscle contractile conditions. Fig. 3 shows estimates of the instantaneous muscle force as a function of the instantaneous muscle length and velocity of m. gastrocnemius medialis during the support phase in running. High muscle forces occurred at a longer muscle length and at a rate of muscle length change close to zero. Taking into account that the ability of a muscle to produce force increases with increasing muscle length up to the optimal length (Blix, 1891) and with decreasing the muscle shortening velocity (Hill, 1938), and assuming that the muscles function on the ascending limb and plateau of the force-length relationship (Zajac, 1989), one may conclude that the observed instantaneous force-length and force-velocity relationships during locomotion allow the muscles to produce the required force with less activity.

The use of external forces. During the early stance phase in running and the long jump, powers of the net moments at the leg joints were typically negative. The active leg extensor muscles were stretched by the ground reaction force. This stretch might allow the knee extensor muscles to produce extremely high positive power during the subsequent shortening in the long jump (10.780 kW), which is many times higher than the maximum power produced by the knee extensor muscles during isokinetic knee extension without a pre-stretch. In running, the preliminary muscle stretch may be a reason for a high economy of running (Cavagna et al., 1964). Thus, it may be suggested that the effective use of the ground reaction force during locomotion increases power output of the muscles per unit of their activity.

The use of inertial forces. During the second half of the swing in walking, running, and the long jump, the knee joint is extended without any moment produced or positive work done by the knee extensor muscles. The extension of the knee is caused by the hip extensor muscles which contracting eccentrically decelerate the thigh that causes the knee extension. Taking into account that producing force during the eccentric contraction requires less muscle activity than during concentric contraction (Bigland and Lippold, 1954), it may be suggested that the observed organization of movement of the swing leg allows muscles to reduce their activity.

The use of two-joint muscles. During walking and running, there are phases where the flexion and extension moments at the adjacent joints should be produces simultaneously. For example, in the second half of the stance phase of walking and running, the hip moment tends to flex the hip, and the knee moment tends to extend the knee; in the second half of the swing phase of walking and running, the hip moment tends to extend the hip, and the knee moment tends to flex the knee. These combinations of joint moments are efficiently produced with the participation of two-joint m. rectus femoris (Fig. 1, second half of stance) and m. hamstrings (Fig. 1, second half of swing) which produce the desired joint moments with less total force of all muscles crossing these joints. Thus, the features of the movement organization derived from the optimization problem formulation were found experimentally in highly skilled locomotor movements. This result supports Bernstein's hypothesis that completely acquired motor skills are performed with the minimum necessary muscle activity.

REFERENCES

Aruin et al. Arch. Anat. Histol. Embriol., 94, 52-55, 1988.
Bernstein, N.A. On construction of movements. (In Russian), 1947.
Bigland, B., Lippold, O.C.J. J. Physiol., 123, 214-224, 1954.
Blix, M. Scand Arch Physiol., 3, 295-318, 1891.
Cavagna, G.A. et al. J. Appl. Physiol., 19, 249-256, 1964.
Davy, D.T., Audu, M.L. J. Biomech., 20, 187-201, 1987.
Hill, A.V. Proc. R. Soc. Lond. Biol., 126, 136-195, 1938.
Pierrynowski, M.R. Ph.D. Thesis. Simon Fraser University, 1982.
Prilutsky, B.I., Raitsin, L.M. (1993) Proc. ASB, (119-120), 1993.
Prilutsky, B.I., Zatsiorsky, V.M. J. Biomech., 27, 25-34, 1994.
Prilutsky, B.I. Proc. ISB, (1076-1077), Paris, 1993.
Zajac, F.E. Crit.Rev.Biomed Eng., (359-411),CRC Press, Inc., 1989.
Zatsiorsky, V., Seluyanov, V. Biomechanics IXB, (233-239), 1985.

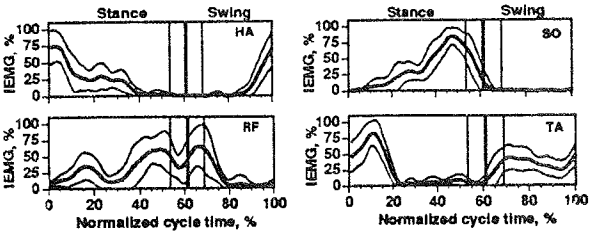

Figure 1: Normalized IEMG of two pairs of antagonistic muscles -- hamstrings (HA) and rectus femoris (RF), and soleus (SO) and tibialis anterior (TA) -- as a function of the normalized cycle time during walking. Thick lines represent the average values of ten subjects; thin lines represent the standard deviation. The vertical lines separate the stance and swing phases. The nominal speed of walking was 1.82 m/s.

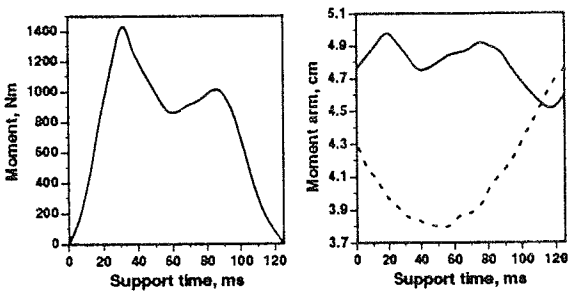

Figure 2: The net moment at the knee joint and the moment arm of the knee extensor muscles (quadriceps) during the support phase of the running long jump. The solid and dashed lines represent the moment arm in the support and swing leg, respectively. Positive moment corresponds to extension at the knee. The result of the long jump was 7 m.

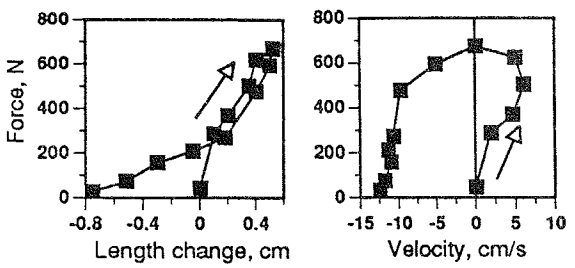

Figure 3: The force of m. gastrocnemius medialis as a function of muscle length change (left) and the rate of muscle length change (right) during the stance phase of running. The arrows show the direction of force, length, and rate changes. The positive rate of length change corresponds to muscle elongation.

THE EFFECT OF EXTREME WALKING SPEEDS ON NET KNEE JOINT MOMENTS

John P. Holden[1], Gloria Chou[1], Steven J. Stanhope[2]
[1]National Institute of Arthritis and Musculoskeletal and Skin Diseases
[2]Rehabilitation Medicine Department, Clinical Center
Biomechanics Lab, National Institutes of Health, Bethesda MD 20892-1604

INTRODUCTION

Neuromuscular function and adaptation are often evaluated by comparing a patient's kinematic and kinetic gait patterns with those obtained from healthy individuals. A feature of many patients' gait, however, is a much slower than normal walking speed which affects many other gait variables. It is important when interpreting a patient's gait data to distinguish which variations from normal are due solely to differences in walking speed and which are due to neuromuscular abnormalities or adaptations other than speed. The current study examined the effects of dramatically different walking speeds on the net flexion-extension moment patterns at the knee during walking by healthy adults.

REVIEW AND THEORY

The effect of walking speed on net moment patterns at the knee is not entirely clear. Winter (1991) reported that, despite high inter-subject variability, the shape of average knee moment patterns remains essentially the same at slow, natural, and fast cadences, with moment amplitudes decreasing as cadence decreases. Andriacchi et al. (1985) identified three different patterns of normal knee moments, and the frequency of occurrence of each pattern depended on walking speed (slow, normal, fast). As speed decreased, there was an increase in the percentage of subjects with a net internal flexor moment present throughout early and mid stance phase. This pattern was similar to the "quadriceps avoidance" gait that Berchuck et al. (1990) later reported for 75% of the ACL-deficient patients they studied. The mechanism of this "quadriceps avoidance" adaptation remains uncertain because the walking speeds of the subjects and patients were not reported.

The purpose of the current study was to examine net flexion-extension moment patterns at the knee to determine if a "quadriceps avoidance" gait can be demonstrated by healthy subjects walking at slower speeds. It was hypothesized that two different modes of walking exist, i.e., that there is a walking mode at slow speeds which requires net knee flexor moments rather than extensor moments in early to mid stance phase.

PROCEDURES

Data were collected from 18 healthy subjects (9 male, 9 female) who walked barefoot at 25%, 50%, 75%, 100%, and 125% of a normalized speed of 0.785 statures/s (± 2.5%). The means (and range) of the subjects' age, height, and body mass were 28.8 yrs (21-37), 1.719 m (1.549-1.848), and 68.5 kg (48.2-96.5), respectively. During data collection, speed was measured over a 2.28 m distance using two photocells (at head height) and a gait speed indicator circuit, which was used to provide feedback to the subjects and to determine if the speed for a given walk fell within the required range. The calibrated data collection volume extended 2.08 m in the direction of progression and was 1.00 m high and .61 m wide. A four-camera, 50 Hz video-based system was used to measure the 3-D locations of reflective targets mounted on polyform shells on the foot, shank, and thigh of the right lower limb. A static subject calibration trial employing landmark targets and two additional cameras was used to create anatomically-based, orthogonal coordinate systems for each segment. A force plate sampled at 200 Hz measured the ground reaction forces and moments. Low-pass digital filtering was applied to target trajectories at 6 Hz and to force plate data at 15 Hz. The six degree-of-freedom motions of the body segments were estimated using a least squares technique, and inverse dynamics analysis was performed to calculate net knee joint moments (reported relative to the thigh coordinate system) throughout the stance phase (defined by 20 N of vertical loading on the force plate) for three trials by each subject at each speed. For inter-subject comparisons, moments were normalized to percent of body weight times height.

RESULTS

Two-thirds of individual subjects had knee flexion-extension moment patterns that were similar across all five walking speeds, with no evidence of a

distinctly different mode of walking (Fig. 1a). One-third of the subjects, however, did demonstrate a quadriceps avoidance strategy (net flexor moment or zero moment) in at least one trial at the slowest speed (Fig. 1b). On average, peak knee extensor moments during early to mid stance phase decreased progressively from 6.7 at the fastest speed to 1.2 at the slowest. (Compare with -1.3 reported by Berchuck et al. for ACL patients utilizing "quadriceps avoidance".) Decreased moment amplitude was related to decreased knee flexion during the "loading response" phase in early to mid stance. Absence of knee flexion during this period produced the quadriceps avoidance pattern at the slowest speed (Fig. 2).

DISCUSSION

Averaged across subjects, knee moment patterns were similar in shape across a wide range of speeds (consistent with Winter, 1991). For several individuals, however, a quadriceps avoidance strategy was demonstrated at the slowest walking speed. In these trials, the subject used a different mode of walking in which the knee was maintained near full extension throughout the early and mid stance phase. This finding for net knee moments is consistent with Andriacchi et al. (1985), who reported a quadriceps avoidance pattern in 27% of their 29 healthy subjects walking at slow speeds. The use of such an adaptation, and the speed at which it is implemented, may depend on a variety of factors that are affected by specific injuries or pathologies. Similar kinds of adaptations may also occur at the other joints in the lower limb.

REFERENCES

Andriacchi, T.P., et al. *Biomechanics of Normal and Pathological Human Articulating Joints*, (pp. 83-102), 1985.

Berchuck, M., et al. *J. Bone Joint Surg.*, 72-A, 871-877, 1990.

Winter, D. A. *The Biomechanics and Motor Control of Human Gait: Normal, Elderly, and Pathological*, (pp. 41-43), University of Waterloo Press, 1991.

ACKNOWLEDGMENTS

The authors wish to acknowledge the assistance of the staff of the NIH Biomechanics Lab.

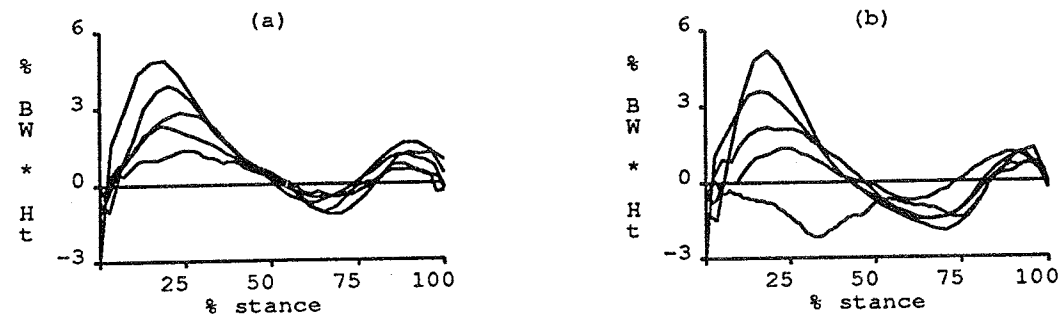

Figure 1: Individual trials of stance phase knee moments from two subjects at five walking speeds, demonstrating decreased moment amplitude (a) and quadriceps avoidance (b) patterns.

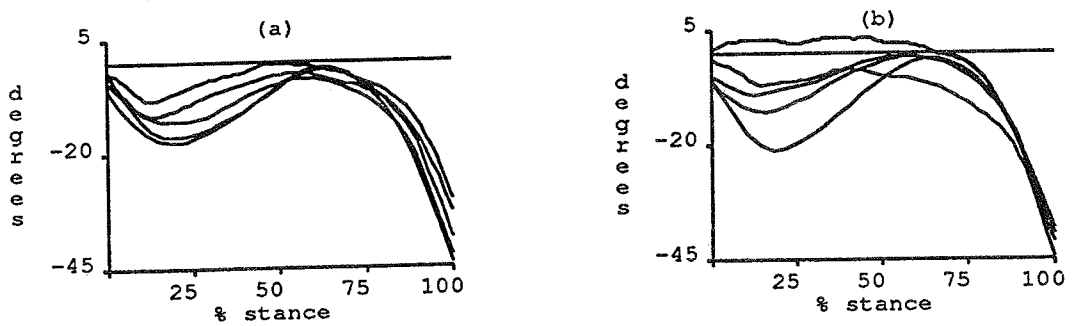

Figure 2: Individual trials of stance phase knee flexion angles from two subjects at five walking speeds. Decreased knee flexion in early stance contributed to decreased moment amplitudes (Fig. 1). The extended knee throughout early and mid stance at the slowest speed (b) produced the net flexor moment in Figure 1b.

MECHANICS OF TURNING IN HEXAPODS

D. L. Jindrich and R. J. Full
Department of Integrative Biology, University of California, Berkeley
Berkeley, CA 94720-3140

INTRODUCTION

Arthropods, such as insects and crabs, present many experimental opportunities for integrating musculo-skeletal mechanics with neural organization. Moreover, studies of 2-, 4-, 6- and 8-legged runners have allowed the discovery of general principles underlying locomotion (Full and Tu, 1990). Experiments on cockroaches, in particular, have shown that insects have a unique combination of stability and maneuverability (Ting at el., 1994). Further study of insect locomotion can aid the construction and control of autonomous legged robots.

The kinematics of straight-ahead locomotion, and of more complex behaviors like turning and climbing, have been described for several species of insects. The kinetics (i.e. the patterns of leg force production) of locomotion have also been studied, but measurements have thus far been limited to cockroaches running straight ahead (Full and Tu, 1990). We investigated the kinematics and kinetics of a more complex behavior, turning during running. We studied the behavior of the cockroach, *Blaberus discoidalis*. Since dynamic adjustments may be necessary to maintain stability, kinematic analysis alone is an insufficient descriptor of a complex and dynamic behavior like turning. We videotaped cockroaches running and turning on a photoelastic gelatin track to measure the ground reaction forces generated by individual legs.

REVIEW AND THEORY

Insects have been shown to employ several kinematic mechanisms to turn in place or to turn while walking. Increasing the distance traveled by the legs on one side of the body will cause the animal to turn away from those legs (the "outside legs"), in the direction of contralateral legs (the "inside legs"). Decreasing the stride frequency, or shortening the stride length, of the inside legs relative to the outside legs will increase the distance traveled by the outside legs relative to the inside legs and turn the animal.

Using a dynamic mechanism (employing kinematic and kinetic adjustments) to turn the body is also possible. Cockroaches could increase the lateral forces produced by the outside legs (simply increasing the yaw observed in straight running; Full and Tu 1990), increase the lateral forces produced by both the outside and inside legs in a force couple (a mechanism proposed for the cockroach escape response; Nye and Ritzmann, 1992), or pull with the inside legs.

Our experiments addressed the following question:
1. Do cockroaches use a kinematic mechanism or a dynamic mechanism to turn their bodies while running?

PROCEDURES

The cockroaches were filmed at 500 frames per second using an intensified high-speed video camera (Kodak EktaPro 1000), as they ran in a circular track. Head, midsection, tail, and tarsal contact points were digitized using a computer motion analysis system (Peak Performance Technologies). Ground reaction forces were measured using the photoelastic technique (Full, Yamauchi, and Jindrich, *J. Exp. Biol.*, in press; Figures. 1 and 2).

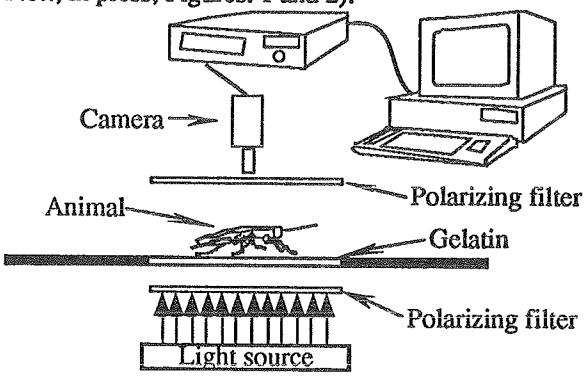

Figure 1. The animals ran across a plate of gelatin between two orthogonally-oriented polarizing filters, and were filmed from above. Each video frame was captured using a video capturing board (Neotech, Inc.) in a Macintosh computer, and analyzed using a specialized image analysis program, implemented using the Ultimage Concept V.i. (Graftek, France) extensions of the LabVIEW data acquisition software (National Instruments).

Data were filtered using a Butterworth low-pass filter with zero phase shift. Body angles and center of mass coordinates were filtered using a 25 Hz cut-off frequency; force data were filtered at 200 Hz.

The location of the animal's center of mass was estimated as a point 54% of distance from the head to the tail of the animal (Kram, Wong, and Full, in review). Data were analyzed using a two-dimensional model that considered only horizontal

forces (those in the surface plane of the gelatin; Figure 3).

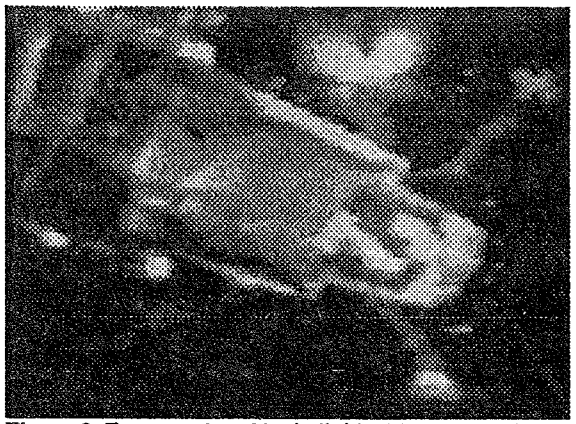

Figure 2. Force produced by individual legs stressed the gelatin and produced clover-shaped light patterns. Given a set of calibrations, the vertical and horizontal components of the force produced by the legs, as well as the direction of the horizontal force relative to the axes of the polarizing filters could be determined.

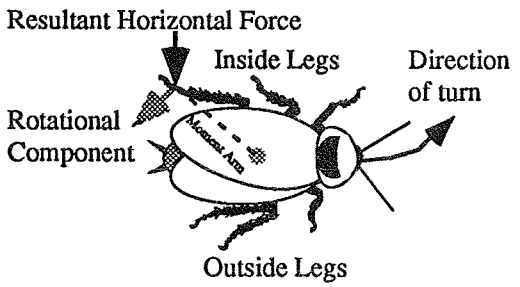

Figure 3. Each leg was modeled as a rigid bar (moment arm) connecting the animal's center of mass to the tarsus. The resultant horizontal force was resolved into components parallel and perpendicular to the bar. The rotational moment (a torque) was calculated by multiplying the force component perpendicular to the moment arm by the length of the moment arm. Positive rotational work was calculated by integrating the positive moment with respect to the angle of the body during periods when the body was rotating in the direction of the turn.

RESULTS

Cockroaches were able to turn through a yaw angle of over 20 degrees within one stride. The alternating tripod gait (characteristic of insects, in which the front and hind legs on one side of the body and the contralateral middle leg form a tripod) was maintained throughout the turn. Stride frequency therefore did not differ between the inside and the outside legs. Measured stride length differences could only account for 25% of the observed turn, suggesting a dynamic turning mechanism. The outside middle legs contributed the most to turning the body (Figure 4). Front legs produced small forces. Hindlegs produced large forces that tended to accelerate the body without rotating it.

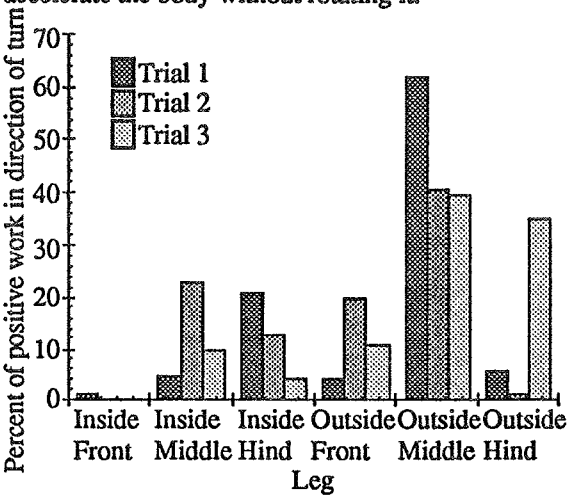

Figure 4. Positive work in the direction of the turn contributed by each leg. Values are expressed as a percentage of the sum of the positive work in the direction of the turn produced by all legs.

DISCUSSION

Cockroaches turned using a dynamic mechanism. Leg forces appear similar to those predicted during the escape behavior (Nye and Ritzmann, 1992). However, the front legs contributed little to turning the body. The dynamic nature of cockroach turning appears to be more similar to the equivalent behaviors of quadrupeds or bipeds than the turning behaviors of slow, statically-stable hexapods (including hexapedal robots; Angle, 1991). Discoveries about many-legged locomotion, such as those yielded by the present study, are being used in the design of autonomous legged robots (Binnard, 1995).

REFERENCES

Angle, C. M. M.S. Thesis. Massachusetts Institute of Technology, 1991.

Binnard, M. M.S. Thesis. Massachusetts Institute of Technology, 1995.

Full, R.J. and Tu, M.S. *J. Exp. Biol.* 148:129-146, 1990.

Full, R. J., Yamauchi, A. and Jindrich, D. L.*J. Exp. Biol.* In press.

Kram, R., Wong, B. and Full, R. J. *J. Exp. Biol.* submitted.

Nye, S.W. and Ritzmann, R.E. *J. Comp. Physiol*, 171:183-194, 1992.

Ting, L.H. et al. *J. exp Biol.* **197**, 251-26, 1994.

ACKNOWLEDGMENTS

We would like to acknowledge Rodger Kram for his assistance at all stages of this project. Supported by ONR Grant N00014-92-J-1250.

THE KINETICS OF CENTIPEDE LOCOMOTION

B.D. Anderson and R.J. Full
Department of Integrative Biology, University of California, Berkeley CA 94720-3140

INTRODUCTION

Much attention has been given to understanding the energetics and mechanics of terrestrial locomotion in animals using symmetrical gaits. Although symmetrical gaits are common, many animals use metachronal or wave gaits. Metachronal gaits have received little attention in the literature and no real quantification of their mechanics has been attempted. We quantified the mechanics of locomotion in a centipede, *Scolopendra heros*, that uses a metachronal gait.

REVIEW AND THEORY

Symmetrical gaits are characterized by two sets of propulsers alternating out of phase. Two-legged walking humans and six-legged cockroaches, using an alternating tripod, both use symmetrical gaits. Metachronal gaits are best characterized by legs being picked up and set down more closely in time than in symmetrical gaits. In metachronal gaits it appears as if a wave of leg movement passes down along the body.

Full (1989) has shown that pedestrians, using symmetrical gaits, which vary greatly in morphology can have similar whole body locomotor mechanics during constant speed locomotion. Gray (1953) suggested that animals with many legs using metachronal gaits, such as in millipedes and centipedes, will function more like wheels than other animals. If one leg hits the ground soon after another, body weight can be supported almost continuously. Thus, we hypothesized that the center of mass of animals using metachronal gaits undergo little fluctuation during constant speed locomotion. This implies that the whole body ground reaction forces in the vertical, horizontal and lateral directions should not vary from a steady-state value.

While whole body mechanics are similar, individual legs have different functions in animals using symmetrical gaits. In humans and dogs each leg shows a similar pattern of ground reaction forces. In these animals each leg first decelerates the animal and then accelerates it in the horizontal direction. In the 6-legged cockroach, each leg has a different pattern of ground reaction forces (Full et al., 1991). This lead us to address the question of how individual legs function in metachronal gaits.

PROCEDURES

We used centipedes of the species *Scolopendra heros*, from the Arizona dessert. This species has 22 sets of legs, a total of 44 legs, and is 5-6 inches in length. The mean mass of our animals was 7.56 ± 1.54 (SE) gm.

Centipedes were run across a force platform capable of simultaneously measuring whole body ground reaction forces in three directions. Trials were videotaped using a high-speed video cameras (Kodak EktPro 1000). Video and force records were synchronized by matching the first frame in the video that the animal touched the force plate with the beginning of the vertical force record.

To measure forces for individual legs, a thin balsa wood cover with two rectangular holes was suspended above the force plate. These holes were the only place were the animals legs touched the active plate. These trials were also videotaped.

RESULTS

The whole body ground reaction force in the vertical direction oscillated around body mass. The lateral force oscillated around zero as the animals pushed from side to side. The horizontal force also oscillated around zero as the animal accelerated and decelerated the body as it locomoted.

Single legs of the centipede are only on the ground for a brief period of time before the next leg is set down. Since the centipedes very nearly generate a standing wave relative to the ground, a leg touches down in the same footprint as the leg ahead of it. Legs hit the ground on the inner portion of a concave bend in the body and radiate around a focal point (Fig. 1).

We therefore considered these focal points or foci as effective legs that generate force as they travel along the body. A single focus force recording is shown in Figure 2.

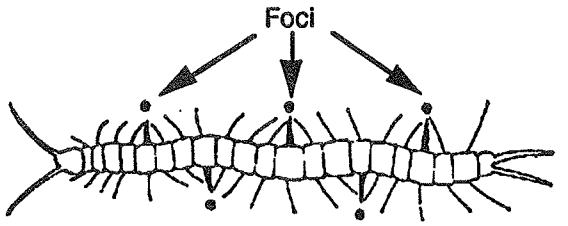

Fig 1: The dark legs and spots indicate which legs are in contact with the ground. Each of these points on the concave side of the body is a focus.

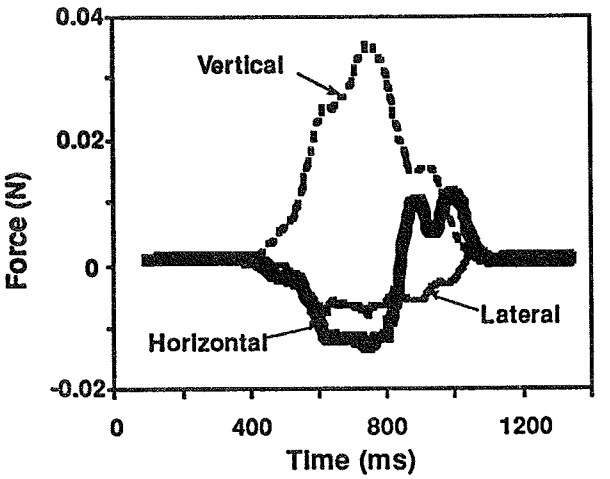

Figure 2: Example of the ground reaction forces from the legs passing through a single focus.

When the single focus horizontal force was correlated to the leg which generated the force, we found that the anterior legs (legs 3-9) decelerated the body (negative values), the middle legs (10-14) could either accelerate or decelerate the body and the rear legs (15-20) tended to accelerate the body (Fig. 3).

DISCUSSION

The oscillation of the whole body ground reaction forces indicates that the Arizona centipede does accelerate and decelerate its center of mass as it locomotes at constant speed. This implies that animals using metachronal gaits do not necessarily roll like wheels as Gray (1953) hypothesized. Instead, the center of mass of animals using metachronal gaits undergo significant fluctuations during constant speed locomotion, just as in animals using symmetric gaits.

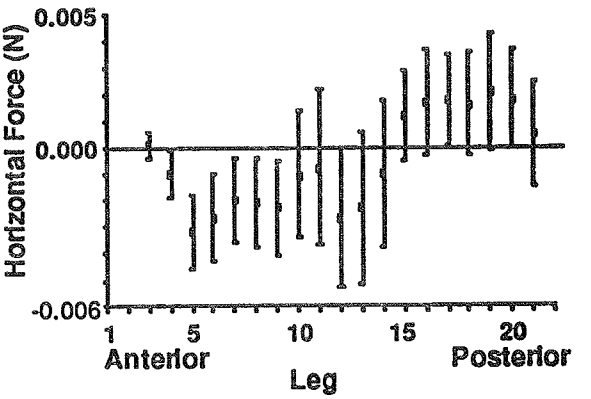

Figure 3: The average horizontal force as a function of leg number. Leg number increases from anterior to posterior. Error bars are ± 1 SE.

The single focus force measurements reveal that anterior legs decelerate the centipede and the posterior legs accelerate it. There is a switch from decelerating to accelerating horizontal force in the middle legs. This is analogous to the cockroach where during ground contact the anterior leg decelerates the body, the middle first decelerates and then accelerates it and the rear leg accelerates the animal (Full et al., 1991).

In running humans, a leg first decelerates the body during landing and accelerates it during takeoff. The same force pattern is seen in trotting dogs, cockroaches and crabs, but is produced by more legs acting synchnously. Two legs of a trotting dog, 3 legs of a cockroach and 4 legs of a crab sum to function as a single leg of a human. In centipedes, 22 legs generate the characteristic ground reaction force pattern. The effective leg of a centipede is a wave of 22 legs passing along the body.

REFERENCES

Full, R.J. et al. *J. Exp. Biol,* 158, 369-390, 1991.
Full, R.J. Energy Transformations in Cells and Organisms, (pp. 175-182), Verlag, 1989.
Gray, J. How Animals Move, (pp.13-36), Cambridge Univ. Press, 1953.

ACKNOWLEDGMENTS

This work was supported by NSF Grant DCB 89-04586 and NSF Presidential Young Investigator Award DCB 90-58138. to R.J. Full.

THE STIFFNESS OF THE HUMAN LEG AS A FUNCTION OF SURFACE STIFFNESS

D.P. Ferris, C.T. Farley, and G. Chen
Department of Human Biodynamics, University of California, Berkeley CA 94720

INTRODUCTION

This study examined the effects of surface compliance on the leg stiffness of humans. Subjects hopped in place on both a hard surface and a compliant surface over a range of frequencies to test the hypothesis that humans would maintain a constant leg stiffness regardless of the stiffness of the surface. Our findings show that this hypothesis is incorrect. We find that humans increase their leg stiffness on compliant surfaces. As a result, the total stiffness of the combination of the leg and the surface is similar regardless of the surface stiffness.

REVIEW AND THEORY

When humans and other animals hop or run, they literally bounce along the ground using muscles, tendons, and ligaments to store and return elastic energy. The mechanics of these bouncing gaits can be accurately described by a simple spring-mass system consisting of a single linear leg spring and a point mass equivalent to the body mass (McMahon and Cheng, 1990). Over a wide range of speeds, the stiffness of the leg spring remains nearly the same in a variety of running, hopping and trotting mammals, including humans (Farley et al., 1993; He et al., 1991). However, humans can alter their leg stiffness to accommodate changes in stride frequency (Farley et al., 1991; Farley and Gonzalez, in press) and surface slope (Iverson and McMahon, 1992).

The goal of this study is to determine whether the stiffness of the leg spring is adjusted to accommodate surfaces with different properties. Previous research has shown that surface properties affect the mechanics of running (McMahon and Greene, 1979). However, it is not known whether the stiffness of the leg is altered to accommodate different surfaces. Our study tests the hypothesis that humans maintain a constant leg stiffness regardless of surface stiffness during bouncing gaits. We test this hypothesis by having humans hop in place on a hard surface and on a compliant surface. Hopping in place is a convenient experimental system because the musculoskeletal system behaves like a simple spring-mass system much like it does during forward running (Farley et al., 1991).

PROCEDURES

We collected ground reaction force data as three subjects hopped in place at a range of frequencies (2.0 - 3.2 Hz) on both a hard surface and a compliant surface. A force platform served as the hard surface. The compliant surface was an area elastic surface constructed from plywood and steel springs. It was mounted on a force platform. The compliant surface had a constant stiffness (k_{surf}) of 57,300 N m^{-1} and a damping ratio of 0.01. The inertial force due to the surface acceleration was less than 5% of the peak vertical ground reaction force during hopping in place. The inertial force due to the surface was calculated from the surface acceleration and the effective mass of the surface. We determined the surface acceleration by videotaping (120 images/second) the surface while a person hopped on it, and we determined the surface effective mass from the natural frequency of loaded free vibration. Because of the small surface inertial forces compared to the vertical ground reaction force, we used the vertical ground reaction force as an approximation of the force experienced by the leg spring during hopping in place on the compliant surface.

Hopping in place was modeled as a simple spring-mass system consisting of a single linear leg spring and a point mass, equivalent to the mass of the subject (Blickhan, 1989; Farley et al., 1991; McMahon and Cheng, 1990). Using force platform measurements, we calculated the stiffness of the total system (i.e., compliant surface in series with leg spring) as well as the stiffness of the leg spring.

The total stiffness of the system (k_{tot}) was defined as the ratio of the peak force (F_{peak}) to the peak displacement (ΔX_{tot}) of subject and the compliant surface during the ground contact phase.

$$k_{tot} = F_{peak} / \Delta X_{tot} \qquad (1)$$

The total vertical displacement of the system (ΔX_{tot}) during the ground contact phase was calculated from the vertical ground reaction force as described by Cavagna (1975). On the compliant surface, this displacement (ΔX_{tot}) was the sum of the displacement of the surface (ΔX_{surf}) and the displacement of the leg spring (ΔL).

$$\Delta X_{tot} = \Delta X_{surf} + \Delta L \qquad (2)$$

The displacement of the compliant surface (ΔX_{surf}) was calculated from the ratio of the peak vertical force to the surface stiffness. The displacement of the leg spring could then be found using Equation 2. Given the peak force and the displacement of the leg spring, the leg stiffness (k_{leg}) was calculated using Equation 3:

$$k_{leg} = F_{peak} / \Delta L \qquad (3).$$

RESULTS

On both surfaces, the stiffness of the leg spring increased at higher hopping frequencies (Figure 1). When the subjects hopped at the higher frequencies, the stiffness of the leg spring was as much as 64% greater on the compliant surface than on the hard surface. At the highest hopping frequency (3.2 Hz), k_{leg} was 54 kN/m on the compliant surface and 33 kN/m on the hard surface. By contrast, at the lowest frequency (2.0 Hz), k_{leg} only slightly higher on the compliant surface than on the hard surface.

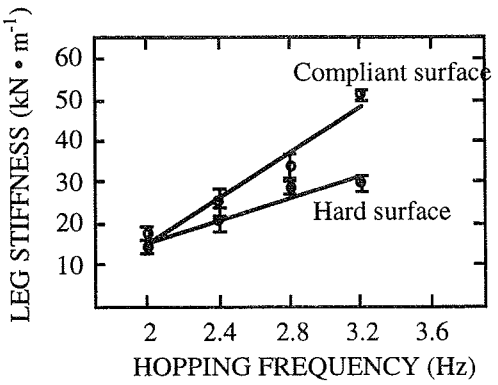

Figure 1: Leg stiffness as a function of hopping frequency. Each point is the mean for the three subjects. Error bars are the standard error of the means.

The total stiffness of the system (the series combination of the leg stiffness and the surface stiffness) was only slightly less on the compliant surface compared to the hard surface at each frequency (Figure 2). For example, during hopping at 2 Hz, the total stiffness was 27.0 kN/m on the compliant surface and 30.1 kN/m on the hard surface. On average over all of the frequencies, the total stiffness was only 15% less on the compliant surface than on the hard surface.

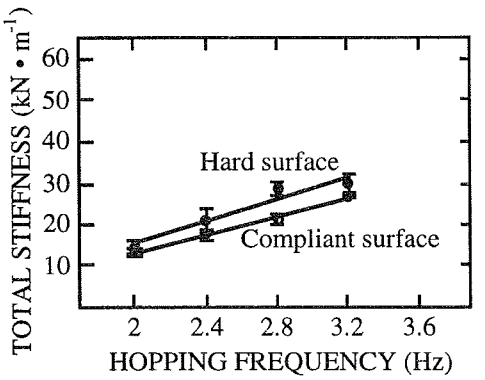

Figure 2: Total stiffness as a function of hopping frequency. Each point is the mean for the three subjects. Error bars are the standard error of the means.

DISCUSSION

We conclude that the stiffness of the leg spring is adjusted to accommodate changes in surface properties. We find that the leg spring stiffness during hopping in place can be increased to accommodate a more compliant surface. As a result, at a given hopping frequency, the total stiffness of the series combination of the leg spring and the compliant surface remains nearly the same regardless of surface stiffness. Our future research will examine adjustments to leg spring stiffness to accommodate surfaces with a broad range of stiffnesses. We predict that the stiffness of the leg spring will be increased at all hopping frequencies when humans hop on surfaces that are less stiff than the one used in the current study.

Our findings about the adjustment of the musculoskeletal system to accommodate different surfaces may provide insight into the prevention, diagnosis, and treatment of locomotion-related injuries. In addition, they will provide insight into the design of spring-based prostheses and legged robots intended to traverse a variety of terrain.

REFERENCES

Blickhan, R. *J. Biomech.* 22: 1217-1227, 1989.

Cavagna, G.A. *J. Appl. Physiol.* 39, 174-179, 1975.

Farley, C.T. et al. *J. Appl. Physiol.* 71:2127-2132, 1991.

Farley, C.T. et al. *J. Exp. Biol.* 185:71-86, 1993.

Farley, C.T. and O. Gonzalez *J. Biomech.* In Press.

He, J. et al. *J. Appl. Physiol.* 71:863-870, 1991.

Iverson, J.R., and T.A. McMahon *J. Biomech. Eng.* 114:435-441, 1992.

McMahon, T.A. and G.C. Cheng *J. Biomech.* 23(Supp. 1):65-78, 1990.

McMahon, T.A. and P.R. Greene *J. Biomech.* 12:893-904, 1979.

CORRELATIONS BETWEEN "LEG SPRING" CHARACTERISTICS AND RUNNING ECONOMY

G.D. Heise[1] and P.E. Martin[2]

[1]Department of Kinesiology, Louisiana State University, Baton Rouge, LA 70803

[2]Department of Exercise Science and Physical Education, Arizona State University, Tempe, AZ 85287

INTRODUCTION

By applying a simple, linear mass-spring model to running, the leg spring stiffness, the effective vertical stiffness, and the work rate of the spring were determined and correlated with running economy (RE). Recreational runners (n=16) ran on a treadmill at 3.35 $m \cdot s^{-1}$ for physiological measures and overground for biomechanical measures. The latter included a sagittal plane video record of the running motion and ground reaction data. The stiffness coefficients and the work rate of the leg spring model were determined from computations presented by McMahon and associates (e.g., McMahon & Cheng, 1990). Both coefficients were inversely related to aerobic demand. The work rate of the spring was positively correlated to aerobic demand. Although the model greatly simplifies the mechanics of running, the effective vertical stiffness accounted for nearly 25% of the inter-individual variability in RE. The inverse relationships found in the present investigation are in agreement with similar results from studies which examined relationships between static measures of flexibility and aerobic demand.

REVIEW AND THEORY

Biomechanists have identified several variables describing structural characteristics and running mechanics which are related to RE. Many of these relationships are weak and inconsistent from one study to the next (Martin & Morgan, 1992). For example, when several modeling schemes for calculating overall mechanical power output were examined, no single approach was found to be superior in explaining inter-individual variability in RE (Martin et al., 1993).

McMahon and associates (Farley et al., 1993; McMahon & Cheng, 1990; McMahon et al., 1987) have shown that a simple linear spring model of the leg can accurately predict running mechanics. The model consists of a mass and a simple leg spring (Fig. 1). He et al. (1991) showed that as humans run faster the stiffness coefficient of the leg spring does not change. Farley et al. (1993) have shown this effect to hold for a variety of trotting and hopping animals.

This simple model describing overall stiffness of the musculoskeletal system during running in combination with recent experimental evidence showing that more flexible runners may be less economical (Craib et al., 1994) led us to the following hypothesis: The coefficients describing stiffness in the model developed by McMahon and associates should be inversely related to $\dot{V}O_2$ (i.e., greater stiffness associated with greater economy). In addition, $\dot{V}O_2$ should be positively correlated with the work rate of the spring if the model can accurately predict overall mechanical output.

PROCEDURES

Sixteen well-trained men (mean $\dot{V}O_{2max}$ = 62.2 $ml \cdot kg^{-1} \cdot min^{-1}$) performed treadmill running for determination of running economy and overground running for which biomechanical measures were determined (running speed = 3.35 $m \cdot s^{-1}$). Specifically, time of contact (t_c), peak vertical ground reaction force (F) and peak vertical displacement during stance (Δy) were determined from force platform data and leg length at foot contact (L_o) was determined from a sagittal plane video image. These measures correspond to descriptors of the leg spring model (Fig. 1) and were used to calculate dependent measures.

The leg spring model contains a mass and a single linear spring (Fig. 1). The figure depicts a runner going from left to right and shows the mass-spring model at three positions during the stance phase (foot contact, mid-stance, toe-off).

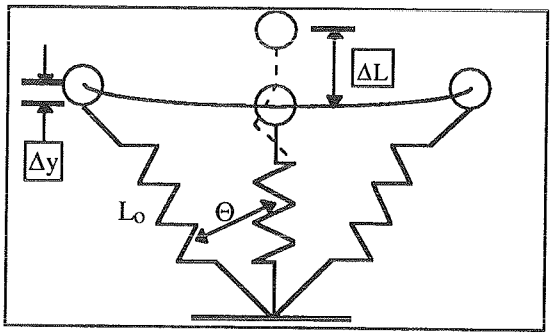

Figure 1: Leg spring model (adapted from McMahon & Cheng, 1990). Θ is half the angle swept by the leg spring during stance.

The stiffness of the leg spring, k_{leg}, was defined as the ratio of F to ΔL, where

$$\Delta L = \Delta y + L_o * (1 - \cos \Theta) \qquad \text{and}$$

$$\Theta = \sin^{-1} [(3.35\ m \cdot s^{-1} * t_c) / (2\ L_o)]$$

The effective vertical stiffness, k_{vert}, was defined as the ratio of F to Δy. This does not correspond to an actual spring in the model, but instead describes the vertical compliance of the running gait (McMahon et al., 1987). Both stiffness coefficients were multiplied by the ratio of L_o to body weight resulting in unitless meaures which were then correlated with $\dot{V}O_2$. The work rate of the spring was determined from the following equation (Farley et al., 1993):

$$P_{sp} = [(0.5 * F^2\ f) / (k_{leg} * M)]$$

where f is the step frequency and M is body mass.

RESULTS AND DISCUSSION

The magnitudes of the stiffness coefficients before normalization (mean k_{leg} = 12.6 kN·m^{-1}; mean k_{vert} = 34.5 kN·m^{-1}) were similar to previously reported values (e.g., Farley & Gonzalez, 1994; He et al., 1991). The normalized leg spring stiffness appeared to be a poor indicator of $\dot{V}O_2$ with several outliers influencing the already poor relationship (Fig. 2). However, the effective vertical stiffness displayed a moderately strong inverse correlation (Fig. 3) with $\dot{V}O_2$, whereas the work rate associated with the leg spring showed a moderate positive relationship (Fig. 4).

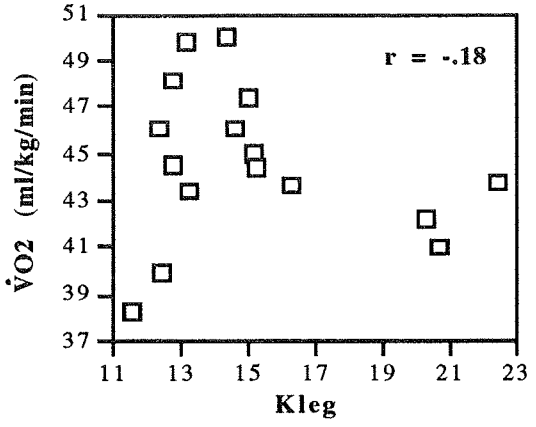

Figure 2: Scatterplot of aerobic demand and unitless coefficient of stiffness for the leg spring (K_{leg}).

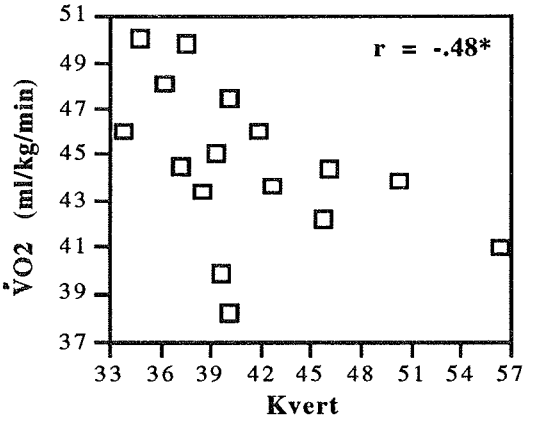

Figure 3: Scatterplot of aerobic demand and unitless coefficient describing the effective vertical stiffness of the leg spring (K_{vert}). * $p < .05$ (one-tailed)

The inverse relationships between $\dot{V}O_2$ and both stiffness coefficients were expected and agree with studies which have examined the link between RE and static flexibility. Craib et al. (1994) and Gleim et al. (1990) found negative relationships between some flexibility measures and $\dot{V}O_2$. Both studies, however, noted significant inverse correlations between the amount of trunk rotation and $\dot{V}O_2$. This potential store of elastic energy during running was not accounted for in the leg spring model examined in the present study. More generally, how $\dot{V}O_2$ changes with manipulations of flexibility remains unknown.

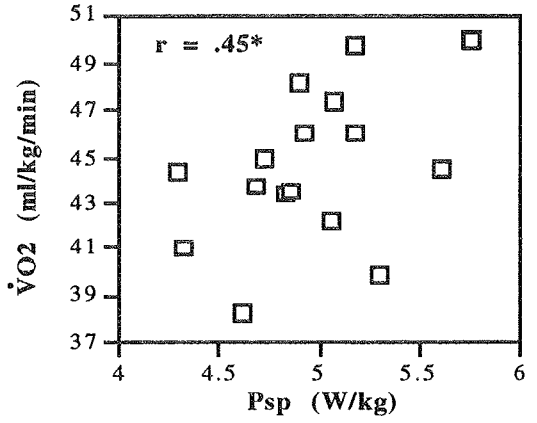

Figure 4: Scatterplot of aerobic demand and the work rate of the simple linear leg spring. * $p < .05$ (one-tailed)

McMahon et al. (1987) manipulated k_{vert} by having subjects run with exaggerated knee flexion during stance (Groucho running) and found that k_{vert} was reduced to 82% of its original value. The effects of this decreased vertical stiffness were twofold: a dramatic decrease in the shock transmission to the head (to 20% of its value for normal running) and an increase in $\dot{V}O_2$ (by as much as 50%).

The positive correlation between $\dot{V}O_2$ and P_{sp} was greater than any correlation reported by Martin et al. (1993) when we examined several biomechanical expressions for total mechanical power output with these same data. In that study, the correlation between $\dot{V}O_2$ and power based on the kinematics of the center of mass, assuming no exchange between potential and kinetic energy, was 0.40.

Collectively, the results reported here suggest that greater vertical stiffness and lower work rate of the leg spring are associated with better economy. Consequently, the directions of these associations are consistent with our stated hypotheses. Whether stiffness characteristics of the body change as a result of increased or decreased flexibility remains unanswered.

REFERENCES

Craib, M. et al. Med. Sci. Sports Exerc., 26(Supp), S113, 1994.

Farley, C.T. et al. J. exp. Biol., 185, 71-86, 1993.

Farley, C.T. & Gonzalez, O. ASB Proceedings, Columbus, OH, pp. 117-118, 1994.

Gleim, G.W. et al. J. Ortho. Res., 8, 814-823, 1990.

He, J. et al. J. Appl. Physiol., 71, 863-870, 1991.

Martin, P.E. et al. Med. Sci. Sports Exerc., 25, 508-515, 1993.

Martin, P.E. & Morgan, D.W. Med. Sci. Sports Exerc., 24, 467-474, 1992.

McMahon, T.A. & Cheng, G.C. J. Biomech, 23(Supp), 65-78, 1990.

McMahon, T.A. et al. J. Appl. Physiol., 62, 2326-2337, 1987.

STRUCTURAL FEATURES AND THICKNESS OF THE VERTEBRAL CORTEX IN THE THORACOLUMBAR SPINE

Y.G. Zheng, L.A. Fay, H.A. Yuan, W.T. Edwards

Orthopedic Research Laboratory, SUNY-Health Science Center
Syracuse, NY 13210

INTRODUCTION

The strength of the vertebrae is dependent on the thickness of the cortex of the vertebral body and the density of the trabecular centrum (McBroom et al. 1985). The thickness and structure of the cortex and the endplates were measured to provide a mode accurate basis for the mathematical modeling of the vertebral strength. Previous analyses have overestimated cortex thickness and have overlooked common structural variations along the endplates.

REVIEW AND THEORY

Few studies have directly examined the thickness of the human vertebral cortex. Non-invasive techniques, such as quantitative computed-tomography and dual-energy x-ray absorptiometry, commonly applied in the study of osteoporosis, cannot directly quantify cortex thickness and variation in comparison to the underlying trabecular structure. In mathematical models it is generally assumed that the cortex and the endplates are uniform with a thickness of about 1 mm. The objectives of this study were: 1) to identify principal structural features of the cortex, 2) to directly measure the minimum and maximum thicknesses of the cortex along the thoracolumbar spine, and 3) to compare the regional variations in cortical structure.

PROCEDURES

The vertebral bodies of the thoracolumbar spine (T1, T5, T9, L1 and L5) were obtained from 20 fresh cadaver spines, aged 49-82 years (mean 70.4 years). Specimens were examined by radiograph to rule out gross defects, and frozen at -20° C. Any specimen which exhibited bony abnormalities or had a history of metastatic disease was eliminated from the study. The specimens were thawed and stripped of all muscle and soft tissue leaving only the ligamentous structures. The specimens were then dried and sectioned. Each vertebral body was encased in an epoxy block and sectioned at 8 mm increments from the mid-sagittal to lateral-sagittal regions. The medial surface of each section was then ground smooth, cleaned of residue, and air dried. The sections were then stained with India ink and dried. After drying each section was brushed with Confectioner's sugar to provide a sharp contrast between bone and non-bone, as the final step of section preparation. Color 35 mm slides of each of the mid-sagittal sections were obtained and scanned. The images of the vertebral sagittal sections were digitized by a high resolution video system with a resolution better than 0.063 mm/pixel. Cortex thickness were obtained from the images using the NIH-image computer program (v1.55). The minimum and maximum thickness was measured at twenty regions along the cortical margin, five along each endplate (labeled Regions 1-5, from anterior to posterior) and five along the anterior and posterior cortex (labeled Regions 1-5, cephalad to caudal). The regional variations in cortical thicknesses were statistically compared using Student's t-test and ANOVA assessment.

RESULTS

The mean thickness of the cortex was less than 1 mm along the endplates and the anterior and posterior surfaces. There was a decrease in thickness of about 0.25 mm over the central portion of the endplates. The eight corner regions of the specimens where the cortex shell and the endplates intersect had an increased thickness in comparison to the other twelve regions. Structurally, a double-layer of bone formed the endplates in a significant number of specimens. The percentages of double-layers at the superior and inferior endplates in the vertebrae T9 and L1 were 32% and 80%, respectively. The highest percentage of the double-layered endplate was observed at the super L5 level in 88% of specimens.

The anterior surface was significantly thicker (Tmin and Tmax were greater anteriorly) than the posterior surface, $p<0.0001$. The cortex was significantly thicker for the lumbar vertebrae in comparison to the thoracic vertebrae, $p<0.0008$. The overall range for the minimum thickness was 0.10-1.53 mm, and for the maximum

thickness was 0.19-2.42 mm, 0.63±0.26 mm (mean±1 SD).

DISCUSSION

The vertebral cortex supports 15-30 percent of the compressive force of the spine (McBroom, 1985). The strength of the compact bone within the cortex is dependent on the thickness and support from the underlying trabecular structure. Unfortunately, the thickness of the cortex can not be measured by CT and other non-invasive techniques and therefore has been estimated in strength analyses and in finite element modeling. In analyses of the vertebral strength it has been generally assumed that the bone of cortex is uniform and 1.0 mm thick (Shirazi-Adl et al. 1986). Our measurements showed that the mean minimum and maximum cortical thicknesses varied and may be as thin as 0.4 mm or as thick as 0.85 mm, with an overall mean of 0.63 mm. The thicker anterior cortex appears to reflect the normal loading patterns of a compression-flexion stresses through a vertebral body. Since most injuries in the sagittal plane are the results of some combination of a compressive force and a bending moment (White et al. 1990), the thickened anterior cortex would reduce the risk of compression fractures and contribute to added vertebral body strength. The thickened cortex in the lumbar vertebrae suggests a remodeling process with age. With a reduction in trabecular bone content which occurs predominantly in the lumbar spine and lower thoracic vertebra, the cortex may thicken to provide adequate vertebral strength. In addition the structure of the endplate may contribute to strength. The endplate, a solid compact bony ring, is formed by the fusion of primary and secondary ossification centers at the cranial and caudal ends of the vertebral body (Edelson & Nathan 1988). It appears that this double-layered structure may provide added strength in the lower thoracic and lumbar vertebrae. However, the biomechanical properties of the double-layered endplates have not been previously been presented.

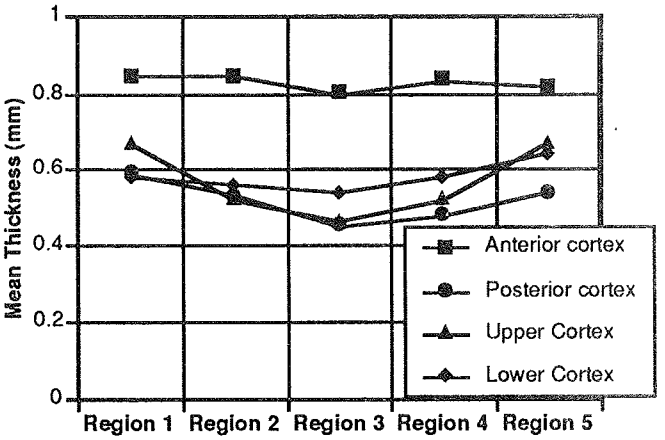

Fig. 1 Mean cortex thickness at five positions along the four vertebral faces.

REFERENCES

McBroom, RJ et al. JBJS 67A:1206-1214, 1985. Shirazi-Adl, A et al. J Biomech 19:331-350, 1986. White, AA, III et al. *Clinical Biomechanics of the Spine, 2nd edition.* (pp. 170-171), 1990. Edelson, JG and Nathan, H: Spine 13(1):21-26, 1988

ACKNOWLEDGMENTS

This study was supported in part by funding from PHS-NIH AR-33066 and the Department of Orthopedic Surgery, SUNY-HSC, Syracuse.

ABDOMINAL EXERCISES: SEARCHING FOR THE OPTIMAL MUSCLE CHALLENGE WITH MINIMAL SPINE LOADING

Craig T. Axler and Stuart M. McGill
Occupational Biomechanics and Safety Laboratories, Department of Kinesiology, University of Waterloo, Waterloo, Ontario, Canada

INTRODUCTION

Weak torso musculature is highly correlated with the presence of chronic low back pain (LBP) (Addison and Schultz, 1980; Biering-Sorensen, 1984; Smidt, et al., 1983). Although it has not been established if the weak musculature leads to LBP or vice versa, it has been shown that reduced abdominal and spinal extensor strength is a factor in the recurrence and/or persistence of chronic LBP (Biering-Sorenson, 1984;). Because of this relationship, abdominal exercises are used to strengthen the abdominal portion of the torso musculature in clinical settings, as well as for general fitness purposes and for athletes. The abdominal exercises most often recommended are those which maximize abdominal muscle activity (Flint, 1965). However, the load cost on the lumbar spine from these exercises has not been sufficiently examined.

The purpose of this study was to **quantitatively** identify abdominal exercises that optimize the challenge to the abdominal muscles with minimal loading penalty to the lumbar spine. This would provide clinicians with the information necessary to choose which exercise would be most appropriate for a given stage in either the rehabilitation or training process.

PROCEDURES

Nine male university students (mean age 23 years, SD=4.8, height 1.78m, SD=0.07, weight 85.1kg, SD=19.0) volunteered to perform five repetitions of twelve different abdominal exercises. The exercises represented a variety of techniques used to exercise the abdominal muscles, such as lifting the legs vs. lifting the torso, full situps vs. partial curlups, twisting actions, etc. The twelve exercises were as follows:

1) straight-leg situp (STRLSP)
2) bent-leg situp (BNTLSP)
3) Canadian Standard Test of Fitness partial curlup with feet fixed (CSTFFIX)
4) Canadian Standard Test of Fitness partial curlup with feet free (CSTFFREE)
5) quarter situp (curlup with bent knees raised in the air) (QSP)
6) straight-leg raise (STRLRS)
7) bent-leg raise (BNTLRS)
8) dynamic cross-knee crunch (XKNEEDY)
9) static cross-knee crunch (XKNEEST)
10)hanging straight-leg raise (HANG)
11)hanging bent-leg raise (BNTHANG)
12)isometric side support (ISOCSS).

Surface EMG was recorded from the rectus abdominis (upper and lower), external and internal oblique, rectus femoris, latissimus dorsi, and erector spinae (upper and lower) from both the right and left sides. Lumbar spine kinematics were obtained using the 3SPACE ISOTRAK magnetic source and sensor system. Video data was used to generate a link-segment model of each subject for each trial. These three sources of information were combined to generate compression and shear values at the L4/L5 lumbar spine level, using an anatomically detailed EMG-driven computer model (McGill and Norman, 1986). Using the biological signals of spine kinematics and muscle activation signals to drive the model enabled a sensitivity to the different motor control strategies that each subject employed to accomplish each exercise.

The maximum electrical activity from each abdominal muscle during a trial (normalized to 100%MVC), was incorporated into a ratio with the maximum model-generated compression value for that trial. The activity level was used as the numerator for this index, and the compression value formed the denominator, resulting in an index of muscle activity versus lumbar spine compression. Substituting different abdominal muscle values into the numerator provided an index for each muscle of interest, for each trial. This information facilitated the ranking of muscle challenge versus load penalty imposed on the spine form each exercise.

RESULTS AND DISCUSSION

In the figures below, the trials are presented in increasing order of maximum EMG signal for the muscle of interest, with the corresponding activity versus load ratios immediately below. The values obtained using the Rectus Abdominis muscle (See Figure #1 and Figure #2) reveal that although some exercises elicit greater muscle activity than others, these tasks do not always optimize the activity-to-load ratio. Essentially, some of the tasks also generate considerable compression values, decreasing the effectiveness of an activity if spinal compression were a concern (e.g. for a recovering LBP patient).

When the trials are presented in order of increasing activity for the other abdominal muscles (internal and external oblique), the order in which the trials appear is not the same as the rectus abdominis (See Figure #3 and Figure #5). From this result it could be concluded that different exercises activate each abdominal muscle to different degrees. The corresponding activity-to-load ratios of the internal oblique and external oblique, show the same effect as with the rectus abdominis; that the activity versus load ratios do not mirror the pattern of the maximum EMG values (See Figure #4 and Figure #6). The fact that the order of increasing EMG activity does not match the order of increasing activity-to-load ratio for three of the main abdominal muscles illustrates that one should not evaluate an abdominal flexion exercise on EMG activity alone. Also, although an exercise may not elicit the largest EMG activity, it is possible that considerable activity can be effected with relatively low loads on the lumbar spine, and vice versa.

This experiment has revealed that no one abdominal exercise is best suited for every person, nor for every situation. Some exercises may generate high activation of the abdominal musculature, but also generate considerable lumbar spine compression forces. This type of exercise may be suitable for an athlete who is seeking maximal muscle challenge and is able to support high spine forces. In contrast, this type of exercise is contraindicated for someone who is being rehabilitated from a low back injury. Conversely, exercises which optimize the muscular activity versus spine load index may be very useful to someone with LBP, but they may not challenge the abdominal musculature to the degree that is required for intensive training. The quantitative information obtained from this experiment should provide a more comprehensive overview regarding which exercises are appropriate for certain people and/or situations.

REFERENCES

Addison, R. & Schultz, A. *Spine*, **5**, 539-544, 1980.
Biering-Sorensen, F. *Spine*, **9**, 106-119, 1984.
Flint, M.M. *Am. J. of Phys. Med.*, **44**, 224-233, 1965.
McGill, S.M. & Norman, R.W. *Spine*, **11**, 666-678, 1986.
Smidt, G. et al. *Spine*, **8**, 211-219, 1983.

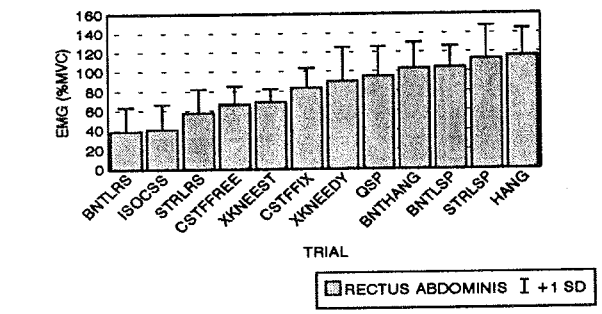

Figure #1: Maximum Rectus Abdominis EMG levels.

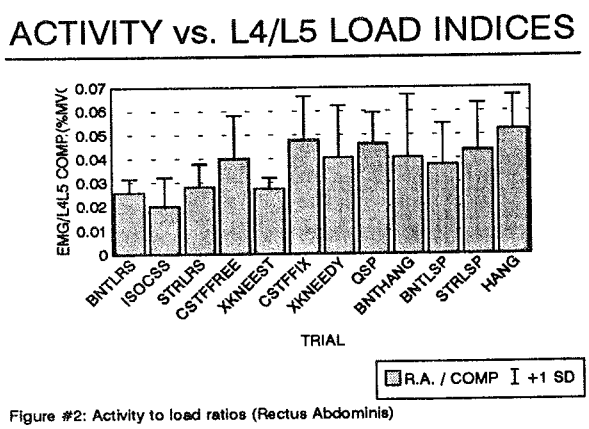

Figure #2: Activity to load ratios (Rectus Abdominis)

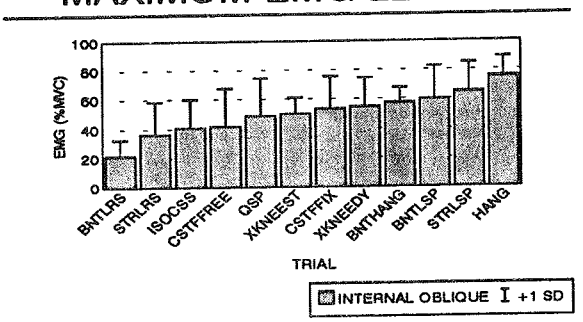

Figure #3: Maximum Internal Oblique EMG levels.

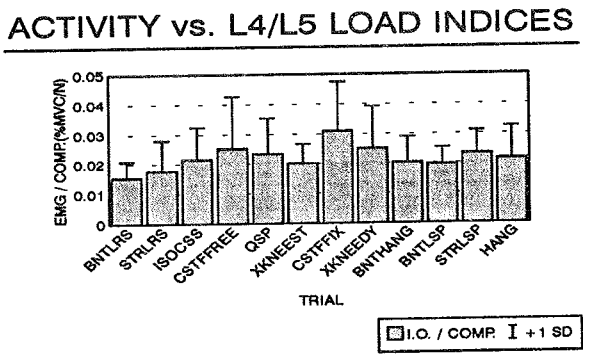

Figure #4: Activity to load ratios (Internal Oblique)

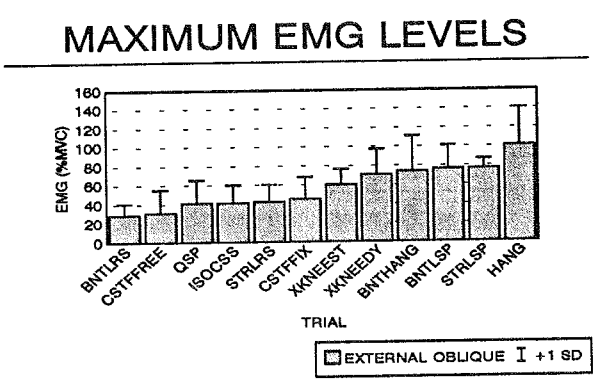

Figure #5: Maximum External Oblique EMG levels.

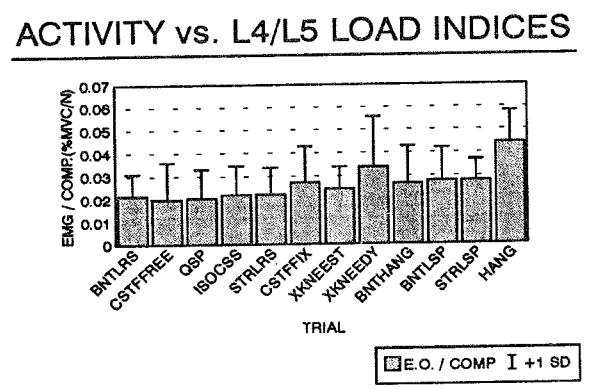

Figure #6: Activity to load ratios (External Oblique)

MUSCLE ACTIVITY AND LOW BACK LOADS UNDER EXTERNAL SHEAR AND COMPRESSIVE LOADING

Jack P. Callaghan and Stuart M. McGill
Occupational Biomechanics & Safety Laboratories, Department of Kinesiology
University of Waterloo, Waterloo, Canada

Introduction:

There has been considerable work in recent years to determine the loads on low back tissues. Knowledge of these loads are necessary for understanding spine mechanics and to elucidate injury mechanisms. Estimating tissue loads has required the development of sophisticated, anatomically detailed models that capture the architecture of the load bearing tissues. Recognizing the architecture of the muscles, specifically their moment arm length and line of action, can result in substantial differences in joint loads. Clearly, the two erector spinae muscle groups (thoracic and lumbar) have very distinct functions; the thoracic group would be preferential to support moment and minimize joint compression while the lumbar group is better suited for supporting shear loads. Given the dramatic differences in lines of action of various groups of muscles within the low back extensors, we were motivated to examine whether the motor control system recognizes the benefit of certain architectural features and chooses to minimize joint loading during different moment, compression, and shear support requirements by assigning muscle activation in the most appropriate way.

Therefore, in this study, the migration of EMG activity between the thoracic and lumbar erector spinae groups was examined while the applied compression and shear loads on the spine were manipulated but the external reaction moment was held constant. Activity in the abdominals and the multifidus at the L5 level was also monitored.

Methods:

Two experiments were performed to assess activation levels of various trunk muscles. The first experiment examined loading on eleven male subjects. The second experiment followed the same paradigm but intra-abdominal pressure (IAP) and an increased range of applied compressive and shear loads were examined on 4 additional male subjects.

Seven surface electromyogram (EMG) channels were recorded (rectus abdominis,internal and external oblique, latissimus dorsi, lumbar and thoracic erector spinae, and multifidus). Data was normalized to maximal isometric contractions for all monitored muscle groups following the methods of McGill (1991). A video monitor and a 3SPACE ISOTRAK were used to provide feedback to the subject, enabling them to maintain a constant posture, which also served to monitor lumbar curvature after Sutarno et al. (1995). The posture maintained throughout the task was similar to that adopted in upright standing. The hip angle was maintained at approximately 135° to create passive elastic equilibrium of the anterior and posterior hip muscles (Keegan, 1953) thus eliminating any possibility of lumbar posture change through pelvic rotation. IAP measurements were made using a pressure catheter placed in the stomach via the naso-oesophageal pathway.

Subjects were positioned into a restraint jig where they were loaded with shear and compressive loads. An equal extensor moment about the L4/L5 joint was ensured with similar load moment arms and body posture. The low back reaction moment was examined post-hoc via a planar-static linked segment model (WATBAK, Norman, 1984). Examination of the computed reaction moment verified that the low back moments were of equal magnitude between shear and compressive trials. Muscle forces and low back joint loads were estimated from a three-dimensional myoelectrically assisted model (McGill, 1992, McGill et al., 1986).

The first experiment examined six trials (3 compression and 3 shear) at the maximum load the subject could hold for the 5 second task (isometric). The same methodology was followed for experiment two, but with the inclusion of monitoring (IAP), and manipulating different levels of shear (5-25 kg in 5 kg increments) and compression (5-15 kg).

Results:

Activation levels for all muscles and all subjects from experiment one demonstrated higher activation in the compression trials than the shear trials (figures 1 &2). The same trend was also evident in experiment 2. In every muscle the compressive trials resulted in much higher levels of activation than corresponding shear trials reinforcing the finding of part one of the study. Even with the wide range of inter-subject variation, statistical analysis showed that the level of activation was significantly larger ($p > 0.01$) for all channels, in the compressive trials.

The IAP data from the four subjects was averaged (mean and standard deviation contained in figure 3). The shear tasks show little change from the lowest to highest load (5-25 kg) while the IAP levels are substantially higher for the compressive tasks (5-15 kg) with the lowest compressive load of 5 kg resulting in an IAP value close to that produced by the highest shear load of 25 kg.

The mean L4/L5 joint compressive and shear forces estimated from the model, of the four subjects examined in part two of the study, are presented in figure 4 and 5 respectively. The increased levels of activation observed in the compressive trials resulted in an increased joint compressive penalty. The 15 kg compressive load created almost 800 N of increased load on the L4/L5 joint when compared to the same magnitude of shear load. Similarly the net anterior shear load at L4/L5 was higher for the 15 kg compressive load than the 25 kg shear load.

Discussion:

It appears that the motor control system does not arrange muscle activation levels in a way to minimize lumbar spine loading at least for the relatively low levels of loading in this study. Even though some muscle groups are architecturally arranged to sustain moments and contribute support to offset applied shear loads, this potential for minimization of joint loading was ignored. Optimization procedures, to solve for mathematical indeterminacy, have assumed that the motor control system works to minimize joint load. Given this data, this may not be appropriate. The increases seen in both extensor and abdominal muscles with rising levels of applied compressive suggest that some other mechanical requirement must be met. Perhaps the abdominals are working to offset changes in lumbar posture as compressive loading would tend to accentuate lordosis requiring additional flexor effort. On the other hand Crisco et al. (1992) demonstrated a need for muscular coactivation under compressive loading to stabilize the spinal column to prevent buckling. A lumbar spine, stripped of muscle will buckle under compressive loads as low as 90 N. Perhaps at low loading levels the motor control system is preventing buckling at the expense of increased joint compressive load. Perhaps the applied compressive load must be increased to critically dangerous levels before the motor control system will utilize the architectural advantages of certain portions of the extensor musculature to

optimize safety.

The shear forces supported by the low back were found by Potvin et al. (1991) to remain at approximately 200 N regardless of the mass lifted. Potvin et al. (1991) concluded that the low levels of joint shear left to be supported by passive tissues (facets and disc) suggests that the musculature acts to reduce the amount of joint shear. In the present study the values of joint shear in the shear trials are well below the external applied force due to the shear support provided by the pars lumborum laminae of the extensors. However, it appears that while shear support is provided, it is not optimized at the loading levels tested in this study.

In summary, it would appear that the collective role of the various components of the extensor muscles of the low back is to support extensor moments and that minimum joint loading is not optimized.

References

Crisco III JJ et al.(1992) *Clin Biomech* **7**:19-26.
Keegan, J.J.(1953) *J Bone and Jt Surg* **35A**:589-603.
McGill SM et al.(1986) *Spine* **11**:666-677.
McGill SM et al.(1987) *J Biomechanics* **20**:591-600.
McGill SM.(1991) *J Orthop Res* **9**:91-103.
McGill SM.(1992) *J Biomechanics* **25**:395-414.
Norman RW.(1984) Report to the Canadian Defence and Civil Institute of Environmental Medicine 1984.
Potvin JR et al.(1991) *Clin Biomech* **6**:88-96.
Sutarno CG et al.(1995) *Eur J Appl Physiol* (In Press).

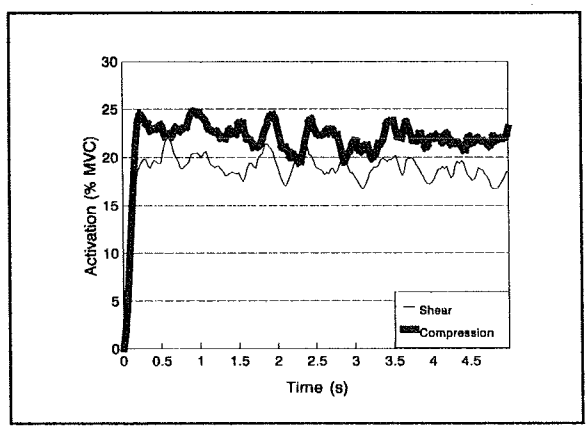

Figure 1: Lower erector spinae EMG signals as a result of applied external compressive and shear loads, with equal extensor moments, in experiment 1.

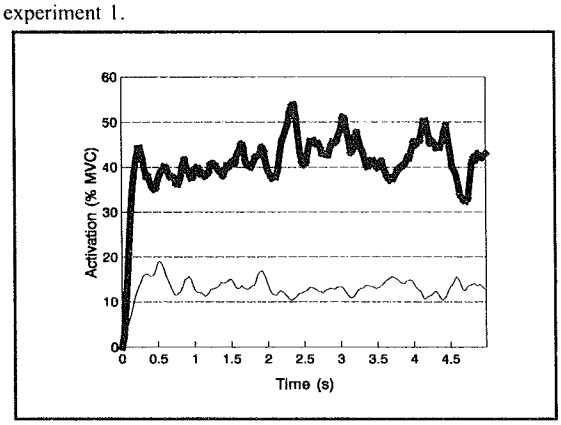

Figure 2: EMG signals for the upper erector spinae during the same task as figure 1.

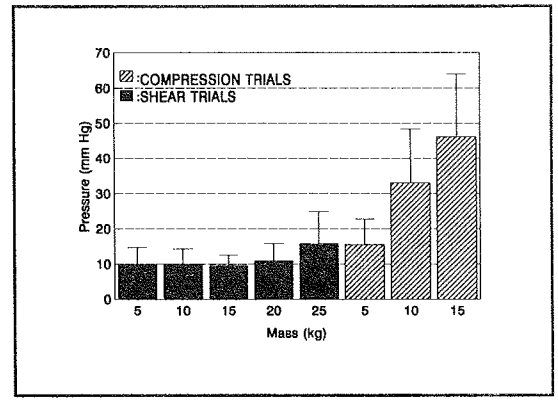

Figure 3: IAP mean and SD for each of the eight load conditions in experiment 2.

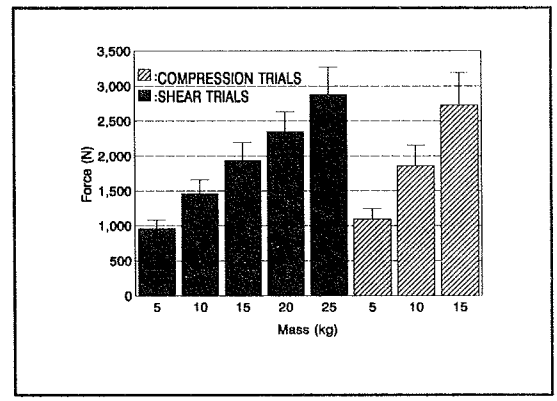

Figure 4: Joint compressive force (mean and SD) for all loading conditions in experiment 2.

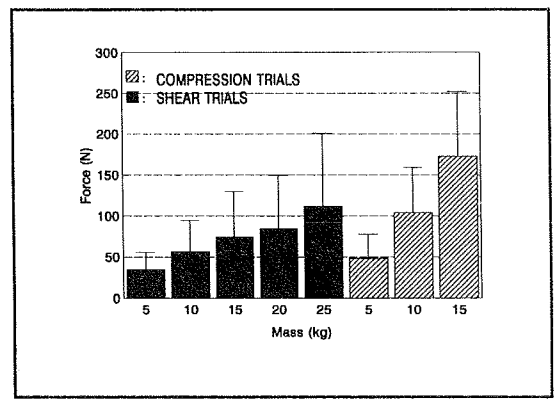

Figure 5: Mean joint shear forces, and SD, for each load condition in experiment 2. A positive value indicates a net anterior shear force.

THE EFFECT OF LOAD RATE ON THE MECHANICAL PROPERTIES OF PORCINE SPINAL MOTION SEGMENTS

Vanessa R. Yingling, Jack P. Callaghan, Stuart M. McGill

Occupational Biomechanics and Safety Laboratories
Department of Kinesiology
University of Waterloo

Understanding mechanical properties of biological tissues is a necessary component for optimizing injury prevention and rehabilitation of the injured. Few studies have examined the effects of load rate on spinal motion segment behaviour; these studies indicate a trend toward load-rate dependence in an uncontrolled non-homogenous population and under position control loading which clouds the interpretation of stiffness and energy storage. The purpose of the current study was to augment the available data but more specifically, to vary the load rate on a homogeneous group of spine specimens under load control loading.

METHODS

Twenty-five cervical spines were collected immediately post mortem with all soft tissue in place. The spines were loaded to failure under five loading rates (100, 1000, 3000, 10,000 & 16,000 N/s) using a servohydrolic dynamic testing machine. After the specimens failed they were dissected to determine the mode of failure using the classifications of Brinckmann et. al. (1989).

A two-way ANOVA design was used to detect effects of load rate and spinal level (C24 & C57) on the energy stored at failure, deformation to failure, ultimate compressive load at failure and the stiffness of the specimen. Post hoc tests (LSD) were utilized to identify the load rates that accounted for the differences recognized by an ANOVA.

RESULTS

Ultimate compressive load was found to increase with increases in loading rate ($p < .05$). Post hoc analysis revealed that the increase occurred at low loading rates and higher loading rates did not augment the effect (Figure 1). Stiffness behaved in a similar manner (Figure 3). The displacement to failure of specimens decreased as load rate increased but again the significant ($p < .05$) effects occurred at low loading rates and not at higher loading rates, at least up to 16,000 N/s (Figure 2). Energy stored in the segments at failure was unaffected by load rate (Figure 4). Furthermore, failure at low load rates occurred exclusively in the cartilaginous endplate while failure of the bony vertebrae appeared with greater frequency at higher load rates (Figure 5).

DISCUSSION

The strain rate response of isolated cortical and cancellous bone is well established (McElhaney, 1966). Failure in bone appears to be dependent more on deformation than on the amount of internal stress resisted by the specimen (McElhaney, 1966). Specifically, bone has been found to become stiffer and to resist higher ultimate compressive loads before failure as strain rate increases. The displacement to failure has been found to remain constant in bone until a critical velocity occurs where the displacement at failure decreases significantly. The effect of load rate on the composite tissues of the vertebral column is less defined. Kazarian et. al. (1977) tested isolated human thoracic vertebral bodies and found that the ultimate compressive load before failure and stiffness increased in a similar trend to the current results. Hutton et. al. (1979) in a study of isolated human lumbar vertebral bodies also found a significant increase in ultimate compressive load at higher load rates. The previous studies reported trends similar to the current study, which tested homogenous motion segments, but they tested uncontrolled non-homogeneous populations over relatively few load rates.

Porcine spinal motion segments were found to be affected by increasing load rate but not in a manner similar to bone. In fact, increases in load rate resulted in a decrease in displacement, while isolated bone has been found to have constant displacements at failure (McElhaney, 1966). The failure in bone may be determined by deformation, but the interaction of the mechanical variables that regulate failure in the composite vertebral motion segment remains unknown. The data of this study which produced mechanical failure under load control on a homogenous set of spines further defines the effect of load rate on injury behaviour.

ACKNOWLEDGEMENTS

Financial support from the Natural Sciences and Engineering Research Council of Canada (NSERC) is gratefully acknowledged. Special thanks to the statistic consulting of D. Capatos.

REFERENCES

Brinckmann, P., Biggemann, M., Hilweg, D. (1989) *Clin. Biomech.* 4(supp 2):s1-s27.

Hutton, W.C., Cyron, B.M., Stott, J.R.R. (1979) *J. Anat.* 129(4): 753-758.

Kazarian, L. & Graves, G.A. (1977) *Spine.* 2(1): 1-14.

McElhaney, J.H. (1966) *J. Appl. Physiol.* 21(4): 1231-1236.

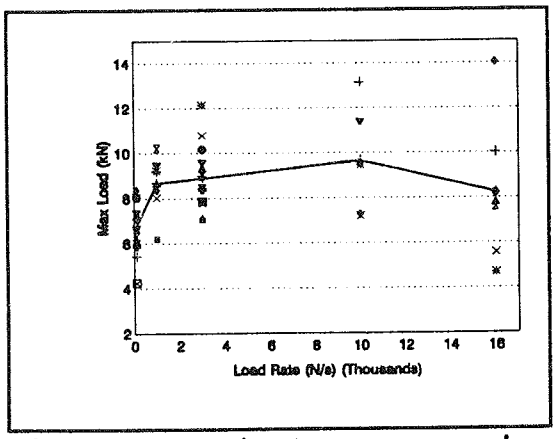

Figure 1: Ultimate compressive load to failure increased with higher load rates.

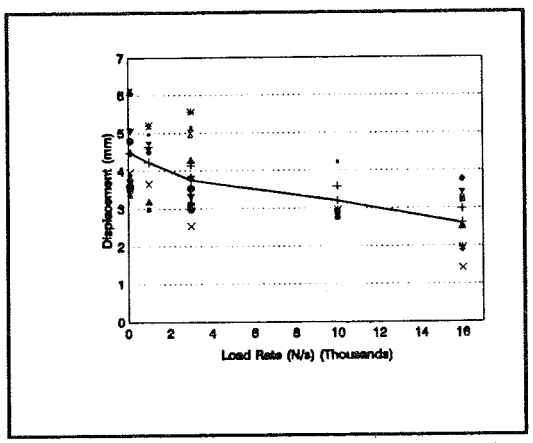

Figure 2: Displacement to failure decreases as load rate increases in a spinal motion segment.

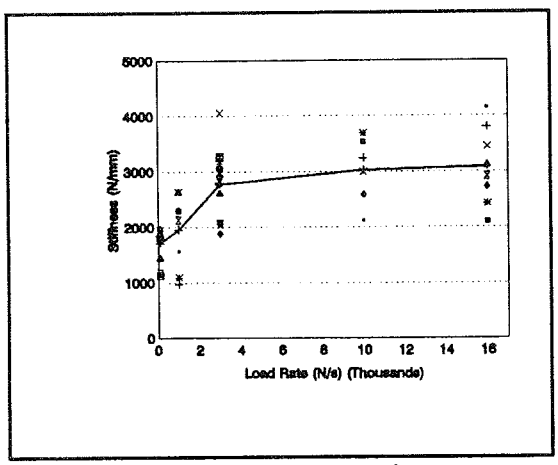

Figure 3: Stiffness increases significantly ($p < .05$) as load rate increases.

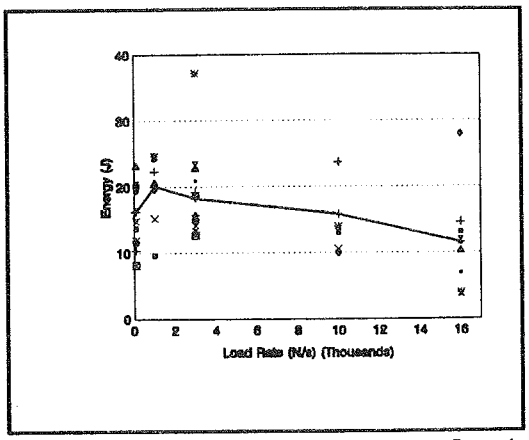

Figure 4: Energy stored at failure was not significantly affected by load rate.

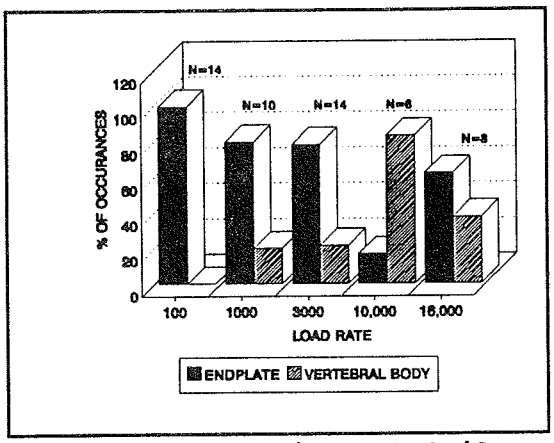

Figure 5: The site of failure was exclusively in the cartilaginous end-plate at 100 N/s but edge fractures occurred in the vertebral body with greater frequency at higher load rates.

DYNAMIC FLEXION RESPONSE OF THORACIC SPINAL SEGMENT

L. Voo[1], Y.K. Liu[2], F.A. Pintar[1], N. Yoganandan[1], J. Reinartz[1]

[1]Department of Neurosurgery, Medical College of Wisconsin 53226
and Veterans Affairs Medical Center, Milwaukee, Wisconsin 53295

[2]University of Northern California, Petaluma, California 94952

INTRODUCTION

Unembalmed cadaver thoracic spinal motion segments (two vertebrae and one joint) were tested in sagittal flexion with both quasistatic and high rates of loading. The resulting moment-angulation characteristics were analyzed to examine their sensitivity to the rate of loading.

REVIEW AND THEORY

Spinal injuries commonly occurring in motor vehicle accidents, contact sports, falls, and diving are often related to high speed loading. In addition to factors such as the load magnitude, the structural behavior and failure of the spine is also related to the speed of loading in these incidents. Studying the structural and failure characteristics of a spinal functional unit in isolation and under a well-controlled setting is an essential step toward understanding its behavior *in vivo*. Although many biomechanical studies have been conducted in the past, they are primarily focused on the response of the structure under low level, sub-injury physiologic, and slowly applied quasi-static loads. Kazarian (1972) tested human vertebral body-disc-body units (without posterior components) in cyclic axial compression up to 50 Hz and found the structural properties. The dynamic stiffness, appeared to be higher at higher loading frequencies. McElhaney et al. (1988) reported no significant differences in bending stiffness of the cervical spine under 0.01, 0.1, and 1 Hz load-unload frequencies. A similar conclusion was reached by Doherty (1990) for the cervical and lumbar spines subjected to combined cyclic bending and axial loading within the same range of loading rates. However, most of the spinal injuries are associated with much higher rates of loading. The only high-speed bending test of the spinal segment was reported by Gadd et al. (1971) on the cervical segments (three vertebrae with two intervertebral discs) in combined bending and axial loading. The rate of flexion angulation ranged from quasistatic to as high as 500 deg/s. Only two specimens were tested in their study and the effect of loading rate on the bending response of the cervical spinal segment was not conclusive. Yoganandan et al.(1989) found that the tensile stiffness of cervical anterior longitudinal ligament and ligamentum flavum increases with the stretch rate in the range from 8.89 to 2500 mm/s.

The spinal motion segment in flexion subjects its anterior aspect (intervertebral disc) in compression and its posterior components (ligamentum flavum, capsular ligaments, interspinous ligament) in tension. In view of the works of Kazarian (1972) and Yoganandan et al. (1989), it was hypothesized that the bending stiffness of the spinal motion segment in flexion was also likely to be higher for higher rates of loading. It is the purpose of this study to examine the moment-angulation characteristics of a single spinal motion segment in sagittal flexion with low and high rates of loading through *in vitro* experiments.

PROCEDURES

Fresh cadaveric thoracic spines were determined to be of good structural integrity based on a review of medical history and by radiographic evaluation. The functional unit (vertebra-joint-vertebra) was isolated and potted in rigid fixation at both ends. The inferior mount of the preparation was then bolted to a six-axis load cell on a custom-designed servo-controlled electrohydraulic testing machine (MTS Systems Corp., Minneapolis, MN). Compressive force was applied by the piston approximately 240 mm anterior to the posterior margin of the vertebral bodies through a lever arm which was rigidly attached to the superior mount of the preparation. The other end of the lever arm was attached to a string potentiometer for the measurement of its end deflection in both quasistatic loading and high-speed dynamic loading.

Each specimen was subjected first to quasistatic load-unload for three cycles at a rate of 7.6 mm/s and then to a single impulsive loading to failure at a piston speed of 3800 mm/s. Compressive force, shear force (posterior-anterior) and sagittal plane bending moment were measured by a six-axis load cell underneath the specimen. Lever arm free-end deflection, piston displacement, and piston contact force were also measured. Data sampling rates were 60 Hz for quasistatic tests, and 20 kHz for dynamic tests.

Force-time and displacement-time data were simultaneously collected into a 486 computer for analysis. The specimen behavior in dynamic loading was recorded at a rate of 4500 full frame/s by a high-speed video camera system (Kodak, Rochester, NY).

Vertebral angulation-time data were derived from lever-arm deflection-time data. Moment-angulation characteristics were obtained by eliminating the time variable. The flexion stiffness of the structure was defined as the slope of the moment-angulation response in its most linear phase. Specimen failure in the study was considered to be the point where the moment decreased markedly while the angulation was still increasing.

RESULTS

Six T3-4 specimens, with age ranging from 50 to 72 years, were tested for this study. The speed of angulation ranged from 1.8 to 2.5 deg/s in quasistatic tests and from 1088 to 1450 deg/s in dynamic tests. The specimens were slightly stiffer under dynamic loading than under quasistatic loading (Table 1). A paired t-test showed that mean stiffness values were different at the level $p < 0.05$.

Table 1: Flexion stiffnesses (Nm/deg)

Sample	Ks*	Kd*	Kd/Ks
1	1.82	2.15	1.18
2	4.37	4.50	1.03
3	5.06	6.08	1.20
4	6.94	6.96	1.00
5	3.40	4.79	1.41
6	4.63	5.56	1.20
Mean	4.37	5.01	1.17
S. D.	1.71	1.66	0.15

* Ks = static stiffness ; Kd = dynamic stiffness; S.D. = Standard Deviation.

DISCUSSION

Flexion bending stiffnesses Ks (static) and Kd (dynamic) had standard deviations greater than 30% of the mean value (Table 1), mainly due to the biological variation in the structural properties of the specimens. When Kd is normalized by its corresponding Ks, the standard deviation reduced to less than 13% of the mean (Table 1). Although the dynamic bending stiffness proved to be higher than quasistatic with a relatively high level of statistical confidence, their relative difference in the mean was only 17%.

The dynamic loading rates in this study fell in the estimated velocity range of neck angulation (up to 1784 deg/s) in the human volunteer sled-impact experiments by Ewing et al. (1969), as quoted in Gadd et al. (1971). In their study of responses and tolerances of human neck, Gadd et al. (1971) reported similarly shaped moment-angulation curves from quasistatic and dynamic sagittal bending tests of two multi-segment cadaveric cervical spinal columns. Their effective angular velocity of the top vertebra ranged from quasi-static to nearly 500 deg/s. The loading rate effect could not be discerned from that study due to the small sample size of only two specimens.

The difference between the dynamic bending stiffness and quasistatic was not found conclusively in the reports by McElhaney et al. (1988) for cervical spine and by Doherty (1990) for cervical and lumbar spines. The range of loading rates in their study were probably too low (0.01 to 1 Hz) show any dynamic effects. The loading rates in our dynamic tests were at least two orders of magnitude higher than their highest rate.

In conclusion, flexion bending stiffness of the thoracic intervertebral joint is higher under high speed dynamic loading comparing to its quasistatic value. The ratio of the dynamic stiffness to static stiffness is relatively constant while the stiffness values themselves vary widely among specimens. Further studies on the cervical and lumbar spines will likely confirm that similar patterns exist in the cervical and lumbar intervertebral joints as well, since their structural and material properties are similar with respect to the responses in sagittal flexion.

REFERENCES

Doherty, B. J. *Ph.D. Dissertation*, Duke University, 1990.

Gadd, C. W. et al. *Proc. 15th Stapp Car Crash Conf.*, 256-268, 1971.

Kazarian, L. *Acta Orthop. Scandinavica*, S146, 1972.

McElhaney, J. H. et al. *SAE Transaction*, 4(97), 1090-1097, 1988.

Yoganandan, N. et al. *Spine*, 14(10), 1102-1110, 1989.

ACKNOWLEDGMENTS

This research was supported in part by PHS CDC Grants R49CCR-507370 and 703640, DOT NHTSA Grant DTNH22-93-Y-17028, the Department of Veterans Affairs.

VARIATION OF HIP ROTATION MOMENT ARMS WITH HIP FLEXION

William E. Hess and Scott L. Delp

Departments of Rehabilitation Medicine and Biomedical Engineering, Northwestern University
Sensory Motor Performance Program, Rehabilitation Institute of Chicago
345 East Superior Street, Chicago, IL, USA, 60611

INTRODUCTION

Excessive internal rotation of the hip is a important problem for individuals with cerebral palsy. To analyze causes and treatments of this problem, we have undertaken a set of computer simulations and anatomical studies to determine which muscles contribute to internal and external rotation of the hip. We have studied how muscle contributions to rotation are altered by excessive hip flexion, which often accompanies exaggerated internal rotation. The goal of this study was to determine how the rotation moment arms of the muscles about the hip vary with hip rotation and flexion. Our results indicate that the internal rotation moment arms of many muscles increase as the hip is flexed, whereas the external rotation moment arms decrease. These results have important implications for the treatment of flexed, internally rotated hips.

REVIEW AND THEORY

Persons with cerebral palsy frequently walk with excessive flexion, adduction, and internal rotation of the hip. Although the muscles that contribute to flexion and adduction are well defined, the muscles that potentially contribute to rotation have not been clearly identified. Few investigators have attempted to quantify hip rotation moment arms (Dostal et al., 1986, Mansour et al., 1987), and none have given a full account of how rotation moment arms vary with hip rotation and flexion. As a result, the rotational function of the muscles about the hip remains unclear, and the success of derotational procedures is limited. The long-term goal of our work is to determine which muscles have the greatest potential to rotate the hip and to develop more effective methods to treat excessive internal rotation.

We developed a computer model to study the rotation capacity of muscles about the hip (Delp et al., 1990). Analysis of this model suggested that maximum isometric rotation moments at the hip were altered with hip flexion; the maximum moment-generating capacity increased for the internal rotators and decreased for the external rotators. Based on this analysis, we hypothesized that the internal rotation moment arms increase and the external rotation moment arms decrease with hip flexion. To test this hypothesis, we measured the rotation moment arms of selected hip muscles in four anatomical specimens at a variety of hip flexion angles.

PROCEDURES

Moment arms were estimated from measurements of muscle length change throughout a range of internal and external rotation. Four anatomical specimens were dissected and the areas of muscle attachments were marked. The following muscles were analyzed: gluteus maximus (Gmax), gluteus medius (Gmed), gluteus minimus (Gmin), iliopsoas (Ilps), piriformis (Pirif), quadratus femoris (Quad Fem), obturator internus (Obt Int), and obturator externus (Obt Ext). Muscles with broad areas of attachment were divided into several compartments to accurately represent their geometry. Wires were used to represent the compartments of each muscle. The gluteus maximus was represented with six wires, gluteus medius with four wires, the gluteus minimus with three wires, and all other muscles with one wire each. The length of the wire was measured using a Celesco position transducer for a range of hip rotation angles (35° internal rotation to 35° external rotation). These measurements were repeated at five different flexion angles (0°, 20°, 45°, 60°, 90°). Fourth order polynomials were fit to the muscle length vs. rotation angle records with a least-squares fit. The derivative of the polynomial fit was taken as an estimate of the moment arm (An et al., 1984). The polynomial fit was chosen because it effectively smoothed noise evident in the numerical derivatives of the muscle length vs. joint angle data. In our analysis, the experimentally derived moment arms were compared to the moment arms estimated with the computer model.

RESULTS

Our results demonstrate that the rotation moment arms of hip muscles vary substantially with hip flexion. For example, at 0° hip flexion the intermediate compartment of the gluteus medius (Gmed2 in Table 1) has a slight external rotation moment arm (Fig. 1). However, with the hip flexed to 45°, which frequently occurs in cerebral palsy, the gluteus medius has an internal rotation moment arm.

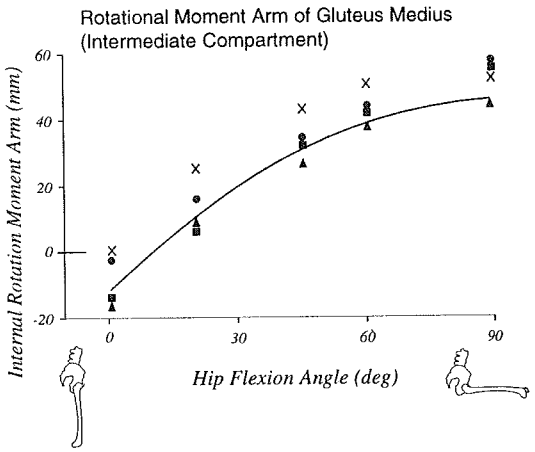

Fig. 1 Internal rotation moment arms at 0° hip rotation vs. hip flexion for the gluteus medius. Each specimen is shown with a different symbol. Results from the computer model are shown in the solid line. Note that the internal rotation moment arm increases with hip flexion.

Table 1. Change in Rotation Moment Arm from 0° to 90° Hip Flexion.

Muscle	Δ m.a. (mm)	Muscle	Δ m.a. (mm)
Gmax1	66±7	Gmin1	23±9
Gmax2	58±18	Gmin2	52±10
Gmax3	41±7	Gmin3	56±21
Gmax4	29±14	Pirif	43±5
Gmax5	12±3	Ilps	-6±4
Gmax6	6±3	Quad Fem	14±5
Gmed1	51±12	Obt Int	23±3
Gmed2	66±10	Obt Ext	-12±4
Gmed3	59±9		
Gmed4	63±25		

1. The average change for the four specimens ± one standard deviation is reported.
2. Rotation moment arms were measured over a range of hip rotation , but only the change in moment arm at 0° hip rotation is reported here.
3. Gmax1 is superior, and Gmax6 is inferior. Gmed1 is anterior, and Gmed4 is posterior. Gmin1 is anterior, and Gmin3 is posterior.
4. A positive number indicates an increasing internal rotation moment arm or a decreasing external rotation moment arm.

Thus, as the hip is flexed, the intermediate compartment of the gluteus medius switches from an external rotator to an internal rotator. Almost all of the muscle compartments we have examined thus far show a trend similar to the intermediate compartment of the gluteus medius (Table 1). A positive number in Table 1 indicates an increase in internal rotation moment arm (or a decrease in external rotation moment arm) as the hip is flexed from 0° to 90°.

DISCUSSION

This study provides new data needed to understand the biomechanics of normal and pathological hip rotation. For 16 of the 18 muscle compartments we have studied, the internal rotation moment arms increase (or external rotation moment arms decrease) with hip flexion. Flexion deformities frequently accompany rotational deformities in individuals with cerebral palsy. The variation in hip rotation moment arms demonstrated in our results suggest that excessive internal rotation may decrease if excessive hip flexion is corrected.

There are several important limitations of this analysis that will be addressed in future studies. First, we have examined only a subset of the muscles that potentially contribute to hip rotation. Specifically, the adductors and hamstrings must be examined in detail since they are commonly lengthened surgically in an attempt to correct internal rotation. Second, we now need to consider how changes in femoral anteversion, which occur frequently in persons with cerebral palsy, affect hip rotational function. Third, we have used a computer model of an adult skeleton and adult-size cadavers to estimate rotation moment arms. Additional work is needed to determine how these compare to the rotation moment arms in children. Finally, it is essential to determine how the moment-generating capacity of the rotators is altered by surgical procedures such as derotational osteotomies of the femur which are performed to correct excessive internal rotation.

REFERENCES

An et al. *J. Biomech. Engng.*, 106, 280--282, 1984.
Delp et al. *IEEE Trans. Biomed. Eng.* 37, 757-767, 1990.
Dostal et al. *Phys. Ther.*, 66, 351-361, 1986.
Mansour, J.M. et al. *J Biomech.*, 20, 51-58, 1987.

ACKNOWLEDGEMENTS

We gratefully acknowledge the assistance of Lynne Jones and David Hungerford and the support of NSF, the Division of Arthritis Surgery Research Fund at Johns Hopkins University, and the Good Samaritan Hospital in Baltimore, Maryland.

FORCE-LENGTH PARAMETERS OF LOWER EXTREMITY MUSCLES DERIVED FROM MAXIMAL ISOMETRIC STRENGTH TESTS

K.G.M. Gerritsen and A.J. van den Bogert
Human Performance Laboratory, University of Calgary, Canada

INTRODUCTION

Musculoskeletal modelling has been shown to be a useful tool to answer questions with respect to neuro-muscular coordination of movements (Zajac, 1993). A good estimation of muscle model parameters is crucial for the model to be successful. When a musculoskeletal model of an elite athlete is used to study a performance task, it is clear that parameters from literature data (usually cadaver measurements) do not reflect the muscle properties of a high performance athlete. The same problem occurs when a musculoskeletal model of a spinal-cord injured patient is used to simulate FES (Functional Electrical Stimulation) assisted locomotion. Due to muscular atrophy and spasticity, these patients are likely to have different muscle properties. For a standard subject some muscle parameters can be relatively easy determined from literature data. For instance, an estimation of maximal muscle force can be made using physiological cross sectional area (PCSA) data. Other parameters such as slack length of the tendon and width of the force-length relationship of a group of muscles are not easily determined.

REVIEW AND THEORY

Literature data on maximal voluntary isometric joint moments as a function of joint angle are available for the six lower extremity tasks (ankle plantar/dorsiflexion, knee extension/flexion and hip extension/flexion). It is however impossible to extract force-length information of bi-articular muscles from these data, because often only one joint angle has been varied systematically. Extracting muscle properties from bi-articular muscles is only possible when for instance, knee extension is executed not only over a range of several knee joint angles, but also over a range of several hip joint angles. *Purpose* - To find a set of model parameters for lower extremity muscles that generate maximal isometric moment angle surfaces comparable to experimental measurements.

PROCEDURES

Four female cyclists performed dorsiflexion for different ankle angles, plantarflexion for different combinations of ankle and knee angles, knee extension, knee flexion, hip extension and hip flexion for different combinations of knee and hip angles in a randomized order. Torques were measured with a Cybex II dynamometer, and the average torque during a one second maximal voluntary contraction, corrected for weight and passive torque, was used for further analysis.

A standard two-element Hill-type muscle model was used to simulate maximal isometric contractions. The force-length relationship of the contractile element *CE*, was assumed to be symmetrical and parabolic. Maximal isometric muscle force (F_{max}) was determined using PCSA data from Friedrich and Brand (1990) summed over all muscles belonging to a functional group (e.g. all mono-articular knee extensors = vasti). Optimal length of the contractile element (L_{CEopt}) was calculated by multiplying sarcomere numbers by sarcomere optimal length. The force-length relationship of the series elastic element *SEE*, is modeled as a non-linear spring (2nd order), with 4% strain at F_{max}. Linear equations were used to calculate muscle length (L_M) as a function of joint angles (φ_j) in radians (full extension = π) according to:

$$L_M(\varphi) = A_0 + d_{ankle}\varphi_a + d_{knee}\varphi_k + d_{hip}\varphi_h$$

where A_0 is determined from typical anatomical data and d_{joint} are moment arms that are assumed constant.

The maximal shortening and lengthening (*width*) of the force-length relationship of the *CE* and the slack length (*lslack*) of the *SEE* are two parameters for each muscle that were optimized to fit the measurements using a least squares fit. F_{max} was not optimized, but scaled inversely proportional to *width* in order to maintain a constant amount of work. The dorsiflexion task could be optimized by itself to find parameters for the tibialis anterior. Knee extension and hip flexion had to be optimized simultaneously, because of the bi-articular rectus femoris. Further, ankle plantarflexion, knee flexion and hip extension were combined to find parameter values for soleus, gastrocnemius, hamstrings and glutei muscles.

RESULTS

Figure 1 shows a maximal isometric plantar flexion surface of one subject together with the simulated surface with optimized parameters. Table 1 provides values of all muscle parameters that were used to simulate all six isometric lower extremity tasks. The parameters that were optimized are averaged over those subjects for which the optimization process resulted in reasonable solutions.

DISCUSSION

Hatze (1981) determined maximal isometric force, optimal fibre length, *SEE* stiffness, as well as *width* for three muscles from a single isometric moment-angle relationship for elbow extension. Although reasonable parameter values were obtained, it is our experience that this procedure is not generally applicable to the lower extremity. Typically, many possible parameter combinations are possible that produce very similar moment-angle relationships. Pandy et al. (1990) used isometric strength data from the literature to obtain the *lslack* parameters in a lower extremity model. Two problems became apparent from this work: (1) It is difficult to extract separate force-length properties for synergistic muscles. (2) Predicted moment-angle relationships tend to be narrower than experimental results.

Address for correspondence:
kggerrit@acs.ucalgary.ca

Table 1: Muscle model parameters. *lslack* and *width* are optimized to fit experimental data. Other muscle parameters are derived from literature data (see text). *N* is the number of subjects used to obtain average values for *lslack* and *width*.

muscle (group)	A_0 [m]	d_{ankle} [m]	d_{knee} [m]	d_{hip} [m]	L_{CEopt} [m]	F_{max} [N]	*lslack* [m]	*width* [%]	*N*
tibialis anterior	0.348	0.037	0	0	0.087	1527.9	0.317±0.004	44.2±5.6	4
soleus	0.367	-0.053	0	0	0.055	3883.2	0.245±0.015	103.9±2.0	3
gastrocnemius	0.508	-0.053	0.020	0	0.055	1638.7	0.420±0.023	88.8±24.2	2
vasti	0.403	0	-0.042	0	0.093	7403.0	0.223±0.006	62.7±6.6	3
rectus femoris	0.524	0	-0.050	0.034	0.081	662.9	0.398±0.013	144.3±32.7	3
glutei	0.465	0	0	-0.062	0.200	1704.8	0.157±0.016	62.5±4.3	4
hamstrings	0.503	0	0.034	-0.072	0.104	1769.3	0.334±0.023	119.7±15.0	4
iliopsoas	0.091	0	0	0.050	0.102	821.3	0.142±0.007	129.8±12.4	4

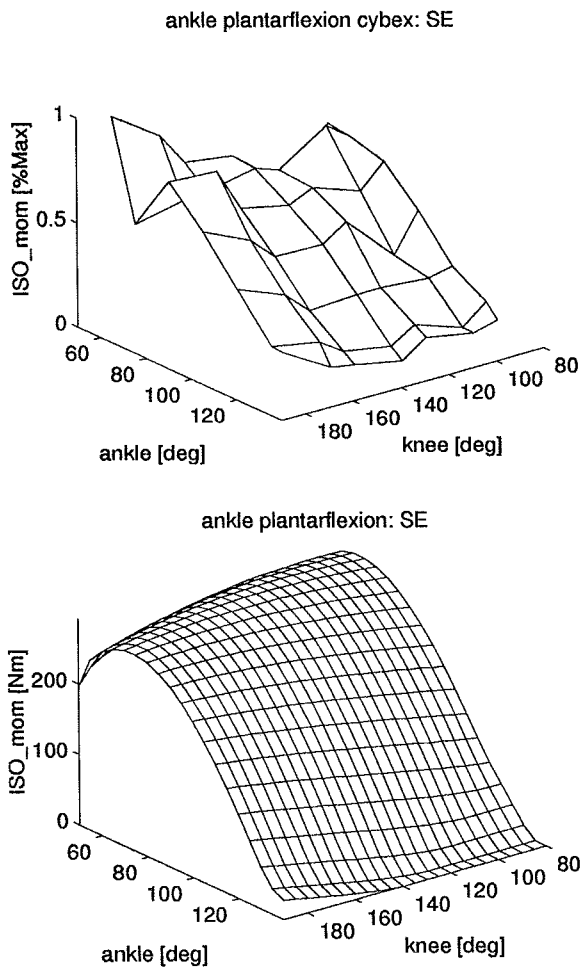

Figure 1. maximal isometric plantar flexion task of one subject (top) and simulated with optimized parameters (bottom). 180 degrees is full extension.

In the present study, the first problem was solved by measuring isometric torque as a function of two joint angles, which allows separation of the properties of mono-articular and bi-articular synergists as shown by Herzog et al. (1991). In addition, information about force production by bi-articular muscles was obtained from isometric moments at both joints. This approach proved to be successful for all muscles, except for the rectus femoris where *lslack* was often increased until the muscle disappeared completely out of the moment angle surfaces. In order to solve the second problem, the *width* parameter was optimized together with *lslack*. This improved the agreement between measurements and model considerably. The optimized *width* was for many muscles much larger than the theoretical value of 54%, based on filament overlap in a sarcomere. This may be a result of the fact that muscles within a functional group, or fibres within a muscle do not reach their optimal length simultaneously.

The parameter values listed in Table 1 represent the maximal amount of information that can be extracted from these isometric strength data. Two aspects of the data collection should be improved in order to increase the reliability of the results: (1) A wider range of angles should be used, especially for the hip joint. This will increase the reliability of the *width* parameter. (2) Random fluctuations in the data, as shown in Figure 1, should be reduced, either by training the subject or by repeating the test protocol on different days and averaging the results. This will facilitate the separation between synergistic mono-articular and bi-articular muscle groups.

REFERENCES

Friedrich, J.A. and Brand, R.A. *J Biomech* 23, 91-95, 1990.
Hatze, H. *Eur J Appl Physiol* 41, 325-338, 1981.
Herzog, W. et al. *Med Sci Sports Exerc* 23, 1289-1296, 1991.
Pandy, M.G. et al. *J Biomech* 23, 1185-1198, 1990.
Zajac, F.E. *J Biomech* 26, Suppl. 1, 109-124, 1993.

ACKNOWLEDGMENTS

The authors would like to thank NSERC of Canada for financial support and C. Janssen for collecting the data.

The Effects of Connective Tissue on Muscle Force Enhancement

D. Hawkins, M.J. Bey
Department of Exercise Science
Biomedical Engineering Graduate Group
University of California, Davis CA 95616

INTRODUCTION

This project was designed to test the effects that changes in collagen content within a muscle have on the muscle's mechanical response to stretch and its potential for force enhancement. This was accomplished by comparing the force enhancement values recorded from the tibialis anterior muscles of normal cage activity rats to force enhancement values obtained from hind limb suspended rats. Hind limb suspension has been shown to alter the ratio of collagenous to non-collagenous protein within the muscle and thus served as a good model for testing the ideas stated above.

REVIEW AND THEORY

Stretch-shortening cycles (SSCs), stretch of an activated muscle followed by muscle shortening, occur in many common human movements (e.g. running and jumping) and they are considered to be important in movement efficiency and for the execution of certain motor tasks. Though the importance of SSCs to human movement has been known for many years, the exact mechanisms responsible for the observed muscle force enhancement continue to be debated [Abbot et al, 1952; Asmussen, 1953; Cavagna, 1977; Thys et al, 1975; Alexander and Bennet-Clark, 1977; Edmond et al., 1978]. It has been proposed that force enhancement may be due to storage and subsequent release of elastic energy within the tendon or muscle, or potentiation of the force generated per individual cross-bridge, or a combination of the two. To investigate the relative role that these two factors play it was hypothesized that cross-bridge force potentiation is the primary source of force enhancement during a single active stretch. For this hypothesis to be true changes in the relative amount of connective tissue within a muscle should not effect force enhancement. This hypothesis was tested by comparing the force enhancement recorded during stretch of rat tibialis anterior (TA) muscles from two groups of rats, a normal cage activity (NCA) group, and a four week hind limb suspended (HLS) group.

PROCEDURES

The work station used to collect the data for this study consisted of several components described in detail elsewhere (Hawkins and Bey, 1994). Briefly, the hardware included an arbitrary waveform generator (Model 75 supplied by WaveTek) for controlling muscle activation, an ergometer lever system (Model 305B supplied by Cambridge Technologies) for controlling muscle kinematics and recording the force developed, a video-based motion analysis system (Motion Analysis Corporation) for determining localized muscle and tendon strains, and a microcomputer containing a Lab Master DMA data acquisition board (Scientific Solutions).

Tibialis anterior (TA) muscles from two activity groups of rats (normal cage activity and fours weeks of hind limb suspension) were tested under a variety of eccentric contraction conditions. Tissue covering the TA was carefully removed. The nerve innervating the TA was exposed and a small electrode cuff was attached to it. Three small black silicone markers were located along the length of the muscle-tendon-bone (MTB) complex The distal end of the TA was dissected free with a small section of bone retained for use in attaching the MT complex to the lever arm. The partially intact TA was positioned in front of the video camera and the tibia secured to a fixture to minimize movement of the limbs during testing. A saline drip system was used to maintain the TA moist at all times. All mechanical tests were conducted at room temperature, 24 $\pm$ 2 °C.

The TA nerve was stimulated via the nerve cuff and the force generated by the muscle was determined for various stretch amplitudes, stretch rates and initial muscle lengths. The lever arm was moved either 1 mm, 2 mm, 3 mm, or 4 mm at rates of either 1 mm/s, 10 mm/s or 100 mm/s. Muscle kinematics associated with each test were determined using the video system to digitize the relative location of the silicone markers located along the MTB complex.

Data were grouped into categories based on the combination of initial muscle length, muscle stretch velocity and muscle stretch amplitude. A total of 36 groups were considered; 4 ranges of initial muscle lengths (< 0.8 %Lo, 0.8-0.9 %Lo, 0.9-1.0 %Lo, > 1.0 %Lo: "Lo" being the muscle length at which maximum active force was developed), 3 ranges of stretch velocities (< 5.5 mm/s, 5.5-15.5 mm/s, > 15.5 mm/s), and 3 ranges of stretch amplitudes (< 1.5 mm, 1.5-2.5 mm, > 2.5 mm). Muscle force enhancement (MFE) was defined as the force generated at the end of the eccentric contraction divided by the isometric

force developed by the muscle at a comparable muscle length. MFE values were compared between the NCA and HLS groups for each of the kinematic categories listed above.

RESULTS

The HLS group had on average a smaller muscle mass, lower maximum isometric force, and a higher percentage of connective tissue per wet weight of muscle compared to the NCA group. Initial comparisons of force enhancement between the two groups yielded significantly ($p<0.05$) higher force enhancement values for the HLS group for initial lengths less than 80% of Lo. However, the NCA group demonstrated higher force enhancement values for initial lengths near 100% Lo. Results from 12 of the kinematic categories analyzed are summarized in Figure 1 and Figure 2 for the NCA and HLS groups respectively.

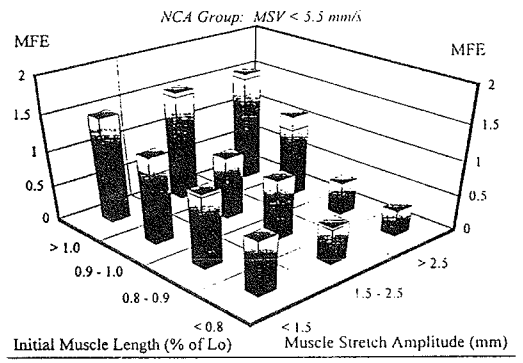

Figure 1: MFE results for the NCA activity group for muscle stretch velocities (MSV) < 5.5 mm/s.

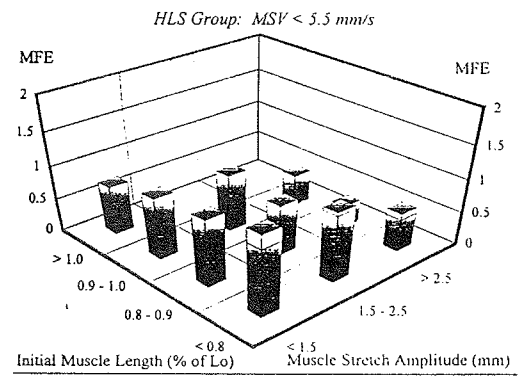

Figure 2: MFE results for the HLS activity group for muscle stretch velocities (MSV) < 5.5 mm/s.

DISCUSSION

It was believed that the difference in force enhancement between the two groups would always be skewed toward one group, or zero. Thus, the fact that the trend of the MFE values changed as a function of the initial muscle length was not expected. It may be that altering the relative percentage of connective tissue within the muscle altered the force-length relationship causing the ascending portion of the curve to be less steep for the HLS group. If this occurred, then the HLS group would appear to have a higher force enhancement for initial lengths corresponding to the ascending portion of the force-length curve though the absolute increase in force might be less than the NCA group. A similar argument could be made for the higher MFE values observed for the NCA group for initial lengths greater than 0.9 %Lo. Another consideration which might explain the results are the effects of connective tissue "quality". It may be that different results would be obtained from muscles that have a greater percentage of connective tissue resulting from endurance-type training. The "quality" of this connective tissue may alter the force-length curve in a different way compared to that observed for the HLS group. At this time it can be stated that the relative percentage of connective tissue within a muscle does have an effect on its ability to generate force enhancement. However, relative to the initial hypothesis it can not be concluded that cross-bridge force potentiation did not play a major role in force enhancement.

REFERENCES

Abbot, B.C., et al. *J. of Physiolo.* **117**(3), 380-390, 1952.

Alexander, R. and Bennet-Clark H.C.. *Nature.* **265**, 114-117, 1977.

Asmussen, E. *Acta Physiol. Scand.* **28**, 364-382, Fasc 4, 1953.

Cavagna, G.A. *Ex. and Sports Science Reviews.* Ed. by R.S. Hutton. Journal publishing affiliates, Santa Barbara, CA. **5**, 89-129, 1977.

Edman, K.A.P., et al. *J. of Physiol.*. **281**, *139-155, 1978.*

Hawkins, D.A. and M. Bey. *J. of Biomech.Eng.*. **116**, 51-55, 1994.

Thys, H., G.A., et al. *Pflugers Archives*, **354**, 281-286, 1975.

ACKNOWLEDGMENTS

The author is grateful to the Whitaker Foundation for supporting this project.

THE EFFECT OF TENDON LOADING AND WRIST POSTURE ON CARPAL TUNNEL PRESSURE IN CADAVERS

P.J. Keir and R.P. Wells

Department of Kinesiology, University of Waterloo, Waterloo, Ontario, Canada N2L 3G1

INTRODUCTION

The pathophysiology of carpal tunnel syndrome (CTS) has long been associated with increased intracarpal canal pressures. Pressures have been measured under a variety of conditions using a variety of devices. Hydrostatic pressures are known to increase with passive wrist flexion and extension, more so with extension (Rojviroj *et al.*, 1990; Okutsu *et al.*, 1989). Similar findings have been found with bulb/balloon type transducers, notably Smith, Sonstegard & Anderson (1977). Muscle force has been shown to affect carpal tunnel pressure (CTP) whether described in gross terms (*cf.* Okutsu *et al.*, 1989) or due to specific muscle loading (Smith *et al.*, 1977).

The difference between the catheter measures (slit, wick, perforated, needle) and bulb measures appears to be a difference between measuring a hydrostatic pressure and a combination of hydrostatic pressure and contact stress. Compression (contact stress) as a mechanism is supported by Phalen's test which places the wrist into flexion (known to decrease CTP) and if the modified test is used the fingers pinch until symptoms arise.

While it has been shown that increased flexor muscle forces lead to increased pressures within the carpal tunnel, the extent and manner of this relationship is unknown. The purposes of this study were to determine the effects of loading different muscles in many functional wrist postures and to examine the similarities and differences between the techniques of the bulb and catheter pressure measurement.

METHODS

Eight fresh/frozen cadaver arms (4 pairs) were used in this study. Pressures were measured using two techniques, a catheter and a bulb. Each arm was secured as seen in Figure 1. The wrist angles were maintained via a rod anchored into the third metacarpal shaft. Nine wrist angles from 45° extension (-45°) to 45° flexion were used (-45, -30, -20, -10, 0, 10, 20, 30, 45). Four loading conditions were tested: 1. no tendon loading, 2. combined loading of flexor digitorum profundus and flexor digitorum superficialis to the index and long fingers (FDP2+3 + FDS2+3), 3. loading of palmaris longus (PL), and 4. loading of flexor pollicis longus (FPL). Due to the exploratory nature of the last two loading conditions, the number of flexion-extension angles was reduced to five by eliminating the 10° and 30° angles.

The skin on the flexor side of the forearm was opened no closer than 10 cm proximal to the distal wrist crease and the deep flexors to the index and long fingers (FDP2 and FDP3, respectively), the superficial flexors (FDS2, FDS3), palmaris longus (PL) and flexor pollicis longus (FPL) were identified and sutured to a cord. The cord was run over a ball-bearing pulley and a kilogram mass hung from it.

Hydrostatic intracarpal canal pressure was measured using an open ended polyurethane catheter with 3 side holes connected to a pressure transducer (Gould Electronics, model P23Db). A slow infusion of Ringer's solution at a rate of approximately 0.5 ml/min was maintained between measurements.

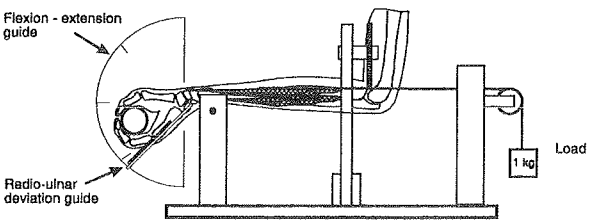

Figure 1. Schematic of the forearm secured in the testing jig. The wrist posture was defined by two orthogonal protractors and a rod anchored into the shaft of third metacarpal.

After all tests for hydrostatic pressure were completed, the median nerve was replaced by a bulb made from of thin walled rubber tubing, with a measuring zone of 30 mm. For the bulb readings, zero was considered the pressure with the wrist neutral position with the no loads acting on it.

The data were analyzed using repeated measures ANOVAs (SAS). The angles used in the analysis included only those that were used in all loading conditions (i.e. -45°, -20°, 0, 20°, 45°).

RESULTS

The effect of differential tendon loading was significant using both measurement techniques (Figure 2). The pressures obtained via the catheter show a "U" shape for all load conditions (Fig. 2) with higher values in extension and a minimum in neutral or in slight flexion. There were statistically significant main effects due to load ($F = 9.51$, $p = 0.0005$) and wrist angle ($F = 13.28$, $p = 0.0001$). The loaded PL created higher pressures than loading the flexors which were both significantly higher ($p < 0.05$) than FPL and the unloaded condition. The bulb technique showed responses similar in shape to the catheter. Significant main effects of load and angle were found ($F = 19.98$, $p = 0.0001$ and $F = 6.50$, $p = 0.0008$, respectively). The pressure response due to the flexors to be greater ($p < 0.05$) than the response from loading PL which created significantly higher pressures ($p < 0.05$) than loading FPL or the unloaded condition. As a point of note, the loading the flexor tendons condition appears to have a very large effect (twice as great as PL, the next highest pressure condition) on carpal tunnel pressure at wrist flexion angles beyond 20°(Fig. 2). However, the pressure response to PL loading was greater than that in the flexor loading condition with the wrist extended beyond 20°.

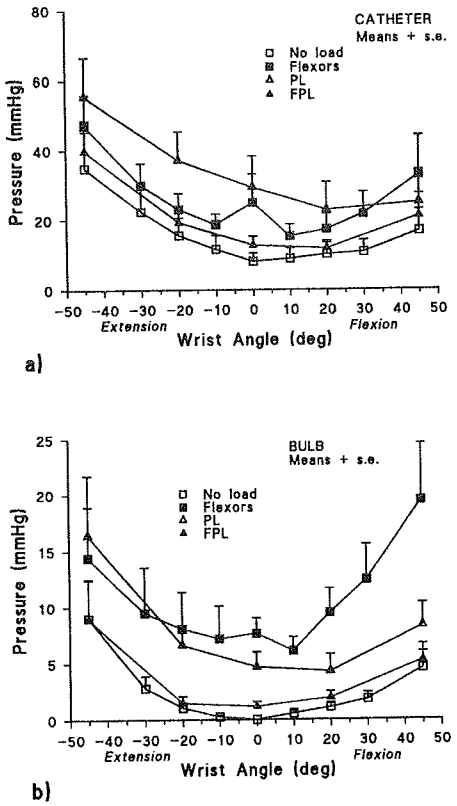

Figure 2 Pressures measured in each of the loading conditions in angles of flexion and extension, a) Hydrostatic pressures measured using the catheter. b) Contact pressures measured using the bulb.

DISCUSSION

Carpal tunnel pressures are dependent on wrist posture and the tendons carrying load through the carpal tunnel. Regardless of loading condition, catheter pressures were higher in extension than in flexion, this has been shown previously for the passive condition (Rojviroj *et al.*, 1990; Okutsu *et al.*, 1989). The magnitudes of the unloaded catheter pressures, as well as the standard errors were in agreement with those values in the literature (Rempel, Horie & Tal, 1994). This indicates that the cadaveric carpal tunnel pressure undergoes similar changes to the *in vivo* wrist when subjected to changes in posture despite possible changes in tissue fluid content due to the freezing and thawing process.

The measures from the bulb and catheter techniques indicate that they may be measuring different phenomena. Based on the characteristics of the bulb transducer, it may be appropriate to separate the findings of the bulb and catheter and discuss them separately. If these measures are indeed independent, they may be considered additive, thus both measures are necessary to describe the condition of loading on the intracarpal canal contents.

Histological investigations of the effects of direct nerve compression have provided strong support for mechanical trauma being a greater etiological factor than ischemia (Rydevik & Lundborg, 1977) although it has been shown that nerve conduction is regained after the release of compression but full amplitude of the action potential is gained upon restoration of blood flow (Lundborg *et al.*, 1982). These findings regarding mechanical compression have also been noted in patients with CTS (Schuind, Ventura & Pasteels, 1990) and in cadaveric wrists which had no history of CTS (Armstrong *et al.*, 1984). In the present study, using the bulb pressure as measure of contact pressure, evidence of direct loading in the carpal tunnel was found with the wrist flexed and flexors loaded (Fig. 2). As the flexion angle increased, the bulb pressure increased drastically, to pressures of about 250% of those of the lowest pressure seen with the flexors loaded in the neutral position and the next highest pressure at those angles (PL). These findings provide a sound mechanical basis for a positive modified Phalen's test in which the wrist is acutely flexed and the digital flexors loaded by means of an active pinch.

Palmaris longus loading had a greater effect on carpal tunnel pressure than expected. The pressures associated with loading palmaris longus were generally the largest of all conditions of loading when measured with the catheter and second highest (flexors) when measuring with the bulb. The highest pressures for both methods were found in extension, thus the insertion of the PL into the palmar aponeurosis (which should be considered the distal portion of the flexor retinaculum (Cobb *et al.*, 1993)) may have an effect on the carpal tunnel shape. For example, in extension, the pull of PL may flatten the retinaculum thereby increasing the pressure within the tunnel. At the level of the pisiform, the cross-sectional area and the depth of the carpal tunnel have been shown to decrease with wrist extension (Yoshioka *et al.*, 1993). This effect may be further intensified with significant loading of the palmaris longus. The opposite may occur with the wrist in flexion as we found the lowest catheter pressures for the PL loading condition in flexion. Other muscles inserting onto the retinaculum, such as the thenar muscles, may also strongly influence pressure by a similar mechanism. Palmaris longus is a weak wrist flexor with limited force production capability, its connections with the palmar aponeurosis and tight coupling with the flexor retinaculum provide insight to its possible function to control the shape of the carpal tunnel.

This study was the first attempt to determine the effects of differential muscle loading on carpal tunnel loading. Muscular loading elevates intracarpal canal pressure, particularly PL in extension and the flexor tendons in flexion. Bulb pressure measurements seem to be due to direct local contact and were found to be greatest in flexion with the digital flexors carrying load.

REFERENCES

Armstrong, T.J. et al. (1984) *J. Occup. Med.* **26(3)**, 197-201.
Cobb, T.K. et al. (1993) *J. Hand Surg.* **18A**, 91-99.
Lundborg, G.N. et al. (1982) *J. Hand Surg.* **7(3)**, 252-259.
Okutsu, I. et al. (1989) *J. Bone Joint Surg.* **71-A (5)**, 679-683.
Rempel, D. et al. (1994) *Marconi Keyboard Research Conference*
Rojviroj, S. *et al.* (1990) *J. Bone Joint Surg.* **72B(3)**, 516-518.
Rydevik, B. & Lundborg, G. (1977) *Scand. J. Plast. Reconstr. Surg.* **11**, 179-187.
Schuind, F. et al. (1990) *J. Hand Surg.* **15-A**, 497-503.
Smith, E.M. et al. (1977) *Arch. Phys. Med. Rehabil.* **58**, 379-385.
Yoshioka, S. et al. (1993) *J. Hand Surg.* **18B**, 620-623.

ACKOWLEDGEMENTS

The authors wish to thank Anne Moore and Warren Lavery. This work was supported by NSERC grant #A2785.

INTERPLAY OF MUSCULOSKELETAL GEOMETRY AND MUSCLE ARCHITECTURE IN THE HUMAN WRIST

Roger V. Gonzalez, Scott L. Delp, Anita E. Grierson, and Thomas S. Buchanan

Departments of Rehabilitation Medicine and Biomedical Engineering, Northwestern University, and Sensory Motor Performance Program, Rehabilitation Institute of Chicago, 345 East Superior Street, Chicago, IL, 60611

INTRODUCTION

Measuring the moments generated by muscles under conditions of maximum voluntary contraction is the most common method used to assess muscle strength. Several factors contribute to the peak isometric moment generated by an individual muscle, including its physiological cross-sectional area (PCSA), moment arm (MA), and activation. Other factors contribute to the change in the isometric moment with joint angle, such as variation of MA with joint angle, and the muscle's force-length (F-L) behavior. Since measured joint moments represent the sum of the moments generated by individual muscles, a biomechanical model is needed to analyze the contributions of individual muscle architectures (the arrangement of muscle fibers in a muscle-tendon complex) and MAs to the moment-generating capacity of muscles about the wrist. In this study we have used a model that characterizes the architecture and geometry of 15 muscles to analyze measured maximum voluntary moments about the wrist.

REVIEW AND THEORY

We recently reported the maximum isometric wrist moments generated by 10 healthy subjects (Grierson et al., 1995). This experimental study demonstrated that the peak flexion moment was significantly greater than the peak extension moment. The study also showed that the flexion moment peaked with the wrist in the flexed position, where muscle fibers of the flexors are relatively short.

The purpose of this study was to determine if the measured moments about the wrist could be explained by the relationship between the architecture and MAs of the wrist muscles. We hypothesized that the peak flexion moment was greater than the peak extension moment because the sum of PCSA-MA products is greater for wrist flexors than extensors. We also hypothesized that flexion moment peaked with the wrist in flexion because the moment arms of the major flexors increase as the wrist is flexed. To investigate these issues we developed a detailed biomechanical model of the wrist and the surrounding muscles.

PROCEDURES

This wrist model represents the three-dimensional geometry of the bones, kinematics of the joints, and the lines of action and force-generating properties of 15 muscles. These muscles were: abductor pollicis longus (APL), extensor carpi radialis brevis (ECRB), extensor carpi radialis longus (ECRL), extensor carpi ulnaris (ECU), extensor digitorum communis (EDC), extensor digiti minimi (EDM), extensor indicis proprius (EIP), extensor pollicis brevis (EPB), extensor pollicis longus (EPL), flexor carpi radialis (FCR), flexor carpi ulnaris (FCU), flexor pollicis longus (FPL), flexor digitorum profundus (FDP), flexor digitorum superficialis (FDS), and palmaris longus (PL). The model was implemented using the musculoskeletal modeling system (SIMM) described by Delp et al. (1990). The bone geometry was obtained by digitizing an average size male skeleton. The kinematics of the wrist were represented as two revolutes to account for motion at the radiocarpal and midcarpal joints (Ruby et al., 1988). Muscle-tendon paths were defined based on the anatomical landmarks of the bone models. In addition to the muscle origins and insertions, "via points" were used to represent muscles that wrap over bones and to simulate the constraints imposed by retinacula. The isometric force-generating properties were derived by scaling a generic Hill-type muscle model (Zajac, 1989). Parameters to scale the model were derived from Lieber et al. (1990), Jacobson et al. (1992), and Lieber et al. (1992). Different factors were used to scale the PCSAs of the flexors (30 N/cm^2) and extensors (45 N/cm^2). These factors were derived by comparing the joint moments computed with the model to the maximum moments reported by Grierson et al. (1995).

RESULTS

MAs for the 15 muscles were estimated with the model and compared with MAs in the literature (Brand et al., 1993; Loren et al., 1995). In general, the magnitudes of the computed MAs and their variation with joint angle corresponded well with the experimental data. Flexor MAs were on average 18% larger than extensor MAs throughout the range of motion. The flexor moment arms varied more with joint flexion; the difference between the maximum and minimum moment arms was 2.7 times greater for the flexors. Flexor MAs also tended to peak toward full flexion while the extensor MAs tended to peak in the mid-range to slightly extended position, except the ECRL, EPL, and EDC, which peaked near full extension.

The maximum isometric moments computed with the model correspond well with the experimentally measured moments over most of the range of motion (Figure 1). The model replicated the experimental magnitude of the peak flexion moment to be approximately twice as large as the peak extension moment. This occurred because the total PCSA of the flexors is 111% larger than the PCSA of the extensors. In the model, the sum of the peak isometric forces is 37% larger for the flexors than the extensors because a smaller factor was used to scale PCSA to peak force for the flexors (see Procedures).

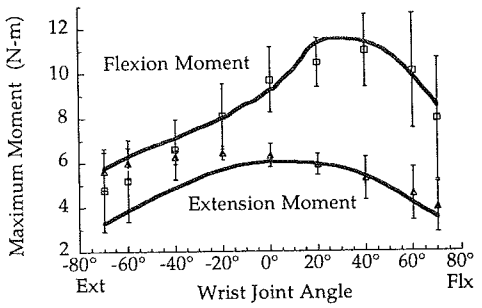

Figure 1: Average maximum isometric flexion and extension moment vs. wrist joint angle. Points (empty squares, triangles) represent subject data with the error bars representing the 95% confidence interval. Lines represent the model's calculated moments. Flexion angles are positive, extension angles are negative.

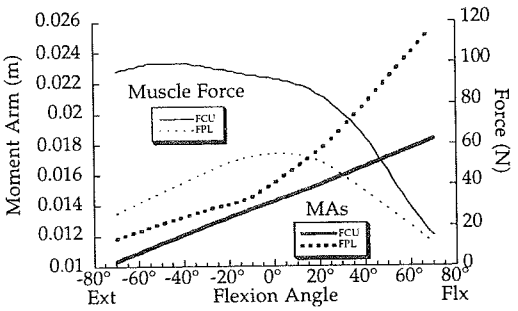

Figure 2: Moment arm and muscle force versus flexion angle for two muscles. Light curves are muscle forces, bold curves are MAs. Solid curves are flexor carpi ulnaris (FCU) and dashed curves are flexor pollicis longus (FPL). Flexion angles are positive.

The model revealed why the flexion moment peaks with the wrist in a flexed position, in accord with experimental data (Grierson et al., 1995). Flexion moment peaks in this position because the moment arms of the major flexors increase as the wrist is moved toward full flexion. Figure 2 shows the force-angle and MA-angle behavior of two important flexors (FCU and FPL). Although the flexor muscle forces decrease with flexion beyond the neutral position, the product of muscle force and MA produces a larger joint moment at a slightly flexed position. This occurs because the flexor forces decrease slightly with flexion (i.e., they are on the plateau region of F-L curve in a slightly flexed position), and then much more steeply from a slightly flexed position through full flexion (i.e., as they reach the ascending region of the F-L curve).

The model underestimates the moment-generating capacity of the extensors with the wrist near full extension because the fibers are very short in this position. These short fibers affected 4 (ECU, ECRB, EDC, EIP) of the 7 extensor muscles substantially.

DISCUSSION

The interplay of the MAs and architecture of the wrist muscles accounted for the experimental observations of maximum flexor and extensor moments about the wrist. We found that the greater PSCA and MAs of the flexors are responsible for the greater flexion moment. The position of the peak flexion moment was determined by the increasing flexion moment arm and decreasing flexor force with flexion. That is, the interplay of the flexor MAs increasing toward full flexion and the muscle forces slowly decreasing up to a slightly flexed position resulted in the peak moment occurring at a slightly flexed position.

Even though the computer model replicates the measured joint moments well, it is difficult to have confidence in the individual muscle force estimates because many muscles contribute to the measured moments. Fortunately, there have been excellent measures of muscle architecture (Lieber et al., 1992) and detailed reports of muscle moment arms

(Brand, 1993; Loren et al, 1995) to test the model. However, additional data is needed to test the variation of muscle force with joint angle. Our simulations suggest that some of the flexors operate on the ascending limb of the F-L curve for neutral and flexed positions, while the extensors operate on the ascending limb for extended positions only. Similar operating ranges were reported by Loren et al. (1995). Detailed measurements of sarcomere length and joint angle are needed to further test these simulation results.

We believe that the development of a detailed model of the wrist will elucidate the factors that contribute to normal muscle function, reveal the causes of deformities that arise in rheumatoid arthritis, and help design surgical corrections and joint replacements to restore joint function. This initial report is a first step in the development of this model.

REFERENCES

Brand, P.W. et al. *Clinical Mechanics of the Hand:*, Mosby Year Book, 1993.

Delp, S.L. et al. *IEEE Trans. Biomed. Eng.* 37, 757-67, 1990.

Grierson, A.E. et al. *J. of Biomech.* (accepted).

Jacobson, M.D. et al. *J Hand Surg.* 17A, 804-9, 1992.

Lieber, R.L. et al. *J Hand Surg.* 15A, 244-50, 1990.

Lieber, R.L. et al. *J Hand Surg.* 17A, 787-98, 1992.

Loren, G. J. et al., *J. of Biomech.* (accepted).

Ruby, L.K. et al. *J Hand Surg.* 13A, 1-10, 1988.

Zajac F.E. *Crit. Revs. Biomed. Eng.* 17: 359-411, 1989.

ACKNOWLEDGMENTS

This work is supported, in part, by NIH R29-AR40408.

IN SITU MECHANICAL BEHAVIOR OF CORALLINE HYDROXYAPATITE AFTER SHORT AND LONG-TERM IMPLANTATION IN THE CANINE PROXIMAL HUMERUS

B. K. Bay, N.A. Sharkey

Orthopaedic Research Laboratories, University of California Davis, Sacramento, CA 95817

INTRODUCTION

Coralline hydroxyapatite (CHA) is coral chemically converted from calcium carbonate to hydroxyapatite. When implanted into defects in the mammalian skeleton it is readily infiltrated by bone tissue and becomes an integral part of the host bone. Our laboratory has studied CHA implanted in the canine proximal humerus. After 1 year of ingrowth material properties of the explanted graft are similar to published values for canine trabecular bone.

There is evidence, however, that bone surrounding the implant undergoes considerable remodeling and may have significantly altered material properties. The mechanical interaction of the implant and surrounding trabecular bone, and how this changes over time, are therefore uncertain.

Texture correlation is a technique recently developed in our laboratory for the measurement of deformation patterns within trabecular bone samples (Bay, B.K., 1995). In was used here to directly visualize the interaction between CHA and trabecular bone in the canine proximal humerus model. It is shown that the CHA implant is initially considerably weaker than the host trabecular bone. In contrast, after 1 year of implantation the graft is substantially stiffer and acts as a strong stress concentration.

REVIEW AND THEORY

Coral-based bone graft materials are attractive because certain coral genera (*Porites and Goniopora*) have interconnected pores of a suitable size for bone ingrowth, and the calcium carbonate skeleton can be converted to hydroxyapatite without altering the overall architecture. CHA securely anchors within trabecular bone defects, and is rapidly infiltrated with bone tissue (Holmes, R.E. et al., 1986).

Our laboratory has studied CHA in a canine model, focusing on the histology and material properties of retrieved implants (Martin, R.B. et al., 1993). The model consisted of a 1 cm diameter hole cored in the proximal humerus and filled with a slightly undersized plug of CHA (Fig. 1A). After 1 year the implants were removed with a coring tool and tested in compression. Elastic modulus was 593 ± 175 MPa. Virgin CHA elastic modulus ranges from 30 to 75 MPa, and canine trabecular bone ranges from 230 to 430 MPa.

While CHA grafts generally fared well in these animal models, questions remain. How does CHA interact mechanically with the host bone? Does the graft need protection from load immediately after implantation? Are there potential consequences of implantation below articulating surfaces? Deformations in loaded sections cut from implanted bones provide information concerning these issues.

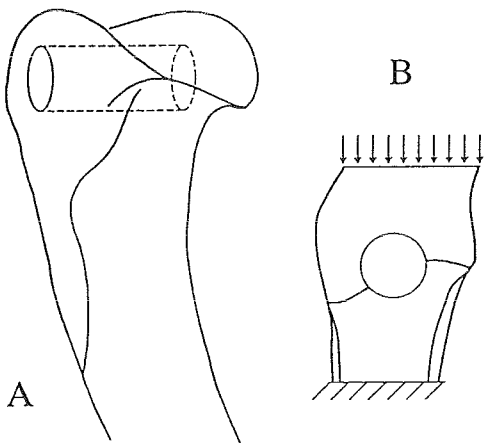

Figure 1: Implant location and test sample.

PROCEDURES

Samples were prepared from two bones harvested from dogs with humeral CHA implants (remaining bones were committed to other tests). The short-term bone came from an animal sacrificed 1 week after surgery due to complications unrelated to the implant. The long-term bone came from an animal sacrificed 1 year after surgery. Slabs 5mm thick were cut from each bone perpendicular to the long axis of the implant (Fig 1B). A Faxitron was used to radiograph the samples unloaded and with a nominal compressive strain of 0.008 in the superior-inferior direction.

Texture correlation measures displacements by comparison of unloaded and loaded contact radiographs digitized with standard video grabber techniques. The displacement for any point within the sample is measured by locating the point with a pattern matching algorithm in both images and calculating the difference in position. An evenly spaced 64x48 grid of points is analyzed in this way, then processed with a Savitsky-Golay convolution filter to remove high frequency noise.

RESULTS

Lines of constant displacement magnitude concentrating within the center of the implant for the short-term sample (Fig. 2) are consistent with collapse of the virgin graft material. A similar pattern would be expected for an unfilled defect.

Contour lines concentrating in the trabecular bone surrounding the long-term implant (Fig. 3), and widely-spaced lines within the implant itself, are consistent with a graft substantially stiffer than the surrounding bone. In addition to the stress concentration effects within the trabecular bone, high shear strains at the bone-implant interface are expected under these conditions.

DISCUSSION

The strain patterns after short-term implantation illustrate the need to protect the CHA implants during the time interval before ingrowth of bone tissue. In this canine model the graft is sufficiently shielded from strain *in vivo* to prevent spontaneous fracture. This would not generally be the case in clinical use.

The stiffness mismatch between graft and host bone at 1 year has two possible consequences. First, the altered strain environment in the host bone could lead to subsequent alterations in bone density through remodeling. Second, subchondral bone stiffening has been implicated in osteoarthritis. One of the most common applications of CHA is the replacement of epiphyseal bone lost to crush fractures, therefore high graft modulus may have a detrimental effect on the overlying articular cartilage. Further studies are required to evaluate this potential complication.

There are several limitations in a study of this type. Dogs are aggressive bone formers, and their response to CHA is not identical to the human response. The texture correlation technique requires sections cut from the whole bone and measures deformation in two-dimensions only. Interpretation of results is limited to the relative behavior of tissues under simple loading conditions. A three-dimensional version of the texture correlation technique, currently under development, will relax these limitations.

REFERENCES

Bay, B.K., J. Ortho. Res., in press.
Holmes, R.E. et al., JBJS, 68A, 904-911, 1986.
Martin, R.B. et al., Biomaterials, 14, 341-348, 1993.

ACKNOWLEDGMENTS

Results presented here derive from experiments funded by Interpore International of Irvine, California.

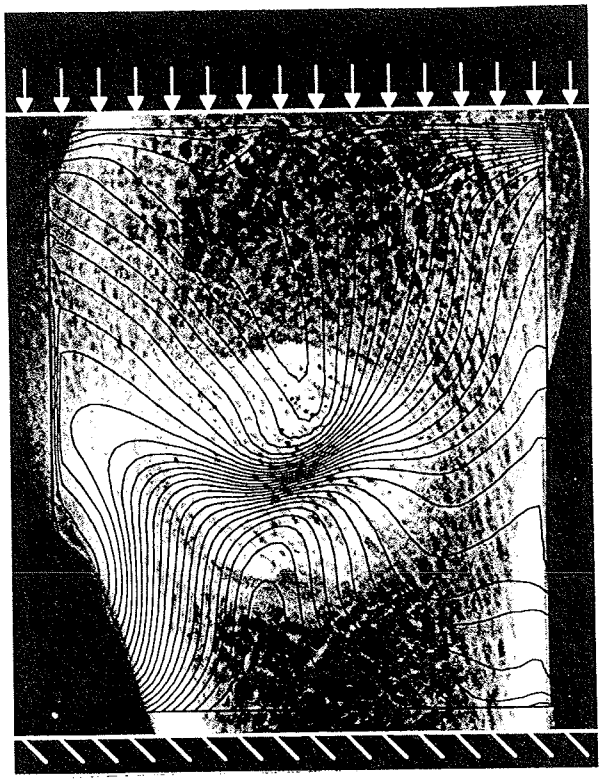

Figure 2: Displacement pattern for short-term sample. Each line represents 14 μm of displacement.

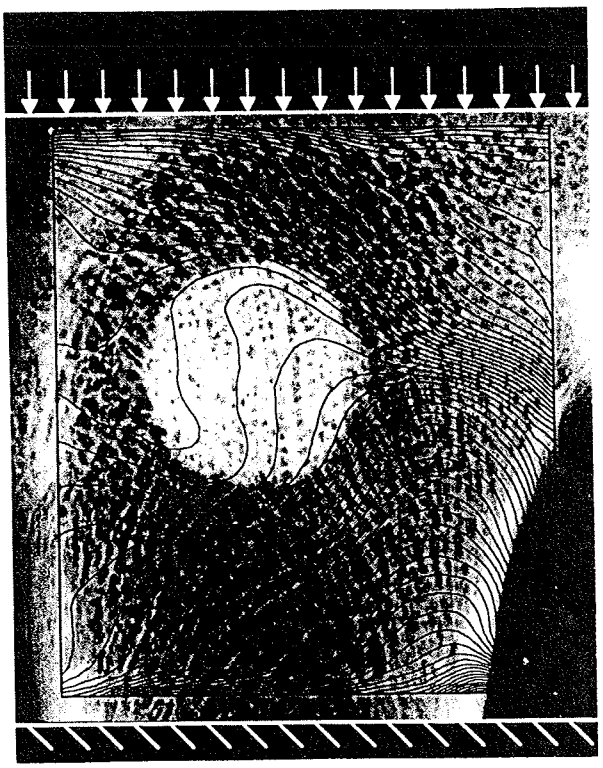

Figure 3: Displacement pattern for long-term sample. Each line represents 14 μm of displacement.

Quantification of 24-Hour Skeletal Loading History in Relation to Treadmill Exercise

A. Biewener, D. Konieczynski, M. Temaner, M. Truty

Department of Organismal Biology & Anatomy, The University of Chicago, Chicago, IL 60637

INTRODUCTION

Quantification of a bone's loading history, *the summed loading that a structure experiences over a period of time*, is important in relation to assessing various approaches for investigating the adaptive remodeling response of bone to changes in mechanical loading. Carter (1) and Beaupre (2) have defined the 'daily osteogenic stress stimulus' as the summed effect of stress cycles experienced by a bone over a 24-hr period. In their formulation, stress magnitudes are weighted by an exponent (typically having a value of four) that emphasizes higher magnitude loading events in relation to lower magnitude, but more frequent loading events. The formulation of a daily osteogenic stimulus can also be made in terms of strain magnitude or strain energy density.

Despite the accepted importance of the need to quantify a bone's loading history for assessing the remodeling response of bone tissue to changes in functional strain patterns, little quantitative data exists that describes a bone's loading history. Recent studies of avian leg (3) and wing (4) bones have shown that the relative frequency of strain magnitude measured at different sites within a bone generally fits a normal or lognormal distribution, that the magnitude of peak strain can differ considerably among sites when sampled over a wide range of activity, and that, when sampled over a 24-hr period of activity, low magnitude - high frequency components of the strain signal tend to dominate the summed loading history of a wing bone element (4).

We have previously used a load-carrying treadmill exercise regimen to study the effect of physical activity on bone modeling during growth in the avian tibiotarsus (5). However, a potential difficulty of this approach is the possibility that "background" loading, while the animals are housed in a cage during 95% of the day, may overwhelm the osteogenic signal generated by the much briefer exercise bout on the treadmill. The goal of this study, therefore, was to reconstruct the 24-hr loading history of the tibiotarsus for animals subjected to the load-carrying exercise regimen versus that during cage activity, in an attempt to determine whether the background "noise" of cage activity obscures the "signal" engendered by treadmill exercise.

METHODS

Ten young adult male and female white leghorn chickens (1.1 to 1.45 kg) were used in the study. Animals were trained to run on a treadmill over a range of speed and gait. Following two to three weeks of training, each animal underwent aseptic surgery to attach strain gauges to three midshaft sites (anterior: AM, posterior: PM & medial: MM) and three distal sites (anterior: AD, posterior: PD & medial: MD). At the PM and AD sites, a small rosette strain gauge (type FRA-1, Tokyo Sokki Kenkyujo) was attached; at the remaining four sites single element (FLA-2) gauges were attached to record longitudinal strain.

Following recovery from surgery, *in vivo* cortical strains were recorded over a two-day period while the animals exercised on the treadmill at speeds from 0.45 to 2.1 m/s. Strains were also recorded while the animals were housed in their cage and during transport in a carrying kennel. Recordings during cage activity were typically carried out over long periods (6 min runs sampled at multiple times). Cage activity took into account daily periods in which the animal's activity might be stimulated by water and food changes, bi-weekly events of bedding changes and movement of investigative staff into and out of the animal's room. After all recordings were completed the animals were sacrificed and the bones excised to confirm gauge orientation using a dissecting microscope and to determine bone areal properties.

RESULTS

Figure 1 shows the results for the two medial (midshaft, MM and distal, MD) sites that were sampled during treadmill activity, corresponding to exercise at 60% of the animal's maximal speed (1.65 m/s) while carrying an additional weight, equal to 20% of the animal's body weight, on their back. Peak strain magnitudes are binned at 100 $\mu\varepsilon$ (strain $x10^{-6}$) intervals. The frequency distribution for treadmill exercise (open bars) reflects the distribution obtained by sampling 2500 loading cycles, the number of cycles experienced by the daily treadmill exercise treatment group. The frequency distributions for cage activity (hatched, 240 cycles/day) and transport (solid) to and from the

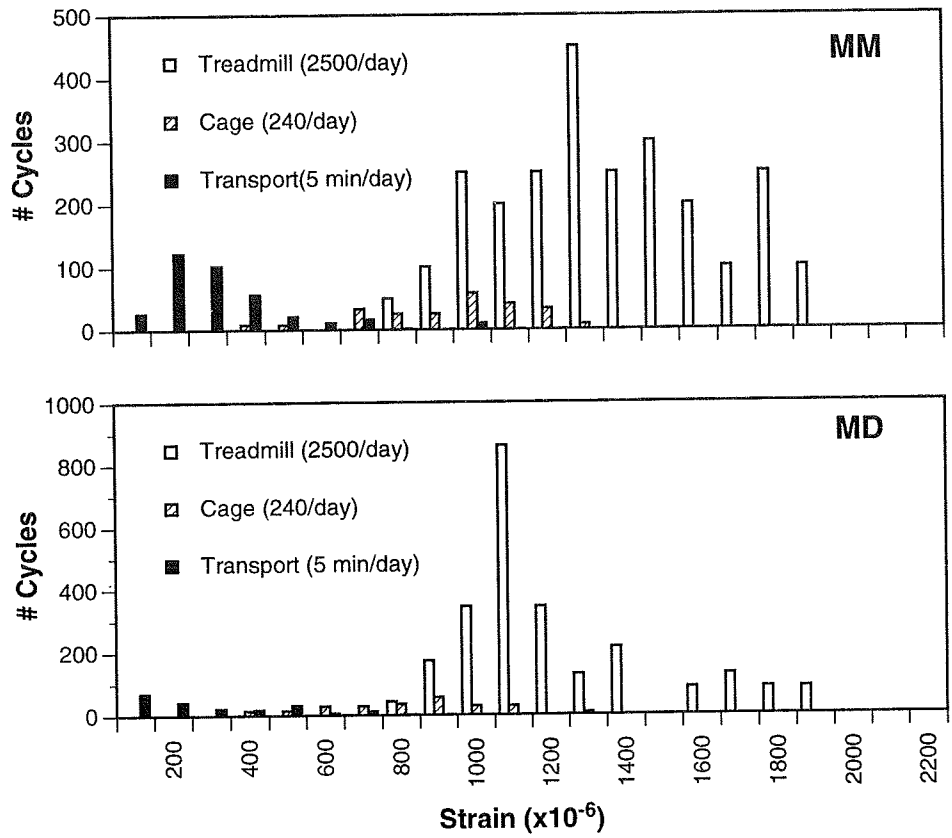

FIGURE 1.

animal facility to the laboratory treadmill are also shown. It is clear from these data that the treadmill exercise of 2500 cycles/day can easily be distinguished from the 'loading history components engendered by background cage activity and animal transport. Whereas treadmill exercise at 60% max/20% load carrying engenders strains in the range of 1000 to 1800 με (75% of all values recorded), strains developed during cage activity are generally well below 1000 με and considerably less frequent. Strains produced during transport are generally of low magnitude and likely reflect the oscillatory effect of the animals keeping their balance while being carried. Similar comparisons of the frequency components of the bone's loading history at the other recording sites for both longitudinal and principal strains are observed.

DISCUSSION

Our results support the view that daily treadmill exercise activity can be used to evaluate remodeling responses of the skeleton to physiological changes in loading. Such daily activity periods, even if carried out over a brief period of time (15-20 min), can readily be distinguished from background loading events while the animals spend most of their time in a cage. In this instance, load carrying treadmill exercise provides a clear strain signal compared with the background 'noise' shared by sedentary control animals housed in cages. The inability to impose major changes in loading distribution and the variability in strain patterns among exercise animals (CV: 20 - 35%), however, remain important limitations of this approach. Future work needs to address other load-related parameters, such as strain energy density, shear strain and bending:axial strain gradient, to evaluate how changes in loading history may influence the skeletal response to exercise.

REFERENCES

1. D. Carter, D. Fyhrie & R. Whalen (1987) *J. Biomech.* 20:785-794.
2. G. Beaupre, T. Orr & D. Carter (1990) *J. Orthop. Res.* 8:651-662.
3. A. Biewener, D. Koneiczynski, M. Temaner & M. Truty (1995) *Trans. ORS* 20:199.
4. S. Fritton, K. McLeod, J. Fritton, R. Brand & C. Rubin (1995) *Trans. ORS* 20:547.
5. A. Biewener & J. Bertram (1994). *J. appl. Physiol.* 76:946-955.

ACKNOWLEDGEMENTS

This work was supported by NIH Grant AR-39828.

A REEXAMINATION OF ULTRASOUND ATTENUATION IN PREDICTING BONE PROPERTIES

S. Han[1,2], J. Medige[1,2], I. Ziv[1,2,3]
[1]Department of Orthopaedic Surgery, University at Buffalo
[2]Department of Mechanical & Aerospace Engineering, University at Buffalo
[3]Department of Veterans Affairs Medical Center, Buffalo, NY 14214

INTRODUCTION

This study was undertaken to compare ultrasound attenuation at a particular frequency (0.5 MHz) and broadband ultrasound attenuation (BUA) in assessing bone mineral density (BMD) and elastic modulus. The application of ultrasound to the non-invasive assessment of bone properties has become increasingly popular over the past decade. Not only does ultrasound allow for inexpensive and radiation-free measurements, it also provides information on bone structure and strength independently of BMD.

Ultrasound velocity , ultrasound attenuation at a particular frequency (0.5 MHz), and BUA were measured in the three orthogonal directions of human trabecular bone cubes. Measurements of BMD were made using quantitative computed tomography (QCT) and apparent density by weighing bone specimens and measuring their volume. The "ultrasonic elastic modulus" was calculated from ultrasound velocity and apparent density. Ultrasound attenuation, at a frequency of 0.5 MHz, and BUA were associated with BMD and ultrasonic elastic modulus in the anterior/posterior (AP), medial/lateral (ML), and superior/inferior (SI) directions.

REVIEW AND THEORY

The assessment of ultrasound techniques in the medical field originally focused on BUA measurements (Langton et al., 1984, Baran et al., 1988). Langton et al. (1984) described a BUA technique for the diagnosis of osteoporosis, suggesting that BUA provides direct information on trabecular bone structure as well as mineral density. Many subsequent studies have attempted to correlate BUA with BMD acquired through traditional radiographic measurements.

Ultrasound attenuation (dB/cm) is, in general, expressed as the spatial rate of decrease in signal amplitude of waves propagating through a medium at a particular frequency, while BUA (dB/MHz-cm) is determined as the rate of change with frequency of attenuation over a selected range of frequency. Although BUA is favored over attenuation, little is found in the literature concerning why. In fact, in an earlier study (Evans and Tavakoli, 1990), it was reported that bone density appeared to correlate better with attenuation than with BUA. This, however, was not emphasized.

Ultrasound velocity has been successfully applied to determining the elastic properties of cortical bone (Ashman et al., 1984). Efforts to extend the wave theory of ultrasound to assessing the elastic modulus and strength of cancellous bone were also made ***in-vitro*** (Ashman et al., 1987, Turner et al., 1991). Ashman et al. (1987) reported that Young's modulus obtained from mechanical testing was highly correlated with the ultrasonic elastic modulus.

PROCEDURES

Seventy-one trabecular bone cubes (approximately 9.5 x 9.5 x 9.5 mm) were obtained from four human proximal tibiae. Three orthogonal axes of these specimens were aligned in the SI, ML, and AP directions and marked.

Measurements of apparent density were accomplished by weighing the trabecular bone specimens and measuring their volume. The BMD of cubic specimens was measured by QCT. The CT images were transferred to a computer and analyzed using profile imaging software (C-MED, Virtual Vision, Cupertino, CA). The average pixel intensity of at least three consecutive slices for each specimen was related to a BMD value (mg/cc).

The ultrasound velocity was measured by a pulse transit time approach. A pair of contact transducers with a center frequency of 0.5 MHz was placed at opposite ends of the specimens. The ultrasonic elastic modulus ($E_{ultr}=\rho V^2$) was calculated from ultrasound velocity and bone density.

A pulse transmission technique with a pair of broadband ultrasound immersion transducers having 0.5 MHz nominal center frequency was used to measure BUA and ultrasound attenuation at a frequency of 0.5 MHz. Identical transmitting and receiving transducers were mounted coaxially on opposite sides of a water-filled Plexiglas® tank and remained fixed. In order to exclude unattenuated signals passing alongside a specimen, a wave-blocking holder with holes slightly smaller than the specimen was used. Time-based signals captured by an oscilloscope were converted to the frequency domain using fast fourier transformations (FFT). A spectrum obtained with a specimen in place was subtracted from a spectrum obtained with water only. This difference, in dB, was plotted vs. frequency. The slope obtained from the best linear fit of the plot between 0.3 and 0.7 MHz was normalized using the specimen thickness. This value was expressed in units of dB/MHz-cm and is referred to as the BUA. Ultrasound attenuation of each specimen was measured at the center frequency of the transducers (0.5 MHz) and normalized to the specimen thickness. Ultrasound measurements for each specimen were made in the three orthogonal directions.

RESULTS

The correlations between the variables were highly significant in all cases (P<0.0001) (Table 1). Attenuation at 0.5 MHz was better associated with both BMD and ultrasonic elastic modulus in all three directions than was BUA. Its enhanced correlation was pronounced in the AP and ML directions. Figure 1 describes the general trend of the relationship between BMD and attenuation. Ultrasound attenuation tended to increase linearly with increasing BMD. The ultrasonic elastic modulus correlated well with attenuation at 0.5 MHz, in the AP and ML directions.

Table 1: Coefficients of determination, r, from linear regression analysis applied between variables.

	BUA			Attenuation (.5MHz)		
	AP	ML	SI	AP	ML	SI
BMD	.664	.524	.659	.803	.794	.680
E_{ultr}	.717	.612	.437	.820	.854	.469

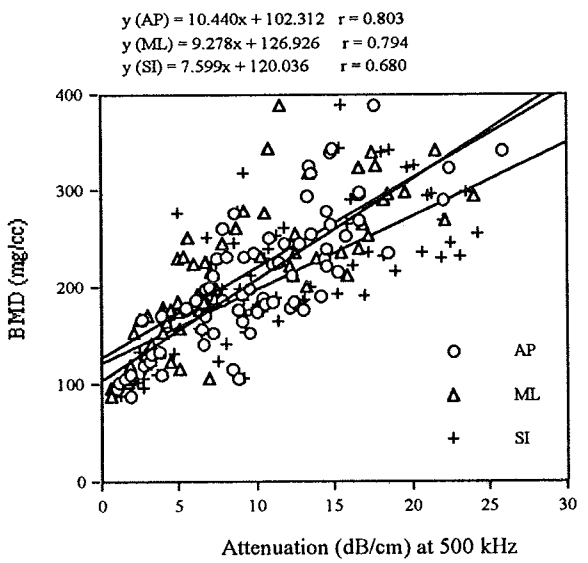

Figure 1. Correlation of BMD and attenuation at 0.5 MHz in the AP, ML, and SI directions. Significant linear relationships were obtained for all directions (p<0.0001).

DISCUSSION

The results demonstrated that ultrasound attenuation at a frequency of 0.5 MHz was superior to BUA in the prediction of BMD and elastic modulus. Most published reports on the clinical assessment on bone using ultrasound show a wide range of coefficients of determination (0.29<r<0.92) for correlations between BMD and BUA. This questioned the reliability of ultrasound to predict BMD.

Until recently, there has been little discussion on preference of BUA over attenuation. The results of this investigation suggest that the current methodology of ultrasound measurements should be altered for more accurate ultrasound assessment of bone properties. Since the correlations of BUA and attenuation with modulus were significantly better than with BMD in the AP and ML directions, these attenuation parameters might reflect properties of the trabecular architecture, which is independent of BMD but contributes to elastic modulus. It was shown by Gluer et al., 1994 that the mean attenuation across the selected frequency range reflects trabecular separation, while BUA reflects a combination of trabecular separation and connectivity. Although BUA and attenuation might be influenced by different aspects of trabecular architecture, ultrasound attenuation surpassed BUA in the predictability of BMD and elastic modulus. The combined effect of attenuation and BUA may improve ultrasound diagnostic measurements.

Consequently, the results of the present study suggest that the BUA technique should be complemented or replaced with attenuation. Future studies are needed to apply our findings to ***in-vivo*** bone and should concentrate on the improvement of current BUA techniques.

REFERENCES

Ashman, R. et al. J Biomech, 17, 349-61, 1984. Ashman, R. et al. J Biomech, 20, 979-86, 1987. Baran, D.T. et al. Calcif Tissue Int, 43, 138-42, 1988. Evans, J.A. et al. Phys Med Biol, 35-10, 1387-96, 1990. Gluer, C. et al. Calcif Tissue Int, 55, 46-52, 1994. Langton, C.M. et al. Eng Med, 13, 89-91, 1984. Turner, C.H. et al. Calcif Tissue Int, 49, 116-9, 1991.

MODE III FRACTURE TOUGHNESS OF CORTICAL BONE

Zude Feng, Arie Salzman

Department of Orthopaedic Surgery, SUNY at Buffalo, Buffalo, NY 14214

INTRODUCTION

The majority of our understanding about bone fracture toughness has focused on the initiation and propagation of cracks subject to tensile loading (mode I) [1-4]. However, failures seldom occur under pure tensile loading. Fracture may rise under shear loading (mode II), tear or out-of-plane shear loading (mode III) [5], or complex loading conditions (various combinations of mode I, II, and III) . In addition to the study of fracture toughness under tensile loading its characterization under shear and tear loading is an important step to correctly estimate bone damage tolerance.

The purpose of this study is to investigate fracture toughness under tear loading (mode III) of bovine mid-shaft tibiae, using the Triple Pantleg (TP) method. Preliminary data on the difference between mode I and III fracture toughness will be reported.

MATERIALS AND METHODS

Five fresh bovine tibiae were acquired within 24 hours of slaughter. The tibiae were kept frozen at -20° C until machining. A total of eight Compact Tension (CT) and Triple Pentleg (TP) specimens were cut from the lateral and medial cortices of the tibia mid-shaft with a band saw and shaped using a vertical milling machine. The CT specimens were shaped according to the method described by Norman [6]. As no method is available to test bone fracture toughness under tear loading, the authors adapted the TP technique used in material science by Manoharan and Kumar [7,8], (Fig.1). In each sample, a chevron notch was created in the longitudinal direction and a 1 mm deep V-notched groove was machined on both sides of the sample, along each chevron notch, leaving a 3 mm bone bridge between the grooves (B_{net}). Before testing, a precrack was initiated into the chevron notch using a razor blade. The orientation of all the samples corresponded to longitudinal crack propagation [3]. After machining, and prior to testing the specimens were stored in physiological saline at 4° C.

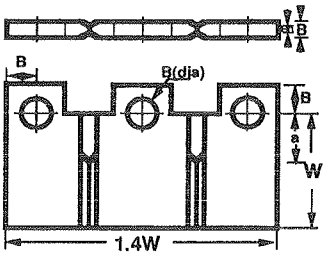

Figure 1. Triple Pantleg specimen. The dimensions (mm) are, a=8, W=14, B=5 and B_n=3.

All specimens possessed the same thickness (B = 5 mm) and width (W = 14 mm). The overall dimensions of CT and TP specimens were 17.5 mm x 16.8 mm and 20.4 mm x 18 mm, respectively. The a/W ratio expressed as the proportion of crack length (a) to specimen width (W) ranged from 0.55 to 0.60 in all specimens.

A test specimen was placed in mode I or mode III fixture and mounted on an MTS machine (MTS T22K). Specimens were loaded under stroke control at a crosshead displacement rate of 0.2 mm min^{-1}. Three CT specimens were used for tensile loading (mode I), and five TP for tear loading (mode III). CT specimens were loaded through loading pins that passed through holes in the specimens. The outer two legs of the TP specimens were bolted to a U-shaped base through 4mm holes. Load was applied to the central leg in the vertical direction. Load and displacement were recorded using a PC data acquisition system.

Critical load P_{IQ} and P_{IIIQ} were determined by a 5% scant offset procedure according to ASTM E399 (1985). The mode I fracture toughness (K_{IC}) was calculated according to the formula used by Bonfield [9]. The P_{IIIQ} value was used to obtain the mode III fracture toughness (K_{IIIC}), according to the following formula:

$$K_{IIIQ} = \{P_{IIIQ} / B_{net} W^{1/2}\} f(a/W) h_{iii}(\phi)$$

where B_{net} is the grooved thickness, f(a/W) is the geometry correction function as defined in the ASTM E 399, and $h_{iii}(\phi) = (2.24 - 1.04 \sin\phi)$ is the angular correction function. In mode III loading

$\phi = 90°$, thus hiii (ϕ) = 1.2. The remaining terms were defined earlier.

RESULTS AND DISCUSSION

Representative load versus displacement plots obtained from mode I and mode III test is illustrated in Fig. 2. The mean value of Mode III fracture toughness K_{IIIC}, was 10.68 MN $m^{-3/2}$ (SD = 1.677)], and that of K_{IC} was 2.554 MN $m^{-3/2}$ (SD = 0.072). These results indicate that fracture toughness of bovine tibiae under tear loading is greater than under tensile loading. A larger number of specimens is required for statistical analysis.

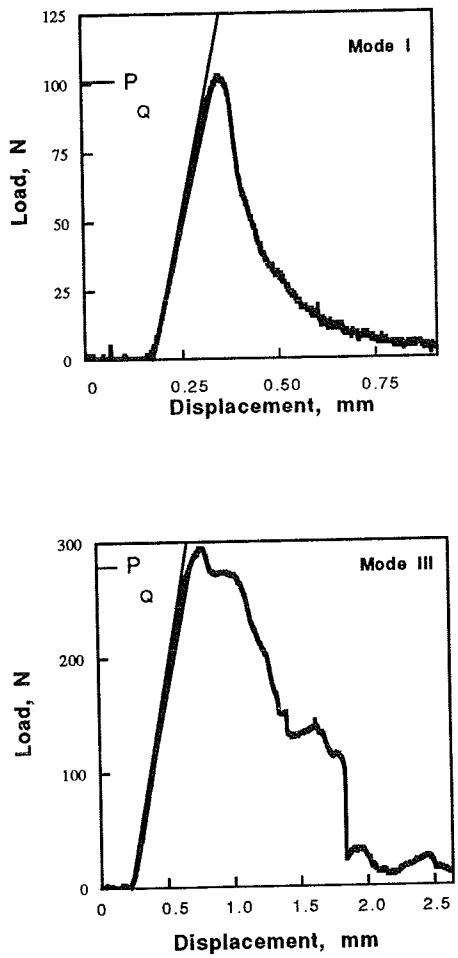

Figure 2. Representative load *vs.* load-line displacement plot obtained from mode I and mode III fracture toughness test.

This study suggests that analysis of bone fracture toughness under tear loading using the TP model is adequate for the following reasons [8]: 1) Two crack fronts are provided to balance the bending forces to avoid rigid body rotation of the specimen. 2) The side grooves allow crack propagation before the occurrence of general yield in the cantilever beam arms of the specimen. 3) The grooves increase the stress triaxiality at the edges of the advancing crack, promoting planar crack extension without shear lip formation at the specimen faces.

Rosenfield suggested that fracture toughness of brittle materials under tear loading is greater than under tensile loading [10]. Since cortical bone is a brittle material [11] it may behave in a similar way as shown in this study. This important variable is to be considered in analysis of actual failure processes in bone. Further study of bone fracture mechanisms under tear loading is required.

REFERENCES

1. Wright, T.M. *et al.* J Biomech, 10, 419-30, 1977. **2.** Behiri, J.C. *et al.* J Biomech, 17, 25-34, 1984. **3.** Melvin, J.W. J Biomech Eng, 115, 549-54, 1993. **4.** Norman, T.L. *et al.* J Biomech, 28, 309-20, 1995. **5.** Anderson, T.L. Fracture Toughness Fundamentals and applications, (pp.64), CRC Press, 1991. **6.** Norman T.L. *et al.*, J. Biomech 25, 1489-92, 1992. **7.** Manoharan, M. *et al.* JTEVA, 18, 106-14, 1990. **8.** Kumar, A.M. *et al.* JTEVA, 22, 327-34, 1994. **9.** Bonfield W *et al.*, J. Biomech 22: 863-72, 1989. **10.** Rosenfield, A.R. Fracture Behavior and Design of Materials and Structure, (pp. 501), EMAS, UK, 1990. **11.** Bonfield, W. J Biomech, 20, 1071-81, 1987.

ACKNOWLEDGMENTS

The authors would like to express their sincere gratitude to Dr. Israel Ziv for his support of this work and helpful discussion.

A MODEL OF HUMAN TIBIA VIBRATION FOR NON-INVASIVE MEASUREMENT

S.G. Roberts and C.R. Steele
Department of Mechanical Engineering, Stanford University, Stanford CA 94305

INTRODUCTION

A biological vibration response technique, Mechanical Response Tissue Analysis (MRTA), has shown promise in tests of human ulnas and monkey tibias, but the human tibia has a more complex structure, requiring specialized description. In this study, an embalmed human tibia is tested using MRTA in order to gain a better understanding of the bone's dynamic behavior. The findings are then incorporated into a biomechanical model of the vibrating bone which will be used in non-invasive tests *in vivo* to determine the cross-sectional bending stiffness of the bone.

REVIEW AND THEORY

With the MRTA technique, the bone is positioned firmly in proximal and distal supports, producing simply-supported end conditions, and a shaker probe transcutaneously delivers low frequency random vibration to the center of the bone. Force and acceleration, measured at the probe, are transformed to construct the complex frequency response. A curve-fitting algorithm is used to determine the values of the physical parameters in the mathematical model of the skin, bone, and support system. One of the physical parameters, bone cross-sectional bending stiffness, is highly correlated (R^2 = 0.98) with breaking strength (Roberts *et al.*, 1995).

Previously, a planar model of the long bone was used; there is one single bending mode (Steele *et al*, 1988; Roberts *et al*, 1995). Others have found using modal analysis that such an assumption is not valid for the human tibia with free-free boundary conditions (Van der Perre *et al.*, 1983). Based on these findings, we hypothesize that there are two single-bending modes for the simply-supported human tibia that should be accounted for in the mathematical model.

PROCEDURES

An embalmed human tibia was simply-supported in a rigid test fixture. The supported length was 0.23 m and included primarily the diaphyseal region. The MRTA probe was centered between the supports, and five frequency response measurements were made before repositioning.

A mathematical model of the simply supported bone was developed to allow for two single-bending modes. The two planes of vibration are assumed perpendicular and are in principal directions.

For the static case of a beam loaded through the centroid at any arbitrary angle, θ, to the maximum principal direction, the effective bending stiffness, k_{eff}, is

$$(1) \qquad k_{eff} = \frac{k_{max}\, k_{min}}{k_{min} \cos^2\theta + k_{max} \sin^2\theta}$$

where the subscripts refer to the principal directions.

This can be applied to the dynamic equations in the two directions (Eqn. 2), and the resulting equations can be added like springs in series to formulate the complex frequency response in the direction of forcing (Eqn. 3).

$$(2) \qquad K_j = -m_j \omega^2 + i\, b_j\, \omega + k_j$$

$$(3) \qquad K_{eff} = \left(\frac{\cos^2\theta}{K_{max}} + \frac{\sin^2\theta}{K_{min}} \right)^{-1}$$

where m, b, and k, are mass, damping, and stiffness, and the index, j, refers to principal direction.

The model was fit by hand to the experimental response curves.

RESULTS

The experimental results indicate that there are two significant vibration modes for the simply-supported human tibia in the frequency range specified (100 - 1400 Hz). This is most easily seen in the curve of Imaginary Compliance versus Frequency (Fig. 1, gray curve). The two sharp negative peaks occur at the resonant frequencies.

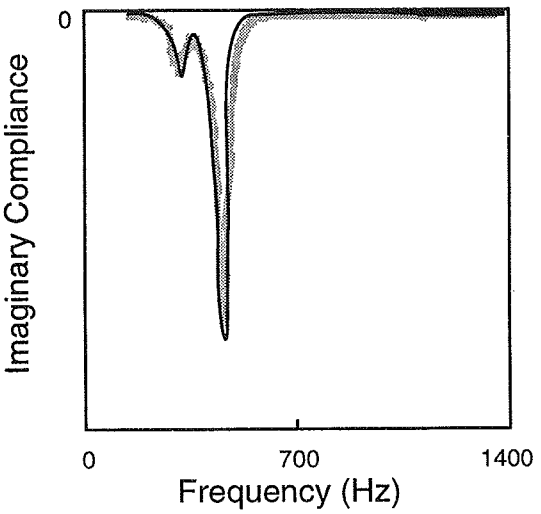

Figure 1: The experimental frequency response curve (gray) clearly shows two resonances of the simply-supported embalmed human tibia. The mathematical model (black) exhibits the same behavior as the test specimen.

The novel mathematical model of the tibia is capable of reproducing the behavior seen experimentally. The real and imaginary parts of the stiffness and compliance curves can all be fit by the model, as exemplified in the curve of imaginary compliance (Fig. 1, black curve). The location and amplitude of the peaks is matched by the model, and both curves approach zero beyond 500 Hz. The value of effective bending stiffness determined using the model is 190 Nm^2.

DISCUSSION

The two distinct resonances identified from the frequency response were compared to those found for the fresh tibia with free-free boundary conditions (Van der Perre *et al.*, 1983). Taking into account the 0.11m difference in tibia length, and assuming stiffness and mass to be the same, the theoretical ratio of the frequencies for the first single bending modes in the simply-supported to free-free case is 0.96 (Eqn. 4).

$$(4) \qquad \frac{\omega_{s\text{-}s}}{\omega_{f\text{-}f}} = \frac{1}{1.5^2}\left(\frac{L_{f\text{-}f}}{L_{s\text{-}s}}\right)^2\left(\frac{EI_{s\text{-}s}\, m_{f\text{-}f}}{EI_{f\text{-}f}\, m_{s\text{-}s}}\right)^{\frac{1}{2}}$$

ω, L, EI, and m are frequency, length, cross-sectional bending stiffness, and mass, and the subscripts refer to the end conditions.

The tibias in the modal analysis study were fresh, while the tibia in the present study was embalmed. The additional fluid and marrow mass of the fresh tibia would decrease the natural frequencies by the square root of the mass.

Considering the 25 percent greater mass of the fresh bone, the natural frequencies found in the present study are in agreement with those found for the single-bending modes of the fresh tibia (Table 1). This provides evidence that the two modes found for the simply-supported tibia are single bending modes in planes of maximum and minimum stiffness as in the free-free case.

Table 1: Natural frequencies of the single-bending modes in the principal directions of fresh (Van der Perre *et al.*, 1983), predicted from fresh, and embalmed tibia.

	minimum	maximum
free-free		
fresh	301 Hz	417 Hz
simply-supported		
predicted	289 Hz	400 Hz
embalmed	320 Hz	450 Hz

By manipulating the values of the mass, stiffness, and damping parameters in the mathematical model, we were able to produce the same behavior as the test specimen. Further, the value of effective bending stiffness found using this model is within 4% of that found by Katz (1995) in a static test of the same bone, 196 Nm^2. This model of the bone will now be incorporated into the larger model of the skin, bone, and support system that is used for MRTA tests *in vivo*. As a result, more accurate characterization of long bone mechanical properties can be made *in vivo*.

REFERENCES

Katz, BA., *et al.* (1995) Dependence of long bone flexural properties on bone mineral distribution. *Proc, ASME Summer Bioeng Conf* (submitted).

Roberts, S. G., *et al.* (1995) Non-invasive determination of bone mechanical properties using vibration response: a refined model and validation *in vivo*. *J Biomech* (in press).

Steele, C. R., *et al.* (1988) *J Biomech Eng* **110**, 87-96.

Van der Perre, G., *et al.* (1983) *J Biomech Eng* **105**, 244-8.

ACKNOWLEDGMENTS

The authors wish to thank Robert Whalen and Teresa Hutchinson for their contributions. The experimental work was supported by NASA grant # 199-26-12-34.

DECREASE IN CANINE PROXIMAL FEMORAL ULTIMATE STRENGTH AND STIFFNESS DUE TO FATIGUE DAMAGE

S.J. Hoshaw,* D.D. Cody,** A.M. Saad,* and D.P. Fyhrie*
*Breech Research Laboratory, Bone & Joint Center and **Department of Radiology
Henry Ford Hospital, Detroit, MI 48202

INTRODUCTION

Fractures of the proximal femur represent a significant health concern especially in the elderly. This study examined the relationship between whole bone stiffness and strength following fatigue loading using paired canine proximal femurs. One femur from each of 8 pairs was monotonically loaded to failure to determine the ultimate strength. The contralateral femur was then cyclically loaded at 50% of the ultimate load value for either 3600 cycles or until a 40% reduction in stiffness was achieved. This femur was then monotonically loaded to failure. The data demonstrated decreased residual strength and whole bone stiffness following cyclic loading. In addition, damage (microcracks) in the cortical bone and broken trabeculae were observed in the neck and head region. The relationship between strength loss and stiffness loss was linear (R^2=0.79).

REVIEW AND THEORY

A major challenge in the prevention of hip fracture is identifying individuals whose bones have a decreased load bearing capacity and, consequently, who are at risk for fracture. Measures of bone mass or density have been shown to be limited predictors of fracture risk (R^2 =0.6-0.7; Cody et al., 1994) and individuals with measured density values within the normal range for their age and gender have gone on to fracture. The quality of the bone tissue may be a factor in these cases. The accumulation of bone microdamage in both cortical and trabecular bone due to repetitive loading may play a role in reducing bone quality and strength. The purpose of this study was to investigate the hypothesis that fatigue loading of the proximal femur results in decreased whole bone stiffness and strength. Furthermore, it was postulated that this strength reduction was due to bone microdamage in both the cortical and trabecular bone envelopes.

PROCEDURES

Both femurs were collected from 8 canines (22.9 ± 4.4 kg), cleaned of soft tissue, and stored frozen. After thawing, each femur was sectioned 5 cm distal to the lesser trochanter and potted in an aluminum test fixture with low melting point alloy and methyl methacrylate (MMA). Compressive loads were applied to the femoral head using a servohydraulic test system. A custom loading cup consisting of MMA with a metal backing was made for each femur. The femur was positioned so that the load was applied in line with the principal compressive trabecular band, as determined from radiographic images. A steel strip was attached between the greater trochanter and table of the testing machine to counter balance the applied load (Figure 1).

The femurs from each dog were randomly allocated to one of two test protocols: single cycle or fatigue. In the single cycle protocol, the femur was loaded in compression at a rate of 0.01 mm/sec until failure and the ultimate load was recorded using a computer data acquisition system. In the fatigue protocol, femurs were cyclically loaded in compression at 1 Hz with a load magnitude equal to 50% of the ultimate load of the contralateral femur. In 5 cases, cyclic testing was stopped after 3600 cycles. For the other 3 femurs, cyclic testing was stopped when the stiffness of the femur, defined by the moving average over 200 data points of the load divided by the actuator position, reached 60% of its value at the start of the test. The residual strength of each fatigued femur was then determined in a monotonic compression test to failure at 0.01 mm/sec.

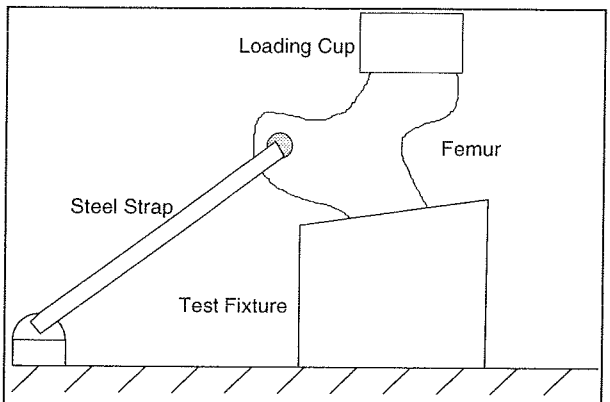

Figure 1. Schematic diagram of loading configuration showing the loading cup, steel strap and aluminum test fixture.

Two additional femur pairs were tested as described previously. However, instead of determining the residual strength following either 3600 cycles or a 40% reduction in the femur's stiffness, the fatigued bones were bulk stained in basic fuchsin to demonstrate microscopic damage (Burr and Stafford, 1990). After staining, the bones were embedded in MMA and coronal sections of 100 μm thickness were obtained using a slow speed diamond saw.

RESULTS

Both test protocols consistently produced cervical fractures. Two femurs in the fatigue group fractured prior to finishing the fatigue portion of the loading protocol. One of the femurs in the 3600 cycle group broke at 1504 cycles and the other broke just as its stiffness had fallen the desired 40%.

The data were plotted in terms of the ratio of the residual and ultimate strengths for each femur pair and the ratio of the final and initial stiffness of the cyclically loaded femur (Figure 2). A linear relationship was found between the strength and stiffness ratios (R^2= 0.79).

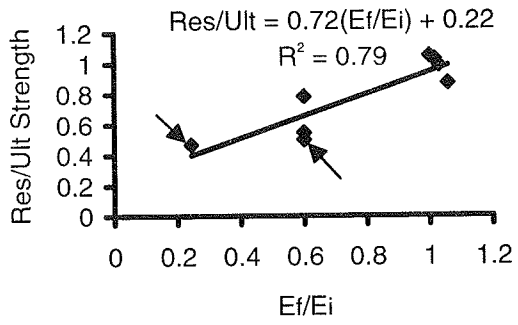

Figure 2. Ratio of the residual strength of the fatigued femur (Res) to the ultimate strength of the contralateral femur (Ult) versus the ratio of the final (Ef) and initial (Ei) whole bone stiffness of the fatigued femur. The arrows identify data from the two bones that broke during fatigue testing.

No microdamage was found in the bone fatigued for 3600 cycles. However, bone microdamage was observed in both cortical and trabecular bone regions in the fatigued femur with a 40% reduction in stiffness. Regions of cross-hatched cracks were found in the inferior femoral neck cortex (Figure 3A). In the trabecular bone of the femoral head and neck, numerous broken trabeculae were observed (Figure 3B). Bands or zones of damaged bone were also noted in the trabecular bone.

DISCUSSION

This study demonstrated a decrease in whole bone stiffness and residual strength in canine proximal femurs following fatigue loading. Fatigue testing of machined compact bone specimens have also shown decreases in residual strength and stiffness following periods of fatigue loading (Carter and Hayes, 1977). Similar fatigue behaviors have also been observed in composite materials and attributed to accumulated microdamage. In this study, microstructural damage was identified in both cortical and trabecular bone elements in bone fatigued until a 40% reduction in stiffness was achieved. The cross-hatched cracks and broken trabeculae are indicative of shear failure of the bone. The non-crack damage observed in the trabeculae may be kink bands caused by micro-buckling at the collagen-mineral level (Hahn et al., 1986) which will proceed to absolute fracture with continued loading.

If a similar relationship between stiffness and strength can be demonstrated for human proximal femurs, then it may be advantageous to develop an *in vivo* stiffness measurement technique that could identify patients with reduced femoral strength so that aggressive preventative therapies could be initiated.

REFERENCES

Cody DD et al., Bone, 16(Suppl 1), 1508, 1994.
Burr DB, Stafford BS, CORR, 260, 305-308, 1990.
Carter DR, Hayes WC, J Biomech, 10, 325-337, 1977.
Hahn HT et al., NASA Contractor Report, 3988, 1986.

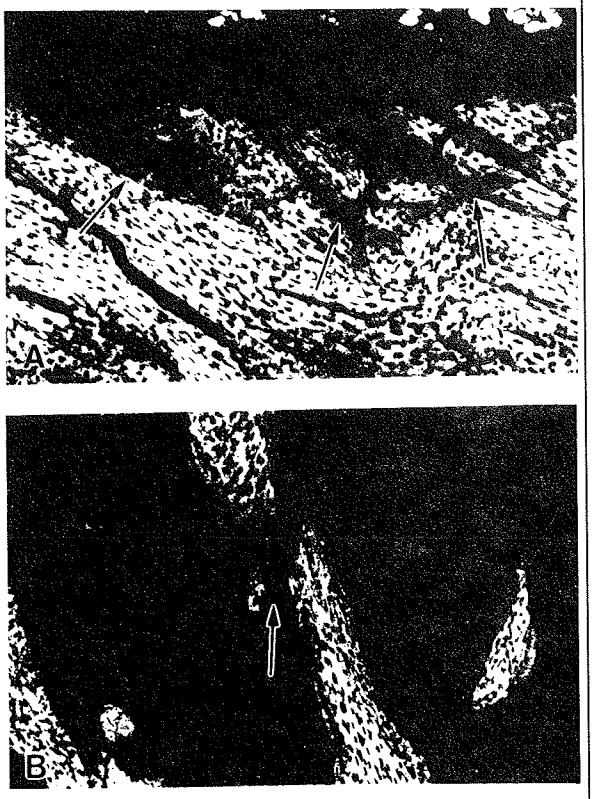

Figure 3. Photomicrographs of damaged cortical and trabecular bone from a canine femur following fatigue loading. A) Microdamage observed in the inferior femoral neck cortex. Note cross-hatched cracks near the periosteal surface of the neck (arrows). B) Broken trabecula located in the femoral head. (————100 μm).

ACKNOWLEDGMENTS

NIH AR40776 (DPF) and NIH AG08776 (DDC)

A NEW METHOD FOR DETERMINING RAT FEMORAL NECK MECHANICAL COMPETENCE

B. Katz[1], E. Hendley[1], G. Watanabe[1], C.M. Bagi[2], M.C.H. van der Meulen[1,3]
[1]Department of Mechanical Engineering, Stanford University, Stanford, CA 94305
[2]Celtrix Pharmaceuticals, Inc., Santa Clara, CA 95052
[3]Palo Alto VAMC, RR&D Center, Palo Alto, CA 94304

INTRODUCTION

A new method has been developed for testing the mechanical competence of the rat femoral neck. Mechanical competence was characterized during external mechanical loading *in vitro*. As a preliminary assessment of the ability of the mechanical test to detect changes in trabecular content, paired femurs were tested, in which the trabecular core of one femur from each pair was removed, while its contralateral remained intact.

BACKGROUND

Studies that have investigated the effects of parathyroid hormones and bisphosphonates (Søgaard, et al., 1994) and strenuous exercise (Hou, et al., 1990) on the structural integrity of the femoral neck, particularly the trabecular component, have tested the femoral neck in a vertical configuration. This loading configuration resulted in fractures which extended beyond the femoral neck and into the cortical diaphysis. As a result, measurements may reflect not only the strength of the femoral neck, specifically changes in the trabecular component, but the strength of the cortical bone in the diaphysis as well.

The purpose of this study was to design a repeatable and reliable testing method that exclusively tested the strength of the rat femoral neck. In an effort to produce a site-specific test configuration, preliminary studies done in our lab have investigated various loading configurations and the locations and types of fractures produced. We tested the femurs in an inclined configuration, in which the diaphyseal axis was oriented at 30° to the plane perpendicular to the applied loads, a vertical configuration, with the applied load parallel to the femoral shaft, and a "single-limb-stance" configuration, a simulation of the human physiological loading state, where the resultant load is directed at an angle to the long axis of the femur. The inclined configuration was chosen for further study, and is presented here, due to the characteristic mid-neck fractures that were produced.

PROCEDURES

Paired femurs from eight female Sprague Dawley rats were tested in an inclined configuration. The left femur of each pair was evacuated of its trabecular core using a fine dental drill. An entrance hole was made on the lateral side of the diaphysis oriented co-linearly with the neck axis. The entrance hole extended into the intertrochanteric region. The trabecular core of the neck was then removed to the level of the base of the head using a .35mm diameter drill bit (Figure 1).

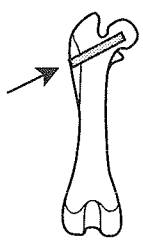

Figure 1. Femur showing extent of trabecular evacuation (arrow indicates entrance hole).

Both left and right femurs of a pair were potted and tested in the inclined configuration. Based on the method of Lotz and Hayes (1990) for mechanical testing of the human femoral neck in a fall simulation, the femoral diaphysis was aligned at an angle of 30° with respect to the plane perpendicular to the applied loads. The medio-lateral plane of the femur was oriented parallel to the load. To achieve this configuration, a straight pin was initially potted in polymethylmethacrylate (PMMA) in a delrin potting mold using a coverplate with a guide hole to precisely align the pin. The mid-diaphysis of each bone was then sectioned at 2.0cm from the proximal end and the exposed medullary canal was positioned on the guide pin and fixed in the potting mold using PMMA. The femur was then positioned in a larger potting mold and potted in PMMA to the level of the greater trochanter. This established the 30° inclined loading configuration (Figure 2).

After the desired loading configuration had been established, rat femurs were mechanically tested using a MTS Bionix 858 servo-hydraulic testing machine. The femurs were loaded under displacement control of 1 mm/sec. A sampling rate of 50 Hz was used to record time, displacement, and force.

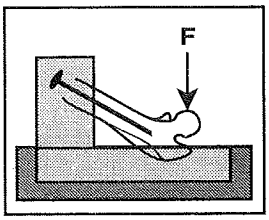

Figure 2. Inclined potting configuration indicating direction of load application.

RESULTS

The inclined testing configuration produced repeatable and noncomminuted fractures within the femoral neck. All femoral neck fractures were transcervical and did not extend into the cortical shell of the femoral diaphysis (Figure 3a and 3b).

a.

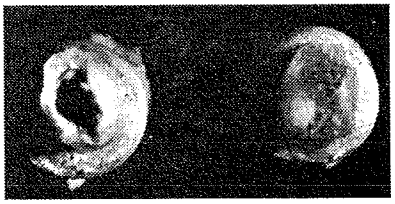

b.

Figure 3a, b. Typical fracture surfaces of evacuated (left) and intact (right) femurs.

The results from the paired femur test are shown in Table 1, expressed as the percent decrease in the measured variables between the intact and evacuated femurs. The evacuated femur of each pair was compared only to its contralateral. The force required to fracture the evacuated femurs and the total energy to fracture were significantly less than that of the intact femurs (p=.029 and p=.002, respectively). The percent decrease in structural rigidity of the evacuated femurs was not significantly different (p=.74) from intact femurs.

Table 1. Comparison of Intact and Evacuated Femurs

	Force (N)	Structural Rigidity (N/mm)	Energy (mJ)
% decrease between intact and evacuated femurs	16.6±13.6*	5.8±35.4	26.4±13.7*

values are mean±SD for 8 pairs of femurs

*evacuated femur significantly different from intact femur(p<0.05)

DISCUSSION

The advantage of this testing configuration lies in its site-specific nature, in which fracture is confined within the femoral neck only. Preliminary studies have shown that the 30° inclined configuration produces clean, transverse fractures within the neck, in contrast to the vertical configuration, which produces oblique fractures extending into the femoral diaphysis. Based on the nature of the resultant fracture location and type, the inclined configuration provides a more direct method of evaluating only the structural integrity of the femoral neck, without the contribution of the cortical diaphysis. For the purpose of investigating the pharmacological, hormonal, and activity-related effects on the structural integrity of the rat femoral neck, our results indicate that the 30° inclined configuration may be a reliable method for quantifying trabecular-specific structural changes in the rat femoral neck.

REFERENCES

Hou, J.C.H. et al. *Amer. Physiol. Soc.* 1309-1314, 1990.

Lotz, J.C. and Hayes, W.C. *J. Bone Jt. Surg.*, 72A, 689-699, 1990.

Søgaard, C.H. et al. *J. Bone Min. Res.*, 9, 409-416, 1994.

ACKNOWLEDGMENTS

We would like to thank Dennis Carter for his help and support throughout this study.

Toward a Description of Cortical Strain Distribution during Functional Loading Activities

D. D. Konieczynski, A. A. Biewener

Department of Organismal Biology & Anatomy, The University of Chicago, Chicago, IL 60637

INTRODUCTION

It is generally accepted that mechanical strains play an important role in bone development during growth and adaptive bone modeling at maturity Further, it has been suggested that mature bone represents a final adaptive state which is optimized to achieve a uniform measure of mechanical strain at all cortical sites [1]. Such a measure likely reflects the combined effects of many *in vivo* loading activities. Previous strain gage studies have determined peak strain magnitudes at specific cortical sites for various functional *in vivo* loading activities [2,3]. To evaluate the uniformity of cortical strain at all cortical sites, however, it is necessary to better understand the cortical *strain distribution* for these functional *in vivo* loading activities.

In the present study, we develop a method to evaluate the distribution of longitudinal strains about an axial cross-section of bone for a variety of functional *in vivo* loading activities. Specifically, we used strain gage data of the midshaft of a mature chicken tibiotarsus to answer the following questions. How does the longitudinal strain distribution change during a loading cycle of gait? How do longitudinal strain distributions for treadmill and more general activities compare?

METHODS

Strain gage rosettes were positioned at the medial, anterior, and posterior aspects of the midshaft of the left tibiotarsus of a white leghorn chicken aged 13 weeks (Fig. 1). Symmetric weight bearing was ensured by positioning three strain gage rosettes on the tibiotarsus of the contralateral leg for use in a related study. Following 24 hr recovery from surgery, strain was recorded at these sites for treadmill activity (1.1 m/s gait) and for general activity (running, turning, jumping, standing, and 1 m dropping) as the chicken moved freely within a 4 × 5 m exercise arena. Strain recordings were synchronized with activity through use of simultaneous video recording. Several 60 s bouts of activity were sampled at 100 Hz over a two or three day period. The chicken was then sacrificed and the tibiotarsus dissected to determine gage orientation. The tibiotarsus was embedded within a polyester matrix and cross-sectioned into 100 μm axial slices to determine gage positions and cross-sectional geometry of the midshaft (Fig. 1).

Longitudinal strains at each rosette were then calculated at each data sample for both treadmill and general activities. From this, the strain distributions were determined using beam theory in a method similar to that described previously [4]. This data was processed further to determine the components of longitudinal strain due to both axial and bending loads as well as the orientation of the peak compressive strains. To simplify the analysis, the component of longitudinal strain due to bending was calculated at an average radius (3.0 mm) of the medial, lateral, anterior, and posterior radii (Fig. 1).

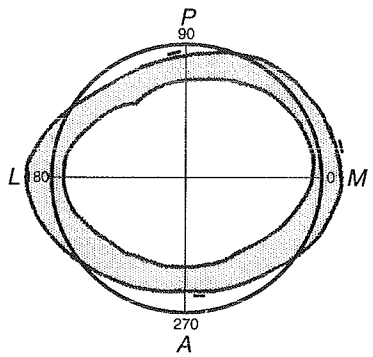

Figure 1: Midshaft Orientation

RESULTS

Data for twelve representative load cycles of gait during treadmill activity were normalized and averaged to represent a composite gait cycle (Fig. 2). It was not possible to construct a meaningful composite load cycle for general activity, due to the wide range of walks, runs, turns, jumps, and drops. For treadmill activity, longitudinal strains due to bending predominated and resulted in a bimodal history of compressive longitudinal strain. The orientation of the peak compressive strains ranged from about 20° to 150° throughout the composite load cycle, with the bimodal peaks occurring at 25° and 135°.

The frequency distributions of the orientations of peak compressive strain were then determined for longitudinal strains greater than 75% and 90% of peak magnitudes for all sampled data from the treadmill and general activities (Fig. 3). For treadmill activity, nearly all peak compressive longitudinal strains greater than

90% of the peak magnitudes occurred at orientations between 10° and 40°, while for the general activity, these were distributed between 10° and 160° with most occurring between 20° and 50°. For peak longitudinal strains greater than 75% of peak magnitudes, treadmill activity exhibited a second peak in the frequency distribution at an orientation of approximately 140°, consistent with the bimodal history of strain shown in Fig. 2. This did not develop for general activity; instead the frequency distributions were similar for both the 75% and 90% thresholds.

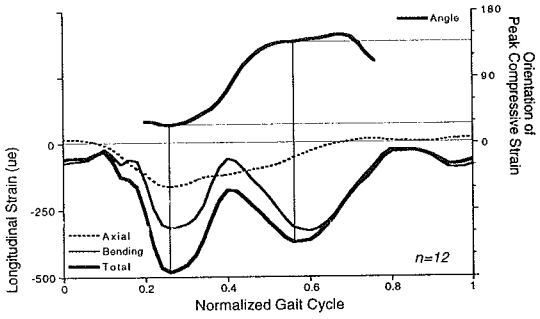

Figure 2: Composite Load Cycle

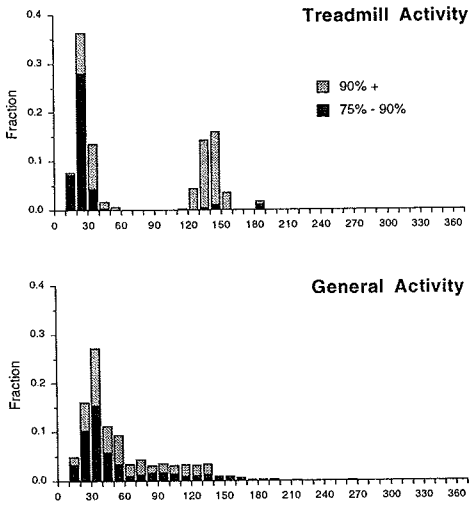

Figure 3: Orientation of Peak Compress Strain

DISCUSSION

These results demonstrate that both strain magnitude and bending orientation evolve during a loading cycle of gait and influence the longitudinal strain distribution. In particular, the orientation of peak compressive strain varied over 120° from heel strike to toe off, in contrast to a 20° range reported during the late stage of stance for an equine metacarpal [4]. This, in combination with the bimodal distribution of bending strain, resulted in *two* orientations of peak compressive strain, instead of the *single* orientation which would develop if bending occurred about a single axis. While the introduction of a wider variety of loading events during general activity did result in a broader orientation of peak compressive longitudinal strains, most were again oriented at 30°. These data suggest that most peak compressive strains occur at well-defined and distinct orientations associated with peak bending loads, and are generally consistent for both treadmill and general activities.

Interestingly, although the orientation of peak compressive strains was approximately 30° for all activities, the radius of cortical bone at 30° was greater than the average radius. Because longitudinal strains due to bending increase with distance from the centroid, strains at this region of the periosteal surface would be *greater* than those reported using an average radius. If mature bone were optimized to minimize differences in longitudinal strain magnitude at different cortical sites, the radius of mature cortical bone should be *inversely* related to the longitudinal strain magnitude at all orientations of peak compressive strain.

It should be recognized, however, that the current results are limited to distributions of longitudinal strain and do not incorporate out-of-plane or torsional components. Current ongoing work is focused on utilizing finite element methods in conjunction with strain gage data to provide a more complete description of these strain components for a variety of functional *in vivo* loading activities.

REFERENCES

1. G. Beaupre, T. Orr & D. Carter (1990) *J. Orthop. Res.* 8:651-662.
2. A. Biewener, S. Swartz, J. Bertram (1986) *Calcif. Tiss. Int.* 39:390-395.
3. D. Konieczynski, A. Biewener, M. Temaner & M. Truty (1995) *Trans. ORS* 20:203.
4. T. Gross, K. McLeod, C. Rubin (1992). *J. Biomech.* 25(9): 1081-1087.

ACKNOWLEDGEMENTS

This work was supported by NIH Grant AR-39828.

MECHANICS AND MECHANISMS OF CRACK GROWTH AT OR NEAR INTERFACES IN CEMENTED LOAD BEARING PROSTHESES

[1]Reiner H. Dauskardt, [1]N. Christine Nguyen, and [2]William J. Maloney

[1]Department of Materials Science and Engineering
[2]Department of Functional Restoration
Stanford University
Stanford, CA 94305-2205

INTRODUCTION

Self-curing polymethylmethacrylate (PMMA) bone cements are extensively employed to affix load bearing prosthetic components to bone in the musculoskeletal system. In this role, the PMMA bone cement must not only secure the prosthetic component in place, provide a mechanically compliant buffer layer between the stiff metallic prosthetic substrate and the significantly less stiff bone to which it is attached [1], but also effectively transfer complex, and in most cases, time-varying physiological loads from the prosthesis to the bone [2].

REVIEW AND THEORY

Failure of cemented prostheses is most frequently associated with progressive "loosening" of the joint [see e.g. 3]. In service lifetimes are dictated by the *initiation* and *subcritical growth* flaws or cracks in any of the constituents of the prosthetic/cement/bone composite system, or debonding of either of the typically weak interfaces separating them.

Despite the importance of such fracture behavior, it is somewhat surprising that few studies have provided a detailed and valid* measure of the fracture and subcritical crack-growth behavior of the prosthesis/cement/bone structure, and particularly in the weak PMMA cement and adjacent interfaces. Accordingly, the intent of the present work is to provide a detailed study of the fracture and subcritical fatigue crack-growth behavior of PMMA bone cement in both air and simulated physiological environments. In addition, methods for the measurement of interface fracture resistance and subcritical growth of interface cracks or debonds are explored.

PROCEDURES

Material: A two-component PMMA cement consisting of a powder polymer and a liquid monomer (Surgical Simplex-P, Howmedica Inc., Rutherford, New Jersey) was prepared under controlled conditions by stirring at room temperature at a slow mixing rate to minimize porosity, and cured under pressure in a Delrin mold. The specimen was removed from the mold and stored in air for 24 hours. Both 50 mm diameter blanks (2 to 16 mm thick) and composite samples containing interfaces between the cement and either the prosthetic substrate or bovine bone (with various surface preparations) were prepared to facilitate fabrication of fracture mechanics samples described below.

Fracture Mechanics Experiments: Disk-shaped compact-tension DC(T) fracture mechanics samples were prepared from the round PMMA blanks according to the specifications of ASTM Standard E399-90, for *Plane-Strain Fracture Toughness of Metallic Materials*. Thin metallic foils were bonded onto the specimens to facilitate accurate and continuous measurements of the crack length using electrical potential drop techniques. The foils were protected with a thin layer of waterproof polysulfide epoxy to allow testing in the conductive Ringer's lactate solution.

Cyclic fatigue crack-growth rates per cycle (da/dN) were characterized in terms of the applied stress intensity range (ΔK) in general accordance with ASTM Standard E647-85A for *Measurement of Constant-Load-Amplitude Fatigue Crack Growth Rates*, using the procedures outlined for brittle materials by Dauskardt, et. al. [4]. The stress intensity is considered the "driving force" for crack advance, providing a measure of the local stress and deformation field in the vicinity of the crack tip. Fatigue tests were performed with a cyclic sinusoidal frequency of 25 Hz at a load ratio R = 0.10.

The fracture toughness (i.e., critical stress intensity K_{IC} for instability) was determined under displacement control from the resistance-curve (R-curve) behavior, using a specimen containing a sharp fatigue pre-crack. Procedures essentially conform to ASTM Standard E399-90, and are considered to be more precise than many used previously where cracking was initiated from a machined notch (rather than from a fatigue crack) in samples too small to satisfy small-scale yielding requirements.

Interfacial fracture resistance and subcritical crack growth behavior was assessed using a novel four point bend fracture mechanics sample containing the

* Valid in this context is used to indicate that fracture mechanics tests have been conducted under nominally standard conditions (e.g., as specified by ASTM E399 and E642 described in the experimental section) and that results are not a function of specimen geometry and other configurational effects.

interface of interest (Fig. 1). After prenotching of the top layer, the specimens were loaded in four-point bending in a high-resolution miniature mechanical test system. Fracture proceeds from the machined notch, through the PMMA layer, until the crack encounters the weak interface, bifurcates and proceeds along the selected interface. Fracture energies for both critical and subcritical debonding were measured under representative loading and physiological conditions. The effect of mode mixity (ratio of shear to normal stress at the interface) was examined by changing the sample configuration.

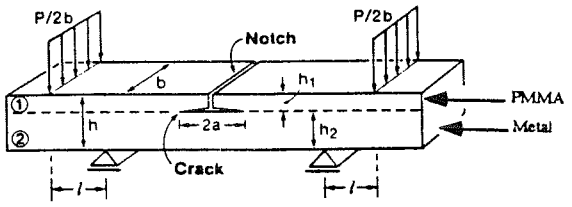

Fig. 1: Four-point bend fracture mechanics sample. The fracture energy is expressed in terms of the strain energy release rate, G, which is a function of the applied loads P, elastic properties, E_i, and moments of inertia, I_i.

RESULTS AND DISCUSSION

Fatigue crack growth: Selected results of the cyclic fatigue-crack growth tests are plotted in Fig. 2. Crack growth rates span four orders of magnitude, exhibit a Paris law dependence similar to that observed in other engineering polymers ($da/dN \propto (\Delta K)^m$), and display an apparent fatigue threshold (ΔK_{TH}), below which crack growth is presumed dormant. The striking effect of Ringer's lactate solution on decreasing crack growth rates by almost two orders of magnitude are clearly apparent. Data obtained for cracks located near, or at, the interface between PMMA and either the metallic substrate or bone are also discussed. Behavior is rationalized in terms of the plasticizing effect of the Ringer's solution, fluid wedging effects in the crack wake under cyclic loads, and interface strength for cracks located at bi-material interfaces.

Fracture Toughness: Fracture toughness values were determined by characterizing the complete crack-growth resistance (R-) curves of fatigue pre-cracked samples (Fig. 3). Similar to fatigue crack-growth behavior, R-curves of PMMA bone cement were critically dependent on testing environment. Steady-state fracture toughness values taken from the plateau of the R-curves were almost four times as great for cement tested Ringer's solution. Similarly, interface fracture resistance was also sensitive to the testing environment and interface morphology. The results of several surface preparations resulting in different interface morphologies are reported. Based on the findings of this work, interface engineering strategies to promote optimum resistance to debonding and subcritical crack growth are discussed.

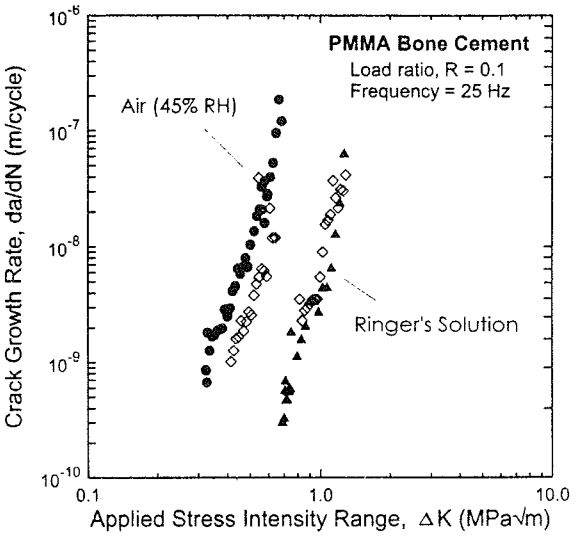

Fig. 2: Fatigue crack growth rate behavior in PMMA cement

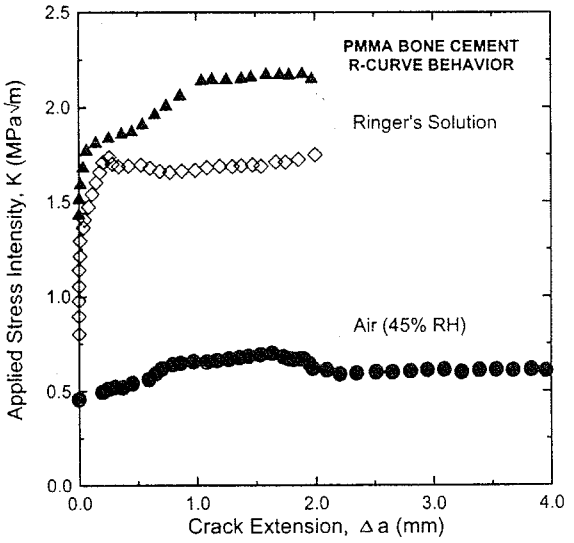

Fig. 3: Fracture toughness (R-curve) behavior.

REFERENCES

1. J. Charnley, Acrylic Cement in Orthopedic Surgery, Williams and Wilkins, Baltimore, 1970.
2. A.M. Ahmed, et. al., J. Orthop. Res., 8, 435-47, 1990.
3. W.J. Muralijasty, et. al., J. Bone Joint Surg., 73-B, 551-58, 1991.
4. R.H. Dauskardt, et. al., J. Biomed. Mat. Res., 28, 791-804, 1994.

ACKNOWLEDGMENTS

Griffin Award through the McCutchen Foundation.

THE EFFECT OF ULTRASONICALLY DETERMINED ANISOTROPY ON FRACTURE TOUGHNESS OF CORTICAL BONE

S. Han[1,2], J. Rho[1,2], J. Medige[1,2], I. Ziv[1,2,3]
[1]Department of Orthopaedic Surgery, University at Buffalo
[2]Department of Mechanical & Aerospace Engineering, University at Buffalo
[3]Department of Veterans Affairs Medical Center, Buffalo, NY 14214

INTRODUCTION

The objective of this study was to determine the effects of bone density and microstructure on fracture toughness using ultrasound. Bovine cortical bone samples were demineralized by acid attack, producing specimens with a wide range of bone density. Ultrasound velocity was measured in the radial and longitudinal directions of specimens using a pulse transit time approach. A microstructural anisotropy parameter was introduced and evaluated as a function of these ultrasound velocities. The critical stress intensity factors K_{IC} of these specimens were determined by mechanical fracture tests. The dependence of fracture toughness on density, on microstructural anisotropy and on the combination of the two was investigated.

REVIEW AND THEORY

Fracture of compact bone is dependent on the nature of intrinsic cracks as well as the stress level (Evans et al., 1973, Bonfield et al., 1987). For many years, the mechanical properties of bone have been characterized primarily by strength, Young's modulus, etc. (Lindahl et al., 1967, Wall et al., 1979, Martin, 1993). However, a precise assessment of bone fracture risk can best be achieved by its fracture toughness (Evans et al., 1973, Melvin et al., 1993) . Behiri et al. (1984) reported that fracture toughness significantly increased with relatively small increases of density in human cortical bone. Although bone density in fracture is of great importance, there has been a strong desire to determine the effect of the microstructure of compact bone tissue on fracture. The combined effect of density and microstructure will likely provide a more accurate predictor.

PROCEDURES

Twenty cortical specimens (4.5 x 18.5 x 19.3 mm) were taken from four bovine tibiae. Seventeen specimens were immersed in 0.6 N hydrochloric acid for several time periods to reduce mineral content by various amounts. The density of each specimen was measured using Archmedes' principle. Ultrasonic velocities were then measured in the longitudinal and radial directions to determine the microstructural anisotropy of each cortical specimen. A pair of 2.25 MHz transducers was used to transmit and receive the ultrasonic waves. A structural anisotropic parameter, referred to as the "longitudinal anisotropy index" (LAI), was developed. This parameter is defined as the square of the ratio of ultrasonic velocities in the radial and longitudinal directions, or $LAI=(V_{rad}/V_{long})^2$, where LAI is the longitudinal anisotropy index and V_{rad} and V_{long} are the ultrasound velocities in the radial and longitudinal directions, respectively. After ultrasonic measurement, the samples (compact tension specimens) were prepared for fracture toughness tests with 0.5 mm wide slots and 3.2 mm diameter holes. The crack length was 7.2 mm and all other parameters were in accordance with ASTM Standard E399-70T. Mechanical fracture tests were performed on an axial testing machine (MTS T22K) at the crosshead rate of 0.05 mm/sec to determine the critical stress intensity factor (K_{IC}, $MNm^{-2/3}$). Correlation studies of fracture toughness with density, the longitudinal anisotropy index and combinations of the two were performed.

RESULTS

Specimens were demineralized up to 25 % by the acid attack. As a result, density was distributed from 1.52 to 2.08 g/cc. The mean fracture toughness value (K_{IC}) for the three specimens that were not cured in HCl solution was calculated to be 3.90 $MNm^{-2/3}$. Bone density was highly correlated with the fracture toughness parameter (r^2=0.913). The relationship between LAI and K_{IC} was also significant (r^2=0.776). The fracture toughness parameter was most strongly dependent on the combined effect of bone density and longitudinal anisotropy index, defined as the bone density multiplied by LAI (r^2=0.951).

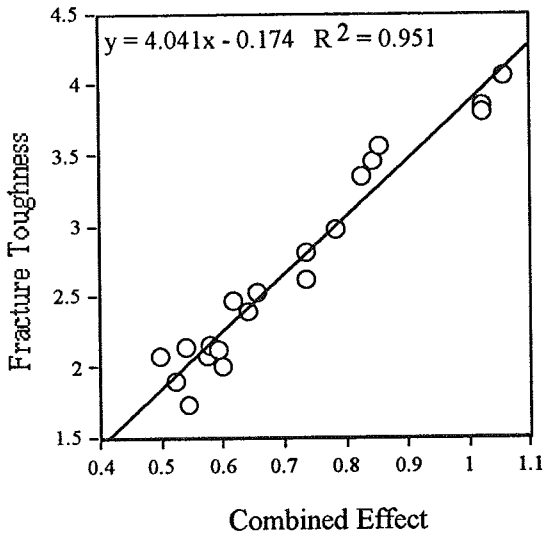

Fig.1: Measured fracture toughness (K_{IC}, $MNm^{-2/3}$) vs. the combined effect (product) of the anisotropy index and density

DISCUSSION

The value of 3.90 $MNm^{-2/3}$ obtained for the control specimens agrees with those of previous studies (Behiri et al., 1980, Behiri et al., 1984). Results showed that the fracture of cortical bone is related to the microstructural properties of the bone as well as to its density. The fact that the bone density significantly affects the critical stress intensity factor (K_{IC}) may indicate that the density is related to the number of flaws per unit volume, which induces bone's microcracking. Behiri et al. (1984) reported that fracture toughness could be evaluated by bone density alone. However, their study did not examine the effect of microstructural anisotropy within the bone. Despite the need of incorporating the anisotropic chracteristics of bone in fracture toughness assessment, the difficulty of its measurement has hampered its application. With the use of ultrasound measurement in bone, the effect of microstructure on fracture toughness can be evaluated. The parameter LAI reflects the anisotropy of osteon alignment in cortical bone. Although the density alone can predict fracture toughness with relatively high accuracy, the combined effects of density and microstructure increase the predictability of fracture toughness. The inclusion of this microstructural effect enhances the understanding of fracture mechanics in compact bone.

REFERENCES

Behiri, J.C. et al. J Mater Sci, 15, 1841-9, 1980. Behiri, J.C. et al. J Biomech, 17, 25-34. Bonfield, W.J. et al. Biomech, 20, 1071-81, 1987. Evans, F.G. et al. Mechanical properties of bone, Thomas, Springfield, IL, 1973. Lindahl, O. et al. Acta Orthop Scand, 38, 141-7, 1967. Martin, B. Calcif Tissue Int, 53, S34-9, S39-40. Melvin, J.W. et al. J Biomech Eng, 115, 549-54, 1993. Wall, J.C. et al. Calcif Tissue Int, 27, 105-8, 1979.

ACKNOWLEDGEMENT

This work was supported in part by the Whitaker Foundation.

POTENTIAL INJURY PATTERNS OF CERVICAL SPINE DUE TO VERTICAL LOADING – A MODAL ANALYSIS

L. Voo[1], Y. Liu[2], F. Pintar[1], N. Yoganandan[1],

[1]Department of Neurosurgery, Medical College of Wisconsin 53226
and Veterans Affairs Medical Center, Milwaukee, Wisconsin 53295

[2]University of Northern California, Petaluma, California 94952

INTRODUCTION

Cervical spinal injury occurs in motor vehicle accidents, falls, diving, tackle football, hockey, and other contact sports. Consequences of severe neck injuries range from fatality to complete or incomplete quadriplegia. Understanding the mechanisms of cervical spine injury has been the focus of many clinicians and biomedical engineers. Buckling response of the head and neck has been suggested as a potential mechanism for neck injuries of compression-flexion type, which are most common and severe. This study examined the buckling behavior of the head and neck using a simple segmented column model and structural analysis computer software. Buckling mode shapes and their corresponding critical loads provided an estimated potential neck injury patterns.

REVIEW AND THEORY

Epidemiological studies have shown that the majority of severe neck injuries occur due to compression-flexion loading resulting in vertebral body fractures and intervertebral joint dislocations (Yoganandan et al., 1990). Reviews of cervical spine injuries in contact sports (Burstein et al., 1982) and experimental studies in cadavers indicate that the elimination of the natural cervical lordosis is often necessary for a vertical head impact to produce clinically-seen severe neck injuries (Pintar et al., 1990b; Yoganandan et al., 1991).

Liu and Dai (1989) theorized, with the concept of the stiffest axis, that the straightened cervical spine subjected to a axial impact may buckle in the sagittal plane and initiate the injury. Idealizing the straightened human neck to be a homogeneous beam-column, the stiffest axis concept provided insight into the possible underlining mechanisms and predicted that the cervical column pre-alignment (unloaded configuration and load alignment) was the key parameter for the production of compression-flexion type of vertebral injury. That theoretical prediction was later supported by the success of *in vitro* dynamic head and neck experiments (Pintar et al., 1990b; Yoganandan et al., 1991). However, the homogeneous column representation did not account for the structural inhomogeneity of the cervical spine and can not be used for quantitative analysis with available experimental data. These goals can be achieved by treating the ligamentous human cervical spine as a segmented column.

The objective of the present study was to investigate the correlation between the buckling mode shapes, critical loads, and potential injury patterns of the head and neck using a segmented column model and *in vitro* experimental data of the cervical intervertebral joints.

PROCEDURES

The head was represented by a rigid body with its height equal to the height from occipital condyle to the crown. The occipito-atlanto-axial (C0-C1-C2) joint was simulated by an elastic joint which allowed the two connected bodies to have relative rotations and translations with stiffnesses. Data from *in vitro* experiments of cadaver C0-C1-C2 joint were used as the input for those stiffnesses. The straightened cervical column (C2-T1) was idealized as seven rigid segments (cylinders) representing the vertebrae interconnected by elastic joints. The vertebrae were 15 mm in height based on an earlier study (Sherk et al., 1989). The actual experimental data for the cadaveric cervical intervertebral joints in the literature were used as the input for the stiffnesses of those elastic joints, which included axial compression (normal), anterio-posterior shear, and flexion-extension bending. A general purpose structural analysis software, ANSYS®, was used for the numerical solution. The model was constrained to have only planar motion to simulate the sagittal buckling of the head and the straightened cervical spine. Linear eigenvalue buckling analysis were performed to obtain the critical loads and corresponding buckling mode shapes for the segmented column model. The equation to be solved is:

$$([K] + \mu_i[S])\{u\}_i = \{0\}$$

where [K] = elastic stiffness matrix; [S] = stress stiffness matrix (based on a preload); μ_i = ith eigenvalue or critical load; $\{u\}_i$ = ith eigenvector of nodal displacements (used to construct buckling mode shapes). The critical loads obtained by this analysis gives the upper bound of the load carrying ability of the structure. T1 segment was assumed kinematically fixed while different constraint conditions of the head were simulated to examine their effects on the column behavior.

RESULTS

The buckling mode shapes of the model showed the following potential behaviors of the head and neck when excited by axial impact load:

1) large head rotation occurred with maximum compressive load of only 61 N (head unconstrained);
2) large head lateral translation and cervical spine bending with a critical load of 1001 to 1100 N depending on the head constraints and/or the order of the buckling modes;
3) joint dislocation with some degree of bending when the compressive reached 3011 N (head constrained to allow only axial translation);
4) single-bow cervical column buckling with head translated axially and a critical load of 3394 to 3633 N depending on the head constraints and/or the order of the buckling modes;
5) double-bow buckling of the cervical column with head translated axially and a critical load of 5620 to 6173 N depending on the head constraints.;
6) hyperextention injuries to the occipito-atlanto-axial (C0-C1-C2) complex is possible if the higher modes are excited.

DISCUSSION

The critical load increases with an increase in end constraints or order of buckling mode. Higher critical load magnitude means higher stress level in the materials of the structure. Cervical spine injuries include vertebral body wedge or burst fracture, joint dislocation, and rupture of ligaments. In the case of unconstrained head subjected to crown impact, large head rotation tend to deflect the head away from the load path, reduce contact duration and result in sub-injurious load in the cervical spine (mode 1 in the results). Critical load of 1001 to 1100 N is below the load level for vertebral fractures before the column buckles out of its initially straight configuration. Post-buckling of the column beyond the 1100 N critical load level may induce hyperflexion or hyperextension of the cervical spine resulting in injuries to various ligaments in tension. When the head is constrained to move only axially, a quasistatic compressive load or low-speed impact may cause dislocation of intervertebral joints with a critical load around 3000 N. Pintar et al. (1990a) reported compressive loads of 1355-3613 N for cervical joint dislocation in their in vitro experiments. The single-bow and double-bow buckling mode shapes of the cervical column requires higher-speed of impact to excite and more difficult to reproduce in experiment unless it is pre-configured in those shapes. Compressive load in the straightened cervical spine at 3394 to 3633 N may induce vertebral fracture before the cervical column buckles into the single-bow bending curve. Yamada reported compressive breaking load for cervical vertebral body to be an average of 4096 N for 20-39 year age group and 3303 N for 40-59 group. In dynamic head/neck vertical impact experiments, Yoganandan et al., (1991) reported an average peak load of 4467 N, with a range of 3300-5600 N. Post-buckling behavior of the single-bow mode shape may cause fracture of the spinous processes and/or anterior longitudinal ligaments in the cervical column. If the cervical column is forced to buckle only into the double-bow mode shape, one of the vertebral bodies will most likely fracture before the compressive load reaches the critical load of 5620 to 6173 N for buckling.

REFERENCES

Burstein, A.H. et al. *Athletic Injuries to the Head, Neck and Face,* (pp.139-154), Lea & Febiger, 1982.

Liu, Y.K. and Dai, Q. *J. Biomech. Eng.,* 111, 122-127, 1989.

Pintar, F.A et al. *SAE Transactions*, 98(6), 1766-1789, 1990a.

Pintar, F.A. et al. SAE paper #902309, 1990b.

Sherk, H.H.et al. *The Cervical Spine*, J. B. Lippincott, 1989.

Yamada, H. *Strength of Biological Materials*, Williams & Wilkins, (pp. 76-78), 1970.

Yoganandan, N. et al. *SAE Transactions*, 98, 1790-1807, 1990.

Yoganandan, N. et al. *Spine*, 16, S511-517, 1991.

ACKNOWLEDGMENTS

This research was supported in part by PHS CDC Grants R49CCR-507370 and 703640, DOT NHTSA Grant DTNH22-93-Y-17028, the Department of Veterans Affairs, and the Helen Streiffer Fund at the University of Iowa Foundation.

MULTIDIRECTIONAL INSTABILITY OF THE THORACIC SPINE RELATED TO IATROGENIC PEDICLE INJURIES DURING TRANSPEDICULAR FIXATION: A BIOMECHANICAL INVESTIGATION

MM Panjabi, R Kothe, W Liu
Biomechanics Laboratory, Yale University School of Medicine,
New Haven CT 06510

INTRODUCTION

Pedicle screw fixation is probably one of the most advanced fixation techniques in spine surgery. Although widely used, the insertion of the pedicle screws still involves a high amount of complications, i.e. pedicle fracture during insertion. This is especially true for the thoracic spine, where the pedicle width is often only slightly bigger than the screw diameter. Unfortunately, little is known about the biomechanical affect of an intra-operative pedicle injury during screw insertion.

AIM OF THE STUDY

The purpose of this study was to investigate the effect of an intra-operative fracture of the pedicle during screw insertion on the multi-directional stability of pedicle screw plate fixation in the thoracic spine.

MATERIALS AND METHODS

Eight fresh human cadaveric spine specimens were dissected and prepared for mechanical testing. Each specimen consisted of five vertebral segments, four specimens of the middle thoracic spine (MTS) and four specimens of the lower thoracic spine (LTS). The mechanical properties of the intact specimens were determined with a multi-directional flexibility test, in which the loads applied were pure moments. Then a burst fracture was produced in the middle vertebra, using a high speed trauma apparatus. The fracture was stabilized with the Dorsal Fixation System (Howmedica). It consisted of profiled plates with elongated holes, pedicle screws and threaded rods which were added to the screw heads as diagonal cross-linkages. To simulate an intraoperative pedicle fracture, all instrumented pedicles were cut in four steps, i.e. (1) lateral wall at one level, (2) lateral wall at two levels, (3) entire pedicle at one level, and (4) entire pedicle at two levels. After each step, the multidirectional instability was determined with the flexibility test. Statistical analysis was performed with ANOVA for repeated measurements and the Fisher test at 95% confidence level.

RESULTS

In flexion and extension, neither the range of motion (ROM) nor the neutral zone (NZ) increased when the lateral wall of the pedicle was resected. Even when all the pedicles were cut there was only an insignificant increase of ROM and NZ in the MTS specimens while the LTS specimens were not affected at all. In axial rotation, ROM and NZ significantly increased in the MTS when the lateral wall was resected, while in the LTS, ROM and NZ did significantly increase only when all the pedicles were cut. In lateral bending, the lateral cut of the pedicle resulted in a significant increase of ROM and NZ in both the MTS and LTS. With all the pedicles cut, the instrumentation was severely unstable in lateral bending.

DISCUSSION

In the thoracic spine, the intra-operative fracture of the pedicle does not affect the stability of the system in flexion and extension. However, in axial rotation and especially in lateral bending, a pedicle fracture results in a significant decrease in the stability provided by the instrumentation. This effect was higher in the middle than the thoracic. Therefore, one should consider smaller pedicle screws (less than 5.0 mm) and different techniques of insertion, e.g. insertion of the screw through the transverse process, for the pedicle screw instrumentation of the thoracic spine.

Table 1: Mean ± SD of motion for the Middle Thoracic Spine

Pedicle Injury					Statistical Analysi	
	1	2	3	4	P-value	Fisher
Flexion/Extension (degrees)						
NZ	0.4 ± 0.1	0.2 ± 0.2	0.7 ± 0.4	1.4 ± 0.4[A]	0.018	0.497
ROM	6.2 ± 1.4	1.5 ± 0.4[A]	2.9 ± 2.9[A]	5.5 ± 4.4	0.051	3.298
Axial Rotation (degrees)						
NZ	1.4 ± 0.7	1.1 ± 0.3[D]	2.4 ± 1.5	4.4 ± 2.7[A]	0.078	2.174
ROM	12.1 ± 2.	3.6 ± 1.7[A,D]	8.2 ± 4.2	12.4 ± 7.9[	0.036	5.746
Lateral Bending (degrees)						
NZ	1.2 ± 0.3	2.6 ± 1.1[C,D]	5.6 ± 1.8[A,B]	6.5 ± 2.3[A,B]	0.001	1.817
ROM	10.6 ± 3.	10.0 ± 3.9[C,	19.0 ± 7.1[B]	25.4 ± 11.8	0.013	8.559
Note: ANOVA and Fisher-test were performed to determine the significant differences ($P < 0.05$), which are indicated by the superscript A,B,C,D.						

BIOMECHANICAL SYMMETRY OF THE RABBIT ACL

S. Chelikani, M.M. Panjabi
Biomechanics Laboratory, Yale University School of Medicine,
New Haven, CT 06510

INTRODUCTION

The assumption of bilateral symmetry is crucial to biomechanical experimentation, where one limb of a pair serves as a control for the other. The purpose of this study was to determine whether the symmetry assumption can be applied to the rabbit anterior cruciate ligament (ACL). Ten pairs of rabbit ACLs were stretched to failure, and the load-displacement readings were collected and analyzed. The parameters compared were, the failure load, failure displacement, stiffnesses and energies absorbed. The results of our study assert that there is a remarkable similarity in the mechanical properties within each pair.

REVIEW AND THEORY

Symmetry studies on soft tissues are practically non-existent, though the assumption itself is widely used. A review of past research reveals that some studies have inquired into questions of symmetry of long bones. Mather (1967), determined that human femoral pairs are mechanically symmetrical in the ultimate load, energy to failure, elastic modulus and failure stress. White and Panjabi (1974), found that rabbit long bones exhibit symmetry in torsional strength. On the other hand, Dogra and Singh (1971), found that a statistically significant asymmetry exists in bone and muscle weights of paired human humeri, in keeping with the incidence of 'handedness'. Singh (1971), concluded that in rabbits and frogs, one-sided dominance exists in both fore and hind limb bone weights. In view of the lack of symmetry data concerning soft tissues, we designed this study to determine whether paired ACLs exhibit symmetry.

PROCEDURES

Ten New Zealand white rabbits, euthanized for reasons unrelated to this study, were obtained from other research groups. The average weight and ages were 3 kg and 12 months respectively. The hind limbs of each animal were amputated distal to the hip joint, tagged left and right, and bagged as a pair in heavy gauge plastic and frozen at -20^{o} C until testing. On thawing, the specimens were dissected of all soft tissues except the anterior cruciate ligaments. To facilitate testing the femur and tibia were cut about 1 cm distal to the joint line, leaving in effect a femur-ACL-tibia complex. Into each bone-end two K-wires were drilled, perpendicular to each other. Each bone-end was then mounted in a water based dental cement [Die Keen, Columbus Dental, St. Louis, Missouri].
While mounting, the angles of the femur and tibia were adjusted, to align the ligament to the load axis. The K-wires ensured that the bone end was rigidly anchored into the cement, and prevented any slippage from occurring (Fig. 1). From the time of thawing, until the failure test, the ligament was kept moist by gauze soaked in 0.9% normal saline.

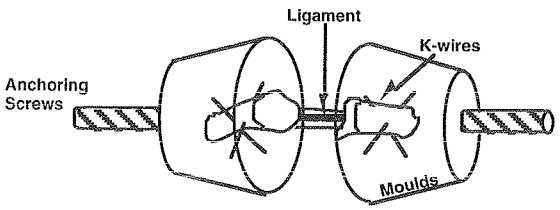

Figure 1. Femur-ACL-Tibia unit.

The testing machine was custom built and computer controlled using software specifically written for the purpose. The specimen was mounted in the machine with one end fixed to an immovable frame, in series with a load cell, while the other end was attached to a moving platform. Once mounted, the ligament was checked for alignment with the loading axis of the machine, and adjustments were made if needed. A speed of 1 mm/sec was chosen for the present experiments. The load cell measured the ligament force, while the ligament stretch was recorded via an LVDT (Linear Variable Differential Transformer). Both transducers were sampled at 100 samples per second by a computer which also ran the testing machine. Once mounted, the initial length of the specimen was standardized at a displacement which applied a tension of 2 N. The ligament was then preconditioned by cyclically stretching it to a maximum displacement of 0.5 mm from the initial position, for 21 cycles. In the 22nd cycle, the ligament was stretched to failure. A similar protocol was observed for the contra lateral ligament.

Load and deformation data from the 22nd cycle were analyzed. Two distinct regions, the 'toe' and the linear segment were identified for analysis (Fig. 2).

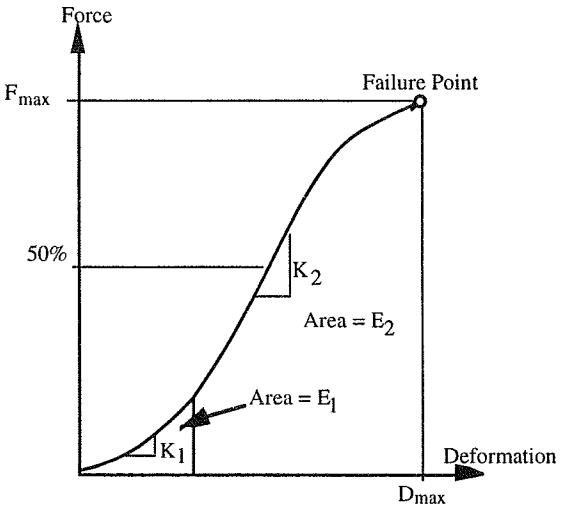

Figure 2. Various parameters used for comparison.

The parameters for comparison were: failure force F_{max}, failure deformation D_{max}, and stiffnesses K_1 and K_2, energies E_1 and E_2, corresponding to the toe and linear regions. Paired Student's t-test was used at 95% confidence level to determine any significant differences. Statistical analyses were done using Statview™ (Abacus Concepts, Inc., Berkeley, California).

RESULTS

The aim of this study was to determine whether the left and right anterior cruciate ligaments salvaged from the same animal exhibit similar mechanical properties. The average and standard deviation values for the various parameters for the left and right ACLs are given in Table 1. We were unable to disprove the null hypothesis for any of the parameters, as indicated by the p-values in Table 1. Consequently, we assert that left-right differences in mechanical properties among ACL pairs are statistically insignificant.

DISCUSSION

The results of our study prove that paired ACLs do exhibit mechanical symmetry. This was verified by the high p-values for significance of differences. The parameters compared were the failure force and deformation. In addition, the stiffness and energy values were computed from the load-deformation data, for distinct regions of the curve. One is the toe region, when the ligament is aligning itself internally, to the load direction. This is assumed to happen by the mechanism of 'uncrimping' of fibers in the ligament. By the nature of the process, this region is highly non-linear. The next region is the linear segment when the ligament is a load bearing structure and exhibits higher values of stiffness and energy absorption. We deemed it necessary to demarcate these regions and separately compute the values. The similarity in values demonstrates that paired ligaments exhibit comparable nonlinearity, as well as linearity. The lack of difference in energy values is a measure of the extent to which they are similar elastic structures, as defined in theories in classical mechanics.

The symmetry hypothesis is crucial to many biomechanical experiments which require a control. The idea of symmetry can be employed in planning biomechanical experiments, where variables under study can be introduced on one specimen, while the other (the contra lateral) can serve as a control. By using the symmetry criterion, a substantial saving in experimental animals and time can be achieved, while obtaining the same statistical power.

Table 1. Means and standard deviations of experimental parameters and the corresponding p-values.

	Right	**Left**	**p-values**
F_{max},N	248.97 ± 27.	251.11 ± 16.	0.67
D_{max},mm	2.37 ± 0.3	2.38 ± 0.25	0.87
K_1,N/mm	70.7 ± 15.6	73.6 ± 15.8	0.86
K_2,N/mm	124.1± 16.3	123.5 ± 12.6	0.84
E_1,N.mm	12.2 ± 3.2	13.7 ± 3.1	0.89
E_2,N.mm	67.9 ± 9.7	70.9 ± 8.7	0.82

REFERENCES

Dogra, S.K., Singh, I. *Anat. Anz*, 128, 278-280, 1971.

Mather,S. *Journal of Surgical Research* 7, 222-225, 1967.

Panjabi, M.M. et al. *Journal of Orthopedic Research* (Submitted), 1995.

Singh, I. *Journal of Anatomy*, 109, 271-275, 1971.

White, A.A., Panjabi, M.M. *Acta Orthop Scand*, 45, 328-336, 1974.

Acknowledgments:

This research was funded in part by NIH grant AR42211.

AN IMPROVED KNEE-ANKLE-FOOT ORTHOSIS FOR ENERGY EFFICIENT GAIT

K.R. Kaufman[1,2], S.E. Irby[2], D.W. Ussell[2], R.W. Wirta[2],
J.W. Mathewson[3], D.H. Sutherland[1,2]
[1]University of California-San Diego
[2]Motion Analysis Laboratory and [3]Cardiovascular Stress Laboratory
Children's Hospital, 3020 Children's Way, San Diego, CA 92123

INTRODUCTION

Patients with paralysis of the lower limb due to poliomyelitis, Duchenne muscular dystrophy, spinal cord injury, or spinal defects often require a knee-ankle-foot orthosis (KAFO). Conventional orthoses are one of two fundamental types (Yang, 1975). One type is a joint in which the knee remains locked to provide maximum stability during stance but offers no swing phase flexibility. The other type has a knee joint that gives freedom to flex during swing but offers limited stability during stance. Neither of these two types of knee orthoses are optimal. There is a need for a KAFO which will control the external moment at the knee during stance while adjusting the limb length by allowing the knee to flex during swing.

PROCEDURES

A small, lightweight, electronically controlled knee lock has been developed that can be installed on a conventional KAFO. The system is composed of two major parts: mechanical hardware and an electronic control system. The mechanical hardware portion consists of a polypropylene long-leg brace design, a mechanical knee flexion restraint mechanism, and a knee release actuator solenoid. To adapt the electro-mechanical components to a standard orthosis, the medial side knee hinge struts are left intact and the lateral side struts are replaced with matching sized aluminum uprights containing a clutch mechanism. The knee hinge clutch mechanism is a wrap-spring clutch which is a special class of overrunning clutches. A solenoid is used to activate the clutch. The electronic control system is composed of digital logic integrated circuits. A combinational logic network monitors input data and produces electrical output commands based on the input states. The inputs to the control circuitry are signals generated by strategically located foot contact sensors. Based on the input, the controller algorithm generates an actuation signal that is sent to the solenoid for release of the electromechanical knee joint mechanism during the swing phase of gait.

A 40 year-old subject with poliomyelitis was studied using the brace in both the locked and unlocked configurations. The subject underwent bilateral motion analysis using a VICON movement measurement system with retro-reflective markers placed on the subject. The energy costs of walking were evaluated on a treadmill at speeds of 1 to 5 km/hr and slopes of 0% and 5%. While the subject exercised, continuous breath-by-breath expired gas analyses were obtained. Measurements were taken when a steady metabolic state was reached. Regression analysis was used to test if the two straight line regression equations (locked vs. unlocked) were coincident.

RESULTS

The gait analysis demonstrated differences in hip, knee, and ankle motion. When the brace was used in the locked position (similar to a conventional KAFO), the subject displayed circumduction at the hip and vaulting on the contralateral leg. The knee swing-phase motion approached that of a normal individual when the brace was switched from the standard knee locked condition to the unlocked condition (Fig 1).

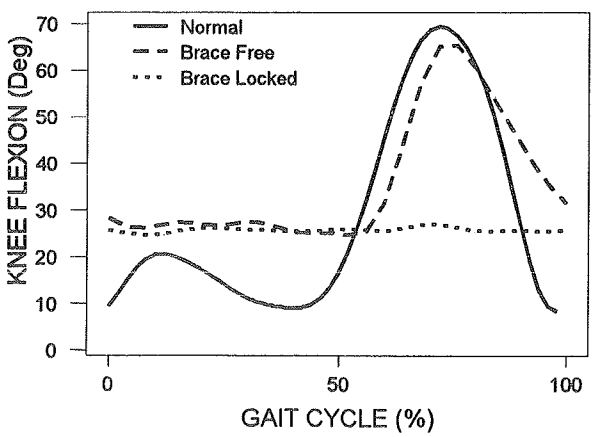

Figure 1: Knee Motion

At each treadmill speed, oxygen consumption increased in a linear manner for both brace locked and unlocked conditions (Fig. 2). However, at each speed, oxygen consumption was always greater with the brace locked. Comparison of the regression lines showed that the intercepts were not significantly different ($p > 0.05$), but the slope of the brace locked condition was significantly greater than the brace unlocked condition ($p < 0.025$). Thus, the brace unlocked configuration reduced metabolic energy requirements.

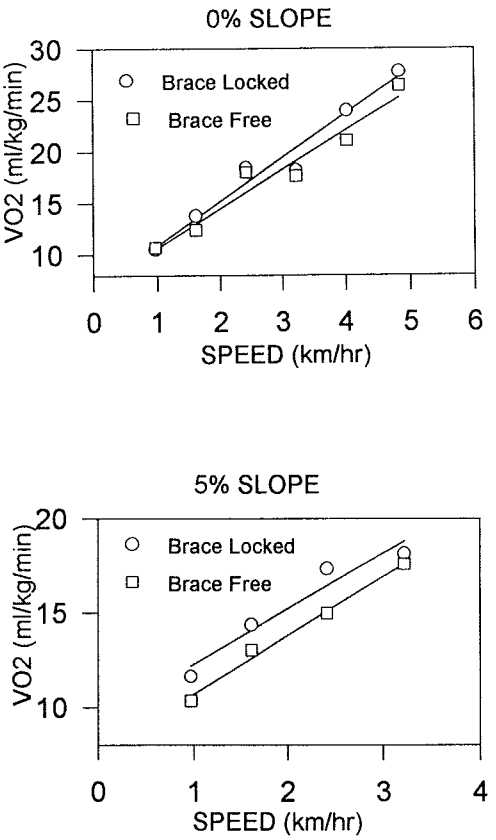

Figure 2: Oxygen Consumption

DISCUSSION

Most of the research and development efforts that are aimed at improving impaired gait have been directed at prosthetic systems. This is because design engineers face fewer technical problems in developing a prosthetic limb replacement, as compared to the development of an orthotic brace system. The difficulties of an orthotic device include the added weight and volume of the lower extremity which limits the size and weight that is available for accommodating the orthotic device. Other than the application of modern plastics to orthotic designs, there have been no real changes in the function of conventional long-leg braces for decades. Surveys show the rejection rate for long-leg braces range from 60% to nearly 100% (Kaplan et al, 1966; Rosman and Spira, 1974; Phillips and Zhao, 1993). Patients who require KAFO's typically accept braces for a very short period following injury or disease, but soon choose to stay in wheel chairs because walking with locked knees is so energy inefficient.

The improved knee-ankle-foot orthosis described in this abstract meets the mobility needs of patients suffering from lower extremity dysfunction, by providing an articulated knee joint system for long-leg braces which reduces the metabolic energy requirements for gait. Six key motions, termed the determinants of gait (Saunders et al, 1953), have been described that optimize the vertical displacement of the body during normal gait. Long-leg bracing may improve static posture, but fails functionally because the determinants of gait are constrained. The brace system described above permits knee stability during stance, while allowing free knee motion during the swing phase of gait. The ability for the leg to move freely during the swing phase of gait results in a gait which is more energy efficient.

REFERENCES

Kaplan, L.K. et al. *Arch Phys Med Rehabil*, 47, 393-405, 1966

Phillips, B. et al. *Assist Technol*, 5, 36-45, 1993

Rosman, M. et al. *Arch Phys Med Rehabil*, 55, 310-314, 1974

Saunders J.B. et al. *J Bone Joint Surg*, 35A(3),543-558, 1953.

Yang P.Y. PhD Dissertation, Ohio State Univ., 1975

ACKNOWLEDGMENT

This work was supported by NIH Grant HD30150.

CORE SUTURE-TENDON INTERFACE AS A FACTOR AFFECTING THE STRENGTH OF TENDON REPAIR - A Biomechanical Analysis

E. Diao, MD, J.S. Hariharan, MD, J.C. Lotz, PhD
Department of Orthopedic Surgery, University of California San Francisco, San Francisco, CA 93143-0728

INTRODUCTION

To determine whether the number of locking loops of the core suture significantly affects the strength of the tendon repair, we performed tensile tests on two paired groups of flexor digitorum profundus (FDP) tendons: one group had modified Kessler[1] suture (MKS) repair with a single loop suture-tendon interface, while the other group had modified Strickland[2] suture (MSS) repair with a double loop suture-tendon interface.

REVIEW AND THEORY

Several different suturing methods have been proposed for primary repair of flexor tendons in an effort to improve results; however, the modified Kessler technique of Kleinert[1], with single locking loops, supplemented by the peripheral running suture, is currently the most popular repair technique. Recently, Strickland et al.[2] have described a core suture with double loops with the aim of improving clinical results. Current studies, including those in our laboratory have focused on developing tendon repair methods that are strong enough to start early active mobilization. Although gap formation and core suture pullout are recognized complications of repair failure, few studies have specifically investigated the biomechanical properties of the core suture-tendon interface.

PROCEDURES

12 fresh-frozen human cadaver FDP tendons were isolated from their insertion to a point 16 cm. proximal to it. To overcome the large biological variability that occurs between individual specimens, we divided each tendon into two equal lengths, forming a matched pair to act as an internal control. One tendon from each pair was repaired by MKS technique using 4-0 Dermalon, while the other was repaired by MSS technique. The tendons were mounted on a servohydraulic materials testing machine (MTS) and distracted at the rate of 2 mm/s to failure, with continuous recording of tendon loads and grip displacements, with the specimens kept immersed in physiologic saline. We recorded each test on video (Kodak P6-120) to allow the analysis of the failure pattern of each repair. We tested differences between two means for statistical significance by a paired Student's t test.

RESULTS

The mean failure load of the MKS repair was 11.7 N $\pm$ 1.89 (SD), while that of the MSS repair was 19.5 N $\pm$ 2.1 (SD) [Figure 1]. The MSS group had 66% higher tensile strength than the MKS group ($P<0.001$). The core suture failed by interface failure, pulling out of the substance of the tendon in each case, and not by suture or knot failure.

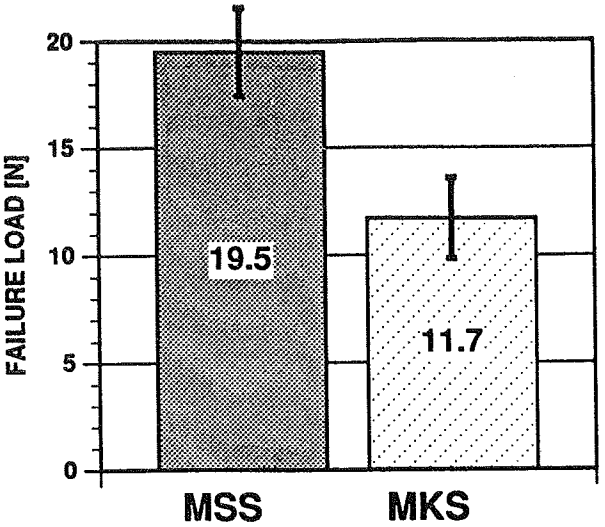

Figure 1: Relative strength of MSS and MKS repairs

DISCUSSION

Prior cadaver studies have established that a double modified Kessler suture is stronger than a single modified Kessler suture for flexor tendon repair[3]. In this study, we found that the number of loops at the suture-tendon interface has a great influence on tensile strength of the core suture. We infer from this study that the number of strands of core suture may be secondary to the number of loops. In terms of the 2 groups we studied, the MSS repair with its double loop is superior in strength to the conventional MKS repair. Expanded use of the MSS technique clinically is supported by our study.

REFERENCES

1] Kleinert, et al. Surg Clin, 61, 2, 267-8, 1981.
2] Strickland, et al. The Indiana Hand Center Newsletter,1, 1, 1-19, 1993.
3] Li X, et al. Orthop Res Soc Trans, 20, 616, 1995.

ACCURATE 3-D MEASUREMENT OF DYNAMIC KNEE REPLACEMENT MOTIONS USING SINGLE-PLANE FLUOROSCOPY: VALIDATION AND *IN VIVO* APPLICATION

S.A. Banks and W.A. Hodge
Orthopaedic Research Laboratory, Good Samaritan Medical Center
West Palm Beach, FL 33401

INTRODUCTION

A new measurement technique has been developed to permit accurate assessment of the three-dimensional motions of knee replacements during dynamic weight-bearing activities. This technique provides a direct kinematic measurement of prosthetic motion which is not affected by skin or muscle motion relative to bone. Studies using this capability are, for the first time, providing detailed objective information on the mechanical function of knee replacements *in vivo* during dynamic activities. This information is critical to improving the understanding of knee replacement function, surgical techniques and the design of longer lasting devices.

REVIEW AND THEORY

Approximately 200,000 total knee replacements (TKR) are performed annually in the U.S. For these operation surgeons choose from well over twenty different designs of TKR. These numbers belie the fact that almost no quantitative information exists on the function of TKR's *in vivo*, and that the majority of device design has been based on trial and error, *in vitro* simulation studies, computer models, and observations of failed components. Although TKR enjoys excellent clinical success, it is clear that accurate *in vivo* kinematic information would enhance the understanding of TKR function and failure, with the prospect of improved surgical approaches, longer lasting devices, and broadened clinical indications.

The kinematic measurement techn que is based on the principles of perspective projections and shape matching; given the source-to-screen imaging distance and the surface geometry of the object, it is possible to estimate the object's position and orientation from its projection (shadow). Rather than implementing a direct model and match approach requiring six dimensional searches, we extended an efficient two-dimensional object recognition technique (Wallace et al.,1980) to a full six degree-of-freedom position/orientation estimator using simple approximations to perspective geometry.

The boundary contours of experimentally acquired silhouettes are first transformed into the Fourier domain and normalized for position, size, and in-plane rotation (Wallace et al., 1980). These Normalized Fourier Descriptors (NFD's) are then compared with a library of precomputed NFD's based on similarly normalized silhouettes of the prosthetic component's 3D CAD model. The library represents the silhouettes of the component over a regular grid of out-of-plane rotations, so that matching between the library and the experimentally determined contour results in estimates of the two out-of-plane rotations. The remaining four degrees of freedom (three translations, and the in-plane rotation) are then estimated by comparing the normalization coefficients of the data and the best matched library contours.

The purpose of this investigation was to evaluate the accuracy of this technique for performing kinematic measurements with knee replacements, and to characterize the knee kinematics in three groups of clinically successful patients with TKR.

PROCEDURES

Simulation Study: The accuracy of the technique was first assessed under ideal conditions using a computer simulation study. CAD models of two TKR components were projected in 100 random poses each to generate the input contours. Library matching and position/orientation estimation were carried out as outlined above.

In Vitro Study: The accuracy of the technique was also assessed using fluoroscopic imaging and post-processing hardware under controlled conditions. TKR components were mounted on a two-axis hydraulic manipulator, and fluoroscopic images were recorded as the components were incrementally translated and rotated over ranges expected for *in vivo* activities. The same image distortion correction, geometry calibration, and image processing procedures were used for the *in vitro* and human studies. Library matching and position/orientation estimation were carried out as outlined above.

Human Study: The motions of subjects' knees were recorded at 30Hz using video-fluoroscopy as they performed a stair-rise maneuver with their knee positioned in front of the fluoroscope image intensifier (sagittal plane parallel to the image plane). The motions of 17 knee replacements in twelve subjects were recorded for four trials each of the stair rise maneuver. All subjects had excellent clinical results, could climb stairs in a reciprocal manner, and gave informed consent to participate in the study. Six knees had posterior cruciate ligament (PCL) retaining AMK (DePuy) knee replacements where the PCL was maintained intact with a tibial bone block. Six knees had PCL retaining Series 7000 (Osteonics) knee replacements where the PCL was partially recessed using a flat tibial plateau bone resection. Five knees had PCL substituting Series 7000 PPSK (Osteonics) knee replacements. The PCL retaining knees utilized relatively flat, non-constrained tibial inserts.

RESULTS

Table 1 shows the average accuracy results for the computer simulation and controlled *in vitro* studies performed with both tibial and femoral knee replacement components. The computer simulation studies demonstrated that the measurement technique was unbiased for rotations, but did exhibit a (negligible) bias of approximately 60μm for translations parallel to the image plane. Given unbiased estimates, the technique's accuracy is expressed in terms of the standard deviation of the error, or standard error. Both validation studies exhibited much larger errors for translation

measurements perpendicular to the image plane than for translations parallel to the image plane.

Table 1. Standard errors for position and orientation measurements from validation studies.

	Rotational Accuracy (deg)	Translational Accuracy (mm)
Computer Modeling	0.3	0.2 (in-plane) 2.0 (out-of-plane)
In Vitro Studies	1.1	0.5 (in-plane) 6.6 (out-of-plane)

The human knee kinematic data are presented as the locations of femoral condylar contact on the tibial component. This convention is used because it is independent of how the local coordinate systems are defined, has obvious anatomical relevance, and is critical to understanding the mechanisms of polyethylene wear in TKR. Table 2 lists the average positions of anterior/posterior condylar contact of the femoral component on the tibial plateau at various points during the stair-rise maneuver (NOTE: Table 2 reports data for only 2 PPSK knees, since CAD models were not available for the remaining 3 knees at the time of writing).

Table 2. Average positions of condylar contact on the tibial plateau. Positions are relative to the anterior/posterior midpoint of the tibial plateau, with negative numbers indicating contact posterior to the A/P midpoint.

	Range of Condylar Translation (mm)	Contact at Max Flexion (mm)	Contact at Max Extension (mm)	Maximum Posterior Contact Point-MPC (mm)	Knee Flexion at MPC (deg)
AMK - Medial Condyle	9.5	-2.2	-2.1	-9.9	41
AMK - Lateral Condyle	11.4	-6.5	-0.3	-9.7	42
7000 - Medial Condyle	8.3	-1.1	-7.5	-9.3	14
7000 - Lateral Condyle	6.3	-3.5	-7.5	-9.2	30
PPSK - Medial Condyle	2.2	-6.9	-6.6	-7.6	53
PPSK - Lateral Condyle	2.7	-5.4	-3.7	-5.5	54

All knees exhibited an external rotation of the tibia as the knee extended. This can be seen in Table 2 by noting that the point of lateral condylar contact moves anterior relative to the point of medial condylar contact as the knee moves from flexion into extension. The three groups of knees exhibited distinctly different patterns of condylar translation. The AMK knees, with a surgically unaltered PCL, showed net anterior translations of the condyles from flexion to extension, with larger anterior translations of the lateral condyle. The Series 7000 knees, with a surgically recessed PCL, showed net posterior translations of the condyles from flexion to extension, with larger posterior translations of the medial condyle. The PCL substituting knees demonstrated small anterior translations of the condyles from flexion to extension, with greater anterior translations of the lateral condyle. All knees exhibited average condylar contact which was contained entirely on the posterior half of the tibial plateau.

DISCUSSION

The computer simulation and *in vitro* studies demonstrated that the measurement technique has the potential to provide very accurate information on all the rotations occurring within the knee, as well as the translations which occur parallel to the image plane. Translations which occur perpendicular to the image plane result primarily in magnification of the silhouette, which is a much more subtle change than those for the other translations and rotations, resulting in poorer measurement accuracy. For typical testing situations, these out-of-plane translations correspond to medial/lateral motions within the knee, which are typically less than several millimeters due to the geometric constraints of knee replacements. Thus, five of the six degrees of freedom of the knee can be measured directly with high accuracy, unaffected by motions of soft tissue relative to the joint.

The results from the human studies are of great interest for several reasons. First, it appears that the surgical handling of the PCL can have a dramatic effect on the resulting kinematics of the PCL retaining knee. This finding is contrary to the commonly advanced viewpoint that surgically recessing the PCL has little effect on its mechanical function. Second, sliding was the dominant contact condition between the components in most knees, and all knees exhibited some sliding over the range of motion. Blunn et al. have shown that cyclic sliding is the dominant mechanism for polyethylene wear in knee replacements, particularly in the relatively non-conforming designs evaluated for this study. Third, condylar contact was confined entirely to the posterior half of the tibial plateau in all knee designs. This is due, at least in part, to the absence of the anterior cruciate ligament (ACL) , and may explain the variable function of the PCL observed in the PCL retaining knees. Furthermore, numerous recent studies have reported severe posterior wear in retrieved tibial inserts. The kinematic data confirm that posterior contact is occurring throughout the range of motion, and that in cases where the PCL is apparently under-tensioned, the most posterior contact is occurring during full weight-bearing knee extension.

This fluoroscopic measurement technique appears to be well suited for performing accurate measurements of knee replacement motions *in vivo*. The preliminary human studies data indicate that accurate kinematic information will elucidate the function of implanted knee replacements, which may ultimately lead to better, longer lasting clinical results.

REFERENCES

Blunn, G.W. et al. C.O.R.R., 273, 253-260, 1991.
Wallace, T.P. et al. IEEE Trans. P.A.M.I.,2:6, 583-588, 1980.

ACKNOWLEDGMENTS

The authors wish to acknowledge the support of The Biomotion Foundation and the Good Samaritan Foundation.

MOMENT ABOUT THE LOWER LEG DURING GAIT OF CHILDREN WITH DOWN SYNDROME: THE EFFECT OF FOOT ORTHOSES

S. Bhimji[*], M. P. Besser[*#], L. Selby-Silverstein[*#], H. Hillstrom[*#ψ⊕], W. Freedman[*]
[*] Drexel University, Philadelphia, PA 19104
[#] Thomas Jefferson University, Philadelphia, PA 19107
[ψ] Pennsylvania College of Podiatric Medicine, Philadelphia, PA 19107
[⊕] University of Pennsylvania, Philadelphia, PA 19104

INTRODUCTION

A method to calculate the moment about the long axis of the lower leg during gait has been formulated. Typically, children develop approximately twenty three degrees of lateral tibiofibular torsion by puberty.[1] Some children, such as those with Down Syndrome (DS), however, do not develop this torsion. As it is difficult to predict whether a child will develop enough lateral tibiofibular torsion for normal gait, clinicians may disagree as to whether or not to treat these children. According to Wolff's law, bone remodels in the direction of the maximum time averaged stress.[2] These physical forces have been described to be from muscular pull. We postulate that external moments produced during gait play a role in the development of tibiofibular torsion. Therefore, calculating the moment about the lower leg during gait may be a tool which could be used by clinicians to help predict which children will and which will not develop the correct amount of tibiofibular torsion.

REVIEW AND THEORY

The tibiofibular moment was calculated by separating the foot and shank into two separate segments. Each segment was then labeled with all the external forces and moments acting on it. See figures 1a and 1b for the free body diagrams of the foot and shank, respectively.

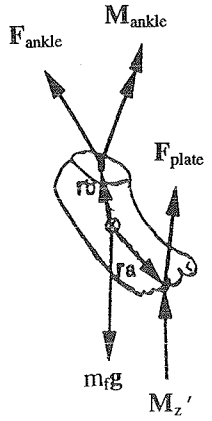

Figure 1a - Free Body Diagram of the Foot

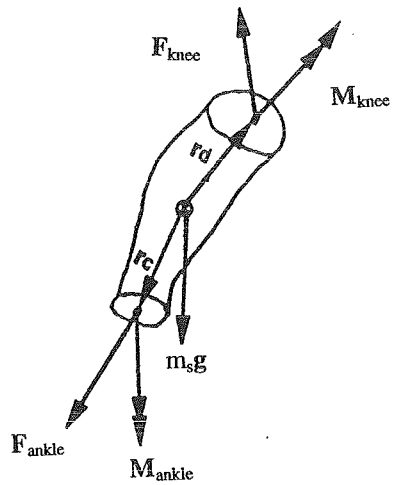

Figure 1b - Free Body Diagram of the Shank

Free body diagram of the foot

The free body diagram of the foot includes the weight of the foot ($m_f g$) originating at its center of gravity (CG), the ground reaction force vector ($\mathbf{F}_{plate}$) originating at the center of pressure, the forces acting at the ankle ($\mathbf{F}_{ankle}$), the moments acting at the ankle ($\mathbf{M}_{ankle}$), and the free moment ($\mathbf{M}_z'$). Summing the moments about the CG of the foot yields the following equation:

$$\Sigma M^{CG} = I_f \times \alpha_f \quad (1)$$

$$M_{ankle} + M_z' + (r_a \times F_{plate}) + (r_b \times F_{ankle}) = I_f \times \alpha_f \quad (2)$$

where I_f is the moment of inertia of the foot; α_f is the angular acceleration of the foot; r_a is a position vector from the CG of the foot to the center of pressure; and r_b is a position vector from the CG of the foot to the center of the transmalleolar axis. Solving equation (2) for the moments acting about the ankle yields:

$$M_{ankle} = I_f \times \alpha_f - M_z' - (r_a \times F_{plate}) - (r_b \times F_{ankle}) \quad (3)$$

F_{ankle} can be found by applying Newton's second law:

$$F_{ankle} = m_f (a - g) - F_{plate} \quad (4)$$

where **a** is the acceleration of the foot.

Free body diagram of the shank

The free body diagram of the shank includes the weight of the shank ($m_s g$) originating from its CG, the forces and moments acting at the ankle ($\mathbf{F}_{ankle}$ and $\mathbf{M}_{ankle}$), and the forces and moments acting at the knee ($\mathbf{F}_{knee}$ and $\mathbf{M}_{knee}$). Summing the moments about CG of the shank yields the following equations:

$$\Sigma M^{CG} = I_s \times \alpha_s \quad (5)$$

$$M_{knee} - M_{ankle} - (r_c \times F_{ankle}) + (r_d \times F_{knee}) = I_s \times \alpha_s \quad (6)$$

where $\mathbf{I}_S$ is the moment of inertia of the shank; α_S is the angular acceleration of the shank; $\mathbf{r}_C$ is a position vector from the CG of the shank to the center of the transmalleolar axis; and $\mathbf{r}_D$ is a position vector from the CG of the shank to the knee. Solving equation (6) for the moment about the knee yields:

$$\mathbf{M}_{knee} = \mathbf{I}_S \times \alpha_S + \mathbf{M}_{ankle} + (\mathbf{r}_C \times \mathbf{F}_{ankle}) - (\mathbf{r}_D \times \mathbf{F}_{knee}) \quad (7)$$

Moment about the Lower Leg

The moment about the lower leg is equal to the dot product of the moment at the knee with a unit vector in the tibial direction:

$$\mathbf{M}_{tibia} = \mathbf{M}_{knee} \bullet \mathbf{u}_{tibia} \quad (8)$$

where $\mathbf{M}_{tibia}$ is the moment around the lower leg and $\mathbf{u}_{tibia}$ is a unit vector in the tibial direction. Substituting equations (3) and (7) into equation (8) yields the following:

$$\mathbf{M}_{tibia} = \mathbf{I}_S \times \alpha_S \bullet \mathbf{u}_{tibia} + \mathbf{I}_f \times \alpha_f \bullet \mathbf{u}_{tibia} - \mathbf{M}_Z' \bullet \mathbf{u}_{tibia} - (\mathbf{r}_a \times \mathbf{F}_{plate}) \bullet \mathbf{u}_{tibia} - (\mathbf{r}_b \times \mathbf{F}_{ankle}) \bullet \mathbf{u}_{tibia} + (\mathbf{r}_C \times \mathbf{F}_{ankle}) \bullet \mathbf{u}_{tibia} - (\mathbf{r}_D \times \mathbf{F}_{knee}) \bullet \mathbf{u}_{tibia} \quad (9)$$

The following assumptions have been made to simplify equation (9):

- $\mathbf{I}_S \times \alpha_S \bullet \mathbf{u}_{tibia} = 0$, assuming that $\mathbf{I}_S$ is small compared to that of other segments in children.
- $\mathbf{I}_f \times \alpha_f \bullet \mathbf{u}_{tibia} = 0$, assuming that $\mathbf{I}_f$ is small compared to that of other segments in children.
- $(\mathbf{r}_C \times \mathbf{F}_{ankle}) \bullet \mathbf{u}_{tibia} = (\mathbf{r}_C \times \mathbf{u}_{tibia}) \bullet \mathbf{F}_{ankle} = 0$, assuming $\mathbf{u}_{tibia}$ and $\mathbf{r}_C$ are approximately parallel to each other.
- $(\mathbf{r}_D \times \mathbf{F}_{knee}) \bullet \mathbf{u}_{tibia} = (\mathbf{r}_D \times \mathbf{u}_{tibia}) \bullet \mathbf{F}_{knee} = 0$, assuming $\mathbf{u}_{tibia}$ and $\mathbf{r}_D$ are approximately parallel to each other.
- $\mathbf{F}_{ankle} = -\mathbf{F}_{plate}$, assuming $m_f(\mathbf{a}-\mathbf{g})$ is small in comparison to $\mathbf{F}_{ankle}$ and $\mathbf{F}_{plate}$.

Thus, equation (9) can be reduced to

$$\mathbf{M}_{tibia} = (-\mathbf{M}_Z' - (\mathbf{r}_e \times \mathbf{F}_{plate})) \bullet \mathbf{u}_{tibia} \quad (10)$$

where $\mathbf{r}_e = (\mathbf{r}_a - \mathbf{r}_b)$. Equation (10) is the final solution for the moment about the lower leg.

The purpose of this research is to determine the effect of wearing neutral position foot orthoses (NPFOs) on the tibiofibular moment during gait of children with DS. The hypothesis is as follows: If NPFOs, by modifying foot alignment, modify the lever arm between the ground reaction force vector and the long axis of the tibia and fibula during gait, then NPFOs will also modify the moment about the tibia and fibula.

PROCEDURES

Thirteen 3-6 year old children with DS were evaluated during comfortable cadence locomotion using kinetics and kinematics. Data was collected across three conditions for each subject: in shoes alone, in NPFOs after a 1 week wearing period, and in NPFOs after a 6-8 week wearing period. Kinematic data was collected at 60 Hz using the Podiatric Telefactor Motion Analysis System, and kinetic data was collected from Kistler force plates at 200 Hz using a PDP 11/24 minicomputer. Velocity data was also collected from a tachometer at 200 Hz.

RESULTS

A typical tibiofibular moment curve has an external moment followed by an internal moment with the zero crossing between 30% and 40% of stance (figure 2). Using a repeated measures ANCOVA with velocity as the covariate, the peak external moment amplitude was significantly different for children with DS before and after wearing orthoses.

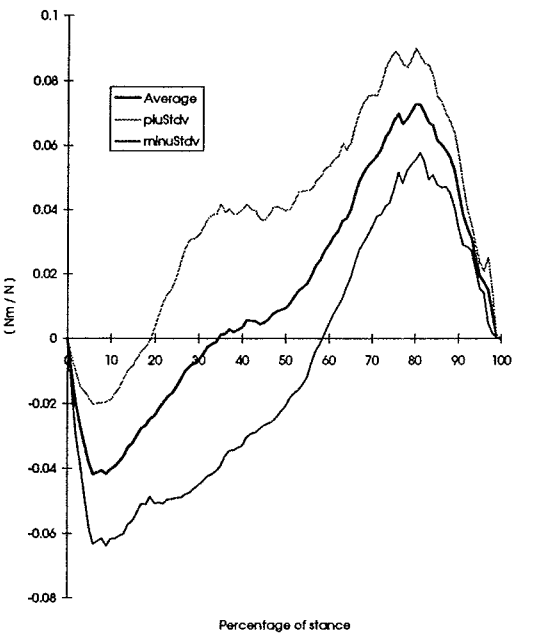

Figure 2 - Typical tibiofibular moment (normalized by BW) from a child without disability, n=3

DISCUSSION

Traditionally in gait analysis, moments are calculated about joint axes. We have demonstrated a purpose and method for quantifying moment about the long axis of the lower leg. Because young children's bones are malleable, they are probably affected by this torsional moment. Our results show that the hypothesis is accepted for the peak external tibiofibular moment.

REFERENCES

1. Yagi T. *Clin.Orthop.*, 213: 117-182, 1986.
2. Fung YC. *Biomechanics: Motion, Flow Stress and Growth.* 1990.
3. Vaughan CL, et al. *Dynamics of Human Gait.* 1992.

ACKNOWLEDGEMENTS

American Podiatric Medical Association for funding this project

THE EFFECT OF FEMORAL COLLAR ON SURFACE STRAINS IN THE PROXIMAL FEMUR AFTER CEMENTED HIP ARTHROPLASTY

V.L. Giddings[1,2], M.C.H. van der Meulen[1,2,3], S.B. Goodman[3], G.S. Beaupré[1,2,3]
[1]VA Medical Center, RR&D, Palo Alto, CA 94304
Stanford University, [2]Biomech. Eng. Prog., [3]Div. Ortho. Surg., Stanford, CA 94305

INTRODUCTION

The effect of a collar in cemented hip replacements has long been debated and is still a controversial issue [1,2]. Proponents of collared designs believe that the collar will transfer the applied load directly to the proximal calcar region, thereby loading the femur more physiologically [1]. Critics argue that the beneficial effects of the collar are never realized in practice, since the ability of a collar to transfer load directly to the bone relies on the difficult task of achieving and maintaining calcar collar contact [2,3]. Additionally, critics contend that the collar will neither increase the femoral loading to the degree necessary to maintain bone stock nor will a collar load the bone in a truly "physiological" manner [2].

While experimental and analytical studies suggest that the collar does increase the load transferred to the proximal femur as compared to a collarless implant [3,4], it is still unclear whether the results of these studies have clinical applicability. Oh and Harris [4] performed a strain gage experiment that demonstrated increased load transfer with the use of a collared implant; however, the implants they used had fundamental differences in addition to collar type. The specific design variable of a collar was not isolated and therefore it is unclear whether differences were a result of other design variations. Crowinshield *et al.* [3] conducted a finite element analysis that demonstrated an increase in femoral loading for a collared implant; however, assumptions made to construct the model, in particular the ideal representation of interface conditions, leave the question of whether a collar will actually increase the femoral loading in a clinical setting as yet unanswered.

The effect of an implant collar was evaluated by measuring the femoral surface strains for two implants that were identical except for the presence of a collar on one of the implants. Preliminary experimental and finite element analyses indicate that in a *non-cemented* model, the conically shaped collar used for this study could provide adequate mechanical stimulus to maintain proximal bone by generating hoop stresses in the femur [3,4]. The goal of this study was to explore the effect of a collar in a *cemented* model.

MATERIALS AND METHODS

Two prosthesis designs, one with a conically shaped collar and the other with no collar (otherwise they were identical), were manufactured for this study (Figure 1). Eight composite femora (Pacific Research Labs, Vashon, WA) were instrumented with strain gages (Micro-Measurements, Raleigh, NC). A total of six strain gages were used: 3 three-element

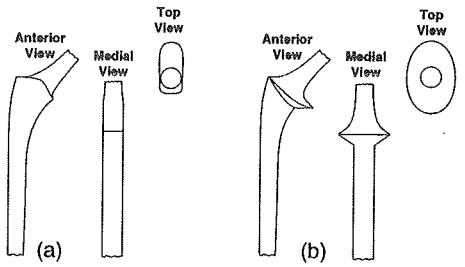

Figure 1: Femoral Implant Designs: (a) Collarless and (b) Conical Collar

stacked rosettes were applied on the anterior, medial, and posterior aspects 5 mm distal to the resection line; one three-element stacked rosette was mounted on the medial aspect 25 mm distal; and 2 two-element stacked rosettes were applied on the medial aspect at 85 and 145 mm distal. One of the two most distal gages was located proximal and the other distal to the implant tip.

The load was applied to the femora by a servo-hydraulic testing machine (MTS, Minneapolis, MN) using a lever mechanism that applied a load to the femoral head and to the greater trochanter (Figure 2). The loading set-up simulated single limb stance phase of gait by applying the load at 20° from the vertical. The load transmitted to the trochanter was monitored with a miniature load cell. A ramp load from 0 to 2000 Newtons was applied at a frequency of 1 Hz to precondition the system for four cycles; data were taken on the fifth cycle. Strain gage data were sampled continuously throughout the test, as were the abductor and MTS loads. The femora were tested intact and then prepared for implantation using standard surgical procedures and instrumentation. The femoral canal was prepared using precision reamers to match the proximal surface to the collar geometry prior to cementing. Four femora were implanted with the conically collared implants and four received the collarless implants. Strain gages remained in place between the intact and implant tests.

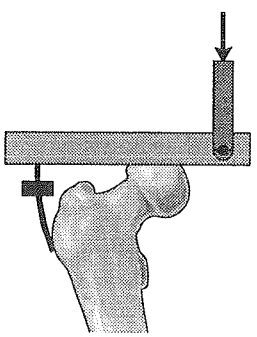

Figure 2: Load Application

Strain measurements were compared between the intact and the different implant types for a resultant head load of 2000 N (3 x bodyweight). Maximum and minimum principal strains were calculated for all three-element rosettes.

Strain energy density (SED) was calculated for all gages. SED was calculated from the biaxial gages by assuming that the gages were aligned along the principal axis.

One factor ANOVA was used to test for statistical significance ($p<0.05$) between the measured strains and the calculated principal strains and SED for all gage locations.

RESULTS

The principal strains measured at the gage locations on the anterior and posterior surface did not demonstrate much variation between the intact and two implant models. Figure 3 shows the minimum principal strains for the three-element rosettes located on the medial aspect at 5 mm and 25 mm distal to the resection line. The intact and arthroplasty groups were significantly different for both gage locations ($p<0.002$). The difference between the two implant groups was significant only for the gage located at 25 mm, with the conically collared implant producing strains of 39.0% of intact and the collarless group producing strains of 26.7% of intact. Figure 4 shows the results for SED along the medial side. All differences between the intact and arthroplasty groups were significant; however, none of the differences between the two implant groups were. The location 5 mm distal to the resection line, for both implant types, experienced 5% of the intact SED. The 25 mm distal location for the conically collared implant had an SED of 15.5% of intact, while the femur with the collarless implant had an SED of 7.5% of intact.

DISCUSSION

The two implants used in this study significantly reduced the surface strains in the proximal femur from the intact model along the medial aspect of the femur. The increase in principal strain for the conically collared implant, while being significant statistically, is probably not large enough to be clinically meaningful. SED, which is used as the basis for bone remodeling algorithms [5,6], is dramatically decreased between intact and implant groups, but demonstrates no difference between implant groups. The differences in SED at the location below the tip of the implant (145 mm) could be explained by the presence of cement in the femoral canal or by changes in femoral head offset resulting in differences in loading conditions between the intact and arthroplasty models. The significant reduction in proximal SED is clearly the result of stress shielding.

This study demonstrates that, in the case of a cemented implant, the presence of a collar does not substantially increase the proximal strain energy density in comparison with a collarless implant. Thus, from a purely mechanical perspective, we would predict no clinical benefits due to the addition of a collar in cemented hip arthroplasty.

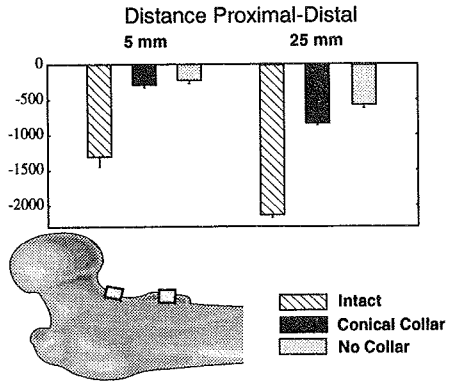

Figure 3: Minimum Principal Strain (μstrain, mean ± SEM)

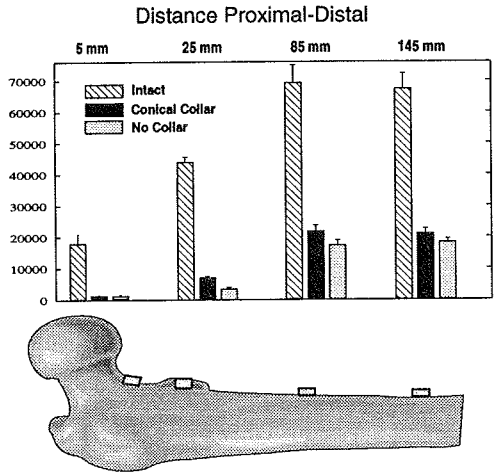

Figure 4: Strain Energy Density (J/m^3, mean ± SEM)

REFERENCES

[1] Harris (1992), *Clin. Orthop.*, 285:67-72. [2] Ling (1992), *Clin. Orthop.*, 285:73-83. [3] Crowninshield *et al.* (1981), *Clin. Orthop.*, 158:270-277. [4] Oh and Harris (1978), *J. Bone Jt. Surg.*, 60A:75-85. [3] Caler *et al.* (1990), *Trans. ORS*,15:468. [4] Mandell *et al.* (1994), *Trans. ORS*, 19:224. [5] Huiskes *et al.* (1987), *J. Biomech.*, 20:1135-1150. [6] Beaupré *et al.* (1990), *J. Orthop. Res.*, 8:651-661.

ACKNOWLEDGMENTS

We would like to thank Dennis Carter for his advice and guidance. We also thank Dave Schurman, Jay Mandell, and Jim Anderson. Funding for this project was provided by VA Merit Review Grant A652-RA and Kirschner Medical Corporation.

SELF-FIXATION CHARACTERISTICS OF A NEW SWELLING TYPE COMPOSITE MATERIAL IN BONE

A. Abusafieh[1], R. Nobilini[2,3], S.Siegler[2,3], I. Kamel[1], A. T. Berman[4], and S. Kalidindi[1]

[1]Department of Materials Engineering, Drexel University, Philadelphia, PA 19104

[2]Department of Mechanical Engineering and Mechanics, Drexel University, Philadelphia, PA 19104

[3]Hahnemann/Drexel Biomechanics Laboratory, Philadelphia, PA 19107

[4]Department of Orthopedics, Hahnemann University Hospital, Philadelphia, PA 19102

INTRODUCTION

A new swelling type composite material system capable of self-fixation to bone has been recently developed for bioimplant applications (Greenberg and Kamel, 1978; Sharda and Kamel, 1993; Ahmad and Kalidindi, 1994). Self-fixation is achieved after implantation by swelling of the implant material which results in an expansion-fit mechanism. Swelling of the implant material is accomplished by absorption of surrounding body fluids. The proposed material system for the swelling type implant applications comprises of a copolymer matrix reinforced by three-dimensionally braided graphite fibers. The copolymer matrix is designed to be slightly hydrophilic and provides the swelling characteristics to the material while the 3-D braided graphite fibers provide excellent mechanical properties which include modulus, strength, fracture toughness, fatigue strength, and impact resistance.

A detailed experimental study was conducted to investigate the swelling and self-fixation characteristics in bone of this new class of composites. The main variable in the study was the composition of the matrix which governs the swelling behavior of the material. The major goal of the study was to optimize the composition of the matrix to yield the best fixation characteristics in bone. The swelling characteristics studied included saturation swelling strains, diffusion coefficients, degree of degradation of mechanical properties with swelling, and the effect of pressure on swelling. The self-fixation characteristics of the proposed material in bone were evaluated through a series of push-out tests.

REVIEW AND THEORY

The idea of swelling type implants was originally introduced by Greenberg and Kamel (1978). Sharda and Kamel (1993) have recently developed a textile composite material system comprising of Polyacrylic Acid and graphite fibers. Although, this material system has good mechanical properties in the dry state, it showed a substantial loss in modulus and strength at saturation, making it unsuitable for the swelling type implants. A comprehensive study of the stress fields and interfacial micromotions in the swelling type implant-bone system was recently conducted by Ahmad and Kalidindi (1994) using finite element techniques. Their study led to the development of a new matrix material, which swells in a controlled manner and at the same time limits the degradation of mechanical properties of the composite to fairly low values. The matrix proposed by Ahmad and Kalidindi (1994) is a copolymer comprised of a hydrophobic and a hydrophilic polymer. Swelling behavior can be controlled by varying the ratio of the copolymer components. The major purpose of this study is to experimentally determine the effect of the matrix composition on the swelling and fixation characteristics in bone of the newly proposed composite material.

PROCEDURES

Cylindrical samples of the material (both matrix material and the composite) were machined and immersed in saline solution for extended periods of time, while monitoring weight and volume changes in the samples due to absorption of fluids.

Simple compression tests were performed on different sets of samples in both dry and saturated conditions. Elastic moduli and strengths of the material were estimated from these tests.

Two types of pushout tests were performed. In the first set of tests cylindrical coupons of the material were slip fitted into cylindrical rings machined out of cortical bovine bone. These samples were placed in saline solution and the implant material was allowed to swell. Push-out tests were conducted at various intervals on these samples covering a period of up to two months of exposure to saline solution. The maximum load required for pushing the implant out of the bone-implant assembly was recorded and the frictional shear strength of the bone-implant interface was computed. In the second set of tests cylindrical samples of the implant material were implanted into holes drilled in the midshaft region of the cortical wall of swine femurs and immersed in saline solution for three days. Push-out tests were once again conducted (see Figure 1) on these samples. The bones were then sectioned to measure the bone thickness at the sample site and the frictional shear strength of the interface was computed.

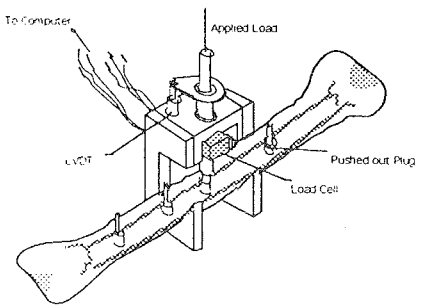

Figure 1. Setup for pushout test on swine femurs.

RESULTS AND DISCUSSION

Although a number of matrix compositions (i.e. the ratio of hydrophobic to hydrophilic components of the copolymer) were evaluated in this study, for brevity, we report here the results of only two compositions. These will be identified as 'ratio1' (80:20)and 'ratio2' (60:40) in the following discussion.

Figure 2 shows plots of volumetric swelling strain in the copolymer matrices as a function of time. It is seen that the swelling strain in the material reaches an asymptotic value at saturation, and that this value is strongly influenced by the matrix composition. Typical stress-strain plots on dry and saturated matrix samples are presented in Figure 3 and indicate that there is a significant loss of modulus and strength with swelling. This degradation in mechanical strength was observed to be strongly dependent on the degree of swelling in the matrix.

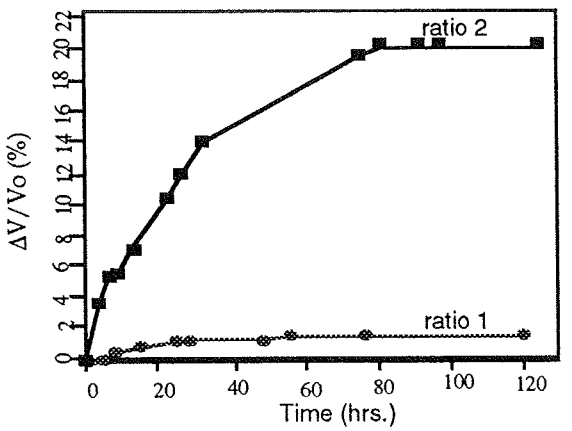

Figure 2. Swelling behavior of two matrix ratios.

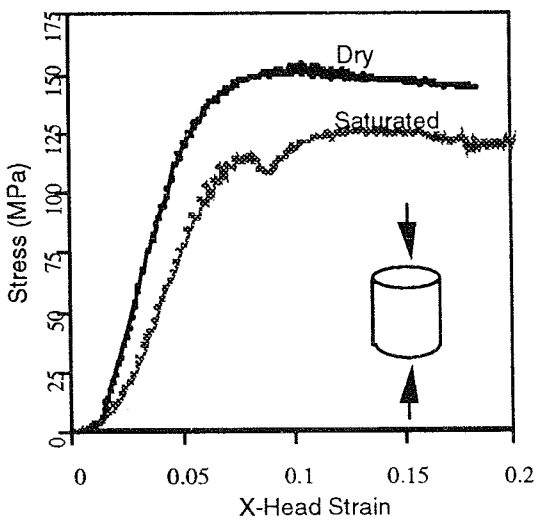

Figure 3. Stress Strain curves for identical dry and saturated copolymer samples.

The load-displacement curves obtained from push-out tests are shown in Figures 4 and 5. The data shown in Figure 4 corresponds to a single matrix composition and indicates that the fixation improves with exposure time. The data shown in Figure 5 indicates that better fixation is obtained with ratio 1 compared to ratio 2, in spite of the fact that ratio 2 actually has a higher swelling strain compared to ratio 1 (see Figure 2). This can be explained by the higher degradation associated with ratio 2. Similar data was obtained for a number of other compositions and will be presented.

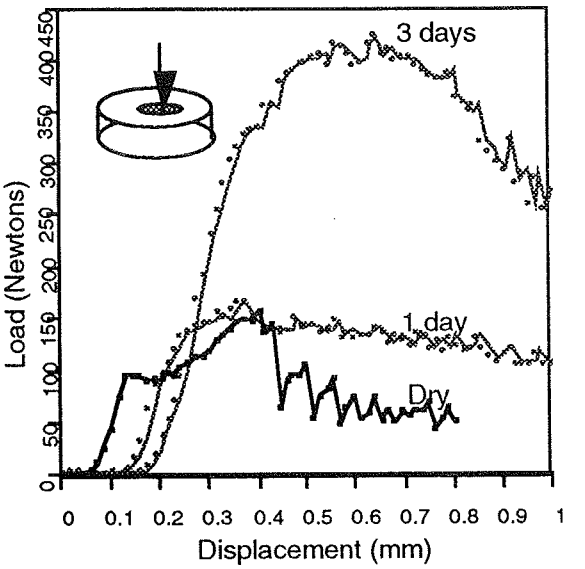

Figure 4. Pushout Load Displacement curves at different swelling rates.

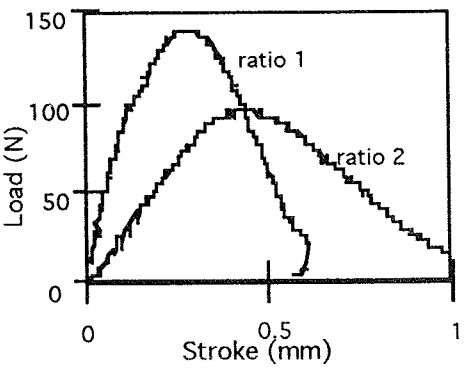

Max Shear Stress (ratio 1) = 8.03 MPa
Max Shear Stress (ratio 2) = 2.29 MPa

Figure 5. Typical data for pushout tests on swine femurs.

REFERENCES

Greenberg and Kamel (1978), Ph.D. Thesis, Drexel University.

Sharda and Kamel (1993), Ph.D. Thesis, Drexel University.

Ahmad and Kalidindi (1994), submitted to J. Biomechanics.

ACKNOWLEDGMENTS

The authors gratefully acknowledge partial support for this work through a grant from Whitaker Foundation.

A NUMERICAL INVESTIGATION OF THE MECHANICS OF SWELLING-TYPE INTRAMEDULLARY HIP IMPLANTS

Parvez Ahmad and Surya R. Kalidindi
Department of Materials Engineering
Drexel University, Philadelphia, Pa 19104.

INTRODUCTION

A novel design for intramedullary hip implants that attain self-fixation by an expansion-fit mechanism due to controlled swelling of the implant (by absorption of body fluids) was examined in detail using a finite element model of the femur-implant system. Some of the potential advantages of this technique over traditional techniques include enhanced fixation, lower relative micromotions, bone calcification, improved bony ingrowth, and elimination of acrylic cement. The finite element model created in this study incorporated (i) the complex three dimensional geometry of the femur and implant, (ii) the anisotropic elastic properties of bone and implant materials and the changes in orientation of the principal axes of anisotropy along the length of the bone-implant system, (iii) a layer of cancellous bone between the implant and cortical bone in the proximal-medial femoral region, and (iv) frictional sliding between the bone and implant. The model was used to study quantitatively the influence of various material and geometric design variables in the bone-swelling type implant system. Based on the results of the finite element analyses, ideal ranges of values for the design variables were established to produce optimal stress patterns and interfacial micromotions. It was observed that swelling of the implant results in enhanced fixation characteristics and greatly reduced interfacial micromotions.

REVIEW AND THEORY

A new self-fixation technique using the concept of a swelling-type implant was introduced by Greenberg and Kamel (1978) in an attempt to provide a viable alternative to both the traditional cemented and non-cemented techniques. This implant swells in a controlled manner by absorption of body fluids and achieves fixation at the implant-bone interface by an expansion-fit mechanism. Controlled swelling of the implant produces a compressive pressure on the entire bone-implant interface which is expected to enhance frictional resistance to sliding between bone and implant. Therefore, enhanced fixation can be obtained in a short time when compared against conventional cemented and non-cemented implants. The better fixation would, in turn, result in lower micromotions and reduce disruption in bone ingrowth. Additionally, a tensile hoop stress is introduced in the femur due to the swelling implant, and this stress mitigates bone resorption. In fact, Greenberg *et al.* (1978) have shown that the tensile hoop stress in bone promotes bone densification, thereby providing excellent long term fixation characteristics.

Although research on the swelling type implants has begun circa 1978 (Greenberg and Kamel, 1978; Greenberg *et al.*, 1978), progress leading to design and commercial utilization of this novel concept has been greatly hampered by lack of quantitative understanding of the influence of swelling of the implant on the resulting stresses and relative micromotions in the bone-implant system. Such an understanding is very important to establish a set of optimal hygro-mechanical properties (such as saturation swelling strain, anisotropic elastic moduli and strengths, etc.) for the material development and evaluation studies. For example, it was not clear what should be the magnitude of swelling strains in these implants. Kamel and co-workers have, in recent years, experimented on a textile composite comprising of three-dimensionally braided carbon fibers in a Polyacrylic Acid matrix (Sharda and Kamel, 1993) which typically swells upto about 10% by volume when left in water for a long time (under free swelling conditions). However, an experimental investigation of the mechanical properties of these composites in dry and saturated conditions revealed substantial degradation of mechanical properties (i.e. loss in modulus and strength) in the composite after swelling, making the material system unsuitable for implant applications. Since, swelling of any material by absorption of water is likely to be accompanied by degradation of mechanical properties, it follows that the only viable approach to realization of the novel implants described here is to limit the swelling strain in the material to a sufficiently low value such that the degradation is minimal while achieving the necessary fixation. The magnitude of swelling strains necessary for good fixation characteristics and the range of elastic moduli and strengths required from the material in its saturation state need to be established before further progress can be made in the development of these implants.

The goals of the present study are to (i) develop an understanding of the mechanism of load transfer in bone-swelling type hip implant system in order to critically evaluate the advantages and disadvantages of the swelling type implants over the traditional implants, and (ii) to establish a range of optimal hygro-mechanical properties that will serve as a target for material development and evaluation studies. A finite element model of the bone-implant system was developed for this purpose, and is described next.

PROCEDURES

A three dimensional finite element mesh was generated using the commercial software COSMOS (COSMOS, 1992). The mesh is shown in Figure 1 with longitudinal and transverse sectional views, and is based on the detailed information on the geometry of a human femur reported by Huiskes *et al.* (1981). Note that we have only modeled one half of the bone-implant system (plane dividing the system into two halves happens to be a plane of mirror symmetry for geometry and loading conditions used

in this study) in order to reduce the memory and CPU requirements.

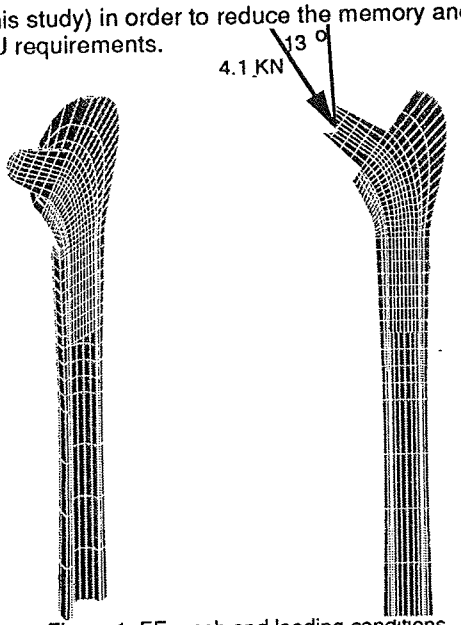

Figure 1. FE mesh and loading conditions.

The generated finite element mesh was transported to the commercial finite element software ABAQUS (1994) and a stress analysis was performed using this mesh. The finite element model shown in Figure 1 has 1440 solid, three-dimensional, continuum elements (C3D8 elements; ABAQUS, 1994), and 192 two dimensional interface elements (INTER4 elements; ABAQUS, 1994). The interface elements permit frictional sliding of the implant with respect to the bone and provide an estimate of the relative micromotions between the bone and implant at various points on the interface.

The bone and implant were assumed to have orthotropic material properties. These properties are best described with respect to a local reference frame aligned with the radial, circumferential, and axial (corresponds to the axis of the intramedullary canal) directions. A user subroutine (ABAQUS, 1994) was written to describe the local orientation of the axes of orthotropy in each of the elements with respect to the global fixed orientation.

A volumetric swelling strain was imposed on the elements representing the implant in our model. This swelling strain was taken to be orthotropic and the axis of orthotropy was chosen to be same as the one described for the elastic properties of the implant and bone. The swelling in the implant and the load are applied sequentially, i.e., the implant is allowed to swell first and then followed by the application of load. The load applied is shown in Figure 1. The loading conditions and properties of the bone have been kept fixed in all of the analyses, however, the hygro-elastic properties of the implant were varied.

RESULTS AND DISCUSSION

A number of finite element analyses were performed using the model described here and the parametric influence of the various design parameters in the implant-femur system were investigated. Design parameters studied included the swelling strain in the implant, the implant elastic properties, the anisotropy of swelling strain, and stem length. Typical results of micromotions obtained from the finite element analyses are shown in Figure 2. Based on the results for the stress fields in the bone-implant system and the micromotions at the bone-implant interface, an ideal range of values was set for all of the important design parameters. This range of values is summarized in Table 1.

REFERENCES

Greenberg, A.R., Kamel, I., Dubin, S., and Miller, *J. Biomed. Mat. Res.* **12**, 929-933.

Huiskes, R., Janssen, J.D., and Slooff, T.J. (1981), *Mechanical Properties of Bone*, ASME, New York, pp. 211, (1981).

Sharda, A.N., (1993) Ph.D. Thesis, Biomedical Engineering and Science Institute, Advisor: I. Kamel.

Variable	Appropriate Range
Swelling Strains	1-2%
Anisotropic Swelling	7:7:1
Orthotropic Modulli	E11=25-35 E22=25-35 E33=45-55 GPa
Stem Length	No major Effects

Table 1. Summary of results from FEM analyses

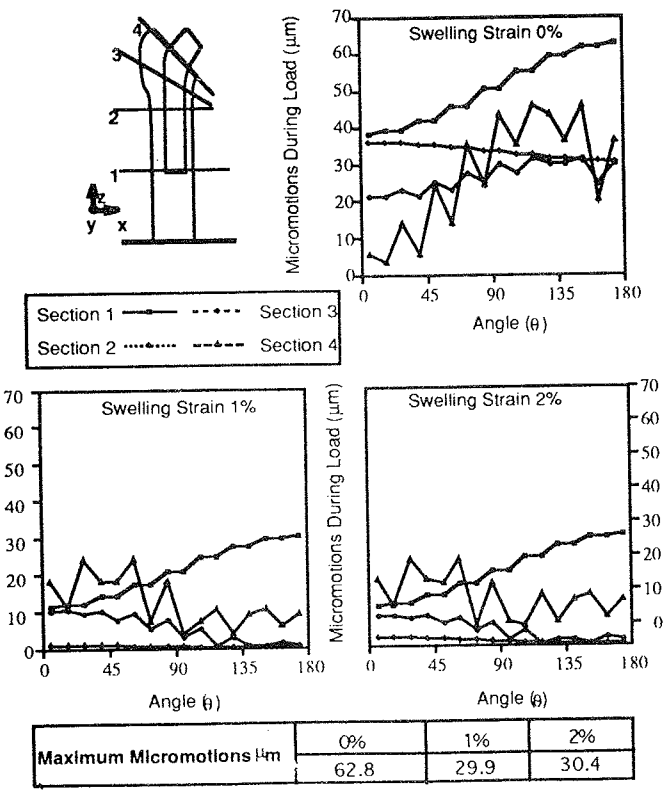

Figure 2. Effect of swelling on interfacial micromotions.

FINITE ELEMENT MODELING OF THE FOREFOOT WITH ACCOMMODATIVE FOOTWEAR ORTHOSES

D. Lemmon, T-Y. Shiang, J. Ulbrecht, A. Hashmi, T. George, P. Cavanagh
Center for Locomotion Studies, The Pennsylvania State University, University Park, PA 16802

INTRODUCTION

Accommodative in-shoe orthoses have been made for many years to alleviate the problems caused by elevated plantar pressure in diabetic neuropathy, principally to prevent plantar ulceration. To date, no biomechanical analysis has been performed to evaluate the effectiveness of current practices. In the present study, two-dimensional, nonlinear finite element (FE) models are used to study the effectiveness of elastomeric foam in-shoe orthoses in reducing peak plantar pressure.

REVIEW AND THEORY

Ulceration in plantar soft tissue has been identified as a major problem in patients with peripheral neuropathy, particularly those suffering from diabetes mellitus. Elevated plantar pressure has been identified as a primary risk factor in ulceration. Current practice is to apply a footwear intervention at the foot-shoe interface to reduce plantar pressure levels. The present study proposes finite element models which can be used in conjunction with clinical measurements to gain insight into the effectiveness of a given orthosis. Finite element models have been successfully employed to simulate the behavior of soft tissues (Oomens et al., 1987) and their interactions with orthotic devices (Vannah and Childress, 1993). This study employs finite element modeling to study the effectiveness of accommodative footwear orthoses in reducing peak plantar pressure.

PROCEDURES

The models in this study are sagittal plane sections of the second metatarsal bone with dorsal and plantar soft tissue, and a section of an accommodative footwear orthosis. Each model extends from the proximal end of the second metatarsal to the joint space at the metatarso-phalangeal joint. The models contain between 1053 and 2025 nodes, and between 880 and 1840 bilinear continuum elements. The relatively stiff bone material is assigned linear elastic material properties with published values of Young's modulus and Poisson's ratio for bone. The much less stiff and highly deformable soft tissue is given hyperelastic material properties with a second order, polynomial strain energy density function. Constants for the strain energy density function are obtained from experimental measurements and verified using simple finite element models. The interface between foot and footwear is modeled by slide line elements. Footwear orthoses (in this case, foam insoles) are represented by hyperelastic, elastomeric foam material using a fourth order strain energy density function. Constants for the strain energy density function for the foam material have been obtained from compression tests of core samples which have been verified by finite element models. Vertical loads are applied to the metatarsal bone.

A pilot validation study was conducted using insoles of varying thicknesses of elastomeric foam. Six different insole thicknesses were modeled for each of the two tissue conditions (normal tissue and reduced tissue), totaling twelve analyses. In addition, clinical measurements have been performed on two subjects (one with normal tissue, one with reduced tissue), and using insoles identical to those of the finite element models. These measurements were taken during normal gait using in-shoe plantar pressure devices (PEDAR, Emed Systems Gmbh), placed at the foot-footwear interface.

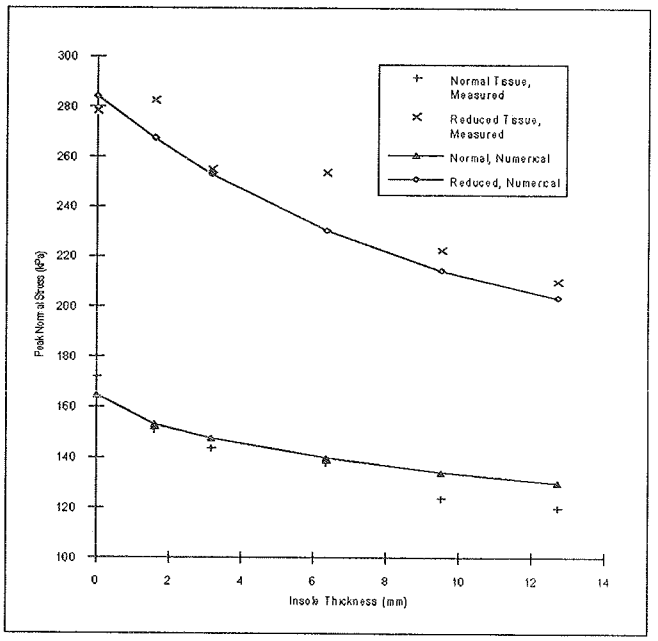

Figure 1: Peak normal stress vs. insole thickness, normal and reduced tissue. Contains both analytical and experimental data.

RESULTS AND DISCUSSION

The peak plantar pressure values predicted by the finite element models compare well with clinically measured values. Figure 1 shows peak normal stress comparisons between the measured and analytical results for both the normal and reduced tissue conditions. Results suggest that the finite element method is a useful tool for studying the relative merits and mechanical characteristics of footwear orthoses as they react with plantar tissue.

REFERENCES

Oomens, C.W.J., Van Campen, D.H., Grootenboer, H.J., *J. Biomechanics, 20(10): 923-935, 1987.*
Vannah, W.M., Childress, D.S., *J. Rehabilitation Research and Development, 30(2): 205-209, 1993.*

ACKNOWLEDGMENT

This research was funded in part under NIH DK-5RO1DK4292.

COMPARTMENTAL LOAD REDISTRIBUTION AND LIGAMENT DISTENSION IN OPENING- vs. CLOSING-WEDGE HIGH TIBIAL VALGUS OSTEOTOMY

T. Aoki*, W.S. Foels#, T.D. Brown+#, J.L. Marsh+, D.S. Tearse+

Departments of +Orthopaedic Surgery and #Mechanical Engineering
University of Iowa, Iowa City IA 52242

*Department of Orthopaedic Surgery, Gifu University, Gifu City, Gifu, Japan

INTRODUCTION

Valgus osteotomy of the proximal tibia is a well accepted method for treating medial compartment osteoarthrosis of the knee. While indications in the elderly have been diminishing with increasing reliability of arthroplasty, the use of high tibial osteotomy (HTO) in conjunction with ligamentous repair procedures has been increasing in younger patient groups. Recently, several authors have advocated medial-side opening wedge procedures as an alternative to the classic lateral-side closing wedge (Coventry) procedure. While technically more difficult to perform, the potential advantages of opening-wedge HTO include avoidance of patellar tendon shortening and patella infera, preservation of proximal tibial bone stock, less intra-operative difficulty in ligament tension balancing, preservation of the proximal fibula and tib/fib joint, and greater ease of conversion to total knee arthroplasty should the need arise. Moreover, if stabilized using an external fixator capable of graded length adjustments, opening wedge HTO's can achieve very precise angular corrections, and can employ the principle of *callotasi* (as developed originally for limb lengthening) to avoid the need for bone graft. Clearly, however, a medial opening wedge involves very different local structural alterations than does a lateral closing wedge, with potentially very different distension/relaxation of major ligamentous structures (MCL, LCL, ACL, patellar tendon, posterior capsule), and different changes of articular contact stresses in the respective tibio-femoral and retro-patellar compartments. Moreover, such structural alterations might well be different depending on whether the medial wedge is opened above or below the level of the tibial tubercle. To systematically investigate these important mechanical considerations, we developed a laboratory cadaver model of opening- vs. closing-wedge high tibial osteotomy.

MATERIALS AND METHOD

Six fresh-frozen cadaver legs free of musculoskeletal abnormality were disarticulated at the hip, and then x-rayed positioned vertically in full extension with a 20-kg weight suspended from the femoral head, for conventional measurement of the mechanical vs. anatomic axes. After subsequent sectioning 20 cm above and below the joint line of the knee (with stripping of all non-periarticular soft tissues), the specimens were loaded in an MTS-based modified Huberti-Hayes apparatus, to flexion angles of 10°, 30°, and 45°. Special fixturing was developed to insure appropriate geometrical offset between the specimen and the loading axis of the test machine. Electromagnetic displacement sensors were used to monitor distensions in the MCL, LCL, ACL, patellar tendon (PT) and at the back of the capsule (BOC). PresSensor contact film, quantitated by digital image analysis, was used to measure contact stress distributions in the medial and lateral tibio-femoral compartments, and at the retropatellar surface. Specimens were tested first as-received, then with 3° and 7° supra-tubercle opening-wedge HTO (stabilized with an Orthofix device), 3° and 7° infra-tubercle opening-wedge HTO (Orthofix), and finally 3° and 7° closing-wedge HTO (plate stabilization).

RESULTS

The data showed that all three modes of HTO performed comparably in terms of achieving lateral shift of the resultant load axis. Series-averaged shifts of the centers of pressure in the medial and lateral tibio-femoral components are illustrated in Figure 1. In all instances, the 7° corrections were more effective than the 3°

corrections. Series-averaged histograms of the contact stress distributions (Fig 2) revealed consistent elevations of contact stress laterally, and reductions medially, the essential clinical goal of HTO. There were no statistically significant differences among osteotomy modes in that regard. All three modes of valgus osteotomy caused increased tensioning of the MCL at any given flexion angle, and increased relaxation of the LCL, again with consistent differences between the 3° and 7° corrections, but not between the respective wedge modes. There were no substantial mode-dependent differences in the ACL or BOC strains, but the supra-tubercle opening wedge caused additional tightening of the patellar tendon. Subjectively, we noted that varus-valgus stability was best for the infra-tubercle opening wedge procedure (and worst for the closing wedge), whereas anterior-posterior stability was best for the supra-tubercle opening wedge. Significantly, several additional specimens were ruined prior to test protocol completion due to fractures at the tibial tubercle for infra-tubercle opening-wedge cases loaded at the higher (45°) flexion angles, apparently due to lack of anterior stabilization by patellar tendon contact.

DISCUSSION

We believe that these data indicate that the medial-side opening wedge HTO does not involve any untoward effects in terms of either articular contact stress concentrations or ligament strains. Moreover, opening wedges seem to be comparable to closing wedges in terms of their ability to achieve clinically-desirable reallocation of load from the medial to the lateral compartment. While some issues of varus-valgus and anterior-posterior instability deserve further investigation, we believe that the results of the study support the use of medial-side opening-wedge procedures, both supra- and infra-tubercle, as a biomechanically reasonable alternative to lateral-side
opening wedges.

ACKNOWLEDGEMENTS

Mr. D.R. Pedersen, Mr. F.C. Barich, and Dr. M.J. Rudert lent valuable technical assistance. Financial support was provided by EBI, Inc., and Orthofix, Srl.

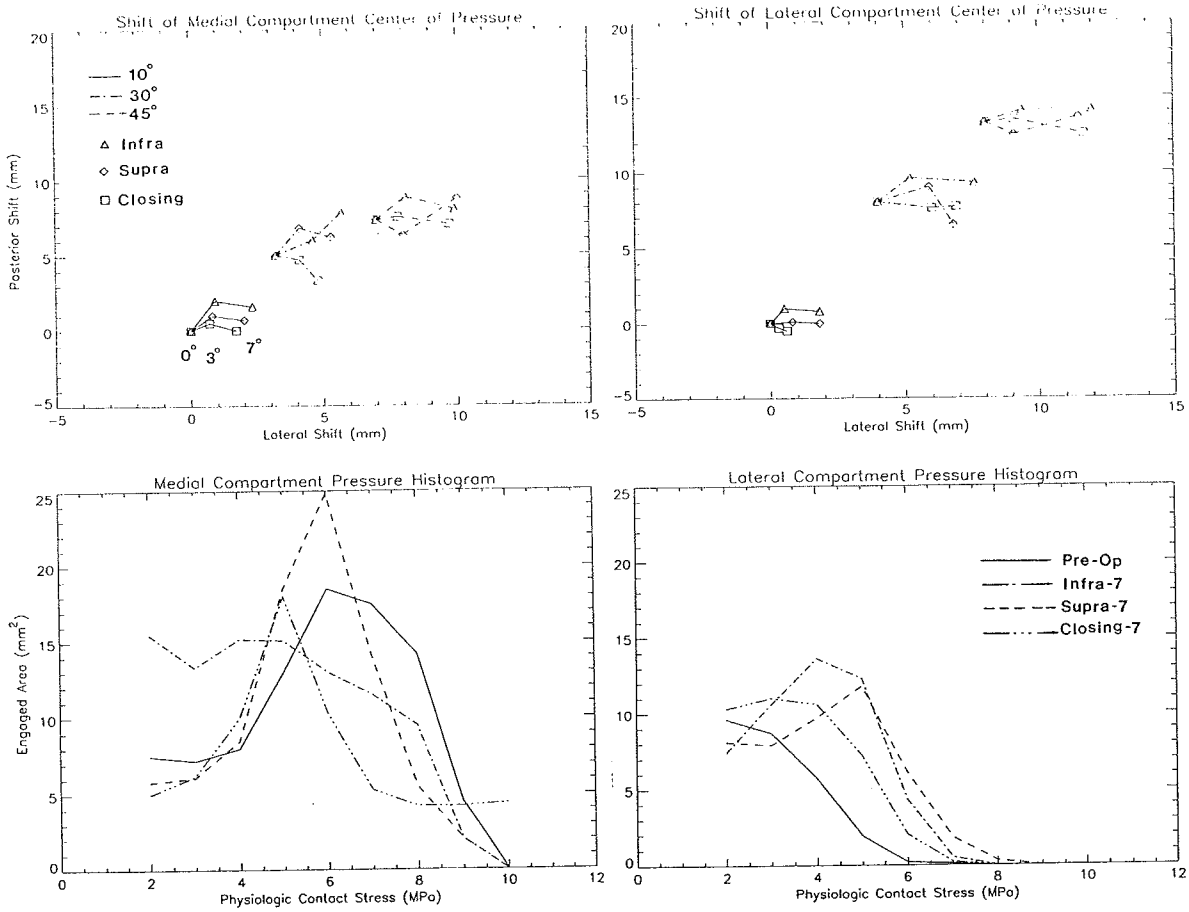

In vivo KINEMATICS OF IMPLANTED AND NONIMPLANTED KNEES DERIVED USING AN INVERSE PERSPECTIVE TECHNIQUE

R.D. KOMISTEK[1], D.A. DENNIS[1], W.A. HOFF[2]
[1]ROSE MUSCULOSKELETAL RESEARCH LABORATORY, DENVER, CO, 80220
[2]DIVISION OF ENGINEERING, COLORADO SCHOOL OF MINES, GOLDEN, CO

INTRODUCTION

After a Total Knee Arthroplasty (TKA), the knee joint undergoes a change in boundary conditions. Therefore, it is important to understand knee kinematics under *in vivo*, weightbearing conditions. Fluoroscopy has been used effectively by researchers to analyze existing TKAs during these conditions [1,2]. By developing a normal knee control, it is possible to compare kinematic results from implants with those obtained from the normal knee group. These comparisons, can be used to determine if there are certain soft-tissue parameters that are altered during surgery which can influence the knee joint, producing poor kinematic profiles. The goal of this study was to derive and compare kinematic profiles for normal knees, ACL deficient knees and TKAs for subjects performing a deep knee bend to maximum flexion.

PROCEDURES

Initially, forty subjects were studied kinematically using fluoroscopy videos. Ten subjects had normal knees, ten had ACL deficient knees, ten had a posterior cruciate retaining (PR) implant and ten had a posterior cruciate substituting (PS) implant. A surgeon control was used, where each TKA analyzed in the study was implanted by the same surgeon. The implants chosen for the study were Press Fit Condylar PR and PS designs (Johnson and Johnson Orthopedics, Raynham, Mass.). Each subject, flexing in the sagittal plane, performed successive deep knee bends for fluoroscopic surveillance. The videos were analyzed using an inverse prespective technique. Each subject's motion was captured on a VHS video and a three dimensional database determined by digitizing three discrete positions on the femur, tibia and patella. These discrete positions were chosen at full extension which was the initial leg position. As a subject flexed, three dimensional coordinates were determined for each of the nine positions relative to fixed position on the computer screen. Using Euler angles, these chosen positions were transformed into the tibia reference frame. Each subject's range of motion (ROM) was also determined using the digitized data.

RESULTS

Fluoroscopic evaluations were first conducted on the normal knees, as shown in Figure 1, to determine a normal control that could be compared to the ACL deficient knees and those implanted with TKA.

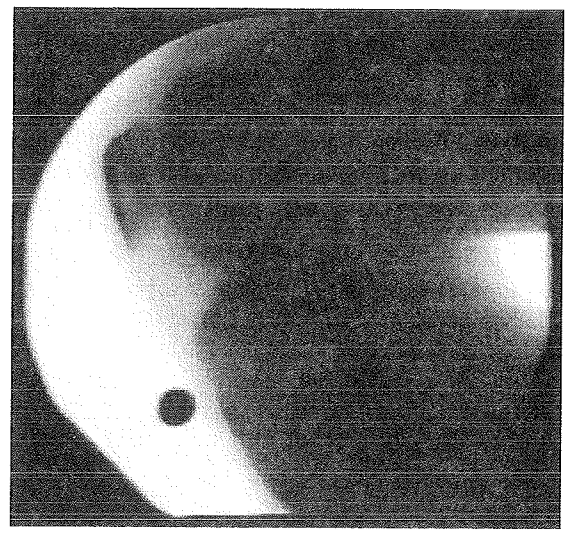

Figure 1. Fluoroscopy of the normal knee.

In Figure 2, the position of the femur on the tibia is shown for a normal, ACL deficient, PS-implanted, and PR-implanted knees. The midline of tibia in the sagittal plane is denoted as the origin position, which is 0 mm. From this midline position, the anterior direction is denoted as positive, and the posterior direction as negative. The normal, ACL deficient and PS femur contacted the tibia anterior to the midline of the sagittal plane in the tibia reference frame. At full extension, the normal knee made contact in the range of 6 to 10 mm, the ACL deficient knee in the range of 3 to 7 mm, and the PS-implanted knee 0 to 4 mm. The PR-implanted knee differed from the other knee types, such that the initial contact was posterior in the range of - 8 to -

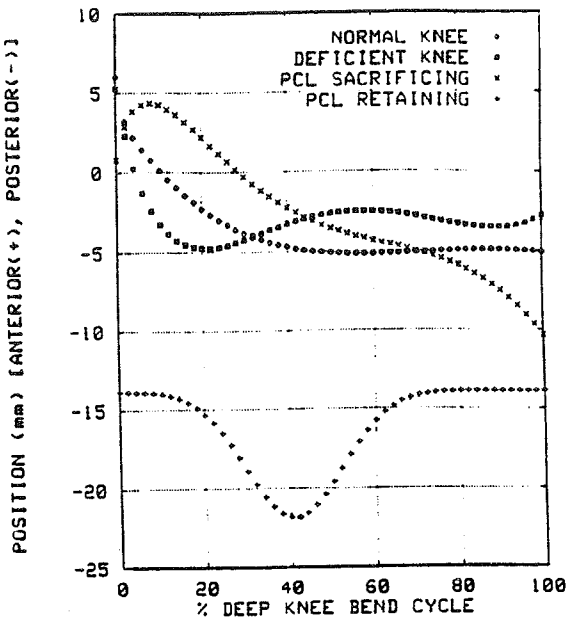

Figure 2. Kinematic profiles of the four knee types in the A/P direction.

15 mm. Table 1 shows a comparison of the position data of each knee type. In Table 1, the minimum, maximum, and median (average) positions of the femur on the tibia are shown.

Table 1
A/P Position Data of the Four Knee Types

KNEE TYPE	MIN. (mm)	MAX. (mm)	MED. (mm)	RANGE (mm)
NORMAL	-5.2	6.0	-4.9	11.2
DEFICIENT	-4.8	5.3	-3.2	10.0
PS DESIGN	-10.3	4.4	-3.6	14.7
PR DESIGN	-21.9	-13.8	-14.5	8.0

Also shown are the range, which is the amount this contact position has translated. In comparing the ROM results of the four knee types, the normal and ACL deficient knees were similar, but the PS-implanted design experienced 10% more knee flexion when compared to the PR-implanted design.

DISCUSSION

The femur of the normal knee contacts the tibia anterior to midpoint in the sagittal plane in full extension and translates in the posterior direction as the knee flexes. The femur of the ACL deficient knee also initially contacts the tibia anterior to the midpoint, but as this type of knee flexes, increased joint laxity is observed as the femur translates further posteriorly then the normal knees. The femur of the PR-implanted knee contacts the tibia posterior to the midpoint in extension. As this type of knee flexes the femur either remains posterior or translates in the anterior direction, which is, kinematically opposite of the normal knees. The femur of the PS-implanted knee contacts the tibia anterior to the midpoint at the initial position and asthe knee flexes the femur does translate posteriorly on the tibia, best simulating the normal knee kinematics.

It must be noted that the data collected from this study was from a single surgeon. The results obtained compared similarly with those results from Stiehl et.al [2] for the PS-implanted design, but were dramatically different for the PR-implanted designs. Stiehl et.al observed that the femur of the PR-implanted designs contacted the tibia posterior at full extension and slid anteriorly as the knee flexed. Their results showed a slide in excess of 20 mm for certain PR-implanted designs. This is suggestive that the PR-implanted designs have a wide variation of knee kinematics and that the implants are very sensitive to surgical technique. In contrast, the kinematics of PS-implanted knees appear less variable and therefore, may be more reproducible. This work to date demonstrates that the PS-implanted knees replicate normal knee kinematics for a deep knee bend better than the PR-implanted knees used in this study.

CONCLUSION

The kinematics of the knee does change when the ACL is damaged or removed. The PS-implanted knees possibly simulate normal knee kinematics better than the PR-implanted knees for this particular design. The authors feel that more data needs to be collected before definite conclusions can be made. They are in the second phase of this work, adding 60 more knees to the study.

REFERENCES

[1] S.C. Banks et. al. 1993. ORS Proceedings, page 428.
[2] J.B. Stiehl et. al. 1995. ORS Proceedings, page 739.

CONTACT PRESSURE ON THE PATELLAR BUTTON FOLLOWING TOTAL KNEE REPLACEMENT

Jean H. Heegaard[1] Alain Curnier[2] and P.F. Leyvraz[3]

[1] Division of Applied Mechanics
Stanford University
Stanford, CA 94305-4040
[2] Ecole Polytechnique Fédérale
Lausanne, Switzerland
[3] Hopital Orthopedique de la Suisse Romande
Lausanne, Switzerland

INTRODUCTION

This study examines the changes occurring in the patello-femoral contact pressures during knee flexion following total knee replacement, using the Insall-Burstein II Total Condylar design (Zimmer, Warsaw, IN). Attention is focused on the effects of a 5° internal or external rotations displacements of the femoral component.

REVIEW AND THEORY

Long term clinical results have demonstrated that replacement of the patello-femoral joint in Total Knee Replacement (TKR) is still the source of many complications, mostly due to instabilities, surface wear, fractures and loosening. Hence, higher stress and strain levels in the resurfaced patella were found to favour wear and fracture of the button (Windsor *et al.*, 1989).

Previous studies on patellar biomechanics following TKR have shown how the natural knee patellar tracking was modified after knee replacement (Anouchi *et al.*, 1993). In particular, the positioning of the femoral component, which unlike design geometry is a factor mainly under the surgeon's control at insertion time, has been recognized as an important factor influencing patellar tracking. However, little is known about the possible effects of femoral component positioning on patellar contact pressure distribution.

Unlike the healthy natural knee, in which conformity between the contacting parts is optimal, the patellofemoral contact zones are significantly reduced after Total Knee Replacement leading to higher pressure distribution which also contribute to accelerated wear of the plastic button (Hsu and Walker, 1989).

The objective of the present study was to determine the effects of various femoral component positioning on the patellar tracking and on patello-femoral pressure distribution using the Total Condylar prosthesis. This could then indicate whether certain positions of the femoral component would favorably decrease or conversely adversely increase the patello-femoral contact pressure.

PROCEDURES

A comprehensive mathematical model of the patello-femoral joint (Heegaard *et al.*, 1995) able to accurately compute the joint's 3D biomechanics was used to investigate the effects of femoral component positioning on patellar tracking and contact pressure distribution. The model consisted of a 3D finite element mesh of the patello-femoral joint (1000 nodes). Geometrical data were obtained from 1 mm thick sagittal slice CT-scans (Somatron DR3, SIEMENS), representing a set of 40 slices for the tested knee joint. The patella was divided into 3 regions: cortex, spongious bone (considered as homogeneous and isotropic) and cartilage (considered as nearly incompressible). The patello-femoral interface was modeled using three-dimensional large slip gap elements (Heegaard and Curnier, 1993).

Prescribed motion of the tibial insertion of the patellar tendon during knee flexion and prescribed quadriceps forces acting on the patella were imposed to the model.

A medium size (A/P 65 mm) femoral component of an Insall-Burstein Total Condylar prosthesis was digitized with an accuracy of 10 μm, into 2000 points (25 slices of 80 points) using a custom made digitizer and was inserted into the model, aligning the component according to the manufacturer's guidelines. A medium sized patellar button (34 mm of diameter), was inserted in such a way as to preserve the original patellar thickness.

Finally, the femoral component was inserted into the model with two non-standard placements, corresponding to a 5° external or internal rotation. These displacements were obtained by rotating the component's surface around the appropriate axis and by translating the rotated surface so as to keep a correct femoral groove depth. The resulting patellar tracking and pressure distributions were computed for each case as a function of knee flexion.

RESULTS

The peak pressures were higher on the lateral compartment than on the medial one (Fig. 1). After TKR

most of the pressure was distributed on the lateral side, with an average 0.5 MPa increase in the peak pressures.

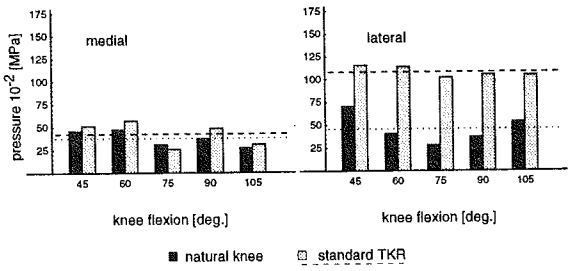

Figure 1: Peak contact pressure natural knee vs. standard TKR

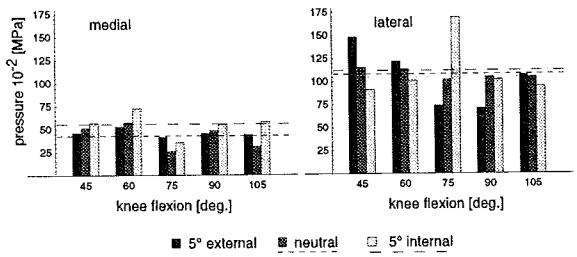

Figure 2: Peak contact pressure standard TKR vs. 5° internal/external rotation of femoral component

Internal rotation of the femoral component produced a small overall increase of peak pressure which was more marked on the medial compartments (+0.15 MPa) than on the lateral one (+0.05 MPa) (Fig. 2).

The mean peak pressure was only slightly increased on the medial compartment (+0.03 MPa) and slightly decreased on the lateral one (-0.04 MPa) (Fig. 2).

DISCUSSION

Fatigue wear of the patellar button is among the most commonly observed problems with incongruent prosthetic designs. Buechel *et al.* (91) have evaluated contact stresses in patellar button of six commonly available designs, including the Insall-Burstein-II, under physiological loads. The peak contact stresses for this prosthesis was higher than the 5 MPa maximum level recommended by polyethylene manufacturers. In the present simulations the same loads were applied on the quadriceps (40 N) as those applied during an earlier experiment (Heegaard *et al.*, 1994). The resulting peak contact pressure were about 1 MPa and represented thus much lower values than the 5 MPa limit. However, when physiological loads would be applied, the contact pressure would increase following a quadratic relation according to Hertzian contact theory. Physiological quadriceps loads typically range between two and three times body weight, in which case contact pressure would raise to the order of magnitude of 10 MPa.

To summarize, none of the applied displacement noticeably altered the contact pressure. Therefore, stability of the patella should be of primary concern to the surgeon, as patellar tracking was affected by positioning of the femoral component. On the other hand, pressure distribution depended mainly on the femoral components geometry as it was not markedly affected by femoral components displacement.

REFERENCES

Anouchi, Y.S., Whiteside, L.A., Kaiser, A.D., and Milliano, M.T. (1993). *Clin Orthop*, **287**, 170–177.

Buechel, F. F., Pappas, M. J., and Makris, G. (91). *Clin. Orthop.*, **273**, 190–197.

Heegaard, J. H., and Curnier, A. (1993). *Int. J. Num. Meth. Engng.*, **36**, 569–593.

Heegaard, J.H., Leyvraz, P.F., van Kampen, A., Rakotomanana, L., Rubin, P.J., and Blankevoort, L. (1994). *Clin. Orthop.*, **299**, 235–243.

Heegaard, J.H., Leyvraz, P.F., Curnier, A., Rakotomanana, L., and Huiskes, R. (1995). *J Biomechanics*, **in press**.

Hsu, H. P., and Walker, P. S. (1989). *Clin. Orthop.*, **246**, 260–265.

Windsor, R.E., Scuderi, G.R., and Insall, J.N. (1989). *J Arthroplasty*, **4 (Suppl)**, 63–67.

ACKNOWLEDGMENTS

This research was supported in part by the Swiss National Fund for Scientific Research, grant no. 32-30013.90.

FAILURE PREDICTION IN THE POLYETHYLENE COMPONENT OF A TOTAL KNEE REPLACEMENT BASED ON STRESS ANALYSIS

Bonnie J. Beard, Raghu N.Natarajan and Thomas P.Andriacchi
Department of Orthopedic Surgery
Rush Presbyterian St.Luke's Medical Center
Farid M.L.Amirouche
Department of Mechanical Engineering
University of Illinois at Chicago
Chicago, Illinois

INTRODUCTION

Damage to ultra high molecular weight polyethylene (UHMWPE) is one of the primary mechanical factors limiting the life of a total knee replacement (TKR). Fatigue failure associated with the cyclic loading during normal walking appears to be a primary source of polyethylene damage. The load distribution (1) changes substantially during the stance phase of gait as the knee undergoes both tractive rolling and sliding.

The purpose of this study was to examine the dynamic changes in the stress distribution in the polyethylene component during the cyclic rolling that occurs during stance phase of gait and thus examine the possibility of fatigue failure of the polyethylene component leading to damage of the component.

THEORY AND PROCEDURE

The loading at the knee joint was taken directly from measurements obtained during the gait of the patient following total knee replacement. A model was used (2) to predict the location and magnitude of normal as well as anterior-posterior shear force acting at the knee during the portion of the gait cycle between heel-strike and pre-swing. The time between two adjacent sample points at which the resultant forces were calculated was 8.3 milli-seconds. Normal and anterior-posterior forces at 20 distinct contact points on the polyethylene were obtained as input to a stress analysis model. The stress analysis model was an adopted Hertzian contact model as described by Smith (3). The femoral component was assumed to be Co-Cr with a radius of 55 mm, while the tibial component was assumed to be flat with a 10 mm polyethylene thickness. The modulus of elasticity of polyethylene was taken as 700 MPa.

The anterior-posterior shear force was posteriorly directed during the initial stance phase and reverses its direction when the contact point between the femur and tibia was at the posterior zone. This force reversal produces cyclic variation of the stresses thus inducing fatigue in the component. The fatigue resistance of the polyethylene when subjected to fluctuating loads was studied using modified Goodman criteria(4) for fatigue failure.

RESULTS

Maximum normal compressive stress always occurred near the surface while the maximum shear stress due to tractive rolling always occurred below the surface. Both the maximum normal compressive and maximum shear stress occurred in the posterior zone of contact. The maximum compressive stress (Fig. 1) in fifteen of the twenty locations exceeded the yield strength (12 MPa) of the polyethylene causing creep deformation of the material.

Large cyclic variations were observed in all three calculated components of stresses in the posterior zone of the polyethylene component (Fig. 1). The normal compressive stress varied from -0.1 MPa to -19.5 MPa yielding a load ratio of 195 within a 2.75 mm range along the tibial surface in the posterior zone of contact. The stresses in the direction of tractive force varied from + 3.2 MPa to -17.2 MPa yielding a load ratio of 5.4 within a 3.3 mm range near the tibial component surface also in the posterior contact zone.

The cyclic compressive stress in the polyethylene component produced a mean stress of 10 MPa and an alternating stress of 10 MPa. Based on an endurance strength of 8 MPa for polyethylene (5), the resulting design factor of safety was found to be less than one. Similar calculations for stresses in the direction of tractive force also showed the design safety factor to be less than unity.

DISCUSSION

The tractive rolling and breaking that occurs in a TKR during the stance phase of gait can produce substantial stresses in the polyethylene. High normal compressive stresses calculated due to forces occurring during the normal stance phase were higher than the yield strength of the polyethylene and thus are responsible for permanent creep deformation observed in the posterior zone of the retrieved tibial components. This permanent deformation forces the knee to move in a constrained fashion.

Reversal of the tractive force in the posterior zone of the implant introduced cyclic variation of the stresses in polyethylene component. The calculations based on Goodman fatigue failure mechanism showed that the polyethylene component is susceptible to failure due to cyclic loading.

Pruitt et al., (6) experimentally found that tension-compression cyclic load in UHMWPE caused fatigue cracks to grow even for a load ratio of 3. Current analysis showed that the tractive forces produced a load ratio of 5.4 and thus are responsible for fatigue failure of the component near the surface in the direction of the tractive force. Similarly Pruitt et al. also found that compression-compression cyclic loading caused fatigue cracks to grow at load ratios greater than 25. Additionally, they noted that with greater unloading toward zero stress, as is the case shown here (-0.1 MPa), the crack length further increases. The load ratios calculated in the current study in the normal load direction also exceeded those reported by Pruitt and thus can cause fatigue failure in UHMWPE. The substantial change in the load on the tibial component during the stance phase of gait can produce fatigue failure in the posterior zone of the component.

ACKNOWLEDGEMENT

University of Illinois at Chicago fellowship

REFERENCES

(1) Wimmer MA et al. ORS, 20:735, 1995.
(2) Schipplein et al. JOR, 9:113-119, 1991.
(3) Smith JO et al. J.App.Mech, 20:157, 1953.
(4) Shigley et al. Mechanical Engineering Design, Mc Graw Hill, pp 296-300, 1989.
(5) Teoh SH, ASTM STP 1173, pp 77-86, 1994
(6) Pruitt L et al. JOR, 13:143-146, 1995

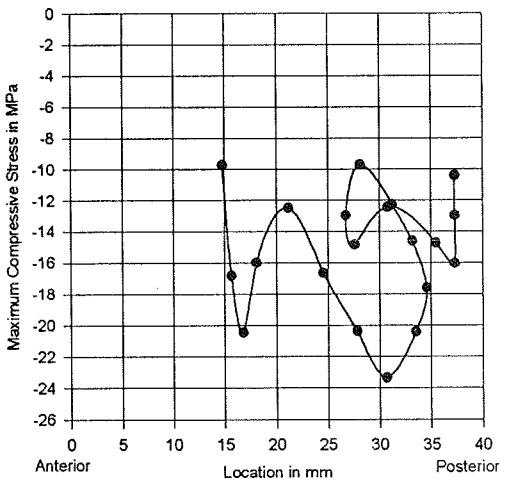

Figure 1. Maximum Compressive Stress Near The Tibial Component Surface

VALIDATION OF F-SCAN PRESSURE SENSITIVE SYSTEM

Z. Luo, L. Bergiund, A. Westreich, E. Growney, K. An
Orthopedic Biomechanics Laboratory, Mayo Clinic/Mayo Foundation, Rochester, MN

INTRODUCTION

This study performed a quantitative validation of the F-Scan sensor, a newly developed pressure sensitive transducer. Our results indicate that with careful calibration, the F-Scan system can suitably determine pressure distribution between soft materials.

REVIEW AND THEORY

The F-Scan pressure sensor system (Tekscan, Inc., South Boston, MA), has recently been developed to measure dynamic, multiple point pressure between two objects and has gained in popularity. The F-Scan system has been marketed as a particularly useful tool for measuring plantar and *in vitro* joint pressure because of its dynamic loading response and multiple sensor cells. However, previous studies have been qualitative due to limited sensor calibrations as well as the complexity of the sensor's material properties[1,3].

This F-Scan sensor consists of two ultra-thin (0.18 mm) Mylar sheets each printed with parallel rows or columns of an electrically conductive ink. Each sheet is then coated with a pressure-sensitive, resistive ink and then assembled so that the rows and columns intersect to form a grid where the electrode intersections form active pressure sensitive cells[2]. Factors affecting the system's pressure response include the pressure normal to the sensor surface, the contact surface hardness, creeping of the resistive ink under pressure, and the ambient temperature. This study examined the sensors' response to each of these variables, as well as the system's linearity and homogeneity. Such data provides a guideline for quantitative use the these sensors.

PROCEDURES

The F-Scan sensor used in this study consisted of an insole sensor designed for plantar pressure measurement. These sensors consist of 955 individual pressure-sensing cells which are evenly distributed at 5.05 mm intervals. In these experiments the sensors were sandwiched between two 6.4 mm thick firm foam pads made of a polymoric foam rubber material (Sorbothane^{TM}, Sorbothane Inc.), and backed by two 12.7 mm thick aluminum plates on each side. An MTS 810 machine (MTS Systems Corporation, Minneapolis, MN) was then used to apply a uniaxial compressive force to the sensor through the rigid plates and immediate soft foam.

The sensor's linearity and homogeneity was evaluated using five pressure levels: 0.048, 0.096, 0.145, 0.193 and 0.241 MPa. From these five levels, a linear regression was performed on each cell as:

$$p = c_0 + c_1 x \qquad (1)$$

where p is the pressure with a unit in MPa, x is the sensor output (represented by the raw electronic signals varying from 0 to 255 levels), and c_0 and c_1 are two regression coefficients.

Because the maximum applied pressure over the entire sensor was only about 0.241 MPa under a force of 11123 N, several randomly selected cells were individually subjected to a much wider range of locally applied force consisting of five pressure levels up to 2.282 MPa.

The influence of the contact surface hardness on sensor output was examined with a uniform pressure of 0.193 MPa under three surface conditions: 1) Two-foam soft contact condition, which was the soft surface sandwich outlined above. 2) One-foam soft contact condition, where the bottom foam was withdrawn. 3) Hard surface condition, where two 1 mm thick Plexiglas plates were inserted between the foams and the sensor.

Resistive ink creeping effects were evaluated by applying a stepped load consisting of a fast (within 1 second) load to 0.193 MPa, and then maintaining that load for 120 seconds.

Temperature effects were evaluated by removing the bottom foam pad and placing the sensor directly on an aluminum plate precooled to below 0^{o}C. The plate was placed on an electric heater and a thermometer monitored the sensor temperature over the course of the test.

In addition to individual curve fitting for each cell, a single linear equation was used for all the cells to check if the result could be represented by a single regression. The output variations among different F-Scan sensors were also tested using three sensors (two additional sensors) under a dynamic slope loading. These sensors were loaded to 0.241 MPa within 1 second, and the results evaluated by the linear regression described by Eq.(1). Standard statistical procedures were used to calculate means and standard deviations throughout the cells. For the tests on the same sensor, the repeated measures analysis of variance (ANOVA) with Tukey test was used to detect any difference; while ANOVA with Tukey test was used for the tests among the different sensors.

RESULTS

The results show that the sensor had an excellent response to the static loadings throughout all the cells (R^2 = 0.97925 ±0.01589). The sensor response also shows a highly uniform distribution with c_0 = -0.04147±0.01659 and c_1 = 0.01157±0.00208. The linear response is valid up to 1.70 MPa (Fig. 1).

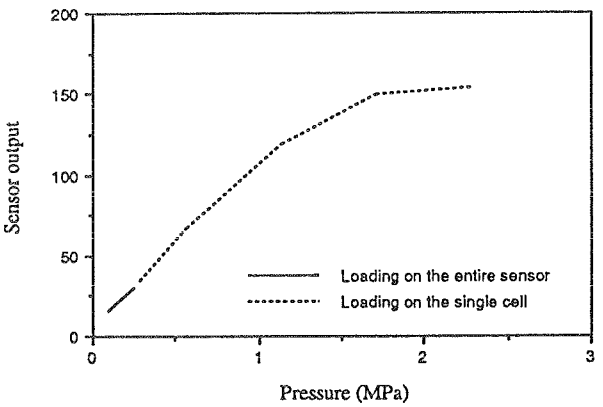

Figure 1: A typical cell response to loadings: The entire sensor loading up to 0.241 MPa (solid line), and the single cell loading from 0.285-2.282 MPa (dash line). The linear response is shown up to 1.70 MPa

The sensor output is highly dependent upon the contact surface hardness (Fig. 2). For the soft surface with two foams, the sensor output had a nearly uniform distribution as 19.93±2.81. When one foam was withdrawn from the top, the uniformity was partially destroyed as the standard deviation increased (20.10±3.97). For the hard surface, the output had significant errors (58.80±17.93) compared to the other two conditions ($p<0.001$)

The sensor output also shows changes under constant pressure probably as a result of creep of the resistive ink. The average whole sensor output slightly increased from 19.4 to 20.5 within 120 seconds. This tendency was continued afterwards (Fig. 3).

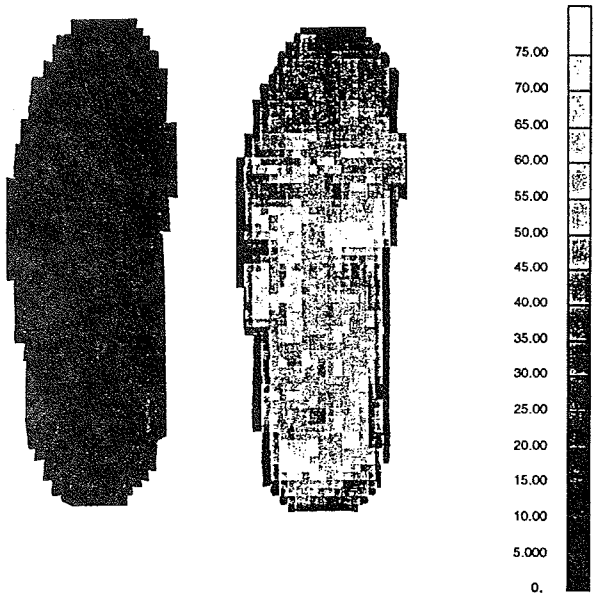

Figure 2: Distribution of the sensor output under a uniform pressure of 0.193 MPa with surface conditions: a) Two foam soft surface condition, the sensor was sandwiched between two 6.4 mm thick firm foams. b) Hard surface condition, two 1 mm thick Plexiglas were inserted between the foams. The output shows a nearly uniform distribution in a), and is completely destroyed with significantly increased mean and standard deviation in b).

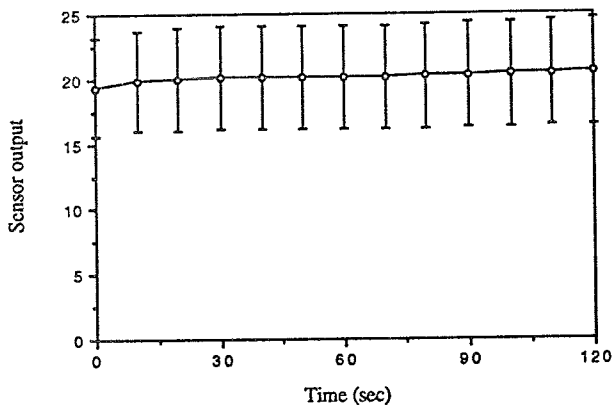

Figure 3: The average sensor output overall the cells under a constant pressure of 0.193 MPa within 120 seconds. The output increase from 17.4 to 20.5 indicates slight creeping of intrinsic pressure-sensitive resistive ink.

The sensor output was found to vary as a function of temperature. A dramatic change occurred above 30°C, where the output increased from 7 at 30°C to 20 at 45°C. While below 30°C, the total change was only 3 (from 4 to 7) (Fig. 4).

When using a single curve fit to describe the output of the entire sensor, the errors were increased. The maximal error at the lower loading level was up to 55.0%, while at the higher level, the error was still acceptable with the maximal error at 0.241 MPa as 16.9%. The results also show that the response varies from sensor to sensor. The three sensors show that c_0=0.0202±0.00357 and c_1=0.01186±0.00143 (R^2=0.98191±0.00642) for sensor one, c_0 = -0.05408±0.04711 and c_1 = 0.01134±0.00328 for sensor two (R^2 = 0.96211±0.02655), and c_0 = -0.04147±0.01659 and c_1 = 0.01157±0.00208 (R^2 = 0.97925±0.01589) for sensor three. The difference among each of the three sensors was statistically different ($p<0.01$).

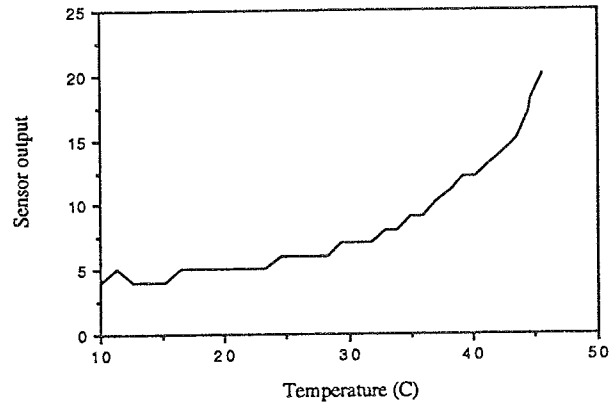

Figure 4: A typical cell response to temperature variation. Notice that the dramatic change occurred above 30°C.

DISCUSSION

The above findings suggest that accurate and consistent measurement is possible provided that each sensor is carefully calibrated under conditions (including temperature, surface hardness, test duration etc.) similar to the actual test conditions. Many differences in sensor output can potentially be explained by the microstructural granularity of the resistive ink[2]. If there are irregular gaps in the resistive ink then under hard surface conditions, the gap at the interfaces will be basically preserved during loading. Resistance will be higher among cells having more peak to peak contact, and lower among those with more peak to valley contact. With the sensor placed between soft contact surfaces, the gaps are substantially eliminated because of the flexibility of the back surfaces, and the cell resistance becomes much more homogeneous throughout the sensor. In addition, ink creeping under pressure and rising temperature may also increase the contact area and therefore change the sensor output.

CONCLUSIONS

The findings that follow from this study are:

1) Contact surface hardness significantly affects sensor output. Placing the sensor on hard surfaces results in significant output errors and cannot be used to accurately resolve loading pressure. When placed on soft surfaces, the sensors demonstrate excellent linear correlation to the pressure to as high as 1.70 MPa.

2) Under constant load these sensors exhibit slight time dependent changes in output.

3) The sensor output is temperature dependent, especially above 30°C.

4) Individual sensors have slightly different responses to the same load.

It is recommended that whenever a sensor is used for pressure measurement, a careful calibration should be performed with awareness of the sensor limitations.

REFERENCES

1. Lord, M.; Hosein, R., *J. Rehabil. Res. Dev.* 31:214-221, 1994.
2. Maness, W. L.; Golden, R. F. Benjamin, Q.; Podoloff, R. M., *United States Patent, No.: 4,734,034,* 1988.
3. Rose, N. E.; Feiwell, L. A.; Cracchiolo, A., *Foot Ankle,* 13:263-270, 1992.

View Order Phase Contrast Magnetic Resonance Imaging: A New Technique for Measuring *in vivo* Muscle Kinematics and Kinetics

F.T. Sheehan[†❖*], J.O. Fredrickson[◆], NJ Pelc[◆], Y Zhu[◆], F.E. Zajac[❖*], J.E. Drace[†◆]

[†]Diagnostic Radiaology Center, DVA Medical Center, Palo Alto, CA, USA.

[❖]Rehabilitation R&D Center (153), DVA Medical Center, Palo Alto, CA, USA.

[*]Mechanical Engineering Department, Stanford University, Stanford, CA, USA.

[◆]Radiology Department, Stanford School of Medicine, Stanford, CA, USA.

INTRODUCTION

Cine Phase Contrast Magnetic Resonance (PCMR) Imaging has proven to be an accurate technique for measuring three dimensional velocity maps (VMs) of musculoskeletal motion *in vivo* (Drace and Pelc 1994a, 1994b) Unfortunately, cine PCMR is limited in temporal resolution and requires over one hundred motion repetitions per data set. To overcome these limitations a new method, View Ordered PCMR Imaging (Fredrickson, 1994), was developed and tested. Since no adequate standard of reference exists for *in vivo* measurement of muscle motion, we tested the accuracy of tracking bidirectional motion using a motion phantom. View Ordered PCMR was approximately 50% more accurate in tracking phantom motion as compared to Cine PCMR. The in-plane motion of a bone phantom was tracked with 0.405 mm and 1.344 mm average absolute error, in the x and y directions, respectively. Out-of-plane motion was tracked with .84 mm and .77 mm average absolute error, in the x and y directions, respectively. The feasibility of using this technique to study *in vivo* muscle motion was tested by studying vasti motion during knee extensions and flexions. Further investigation is warranted.

REVIEW AND THEORY

In order to gather insights into the working of the musculoskeletal system (MSS) numerous models have been designed. Although these models have proven to be quite useful, there is a fundamental lack of accurate *in vivo* muscle, joint and bone kinematic and kinetic data.

PCMR is a valuable tool for the study of the MSS because it provides accurate *in vivo* data during a dynamic task . Presently, both Cine and View Order PCMR are limited to the study of repetitive cyclic motion. Cine's retrospective discretization of the data limits the temporal resolution and requires a minimum of 128 motion cycles per data set (Pelc et al. 1991) View Ordered PCMR allows for a trade-off between these two parameters by discretizing the data as it is collected.

PROCEDURE

A motion phantom, consisting of a series of paired gears connected by a plastic rod that held one end of the sample box, was constructed. The rods holding the top and the bottom of the sample box both moved in a circular path with a circumference ratio of 1:1, 1:2 or 1:3 to each other. All motion was confined to the x-y plane. The first sample box was a solution of $CuSO_4$ in gelatin with a 4x2 grid of fiducials. The second box consisted of a piece of bovine bone soaked in the $CuSO_4$ gelatin solution .

For each data set the images were taken in a single fixed plane. Both Cine and View Ordered PCMR VMs were acquired in the x-y plane of the first sample box. View Ordered PCMR VMs of the bovine sample were taken in both the x-y and x-z planes. The motion rate was 45-48 cycles per minute and the data were divided into 16 or 24 frames.

Regions of interest (ROIs) in each phantom were tracked frame by frame (Drace and Pelc 1994c). For in-plane motion, the ROIs' path, calculated from the VMs, were compared to the ROIs' paths, calculated from the paths of the fiducials, as observed on the magnitude images. For the out-of-plane motion, the ROIs' paths on the x-y plane image at the same y-position as the x-z plane slice was the standard of comparison.

The feasibility of studying actual muscle motion was tested during knee extension/flexion movements. View Ordered PCMR VMs were taken in the axial (x-y) plane, slightly above the vasti's musculotendon junction, during knee

flexions and extensions under two loading conditions in four healthy volunteers and one patient with patellar tracking problems. The motion rate was 27 cycles per minute and the data were divided into 16 frames.

RESULTS

Six ROIs were tracked using the PCMR VMs. For the view ordered data, the average absolute error for all six regions in all 24 frames was 0.401 mm (2.8%) in the x direction and 0.665 mm (2.9%) in the y-direction. For the cine data, the average absolute error for all six regions in all 24 frames was 1.009 mm (6.8 %) in the x direction and 1.317 mm (6.0%) in the y-

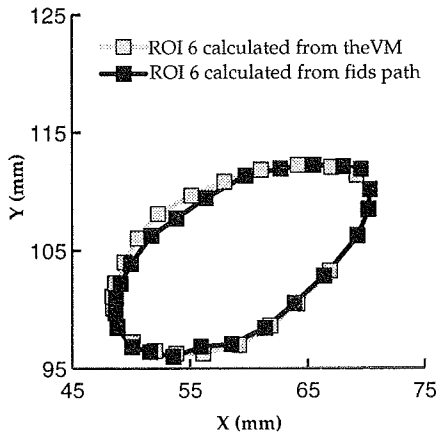

Figure 1: Tracking a ROI

direction. Figure 1 shows an example of this tracking for the view ordered data.

For the in-plane bone phantom motion, the average absolute error for the three ROI's tracked was .405 mm (2.3%) in the x-direction and 1.344 mm (5.8%) in the y-direction. When the same motion was tracked using the x-z plane images there was a discrepancy of 0.84 mm (4.1%) and 0.77 mm (3.0%) in the x and y-directions, respectively.

Vasti data shows similar superior/inferior (z) displacement and velocity profiles for the vasti medialis and lateralis and an increase in the absolute extrema values with increasing load. In the one subject with patellar tracking problems, the two vasti profiles are similar to the normal subjects profiles in the low load case, but not the high load case.

DISCUSSION

Previous work (Drace and Pelc 1994a, 1994b) demonstrated the feasibility and accuracy of measuring tendon length, muscle deformation, translation, rotation, stress and shear using Cine PCMR. View Ordered PCMR offers us the same ability to measure such variables *in vivo*, but has improved accuracy, and better temporal resolution or fewer required motion cycles per data set. Increased temporal resolution is a major factor in the decrease of tracking errors.

PCMR will aid in the measurement of muscle and tendon length, velocity, pennation angle and moment arms *in vivo* during a dynamic task. Accurately tracking bone movement is crucial for this work. Tendons, thus far, have proven to have insufficient signal to measure tendon movement directly. Thus, to measure tendon strain the myotendinous junction and the insertion point of the tendon must be tracked. Another important application of tracking bone movement is in patellar tracking. PCMR may prove valuable in obtaining kinematic details of the patellofemoral and tibifemoral joint during active and passive movements.

Since the movement of the phantom was confined to the x-y plane, the bone phantom data taken in the x-z plane has a large out-of-plane component to the movement. The accurate tracking of both data sets suggests that tracking 3-D bone movement *in vivo* is possible.

Tracking of vasti movement, may prove useful in analyzing patellar tracking problems, since it is often believed that vasti muscle imbalance is the cause of improper patellar tracking. Further work is needed to test if the trends seen thus far are significant.

REFERENCES

1. JE Drace, NJ Pelc, *Radiology* **193**, 423-9 (1994).
2. JE Drace, NJ Pelc, *Radiology* **191**, 835-9 (1994).
3. JO Fredrickson, NJ Pelc, *J Magn Reson Imaging* 4,189-196 (1994)
4. NJ Pelc et al, *Magn Reson Q* **7**, 229-54 (1991).
5. JE Drace, NJ Pelc, *J Magn Reson Imaging* **4**, 773-778 (1994).

ACKNOWLEDGMENTS

This work is supported by NIH grant 1 R29 HD31493-02 and by the Department of Veterans Affairs.

VALIDATION & COMPARISON OF A HAND MARKER SET & MODEL USING SYNCHRONIZED VIDEO FLUOROSCOPY & 3D VIDEO MOTION ANALYSIS

G. Rash[1], A. Gupta[2], P. Belliappa[2], & J. Firrell[2]

[1]Gait & Biomechanic Laboratory, Frazier Rehab Center, Louisville, KY 40202.
[2]Kleinert Institute for Hand & Micro Surgery, Inc, Louisville, LY 40202

INTRODUCTION & REVIEW

Very little work has been conducted in the area of dynamic three dimensional (3D) kinematic analysis of the hand (Darling et.al., 1990, Dennerlein et. al., 1993, & Darling et.al., 1994). Additionally, these studies limited their analysis to only the index finger (2nd digit). Darling et.al. (1990 & 1994) used a marker set which placed active markers over the lateral aspect of the 2nd digit (base of the 2nd metacarpal, centers of the MP, PIP & DIP joints and a thin bar attached to the distal phalanx of the 2nd digit). This marker set is adequate for measuring the motion of the 2nd digit as done by Darling et.al. (1990 & 1994) or even the 5th digit, but would not be adequate if trying to measure the 3rd digit, 4th digit or all five digits simultaneously. Dennerlein et.al., (1993) placed two markers each on the dorsal aspect of the distal & middle phalanx of the 2nd digit and measured the angle of the distal & middle phalanx with respect to the horizontal plane during typing. This marker set allows for measuring the motion of any of the digits separately and may even be adequate for measuring all five digits simultaneously when using an active marker system during a task such as typing. However, Dennerlein's method does not work when analyzing task where the flexion/extension motion does not occur in the vertical plane. Additionally, multiple markers on a segment hindered performing many typical ADL task and over repeated trials in our lab we have not been able to successfully distinguish two or three markers on a segment using a passive marker system in a model which includes the metacarpals and phalanges of all five digits. Thus, we were forced to develop and validate a method of marking all five digits of the hand such that it could be tracked using a passive marker system and allow for accurate measurement of flexion/extension and ulnar/ radial deviation of the digits of the hand.

It was the goal of this study to 1) Evaluate if markers placed on the dorsal aspect of the hand and fingers could accurately measure joint angles & 2) Evaluate the accuracy of the 3D model developed for analysis of hand/ finger motion.

METHODOLOGY

After identification of marker locations on the right hand of the subjects by an orthopedic surgeon specializing in hand surgery, 2.5mm diameter retro-reflective markers were placed on the following anatomical positions of the dorsal aspect of the 1st, 2nd and 3rd digits of the right hand of 5 neurologically normal male subjects: Proximal and distal aspect of the 1st, 2nd, 3rd 4th & 5th metacarpals, PIP joint line of the 2nd digit & DIP joint line of the 1st and 2nd digit, and center of the fingernail of the 1st and 2nd digits (For this validation, only location coordinates needed for the 3D calculations of the 1st and 2nd digit angles were collected).

Data collection for evaluation of the markers placed on the dorsal aspect of the hand/fingers and accuracy of the 3D model developed for analysis of hand/finger motion were collected simultaneously. This was done by simultaneously video-taping (60 Hz) a 2D fluoroscopy view of the 2nd digit of the right hand during flexion/ extension while a three camera 60 Hz Qualisys motion analysis system captured the flexion/extension motion of the 2nd digit and other markers needed for the 3D angle calculations. Both 2D and 3D areas were pre-calibrated.

The subjects were asked to perform numerous flexion/ extension trials at a self selected speed while collecting video images and marker centroid locations. A single flexion/extension trial in the middle of the collection was selected to be analyzed for each subject. From the 2D fluoroscopy video images, the proximal end of the metacarpal bone, centers of the MP joint, PIP joint, DIP joint and tip of the distal phalanx of the 2nd digit were manually digitized for the selected flexion/extension cycle. The same fields of video were manually digitized a 2nd time, however, this time the markers on the dorsal

aspect of the 2nd digit representing the aforementioned anatomical locations were manually digitized. The 2D coordinate data were digitally smoothed using a second order low pass Butterworth filter with a cut-off frequency of 10 Hz and angles from both the digitized joint center and marker locations were calculated using standard geometric techniques. The 3D coordinate data were calculated from the three camera Qualisys motion analysis system and the 3D coordinate data were also digitally smoothed at 10 Hz. A 3D coordinate system was set up in the hand and all coordinates were rotated into this system from the global system established by the calibration frame. The flexion/extension angles of the joints were then calculated using the 3D vector method of projecting a vector onto a plane defined by the coordinate system set up in the hand (i.e. MP flexion/extension in the 2nd digit was computed as the angle between the longitudinal axis of the 2nd metacarpal and proximal phalanx projected onto the plane defined by the 3rd metacarpal and the cross product of the 3rd metacarpal and the vector from the mid point of the 3rd metacarpal to the mid point of the 5th metacarpal.

Since kinematic data over time typically results in a graphic wave form and simple statistics do not yield a meaningful result when describing the similarity or variability of waveforms. A statistical measure called the adjusted coefficient of multiple correlation R_a (Winer, 1971) was used to evaluate the similarity between the flexion/extension waveforms generated by the MP, PIP & DIP joints using the fluoroscopy joint centers (FJC), fluoroscopy dorsal markers (FDM) and the 3D dorsal markers (3DDM) techniques. When the wave forms are similar R_a tends to 1. If the wave forms are dissimilar R_a tends to 0. Thus, R_a yields a measure of the ability of the different techniques to measure the joint angles.

RESULTS & DISCUSSION

Figure 1 shows the graphs of the MP, PIP and DIP flexion/extension angles from one subject for the 3 methods (FJC, FDM & 3DDM). The graphs are very similar, however, the FJC method tends to be a more variable. This is felt to be due to digitizing error as the joint centers had to be estimated in each frame, whereas, both the FDM and 3DDM methods had specific points which were easily located during digitizing.

The average R_a for the MP, PIP and DIP joints for the five subjects were 0.9724 +/- 0.0094, 0.9820 +/- 0.0084 and 0.9840 +/- 0.0089 respectively. This indicates that the 3 methods (FJC, FDM & 3DDM) all yield virtually identical results when measuring joint angles. The MP joint was slightly lower than the PIP and DIP and this may be attributed to a greater difficulty in locating the proximal end of the 2nd metacarpal on the fluoroscopy video images.

From these results it was concluded: 1) Markers placed on the dorsal aspect of the hand/fingers could accurately measure 2nd digit joint angles and 2) The 3D vector model developed for analysis of hand/finger motion was accurate when measuring 2nd digit motion. It is reasonable to assume that the same marker system and vector model would yield similar results when applied to the other 4 digits of the hand.

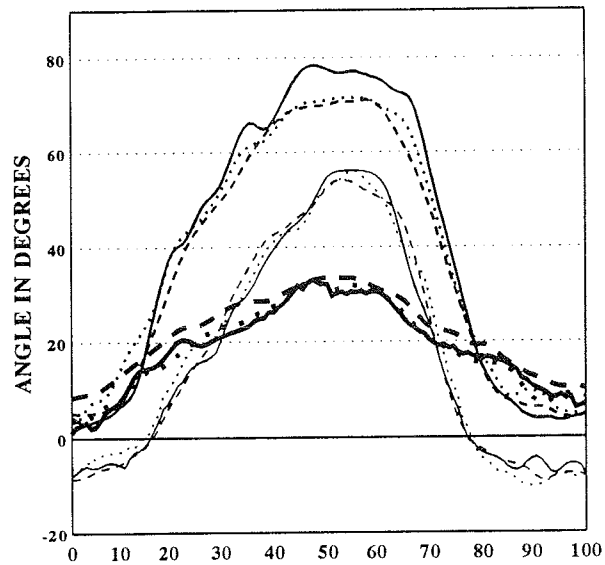

Figure 1. Flexion/Extension Angles of the MP (Thick line), PIP (Medium line) & DIP Joints (Thin line) for the FJC (Solid line), FDM (Dotted line) & 3DDM (Dashed line) techniques respectively.

REFERENCES

Darling, W., et.al. J. Neurophysiology, Vol 63, 1098-1108, 1990.

Darling, W., et.al. J. Biomechanics, Vol 27(4), 479-491, 1994.

Winer, B. Statistical Principles in Experimental Design, (pp. 261-288), McGraw-Hill, 1971.

Dennerlein, J., et.al. Proceedings of the 17th Annual Meeting of the American Society of Biomechanics, Iowa City, Iowa (pp. 27-28), 1993.

A Novel Predictive Technique for 3D Dynamic Lumbar Torso Muscle Tension Estimation Using A Distribution of the Load Moment

U. Raschke, B.J. Martin, D.B. Chaffin
Center for Ergonomics, The University of Michigan, Ann Arbor, MI 48109-2117

INTRODUCTION

Current lumbar torso biomechanical prediction models utilizing static optimization formulations to predict muscle activity do not model observed antagonistic muscle activity well. A conceptually novel method of estimating the activity of the lumbar muscles during dynamic lifting tasks is presented here. In contrast to contemporary static optimization formulations used to solve the muscle indeterminacy problem, this method dynamically distributes the load moment about the reactive load moment direction and uses this distribution to estimate the relative magnitudes of the muscles recruited. A cortical neurophysiology based argument is made for this technique. Both static asymmetric and dynamic sagittal plane predictions were compared with observed EMG data for evaluation of the technique.

REVIEW AND THEORY

Biomechanical models have been developed to understand the underlying factors influencing low back pain. These models estimate the spinal compression and shear forces based on the forces and moments caused by the load of the object, body weight, inertial effects and tissue active and passive tensions. As the anatomical detail of these models has increased, the solution to the muscle indeterminacy problem has become an increasingly important issue. Currently, muscle activation is predicted most often by using a deterministic optimization approach. These optimization methods assume that the central nervous system recruits muscles such that some criterion, such as disc compression or muscle tension, is minimized. Although the optimization techniques tend to predict torso muscle activation in reasonable agreement with observed muscle activities for the sagittal plane, they have generally not been able to predict the variability in antagonistic and synergistic muscle activity present during more complex loading conditions (Hughes, 1991). Furthermore, the torso muscle optimization formulations have traditionally not included modifications to their solutions in response to the velocity of the motion, even though this can influence the tension characteristics of the muscle tissues and the level of lumbar torso muscle antagonistic activity (Mirka et al., 1993). As the speed of a motion seems to be a significant predictor of injury (Marras et al., 1993), a desirable capability of the prediction algorithms is that they model the effect of motion velocity on the muscle recruitment patterns.

The technique described here differs conceptually from the current optimization approaches in that instead of basing the predictions only on the tissue forces at the lumbar torso, it attempts to reflect the motor cortex organization as well. The neuroanatomy literature indicates that the connections from the corticospinal neurons to the individual motor neurons are both converging and diverging in nature. Georgopoulos et al. (1986) found that the range of movement directions to which individual cortical neurons responded was as wide as 300 degrees of arc, with discharge intensities distributed in a bell shaped fashion, leading them to propose that individual cells in the primate motor cortex were "broadly tuned to a particular direction", with the cortical neuron population activity as a whole encoding the direction of movement. It is postulated, therefore, that the central nervous system (CNS) does not select individual, highly specific, motor units for a motion, but instead a distributed pattern of them. The method described here reflects this construct in that it evaluates a distribution of moments about the torso circumference and recruits the muscles in response to this distribution.

METHODS

The technique uses a polar representation to model the muscles and load moment. In order to estimate the relative tensions of the modeled lumbar muscles comprising the Erector Spinae (ES), Latissimus Dorsi (LD), External Oblique (EO), Rectus Abdominus (RA), the load moment is spread in a bell shaped fashion about the reactive load direction (Figure 1) to form a histogram of moments (Distributed Moment Histogram - DMH)

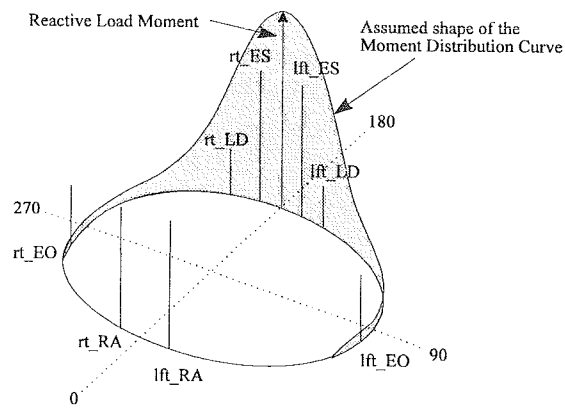

Figure 1. DMH prediction construct showing distributed moment and muscle information.

The intersection of the distribution curve and muscle parameters is used to determine the relative activation of the muscles. The height of the distribution changes with the magnitude of the load, while the width is modulated

with the velocity of the exertion. These modulations model the observed increase in muscle intensity with load amount (Lavender et al. 1992) and increase in muscle antagonism with increased velocity (Mirka et al., 1993). The technique was evaluated under both static and dynamic loading conditions. A bell shaped distribution width of 300 degrees was used to model the CNS recruitment of the muscles, based on the work of Georgopoulos (1986) and Lavender et al. (1992). The data of Lavender et al. (1992), wherein 10 subjects resisted asymmetric moment loads in an upright posture were used for the static tests. The loads were applied in 30 degree increments about the torso using a shoulder harness, producing an estimated lumbar spine moment of 50 Nm for each load direction condition. EMG was measured from the muscles included in the model using surface electrodes. The DMH method was used to predict muscle activation under these loading conditions, and a statistical correlation between the mean normalized EMG response and the predicted tensions was performed. These results were compared against the contemporary BCS (Bean et al., 1988) and SCI (Crowninshield and Brand, 1981) optimization formulations. For the dynamic tests, five male subjects performed dynamic sagittal plane stoop lifts at comfortable rates (<30deg/sec). The predicted muscle activities were compared against estimations using the BCS optimization method and the observed EMG values.

RESULTS

For the static tests, the results indicate that the new method performed on average as well as the SCI method and slightly better than the BCS method for asymmetric loading conditions in the upright posture (Figure 2). For the dynamic tests, the agonistic muscle predictions agreed with the observed EMG activity closely (Figure 3; ES: r^2=0.9, LD: r^2= 0.4). The antagonist RA muscle was found to be silent while the EO muscle had low but significant activity (< 15% MVC). The BCS optimization formulation did not predict any activity for this muscle, while the distributed moment method predicted activity that matched the observed activity well (Figure 4), although with a low correlation (r^2 = 0.07) due to a minimal change in muscle activation throughout the lifts.

DISCUSSION AND CONCLUSIONS

In summary, the Distributed Moment Histogram technique presents a novel rational for both agonistic and antagonistic muscle activity recruitment. Further, it is in agreement with the spatial distribution of neuron activity observed in the motor cortex. The superior predictions of the new method for the antagonist muscles during the studied dynamic sagittal plane extension trials, and the strong correlation with observed muscle activity under static asymmetric loading conditions, suggests this method as an alternative to optimization based approaches in the investigation of low back muscle recruitment strategy.

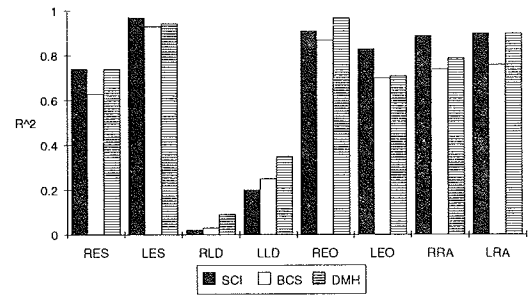

Figure 2. Correlations for static asymmetric loading.

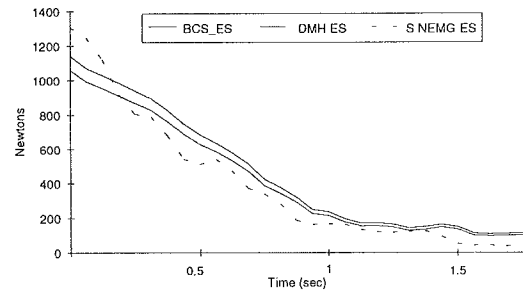

Figure 3. Dynamic lift prediction for the ES muscle from a representative subject.

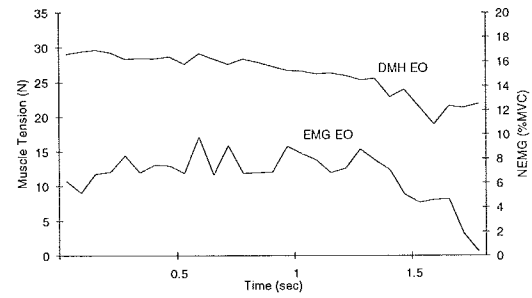

Figure 4. Dynamic lift prediction for the EO muscle from a representative subject.

REFERENCES

Bean, J. C., et al. J. Biomechanics, 21, 59-66, 1988

Crowninshield, D. et al., J. Biomechanics, 14, 793-801, 1981.

Georgopoulos, A. P., et al., Science, 233, 1416-1419, 1986

Hughes, R. E. Ph.D. Dissertation, Univ. of Michigan, 1991

Lavender, S. A., et al. Ortho. Research Society. p141, 1992

Marras, W. S., et al., Spine, 18, 617-628, 1993

Mirka, G. A., et al., Spine, 18, 1396-1409, 1993

ACKNOWLEDGMENTS

This work was supported by Coca-Cola USA and NIH Grant 2R01-AR39599.

FATIGUE RESPONSE OF THE TRUNK MUSCULATURE TO AN ISOMETRIC TRUNK TWIST EXERTION

P.R. O'Brien and J.R. Potvin

School of Human Biology, University of Guelph, Canada, N1G 2W1

INTRODUCTION

Biomechanical models have elucidated muscles having a mechanical advantage for generating axial torque of the trunk. Pope et al. (1986) identified that the relative muscle contributions to a total generated left twist moment were the left internal oblique (IO 59%), rectus abdominis (RA 14%), and the right external oblique (EO 20%) at L3. At L4-5, McGill (1991) identified the left IO (36%), LD (12%), and right EO (45%) as the primary muscles contributing to axial torque production. Muscle antagonism to twist was observed in opposite muscle pairs and bilaterally in the lumbar erector spinae. McGill (1991) suggested that the primary role of muscle coactivation must be to stabilize the lumbar joints because it is achieved at the expense of axial torque production.

The importance of the trunk muscles to the stability of the spine is considerable given that a vertical load of 20 N can buckle the spine in their absence (Lucas and Bresler, 1961). Parnianpour et al. (1988) suggested that the stability of the spine decreased with fatigue. Studies have documented the cocontraction of the trunk musculature during twist exertions under rested conditions but have not explored the effect of muscle fatigue as a perturbation to the system. The purpose of this paper is to present preliminary work investigating the levels of activation and extent of fatigue in the trunk musculature throughout an isometric twist exertion maintained until volitional fatigue.

PROCEDURES

Four male subjects (mean mass 74±2.8 kg, stature 1.77±0.04 m, age 27±3.9 yr.) volunteering from the university population were involved in the experiment. All subjects were free from any type of injury associated with the low back. Subjects were instrumented with surface electrodes at six bilateral muscle sites; the latissimus dorsi (LD), lumbar erector spinae (LES), thoracic erector spinae (TES), rectus abdominis (RA), external oblique (EO), and internal oblique (IO). Electrode placement was similar to McGill (1991).

The test session took place in an isometric twisting apparatus (ITA) (Figure 1). An adjustable harness was clamped to the upper torso of each subject just below shoulder level. The harness consisted of padded boards fastened together with two threaded metal rods. Variations in torso girth were accommodated by adjusting the width of the harness. Handles attached to the front of the harness standardized arm position. Steel cables were fastened at each end of the rear board. The cable on the subjects left side proceeded anteriorly to a wall-mounted pulley whereas the right cable proceeded posteriorly to a pulley attached to a vertical support secured to the floor. Cable heights were adjusted to ensure horizontal force vectors between harness and pulley. The pelvis was immobilized throughout the trial via a strap around the buttocks.

From a neutral standing posture, each subject isometrically resisted a 47.5 Nm external axial torque. The magnitude of external torque represented 50% of the average peak left twist torque generated by males in a neutral standing position as reported by McGill (1991). Left twist refers to rotation of the torso in the transverse plane when the left shoulder moves backwards and the right shoulder forwards, away from a sagittally symmetric trunk position. The external torque created a right twist moment. Volitional fatigue was defined as the point when the subject could no longer maintain the required trunk position.

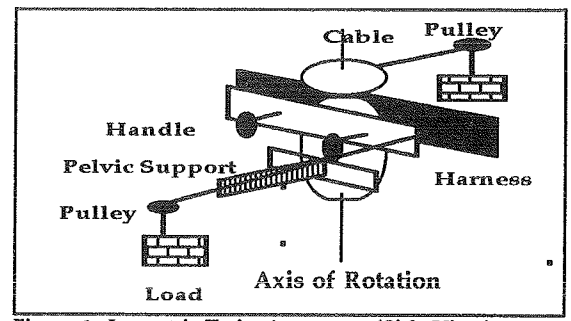

Figure 1. Isometric Twist Apparatus (Side View).

DATA TREATMENT

Mean power frequencies (MnPF) and root mean square (RMS) amplitudes were calculated for each EMG signal throughout the fatiguing protocol. For the 12 channels, 0.5 s of data were sampled at 1024 Hz every 0.75 seconds. A Fast Fourier Transform (FFT) was performed on the 512 samples from each signal and a MnPF was calculated. RMS amplitudes were also calculated for each signal. Decreases in the MnPF and increases in the RMS amplitude over the duration of the protocol were used to demonstrate the presence of fatigue in individual muscles (Petrofsky et al., 1982). For each subject and muscle, average MnPF and RMS amplitude measures were calculated from the samples comprising the first (rested) and last (fatigued) ten percent of the trial duration. RMS amplitudes were normalized to % MVC for each muscle. MnPF measures were expressed as a ratio of the average rested value for each muscle. A two factor ANOVA (muscle*fatigue state) with repeated measures was performed on the MnPF ratios and the % MVC measures.

RESULTS

The ANOVA indicated a significant muscle*fatigue interaction ($P < 0.001$) for both the MnPF ratio and % MVC measures. A means comparison between rested and fatigued values were then performed for each measure and muscle. Significant MnPF ratio decreases were observed in the left TES, LD, and EO muscles. MnPF ratios were not considered to be reliable and were, thus, not used when the rested % MVC values were less than 10% (indicated as na). Significant increases were observed in the % MVC measures for the left TES, LD and IO. Increasing trends in the % MVC values were observed bilaterally in the EO and the right LD but were not significant. % MVC changes were not displayed if the difference between rested and fatigued values were less than 10% (indicated no Δ). Muscles on the left side of the

trunk, as well as the right EO, exhibited significant responses to fatigue (Table 1). These muscles are involved in the mechanism of left trunk twist. Corresponding increases in muscle activity were observed in opposite muscle pairs but were not found to be statistically significant (Table 2).

Table 1. Responses observed in trunk muscles contributing to left twist.

Muscle	↓ MnPf (%)	Rest → Fatigue (↑ % MVC)
Left TES.	15*	26 → 62**
Left LD	17**	18 → 42*
Left IO	9	31 → 54**
Right EO	11*	21 → 34

* $p<0.05$, ** $p<0.01$

Table 2. Responses observed in trunk musculature antagonistic to left twist.

Muscle	↓ MnPf (%)	Rest → Fatigue (↑ % MVC)
Right TES.	na	no Δ
Right LD	na	9 → 22
Right IO	na	no Δ
Left EO	na	9 → 22

The average duration of the protocol was 3.6 minutes (range 1.8-5.5 min). An example of decreases in the MnPF ratios (Figure 2a) and increases in the % MVC (Figure 2b) values for the left twist musculature are displayed for one subject.

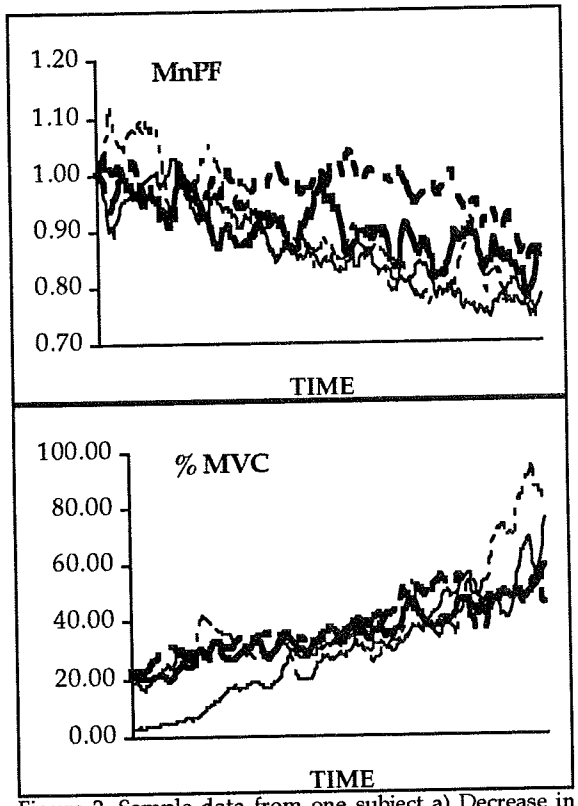

Figure 2. Sample data from one subject a) Decrease in MnPF ratio, and b) Increases in % MVC in muscles generating left twist. *Left TES- thin solid, Left LD - thin dashed, Left IO - thick solid, Right EO - thick dashed.*

DISCUSSION

Based on previous studies, it was expected that the agonist muscles contributing to a left twist would be the left IO, LD, TES and the right EO (McGill, 1991). Conversely, the muscles contralateral to these four muscles were assumed to be antagonists to the task performed.

The large increase in activity levels observed in the left TES and LD may be due, in part, to fatigue effects. Petrofsky et al. (1982) have demonstrated that fatigue will increase EMG amplitudes during prolonged isotonic contractions. However, in the current study, it appears that some of the observed increases in amplitude were too large to be explained solely by this phenomenon. In addition, the initial activation levels of the left LD muscle were quite low and were not at levels sufficient to fatigue the muscle in an average trial duration of 3.6 minutes. By the end of the protocol, the left TES exhibited higher activations and showed significant signs of fatigue based on MnPF decreases. A greater portion of the increased left TES amplitude at the end of the protocol could be attributed to fatigue. McGill (1991) has found that TES has a limited ability to generate lumbar axial torque and states that it may function in a stabilizing role. The left IO and right EO are the trunk musculature primarily responsible for generating twisting moments. These muscles were observed to have progressively increasing EMG amplitudes throughout the trial. Yet, their small decreases in MnPF do not fully explain this observation. Increased neural drive to the left IO and right EO may account for the remaining EMG amplitude increase. As the trunk becomes fatigued, it is possible that the abdominal twist musculature compensates for the fatiguing back twist musculature through increased levels of activation.

The increased activity levels of the left twist abdominal musculature may also be in response to the trend of increasing antagonistic activity in the left EO. This muscle increased its mean activity level by 13% MVC by the end of the protocol. Back muscle antagonism was also observed in the right LD. Its increase in activity was equal to that observed in the left EO. However, the low rested activity of both muscles indicates recruitment rather than changes due to fatigue. The increased antagonism observed in the right LD and left EO may have occured to increase the stability of the trunk.

Future study will attempt to further delineate muscle responses with male and female subjects. In addition, subjects will be tested with a similar protocol where the spine is pre-rotated in the direction of the resistance to investigate the interaction between fatigue and posture effects.

REFERENCES

Lucas, D.B., and B. Bresler. No. Technical Report esr. 11 No. 40. (1961).
McGill, S.M. *J. Orthop. Res.* 9: 91-103 (1991).
Parnianpour, M., et al. *Spine* 13(9): 982-992 (1988).
Petrofsky et al. *Ergonomics*, 25(3): 213-223 (1982).
Pope, M.H. et al. *J. Orthop. Res.* 4: 288-297 (1986).

TRUNK EXTENSOR MUSCLE FATIGUE AND SPINE MECHANICS WHILE HOLDING A CONSTRAINED LOAD IN A SYMMETRIC POSTURE

P.L. Bradshaw & J.R. Potvin
School of Human Biology, University of Guelph, Ontario, Canada, N1G 2W1

INTRODUCTION

Spine flexion has been identified as an important contributor to low back tissue injuries (Marras *et al.* 1993). Flexion increases the stress on passive extensor tissues and it can also influence the injurious effects of compression and shear forces acting on the intervertebral joints (Adams and Hutton 1982, Potvin *et al.* 1991). Potvin *et al.* (1991) have shown that flexion is generally maintained at safe levels during rested lifting. However, recent studies indicate that repetitive and/or prolonged loading of the trunk may precipitate changes in the kinematics of the spine (Parnianpour *et al.* 1988; Potvin and Norman 1992; Trafimow *et al.* 1993). These changes, including increased flexion of the spine or inclination of the trunk, have been associated with an increase in the potential for injury. The above studies however, involved experimental limitations or tasks that were too complex to isolate the specific causes of the fatigue related kinematic adjustments.

The current study has attempted to overcome some of these limitations through the use of a load bearing task with a simple objective and the measurement of the factors that can cause these injury related kinematic responses. The purpose of this study was to investigate the effects of induced trunk extensor muscle fatigue (TEF) on spine mechanics while maintaining a constrained feet/load position in the sagittal plane.

METHODS

Six males (age: 24.2±3.4 years, height: 174.2±4.1 cm, weight: 75.7±4.3 kg) and six females (age: 23.6±3.2 years, height: 165.7±4.9 cm, weight: 58.2±5.2 kg) were studied. Each subject was free from low back or lower extremity injury and signed informed consent.

A total of three sessions were performed at least one week apart. The first two sessions were used as orientation trials, allowing each subject to become accustomed to the task. Isometric maximum voluntary contractions (MVCs) of the trunk extensor (TE) muscles were performed in an upright standing posture. The maximum moment was used to determine a load magnitude relative to each subject's TE strength. The task required the subject to support this load 32.5 cm anterior to their ankles at about knee height, for three 15 second periods (rested phase). Four minutes rest was given between each period to eliminate the effects of any incurred muscle fatigue. Next, the TE muscles were fatigued by maintaining a 50% maximum voluntary isometric contraction for as long as possible. This contraction was repeated four times with 25 seconds of rest given between each contraction. Immediately following the fourth fatiguing contraction, the load was supported for as long as possible (fatigued phase) in the same constrained feet/load location as the rested phase. This concluded the orientation sessions.

The same protocol was completed for the third session. In addition, there was an assessment of lower extremity fatigue, at the beginning and end of the session, using the criteria presented by Potvin and Norman (1994). For the testing session, electromyographic signals (EMG) were collected at three bilateral locations (thoracic and lumbar erector spinae and vastus lateralis). All EMG signals were analog full wave rectified, low pass filtered at 2.7Hz and sampled at 20Hz at the time of collection. Further, an electromagnetic recording device (Isotrak 3SPACE), measuring spine flexion/extension, axial twist and lateral bend, and bilateral goniometers, measuring knee flexion, were sampled continuously at 1Hz.

Three sets of rested phase data (EMG and kinematics) were averaged to create a "Rest" bin, while the fatigued phase values were broken into five equal sized bins (Fat1, Fat2, ...). An amplitude probability density function (APDF) curve was also calculated with all EMG data from each bin. Grand mean values were calculated for males and females, for each kinematic and EMG variable and an ANOVA was performed to determine significant changes.

RESULTS AND DISCUSSION

The results for the individual subject analysis assessing the presence of vastus lateralis fatigue suggest that all subjects (except one) exhibited no substantial fatigue at the conclusion of the session. These results suggest that any modifications made throughout the session were due solely to the effects of the induced isometric fatigue, rather than the combined effects of TE and vastus lateralis fatigue.

All right-left results were averaged as no differences were observed. Further to this, all male-female results were also combined as no substantial sex effects were observed.

In immediate response to the induced TEF (Rest vs. Fat1) subjects significantly increased spine flexion (Figure 1) and significantly decreased the level of thoracic erector spinae (ES)activity (Figure 2). Along with this, both lumbar ES and vastus lateralis activities remained low combined with no changes in knee flexion. These results suggest the occurrence of the flexion-relaxation response (Floyd and Silver 1951; Dolan *et al.* 1994) and subsequent loading of passive tissues (McGill and Kipper 1994). The increased spine flexion may have increased injury risk (Adams *et al.* 1980; Marras *et al.* 1993) compared to the posture adopted during the rested phase.

Once the initial increases in spine flexion had stabilized, subjects were observed to increase knee flexion angle and increase loading of the lower extremities as fatigue progressed later in the session (Figures 1 and 2). In order to maintain a stable spine posture with increasing knee flexion the pelvis may

have rotated backwards. These coupled motions about the hips and knees may have allowed for the maintenance of the current magnitude of spine flexion, indirectly prevented increases in the risk of injury.

In the latest stage of the sessions, with extreme fatigue, both spine flexion and bilateral knee angles were observed to become more extended (Figure 1). In order for the subjects to move in this way and maintain a constant load position, there was likely some forward rotation of the pelvis although this was not quantified. Further to this, no significant increases in EMG levels were shown at the end of the session indicating that postural control at this late stage was modulated by muscles that were not monitored (Figure 2). For example, fatigue of the hamstrings would be likely for this task and a reduction in their force would explain the observed decrease in knee flexion and forward rotation of the pelvis.

The current protocol was designed to accomplish three goals: 1) to isolate fatigue to the trunk extensor muscles, 2) to present a task where the kinematic objective was controlled but the subject was free to modulate postures to meet this objective, 3) to quantify muscle contributions throughout the task. The advantage of meeting the first goal is that the immediate responses to fatigue could be attributed to reductions in TE muscle force generating capacity and/or coordination. (Parnianpour *et al.* 1988). This is not possible with dynamic lifting tasks (Potvin *et al.* 1991). The task was set to maintain the load moment at a relatively constant level so that changes in muscle activation could be attributed to passive/active tissue interactions and/or trunk posture moments. Again, this is not possible with unconstrained dynamic lifting tasks. The measurement of EMG allowed for a determination of the contributions of individual muscle groups to the changes observed. This has been a limitation in previous studies (Parnianpour *et al.* 1988; Trafimow *et al.* 1993).

In conclusion, the subjects responded to the extreme TE fatigue, immediately after the prolonged 50% MVC isometric contraction, by increasing spine flexion to near maximum. However, the degree of this flexion was subsequently reduced to levels that were still above the rested values. This may have been due to recovery of the TE or an unwillingness to maintain the extreme flexion of the intervertebral joints.

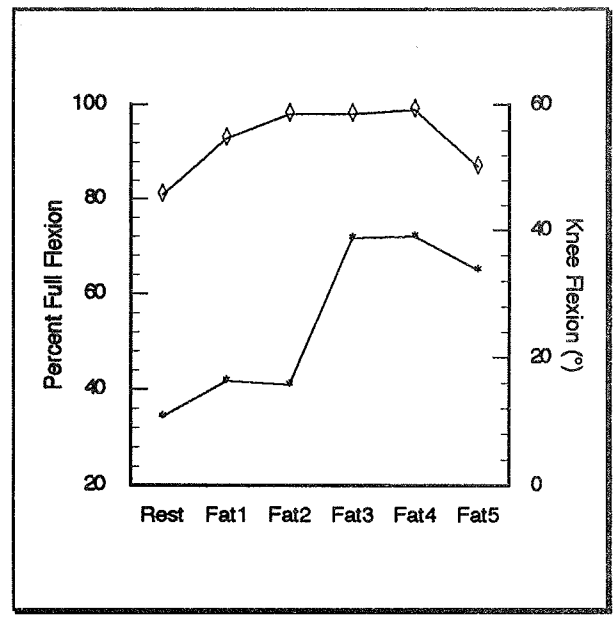

Figure 1: Binned mean spine flexion and mean right-left averaged knee angle. (◊ - spine flexion and * - knee flexion) (n=12)

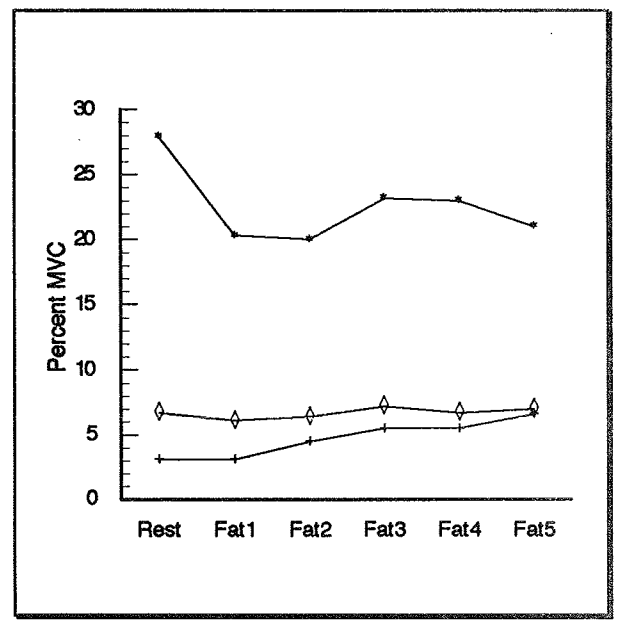

Figure 2: Binned mean 50% amplitude probability density function values. (◊ - lumbar ES; * - thoracic ES and + - vastus lateralis muscles) (n=12)

REFERENCES

Adams M.A. *et al.* (1980) *Spine*, 3, 245-253
Adams M.A. and W.C. Hutton (1982) *Spine*, 7, 184-191
Dolan P., *et al.* (1994) *J. Biomech.*, 27, 1077-1085
Floyd W.F. and P.H.S Silver (1951) *J. Physiol.*, 129, 184-203
Marras W.S. *et al.* (1993) *Spine*, 18, 617-628
McGill S.M. and V. Kipper (1994) *Spine*, 19, 2190-2196
Parnianpour M. *et al.* (1988) *Spine*, 13, 982-992
Potvin (1992) Ph.D. Dissertation, University of Waterloo
Potvin J.R. and R.W. Norman (1992) II NACOB, 513-514
Potvin J.R. *et al.* (1991) *Spine*, 16, 1009-1017.
Potvin J.R. and R.W. Norman (1994) *Eur. J. Appl. Physiol.*, 67, 554-562
Trafimow J.H. *et al.* (1993) *Spine*, 18, 364-367

QUANTIFICATION OF TENDON EXCURSION THROUGH KINEMATIC ANALYSIS OF TYPING MOVEMENTS ON ALTERNATIVE KEYBOARD LAYOUTS

M.M. Flannery[1], R.N. Robertson[2,3], R.A. Cooper[2,3]
[1]Biomedical Engineering Department, California State University, Sacramento 95819
[2]Division of Physical Medicine & Rehabilitation, University of Pittsburgh Medical Center, Pittsburgh PA 15213
[3]Human Engineering Research Laboratories, Highland Drive VA Medical Center, Pittsburgh PA 15206

INTRODUCTION

Cumulative trauma disorders (CTD) account for over 60% of reported occupational illnesses and a large number of these cases are among office workers and keyboard operators (BLS, 1992). CTD's continue to be a problem despite growing attention to workstation ergonomics and other preventative strategies. One might conclude that the standard keyboard layout needs to be analyzed in terms of injury potential. Typing on the standard or 'QWERTY' keyboard layout demands large, awkward movements since the keyboard layout was originally designed to slow typing and prevent jamming of the keys of early typewriters. These large angular excursions of the fingers can translate internally to large excursions of the finger flexor tendons through the confined area of the carpal canal. Evidence suggests that excessive excursion can induce trauma to the connective tissue structures resulting in tendinitis and edema. This becomes particularly serious when swelling of the tissues compress the median nerve causing symptoms typically ascribed to Carpal Tunnel Syndrome. By minimizing range during repetitive motion one may reduce tendon excursion and the reduce probability of cumulative trauma. Minimization of range can be translated in a practical sense to alternative keyboard layouts which map the most frequent keys to the home row. This paper presents preliminary results in quantifying tendon excursion for typing on the QWERTY layout and two alternative keyboard layouts. Data was collected for three subjects through video motion analysis and tendon excursions were calculated through a predictive model. Two subjects showed consistent results with the alternative layouts requiring less total excursion than the standard layout.

REVIEW AND THEORY

Carpal Tunnel Syndrome (CTS) is thought to be caused by compression of the median nerve within the carpal canal. The main structures in close proximity to the median nerve are the finger flexor tendons - Flexor Digitorum Profundus and Superficialis. Thickening of the flexor tendon sheaths, secondary to repetitive motion, has been implicated as a cause for compression of the median nerve (Werner et al., 1983). Cyclic loading tests on the profundus tendons have shown that stress transmitted to the sheath during excursion is significant and a cause of cumulative strain (Goldstein et al., 1987). These findings may indicate that the highly repetitive sliding motion of the tendons through the canal might not only produce tendinitis or tenosynovitis but focal damage to the nerve as well. A number of ergonomic studies also support the findings in correlating repetitive typing motion with a high incidence of CTD. Pascarelli et al. (1993) evaluated 53 disabled keyboard operators and found symptoms of pain and paresthesia in addition to over a third diagnosed with CTS.

Previous biomechanical studies of keyboards include a study by Gerard et al. (1994) which found that the subjects exhibited less muscle activity to maintain a resting posture for typing on a split contoured keyboard with standard layout. Nakaseko et al. (1985) tested the split keyboard with adjustments of opening angle, lateral inclination and forearm support. About 70% of the subjects preferred the split keyboard with a large forearm wrist support. Other studies have focused on the development of a biomechanical model of typing including characterization of impact loading and fingertip kinematics (Dennerlein et al., 1993).

The QWERTY layout is the standard alphanumeric input device for computer entry. Inherent in using the QWERTY layout is the relatively large excursions of the fingers. Ober (1993) calculated that the fingers of a typist on a QWERTY layout would travel 2.6 miles a day during a typical 8 hour day. For the DVORAK layout, the fingers would travel only 1.7 miles. The DVORAK layout is an alternative layout in which the 70-80% of typing is performed on the home row. Another layout is the ASINREDHOT (Finger Relief Co., Stamford, CT) which minimizes the remapping of the keys yet retains the majority of the typing on the home row.

The present study investigated changes in kinematics and flexor tendon excursion for the standard and alternative keyboard layouts. The goal of the study was to characterize total tendon motion for typing a matched sample on the QWERTY, DVORAK and ASINREDHOT layouts and provide a preliminary survey of the results.

PROCEDURES

Fourteen 6 mm reflective markers were adhered to the dorsal surface of each hand at the centerline of the MP, PIP, DIP joints. Markers were also placed at the wrist joint between the styloid processes and at a location 4 cm proximal to the wrist marker. A Peak5 motion analysis system was utilized to calculate the 3-dimensional coordinates and joint angles of the fingers and wrist. Two cameras were positioned at oblique angles on the right and left sides of the keyboard and a third camera was positioned above the monitor for the frontal view of the hands. A custom calibration frame (36 cm x 25 cm x 16 cm) encompassing the volume of the motion was used to accurately calculate the coordinates of the markers within the volume space. A hardware circuit and software program were implemented to synchronize the keystroke data with the 1/60 second video data. Typing speed in wpm was also measured in software during typing trials. An LED was used to synchronize the three cameras at the start of each trial.

Three dimensional coordinates were obtained by digitizing the markers in each camera view. Flexion and extension angle data were calculated at the wrist, MP, and PIP joints. The angle data was incorporated into the predictive model developed by Armstrong and Chaffin (1978). The model relates the finger and two extrinsic finger flexors, profundus and superficialis, as a pulley system dependent on the joint angle and tendon moment arm. Joint thickness measurements were taken of each subject as described in the Collation of Anthropometry (Garrett et al., 1961).

The text sample consisted of nonsense "words" reflecting the frequencies of letters and word lengths of "standard" written English. Statistical representation of letter frequency was critical since the alternative layouts are designed to map the most frequent keys on the home row. The alternative keyboard layouts were "simulated" by replacing the letter location on the alternative layout with the QWERTY equivalent. For example, the first nonsense word in the text sample is "rvw". The letters "r", "v" and "w" correspond to key locations "o", "." and "," respectively on the DVORAK layout. Simulation of layouts does not require keyboard retraining and allows each subject to act as their own control. This is especially important since typing kinematics are unique to the individual.

Data was collected for three subjects with average touch typing speeds of 40 wpm. Each subject typed the 100 character text sample for the three simulated layouts. Valid trials were those with one or no errors to preserve integrity of letter frequencies.

RESULTS

The first 5 seconds of the left index PIP angle and keystroke data for Subject 1 for both QWERTY and DVORAK layouts are plotted in Figure 2. Note the angular deflections in typing of letters "r", "v" and "f" as these keys are assigned to the left index finger on the QWERTY layout. Conversely on the DVORAK layout only slight variations were recorded as only one key on the home row ("f") was typed by this finger in the portion of data shown.

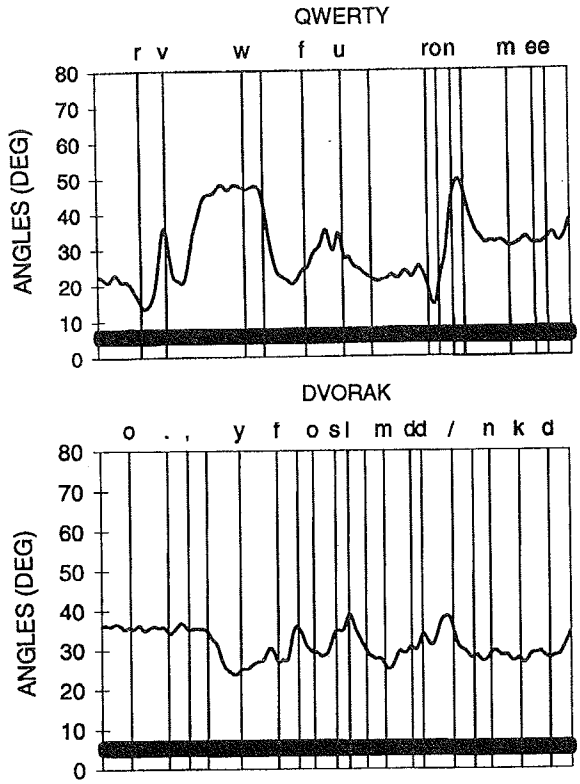

Figure 1. Sample plots of left index PIP angle data and keystroke timing in QWERTY and DVORAK typing trials of subject 1.

The tendon excursion per digit for the profundus tendons of Subject 1 (left hand) is provided in Figure 2. A comparison of total tendon excursion (summation of profundus and superficialis displacement in both hands) of all subjects is provided in Table 1. Calculations for the excursions of the superficialis tendons were relatively similar to those of the profundus.

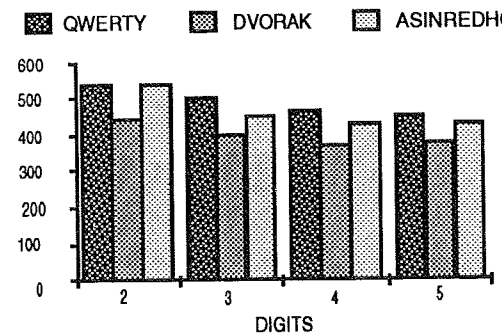

Figure 2. Excursion of the flexor digitorum profundus in digits 2-5 (left hand) of subject 1

Table 1. Total excursion (in mm) and % difference for profundus flexor tendon for each keyboard layout

	QWERTY	DVORAK	ASINREDHOT
Subj. 1	3638	3476	3371
% Diff		4.5 %	7.3 %
Subj. 2	3300	3085	3208
% Diff		6.5 %	2.8 %
Subj. 3	3412	3619	4000
% Diff		- 6.1 %	- 17.2 %

DISCUSSION

Subjects 1 and 2 showed consistent results with the DVORAK and ASINREDHOT layouts requiring less total tendon excursion than typing on the QWERTY layout. Angular displacement plots also correlated with these findings. The third subject, however, showed opposite results, indicating variability of kinematics and/or performance. One of the variables which was not controlled was typing speed. It was noted that subject 3, unlike subjects 1 and 2, typed with significant speed variation between the QWERTY (51 wpm) and alternative layouts (about 38 wpm). Future studies may need to account for digraph effects, or common letter pairs, in the text samples to ensure consistent, natural kinematics for all three layouts. The basic methodology, however, proved to be acceptable in measuring tendon excursion. According to Moore et al. (1991), the best method of studying ergonomic impact is in quantifying the effects on internal structures. Long range goals for these studies may be the establishment of guidelines in keyboard modification and typing techniques for the purpose of reducing the incidence of CTD among keyboard operators.

REFERENCES

Armstrong TM et al. *J. Biomech.*, 11, 119-128, 1978.
Bureau of Labor Statistics, U. S. Government, 1992.
Dennerlein JT, *Proc. Am. Soc. Biomech.*, 27-28, 1993.
Garrett et al., *A Collation of Anthropometry*, (pp. 604-615), Aerospace Medical Research Laboratory, 1971.
Gerard MJ et al. *Ergonomics*, 37(10), 1661-1668, 1994.
Goldstein SA, et al., *J. Biomech.*, 20(1), 1-6, 1987.
Moore A et al. *Ergonomics*, 34(12), 1433-1453, 1991.
Nakaseko M. *Hum. Fact.*, 27(7), 175-187, 1985.
Ober, S. *Delta Pi Epsiolon J.*, 35(1), 1-13, 1993.
Pascarelli Ef et al. *J. Occ. Med.*, 35(5), 522-532, 1993.
Smith, BA et al. *Hum. Fact.*, 23(4), 387-400, 1981.
Werner, CO et al. *Acta Orthop. Scand.*, 54, 312-316, 1983.

ACKNOWLEDGMENTS

Partial funding for this research was provided by the U.S. Department of Education, Rehabilitation Services Administration [H129E00005].

A MODEL FOR CALCULATING LUMBAR COMPRESSION FORCES WITH THE NIOSH EQUATION'S "H" AND "V" FACTORS

J.R. Potvin
School of Human Biology, University of Guelph, Guelph Ontario, N1G 2W1

Introduction

Many criterion have been proposed for determining acceptable loads during various lifting tasks. These criteria generally limit loads based on soft tissue injury risk (biomechanics), metabolic fatigue (physiology) or a perceptual integration of biomechanics and physiology (psychophysics). Ayoub (1992) has proposed that a biomechanical approach is most valid during infrequent lifting where metabolic fatigue is unlikely and psychophysical methods tend to overestimate safe loads. The biomechanical criterion is usually based on intervertebral joint compression forces that do not exceed some threshold level. For example, a limit of 3400 N has been proposed by NIOSH (1981). Unfortunately, the technology to directly measure compression force does not currently exist. This has led to the development of a number of biomechanical models for computing these forces based on assumptions regarding the orientation and recruitment of trunk muscles. These models can be used to determine the compression force consequences of various load/posture combinations although the time required for their use can be limiting, especially as the models become more complex.

NIOSH (1981) have proposed an equation to calculate acceptable loads based on the horizontal distance from the ankles to the load (H), vertical location of the load (V), vertical displacement of the lift (D) and frequency of lifting (F). The H and V factors are primarily responsible for representing the posture and joint moments (biomechanical criterion) associated with the lifting task. The D and F factors are primarily used to represent the work or metabolic cost of lifting (physiological criterion). The advantage of this equation is that it is easy to use, and a large number of ergonomists are familiar with the input measurements required.

The purpose of the current paper was to determine if the H and V factors could be used in regression equations to accurately calculate lumbar compression forces during load bearing tasks. If so, these equations could then be rearranged to determine loads associated with compression forces of 3400 N. Such a method would provide a useful tool for setting acceptable loads based on the biomechanical criterion during infrequent lifting.

Procedures

Eleven male and eleven female young adult subjects were studied. Eight subjects of each sex were used for the development of the regression equations while 3 subjects of each sex were used to test the validity of the equations. An attempt was made to include a wide variety of heights and weights in each group (Table 1).

Table 1: Subject anthropometrics

		Male	Female
Model Subjects	Ht (m)	1.80±0.13	1.66±0.11
	Wt (kg)	79.8±14.5	60.7±9.5
Test Subjects	Ht (m)	1.76±0.10	1.66±0.08
	Wt (kg)	82.7±16.5	65.8±6.4

Each subject was recorded on video tape as they performed movements of the hands in the sagittal plane ranging from the load being on the ground with the hands near the ankles to the arms above the head with the hands reaching forward as far as possible. This movement was first performed with a squat technique where the subjects were instructed to bend the knees as much as possible. The movement was then repeated with a stoop technique where the knees were kept straight throughout. These movements were used to represent a wide variety of lifting postures. Approximately 100 postures were recorded for each subject and each was digitized to determine the position of the hand, forearm, upper arm, head, trunk, pelvis, thigh, leg and foot segments.

For each posture the location of the upper body's centre of mass was determined using linked segment modelling and assuming standard anthropometrics. Regression equations were developed (n=1703) to estimate the horizontal distance from the L4-L5 joint to a) the upper body's centre of mass, and b) the hand held load. Both of these equations required the input of the NIOSH H and V factors and the trunk angle. The regression based moment arm estimates could then be multiplied by the subject's upper body weight and the load weight, respectively, to determine the extensor moment of force about the L4-L5 joint. This moment was assumed to be restored by a single erector spinae force vector acting 6 cm posterior to the flexion/extension axis of the intervertebral joint and parallel to the trunk. The internal muscle force was added to the compression force component of the reaction forces to determine the bone-on-bone compression force acting on the L4-L5 intervertebral joint.

The criterion values for the regression analysis were determined with a linked segment biomechanical model that determined the joint moments and reaction forces.

The internal muscle representation was the same as was described above. A range of loads was iterated for each of the postures analyzed. For males, the loads ranged from 0 to 36 kg in steps of 9 kg and for females, the loads ranged from 0 to 28 in steps of 7 kg. The strength models of Clarke (1966) and Schanne (1972) were used to identify any moments about the knee, trunk, shoulder or elbow joints that exceeded the 95 percentile strength of the subject's gender. These load/posture combinations were considered to be unrealistic and were subsequently eliminated from the assessment of the models. The compression model was tested with the data from the 16 "model" group subjects (n=7003) and the 6 "test" group subjects (n=2409).

Results

The results from both the model and test groups were very encouraging. The model results are presented in Table 2. The RMS error in estimating compression force was observed to be 144 N with a maximum of 573 N over the 7003 conditions studied. Surprisingly, the models appeared to work even better for the independent "test" group when regression model estimates of compression force were compared to those from a biomechanical model (Figure 1). The R^2 was 0.991 with an RMS error of 134 N.

Table 2. Regression model statistics

Model Output	n	Model	RMS
Upper Body CG to L4-L5	1703	0.984	0.018 m
Load to L4-L5	1703	0.979	0.033 m
Compression Force	7003	0.988	143.7 N

One limitation of this method is that trunk angle must be measured. However, an analysis has been performed to determine the range of trunk angles that would be expected for various combinations of H and V. This analysis has resulted in additional regression equations that calculate the maximum and minimum trunk angles observed when the 1703 postures were put into 10x10 cm bins of the horizontal and vertical load locations. These models required H and V as inputs and resulted in acceptable approximations of maximum angle (R^2 = 0.925, RMS error = 8.1°) and minimum angle (R^2 = 0.961, RMS error = 8.2°).

Discussion

A mathematical model has been developed for estimating the horizontal distances from L4-L5 to the load and the upper body centre of mass. The model requires the input of the NIOSH H and V factors and trunk angle. Further, calculations of compression force require the input of load mass and body weight. However, the body weight can be chosen to represent particular percentiles and the various loads can be simulated to determine their effect. The equations can also be rearranged to calculate the load that will result in a compression of 3400 N. Thus, these estimates of acceptable loads can be compared to those from other available ergonomic methods.

The errors associated with this method were found to be within the accuracy range of most biomechanical models given the assumptions and limitations inherent in their development. The major advantage this model is that the inputs are easier to make than most biomechanical models that require the input of multiple joint coordinates or joint angles. The H and V inputs are consistent with those required in the NIOSH equation and, thus, most ergonomists are already familiar with their measurement.

The proposed method has been designed to assess the task and not the lifter. In this way it is similar to other methods involving psychophysical (Snook and Ciriello, 1991), physiological (Garg et al., 1978) and combined criterion (NIOSH, 1981). Most biomechanical models are sensitive to the specific method used by the individual being analyzed. Unless a large number of subjects are studied, it is possible that feasible postures with the highest risk of injury may not be considered when load limits are set. With the current method, the possible range of postures can be determined so that the trunk angle resulting in the highest compression force can be identified. This angle can then be used to determine a load that is safe for all probable postures associated with the task. In addition, the model can also incorporate the NIOSH D factor to consider the entire vertical displacement of the load when limits are set.

Figure 1. Regression vs. biomechanical model compression forces for the test group (n=2409)

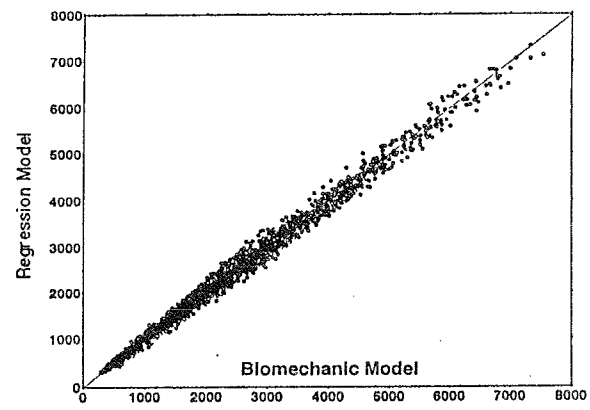

References

Ayoub (1992) *Ergonomics* 35, 713-728

Clarke (1966) *Muscle Strength and Endurance in Man*

Garg et al. (1978) *Am In. Hyg. Assoc. J.* 39(8):661-674

NIOSH (1981) *Work Practices Guide for Manual Lifting*

Schanne (1972) *A Three-Dimensional Hand Force Capability Model for the Seated Operator*

Snook and Ciriello (1991) *Ergonomics*, 34(9) 1197-1213

RELATIVE WORK OF NET JOINT MOMENTS DURING LANDINGS OF FRONT AND BACK SALTOS

Jill L. McNitt-Gray, Dawn M.E. Irvine, James P. Eagle,
Jacklyn G. Heino, Barry A. Munkasy, and Michelle D. Welch
USC Biomechanics Research Laboratory, Department of Exercise Sciences
University of Southern California, Los Angeles, CA, USA 90089-0652

INTRODUCTION

During landing activities, forces and moments generated by muscle-tendon units and reaction forces are applied to the musculoskeletal structures of the lower extremity. Although no causal relationship has been proven between load and injury, the high incidence of injury to the lower extremities of athletes participating in landing activities (NCAA, 1986, 1990; McAuley et al., 1987) suggest injury may be a result of mechanical overload of the musculoskeletal system. Examination of the selective process by which large loads experienced during landings are dissipated and distributed by the lower extremity musculoskeletal system may assist in identifying the contributions of components in reducing the mechanical energy of the body.

REVIEW AND THEORY

Recent changes in the gymnastics code of points encourages performance of more forward rotating skills. Front saltos have been less frequently performed during competition, resulted in shorter contact surface viewing times, and resulted in different anatomical orientation relative to translation direction than back saltos (McNitt-Gray, 1992). No significant differences in peak vertical forces have been observed during landings of front and back saltos performed from the same height (McNitt-Gray, et al., 1991); However, differences in translation direction and segment configurations prior to contact between tasks have produced differences in joint kinetics and muscle activation patterns (McNitt-Gray, et al.,1993).

Examination of work done by net joint moments has assisted in providing an "index of softness" (Zatsiorsky & Prilutsky, 1987), evaluating the consequences of specific landing techniques (Devita & Skelly, 1992), and adjustments in work distribution with increases in mechanical energy at contact and between different subject populations (McNitt-Gray, 1993). The purpose of this study was to determine differences in the work of ankle, knee, and hip net joint moments during landings of front and back saltos. Identification of differences in work distribution between ankle, knee, and hip net joint moments during forward and backward rotating tasks may have implications for training and injury prevention.

PROCEDURES

Six healthy male gymnasts, who were members of a team ranked among the top five of all collegiate gymnastics teams within the United States, volunteered to serve as subjects. During data collection, each subject successfully landed three drop landings (McNitt-Gray, 1991), three front tucked saltos, and three back tucked saltos in a randomized order using their normal competitive landing style. All three tasks were initiated from a height of 0.72 meters above the top surface of two regulation gymnastics mats (100 ILD). These two mats were fully supported by two Kistler force plates. The reaction forces at the mat-plate interface were quantified for each foot using a sampling frequency of 800 Hz. Segment kinematics were recorded simultaneously using high speed video (200 fps; NAC Motion Analysis System). Markers positioned on the body of the subjects were digitized using a video based data acquisition system (Peak Performance, Inc.). Each coordinate of the digitized body landmarks (Zatsiorsky & Seluyanov, 1983) were digitally filtered using a fourth order Butterworth Filter (Saito & Yokoi, 1983) with a cut-off frequency derived by the method of Jackson (1979). The kinematic and reaction force data were synchronized at contact and ankle, knee, and hip net joint moments were calculated using Newtonian mechanics (Nm/kg). Net joint moment power at each joint were computed as the product of the joint angular velocity and the net joint moment. Negative work of each net joint moment was computed as the integral of the negative portion of the net joint moment power curve from contact to 0.2s after contact. Relative negative work for each joint was expressed as a percent of total negative work by the ankle, knee, and hip net joint moments. Absolute and relative negative work of ankle, knee, and hip net joint moments observed during the front and back salto landings were compared within subjects.

RESULTS AND DISCUSSION

Although no significant differences in peak vertical forces were observed between tasks, the orientation of the body relative to the direction of translation produced differences in knee and hip net joint moments. Immediately after contact in the front salto landings, a knee flexor moment was needed to oppose the ankle extensor net joint moment and moments created by the ankle and knee net joint forces. Immediately after contact in the back salto landings, a knee extensor moment was needed to assist the ankle net joint moment in opposing the moments created by the ankle and knee net joint forces.

The differences in knee net joint moments observed between front and back salto landings contributed to the

differences in hip net joint moments. Immediately after contact in the front salto landings, a hip extensor moment was needed to oppose the knee flexor moment and the moments created by the knee and hip net joint forces. Immediately after contact in the back salto landings, a hip flexor moment was need to assist the net joint forces in opposing the knee extensor moment.

During the interval from contact to 0.2s after contact, the ankle, knee, and hip demonstrated flexion resulting in negative joint angular velocities. The net joint moment powers during front and back salto landings performed by a representative subject (Figure 1ab) reflect these differences in knee and hip net joint moments. The magnitude of work by ankle, knee, and hip net joint moments in this study are in line with those reported by Devita and Skelly (1992), McNitt-Gray (1993) and Prilutsky and Zatsiorsky (1994).

Work by the ankle net joint moment comprised a greater percent of the total negative work during front salto landings than during back salto landings (Figure 1c). In contrast, work by the hip net joint moment comprised a greater percent of the total negative work during back salto landings than during front salto landings (Figure 1c). In addition, work by the hip net joint moment occurs throughout the front salto landing, whereas, the work by the hip net joint moment during the back salto landing occurs later (Figure 1ab). These differences in work distribution between forward and backward rotating tasks, although variable within subject, may have implications for training adjustments and injury prevention.

REFERENCES

Devita, P. et al. MSSE, 24 (1):108-115, 1992
Jackson, K.M., IEEE Trans. Bio Eng. 26:122-124, 1979.
McAuley, E. et al., AmJ Spts Med,15,558-565, 1987.
McNitt-Gray, J.L. , J. of Biomech, 1993.
McNitt-Gray, J.L. et al., ASBProc., 1993.
McNitt-Gray, J.L. et al., ASBProc., 1991.
McNitt-Gray, J.L., IJSB, 7, 201-224, 1991.
McNitt-Gray, J.L. & Nelson, R.C., MSSE, Sup, 1988.
National Collegiate Athletic Association,1986,1990.
Prilutsky, B & Zatsiorsky, V., J Biomech, 25-34, 1994
Saito, S. et al., B Hlth Sprts Sci, 5:201-206, 1982.
Zatsiorsky, V etal. , Biomech.VIII-B,1152-1159, 1983.

ACKNOWLEDGEMENTS

US Olympic Committee, Carolina Gym Supply, the USC Biomechanics Research Team, and UCLA Gymnastics.

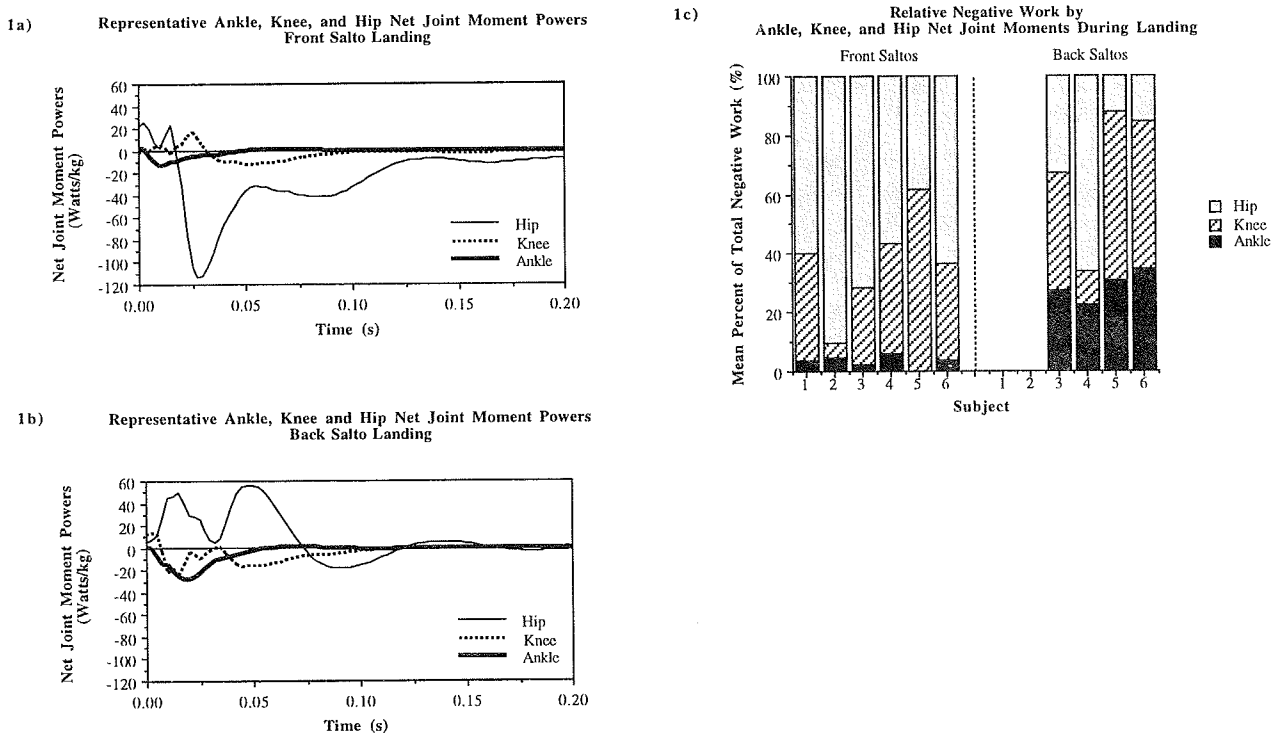

Figure 1. Representative ankle, knee, and hip net joint moment powers for front (a) and back (b) salto landings. (c) Mean percent of total negative work for front and back saltos for each subject. Note: presentation of results only focuses on landings performed without steps or hops.

GOLF SHOE TRACTION: THE EFFECT OF DIFFERENT OUTSOLE SURFACE DESIGNS ON THE STATIC COEFFICIENT OF FRICTION

M.M. Slavin, K.R. Williams
Department of Exercise Science, University of California, Davis, CA 95616

INTRODUCTION

A primary goal of golf shoe outsole design is to minimize the probability of slip between shoe and ground during the downswing. While traction has traditionally been achieved by using relatively long metal spikes, recent designs have included molded projection on the outsole in addition to spikes, and currently there is discussion of replacing traditional spikes with shorter molded polyurethane "spikes" to reduce damage to greens. This study investigated the relative traction characteristics of different golf shoe outsole configurations.

REVIEW AND THEORY

Slip occurs when two surfaces translate with respect to each other in their plane of contact. When the surfaces remain in contact, there are typically two primary factors that affect the force ($F_{s,max}$) that resists shearing translation: (1) the net normal force (N) orthogonal to the plane of contact and (2) the value of a proportionality constant, μ_s, the static coefficient of friction. The equation of equilibrium (when slip is impending) is:

$$F_{s,max} = \mu_s N$$

The surface characteristics of the interface are the primary determinants of $F_{s,max}$.

During a golf swing, the ratio of the shear to vertical force is typically highest during the downswing before ball contact (Williams & Cavanagh, 1983), a time when slip is most likely to occur. As a result of muscle activation, a righthanded golfer applies a relatively large shear force directed generally forward on the left foot and backward on the right foot during the downswing. The ground resists these by applying forces in the opposite direction via the spikes or frictional forces between the ground and outsole. In theory, if this shear force exceeds $F_{s,max}$ for either foot, μ_{actual} exceeds μ_s and a slip occurs. Slip during the swing may adversely affect shot performance.

The purpose of this study was to estimate the static coefficient of friction, μ_s, for different shoe surfaces to evaluate the influence of spike length and outsole design on traction.

PROCEDURES

There were four primary components in the experimental setup (Fig. 1): (1) a Kistler force platform with a shallow tray bolted to the plate in which sod was clamped; (2) a wheeled cart system through which a vertical load could be applied to the shoe with minimal rolling resistance. The normal load was 37 kg (approx. 0.4 typical body weight)

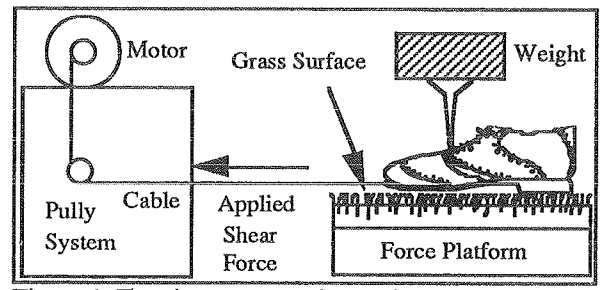

Figure 1. Traction test experimental setup

applied to the forefoot region with the load based on measurements of the shear/vertical force ratio during a typical swing; (3) a high torque, fixed-gear motor that applied a relatively slow but fixed velocity pull through a cable to a bolt mounted in a shoe last placed in and projecting out from the shoe. The pull was applied to the left shoe in a forward direction in the horizontal plane along the long axis of the shoe to mimic the orientation of the force vector seen during the downswing; (4) a data acquisition system to sample the antero-posterior and vertical force outputs. Forces were recorded for 8 seconds at 400 Hz.

The sod and shoe surfaces were characterized as follows:

(A) Sod was a blend of grasses commonly used on driving tees (80% rye/20% blue grass), was mowed low and cut into tray-sized rectangles.

(B) There were nine outsole configurations with various combinations of spike design and length, and with the presence or absence of pyramid structures molded to the outsole surface (Table 1; Fig. 2). A tenth design (condition 8) was a common "spikeless" nubbed outsole golf shoe. The annular and radial designs of the molded spikes were made of polyurethane material.

The maximal static coefficient of friction for each trial was the ratio of horizontal to vertical force at the instant the shoe began to slip (at either peak shear F_s or an inflection point on the F_s-time curve). Eight trials per condition were collected, analyzed, and averaged.

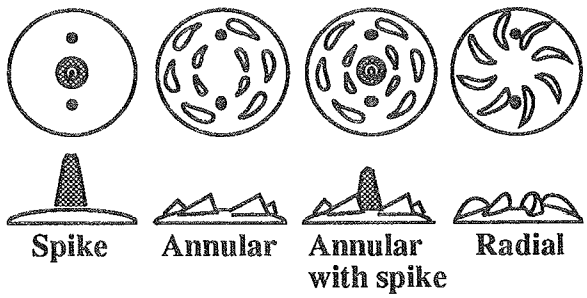

Figure 2: Top and profile views of the removable spikes. Spike length varied.

Condition	Spike length (mm)	Pyramids	Annular	Radial	Spikeless
1	8	Y			
2	8				
3	6	Y			
4	6	Y	Y		
5	4	Y	Y		
6		Y	Y		
7			Y		
8					Y
9				Y	
10					

Table 1: Combinations representing the ten conditions. (shaded indicates presence of feature)

RESULTS

Coefficients of friction ranged from a minimum μ_S = 0.73 for the no-spike, no-pyramid configuration (condition 10) to a maximum μ_S = 1.48 for the 8 mm spike configuration (condition 1; Fig. 3). For the conditions where spike length was identical, the pyramid moldings added 0.06 (4.2%) to the coefficient. With shorter spikes, or the molded spike designs, coefficients were lower. To better convey relative differences in traction between conditions, μ_S values were normalized to the range of difference (Fig. 4).

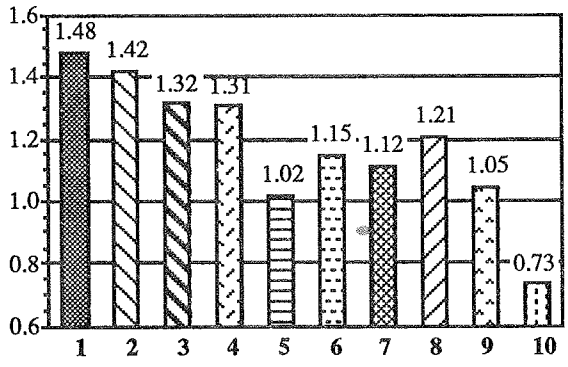

Fig 3: Coefficients of friction for the ten conditions.

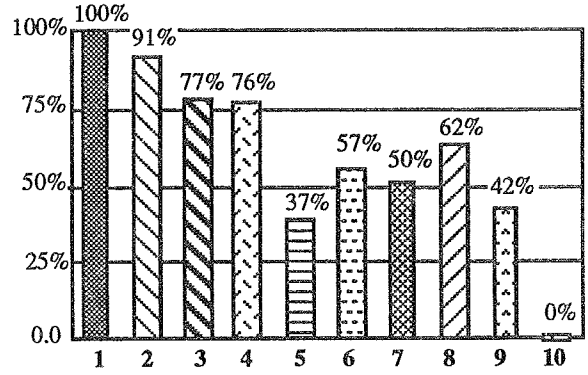

Fig 4: Relative traction for the ten conditions - μ_S values normalized to the range of differences, μ_S= 0.73 (condition 10) at 0% and μ_S= 1.48 at 100%.

A one-way repeated-measures ANOVA with a Bonferroni adjustment to the p=0.005 significance level was used to statistically assess differences. Condition 10, essentially a smooth outsole, was significantly lower than all other conditions, and condition 1, the traditional spike length with pyramids was significantly different from all other conditions except condition 2. Various other significant differences were found but are not described in detail here.

DISCUSSION

The incorporation of spikes, and use of a longer spike significantly improves linear traction on a natural grass surface. Alternative spike designs, alone or in combination with shorter than usual spike lengths, provide greater traction than a flat soled shoe but less traction than when the traditional spikes are used. The low rate of application of force in these tests may be a limitation to the validity of the applying the results to actual golf performance situations.

The performance tradeoff for use of non-traditional or molded spike configurations appears to be a higher probability of slip. If golf swing kinetics demonstrate that the peak horizontal-to-vertical force ratio is consistently below the lower μ_s values in this study, then traditional spikes may not be necessary. Factors such as increased moisture, altered turf conditions, or subject variations in golf swing kinetics may affect the appropriate choice of spike length, spike design, pyramids or other outsole configurations that affect traction.

REFERENCES

Meriam, J.L. *Statics* (pp. 233-235), John Wiley & Sons, 1971.

Williams, K.R. and P. Cavanagh. *Med. Sci. Sports Exerc.*, 15(3), 247-255, 1983.

ACKNOWLEDGEMENTS

Supported in part by a grant from Etonic, Inc.

AN ANALYSIS OF HIP JOINT LOADING DURING WALKING, RUNNING, AND SKIING

A.J. van den Bogert, L. Read, and B.M. Nigg
Human Performance Laboratory, University of Calgary, Canada[1]

INTRODUCTION

Total hip replacement (THR) is one of the most frequent and successful surgical operations for a serious disability. In early years the procedure was typically performed on elderly patients but with improvements in materials, geometry and fixation, THRs are commonplace in younger, more active patients. Several researchers have indicated a relationship between high activity levels and increased rates of implant failure, whereas others have found that low impact activity did not increase the risk of loosening. It is generally recommended that patients do not participate in high-impact activities such as running, but there is controversial opinion as to whether patients should participate in other activities such as cross-country and alpine skiing.

It is the purpose of the present study to quantify hip joint loading during walking, running, cross-country and alpine skiing. Since walking is typically recommended as a "safe" activity for a THR patient, although loosening and failure still occurs over time, and running an "unsafe" activity, the loading conditions of the various skiing activities are compared to walking and running. This information can be used to make recommendations to patients with reference to safe and unsafe activities and to provide the loading conditions for future mechanical testing of hip joint prosthetic components and fixation methods.

REVIEW AND THEORY

Data on hip joint loading has previously been collected using two different methods: direct measurement using an instrumented prosthesis (Davy et al., 1988) and inverse dynamics analysis (Paul, 1971). The first technique has only been applied in a small number of elderly patients, precluding its use for analyzing skiing. The second method typically relies on accurate measurement of forces and movement in three dimensions, which becomes difficult outside a laboratory environment, especially when a large field of view is required. For the purpose of this study, an inverse dynamics analysis method was developed which uses multiple accelerometers attached to the upper body. As described by Kane et al. (1974), accelerometer data can be used to determine the acceleration at the center of mass (CM), angular acceleration, and angular velocity of a rigid body. These variables, combined with inertial properties of the head-arms-trunk (HAT) segment, can subsequently be used to calculate a total force and moment vector, expressed in a segment-fixed coordinate system, from the 3-D equations of motion for a rigid body. Assuming single support, i.e. force and moment exist in only one hip joint, these loads can be attributed to joint and muscle forces acting across the joint.

PROCEDURES

Nine male subjects participated in the study. All subjects had normal, healthy hip joints and were intermediate to expert skiers. Four triaxial accelerometers (ENTRAN EGAX-*-10) were attached to a semi-rigid frame which could be tightly strapped to the upper body. The twelve accelerometer signals were sampled at 300 Hz by a portable data logger (Tattletale 6F, Onset Computer Corp., North Falmouth MA) carried in a pack around the waist. Total mass of the entire system was 1.5 kg. Each subject performed four activities: walking, running, alpine skiing (four conditions) and cross-country skiing (classic and skating technique). In a separate 'calibration' session, the position and orientation of each accelerometer with respect to an upper body coordinate system were measured while standing, using a 3-D video system (Motion Analysis Corp.). At the same time,the location of the CM and of the left hip joint center were obtained from coordinates of markers attached to anatomical landmarks.

Acceleration at CM, angular acceleration, and angular velocity were determined from the accelerometer data in each sample of movement data using a non-linear least-squares method, and the 3-D equations of motion yielded the resultant force and moment vector at the hip joint. By assuming that muscle forces and joint contact force act on the pelvis in opposite directions, joint contact force was estimated from the magnitude of force and moment, according to:

$$F_{joint} = F_{mag} + \frac{M_{mag}}{d} \quad , \qquad (1)$$

where d is an effective muscle moment arm which was estimated from literature data, yielding different values for each activity, depending on the range of hip flexion angles and the major component of the resultant joint moment. After low-pass filtering (20 Hz), the 3-D force and moment vectors were quantified at the time of peak force magnitude in 6-10 loading cycles of each subject in each of the experimental conditions. The peak moment magnitude typically occured simultaneously.

RESULTS

Figure 1 shows a typical result for alpine skiing, without low-pass filtering. The loading cycles of the left and right limb (right and left turns, respectively) could be clearly identified from the negative and positive phases in the medio-lateral force component F_x. A gradual build-up of force and moment can be observed during the turn, after which the load is quickly transferred to the other limb. The force acting on the upper body is oriented lateral, superior, and posterior in the upper body coordinate system, with approximately equal components in each of these three directions. The moment is mainly an extensor moment, with minor contributions from external rotators and adductors.

Results from the peak loading analysis are shown in Table 1. From the four alpine skiing activities, only the extreme loading conditions are shown: long radius turns on a flat slope and short radius turns on a steep slope. The direction of the

1. E-mail: bogert@acs.ucalgary.ca

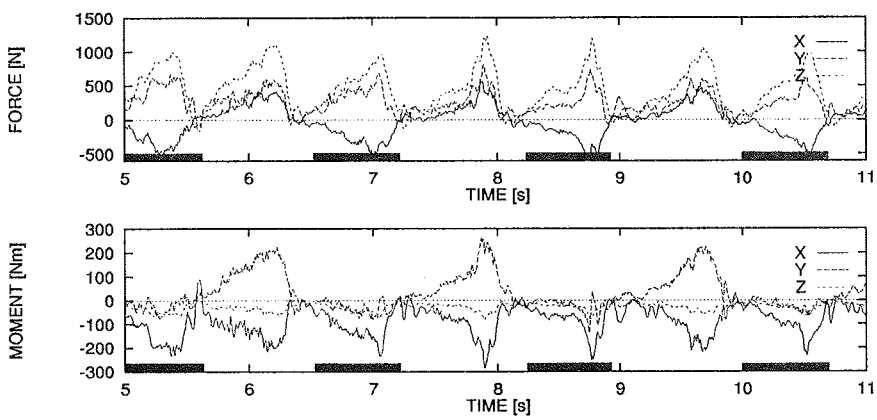

Figure 1: Resultant force and moment at the left hip joint during alpine skiing. The loads are expressed with respect to an upper-body coordinate system. Positive X,Y,Z force compoments represent lateral, posterior, and superior directions respectively. Positive X,Y,Z moment components represent flexor, abductor, and internal rotator moments, respectively. Results for the Y-moment (ab-adduction) are valid for the right turns only, indicated by black bars, when the forces on the right limb can be neglected.

resultant force vector (not shown in the table) during walkin-running was mainly along the Z (inferior-superior) axis of the upper body, while alpine skiing and cross-country skating exhibited large components in medio-lateral and anterior-posterior directions, as illustrated in Figure 1. Specifically, the F_x was already 6 times larger during the easiest alpine skiing condition than during running. Considering only the magnitude of joint contact force, skiing activities can be classified between walking and running, with the exception of the most dynamic alpine skiing activity where the large extensor moment led to a high contact force. Running was the only activity where impact loading was observed; in skiing the increase of force always occurred gradually.

DISCUSSION

The accelerometer system with portable data logger provided a convenient method for collecting data on hip joint loading during various activities. Rigid body kinematics and dynamics were used to obtain resultant joint force and moment from twelve accelerometer signals. The HAT segment was assumed to be rigid, thus neglecting arm movement and non-rigidity of the trunk. Errors due to these assumptions were estimated to be less than 5%. More error was introduced by the assumption that no load was transmitted by the contralateral hip joint. During gait and cross-country skiing, the contralateral limb exerts a mainly downward force, leading to a systematic underestimation (15-20%) of joint force by our method. During alpine skiing, this effect depends on the technique. The subjects were instructed to lift their inside leg during the turn, leading to similar systematic errors as during gait. However, they may have had 10-15% of the total force on the inside ski, possibly leading to overestimation of joint loading on the outside (downhill) hip.

Joint contact forces for walking (Table 1) were comparable to those reported from direct measurements (e.g. Davy et al., 1988). Previous model studies (e.g. Paul, 1971) have typically resulted in much higher values, possibly due to the use of straight-line muscle models which tend to give low moment arms (Brand et al., 1988). The calculation of joint contact force from the resultant force and moment according to equation (1) assumes that no antagonistic activity exists. This is a common assumption for analysis of walking. However, large hip flexor EMG activity has been reported during alpine skiing, in spite of a resultant extensor moment. For the present results, this means that the joint contact force F_{joint} during alpine skiing is systematically underestimated, perhaps by as much as 50%. Literature EMG data on running and cross-country skiing indicate an intermediate level of co-contraction.

The results of this study indicate that cross-country skiing and alpine skiing under controlled conditions are relatively safe activities for a hip prosthetic patient. More dynamic skiing movements and steep slopes should not be recommended. However, it should be noted that, compared to walking and running, large anterior-posterior and medio-lateral force components were observed during all alpine skiing conditions as well as cross-country skating. Such forces may contribute to a torsional load on the prosthetic stem and contribute to the risk of early loosening (Nunn et al., 1989).

REFERENCES

Brand, RA et al., *Proc 35th Ann Meet Orthop Res Soc*, Las Vegas, p. 96.
Davy DT et al., *J Bone Jt Surg 70-A:* 45-50, 1988.
Kane, TR et al., *Biomechanics IV*, University Park Press, Baltimore, pp. 284-290, 1974.
Nunn D et al., *J Bone Jt Surg 71-B:* 452-455, 1989
Paul JP, *Exper Mech 11:* 121-125, 1971.

ACKNOWLEDGMENTS

This study was financially supported by the Swiss Society for Orthopaedics (SGO) and NSERC of Canada...

Table 1: Peak magnitudes of resultant force and moment at the hip joint (average and standard deviation of 9 subjects). Estimated joint contact force is expressed relative to body weight.

Activity/Condition	F_{mag} (N)	M_{mag} (N m)	F_{joint} (BW)
Walking (1.5 m/s)	582±72	72±11	2.5
Running (3.5 m/s)	1203±50	154±19	5.2
Alpine skiing (short, steep)	1196±235	267±62	7.7
Alpine skiing (long, flat)	720±84	139±27	4.1
Cross-Country (diagonal)	751±232	135±48	4.0
Cross-country (skating)	843±133	156±24	4.6

WITHIN-SUBJECT STABILITY OF MULTIPLE REGRESSION MODELS USED TO IDENTIFY LOWER EXTREMITY LANDING STRATEGIES

Philip K. Schot & Michael J. Decker
Department of Human Kinetics, University of Wisconsin-Milwaukee, Milwaukee WI 53201

INTRODUCTION

Nine healthy physically active subjects performed landings from which independent concurrent bilateral kinetic and kinematic records were acquired. Testing involved 25 trials per subject on each of three consecutive days. Multiple regression models were generated using select kinematic measures to predict forefoot and rearfoot impact force magnitudes. The terms entering the models were examined to identify strategies by which joint motion features combined to mediate the impact forces. The concordance of elements combined in a strategy between individual and group models and within subjects between sessions was analyzed.

REVIEW

Biomechanical evaluations tend to generate huge quantities of information. Additional complexity and information load is attributable to the concept of motor equivalence. Even under rigorously controlled lab environments, individuals rarely perform a given task identically. Further, subjects may also utilize idiosyncratic movement strategies. If biomechanics seeks to understand the basic mechanisms of movement, all strategies utilized in solving a particular movement task are deserving of attention for what potential insights might be acquired.

Very subtle, yet critical, aspects of human movement are contained in these mountains of data. A tool is needed that can sift through the less germane material and allow researchers to focus interpretation on the most relevant features. Results from multiple regression models developed for group and single subject data sets have been interpreted to demonstrate that individuals utilize different strategies under a variety of landing conditions (Dufek, 1988; James, 1991). Multiple regression techniques have been used more often to identify critical aspects of technique in groups, primarily to target areas for improvement or optimizing technique, rather than for the purpose of identifying individual strategies of combining joint actions in a particular task.

Projects utilizing multiple regression to identify individual strategies (Dufek, 1988; James, 1991) generally have found every subject to employ a unique strategy. Further, few individuals demonstrate strategies similar to that of the group. This interpretation of the single subject statistical models seems logical, but it has not been shown that this technique identifies stable consistently composed strategies within individuals. This technique offers excellent potential, but for confident application, the internal consistency feature should be evaluated. The purpose of this study was to apply the multiple regression technique to data from individuals performing a highly controlled drop landing task on three consecutive days and evaluate the consistency of the strategies thus identified.

PROCEDURES

Nine healthy physically active subjects performed 25 drop landings (0.6 m) in each of three test sessions conducted on consecutive days. Independent concurrent bilateral ground reaction forces (1000 Hz) and sagittal plane kinematics (200 Hz) were sampled for each landing, resulting in 50 "legs" of data captured for each session. Five landmarks on each side of the body were used to define a four segment lower extremity and trunk model. Video coordinate data were digitally filtered (4th order, zero-lag, low-pass, 16 Hz cut-off) prior to computing angular kinematics. Motion derivatives were calculated using standard digital differentiation techniques. The analysis interval boundaries were from 20 ms prior through 100 ms following initial foot contact.

Fifteen kinematic variables (angular position at contact, angular velocity at contact, range of motion post-contact, maximum angular velocity, and maximum angular velocity time for the ankle, knee, and hip joints each) extracted from each landing (for each leg) were used to develop regression models predicting the first (forefoot: F1) and second (rearfoot: F2) impact peaks. Stepwise regression models were generated for the following groups or clusters: 1) the entire study sample using all 1350 landing trials (GRP), 2) the grand model for each individual using the 150 landings acquired from all three sessions (SS3), and 3) single day (50 trial) models for each individual (SS1). All statistical models utilized entry and removal α levels of 0.05 and a tolerance of 0.5. The tolerance level was selected to address the multicollinearity inherent among the predictor variables. Model significance was also evaluated at the $p < .05$ level.

Contrasts for the agreement of the various models generated were organized as follows: 1) GRP vs each SS3 and 2) SS3 vs each SS1. The following equation was used to capture the % agreement in the elements composing each model:

$$\% = 100 * \frac{2(\#\text{ terms shared in contrasted models})}{(\#\text{ terms in contrasted models})}$$

RESULTS

The GRP models resulted in better predictions for F2 (55.0% explained variance) than F1 (46.1%). The F2 predictions were better for 8 of the 9 subjects, with the explained variance of F2 being 33% greater than F1 on average.

The SS3 models did not strongly agree with GRP models for either F1 or F2 (35.1 and 33.6% agreement, respectively). As shown in Figure 1, only one subject demonstrated more than 60% agreement with the group (S7 for F1).

The within subject model consistencies were varied. Figures 2 and 3 present the SS1 vs SS3 agreements. F2 models were more stable than those for F1 (61.7 vs 28.5%, respectively). Among the 27 SS1 vs SS3 contrasts conducted (each for F1 and F2), 41% of the F1 SS1 models showed no agreement while only 7% of the F2 SS1 models demonstrated this outcome.

DISCUSSION

The poor F1 and F2 model compatibility between individual vs group model contrasts were similar to those reported previously (Dufek, 1988; James, 1991). If this technique is appropriate, this finding highlights the possibility that conclusions drawn from group designs really are not very generalizable.

The primary assumption in this study was that the subjects would utilize similar landing strategies across test sessions. Subjects were instructed to land normally each day, an implicit approval to employ a "preferred" landing style. Indeed, the foundation of the concept of a "preferred" strategy suggests a durable quality to the biomechanical patterning of an individual over time. In addition, a previous analysis of the bilateral performance features of these subjects (Schot, 1994) demonstrated consistent traits. We thus hypothesized that the within-subject models would demonstrate high agreements among the strategic elements combined to mediate impact forces. Such an observation would support the continued use of the technique.

The results of this aspect of the study are equivocal. The stability of F1 models was quite low (28.5%) and the stability of the F2 models (61.7%) might also be viewed as tenuous. The F1 models explained less variance than those of F2, therefore predictions would be more difficult and less consistent. This is at least partly attributable to the predictor variables used, which were arguably more germane to the F2 phenomenon. It has also been suggested that F2 is more susceptible to movement strategy mediation (Caster, 1990; Schot, 1991) and the results of the GRP models offer some support this interpretation. One subject did demonstrate 100% agreement for all F2 models, yet 2 individuals performed such that there was no agreement between one of the SS1 vs SS3 model contrasts.

Given the equivocal consistency of the within-subject models, there are 3 conclusions to consider at this point. First, the technique may be invalid for reasons not related to standard statistical assumptions and guidelines (ie; the single subject design issues). Second, the kinematic predictors used may have been inadequate; the explained variance from similar studies has been higher than achieved here. Third, perhaps humans really do behave as variably as the models tend to indicate. In light of the perspectives evolving from the fields of chaos theory and non-linear dynamics this interpretation suggests that more work be done to assess the potential of this tool.

REFERENCES

Caster, BL. Master's thesis. Univ. of OR, 1990.
Dufek, JS. Doctoral dissertation. Univ. of OR, 1988.
James, CR. Master's thesis. Univ. of OR, 1991.
Schot, PK. Doctoral dissertation. Univ. of OR, 1991.
Schot, PK. Med.Sci.Sports.Exer., 26:1153-1159, 1994.

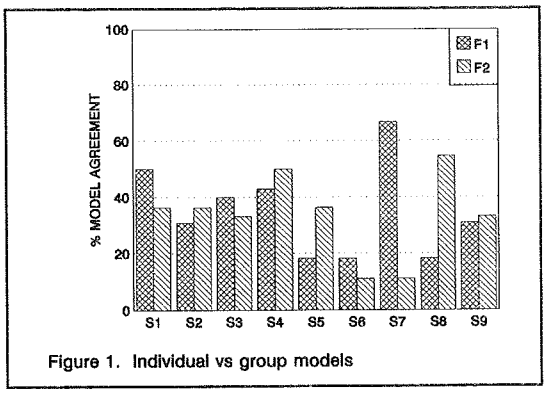

Figure 1. Individual vs group models

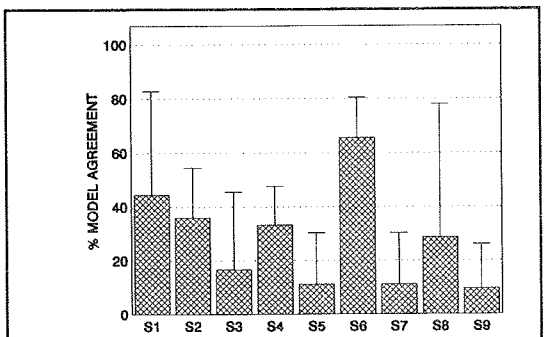

Figure 2. F1 models: average SS3 vs SS1 agreement

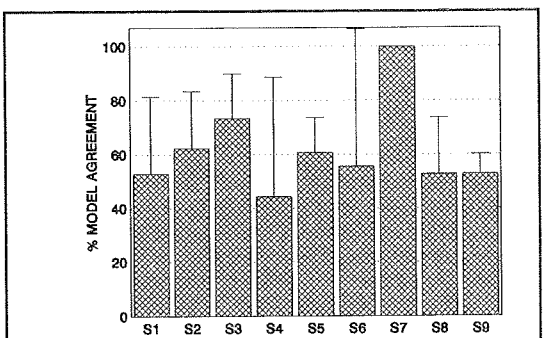

Figure 3. F2 models: average SS3 vs SS1 agreement

Lower Body Mechanics During the Baseball Swing

C. Welch, S. Banks, F. Cook
The Orthopaedic Research Laboratory, W. Palm Beach, FL 33401

INTRODUCTION

Very little scientific effort has been spent developing training and rehabilitation protocols specific to the hitter. In order to successfully address the needs of the hitter, the biomechanics of the baseball swing must be studied and an understanding of physiological and mechanical interaction developed. This study uses three-dimensional kinematic and kinetic data to define and quantify lower body mechanics during the baseball swing.

REVIEW AND THEORY

Movement during the baseball swing is defined by both linear and rotational components (Schmidt M. et al. 1994, DeRenne C. 1993). The linear component is defined by forward movement toward the on-coming pitch. The rotational component is defined by the movement of body segments around the axis of the trunk. Researchers (Messier S.P. et al. 1985, Williams K.R. et al. 1983) have shown that the application of force by the feet to the ground promotes both linear and rotational movement during the swing motion. Other researchers (DeRenne C. 1993, Riley P.O. et al. 1991) have shown the movement of the center of mass of the body can be indicative of forward linear motion. The objective of this study is to utilize biomechanical measurement techniques and hitting theory (Lau C. et al. 1986, Williams T. et al. 1986) to define and quantify both the linear and rotational components of lower body mechanics during the baseball swing.

PROCEDURES

Subjects: Twenty nine professional baseball players were studied. The mean height was 179cm and the mean weight was 85kg. All the subjects batted right handed. At the time of testing the subjects' level of play ranged from minor league (A,AA,AAA) to major league. The mean batting average was .246 and the mean number of 'at bats' was 246.

Data Collection: Three-dimensional motion data were collected using a video based motion collection system (Motion Analysis Corporation, Inc.). The subject was filmed using six cameras at a rate of 200 frames per second. Three-dimensional ground reaction forces were collected using two force plates (Advanced Mechanical Technology, Inc.). Each force plate collected data at a rate of 1000 samples per second. The motion and force collection equipment was electronically synchronized for simultaneous data collection.

Testing: Each subject was tested at an indoor biomechanics facility. The subject was fully informed of testing procedures and asked to read and sign an informed consent prior to data collection. 24 reflective markers were applied to the subject, bat and ball. Anatomical measurements were taken including height and weight. The subject was then allowed to warm up in the data collection area. For the purpose of eliminating the possibility of mechanical variation and adjustment to a pitched or moving ball, the hitter was asked to hit baseballs placed on a standard batting tee. While the hitter warmed up, he was asked to find a comfortable tee position from which line drive hits could be directed toward the middle of the field. During data collection, the researchers, subject and coach observed each hit for solid bat/ball contact, 100% effort and line drive trajectory directed toward the middle of the field. Data from the first three hits that met the fore mentioned criteria were saved.

Calculation: The three-dimensional location of each of the 24 reflective markers was calculated with respect to a global right handed orthogonal coordinate system (global reference frame) (Figure 1). Marker position was mathematically determined based on data collected by each of the six cameras. Kinematic data was then computed using vector mathematics and local coordinate systems which were constructed using the reflective markers placed on the body. All data were filtered using a fourth-order, low pass Butterworth filter with a resultant cut off frequency of 13.3 Hz (Winter D.A. 1979).

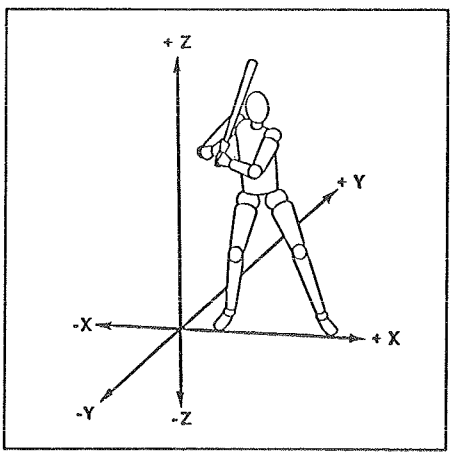

Figure 1: Global reference frame.

Parameters of measurement included stride (length and direction) and the orientation of the front foot. The whole body center of mass and the center of pressure between the feet were determined and their movement relative to each other calculated. The three-dimensional forces applied by the feet to the ground were measured, normalized to body weight and presented with respect to the global reference frame. Compressive forces were applied in the negative Z direction and shear forces were applied in the X and Y direction. The rotation of the hips (as a linked segment) around the axis of the trunk was also measured with respect to the global reference frame.

RESULTS

(Data presented in the results are mean values)

As the hitter began the motion of the swing, he lifted his front foot causing weight to be shifted toward the back foot. The total amount of force applied by the back foot to the ground

was 102%BW (percent of body weight). Shear forces of 19%BW and 2%BW were applied to the ground by the back foot in the global negative X and positive Y directions respectively. At the same time, the center of pressure between the two feet moved toward the back foot to a position 22cm behind the whole body center of mass in the global X direction.

The hitter continued the motion of the swing, by striding forward with the front foot. As the front foot came into contact with the ground, weight was shifted forward. Stride length was 84cm and stride direction was 12° closed with respect to the global positive X direction. Front foot position was 64° closed with respect to the global positive X direction. The total force applied by the back foot to the ground was 73%BW and the front foot was 8%BW. Shear forces were applied by the back foot in the global negative X and positive Y directions. Shear forces were applied by the front foot in the global positive X direction and negative Y direction. The hips were closed 23° with respect to the global positive X direction.

At ball contact, the center of pressure had moved forward in the global positive X direction toward the front foot to a position 27cm ahead of the center of mass. The total forces applied by the back foot and the front foot were 12%BW and 98%BW respectively. The hips were open 76° with respect to the global positive X direction.

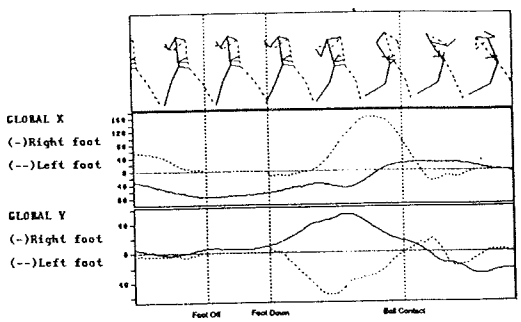

Figure 2: Typical shear force application.

DISCUSSION

General mechanics: As the hitter began the motion of the baseball swing, he 'loaded' both the linear component and the rotational component. 'Loading' the linear component consisted of transferring weight to the back foot. This caused the center of pressure to shift to the rear foot, a position behind the center of mass and thus created a dynamic situation which facilitated forward linear movement. 'Loading' the rotational component consisted of increasing the shear forces applied by the back foot in the global negative X direction and positive Y direction. This created a ground reaction force which facilitated the counter clockwise rotation of the hips.

As the hitter continued the motion of the swing, the front foot made contact with the ground ending the stride. Weight was transferred forward resulting in the forward linear movement of the center of pressure in the global positive X direction from the back foot toward the front foot. Shear force applied by the front foot increased in the global positive X direction and negative Y direction. Ground reaction to the shear forces applied by both back and front feet created a force couple at the hips. The forward linear movement of the hitter combined with the rotational movement of the hips provided a foundation for generating bat speed during the swing.

Mechanical variation: It was observed that different mechanical strategies were used by hitters resulting in a spectrum of interaction between the linear and rotational components of lower body mechanics.

At one end of the spectrum, the hitter emphasized the linear component. As the front foot made contact with the ground a forward weight transfer caused the center of pressure to gradually move to the front foot ahead of the center of mass of the body. At that point, the front foot began to apply shear forces to the ground, which facilitated the rotational acceleration of the hips. The hitter moved in a linear fashion driving his center of mass toward the position of the center of pressure at the front foot. As the hitter continued forward toward his front side, the shear force applied by the rear foot decreased. The force couple generating rotational acceleration at the hips was reduced to primarily the front foot facilitating rotation at the lead hip. The lower body action was then dominated by forward linear motion as the center of mass moved to align itself over the center of pressure at the front foot.

At the opposite end of the spectrum, the hitter emphasized the rotational component. At front foot contact, a rapid weight shift was incorporated causing the center of pressure to quickly move to a position at the front foot. In contrast to the linear hitter, the rotational hitter did not continue forward by driving his center of mass toward the position of the center of pressure, but rather, quickly shifted weight back to the rear foot causing the center of pressure to align directly below the center of mass. In this position, the force couple applied to the hips was enhanced by the combined effect of significant shear force applied by both the rear and front foot. The lower body action was then dominated by the rotational motion of the hips as the application of shear force by both the rear and front foot amplified the force couple generated.

SUMMARY

The data demonstrate a spectrum of lower body mechanics during the baseball swing. The spectrum is defined by variation in interaction between the linear and rotational components of movement. A better understanding of mechanics will allow for more specific and effective training and rehabilitation protocols.

REFERENCES

1.) DeRenne C. High-Tech Hitting: Science vs. Tradition, St. Paul, MN: West Publishing Company, 1993.
2.) Lau C. et al. The Art of Hitting .300, Viking Penguin, 1991.
3.) Messier S.P. et al. Research Quarterly, 56(2): 138-143, 1985.
4.) Riley P.O. et al. J Biomech 24(1):77-85,1991.
5.) Schmidt M. et al. The Mike Schmidt study. Hitting theory, skills, and technique, McGriff and Bell Inc., 1994.
6.) Williams K.R. et al. Med Sci Sports Exerc, 15(3): 247-255, 1983.
7.) Williams T. et al. The Science of Hitting, Simon and Schuster Inc., 1986.
8.) Winter D.A., Biomechanics of Human Movement, John Wiley & Sons, 1979

THREE-DIMENSIONAL KINEMATIC AND KINETIC ANALYSIS OF THE TENNIS SERVE

G. Noffal[1], B. Elliott[1], R. Marshall[1], G. Legnani[2]

[1]Department of Human Movement, The University of Western Australia, Nedlands, W.A. 6009, AUSTRALIA
[2]University of Brescia, Mech. Eng. Dept., Via Branze, 20123, Brescia, ITALY

INTRODUCTION

A powerful first serve has become a valuable and popular weapon in tennis at the expense of producing a greater number of injuries to the contemporary player. In an attempt to serve with more power and precision many players have developed symptoms in the back, shoulder and particularly the medial elbow regions. The tennis serve is truly a three-dimensional skill where many body segments move in mani of their degrees of freedom (d.o.f.) in an attempt to develop greater racket velocity before impact.

This study describes the anatomical rotations of the striking limb, and it calculates the resultant joint moments around elbow joint during a hard and flat first serve. It uses a three-dimensional inverse dynamic model of the upper extremity, consisting of three linked segments: upper arm, forearm, and hand-racket segment. It is hypothesized that medial elbow injuries common to elite players are a consequence of high medial stress seen in the form of varus moments about the elbow.

REVIEW AND THEORY

The main function of the elbow is flexing and extending and this primary task is compromised when an athlete attempts to throw (or hit with a racket) a ball for maximum speed. When the upper arm externally rotates to a maximum prior to the acceleration phase the medial elbow is placed into a position of stress. This can be seen in sports such as baseball, javelin throwing and tennis serving (Harding, 1992).

Most studies that have investigated varus/valgus moments at the elbow have been concerned with baseball pitching. Werner et al. (1993) reported a varus torque of 120 Nm just prior to maximal external rotation (MER) during baseball pitching which decreased in magnitude to approximately 30 Nm at ball release and then became a valgus torque in the follow-through phase. Feltner and Dapena (1986) reported a peak varus torque of 100 Nm $\pm$ 20 Nm just prior to MER (.047 s before release). Although the magnitude of the varus torque decreased it remained as a varus torque throughout the remainder of the pitch. Campbell et al. (1994), reported that an elbow valgus moment was evident throughout the pitch. At MER professional pitchers experienced a valgus moment of 2.2 (moments were normalized by body weight and height) compared to 1.3 for little leaguers. At ball release little leaguers demonstrated a greater valgus moment (1.5) compared to their professional counterparts (0.6). It is possible that this group of authors reported on the moments causing the stress (valgus) and not on the moments resisting the stress (varus). Rash (1994) examined the throwing motion of quarterbacks and introduced two terms referring to the stress placed on the elbow by the throwing of the football. Elbow medial deviation moment and elbow medial deviation loading rate were evident throughout the movement. Bahamonde (1989) reported a large varus torque was present throughout the forward swing in the tennis serve. Maximum value of 74.2 Nm at impact and 43.3 Nm at MER were given.

PROCEDURES

Subjects

Twelve right-handed elite male tennis players were recruited to participate in the study. Subjects selected were deemed by professional coaches to have the best service action in the state. Upon arrival subjects were fitted with lightweight markers, attached to the distal forearm and hand (34 grams and 49 grams respectively), that enhanced the rotational characteristics of the upper limb. Subjects were then permitted as much time as needed prior to the filming to complete their warm-up procedures and become familiar with the upper limb attachments.

Filming

Filming was conducted on a plexipave tennis court and a DLT method for 3-D space reconstruction from 2-D images was used. Three 16mm Photosonics 1PL high speed cameras were used to film a reference structure containing markers of known coordinates in space encompassing the field of movement of the service action. This structure was then removed and the subject was filmed in the same area with identical camera positions. The cameras operated at 200 frames per second (exposure time 1/2400 s) to film each subject hitting flat serves into a 1 meter square area on the service box closest to the center of the court. An electric conic shaped clock with .02 second divisions was positioned in the field of view of all three cameras to enable the speed of the film to be calibrated.

Analysis

The 2-D images of both the reference structure (19 points and dimensions of approximately 2.5 m x 4.0 m x 3.6 m) and subject were digitized, and the unknown 3-D coordinates of each of the subject's markers were determined using a modified version of the Direct Linear Transformation algorithm which allowed the user to

identify hidden points in the movement and a choice of camera combinations. The coordinates of the markers were smoothed using the optimally regularized quintic spline subroutine GCVSPL. The joint angles were obtained using vector calculations and the angular conventions used in Sakurai et al. (1994) were followed. Joint forces and torques were derived using a dynamic model described in Legnani et al. (1993).

RESULTS

At impact the center of the racket-head had a mean velocity of 31.0 ms^{-1} in the direction of the ball. Some of the results are presented in Table 1.

	Int/Ext rot	Abd/add	Hor. Flex/Ext	Elbow Flex/Ext	Pro/Sup	Wrist Flex/Ext
Max	-150.1	88.0	46.1	-124.3	-23.7	-63.0
s.d.	19.3	4.6	6.7	13.0	10.7	10.6
time	0.949	0.907	0.984	0.796	0.861	0.913
s.d.	0.029	0.074	0.026	0.056	0.022	0.018
Impact	-125.2	73.2	42.4	-31.7	36.3	-6.4
s.d.	13.8	9.1	9.1	6.1	15.6	10.7

Table 1: Mean Maximum and impact angles of the upper limb during a tennis serve (degrees) (Impact = 1.00s).

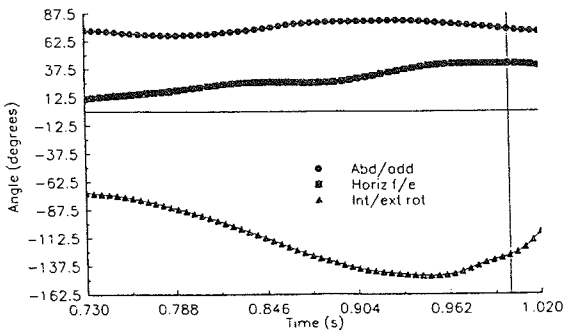

Figure 2: Upper arm angular displacements.

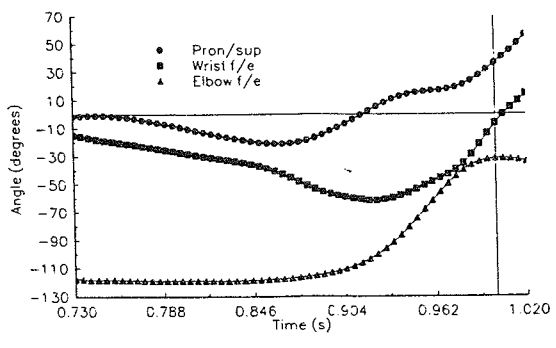

Figure 3: Elbow, forearm and wrist angular displacements.

The tennis serve is characterized by external rotation of the upper arm, and flexing of the elbow in the backswing position. In the acceleration phase the upper arm rapidly moves towards inward rotation, the elbow extends, the forearm pronates, and the wrist flexes. It is speculated that the rotation of the trunk and the external rotation of the upper arm creates an inertial lag of the racket, hand and forearm segments creating a high varus moment at the elbow. This moment reached its mean maximum peak of 103.1 $\pm$ 22.8 Nm at 0.954 $\pm$ 0.012 s which was near the time of MER angle of the upper arm (Figure 1).

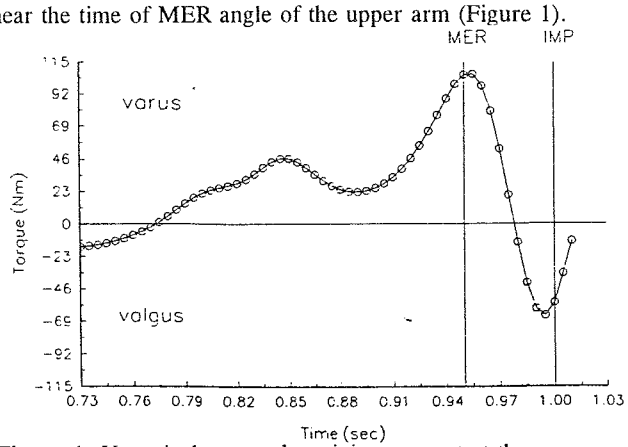

Figure 1: Varus/valgus resultant joint moment at the elbow.

DISCUSSION

This investigation concurs with kinematic information reported in similar three-dimensional studies of the tennis serve. Furthermore, it provides new rotational kinematics, and kinetics of the elbow joint. The varus moment reported in this investigation is higher than that found in the only other previous study of the tennis serve and it is comparable in magnitude to studies of the pitching motion in baseball. This study has also established a base for the modelling of the elbow joint as it relates to loading in the anterior medial collateral ligament. This ligament has been found to be the primary constraint to valgus loading at the elbow (Morrey et al., 1991). The elbow model will investigate not only the dynamic loading of the ligament through the tennis serve, but it will also allow the author to modify the individual d.o.f. involved in any three-dimensional movement and quantify the changes in structure loading as a result of a single or multiple alteration.

REFERENCES

Bahamonde, R. XII Int. Soc. of Biom., Abs. #99, 1989.
Campbell, K. Biom. in Sports XI, ISBS, 23-24, 1994.
Feltner, M. et al. Int. J. Sp. Biom., 2, 235-259, 1986.
Harding, W. Phys. and Sportsmedicine, 20, 65-74, 1992.
Legnani, G. et al. IV Int. Sym. Comp. Sim., Paris 93.
Morrey et al. Clin. Orth. Rel. Res.,265, 187-195, 1991.
Rash, G. Med. Sci. Sp. Ex., 5, S176, 1994.
Sakurai, S. et al. J Appl. Biom., 9, 47-65, 1993.
Werner, S. et al. J Orth. Sp. Phys. Ther., 17, 274-278, 1993.

Lower Extremity Kinematic Comparisons between Forefoot and Rearfoot Strikers

I McClay and K Manal

Motion Analysis Laboratory, University of Delaware, Newark, DE 19716

INTRODUCTION

The manner in which the foot strikes the ground in running is likely to influence the mechanics of the lower extremity during support. There are currently no studies reporting the differences in lower extremity kinematics between rearfoot strikers (RFS) and forefoot strikers (FFS). This study was undertaken with this purpose in mind. The project is currently underway with the results presented here based upon the subjects that have been collected to date. 3-D kinematics were collected on 10 RFS and 10 FFS who were classified based upon their strike pattern. Significant differences were found in both rearfoot and knee movements suggesting that lower extremity kinematics are influenced by strike pattern. It is hoped that these results will begin to generate normative data for runners with a FFS pattern.

REVIEW AND THEORY

Approximately 80% of distance runners strike the ground with the rear portion of their feet (Kerr et al., 1983). The remaining 20% are either midfoot or forefoot strikers. This is likely to result in a different pattern of motion of the foot and lower extremity during support. For example, a forefoot strike pattern places the foot into a more plantarflexed position. It is hypothesized that this will result in a more supinated posture at footstrike (FS) and decreased peak pronation values during support. It is also hypothesized that the knee will consequently be in greater knee flexion at heelstrike to compensate for the plantarflexion at the ankle. However, none of the studies reporting lower extremity kinematics during running have incorporated forefoot strikers. Therefore, normative kinematics for this group of runners has not been established. Without this reference, it is difficult to determine when the mechanics of a person with a forefoot strike pattern is abnormal. As clinicians, this is important to understand as the focus of the treatment may be directed at correcting the mechanics.

Therefore the purpose of this research is to compare the lower extremity kinematics of runners with a forefoot strike pattern to those with a rearfoot strike pattern.

PROCEDURES

20 recreational runners, previously screened for their strike pattern were used in this study. 10 subjects were assigned to the rearfoot strike group (RFS) or the forefoot (FFS) group based upon a visual screen of their strike pattern while running on a treadmill. To be placed in the FFS group, initial contact had to be made in the forefoot region (with heel off the ground at FS). In this group, the foot with the most anterior strike pattern was used. In the RFS group, the foot with normal peak eversion values was used, as this group also served as a control group for comparison to a group of pronators.

Four retroreflective markers were affixed to a velcro-backed polyform shell and attached to the thigh via a neoprene wrap. A similar marker set was attached to the shank. Three markers were attached directly to the heel counter of the shoe: two were placed along the longitudinal axis of the heel and one was placed on the lateral border of the heel. These markers were used to track the motion of the three segments (figure 1). Additionally, markers were placed over the greater trochanter, the medial and lateral femoral condyles, the medial and lateral malleoli, and the head of the first and fifth metatarsals. These markers were used to determine the anatomical coordinate systems in which the motion would be described. After a standing calibration trial was collected and the anatomical transformations calculated, these markers were removed.

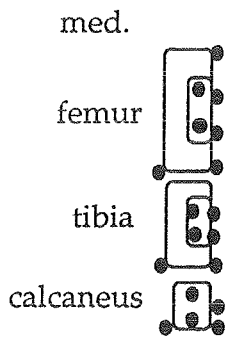

Figure 1. A posterior view of the marker placement on a right lower extremity.

Subjects then ran along a 75 ft runway at a speed of 3.35 m/s. Data were sampled at 120 hz with a 5 camera VICON (Oxford Metrics, UK) Motion Analysis System. Three-dimensional kinematics (position and velocity) were calculated and averaged over 5 trials using MOVE3D software (NIH Biomechanics Laboratory). Angles were computed in a joint coordinate system (Grood and Suntay, 1983) Excursions were computed as seen in figure 2. Coupling parameters such as the ratio of rearfoot eversion to tibial internal rotation (EV/TIR) and timing between peak rearfoot EV and knee flexion (FL) and internal rotation (IR) were also calculated. Independent t-tests were run for the variables of interest and considered significant at the adjusted alpha level of 0.015.

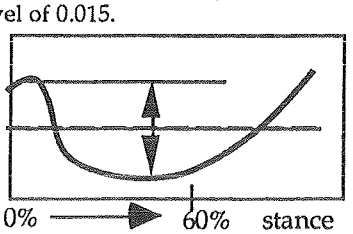

Figure 2. Calculation of excursion values.

RESULTS

Table 1 Ankle Kinematics Results (mean, sd)

	RFS	FFS
Footstrike position		
sagittal (°)	7.6 (5.3)	-4.2 (6.1)*
frontal (°)	2.5 (2.8)	6.1 (2.9)*
transverse (°)	-1.6 (7.1)	3.9 (5.7)
Peak values		
dorsiflexion (°)	25.9 (2.7)	22.3 (4.3)
eversion (°)	-9.2 (2.5)	-7.3 (3.5)
abduction (°)	-8.7 (6.0)	-6.0 (5.2)
Excursions		
dorsiflexion (°)	22.0 (2.9)	26.9 (4.8)*
eversion (°)	-11.5 (1.6)	-13.3 (4.0)
abduction (°)	-7.0 (3.4)	-9.9 (2.7)
Velocities		
dorsiflexion (°/s)	316.2 (32.9)	439.0 (85.5)*
eversion (°/s)	-243.2 (56.6)	-345.6 (97.5)*

* $p<0.015$
df., inv., and add. are positive

Table 2 Knee Kinematics Results (mean, sd)

	RFS	FFS
Footstrike position		
sagittal (°)	-14.0 (5.7)	-22.7 (5.1) *
frontal (°)	0.7 (5.7)	2.6 (3.8)
transverse (°)	-10.9 (5.6)	-17.5 (4.1)*
Peak values		
flexion (°)	-42.9 (6.3)	-44.8(5.8)
adduction (°)	5.0 (4.9)	5.2 (4.1)
int. rot. (°)	1.6 (6.5)	-2.9 (4.2)
Excursions		
flexion (°)	-28.9 (2.3)	-22.0 (3.7)*
int. rot. (°)	12.6 (2.5)	14.5 (4.1)
Velocities		
flexion (°/s)	-480.7 (43.7)	-440.7 (81.9)
int. rot. (°/s)	177.4 (36.7)	247.5 (93.3) *
Coupling		
EV/TIR (ratio)	1.43 (0.73)	1.29(0.55)
EV-FL (ms)	3.9 (8.4)	-5.4 (4.3)*
EV-KIR (ms)	-7.4 (11.2)	-18.6 (8.8) *

* $p<0.02$
ext., add. and int. rot. are positive

DISCUSSION

As expected, the FFS group landed in a plantarflexed position, while the RFS group landed in dorsiflexion. As this position places the subtalar joint into a supinated posture, significantly greater inversion was also seen at FS. They also exhibited greater adduction (the third component of supination), however this was not statistically significant. It was also expected that the RFS would achieve greater pronation. In fact, mean peak values for the three components of pronation (dorsiflexion, eversion and abduction) were greater in this group, however, not significantly so. Dorsiflexion excursion was significantly greater in the FFS largely due to the difference in footstrike position. Another interesting finding was the greater peak dorsiflexion and eversion velocities seen in the FFS group. This is likely to place greater strain rates on the muscles controlling these movements. For example, peak dorsiflexion velocities occur early in the contact phase. During this time, the FFS are eccentrically controlling plantarflexion with the gastroc-soleus. Overuse of this mechanism could potentially lead to an achilles tendinitis.

A plantarflexed position of the ankle at FS functionally lengthens the lower extremity which needs to be compensated for in some way. The results suggest that runners with a FFS pattern compensate, at least in part, through increased knee flexion. internal rotation is typically associated with this motion. However, during gait, knee flexion is normally occurring with rearfoot pronation. In the FFS group, the knee flexion was coupled with rearfoot supination at FS. Supination induces an external rotation of the tibia and may be responsible for the greater external rotation seen in the FFS group at FS, despite the greater knee flexion exhibited. Peak values were similar in all three angular components. Knee flexion excursion was significantly lower in the FFS group as a result of the greater knee flexion seen at FS. The mean internal rotation excursion was greater in the FFS group. This would be expected due to the greater externally rotated posture seen at FS. However, this difference was not significant. Although dorsiflexion velocities were greater in the FFS group, knee flexion velocities were remarkably similar. The trend towards greater internal rotation velocity may be associated with the greater eversion velocity seen in the rearfoot.

Strike pattern did appear to influence the coupling between the foot and knee. Although the relative excursion of rearfoot eversion to tibial internal rotation (EV/TIR) was similar between the two groups, the timing of peak values of EV, KIR (knee internal rotation) and FL was significantly different. It has been suggested that normal synchrony involves rearfoot eversion and knee flexion and internal rotation occurring together in the first half of stance with these motions reversing themselves in the last half and peak values occurring at approximately the same time (Bates et al, 1979) The FFS group shows a clearly greater discrepancy of timing between these motions, especially apparent in the delay in peak internal rotation. This may have implications for injury and warrants further study.

These results have begun to shed light on the influence of strike index on lower extremity mechanics. As more subjects are entered into this ongoing study, further significant findings may become apparent.

ACKNOWLEDGMENTS

The authors would like to acknowledge the Whitaker Foundation for their support of this work.

REFERENCES

Bates, BT et al. MSSE 11(4):328-331 , 1979.
Grood,ES &Suntay, W.J Biom. Eng. 105,136-144. 1983
Kerr, BA et al, Biomechanical Aspects of Sports Shoes and Playing Surfaces, 1983
Lundberg, A, Acta. Ortho. Scandinavica, 1989

Lower Extremity Kinetic Comparisons between Forefoot and Rearfoot Strikers

I McClay and K Manal

Motion Analysis Laboratory, University of Delaware, Newark, DE 19716

INTRODUCTION

It has been reported that 20% of distance runners strike the ground with the mid- or forefoot region of the foot (Kerr et al, 1983). This is likely to result in differences in both movement patterns and ground reaction forces (GRFs) experienced by the lower extremity. Consequently, joint kinetics may also be altered. This study was undertaken in order to examine the influence of strike pattern on joint kinetics in runners. The project is currently underway with the results presented here based upon the subjects that have been collected to date. 3-D kinematics and GRFs were collected on 20 runners; 10 with a rearfoot strike pattern (RFS) and 10 with a forefoot strike pattern (FFS). Differences were found in peak vertical and anteroposterior GRFs and both rearfoot and knee kinetics suggesting a significant influence of strike pattern. It is hoped that these results will begin to generate normative joint kinetic data for runners with a FFS pattern.

REVIEW AND THEORY

It has been demonstrated that differences in strike pattern during running can influence GRFs measured under the foot. Oakley et al (1988) demonstrated that runners with a FFS pattern have attenuated (or absent) vertical impact peaks. Cavanagh et al (1980) reported similar results and reported double peaked braking phases of the anteroposterior (AP) force in the FFS pattern. Harrison et al (1988) reported larger vertical peaks in the FFS group. Runners often alter their strike to a more FFS pattern in attempt to improve their running performance. However, these changes in the force patterns coupled with kinematic differences between a RFS and FFS pattern will likely influence the resultant joint kinetics of the lower extremity. For example, when the foot strikes the ground with a RFS pattern, the ground reaction force is posterior to the ankle joint axis causing an external plantarflexion moment requiring a controlling dorsiflexion muscle moment. In the FFS pattern, the GRF is anterior to the ankle joint axis creating the opposite effect. Additionally, the runner with a FFS pattern is likely to land in greater knee flexion to compensate for the increased ankle plantarflexion. This may also result in a difference in knee kinetics. The variations in joint kinetics between a RFS and FFS pattern have not yet been reported. Alterations in joint kinetics are important to understand as they are associated with changes in muscle force requirements and consequently differences in joint contact forces. Therefore, the purpose of this research was to compare the lower extremity kinetics of runners with a FFS pattern to those with a RFS pattern.

PROCEDURES

20 recreational runners, previously screened for their strike pattern were used in this study. 10 subjects were assigned to the rearfoot strike group (RFS) or the forefoot (FFS) group based upon a visual screen of their strike pattern while running on a treadmill. To be placed in the FFS group, initial contact had to be made in the forefoot region (with heel off the ground at FS). The foot with the most anterior strike pattern was used. In the RFS group, the foot with normal peak eversion values was used, as this group also served as a control group for comparison to a group of pronators.

Four retroreflective markers were affixed to a velcro-backed polyform shell and attached to the thigh via a neoprene wrap. A similar marker set was attached to the shank. Three markers were attached directly to the heel counter of the shoe: two were placed along the longitudinal axis of the heel and one was placed on the lateral border of the heel. These were the markers used to track the motion of the three segments. Additionally, markers were placed over the greater trochanter, the medial and lateral femoral condyles, the medial and lateral malleoli, and the head of the first and fifth metatarsals. These markers were used to determine the anatomical coordinate systems in which the motion would be described. After a standing calibration trial was collected and the anatomical transformations calculated, these markers were removed.

Subjects then ran along a 75 ft runway at a speed of 3.35 m/s. Data were sampled at 120 hz with a 5 camera VICON (Oxford Metrics, UK) Motion Analysis System. Ground reaction forces were collected from the lower extremity of interest from a Bertec (BERTEC Corp, OH) forceplate being sampled at 480 hz. The kinematic and kinetic data were combined mathematically to estimate three-dimensional joint kinetics using MOVE3D software (NIH Biomechanics Laboratory). Only the sagittal plane kinetics will be presented here. Independent t-tests were run for the variables of interest and considered significant at the adjusted alpha level of 0.015.

RESULTS

Table 1. Peak Vertical and Anteroposterior Ground Reaction Forces in bw (mean, sd)

	RFS	FFS
Vertical	2.58 (0.16)	2.87 (0.19)*
Braking	-0.40 (0.04)	-0.44 (0.08)
Propulsive	0.31 (0.04)	0.39 (0.06) *

* $p<0.005$

Table 2 . Peak Sagittal Plane Lower Extremity Kinetics (mean, sd)

	RFS	FFS
Ankle		
PF Moment	-1.39 (0.27)	-1.73 (0.27) *
DF Power	-4.01 (0.96)	-7.76 (1.62) *
PF Power	7.98 (1.18)	10.43 (1.75) *
Knee		
EXT Moment	1.99 (0.42)	1.86 (0.44)
FL Power	-7.45 (0.94)	-5.56 (1.59) *
EXT Power	5.02 (2.03)	4.43 (1.45)

* $p<0.01$ moments = Nm/bw•ht

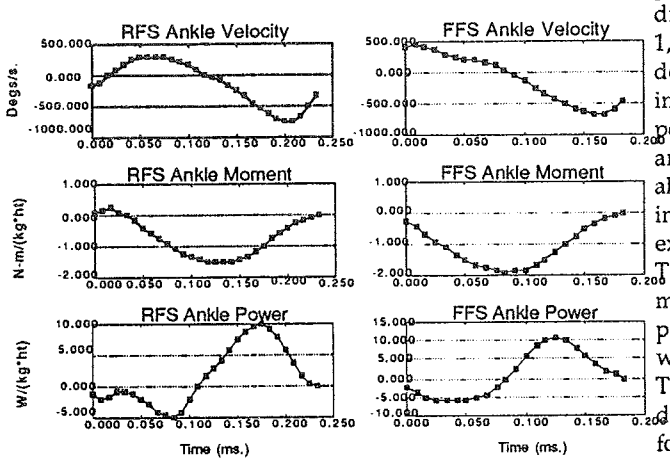

Figure 1. Sagittal plane ankle kinetics for a typical RFS and FFS subject. Positive = dorsiflexion, negative =plantarflexion.

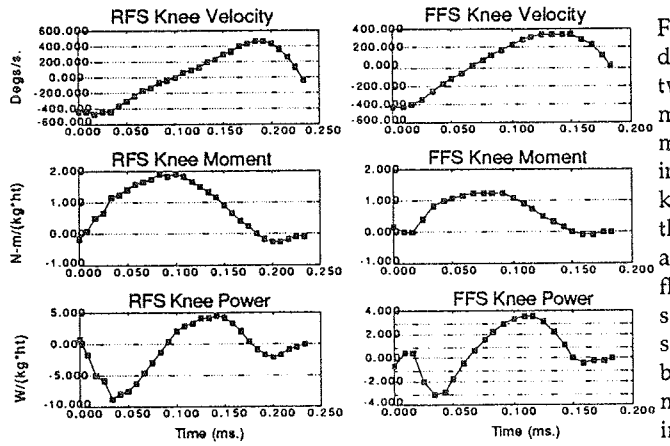

Figure 2. Sagittal plane knee kinetics for a typical RFS and FFS subject. Positive = extension negative = flexion.

DISCUSSION

Peak ground reaction forces were found to be significantly different between the two strike patterns. The larger propulsive peak of the AP force and larger peak vertical force seen in the FFS group suggests that the forefoot strike pattern provides a stronger drive to propel the body upward and forward. This idea is substantiated by the fact that strike index tends to increase with running velocity (Cavanagh et al, 1980, Kerr et al, 1983). Sprinters are almost exclusively forefoot strikers.

The differences in joint kinetics between the two groups can be attributed to differences both in the magnitude of the ground reaction force and the change in angular position. Sagittal plane angular velocity, moment and power for the ankle and knee for a typical RFS and FFS subject can be seen in figure 1. At the ankle, the predominant moment is plantarflexion with the first half of contact being an eccentric, or power absorption phase followed by a concentric, or power generation phase. This general pattern is consistent between the two groups. However, the magnitudes of the peak moment and both power phases were significantly greater for the FFS group. These larger magnitudes translate into larger required forces in the gastrocsoleus muscle.

The primary variations in the ankle kinetic patterns between the two groups are due to the difference in the landing positions of the foot. In figure 1, the ankle moment of the RFS is an initial dorsiflexion moment, whereas in the FFS, it is an immediate plantarflexion moment. This is due to the position of the vertical GRF vector with respect to the ankle joint axis as noted previously. Differences can also been noted in the power curve. The RFS shows an initial decrease in power absorption, whereas the FFS exhibits an immediate increase in power absorption. This is a consequence of the differences in both the moment and the angular velocity at the ankle. A plantarflexion velocity is noted initially in the RFS whereas the FFS has an initial dorsiflexion velocity. This is due to the fact that the RFS typically landed in dorsiflexion, had a brief period of plantarflexion as the forefoot became plantigrade and then proceeded into dorsiflexion. The FFS landed in plantarflexion and immediately moved into dorsiflexion.

Mean peak knee kinetics were lower in the FFS, however only power absorption was significantly different. Differences in kinetic patterns between the two groups can also be seen at this joint (figure 2). The moment in the RFS is immediately an extensor moment. However, the FFS exhibit an initial moment in the direction of flexion. The angular patterns at the knee were similar between the two groups. However, the FFS pattern may position the vertical GRF slightly anterior to the knee joint axis requiring a momentary flexion muscle moment. Knee power curves were also slightly different around footstrike with the RFS showing an immediate power absorption which would be associated with eccentric action of the quadriceps muscle. The FFS demonstrated a power curve with an initial, brief period of power generation, followed by the normal power absorption characteristic of the first half of stance.

In summary, differences in kinetic variables have been noted between the RFS and FFS groups. It is hoped that this will lend insight into the effect of strike pattern on joint kinetics and provide information to both clinicians and sports medicine professionals regarding the potential effect of altering ones strike pattern on lower extremity joint kinetics.

ACKNOWLEDGMENTS

The authors would like to acknowledge the Whitaker Foundation for their support of this work.

REFERENCES

Cavanagh et al, J. Biom, vol 13, pp397-406, 1980
Harrison et al, Biomechanics in Sport, pp81-88, 1988
Kerr et al,BiomechanicalAspects of Sport Shoes and Playing Surfaces, 1983
Oakley et al, Clin. Biom, vol 3, pp159-165, 1988

ALTERATIONS IN HIP JOINT BIOMECHANICS WHILE WALKING WITH A WEIGHTED VEST

[1]G. Salem, [2]J. Young, [3]R. Gregor, [3]M. Ryan, [4]A. Abrahamse, and [2]G. Greendale,

[1]Department of Physiological Science, UCLA, Los Angeles, CA
[2]Department of Internal Medicine, UCLA, Los Angeles, CA
[3]Department of Movement Science, Georgia Institute of Technology, Atlanta, GA
[4]RAND, Santa Monica, CA,

INTRODUCTION

Alterations in hip joint biomechanics during walking were assessed in five subjects after acute application of a weighted (4% body weight) vest, designed to be used in preventative osteoporosis-intervention programs. Sagittal plane kinematic and kinetic parameters of the lower extremities were calculated from film and force-platform data during the support phase of normal gait. The results suggest that significant alterations in hip biomechanics occur after acute applications of the vest.

REVIEW AND THEORY

The success of an exercise program for the prevention of osteoporosis may largely depend upon how easy it is to engage the program. In an effort to minimize the intrusiveness of such programs, an exercise intervention using a weighted vest was designed. Results from a previous study indicated that average lumbar bone mineral density increased by 1.02% in the vest group and decreased by 0.59% in the control group after 20 weeks (Greendale *et. al,* 1993). Because osteoporitic fractures of the hip are major contributors to dysfunction and morbidity in elders, the effects of the vest on hip joint biomechanics and bone tropism remain important research questions. The purpose of the present investigation was to quantify the alterations in hip joint biomechanics during normal walking after the acute application of the weighted vest in seniors. We hypothesize that acute applications of the weighted vest will increase joint reaction forces and moments of force at the hip.

PROCEDURES

The procedures are outlined in chronological order below.

- Five senior subjects were filmed in the sagittal plane (50 frames$\cdot s^{-1}$) as they walked at a normal pace across a force platform, under two conditions: without a weighted vest (CON) and while wearing a weighted (4% BW) vest (VEST). Each subject performed 10 trials (5 right side and 5 left side) for each condition.
- Summed vertical forces were collected onto a 386 computer via an A/D acquisition system at a rate of 500 Hz.
- Coordinate data of reflective markers was obtained by manually digitizing serial film images.
- A cutoff frequency for each coordinate was defined as the frequency representing 95% of the total power as determined by spectral analysis. Raw coordinate data were then filtered using a 4th order zero-lag Butterworth digital filter.
- Center of mass coordinates were calculated from fixed segment length data using body segment parameters from Dempster (1955).
- The smoothed joint and center of mass data were then processed through a quintic spline with zero smoothing to obtain 5th order polynomials for each coordinate.
- Linear and angular velocities and accelerations were then calculated using standard differentiation techniques and known segment lengths.
- Inverse dynamics equations of motion, were used to calculate the peak vertical joint reaction forces (VJRF) and peak moments of force (MOF) about the hip, during the stance phase of gait (Winter, 1990). VJRF'S are normalized to body weight and MOF's are normalized to body mass.
- The last trial (5th) for each side and each condition was chosen for statistical analysis because the 5th trial provided the greatest amount of practice for each subject.
- Standard ANOVA and Mann-Whitney techniques were used to test for differences in the peak VJRF's and MOF's between the

two conditions. A significance level of $P \leq 0.05$ was used for all comparisons.

RESULTS

- Averaged across all subjects and both sides, peak hip VJRF's were significantly greater (6.8%) in the VEST condition (Figure 1).
- Averaged across all subjects and both sides, peak hip flexor MOF's were not significantly different between conditions; however, average peak hip flexor MOF's in the VEST condition were 6.9% greater than in the CON condition. (Figure 2).
- Averaged across all subjects and both sides, peak hip extensor MOF's were significantly greater (34.4%) in the VEST condition (Figure 2).

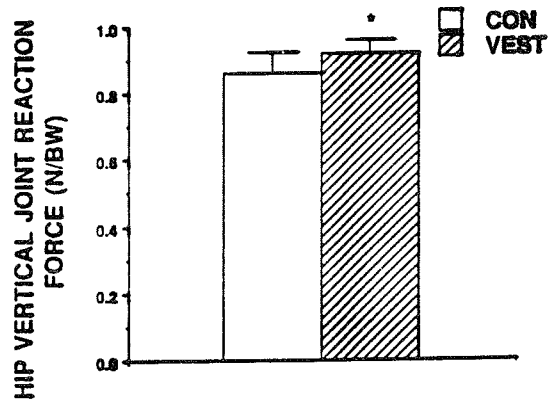

Figure 1. Peak hip vertical joint reaction forces. Mean ± SD are indicated for VEST and CON conditions. * ($p \leq 0.05$)

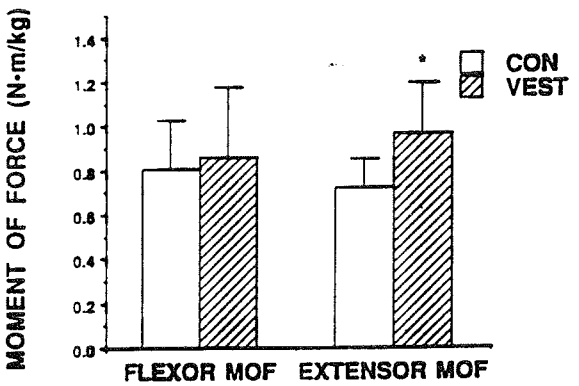

Figure 2. Average peak hip moments of force. Mean ± SD are indicated for VEST and CON conditions. * ($p \leq 0.05$)

DISCUSSION

The results indicated that the addition of a 4% BW vest significantly increased peak hip VJRF's during the stance phase of normal walking in senior subjects. Although not equivalent, increases in peak VJRF's may contribute to increases in bone on bone loading and potentially stimulate bone tropism. Peak extensor MOF were also significantly increased with the vest, and increases in hip MOF's are likely related to increases in muscular and/or periarticular forces. Peak extensor MOF increased by 34% with the vest, whereas peak flexor MOF increased by only 6.9%. This suggests that a greater increase in peak MOF is required during the loading response, when a hip extensor moment is required, than during terminal stance, when a hip flexor moment is required. Future questions to be addressed include: 1) how do JRF's and MOF vary in three dimensions, 2) how are increases in VJRF's and MOF related to changes in bone turnover and bone mass, 3) what are the changes in hip JRF's and MOF's after chronic applications of the vest. Future studies which include a 3D analysis of gait, bone serum markers, and/or hip BMD measurements, and serial analyses of gait may provide further insight into these questions.

REFERENCES

Dempster, W.T. et. al. *Am. J. Phys. Anthrop.*, The anthropometry of manual work space for seated subjects, 17, 289-317, 1959.

Greendale, G.A., et.al. *Qual. Life Res.*, The effect of a weighted vest on perceived health status and bone density in older persons., 2, 141-152, 1993.

Winter, D.W. *Biomechanics and Motor Control of Human Movement*, (pp.77-84), John Wiley & Sons, Inc., 1990.

ACKNOWLEDGEMENTS

UCLA Older Americans Independence Center, NIA

Geriatrics Academic Program, NIA

KINEMATICS OF THE LOWER LIMBS WHEN STEPPING OVER OBSTACLES OF DIFFERENT HEIGHTS

Li-Shan Chou and Louis F. Draganich

Section of Orthopaedic Surgery and Rehabilitation Medicine, Department of Surgery
The University of Chicago, Chicago, Illinois 60637

ABSTRACT

We studied the effects of obstacle height on the kinematics of the lower limbs in twelve healthy young adults when stepping over obstacles of 51, 102, 152, and 203 mm heights. The trailing limb was found to be more challenged than the leading limb and demonstrated less hip joint flexion-extension, more rapid knee flexion, and lower toe-obstacle clearance than the leading limb.

INTRODUCTION

No studies have reported in depth the motion of the trailing limb in response to obstructed gait. Muscle activities and the trajectory of the leading limb during stepping over obstacles of different heights and widths have been investigated (Patla et al., 1993). The differences in lower limb trajectories between healthy young and old adults when stepping over obstacles of different heights have also been studies (Chen et al., 1991). In both of these studies only the kinematics of the leading limb were investigated. The purpose of this study was to investigate the effects of obstacle height on the kinematics of both lower limbs.

METHODS

Gait analysis was performed on twelve healthy young adults (7 males, 5 females) having a mean age of 27.6 years (range, 18 to 34 years). Their average height was 166.6 cm (range, 155 cm to 177 cm), and their average weight was 599.4 N (range, 434.6 N to 741.6 N). Subjects were instructed to walk barefoot along a 9.5 m walkway at a comfortable self-selected speed and step over an obstacle in their usual manner. Five experiments were performed: level walking and stepping over obstacles of heights of 51, 102, 152, and 203 mm. Ground reaction forces were measured with a multicomponent force platform in the center of walkway. Clusters of four infrared light-emitting diodes were rigidly attached to the feet, shanks, thighs, pelvis and torso of the subject. Kinematic parameters were collected with the optoelectronic, 3-D digitizing system. Kinematic and force parameters were sampled at a rate of 100 Hz. The overall accuracy of the system was less than 7 mm for a volume 2 m long, 1.5 m high, and 0.7 m wide.

The mean of three trials for each obstacle height was used in formulating the results. The effects of obstacle height on crossing speed, swing time, stride length, toe-obstacle clearance, and flexion-extension angles of the ankle, knee, and hip were tested using one-way ANOVA with repeated measures and the Tukey test at the α=0.05 level of significance. Paired t-tests were applied to determine differences between the leading and trailing limbs. An α=0.0016 level of significance was used based on a Bonferroni adjustment for comparisons consisting of toe-obstacle clearance, swing time, and flexion-extension angles of the ankle, knee, and hip when the toe was over the obstacle. The temporal-distanceresults were not reported.

RESULTS

When stepping over obstacles the toe-obstacle clearances of both limbs were larger than the toe-ground clearances during level walking at mid-swing (Table 1). The differences were significant ($p<0.03$). When the toe of the leading limb was over the obstacle, the flexion angles of the knee and hip increased with obstacle height (Table 2). Obstacle height was found to significantly affect the flexion angles of the knee and hip but the ankle of the leading limb. When the toe of the trailing limb was over the obstacle, a significant difference was found in the flexion angle of knee only between the lowest and highest obstacles ($p<0.05$). Obstacle height was not found to significantly affect flexion of the hip of the trailing limb. The flexion angle of the ankle joint of the trailing limb changed from plantarflexion to dorsiflexion as obstacle height increased; a significant difference was found between the lowest and highest obstacle ($p<0.02$).

Unlike level walking, the motion of the lower limbs was not symmetric when stepping over obstacles. For the leading limb the average distance between toe-off and the obstacle for any of the obstacle heights was 89.5 (±9.6) cm. The toe of the leading limb was over the obstacle between 51 and 56 percent of the swing time. The average distance between toe-off of the trailing limb and the obstacle for any of the obstacle heights was 21.3 (±4.7) cm. The toe of the trailing limb was over the obstacle

between 28 and 29 percent of swing time. The hip of the leading limb was flexed significantly more than that of the trailing limb ($p<0.001$). The toe of the leading limb was consistently over the obstacle when hip flexion was near maximum (Fig. 1). However, the toe of the trailing limb was over the obstacle well before maximum hip flexion was attained.The dorsiflexion angles of the ankle joint of the leading limb were significantly higher that those of the trailing limb when stepping over the obstacles of 51, 102, and 152 mm heights ($p\leq0.001$). For each height of obstacle, the toe-obstacle clearance of the leading limb was significantly larger than that of the trailing limb ($p\leq0.001$).

DISCUSSION

When stepping over an obstacle, a conservative strategy of significantly slower crossing speed, larger stride length, and larger toe-obstacle clearance than those during level walking was found. These findings were in agreement with those reported in previous studies (Chen et al., 1991; Patla et al., 1993).The toe-obstacle clearance of the trailing limb was only about one-half of that of the leading limb. The primary reason for this difference was that the hip flexion angle averaged 70° for the leading limb (average of 58°, 68°, 75°, and 79°; Table 2) and only 24° for the trailing limb when the toe was over of the four obstacles. This can be explained by the proximity of the swing limb with the obstacle. Therefore, before reaching the obstacle, there was enough space and time to flex the hip of the leading limb and to best configure the leading limb for safe crossing of the obstacle. However, when the trailing limb crossed the obstacle, the obstacle was beneath the subject and between the leading and trailing limbs. It should be noted that flexion of the hip not only elevates the toe but also moves it forward. Thus, flexion of the hip joint of the trailing limb was constrained by its proximity with the obstacle. This was compensated for by greater flexion of the knee joint of the trailing limb over a shorter period of time than that available to the leading limb. Thus, knee flexion became the major contributor to elevating the toe. This resulted in the trailing limb being more challenged than the leading limb when stepping over an obstacle.

Table 1. Clearances between toe and obstacle (mm)

Clearance	Obstacle Free	51 mm	102 mm	152 mm	203 mm	p* value
Leading limb	29 ±8	124 ±25	127 ±33	119 ±39	112 ±48	<0.001
Trailing limb	30 ±5	64 ±23	82 ±33	61 ±19	58 ±26	<0.001

* p-values were for repeated measures ANOVA.

Table 2. Joint angles (in degrees) of the lower limbs when the toe was over the obstacle

Parameters	51 mm	102 mm	152 mm	203 mm	p* value
KFA[1] leading limb	78 ±11	92 ±9	97 ±8	104 ±8	<0.001
KFA trailing limb	80 ±9	88 ±9	91 ±14	93 ±14	=0.029
HFA[2] leading limb	58 ±10	68 ±9	75 ±9	79 ±10	<0.001
HFA trailing limb	20 ±9	23 ±9	26 ±10	26 ±9	n.s.[4]
ADFA[3] leading limb	15 ±6	14 ±8	13 ±6	12 ±8	n.s.
ADFA trailing limb	-8 ±6	-6 ±6	-2 ±8	1 ±9	=0.008

* p-values were for repeated measures ANOVA.
1 KFA= Knee Flexion Angle.
2 HFA= Hip Flexion Angle.
3 ADFA= Ankle Dorsiflexion Angle.
4. n.s.= not significant

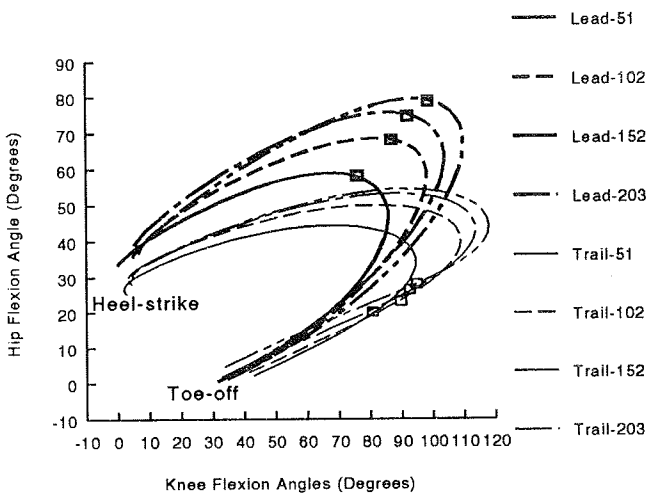

Figure 1. The relationships between the knee flexion and hip flexion of the leading (thick lines) and trailing (thin lines) limbs when stepping over obstacles of 51, 102, 152, and 203 mm heights. The boxes indicated the flexion angles when the toe was over the obstacle.

REFERENCES

1. Chen et al.,*J Gerontology* 46, M196-203, 1991.
2. Patla et al.,*Gait & Posture* 1, 45-60, 1993.

KINETICS OF THE TRAILING LIMB WHEN STEPPING OVER OBSTACLES OF DIFFERENT HEIGHTS

Li-Shan Chou and Louis F. Draganich

Section of Orthopaedic Surgery and Rehabilitation Medicine, Department of Surgery
The University of Chicago, Chicago, Illinois 60637

ABSTRACT

The effects of obstacle height on the kinetics of the hip and knee of the stance limb when stepping over obstacles of different heights were examined in this study. During early stance the external flexion moment at both the knee and hip joints increased as obstacle height increased. During late stance the external flexion moment at the knee and extension moment at the hip decreased as obstacle height increased.

INTRODUCTION

Stepping over obstacles during walking is a common daily activity. Tripping over obstacles is one of the most common causes of falls in the elderly (Tinetti and Speechley, 1989). In order to develop strategies for avoiding falls, it is important to understand how gait patterns are affected by obstacle height.

Muscle activity and the trajectory of the leading limb were studied during stepping over obstacles of different heights and widths (Patla and Rietdyk, 1993). The differences in lower limb trajectory between healthy young and old adults have also been studied (Chen, et al., 1991). The effect of an obstacle with a height of 10% of leg length on the flexion-extension moments of the joints of the lower limb were studied (Mcfadyen and Winter, 1991). However, no statistical differences were found when compared to the moments generated during normal gait. The purpose of this study was to investigate the effects of obstacle height, for four heights ranging from 51 mm to 203 mm (8 inches), on the moments of the hip and knee of the stance limb when stepping over the obstacles.

METHOD

Gait analysis was performed on twelve normal subjects with a mean age 27.6 years (range, 18 to 34 years) and average height of 166.6cm (range, 155cm to 177cm). Subjects were instructed to walk barefoot along a 9.5m walkway at a self-selected speed and step over the obstacle in their usual manner. Five experiments were performed: level walking and stepping over obstacles of heights of 51, 102, 152, and 203mm (standard step height). Ground reaction forces were measured with a multicomponent force platform in the center of the walkway. Clusters of four infrared light-emitting diodes were rigidly attached to the feet, shanks, thighs, pelvis and torso of the subject. Kinematic parameters were collected with an optoelectronic 3-D digitizing system. Kinematic and force parameters were sampled at a rate of 100 Hz. The overall accuracy of the system was less than 7mm for a volume 2m long, 1.5m high, and 0.7m wide.

The human body was modeled as an eight-segment linkage system, six links for the lower extremities, one for the pelvis, and one for the head, arms, and trunk. Each link was assumed to have a point mass at the location of the center of mass. The length, mass, location of mass center, and inertial properties of each link were calculated from data in the literature (Chaffin and Andersson, 1984). The 3-D moments about the hip, knee, and ankle joints of the stance limb were computed using inverse dynamics. The moments were normalized to body weight times lower limb length. We performed repeated measures one-way ANOVA and the Tukey test at the α=0.05 level of significance. Reported here are the flexion-extension moments about the knee and hip joints.

RESULTS

When stepping over the obstacles the patterns of the moments at the joints of the stance limb were similar to those found during level walking. However, for most part, the magnitudes of the moments changed with obstacle height. At the knee, the maximum external flexion moment during early stance increased with obstacle height (Table 1); significant differences ($p<0.001$) in the moments were found between the obstacles of 102, 152, or 203mm heights and level walking and between the obstacles with these heights and the obstacle of 51 mm height. The maximum external flexion moment during late stance decreased as the height of obstacle increased; significant differences ($p<0.001$) were found between level walking and obstacles of 51, 102, 152, and 203 mm heights. Significant differences were also found between the obstacles of 51 and 203 mm height ($p<0.01$) and between the obstacles of 102 and 203 mm height ($p<0.02$). No significant differences was found in the maximum external extension moment.

At the hip, the maximum external flexion moment during early stance slightly increased with obstacle height (Table 2). However, no significant differences were found. The maximum external extension moment during late stance decreased with obstacle height; significant differences ($p<0.01$) were found between level walking and obstacles of 152 and 203 mm heights.

DISCUSSION

During late stance, the decreases in the magnitudes of the maximum external extension moment at the hip and flexion moment at the knee for the higher obstacles were in agreement with the conclusions reported by McFadyen and Winter (1991) for obstacles of low heights. Additionally, we found the magnitude of the external flexion moments about the knee and hip during early stance to increase by 59% and 7%, respectively. This suggest that when stepping over the highest obstacle much greater demands are encountered by the extensor mechanism of the knee and dorsiflexor mechanism of the ankle than of the hip. This leads to the question of whether the increased demand on the muscles of the stance limb would affect the ability of an older individual to avoid tripping.

REFERENCES

1.Chaffin and Andersson,*Occupational Biomechanics*, John Wiley & Sons, Inc., NY, 1984.
2. Chen et al: *J Gerontology*,46: M196-203, 1991.
3. McFadyen et al: *Neuro Rese Com*, 9: 37-44, 1991
4. Patla et al: *Gait & Posture*, 1: 45-60, 1993.
5.Tinetti et al: *New England J Med*, 320:1055-1059,1989.

Table 1. The external moment about knee joint (% of body weight times lower limb length)

Moments	Obstacle Free	51 mm	102 mm	152 mm	203 mm	p* value
Max.Flex at early stance	4.9 ±2.7	6.0 ±2.1	7.5 ±2.4	7.7 ±2.8	7.8 ±3.1	<0.001
Max. extension	6.1 ±2.9	7.1 ±3.5	6.6 ±3.4	6.9 ±3.2	6.4 ±3.4	n.s.[1]
Max.Flex at late stance	2.3 ±0.8	1.5 ±0.7	1.4± 0.6	1.1± 0.4	0.8 ±0.6	<0.001

* p-values were for repeated measures ANOVA.
[1] n.s. = not significant.

Table 2. The external moment about hip joint (% of body weight times lower limb length)

Moments	Obstacle Free	51 mm	102 mm	152 mm	203 mm	p* value
Max.Flex at early stance	10.8 ±1.9	11.2 ±2.3	11.3 ±1.8	11.5 ±2.3	11.6 ±2.1	n.s.[1]
Max.Ext at late stance	14.2 ±3.1	13.5 ±2.3	12.9 ±2.8	12.5 ±3.1	11.3 ±2.7	<0.001

* p-values were for repeated measures ANOVA.
[1] n.s. = not significant.

A METHOD FOR DETERMINING THE PHYSICAL LIMITS TO SINGLE JOINT MOTION: APPLICATION TO MOVEMENT TERMINATION

James Patton[2] and Yi-Chung Pai[1]
[1]Programs in Physical Therapy, Northwestern University Medical School, Chicago, IL 60611
[2]Biomedical Engineering Graduate Program, Northwestern University, Evanston, IL 60208

INTRODUCTION

A method was developed for determining the state boundaries between physically possible and impossible movements, based on the constraints imposed on the system. Both optimal control and switching control were used. Application of this methodology to a simple inverted pendulum model for movement termination was used to illustrate the process.

REVIEW AND THEORY

Most biomechanical tasks involve many possible ways to sufficiently satisfy the objective. Even for the case of single joint motion, the state trajectories possible to execute a task are infinite (Gottlieb et al, 1990). Optimal control techniques are normally used to identify a coordination strategy for a clearly defined task, such as highest jump, but fail to shed light on coordination strategies when the performance criteria is ambiguous (Zajac and Winters, 1990).

An alternative approach that sheds additional light on the coordination strategies is to identify the absolute physical limits. These limits can arise from physiological, anthropometric, or environmental constraints imposed on the body. Gordon (1990) and Kuo and Zajac (1993) have considered the boundaries in the acceleration space which enclose a "feasible space" to torque generation. What can also be considered is the state-space boundaries to feasible motions.

By expressing these constraints in mathematical form, and implementing them in a feedback control system, a simulation can be run whose state trajectory traces out the limits to the mechanical possibilities. The purpose of this study was to outline this procedure, and illustrate it by identifying the regions of the state space in which a fall forward is inevitable during the termination of movement.

PROCEDURES

A two-segment model of the feet (stationary) and the rest of the body (moving in the sagittal plane) was considered. Typical anthropometric proportions were used (Dempster et al 1955; Drillis and Contini 1966 via Winter 1990). The ankle joint was modeled as an ideal frictionless pin joint, and the resultant ankle torque, τ, was assumed to be generated by muscles crossing the ankle (dorsi flexion positive). Static friction was roughly estimated in the middle range of reported values ($\mu = 1.0$)

The base of support (BOS), which the body transmits forces to the floor has limited capabilities, and therefore imposes three constraints on the mechanical behavior:

(1) *Gravity Constraint*: The foot must not leave the floor (the net force on the foot must be positive):

$$F_{gy} \geq 0$$

(2) *Friction (Slip) Constraint*: The friction force of the foot must not exceed the threshold for a given coefficient of friction μ:

$$|F_{gx}| < \mu F_{gy}$$

(3) *Center of Pressure Constraint*: The center of pressure (COP) under the feet must be maintained within the base of support:

$$0 < COP < l_f$$

Note that the friction and center of pressure constraints actually are two constraints each, due to the inequality expressions.

Each of the BOS constraint inequalities were expressed as a *boundary* by taking their equation forms and rearranging them in terms of the angular position Θ, angular velocity $\dot{\Theta}$, and ankle torque τ. Angular acceleration was eliminated by substituting the equation of motion of a pendulum. The resulting expression was a relation between the *states* (Θ and $\dot{\Theta}$) and the torque τ. Thus, the constraints can be interpreted as a limit to the torque τ, given the current states Θ and $\dot{\Theta}$:

$$\tau_{\text{constraint}} = f(\Theta, \dot{\Theta})$$

Each of the constraints can be considered a surface in the *state-torque space*. By combining all constraint surfaces, the intermediate volume between them can be considered a "feasible" space.

For the purpose of simplicity in the present study, a *strength constraint* was considered which was assumed independent of changes in joint position and velocity.. A conservative estimate of maximum plantar flexion torque was made. More complex functions could be added without loss of generality.

A state feedback control system with a state observer switch (Figure 1) was used to force the model to trace the limits of feasible motion. This technique is similar to 'sliding mode control' methodology (Utkin, 1977; Slotine and Li, 1991), but without any *a priori* knowledge if the desired state trajectory.

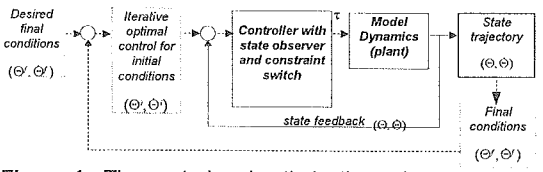

Figure 1: *The control and optimization scheme*

For each instant, the most constraining state-torque surface (dictated by the current state) was used to determine the highest allowable ankle torque. Nonlinear

optimization of initial velocity. Formally stated, the solution $\dot{\Theta}_i$ would be given by:

$$\dot{\Theta}_i = \min_{\Theta}[(\Theta_f - \Theta_d)^2 + \dot{\Theta}_f^2]$$

for an arbitrary initial position Θ_i, where Θ_f and $\dot{\Theta}_f$ represent the final angle and angular velocity of the pendulum, and Θ_d represents the desired final position (over the toe).

RESULTS AND DISCUSSION

Each constraint surface presented a unique limitation (Figure 2). All surfaces were nonlinear, and their intersection formed complex three dimensional curves.

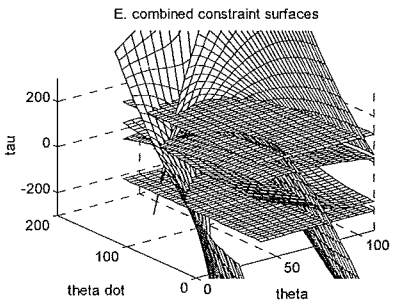

***Figure 2**: The constraint surfaces*

The switching control system effectively constrained the motions and torques to trace out a trajectory that defines the limits of feasible motion. An initial condition was found that begins at the lowest possible angle respect to vertical and highest possible velocity that can still be reduced to zero before the CM exceeds the limit of the BOS (i.e., the toe). The COP constraint was active for the duration of the trial. The two components of the ground reaction force, vertical shear, as well as the center of pressure are plotted against time (Figure 3). Also shown are the corresponding BOS limits (due to the constraints) for each instant of time.

As Bernstien pointed out (1967), the musculoskeletal system can select from many possible movement trajectories to accomplish the same objective, although for many tasks a reduction of such possibilities is likely to occur. We did not attempt to simulate optimal solutions within the infinite feasible possibilities, but instead attempted to identify a boundary to such possibilities.

The task and model chosen were deliberately simple in order to focus the attention on methodology. Similar understanding of the geometric constraints relating states and torque can be implemented using this methodology to define and understand limitations in other tasks.

REFERENCES

Bernstien, N., *The coordination and regulation of movement*, Pegammon Press, Englewood Cliffs, NJ., 1967.

Gordon, M. E., *An analysis of the biomechanics and muscular synergies of human standing.* PhD. Dissertation, Stanford University, 170-192, 1991.

Gottlieb, G. L. et al., In *Multiple Muscle Systems* (Edited by J M. Winters and S. L-Y. Woo), Springer-Verlag, New York, 1990.

Kuo, A. D., and F. E. Zajac, Journal of Biomechanics. 26, 137-150, 1993.

Slotine, J. J. E., and W. Li, *Applied Nonlinear Control*, Prentice Hall, Englewood Cliffs, NJ, 1991.

Utkin, V. I. *Sliding Modes and their Application to Variable Structure Systems*, MIR Publishers, Moscow, 1978.

Winter, D. A., *Biomechanics and Motor Control of Human Movement.* John Wiley and Sons, Inc., New York. 2nd ed, 1990.

Zajac, F., J. Winters, In *Multiple Muscle Systems* (Edited by J M. Winters and S. L-Y. Woo), Springer-Verlag, New York, 1990.

ACKNOWLEDGMENTS

This study was supported by a research grant from the Arthritis Foundation.

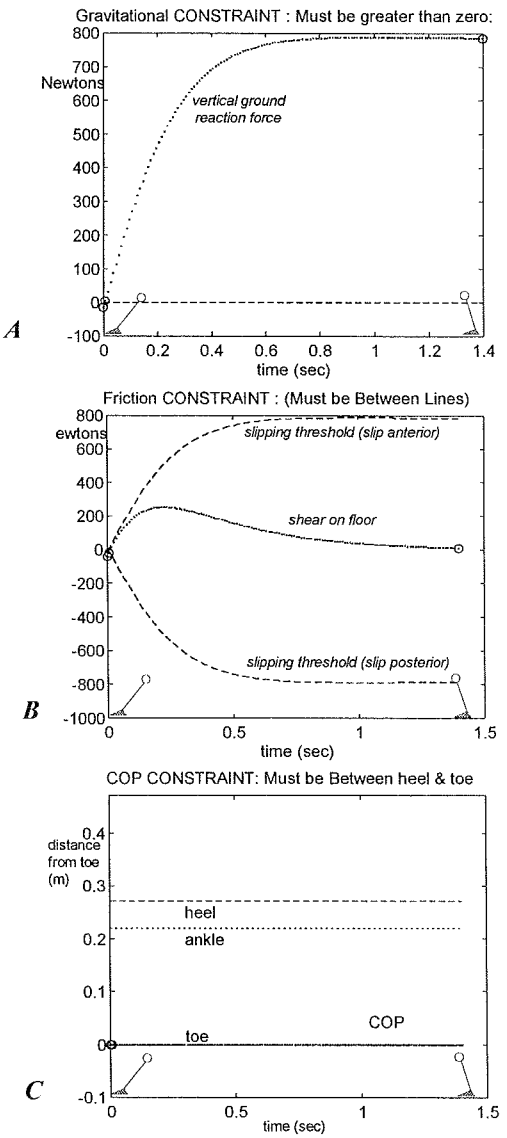

***Figure3**: Time histories for the base of support. A) Vertical force, B) Horizontal (shear) force, C) Center of pressure*

Talocrural and Talocalcaneal Joint Rotations During The Stance Phase of High Heeled Gait

Kyria L. Hontalas, Keith R. Williams PhD
Department of Exercise Science, University of California Davis, Davis CA 95616

Introduction

High heel kinematic studies have described ankle (talocrural) joint motion in the sagittal plane and subtalar (talocalcaneal) joint motion in the frontal plane. In this study, mathematical techniques were used to predict 3D ankle and subtalar joint rotations during the stance phase of high-heeled gait. A two-axis model of the ankle joint complex comprised of three rigid bodies, tibia, talus, and calcaneous linked by two hinge joints (ankle and subtalar) was used to compute respective joint angles.

Review and Theory

The contour of the modern high heel shoe elevates the heel and maintains the foot in a plantar flexed position. It has been established that high heel shoes increase the rate of loading to the metatarsals, elicit postural changes and limit normal supinatory and pronatory movements of the foot during normal walking (Opila *et al.*, 1988; Snow *et al.*, 1992; Snow *et al.*, 1994).

The purpose of this investigation was to present a method to determine 3D joint rotations at the ankle complex during high-heeled gait. A secondary purpose was to compare 3D joint angles computed from the proposed foot model to projected joint angles using traditional 2D analysis methods.

Procedures

Data were collected from fifteen female volunteers from the local university community. The mean age for the 15 subjects was 36.6 years (range, 24-54 years; SD, 9.31). Subjects were required to have worn high heeled shoes at least 4 hours/day and 3 days/week for at least a year.

The shoes used in this study were standard closed toe pumps of two different heights medium (3.81cm) and high (7.62cm). The pump style shoe consisted of a closed toe box with the shoe covering the instep and extending to the toe. The shoes fit snugly in the heel area of each subject to prevent the calcaneous from moving up and down within the heel counter.

Each subject walked at 1.4m/s ± 5% with the speed monitored through the use of photoelectric timing lights placed two meters apart, one on either side of a force plate. An acceptable trial was one in which the subject placed her right foot in the center of the plate without hesitation and met the speed criterion. The procedure of walking across the force platform for five acceptable trials was repeated for each of the heel heights with the order of heel heights randomized among subjects.

Kinematic data were acquired to assess the changes in ankle and subtalar joint kinematics during the stance phase of high-heeled gait. The Motion Analysis ExpertVision Video (MA) System generated the necessary kinematic data and timing information for joint angle measures. Kinematic data were collected at 200Hz using the MA system. A Kistler force plate was used to identify the timing of footstrike.

The position of the shank and foot segments were each defined by a triad comprised of 3 non-collinear reflective spheres. The triads were affixed to the lower right shank and the postero-lateral aspect of the right shoe of each subject. The triad markers were used to establish local coordinate systems for the shank and foot segments from the 3D coordinates of the reflective spheres. An independent reflective marker was placed over the most medial point of the medial malleolus to determine the ankle axis of rotation. The subtalar rotational axes were based on cadaver data published in the literature (Isman and Inman, 1969). They found a mean rotational axis for the subtalar joint that was inclined 41° in the sagittal plane relative to the heel, and medially deviated 23° in the coronal plane relative to the midline of the foot.

Dependent kinematic variables were measured in both 2D and 3D and compared across the independent variable of heel height. An average abduction angle was calculated for the five trials at each heel height condition. Three variables were measured at the ankle joint; angle at heelstrike, angle at maximum plantar flexion and angle at maximum dorsiflexion. Four variables were measured at the subtalar joint; angle at heelstrike, angle at maximum pronation, range of pronation and pronation velocity. Angles were referenced to a standard position of a 90° ankle angle and a subtalar neutral position as determined by palpation of the talus relative to medial and lateral malleoli.

The statistical analysis included three procedures. First, a multivariate analysis of variance (MANOVA) was performed on all the kinematic variables to establish an overall test of significance. Second, post hoc repeated measures analyses of variance (ANOVAS) were conducted on individual variables for statistically significant variable effects from the MANOVA results. Third, the analysis focused more closely at a heel height or dimension effect to determine which of the levels were significantly different.

Results/Discussion

A significant increase in the degree of foot abduction was found during walking in high heels compared to medium heels (high: 10.7, med: 5.4 deg). During high-heeled gait, lateral stability may be enhanced by increasing the degree of foot abduction.

Ankle Joint

As expected, there were significant differences in the ankle joint angle at heelstrike, at maximum plantar flexion and at maximum dorsiflexion with increased in heel height (Table 1). Greater plantar flexion was found for both the 3D and 2D ankle joint variables with increased heel height. Previous 2D studies in the sagittal plane have reported similar results (Snow *et al.*, 1994). All three ankle measures showed significant dimension effects between the 3D and 2D joint angles. The 3D ankle angles were higher (corresponding to more dorsiflexion) relative to the same 2D measure in both the medium and high heel conditions.

Subtalar Joint

The range of pronation (3D) and the maximum pronation velocity (3D) was significantly less in the high heels relative to the medium heels (Table 1). The maximum pronation angle was 3° less in high heels, but differences were not significant. Significant decreases in pronation for the 2D subtalar angle at heelstrike and at maximum pronation were found for the high heel relative to the medium heel. The present 2D results are in agreement with Snow *et al.* (1994) who showed that the rearfoot angle at footstrike was less supinated for the low heels relative to the medium and high conditions.

All of the joint angle measures showed significant differences between the 3D and 2D joint angles except for the range of pronation variable. 3D measures showed greater pronation angles at heel strike and maximum pronation compared to 2D measures. The significant 2D-3D differences found in the present study were influenced by different joint axis orientations and the respective methodologies used to compute joint angles.

The "windlass effect" provides one explanation for the decreased range of pronation and pronation velocity in response to heel height. The contour of a high heel raises the heel and plantar flexes the foot thus resulting in extension of the toes. Because the plantar aponeurosis is wrapped around the metatarsal heads, a windlass effect occurs where tension is increased along the longitudinal arch. The extended metatarsophalangeal joints may have contributed to supination of the foot through their effect on the plantar aponeurosis.

A sensitivity analysis was performed on the subtalar data from one subject in the medium heel condition to determine the potential errors associated with setting the subtalar rotational axis for each subject to the mean data from Isman and Inman (1969). The subtalar axis angles were varied one standard deviation from the Isman and Inman mean (9-11°) and new subtalar angle data was calculated. Resulting subtalar angles showed considerable variation with differences as high as 32%, indicating that data for a given individual may be affected substantially by an assumed subtalar orientation.

Although setting the rotational axis at the average value calculated by Isman and Inman is a recognized limitation, it was assumed that using the average axis orientation for the 15 subjects in the present study would be reasonable since data were averaged across subjects and it was not possible to determine *in vivo* subtalar orientations. These results indicate that the assessment of motion about the subtalar joint for individuals may not be accurate until valid *in vivo* methods are developed for determining subtalar axis orientation.

Table 1. Ankle and subtalar joint kinematic data

Ankle Joint	Med	High
2D angle @ heel strk (deg)	61.7 (6.7)	49.5 (5.4)
3D angle @ heel strk (deg)	68.0 (4.9)	58.9 (4.1)
2D angle-max pl flex (deg)	54.7 (5.8)	42.6 (6.5)
3D angle-max pl flex (deg)	59.0 (5.1)	50.3 (5.3)
2D angle-max dorsi flex (deg)	75.4 (6.8)	64.8 (7.1)
3D angle-max dorsi flex (deg)	83.2 (5.2)	74.4 (6.2)
Subtalar Joint	**Med**	**High**
2D angle @ heel strk (deg)	-1.5 (5.5)	1.5 (3.6)
3D angle @ heel strk (deg)	-6.6 (7.2)	-6.7 (4.3)
2D angle @ max pron (deg)	-8.1 (6.0)	-4.6 (5.5)
3D angle @ max pron (deg)	-14.3 (7.5)	-11.3 (4.8)
2D max pron vel (deg/s)	-114.9 (70.6)	-116.0 (73.6)
3D max pron vel (deg/s)	-249.6 (99.7)	-177.6 (94.8)

References

Isman, R.E. and Inman, V.T. Anthropometric studies of the human foot and ankle. *Bull. Pros. Res.* 11: 97-129.

Opila, K.A.et al (1988) Postural alignment in barefoot and high-heeled stance. *Spine.* **13**, 542-547.

Snow, R.E.et al. (1992) The effects of wearing high-heeled shoes on pedal pressure in women. *Foot Ankle.* **13**, 85-92.

Snow, R.E. et al. (1994) High heeled shoes: Their effect on center of mass position, posture, three-dimensional kinematics, rearfoot motion, and ground reaction forces. *Arch. Phys. Med. Rehabil.* **75**, 568-576.

Acknowledgments

We thank Dr. David Hawkins for his contributions to this study.

The Reliability of an In-Shoe Pressure Measurement System: The Novel PEDAR System

Kernozek, T.W.[1], LaMott, E.E.[2], Dancisak, M.J.[1]
[1] Division of Kinesiology, University of Minnesota, Minneapolis, MN 55455
[2] Department of Health & Physical Education, Concordia College, St.Paul, MN 55104

INTRODUCTION

A growing trend for researchers and clinicians is the measurement of pressure distribution at the interface between the foot and the shoe. The new technology contrasts earlier techniques which allowed only measurement of pressure between the foot and floor. A significant advantage is gained using inshoe techniques rather than platforms eliminate the necessity of "targeting" and enable the bilateral measurement of multiple steps associated with gait and other activities (Lee, 1980). The ability to go within the shoe opens the opportunity to objectively examine the effects of shoe and hosiery modifications for therapeutic effects, orthotic design and the screening of potential foot pathologies.

REVIEW AND THEORY

Initial inshoe technology allowed the measurement of plantar pressure within the shoe with only a limited number of discrete sensors. However, the use of several discrete sensors has several drawbacks due to the placement in predetermined locations (Cavanagh et al., 1992). The sensor placement alone requires some apriori hypothesis about the loading of the foot rather than letting the device determine the load relative to the plantar surface of the foot. Other drawbacks include migration due to shear stress at the foot-shoe interface and the ability to act as a foreign body inside the shoe thus altering movement behavior and subsequently effecting accurate measurement of plantar pressure (Misevich, 1985). The PEDAR is a matrix inshoe device in which to measure pressure. The use of a matrix of sensors in the form of an insole allows the ability to capture the entire plantar surface without the previous drawbacks mentioned. The use of insoles with matrices of sensors has not been without some technical difficulties including mechanical breakage of the sensors or the leads, sensor damage due to repeated loads at high pressure, and poor sensor performance in a warm, moist environment (Cavanagh et al., 1992). Insoles will only measure the force "normal" to each sensor in the matrix. During the initial and late portions of the stance phase of the gait cycle the force vector is altered (Kalpen & Seitz, 1994). Changes in the force vector can also occur when measuring the pressure over curved surfaces such as a foot orthotic. The resultant force may in fact be only a component of the measured force.

The key to measurement with any type of sensor technology whether in a research or clinical setting is having the ability to calibrate each sensor in the matrix. Being able to verify the measurements of each sensor with known loads throughout the measurement range is essential due to each sensors slightly unique characteristics. Previous research has shown reasonable reliability during bench and dynamic testing with the PEDAR system (Xia et al., 1994; McPoil & Cornwall, in press). Reliability of measurement has two factors: the reliability of the measurement device itself as well as the overall variability associated with gait. The purpose of this study is to determine how gait speed effects the loading and timing measures. A second key purpose was to determine an overall number of footfalls needed to obtain to representative force, pressure and timing data for the entire foot and various anatomical regions.

PROCEDURES

Twenty one volunteer participants (age M = 22.9; SD = 4.9) were asked to walk on treadmill at walking speeds of 2.0, 2.5 and 3.0 mph. No attempts were made to differentiate between foot types and lower extremity alignments. Each participant wore his or her own athletic shoes with the original footbed and hosiery during the time of study. The PEDAR inshoe system electronics were attached to the participant by a waist pack with leads going to a laptop computer and each insole. The sampling rate for the insoles was at a fixed rate of 50 Hz. Each insole was approximately 2mm thick containing 99 capacitive sensors. Data was collected for 20 seconds at two seperate times during each walking speed. To provide for the optimal shoe-insole fit, three different sizes of insoles were calibrated. The order of the testing speeds were randomly assigned to each participant. Each participant was allowed to walk for 5 minutes to acclimate themselves to the treadmill prior to data collection. From the bilateral measurements, a maximum of ten right footsteps for each participant were selected for analysis at the 2.0 mph speed from the two data collection cycles. At 2.5 mph, fourteen right footsteps were selected and sixteen at the 3.0 mph speed. Multimask software was used to define the loading variables of seven different anatomical regions or masks of the foot and the total foot. The seven geometric regions of the foot consisted of: one heel mask, one midfoot mask, three forefoot masks and two toe masks. The three forefoot masks under the metatarsal heads were divided into equal thirds with the medial forefoot mask over the first metatarsal, the central forefoot mask over the second and third metatarsal, and the lateral third over the fourth and fifth metatarsal heads. The medial toe mask was over the hallux and the lateral toe mask over the lesser toes. The following dependent variables were calculated relative to the entire foot and to each of the plantar masks of the foot: peak force of the maximum pressure picture (PF), force time integral (FTI), instant of peak force (IPF), peak pressure of the maximum pressure picture (PP), pressure

time integral (PTI), and the instant of peak pressure (IPP). Peak force in percentage of body weight, instant of peak force in ms, force time integral in percentage of body weight * s, pressure in KPa, pressure time integral in KPa*s and the instant of peak pressure in ms.. A repeated measures multiple analysis of variance (RM MANOVA) was performed for each of the dependent variables relative to the loading and timing measures reflecting the total foot and each region. Gait speed served as the independent variable. Reliability coefficients were performed for each of the timing and loading variables at each speed for the right foot. Sequentially steps were added to determine the changes in reliability for each of the force, pressure and timing variables.

RESULTS AND DISCUSSION

Effect of gait speed

The results of the RM MANOVA show a significant effect of gait speed on PF and FTI relative to the total foot with no differences on IPF, PP, IPP and PTI. When performing the same analysis with each mask, different regions of the foot behave similar as the total foot while others did not (Table 1). The results are similar to earlier findings associated with capacitive pressure platform measurements that force increase linearly with an increase in gait speed while the timing variables decrease (Huges et al., 1991). Pressure variables relative to each region of the foot were different with speed. This points to the need for controlling gait speed when performing between subject comparisons on a sample. For example, if comparing the overall effects of orthoses A and orthoses B on the loading characteristics, speed would have to be controlled. However, if performing a within subjects design, (each subject is their own control) speed within each walking trial of a subject's walking performance is of priority to the experimenter or clinician collecting data.

Table 1. Results of the RM MANOVA for the speed effects (based on the means of 10 footfalls) for the total foot and each plantar region.

Region	PF	IPF	FTI	PP	IPP	PTI
Total Foot	15.64*	ns	7.74*	ns	ns	ns
Heel	21.76*	18.08*	3.73*	8.51*	ns	5.15*
Midfoot	61.20*	18.13*	ns	39.44*	ns	ns
Lat. forefoot	64.54*	12.19*	ns	42.84*	ns	ns
Cen. forefoot	74.31*	12.73*	ns	22.55*	ns	ns
Med. forefoot	69.80*	12.81*	ns	17.94*	ns	ns
Lateral toe	67.24*	15.20*	ns	22.99*	ns	ns
Medial toe	63.30*	17.73*	ns	26.30*	ns	ns

* $p < .05$

Reliability

Coefficients of reliability were calculated for each variable for each of the seven anatomical regions for each walking speed. In all cases, the reliability increased as the number of footfalls increased. According to Fleiss (1986), 0.4 to 0.75 shows fair to good reliability while greater than 0.75 indicates excellent reliability. Table 2 depicts the reliability coefficients for 3.0 mph with a maximum of 16 footfalls observed. Some variables such as PF, FTI, PP and PTI are much more reliable than others (IPF and IPP). Total foot results are similar to Hughes et al. (1991) using a capacitive pressure platform. Regional foot areas revealed similar findings as with the total foot. The relative poor reliability of the timing parameters such as IPF and IPP may be explained by the variability of the subjects performance on a treadmill and/or the sampling frequency of 50 Hz of the insoles. However, a regional foot analysis of PF, FTI PP and PTI require a maximum of 3 steps for a 0.75 reliability or 9 steps for a 0.90 reliability.

Table 2

Number of Footfalls to Achieve a Reliability Coefficients of .7 or .9 for the Total Foot and Each Anatomical Region

	PF	IPF	FTI	PP	IPP	PTI
Rel. Coeff.	.7 / .9	.7 / .9	.7 / .9	.7 / .9	.7 / .9	.7 / .9
Total	2 / 2	3 / 4	2 / 3	2 / 6	16 / na	2 / 3
Heel	2 / 2	2 / 6	2 / 2	3 / 6	5 / 16	2 / 3
Midfoot	2 / 2	3 / 7	2 / 3	3 / 9	5 / 12	2 / 3
Lateral forefoot	2 / 7	4 / 7	2 / 2	3 / 6	2 / 6	2 / 2
Central forefoot	2 / 2	2 / 3	2 / 2	2 / 7	2 / 6	2 / 2
Medial forefoot	2 / 3	2 / 2	2 / 6	3 / 8	5 / 12	3 / 7
Lateral toes	2 / 4	2 / 2	2 / 3	3 / 8	5 / 16	2 / 2
Medial toes	2 / 3	2 / 2	2 / 5	2 / 4	2 / 3	3 / 7

Note: NA = Never Achieved

REFERENCES

Cavanagh, P.R., et al. Foot & Ankle. 2.185-194. 1992.

Fleiss, J. L., The Design and Analysis of Clinical Experiments, (pp. 1-32), New York: John Wiley & Sons. 1994.

Hughes, J. et al., Clin Biomech. 6, 14-18. 1991.

Kalpen, A., & Seitz, P., Proc. IVth EMED User Mtng. Ulm. Germany, Post. & Gait. 2. 236-237. 1994

Lee, D.N. Tutorials in motor behavior. In Stelmach & Requin (Eds., pp. 281-295). New York: Elsevier, 1980.

McPoil et al., Lower Extremity, In Press.

Misevich, K.W. ASME Foundation Conf. Sports. Biomechanics. 1985.

Xia, B. it al., Proc. ASB, Ohio State University, 1994

POSTURE DEPENDENT TRUNK STRENGTH AND *i*EMG ACTIVITY

T.S. Keller, M. Nathan, J.B. Lehneman, E.A. Compo, D.C. Guzik

Department of Mechanical Engineering, University of Vermont, Burlington, VT 05405

INTRODUCTION

Trunk muscle function has long been believed to play an important role in low-back pain (LBP), and while muscles may not be a primary source of LBP, they are certainly important for the mechanical functioning of the spine. Consequently, both clinical and basic science investigators are currently using a battery of diverse mechanical and electromyographic techniques to evaluate trunk muscle strength in both the sagittal and coronal planes. The recent literature contains substantial gender-specific information on trunk muscle function during extension activities, but quantitative information concerning task-specific and posture-specific trunk muscle function is much more limited. This paper describes the influence of sagittal plane posture on trunk isometric strength and erector spinae muscle *i*EMG activity in young, healthy men and women.

REVIEW AND THEORY

A considerable amount of literature exists on the assessment of isometric trunk muscle function in normal subjects and in patients with LBP (for a review see Andersson, 1992). Measures of muscle function include electromyographic (EMG) activity, and strength or the ability of the muscle or groups of muscles to exert force. In general, trunk muscle strength has been shown to vary with gender, age, body weight, joint angle and/or task performed, and exhibits a relatively monotonic increase with increasing EMG-activity. The majority of this work is concerned with sagittal plane muscle function.

Relatively few investigations have quantified isometric trunk strength and EMG variations associated with different postures. In seated postures, extension strength (Smidt et al., 1983; Graves et al., 1990) and flexion strength (Smidt et al., 1983) has been found to increase with increasing flexion angle. Similar findings have been reported for extension tasks at three standing postures (Marras et al., 1984).

Of interest is the finding for normal subjects that extensor muscles are stronger than flexors in seated postures, whereas LBP patients show the reverse (Graves et al., 1990 and others). The ratio of extensor muscle to flexor muscle strength is thus thought to be an important clinical determinant of muscle function (Andersson, 1992). Limited data exists, however, concerning the relationship between extension-flexion muscle strength ratios and trunk angles in the upright posture.

The purpose of this study was to quantify the sagittal plane postural dependency of trunk isometric muscle function, and to determine gender-specific and task-specific variations in muscle strength and EMG activity.

PROCEDURES

Ten healthy, young subjects (20-40 yrs) with no history of low back pain were examined (5 men and 5 women). Subjects were positioned and restrained in a triaxial trunk dynamometer (Isostation B-200, Isotechnologies, Inc., Hillsborough, NC). A series of eight flexion and extension tasks were performed through a 70° range-of-motion (50° F to -20° E) with the B200 locked at each angle. Five trials at each trunk angle were performed. For female subjects, rectified and integrated *i*EMG data was also recorded from left and right erector spinae muscles at L3 using a portable EMG amplifier (MioTrace 10, Noraxon, Doraville, IN). A 16 bit A/D system (MP100WS, BIOPAC Systems, Inc., CA) was used to acquire the *i*EMG and B200 torque signals at 50 Hz during testing. Peak values for flexion torque, extension torque, extension/flexion torque ratio, and *i*EMG amplitude (females only) were determined at each posture.

RESULTS

As expected the male subjects exhibited higher peak extension and flexion torque values than female subjects (Table 1). In the upright posture men were only slightly stronger in extension than flexion, with an E/F ratio close to 1. Women, however, were significantly stronger in extension compared to flexion (ANOVA, $P<0.05$), and consequently had an E/F ratio much greater than 1. The ratio of extension/flexion increased in a relatively linear manner with increasing joint angle, and was significantly greater (ANOVA, $P<0.005$) for females compared to males at all angles (Fig. 1). For both males and females, extension moments increased monotonically (about 4-fold) from -20° extension to 50° flexion (Fig. 2a,b). The flexion moment tended to decrease at higher joint angles, particularly in the male subjects (Figs. 2a,b). For the five female subjects, peak erector spinae *i*EMG activity during extension tasks increased with increasing joint angle, and a relatively linear, albeit not 1:1, correspondence between peak isometric extension moments and peak erector spinae activity was noted (Fig. 3).

DISCUSSION

The postural dependence of trunk muscle strength and EMG activity observed for the male and female subjects in

this study has important implications in terms muscle force (gain) calibration and EMG normalization procedures which are adopted for spine biomechanical modeling and analysis. For example, forces and moments obtained from static or dynamic analyses utilizing muscle gains calculated in the upright standing posture will be overestimated (about 2-fold) in extended postures, and will be underestimated a similar amount in flexed postures. The increased E/F ratio observed at all sagittal plane joint angles for females in comparison to males indicates that there are intrinsic differences in trunk function between these groups. Examination of E/F torque ratios at several joint angles may also provide additional insight into spinal abnormalities in low back pain patients.

REFERENCES

Andersson G. *The Adult Spine Principles and Practice*, (pp 242-273), Raven Press, 1992.
Graves, J. et al. *Spine* 15, 289-294, 1990.
Marras, W. et al. *Spine* 9, 176-187, 1984.
Smidt, G. et al. *Spine* 8, 211-219, 1983.

ACKNOWLEDGEMENTS

Research supported by the National Institute of Chiropractic Research and the Foundation for Chiropractic Education and Research.

Table 1. Peak Trunk Strength - Upright Posture (0°) (Mean ± S.D.)

	Men	Women
Flex. (Nm)	203.4 ± 32.0	67.5 ± 15.1
Ext. (Nm)	214.0 ± 67.8	125.6 ± 25.5
Ext./Flex.	1.04 ± 0.25	1.90 ± 0.39

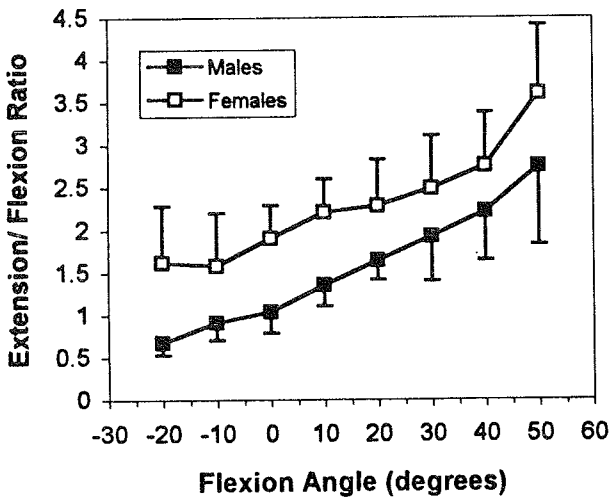

Fig. 1. Extension/Flexion ratio (mean, S.D.) versus sagittal plane joint angle.

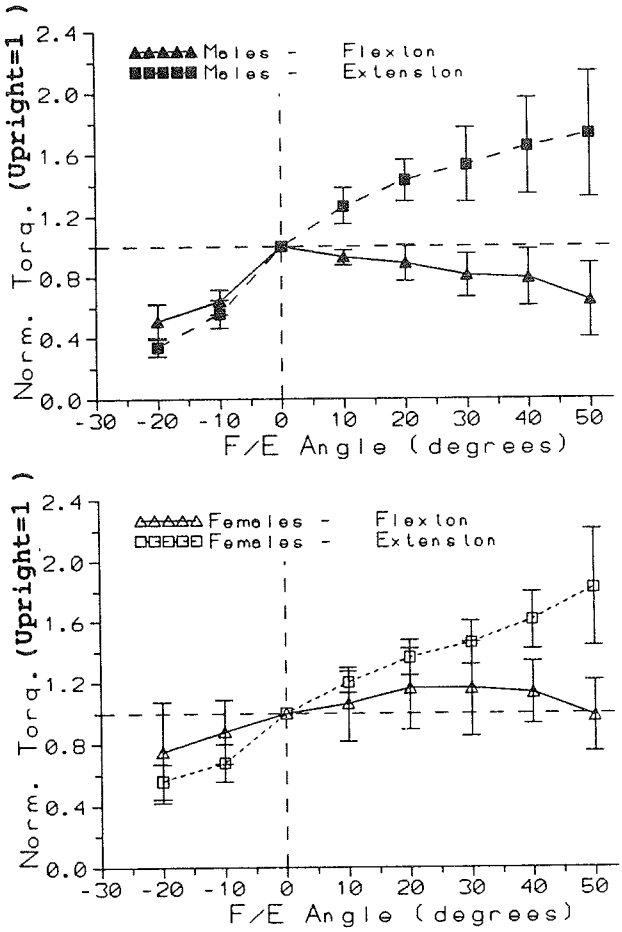

Fig. 2a,b. Isometric torque (normalized to upright posture) versus joint angle for male (top) and female (bottom) subjects. Mean values and standard deviations are shown.

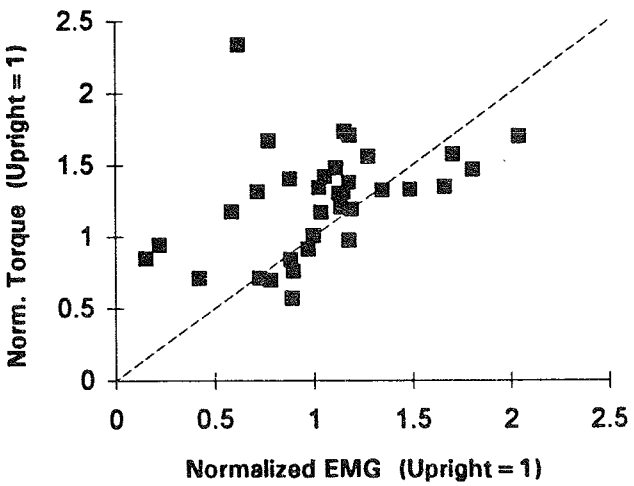

Fig. 3. Peak isometric extension torque vs peak *i*EMG for females. Each point represents average value for 5 trials.

SWAY VELOCITY MAY NOT PREDICT POSTURAL INSTABILITY

T. Lundin and M. Grabiner
Department of Biomedical Engineering, The Cleveland Clinic Foundation
Cleveland OH 44195

INTRODUCTION

Postural stability has received substantial scientific and clinical interest as a factor that may contribute to the predisposition to falls in the elderly population. Age-related muscle weakness, diminished somatosensory, vestibular and visual function are associated with increased postural sway. However, the supportive data for conventionally proposed relationships between increased postural sway, diminished postural stability, and the predisposition to falling are not convincing. This reflects that the generalized measures of postural sway, such as sway amplitude, often presumed to reflect postural stability, are "neither very sensitive nor very specific", (Horak et al., 1989). However, even if sway amplitude adequately described static postural stability there exists a large discontinuity between static and dynamic postural stability and the predisposition to falling in the elderly. The traditionally held belief that aging has a deleterious and *obligatory* effect on postural sway *amplitude* has recently been challenged (Fernie et al., 1982).

Sway velocity has been reported to be higher in elderly subjects than young subjects (Pyykko et al., 1990) and suggested as an index of the predisposition to falling. It has been demonstrated, however that increased sway velocity during static and perturbed stance is not a predictor of falls in "normal" elderly subjects (Baloh et al., 1994).

The aim of this study was to investigate age-related differences in sway velocity during static posture and a more challenging postural task requiring maximum voluntary sway velocity in the anterior-posterior direction. It was expected that sway velocity in the static condition would be higher in the elderly subjects compared to the young subjects and that this relation would be reversed in the dynamic condition. It was not expected, however, that these differences would be functionally significant.

PROCEDURES

Fifteen elderly (age: 73.4±2.0) and eleven young (age: 23.8±3.1) subjects volunteered to participate in this study. A strain gauge force plate was used to measure sway velocities in the anterior-posterior direction under static and dynamic conditions. Sway velocity was calculated by differentiating the center of pressure (COP) data obtained from the force plate.

For both test conditions subjects were positioned on the force plate with their feet as close together as possible and their arms at their sides. Data were collected for 20 seconds at 100 Hz.

For the static condition, subjects were instructed to maintain an upright posture and to remain as still as possible. During the dynamic condition, subjects were instructed to oscillate at the ankle joints from their anterior limit to their posterior limit of stability as rapidly as possible.

Maximum anteriorly and posteriorly directed sway velocities were extracted from both the static and dynamic condition trials. A two by two by two (age by condition by direction) analysis of variance (ANOVA) was performed on the extracted variables. A significance level of $p<0.05$ was selected.

RESULTS

The results of the ANOVA on the sway velocity variables show that during the static condition the elderly did not have significantly higher ($p>0.05$) sway velocities in the anterior or posterior directions than the young subjects. (Table 1). Perhaps more surprisingly, during the dynamic condition, where the subjects were instructed to sway as rapidly as possible, there were no significant differences in sway velocity between the age groups. The maximum sway velocities during the dynamic condition were significantly higher ($p<0.05$) than during the static condition.

Table 1: Maximum sway velocity (cm/s).

	Young	Elderly
Static anterior	3.6(1.6)	5.7(2.6)
Static posterior	3.2(0.9)	6.2(1.8)
Dynamic anterior	39.8(15.8)	32.1(8.0)
Dynamic posterior	38.8(14.0)	35.3(17.1)

DISCUSSION

The findings of this study are inconsistent with those previously reported on sway velocity in elderly subjects. In neither the static nor dynamic conditions, did the elderly subjects obtain maximum sway velocities which were significantly different from that of the young subjects.

The functional significance of the previous reports become less evident, however, when static sway velocities are referenced to maximum voluntary sway velocities. In the present study, during static posture, the elderly subjects reached a maximum sway velocity which was approximately 15% of that achieved during the dynamic condition. It would appear that this value would be trivial if applied in a postural perturbation and stepping response paradigm.

The maximum sway velocity achieved during static posture also seems trivial when related to the COP limits of stability. During static posture, the average COP displacement was 2.9 cm, which represented approximately 21% of the distance elderly subjects reached during the dynamic condition (14 cm). Thus, in elderly subjects, an upright stance in which COP excursion and velocity are small fractions of the maxima available, provides a stable position even if those variables are significantly different from those of young subjects.

REFERENCES

Baloh et al. *J Amer Geriatr Soc*, 42, 405-412, 1994.

Fernie et al. *Age Ageing*, 11, 11-16, 1982.

Horak et al. *Neurobiology of Aging*, 10, 727-738, 1989.

Pyykko et al. *Age Ageing*, 19, 215-221, 1990.

JOINT KINETIC-KINEMATIC RELATIONSHIPS DURING WHEELCHAIR PROPULSION

Rick N. Robertson, Ph.D.[1,2,3], Rory A. Cooper Ph.D.[1,2,3], Greg Ensminger[3], Michael L. Boninger, M.D.[1,2,3]
1Division PM&R, University of Pittsburgh Medical Center, Pittsburgh, PA 15213
2Dept. Rehab. Science & Technology, University of Pittsburgh, Pittsburgh, PA 15261
3Human Engineering Research Labs, Highland Drive Veterans Affairs Medical Center, Pittsburgh, PA 15206

INTRODUCTION

This paper describes the relationship between the joint reaction forces and moments and the position of the upper extremity joints during wheelchair propulsion. Three groups of subjects, categorized by gender and wheelchair use experience, pushed a wheelchair outfitted with a force measuring device on a dynamometer at a set speed. Subsequent analysis of joint reaction forces and moments showed that the 3 groups differed in the level of forces across the joints and when the peak forces occurred in the propulsion cycle. Additionally, the joint angles when peak forces occurred varied among the groups. Wheelchair users experience a high percentage of cumulative trauma injuries. Results from this study will provide information to reduce the level of stresses borne by joint structures by implementing changes in stroke mechanics or improving the fit between the user and the wheelchair.

REVIEW AND THEORY

Manual wheelchair propulsion is used as a means of mobility by approximately 1.2 million people in the US (Philips & Nicosia, 1990). The prevalence of upper extremity injury in the spinal cord injured (SCI) population using wheelchairs is high. Upper extremity injury among wheelchair users has been shown to be as high as 51% with shoulder problems (Nichols et al., 1979), a 30% incidence of persistent, chronic shoulder pain was found during transfers (Bayley et al., 1987), and upper extremity pain (Gellman et al., 1988A) and prevalence of Carpal Tunnel Syndrome (Alijure et al., 1985; Gellman et al., 1988B) increased with greater years post injury.

Net joint moments and forces provide information related to the overall stresses being borne across joint structures. Repetitive overuse trauma to upper extremity joint structures could eventually lead to injuries which prevent manual wheelchair users from being able to push their chairs. Information related to joint motion and the related net joint forces will be used to implement changes in the way the person applies forces to the pushrim through modifying the user-wheelchair ergonomics i.e., fit to chair, or by changing the stroke biomechanics.

Although a number of researchers (Veeger et al., 1992) have studied pushrim forces, the lack of adequate instrumentation has prevented joint moments and forces from being determined. We have described a device (SMART^{Wheel} (Asato et al., 1993)) which allows the measurement of forces and moments applied to the pushrim and the location of the center of pressure (COP) (Robertson & Cooper, 1993); information which is necessary to determine joint kinetics. The present paper analyzes the relationship between joint moments and forces and joint motion at the wrist, elbow and shoulder for 3 different groups of wheelchair users based on level of experience. This information will provide useful information as a first step in determining harmful stroke mechanics.

PROCEDURES

Each of twelve subjects (4 male wheelchair users M-WCU, 4 male non-wheelchair users M-NWCU and 4 female non-wheelchair users F-NWCU) gave informed consent to participate in this study. Subjects were asked to push a Quickie 1 wheelchair (Sunrise Medical, Inc., Quickie Wheelchair), fitted with the Smart^{wheel} (Asato et al., 1993) on the right side, with the chair secured to the wheelchair dynamometer (Vosse et al., 1990). Subjects practiced pushing on the dynamometer until they were comfortable with the set-up. Each subject was then asked to push the wheelchair between 1.5 and 2.0 mph (.67 and .89 m/s). Subjects monitored their speed by viewing an analog tachometer mounted at the front of the dynamometer.

SMART^{Wheel} data were collected at 75 Hz per channel for approximately 10 complete strokes. Processing of the signals from the beam mounted strain gages resulted in a determination of forces in the x and y direction and moment about the z-axis (x - anterior-posterior; y - superior-inferior; z - medial-lateral). Video data were collected at 60 Hz from a right sagittal view of each subject. Video data was synchronized with force data. An interpolating spline was used to match video data to the 75 Hz force data. A Peak 5 System (Peak Performance Technologies, Inc.) was used to generate limb acceleration values following smoothing of the raw data utilizing a Butterworth filter with a 6 Hz cutoff.

Center of pressure (COP) on the push-rim was determined by a method described previously (Robertson & Cooper, 1993). The COP on the hand was assumed to be at the 2nd MP joint. Inertial parameters for the hand, forearm and arm were estimated using data provided in the literature (Winter, 1990). The method described by Cooper et al. (1993) was used to estimate net muscle moments and net joint reaction forces.

RESULTS

Table 1 depicts the maximum moments reached at the elbow (A) and wrist (B) for each group. The joint angles and when in the propulsion phase this peak occurred is shown. The experienced group (M-WCU) had lower moments at these joints and a tendency for the peak to occur earlier in the propulsion phase. Peak reaction forces at the wrist and elbow (not depicted) followed a similar pattern to those found at the shoulder for each group (Figure 1).

Table 1: Maximum Elbow Moment (A) and Maximum Wrist Moment (B) and Corresponding Joint Angles and Percent of Propulsion Phase.

A.

	MaxEl Mom. (N-m)	Elbow Angle (deg)	Shoul Angle (deg)	Wrist Angle (deg)	% Prop
F-NWCU	-22.2	130.1	23.1	177.1	73%
M-NWCU	-29.0	128.5	22.4	183.3	71%
M-WCU	-19.6	130.7	24.5	185.1	69%

B.

	MaxWr Mom. (N-m)	Wrist Angle (deg)	Shoul Angle (deg)	Elbow Angle (deg)	% Prop
F-NWCU	-18.8	176.0	24.6	128.8	71%
M-NWCU	-25.2	181.2	25.7	126.2	67%
M-WCU	-17.2	180.3	30.3	127.8	62%

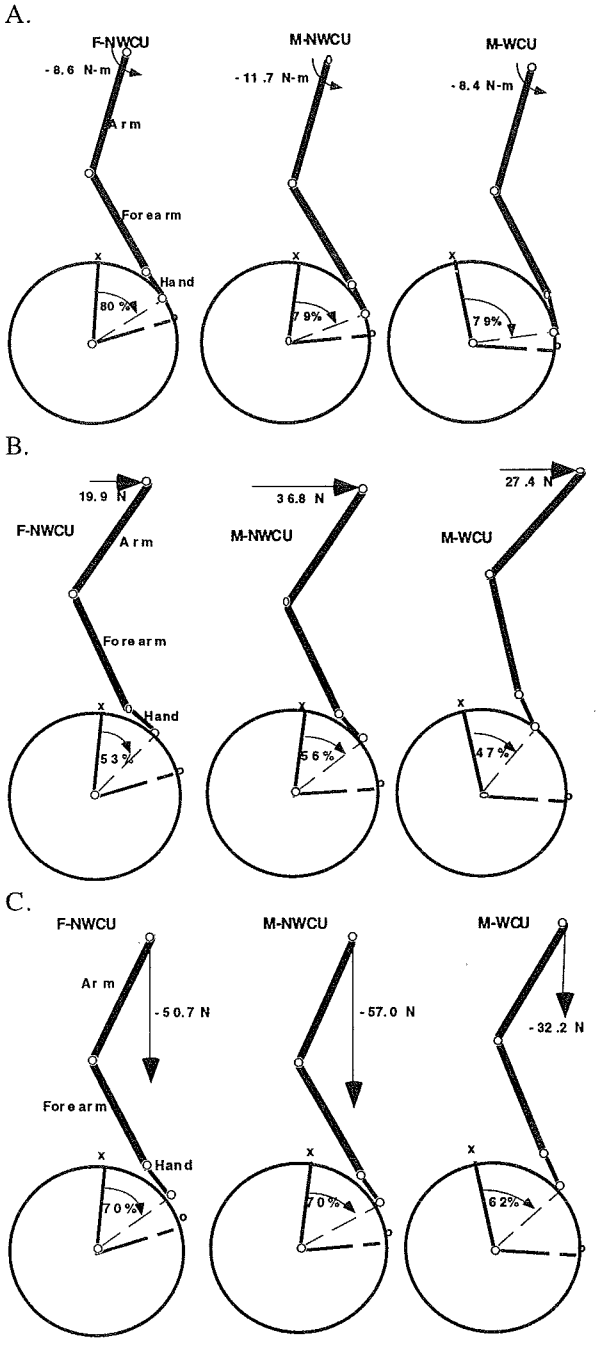

Figure 1: Joint positions and hand-pushrim relationship at peak shoulder moment (A), peak horizontal reaction force Fx (B), and peak vertical reaction force Fy (C).

Figure 1 depicts peak moments (A), and peak horizontal forces Fx (B) and peak vertical forces Fy (C) at the shoulder joint for each group. Each picture represents the mean of 20 strokes (4 subjects x 5 strokes each). At this point in time, percent into the propulsion phase and orientation of each segment is shown. The "x" and "o" on the pushrim indicate where each group on average first contacted the pushrim and when their hand left the pushrim, respectively. The inexperienced male subjects (M-NWCU) had the highest moments and forces at the shoulder. The peak shoulder reaction forces occurred earlier in the propulsion phase of the experienced users (M-WCU) and the peak Fy (vertical) reaction force was lower for both groups. Joint position at peak force was not appreciably different among groups, except that when peak horizontal and vertical reaction forces occurred, the experienced users had more extreme positions of shoulder extension and elbow flexion.

DISCUSSION

Cumulative trauma disorders of the upper extremity have been reported for a large number of manual wheelchair users. The present study showed that experience using a wheelchair resulted in differences in the propulsion phase when net joint peak forces and moments occurred. The greatest differences were found when peak vertical joint reaction forces occurred. The inexperienced male subjects had larger peak forces at all of the joints and they developed them later in the propulsion cycle when compared to the experienced group. At the shoulder, the vertical force has a tendency to drive the humeral head upward into the acromial shelf; a possible mechanism for the development of rotator cuff problems. At the wrist, this component may put carpal canal structures at risk and lead to the development of carpal tunnel syndrome. Changing the stroke mechanics of users or their fit to the wheelchair may have dramatic effects on the joint kinetics. These conditions when studied in relationship to the information provided in this paper will lead to development of strategies by the clinician for reducing the incidence of manual wheelchair propulsion injuries.

REFERENCES

1. Alijure, J. et al.*Paraplegia* , 23, 182-186, 1985.
2. Asato, K.T. et al. *IEEE Trans. Biomed. Eng.*, 40(12), 1320-1324, 1993.
3. Bayley, J.C. et al. *J. Bone & Joint Surgery* (AM), 69, 676-678, 1987.
4. Cooper, R.A. et al. Proceedings of 16th Annual Conference of RESNA, Las Vegas, NV, 277-279, 1993.
5. Gellman, H. et al. *Clin. Orthop.*, 233, 132-135, 1988A.
6. Gellman, H. et al. *J. Bone Joint. Surg. [Am],* 70: 517-519, 1988B.
7. Nichols, P.J.R. et al. *Scand. J. of Rehabil. Med.,* 11, 29-32, 1979.
8. Niesing, R. et al. *Med. & Biological Eng. & Comp.,* 28, 329-338, 1990.
9. Philips, L. & Nicosia, A. *J. of Rehab. Res. and Develop.*-Clinical Supplement No. 2, 1-7, 1990.
10. Robertson, R.N. & Cooper, R.A. Proceedings 17th Annual Meeting of the American Society of Biomechanics, Iowa City, Iowa, pp. 202-203, 1993.
11. Veeger et al. *Europ. J. Appl. Physiol.*, 64, 158-164, 1992.
12. Vosse, A.J. et al. Proceedings RESNA 13th Annual Conference, Washington, D.C., June, pp. 59-60, 1990.
13. Winter D.A. Biomechanics and Motor Control of Human Movement, Second Edition, John Wiley & Sons. 1990.

ACKNOWLEDGEMENTS

Partial funding for this research was provided by the US Department of Veterans Affairs Rehabilitation Research & Development Services (Project #B686-RA) and the US Department of Education, Rehabilitation Services Administration (H129E00005).

Rick N. Robertson, Ph.D.
Division Physical Medicine & Rehabilitation
University of Pittsburgh Medical Center
Kaufmann Building, Suite 901
Pittsburgh, PA 15213
TEL: (412) 648-6976
FAX:(412) 692-4410
EMAIL: RICKR@PITT.EDU

A THREE-DIMENSIONAL ANALYSIS OF FACIAL MOTION

K. Moffatt[1], M. Gross[2], C-A. Trotman[3]
[1]Dept. of Industrial Engineering, [2]Division of Kinesiology, [3]Dept. of Orthodontics & Pediatric Dentistry, University of Michigan, Ann Arbor, MI 48109

INTRODUCTION

The occurrence of cleft lip and palate in the United States is one in every 600-1500 children[1]. By age 25, most patients have undergone on average six surgeries to regain facial function and correct facial disfigurement. Currently, there are no reliable methods to quantify the extent of this facial impairment or the success of the surgical techniques. Our objective is to develop a method to assess facial function in children with a repaired cleft lip and palate.

Few papers have been written on facial animations as they pertain to facial function. Johnson *et al*[2] measured amplitudes of animations using 2D standardized facial photographs taken at rest and at maximal expression. Frey and coworkers[3] conducted a 3D video analysis of ten facial animations. However, their data could not be used to determine the relative accuracy of 2D and 3D methods.

The purpose of this study was to determine whether 3D analysis of facial motion provides a more accurate assessment than 2D analysis over a variety of facial animations.

PROCEDURES

Six subjects were tested, three with unilateral cleft lip and palate (mean age 12.6 yrs.) and three normal subjects (mean age 23 yrs).

Fifteen reflective markers (5 mm in diameter) were placed on each subject's face at specific anatomical landmarks (Fig. 1). Landmarks were: alar base (AB), commissure (CM), infraorbital (IO), medial canthal (MC), supraorbital (SO), and upper lip (UL). Markers had a 2 mm circle punched out of the center to assist in accurate placement. Each subject sat down in a dental chair with an adjustable headrest to assure an upright head posture. Video cameras (60 Hz) were placed in the front of and on either side of the subject's face, at a distance of approximately 0.5 m.

Each subject performed five maximum amplitude facial animations: lip purse (LP), cheek puff (CP), grimace (GR), smile (SM), and eye closure (EC). Each subject executed one trial of each animation and rested before executing another set of animations. Motion Analysis software was used to generate 2D and 3D coordinates for each marker. The 2D coordinates corresponded to the frontal view.

The duration of each facial animation was calculated from the initiation and termination times. To verify stability of the medial canthal markers, intercanthal marker distance was calculated. To eliminate the effects of head motion, the position of each landmark was expressed relative to the ipsilateral medial canthal marker. The motion of each landmark was calculated as the difference between its position at rest and at maximum animation. Analysis of variance was used to determine the effects of animations and markers on motion amplitudes. Paired t-tests were used for posthoc comparisons. A $p < 0.05$ was used to detect significant differences.

RESULTS AND DISCUSSION

To account for potential head motion during facial animations, stable markers were needed for reference.

We hypothesized that the medial canthal points would remain stable during the animations, indicating head movement. To test this hypothesis, we calculated the 3D distance between the right and left medial canthal landmarks. The mean distance over all animations was 0.036 $\pm$ 0.029 cm, ranging from 0.013 cm to 0.142 cm. Because the standard deviations were so small, we concluded that the motion of medial canthal landmarks was due to head motion and not facial motion, and that the land marks could be used for reference markers.

3D motion amplitudes were greater than the 2D amplitudes for all landmarks. However, the difference was significant only for the commissure landmark. In Fig. 2, the 3D and 2D amplitudes are shown for several markers during a smile. Although the 2D analysis was sufficient for some markers, it underestimated the amplitude of the markers in the lower face that tended to move the most during animations.

Similarly, the 3D motion amplitudes were greater than the 2D amplitudes for all animations. However, the difference was significant only for the smile. In Fig. 3, the 3D and 2D amplitudes for the five animations are shown. For animations with extensive mouth motion (i.e, LP, CP, SM), 3D analysis provided a more accurate estimate of motion. For the other animations, the 2D analysis was adequate.

In summary, our results showed greater motion amplitudes for all landmarks and animations when 3D analysis was used. The biological significance of these differences is not yet known. Since the most mobile landmarks were the most affected by analysis type, our results suggest that 3D analysis may be the appropriate method for assessing facial function following surgical intervention.

REFERENCES

1. Ladd, W.E. Boston Med & Surg. J., 194, 1016-1025, 1962.
2. Johnson, P.C. et. al. Ann. Plast. Surg., 32, 171-179, 1994
3. Frey, M. et. al. Plast. Reconstr. Surg., 93, 1334-1349, 1994.

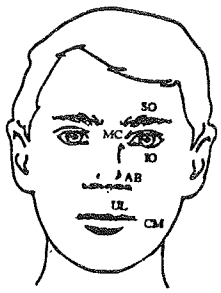

Fig. 1 Location of landmarks

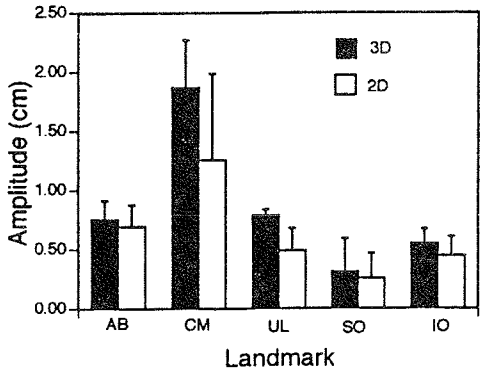

Fig. 2 Motion amplitudes during smile

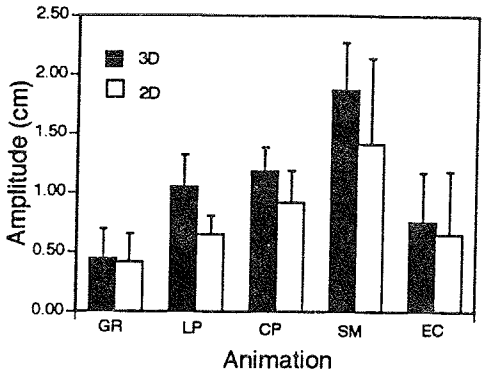

Fig. 3 Motion amplitudes for commissure marker

SAGGING REDUCES TENSION

A. Johnson
Biology Department, Bowdoin College, Brunswick, ME 04011

INTRODUCTION

The long, compliant feeding tentacles of the marine terebellid polychaete Eupolymnia heterobranchia not only stretch out over a sandflat substratum but also extend into flow. Typically, they extend into flow by attaching their tentacles, via mucus and cilia, to floating blades of algae. These tentacles cope with forces due to flow by sagging, much as the cables of suspension bridges sag in response to gravitational forces. The mathematical analogy is such that, when the tentacles are suspended perpendicular to flow, the same equations used to describe tensions in the cables of suspension bridges can be used to understand tension in the tentacles of these terebellid worms. Most studies that examine modification of flow induced forces on marine organisms have focused on modifications of the DRAG experienced by that organism and the contributions of the organism's behavior to drag reduction. The present analysis examines the contribution of sagging not only to drag reduction, but also to the alignment of force vectors acting on the tentacles as they sag in the flow.

REVIEW AND THEORY

The Parabolic Cable Equation: Tension in the cables of suspension bridges is calculated using the force acting on the cables, the distance (or span) between points of attachment of the cable, and the amount of sag in the cable (Figure 1). For tension in parabolic cables (those that carry a uniform distributed load), the maximum tension, T, in the cable occurs at the points of attachment (Steinman, 1942). Drag exerts a force that acts along the horizontal distance (projected area) of a tentacle oriented perpendicular to flow and suspended between two points of attachment. Therefore, tension in the tentacle as a function of drag, D, is

$$T = \sqrt{\left(\frac{D}{2}\right)^2 + \left(\left(\frac{D}{8}\right)\left(\frac{L}{f}\right)\right)^2}$$

where L is the span between points of attachment of the cable, and f is the sag of the cable.

Drag on tentacles is determined from the standard drag equation:

$$D = 0.5\, C_d\, \rho\, S\, U^2$$

where D is drag, C_d is the drag coefficient, ρ is the density of seawater, S is the projected area of each tentacle perpendicular to flow and U is the velocity. The conventional drag coefficient, C_d, was estimated from an empirical formula (for Reynolds numbers (Re) from unity to 10^5) for a cylinder oriented perpendicular to flow (White, 1974 cited in Vogel, 1981) where Re is based on tentacle diameter, d.

Analysis of drag reduction: The equations for tensions in the cables of suspension bridges, as used above, will quantify the influence of sagging on tentacular tension as a consequence of the alignment of force vectors, but neglects the potential effect of sagging on drag reduction. In fact, the estimate of C_d used above will be an overestimate of the coefficient of drag for a sagging tentacle, because portions of the tentacle are oriented at some smaller (lower drag) angle to flow. The coefficient of drag for a cylinder at some angle to flow, C_{d_θ}, can be determined from C_d (for Reynolds numbers to 10^5; Hoerner, 1965) by:

$$C_{d_\theta} = C_d \cos^3 \theta$$

where θ is the smallest angle between a line perpendicular to flow and the surface of the tentacle. The angle θ can be obtained at each point on a tentacle by:

$$\theta = \text{arctangent} \frac{d\left(\left(4 f x^2\right)/L^2\right)}{dx}$$

where x is the distance along the span from the origin (at the point of maximum sag) and $\left(\left(4 f x^2\right)/L^2\right)$ is the parabolic equation describing the sagging tentacles (Steinman, 1942). An estimate of the corrected coefficient of drag for the entire tentacle, C_{d_c} is then:

$$2\frac{C_d}{L}\int_0^{L/2} \cos^3 \theta \, dx$$

This is similar to the method used to determine the drag coefficient of a wing from the sum of the local drag coefficients of infinitesimal sections of the wing (Abbott and Von Doenhoff, 1959).

Drag may be reduced not only because the summed coefficient of drag of a tentacle is reduced as it sags, but also because in a constant volume tentacle diameter will decrease with increasing sag (increasing stretch). A corrected diameter, d_c, was estimated by

assuming that the tentacles maintain a constant volume as they stretch:

$$d_c = d\,\lambda^{-0.5}$$

where λ (the extension ratio) is the ratio of the total length of the tentacle (l) to the span of the tentacle (L).

PROCEDURES

E. heterobranchia, intact within the tubes in which they naturally live, were buried in sand in glass dishes a recirculating flow tank. A micromanipulator was used to lower a probe to the mouth of the worm's tube and, subsequently, to raise the probe after the worm had attached a tentacle using cilia and mucus. In this way, tentacles were oriented perpendicular to the direction of flow, with two points of attachment: one on the probe, the other on the body of the worm.

Experiments were conducted at velocities between 0.5 and 7.0 cm s^{-1}, corresponding to Re between 1 and 7, and representing the natural range of velocities experienced by terebellids in the field. Span (L), sag (f), and tentacle length (l) of each tentacle were measured off photographs taken with a camera oriented perpendicular to the sag of the tentacle.

RESULTS AND DISCUSSION

Although calculated drag on suspended tentacles increased with increasing velocity (linear regression analysis: $F(1,76) = 77.1$, $p = 0.0001$, $R^2 = 0.50$), maximum tension (at the points of attachment) was independent of velocity (linear regression analysis: $F(1,76) = 2.67$, $p = 0.11$), even when using data corrected for C_{d_c} ($F(1,76) = 0.72$, $p = 0.40$) or both C_{d_c} and d_c ($F(1,76) = 2.38$, $p = 0.13$). Tension remained constant because a tentacle of a given length sags more as velocity increases (linear regression analysis of ln (L/f) with ln (U): $F(1,76) = 90.1$, $p = 0.0001$, $R^2 = 0.54$). Thus, sagging decreased the tension a tentacle experienced relative to what it would have experienced if it did not sag.

Drag reduction could potentially enhance this reduction in tension because tentacles thin as they sag and because portions of the tentacles are oriented at angles less than perpendicular to flow. Calculations with the corrected values revealed that although drag reduction by sagging did lower tension in tentacles exposed to the highest velocities, the decrease in tension was less than 2% of that obtained by simple realignment of force vectors.

Thus, drag reduction by reorientation due to sagging and by thinning of the tentacles made a relatively small contribution to the reduction in tension experienced as a result of sagging. The largest contributor to reduction of tension was achieved by closer alignment of force vectors that resist flow (parallel with the length of the tentacle) with force vectors imposed by flow (parallel with the direction of flow). This latter mechanism does have the same ultimate effect as drag reduction: by modifying the effects of flow forces these organisms can function in a wider range of flows.

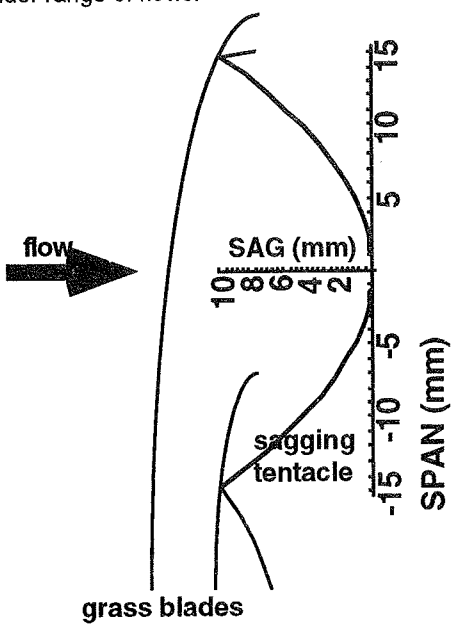

Figure 1: Tentacle in flow.

REFERENCES

Abbott, I. H. and A. E. Von Doenhoff. Theory of Wing Sections, Dover Publications, Inc., New York, 1959.

Hoerner, S. F., Fluid-Dynamic Drag, Hoerner Fluid Dynamics, Bricktown, N.J., 1965

Steinman, D. B. Movable and Long-span Steel Bridges. (pp.289-358), G. A. Hool and W. S. Kinne [Eds.], McGraw-Hill, New York, 1942.

Vogel, S., Life in Moving Fluids, Willard Grant Press, Boston, 1981

ACKNOWLEDGEMENTS

Thanks to O. Ellers, R. Emlet, J. Gosline, M. Koehl, M. LaBarbera, D. Pentcheff, and S. Vogel. This research was supported, in part, by a Libbie Hyman Memorial Field Scholarship, Northeastern University and NATO post-doctoral fellowships, N.S.F. Research Planning Grant OCE 90-09763 to A. Johnson and N.S.F. Grants OCE-8352459 and OCE-8510834 to M. Koehl. This abstract represents work that is published in Biol. Bull. 185: 10-19.

KINEMATICS OF CRABS LOCOMOTING IN WATER VERSUS AIR

M. M. Martinez, R. J. Full, M. A. R. Koehl

Department of Integrative Biology, Univ. of Calif., Berkeley CA 94720-3140

INTRODUCTION

The transition between aquatic and terrestrial habitats has been made in a number of animal lineages (notably the arthropods, molluscs, annelids, and vertebrates). Although pedestrian locomotion in air and swimming in water have been studied extensively, relatively little is known about the biomechanics or physiology of underwater pedestrian locomotion. As an intertidal animal moves from air into water, its effective weight is substantially reduced by buoyancy while the fluid dynamic forces (e.g. lift and drag) are increased 800-fold. The changes in the magnitude of these forces is likely to have substantial consequences for locomotion as well as resistance to being overturned. The 3-D kinematics were measured for intertidal crabs (Grapsus grapsus) as they moved freely over a flat substratum through water and through air.

REVIEW AND THEORY

He et al. (1991) and Newman (1992) have shown that when locomoting under conditions of simulated reduced gravity, people adjust their kinematics and experience greater freedom in gait choice. Since increased buoyancy in water reduces the effective gravitational force on a crab, it was hypothesized that crabs would make the same kinematic adjustments underwater as people do under conditions of simulated reduced gravity. Greater buoyancy and hydrodynamic forces would also increase the likelihood that a crab would overturn or wash away in water. Thus it was also hypothesized that crabs would adopt a more stable posture in water, effected by a lower body position and increased stance width.

PROCEDURES

Crabs were videotaped as they walked freely over a flat substratum through still air and still sea water. 3-D kinematics of one stride per crab were obtained with Peak Performance Motion Analysis software. Air and water trials at matched average velocities (10 cm/s) were analyzed for six individual crabs. Several stride parameters including stride length (distance traversed in one stride), duty factor (time of ground contact/time of stride), and width of stance were analyzed in two ways 1) for each pair of legs, parameters in water were compared to air and 2) data for ipsilateral legs pairs were averaged and the mean values for each individual crab were compared for water versus air trials.

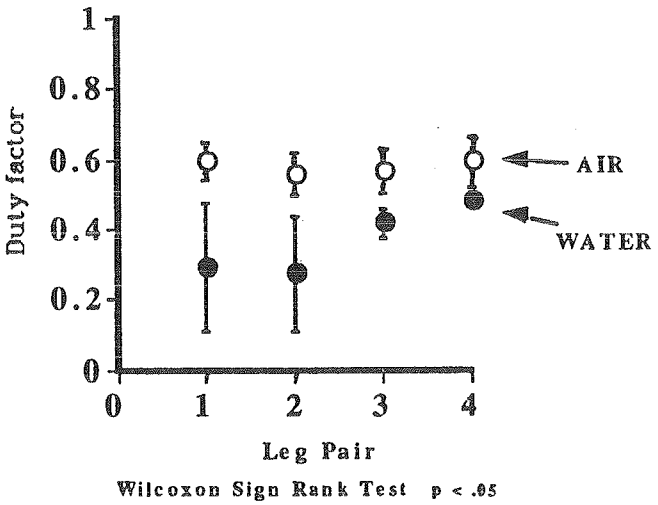

Figure 1: Duty factors were smaller in water than in air for each leg pair. Each point represents the mean value for six individual crabs locomoting sideways at a constant average speed (10 cm/s).

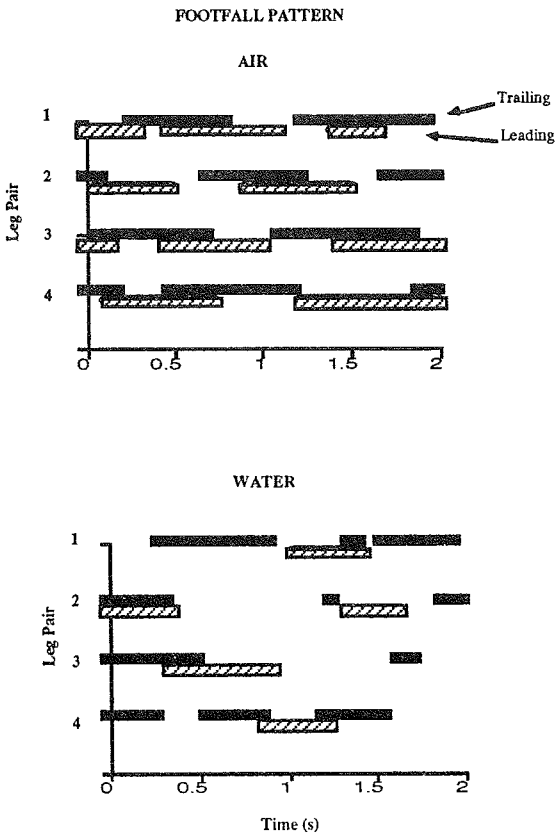

Figure 2: Footfall patterns for an individual crab locomoting in air versus water at 10 cm/s. Bars represent ground contact. Compared to air trials, footfall patterns in water trials were highly irregular, with individual legs cycling at different rates

RESULTS

In water the kinematics were so variable that the conventional definition of a stride (a complete cycle of all leg movements) could not be applied. Legs cycled at different rates, with some legs not cycling at all throughout the time examined. Thus a stride was defined as the complete cycling of whichever leg had the longest stride period in the time examined, usually the third or fourth pair of legs.

Crabs moving under water showed the predicted result of a decreased duty factor compared to locomotion in air, but did not show consistently increased stride length. On average, two more legs were in contact with the substratum under water and contact time was 0.5-33 times that in air. Although the height of the body was not significantly different, the width of the crab's stance was 19% greater in water than air.

Duty factor, number of legs cycling and pitch angle (angle at which the body meets oncoming flow) showed greater variance in water trials than in air trials.

DISCUSSION

Crab locomotion under water differed from that in air in a number of ways. Similar to humans in reduced gravity, crabs locomoting underwater had lower contact times and duty factors. Despite greater stability conferred by a wider base of support, crabs in water pitched more, which may have increased the hydrodynamic forces tending to overturn them. Aquatic locomotion was characterized by use of a greater number of gaits and more variable leg and carapace kinematics.

The mechanics of locomotion by intertidal crabs will provide biological inspiration for the design of autonomous legged underwater vehicles (ALUVs) that must travel both in air and underwater.

REFERENCES

He, J. et al. *J. App. Physiol.* 71(3)863-870, 1991.
Newman, D. *Ph.D. Thesis. M. I. T.*, 1992.

ACKNOWLEDGMENTS

Thanks are due to the Hawaii Institute of Marine Biology, and K. Arfaa. This work was supported by Pauley Fund for Marine Research to M. Martinez and ONR grant #N00014-90-J-1357 to M. Koehl.

EXTENSOR AND FLEXOR FUNCTION IN EXOSKELETONS: MUSCULOSKELETAL MODEL OF AN INSECT LEG

A.N. Ahn, C.M. Eckel and R.J. Full
Department of Integrative Biology, University of California, Berkeley, CA 94720-3140

INTRODUCTION

Joint stiffness is an important property of legs which must respond to uncertain mechanical perturbations. Turning forces or moments on either side of a joint's center of rotation can determine a joint's stiffness. For a simple hinge joint, flexor and extensor muscle groups generate opposing moments. We chose to study joint stiffness by comparing static flexor and extensor muscle function in a cockroach because their legs operate in a plane more parallel to the substratum (center of rotation perpendicular to the substratum) than in most animals. Opposing moments are more likely to be similar in magnitude at the joints of cockroaches than at the joints of animals the primarily resist the effects of gravity. We estimated hind leg, coxa-femur (c-f) joint moments of the cockroach with a 3D musculoskeletal model (Full and Ahn, 1995). In the present study, we compared extensor and flexor muscle function and determined the design of the cockroach roach leg tends to favor rapid flexion over maintenance of high joint stiffness.

REVIEW AND THEORY

High Joint Stiffness Design

1. Flexor moment = Extensor moment
$$F^M_{flex} \times r_{flex} = F^M_{ext} \times r_{ext}$$
2. Angle at Maximum Moment of Flexors, = Angle at Maximum Moment of Extensors
$$\phi_{flex} = \phi_{ext}$$
3. Flexor moment arm = Extensor moment arm
$$r_{flex} = r_{ext}$$

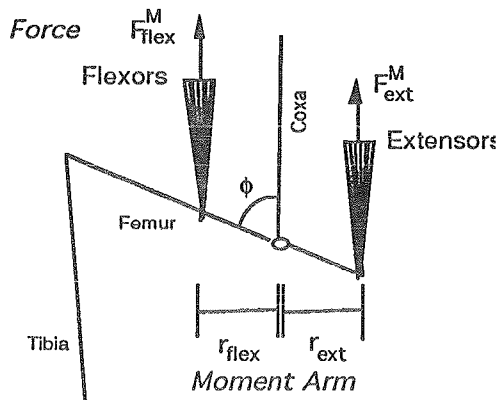

Figure. 1: Hypotheses of leg design which favor maintenance of high joint stiffness.

We examined leg design and static muscle function to determine whether the cockroach leg parameters favored maintenance of high joint stiffness or rapid leg flexion. We hypothesize if (1) flexor moments equal extensor moments, (2) the angle at maximum moment of the flexors equaled the angle observed in the extensors and (3) the flexor moment arm equal the extensor moment arm to maintain joint stiffness (Fig.1).

Rapid Leg Flexion Design

1. Flexor moment < Extensor moment
$$F^M_{flex} \times r_{flex} < F^M_{ext} \times r_{ext}$$
2. Angle at Maximum Moment of Flexors, ≠ Angle at Maximum Moment of Extensors
$$\phi_{flex} \neq \phi_{ext}$$
3. Flexor moment arm < Extensor moment arm
$$r_{flex} < r_{ext}$$

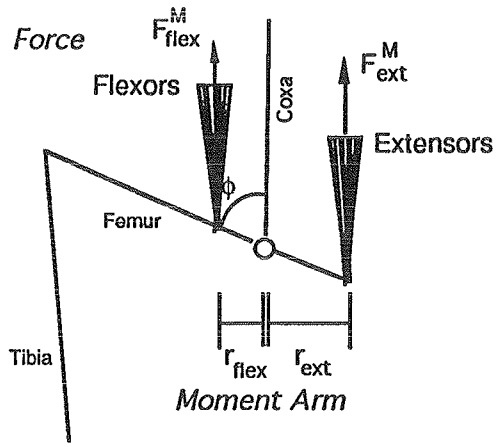

Figure 2: Hypotheses of leg design which favor maintenance of rapid leg flexion.

Alternatively, we hypothesize if (1) the flexor moment are smaller than extensor moments since only small amounts of energy are involved in flexing the leg during running, (2) the angle of maximum moment of flexors is greater than extensors and approximates the joint angle at the beginning of flexion during running and (3) the flexor moment arms are smaller than extensors, then the leg design in cockroach legs favors rapid flexion of the leg in running (Fig.2).

PROCEDURES

MUSCULOSKELETAL MODEL

We constructed a three-dimensional computer model of the hind leg of the cockroach, *B. discoidalis*, using a musculoskeletal modeling program, SIMM (Software for Interactive Musculoskeletal Modeling, MusculoGraphics, Inc.; Delp and Loan, 1995; Full and Ahn, 1995). Within the program, a computer model of jointed framework musculoskeletal structures can be defined by describing the skeletal geometry, joint motions, muscle lines of action, and muscle force-generating parameters.

RECONSTRUCTION

Serial reconstruction of histology sections of the leg segments provided a quantitative, three-dimensional description of the exoskeleton. The 3D coordinates of the muscle attachment points were obtained by video microscopy of muscle dissections. Muscle attachment points were videotaped at three known views (20°, 0°, -20°) using a rotating micromanipulator. Using a video analysis system (Peak Performance Technologies, Inc.), direct linear transformation on the data captured in the three views provided the 3D coordinates. Using pre-determined reference points and several anatomical landmarks on the exoskeleton, we rotated and translated the muscle coordinates to match the exoskeletal coordinates. For the current model, we identified 21 musculo-apodeme actuators (apodemes are the insect equivalent of tendons).

Each segment was contained within its own reference frame. The coxa and femur segments of the cockroach leg are connected by simple hinge or pin joints, with a single axis of rotation. The present study focuses on extension and flexion of the femur at the coxa-femur joint and examines only those joint angles within the normal range of motion in the animal.

We used a Hill-based musculo-"tendon" model after Zajac (1989). Note the model's strong empirical base. We directly measured or calculated from measurements the: maximum isometric force for each femoral extensor and flexor (estimated by multiplying the maximum isometric stress value of 15 N cm^{-2} measured from experiments a c-f extensor [R.K. Josephson and D.R. Stokes, unpublished] by our estimates of physiological cross-sectional area, PCSA); PCSA for each femoral extensor muscle (determined from the muscle mass, length and density) and apodeme slack lengths for each c-f apodeme.

RESULTS and DISCUSSION

Table 1: Mechanical properties of coxa-femur flexor and extensor muscle groups.

Muscle Group	Force (N)	Effective Moment Arm (mm)	Max. Moment (N mm)	C-f joint angle (°)
Flexors	0.13	0.84	0.11	101-111
Extensors	1.4	0.86	1.2	43 - 47

When comparing static function of c-f flexors to that of c-f extensors, flexor force and maximum moment generation are 1/11 that of extensors (reject hypothesis #1; Fig. 1).

The coxa-femur (c-f) joint angle at which the flexors produced maximum total (summed) moment is much greater than the c-f joint angle at which the extensors generate maximum total moment. This joint angle at which moment is maximally generated by the flexors actually approximates the joint angle at the beginning of the swing phase (i.e., beginning of flexion) during running (reject hypothesis #2; Fig. 1).

However, the moment arm lengths (at maximum moment) of the flexors equaled extensor moment arm lengths which supports hypothesis #3 to maintain high joint stiffness. Overall, the data support the alternative hypotheses of a leg design favoring rapid leg flexion over a leg design favoring high joint stiffness.

REFERENCES

Delp, S.L. and Loan, J.P. *Comp. bio. med.* In press.

Full, R.J. and Ahn, A.N. *J. Exp. Biol.* In press.

Zajac, F.E. *Crit. Rev. Biomed. Eng.* 17, 359-411, 1989.

ACKNOWLEDGMENTS

We thank Scott Delp, Peter Loan, Marvalee Wake, Rudy Pipa, Kay Earls, Bob Josephson and Darrell Stokes. The work was supported by NSF PYI Grant DCB 90-58138 to RJF.

MECHANICAL DESIGN OF FIBER-WOUND HYDRAULIC SKELETONS: THE SWELLING NOTOCHORDS THAT ELONGATE FROG EMBRYOS

M. A. R. Koehl[1], K. J. Quillin[1], and C. Pell[2]

[1]Department of Integrative Biology, University of California, Berkeley CA 94720-3140

[2]Biodesign Studio, Department of Zoology, Duke University, Durham NC 27706

INTRODUCTION

We have used physical models to investigate the mechanical consequences of different arrangements of reinforcing fibers in the tensile sheaths surrounding inflating cylinders, both curved and straight. The purpose of the study was to analyze inflation of the swelling notochords that straighten and elongate developing embryos, but the priciples about design of inflatable cylinders are applicable to a wide variety of biological structures.

REVIEW AND THEORY

Many animals and plants inflate fiber-wound hydrostats to change shape or generate forces This includes the hydraulic appendages of many soft-bodied animals (whose inflation depends on pushing fluid into the structure by muscular contractions elsewhere in the body) and the osmotically-inflated cells of plants and notochords of vertebrate embryos.

We have been studying the biomechanics of shape changes in the development of early embryos (Koehl, 1990). One process on which we have focused is the elongation of the late-neurula frog embryo, which is driven by the notochord. We demonstrated that swelling of vacuolated notochord cells is resisted by the collagenous sheath laid down around the notochord, thereby causing increases in the internal pressure and flexural stiffness of the notochord as it inflates and straightens (Adams et al., 1990; Koehl et al., 1990).

The purpose of the present study was to determine the effects of the angle of the fibers reinforcing the tensile sheath of such inflating clyinders (both straight and curved) on their changes in shape and flexural stiffness when inlfated, and on their ability to push or pull as internal pressure rises.

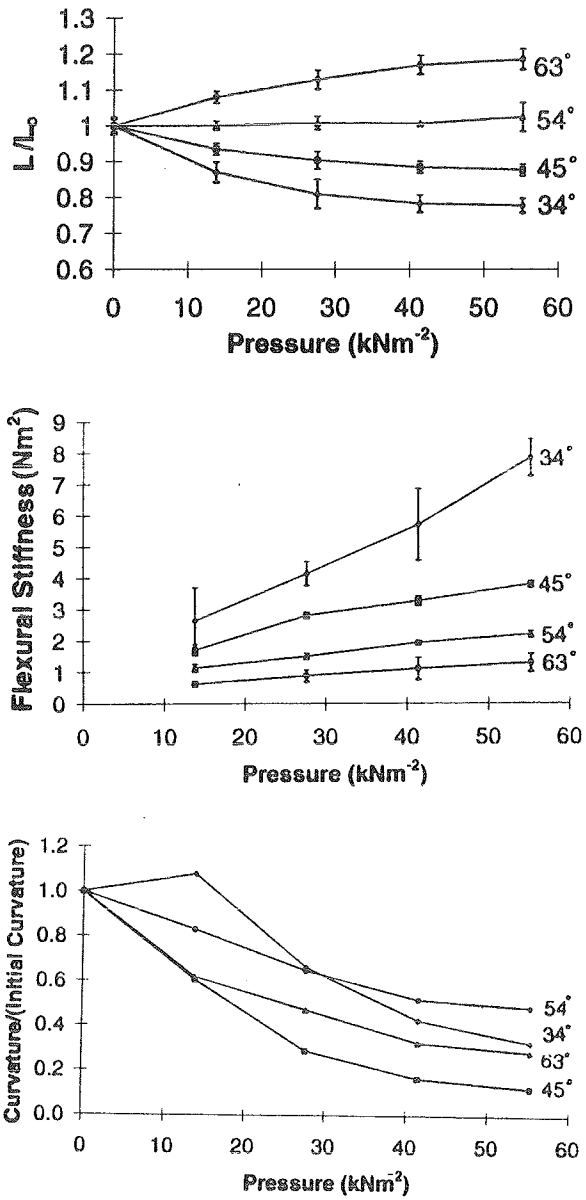

Figure 1: Measured lengths (top graph), flexural stiffnesses (middle graph), and curvatures (lower graph) of models of curved notochord sheaths.

PROCEDURES

We have fabricated latex models of notochord sheaths (curved or straight hollow cylinders) reinforced with nylon fibers at a variety of angles (θ) relative to the cylinder axis. We have inflated these models with air and have measured the shape and size changes, force production, and flexural stiffness changes caused by increases in internal pressure.

RESULTS AND DISCUSSION

The consequencs of inflation depend on fiber angle (θ). Cylinders with θ's above 54° lengthen and narrow upon inflation; although they can push, the forces they exert are limited by their tendency to buckle. Flexural stiffness should increase as internal pressure is raised, but the narrowing of inflating cylinders with high θ's counteracts this. The higher the θ, the smaller the increase in flexural stiffness upon inflation; at $\theta = 63°$ no increase in stiffness is caused by inflation. In contrast, cylinders with θ's below 54° shorten and widen when inflated and show a pronounced increase in flexural stiffness. The lower the θ, the greater the force with which they pull for a given increase in internal pressure. All curved sheaths staighten upon inflation, regardless of initial θ.

We have discovered that fiber orientations that enhance elongation (high θ's) also lead to decreases in stiffness upon inflation and require greater volume changes to produce increases in internal pressure than do fiber orientations characterized by low θ's. The intermediate θ's in notochord sheaths appear to balance these trade-offs.

REFERENCES

Adams, D. S., R. Keller, and M.A. R. Koehl. *Development* 110, 115-130, 1990.

Koehl, M. A. R. *Devel. Biol.* 1, 367-378, 1990

Koehl, M. A. R., D. S. Adams, and R. E. Keller. *Biomechanics of Active Movement and Deformation of Cells*, (pp. 471-485), Springer-Verlag, 1990.

ACKNOWLEDGEMENTS

This research was supported by a MacArthur Fellowship to M. Koehl, and by NSF grant #IBN-9220525 to R. Keller and M. Koehl. We thank S. Wainwirght for inspiration and for support of our work in the Biodesign Studio, and M. Reys for help with constructing models.

Zone-Dependent Biosynthetic and Structural Changes in Adult Articular Cartilage in Response to Static Compression

M. Wong[1], P. Wuethrich[1], M. Buschmann[2], A. Maurer[1], P. Eggli[3], E. Hunziker[1]

M.E. Muller Institute for Biomechanics[1] and the Institute of Anatomy[3]
University of Bern, Switzerland

Institut de génie biomédical, Ecole Polytechnique de Montreal[2]

Introduction

In this study, the zone specific behaviour of articular cartilage under static unconfined compression was investigated. Using new histomorphometry techniques combined with quantitative autoradiography, we were able to obtain spatial information about the structural and biosynthetic changes taking place during compression. The aim of the study was to explore potential correlations between cell and matrix structural changes and changes in chondrocyte biosynthetic activity.

Review and Theory

Chondrocytes have been shown to alter synthesis of matrix macromolecules in response to mechanical load. Static compression applied to cartilage in vitro has been shown by many authors to inhibit biosynthesis of cartilage macromolecules. The pathway(s) by which these mechanical signals are sensed is not clear but may involve changes in cell and matrix structure, matrix pore size, physicochemical changes (pH) or cell-matrix interactions. We used the adult articular cartilage system to investigate possible correlations between cell structural parameters and cell biosynthesis. Adult articular cartilage is a highly stratified, inhomogeneous tissue, whose matrix composition, cell morphology and tissue properties are zone dependent. We anticipated that tissue strains during static compression could vary between zones and hypothesized that the zones undergoing the most deformation may show the greatest inhibition in synthetic activity.

Procedures

Full thickness cylinders of adult bovine articular cartilage (including a thin layer of bone) were cultured for one day and statically compressed 0, 20 or 40% under conditions of unconfined compression.

10μCi/ml of tritiated proline was added to the culture media during the last 18 hours of a 23 hour loading period. Specimens were fixed in 5% glutaraldehyde in the compressed state and were divided into two halves, one for use for stereology measurements and the other for autoradiography.

Stereology: Unembedded, full thickness sections of articular cartilage were 'optically' sectioned using a laser scanning confocal microscope. The following morphometric parameters were measured at eight sites between the superficial layer of articular cartilage and the tidemark.

- chondrocyte number (cells/mm^3)
- cell and matrix volume fraction (%)
- mean cell volume (mm^3)
- mean cell surface area (mm^2)

After processing tissue for autoradiography, silver grains appear on the histologic sections in proportion to the incorporation of radioactive marker by the cells. Using an automated grain counting program, we could measure the grains per unit section volume for eight fields corresponding to the fields used for stereology. Combining this data with the chondrocyte number values, an estimate of cell biosynthetic activity in terms of grains/cell was obtained.

Results

The upper zones of articular cartilage undergo the most significant alterations in biosynthesis and structure during static unconfined compression. Figure 1 shows the synthesis on a per cell basis for the free

swelling controls as well as for 0, 20 and 40% compression (measurements made at center of plug). In the free swelling controls, the radial zone chondrocytes (site 7 and 8) are 10 times more active than cells of the superficial zone (site 1). When the tissue was compressed by 40%, the depth-average synthesis was reduced by 30% compared to the 0% specimens. This change in synthesis occurred primarily in the upper zones of the tissue (sites 2, 3, 4, 5).

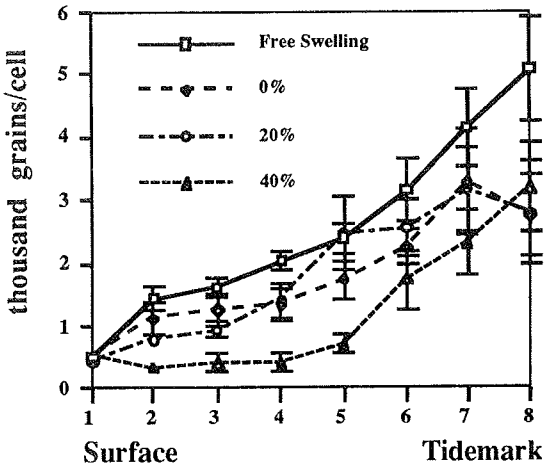

Figure 1: Cell Activity

The results of our measurements for chondrocyte number (cells/mm3) (Figure 2) show that the cellularity is highest in the surface layers. When the tissue is compressed, the cellularity increases predominantly in the upper layers of cartilage whereas the chondrocyte number in the radial zone remains almost unchanged.

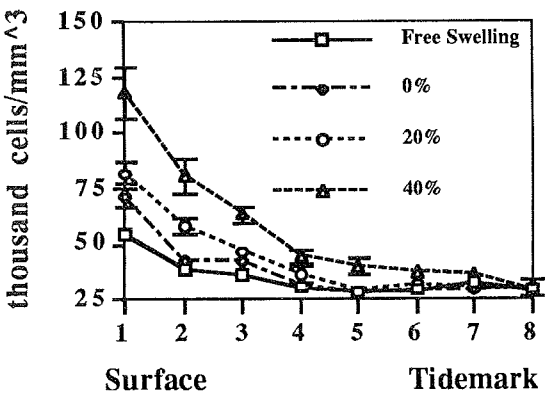

Figure 2: Cell Number

The results of cell volume fraction measurements also reveal interesting properties about the behaviour of articular cartilage under unconfined compression. In uncompressed tissue, the cells occupied a average of 4.6% of the tissue volume. After 40% compression, the cell volume fraction rises to an average of 6.2%, indicating that the matrix preferentially loses volume while the cells tend to maintain their volume. We did not measure a significant change in mean cell volume at any compression level.

The chondrocytes in the center of the plug displayed a very different behaviour in comparison to the cells near the periphery of the plug. Peripheral radial zone chondrocytes were subjected to considerably more distortion and deformation during unconfined compression. Interestingly, these highly deformed chondrocytes often showed an increase in cell activity compared to uncompressed controls.

Conclusions

A new method has been presented which enabled us to obtain morphologic and biosynthetic information about the zone specific response of full thickness articular cartilage to unconfined static compression.

1) The upper layers of articular cartilage undergo the highest tissue strains (as evidenced by cell number). These changes correspond in general to the sites with the greatest inhibition in cell synthesis. The data suggest that matrix and cell deformations are important in the transduction pathways regulating synthetic activity.

2) Biosynthetic and structural behaviour of cartilage is highly dependent on the boundary conditions of the compression protocol and specimen geometry. The difference in behaviour between confined and unconfined compression as well as between specimens with and without a layer of supporting subchondral bone is most likely significant.

CREEP OF MUTABLE COLLAGENOUS TISSUE MODULATES GROWTH IN SEA URCHINS

O. Ellers
Section of Evolution and Ecology, University of California, Davis CA 95616

INTRODUCTION

Echinoderms have a special connective tissue called catch, or mutable collagenous tissue (MCT). The breaking strength, stiffness and viscosity of this viscoelastic tissue can be changed, primarily by changing the viscous components; the material properties are believed to be under nervous control (Motokawa, 1988).

Previous studies have demonstrated many functions for the MCT in echinoderms. Sea lilies (crinoids) use the tissue to hold their arms up into flow while filter-feeding for long periods of time. Sea stars (asteroids) use this tissue to pry open mussels (that they then eat); the MCT is stiffened after muscles have been used to establish a grip on the mussel. Using the MCT in this way reduces the energy expended, and enhances the stamina of sea stars trying to open mussels. Birenheide (1990) suggested that the MCT which attaches the tooth to the jaw in sea urchins may sometimes loosen to allow advancement of the continuously growing teeth.

I propose an additional, new role for the MCT: namely, that it plays a role in determining growth rate in sea urchin skeletons.

REVIEW AND THEORY

Sea urchin skeletons are made of numerous plates that are sewn to each other at the sutures between plates with collagenous fibers (Telford, 1985). Sea urchins grow by adding calcite at the edges of the plates and by adding new plates at the aboral end.

I test whether these sutural, collagenous fibres are MCT, and suggest that adjustable creep of a material that flows over long time periods could be used to control growth of skeletal sutures in urchins.

PROCEDURES

Sea urchins, Lytechinus pictus, were soaked in three treatment solutions: normal sea water, Ca and Mg free sea water, and bleach. Breaking tests were performed on each group of skeletons.

Observations of the looseness of sutures in rapidly vs slowly growing urchins were made. Growth rate was controlled by diet.

RESULTS

Table 1: Average breaking forces of urchin skeletons randomly assigned to different treatments are significantly different.

treat-ment	sea water	CaMg-free	bleach
force,N	45	26	6.0
s.e.,N	3.3	1.6	0.38
n	19	19	17

Sutures of growing urchins are much looser than those of urchins that are not growing. In fact, bleached skeletons of rapidly growing urchins fall apart into their constituent plates under their own weight when bleached, whereas those that are growing less, do not lose skeletal integrity when bleached, because the plate's edges interlock tightly at sutures.

DISCUSSION

The reduction in breaking force of the skeleton when soaked in Ca and Mg free sea water suggests that the collagenous fibres binding the plates together are MCT. The low breaking strength of bleached skeletons shows that the plates of these urchins were quite loose and that the skeleton of loose-sutured urchins derives most of its strength from the tissue binding the sutures.

The observation that sutures of more rapidly growing urchins are looser suggests that the sutures gap first, and then later fill in the gap with accreting calcite. This can be considered analogous to the way in which arthropods (e.g. lobster) inflate themselves during the intermoult period and before re-hardening their shells.

I suggest the following theory. Under suitably good conditions of diet, and perhaps season, urchins reduce the viscosity of the MCT that binds sutures. That tissue then creeps faster under tensile loading from small, fluctuating, internal coelomic pressures that have been measured to be of similar magnitude in fed and starved urchins (Ellers & Telford, 1992). Growth rate could thus be controlled by changes in the rate of creep of the sutural MCT.

That mechanism would also explain the apparent flexibility of the sutures over long time periods. Flexibility of the sutures over long time periods is implied by a model that successfully predicts the shape of sea urchins. This model assumes that shape is determined in sea urchin skeletons by forces, in a manner analogous to the way that shape is determined in water droplets, or water-filled balloons (Ellers, 1993).

Similarly, the collagenous tissue attaching sand dollar teeth to their jaws is a MCT with viscosity and elasticity that is variable in Ca and Mg free seawater. Further, sand dollars have periods during which the collagenous tissue is less strong than is necessary to chew, but slides forward easily, thus enabling growth (Ellers & Telford, in prep.).

Thus, the MCT of echinoderms is not merely a functionally useful tissue, but may also be involved in regulating growth.

REFERENCES

Birenheide, R. 1990. Functional analysis of the tooth support in echinoids. pp. 203-206, in Echinoderm Research, DeRidder et al. , eds., Balkema, Rotterdam.

Ellers, O. 1993. A mechanical model of growth in regular sea urchins: predictions of shape and a developmental morphospace. Proc. R. Soc. Lond. B 254: 123-129.

Ellers, O. & M. Telford, 1992. Causes and consequences of fluctuating coelomic pressure in sea urchins. Biol. Bull. 182: 424-434.

Motokawa, T. 1988. Catch connective tissue: A key character for echinoderm's success. pp. 39-54, Echinoderm Biology, Burke et al, eds., Balkema, Rotterdam.

Telford, M. 1985. Domes, arches and urchins: The skeletal architecture of echinoids (Echinodermata). Zoomorphology 1105: 114-124.

ACKNOWLEDGEMENTS

H. Leddy performed the urchin strength tests. Thanks to A. Johnson and Bowdoin College for providing space, an Instron, and discussions. Thanks to R. Mooi, M. Telford, and E. Pearson for useful discussions. This study was partially funded by an UCD Agricultural Research Station grant to O. Ellers.

IMPACT RELATED DAMAGE TO RABBIT FEMORAL CARTILAGE

Mark S. Vrahas, Gretchen A. Smith, Richard V. Baratta
Bioengineering Laboratory, Department of Orthopaedic Surgery
Louisiana State University Medical Center, New Orleans, Louisiana

INTRODUCTION

It is believed that substantial impacts to articular cartilage and subchondral bone can initiate the pathogenic cascade to post-traumatic arthritis. We are intrested in studying this phenomenon in an *in vivo* rabbit model. To do this it is essential to accurately quntify impacts and to know the damage that results from these. The purpose of this study was to develop the techniques for achieving this goal.

REVIEW AND THEORY

Intra-articular fractures frequently lead to severe and debilitating arthritis, but the exact cause of this post-traumatic arthritis (PTA) is not known. One theory supported by clinical and laboratory studies suggests that residual joint incongruities and malalignments elevate articular contact stresses, initiating the disease cascade (Moskowitz et al., 1984, Hadley et al., 1990). However, this theory is unlikely to be the sole cause of PTA, because PTA is frequently encountered in fractures that have healed without remaining incongruities. An alternative theory suggests that the initial injury damages articular cartilage and launches the disease process leading to PTA. Repo and Finley (1977) described chondrocyte death in an *in-vitro* model with impact stresses of 25 MPa, while Thompson et al. (1991) produced early changes similar to PTA in an *in-vivo* model. Still, no study has documented histologic changes in relation to well-characterized impact parameters. It is therefore the intent of this study to develop a methodology for producing well-characterized impacts to rabbit femoral condyles.

PROCEDURES

The study was conducted on 5 Adult New Zealand White rabbits (10 knees total). After euthanasia according to IACUC guidelines, median peripatellar arthrotomies were performed and the patella deflected laterally to expose the distal femoral condyles. Then the rabbit femur was mounted on an impaction jig using a transfixing pin. A 1 m tall vertical rail was used to guide a sliding weight via linear bearings. The weight struck the superior end of an impactor instrumented with strain gages in a configuration to measure compressive force. The inferior end of the impactor was customized to contour exactly to each medial condyle being tested. This setup insured uniform impact stress distribution over the articular surface. This was cinfirmed through the use of Fuji pressure sensitive film.

The main constituents of impact stress were evaluated in order to estimate this quantity. Impact force was measured by signals amplified from the strain gages attached to the impactor shaft. These signals were calibrated against an MTS Bionix test machine. A linear equation was derived through regression analysis with correlation coefficient in excess of 0.992, and standard error of 12 N over a full scale of 2.2 kN. As an estimate of the impact area, a marker imprint was transferred from the impactor onto paper and measured through a digitizing tablet.

To determine the damage inflicted by these impacts, the joints were retrieved, dehydrated, embedded in Osteobed, sectioned and stained with Safrin O and fast green counter stain. Specimens were then examined under light microscopy for structural damage at 10X. The examiner was blinded as to the impact magnitudes.

To establish the range of mass weights and drop heights necessary to produce impacts of a given force, the peak impact forces were plotted against the product of mass, height and acceleration. The acceleration was estimated by video to account for friction between the mass

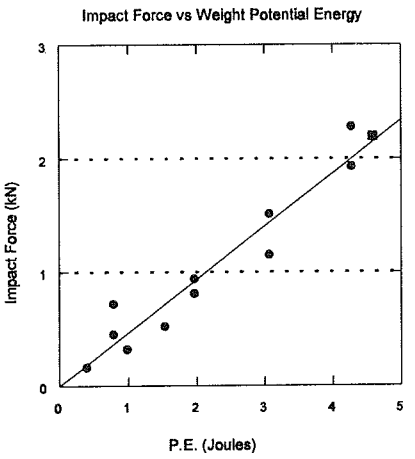

Figure 1: Force vs. Potential Energy

the guide rail at the linear bearing interface.

RESULTS AND DISCUSSION

Impact areas ranged from 0.397±.041 to 0.746±0.054 cm^2. The standard deviations of area measurements suggest that they are reasonably accurate. We thus concluded that these areas can be used to estimate impact stresses.

A range of impacts from 0.2 kN to 3 kN was delivered to the rabbits' condyles. A linear relationship between impact force and the product of mass, height and acceleration was found as shown in Fig. 1. The correlation coefficient was 0.968 with a standard error of 184 N, which suggests that a predictable impact can be obtained with proper adjustment of the weight's mass and height.

One specimen was not evaluated histologically due to poor staining. Four specimens were classified as having mild damage, by virtue of a single superficial crack in the tangential cartilage layer. Within these specimens, the estimated impact stresses averaged 16.8±10.5MPa. Five specimens were graded as having severe damage due to either multiple cracks or fissures extending into the radial and subchondral layers. Among these, the impact stresses averaged 27.3±14.3 MPa. There was no statistically significant difference in stresses between these two groups. Our present studies are aimed at obtaining a larger sample size to more conclusively correlate impact stresses to articular damage. These data will be used to determine graded impacts for future survival experiments.

REFERENCES

Moskowitz, R.., et al.. *Osteoarthritis Diagnosis and Management,* WB Sanders, 1984.

Hadley, N.A.. *J. Orthop. Res.*, 8, 504-513, 1990.

Repo, R.U., Finley, J.B. *J. Bone Joint Surg.*, 59-A, 1068-1076, 1977.

Thompson, R.C., et al. *J. Bone Joint Surg.*, 73-A, 990-1001, 1991.

Supported by: **AO North America**

A DIGITAL RADIOGRAPHIC SYSTEM FOR DETERMINING 3D JOINT KINEMATICS DURING MOVEMENT

S. Tashman[1], K. DuPré[1], H. Goitz[1], T. Lock[1], P. Kolowich[1], M. Flynn[2]
[1]Bone and Joint Center, Henry Ford Health System, Detroit, MI 48202
[2]Department of Radiology, Henry Ford Health System, Detroit, MI 48202

INTRODUCTION

We have developed instrumentation for rapid, accurate assessment of *in-vivo* 3D joint motion during a variety of movements. This abstract describes the system, reports on its accuracy, and provides some preliminary data on the effects of ACL loss on knee kinematics during canine gait.

REVIEW AND THEORY

Traditional motion analysis techniques, based upon markers or devices affixed to the skin, are incapable of accurately measuring joint kinematics. Movement of skin relative to underlying bone introduces artifacts which obscure small changes in bone movement and damp high-frequency motion. To overcome this problem, we have adapted Radiographic Stereophotogrammetric Analysis (RSA), a technique successfully employed to determine static or slow-moving 3D behavior of a variety of human joints using pairs of plane-film X-rays (Selvik, 1990), to study dynamic joint movement by replacing the film with a high-speed digital imaging system and developing software for automated 3D analysis. RSA requires implantation of small spherical markers (typically about 1mm diameter) to enable 3D tracking of bone movement. Percutaneous implantation of these markers is minimally invasive and has resulted in no complications in over 2000 human subjects (Karrholm, 1989).

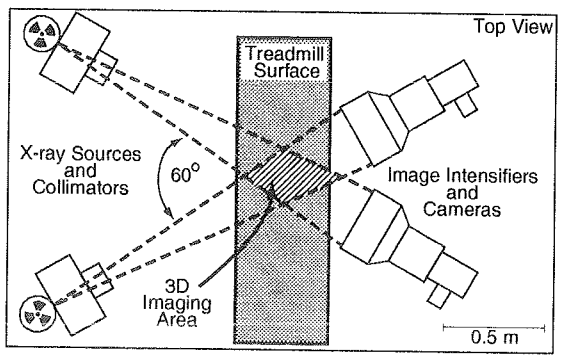

Figure 1: *Top View of Biplanar X-Ray System 60° Configuration showing 3D imaging area and treadmill.*

Our Biplanar X-Ray System consists of two gantries, each containing a 150 kW x-ray source and a 30cm image intensifier, configured to provide two crossing beams parallel to the ground. The beam height, crossing point and inter-beam angle are adjustable. In a typical 60° configuration (Figure 1), this provides a 1m wide, 2.6m tall area with unrestricted access front and back for movement activities, which can be performed on a standard treadmill, force plates or bare floor. The size of the 3D imaging area for the configuration shown is approximately 45cm wide by 30cm long by 25cm high.

The image intensifiers are optically coupled to high-speed (250 frame per second) CCD video cameras. A pair of high performance frame grabbers acquire up to 139 images per camera with a resolution of 500x240 pixels. Radiological details of this imaging system, including dynamic response and subject x-ray exposure, have been previously discussed (Flynn, et al., 1994).

Biplanar x-ray image sequences are acquired for a 567-marker distortion correction grid, a 12-marker 3D calibration cube, and the motion of interest. A pattern recognition algorithm (developed in-house) automatically identifies the marker signatures in each image and performs gray-scale weighted centroid calculations to determine marker positions with sub-pixel resolution. Centroid coordinates from each camera view are written to a file format compatible with the EVa software system (Motion Analysis Corp., Santa Rosa, CA). The EVa software performs distortion correction, DLT-based 3D calibration, tracking and alignment of the centroids from the two views, and 3D reconstructions.

PROCEDURES

Performance was assessed using a 5cm acrylic cube containing three 1.6mm tantalum spheres in a right isosceles triangle with 3cm legs. Static precision was assessed with 125 images acquired at 250 frames/sec for the test object positioned stationary in the center of the field of view. Dynamic accuracy was assessed by suspending the object from a stiff elastic band and then dropping it, allowing it to twist and bounce throughout the field of view. No smoothing or filtering was performed.

Functionality of the system was evaluated with a study of normal and ACL-deficient canine tibial-femoral motion during treadmill gait (1.5m/s). One month prior to kinematic testing, four 1.6mm tantalum spheres were implanted into the right tibia and femur of each of three dogs. 0.5 seconds of biplanar x-ray data were collected at 250 frames/sec before and 8 weeks after ACL transection for each of the 3 dogs. 3D coordinates were smoothed using a 25Hz bidirectional Butterworth lowpass filter. Paw-strike timing information was obtained from a lightweight accelerometer strapped to the lower limb. Six degree-of-freedom tibio-femoral motion was determined using a technique similar to that described by Veldpaus (Veldpaus, et al., 1988).

RESULTS

Performance testing results are provided in Table 1, including means, standard deviations and ranges (maximum-minimum) for 3D vector distances between two of the markers and the angle inscribed by all three markers in the test object (calculated with unfiltered, unsmoothed 3D coordinates). During the dynamic tests, the cube moved through a 550cm^3 volume, reached a peak linear velocity of 70 cm/sec, and underwent rotations of 30 to 135 degrees about each axis.

Table 1: Accuracy Test Results

	Distance (mm)		Angle (deg)	
	Static	Dynamic	Static	Dynamic
True	30	30	90	90
Mean	29.98	29.98	90.14	90.11
S.D.	0.03	0.10	0.10	0.22
Range	0.16	0.53	0.53	0.92

Preliminary results for the dog study are presented in Figure 2. The three relevant degrees of freedom are presented: anterior/posterior translation (anterior drawer), sagittal rotation (flexion/extension), and transverse rotation (internal/external rotation). The remaining motions are not presented because they did not show significant differences before vs. after ACL transection in our study or in other published data (Korvick, et al., 1994).

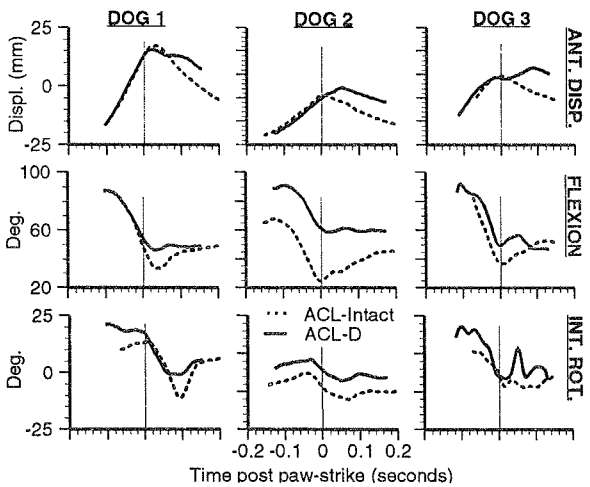

Figure 2: *Knee joint kinematics (tibial motion relative to femur) for ACL-Intact (dotted lines) vs. ACL-Deficient (solid lines) dogs. Vertical line is time of paw-strike. Note increased anterior tibial displacement of ACL-deficient dogs occurring just after limb is loaded.*

All dogs showed an increase in anterior displacement after ACL transection of 7-12 mm from 50 to 100 ms after paw-strike. Post ACL transection, all dogs also showed reduced knee extension (from 15 to 30 degrees), with two different patterns. Dogs 1 and 3 showed similar pre-post patterns, except for reduced peak extension at paw-strike and just after. Dog 2 showed a consistent 20 degree shift towards flexion throughout the gait cycle. Changes in transverse-plane rotations were not consistent across animals.

DISCUSSION

Typical dynamic errors for the Biplanar X-Ray System are in the order of 0.1mm and 0.25 degrees. Dynamic errors are slightly larger than static errors due to small shifts in calculated gray-scale centroid positions as markers cross pixel line boundaries and image features, and variations in distortion correction and 3D calibration accuracy in different areas of the field of view. Worst-case errors are still very small relative to the 5-10mm/0-15 degree differences in knee motion reported to occur between ACL-intact and ACL-deficient dogs (Korvick, et al., 1994).

Our findings for ACL-deficient dogs are quite similar to those reported by Korvick, et. al. (using instrumented linkages rigidly affixed to the bones). The pre-post ACL transection differences in flexion and anterior displacement are nearly identical in magnitude, and their internal/external rotation data also shows large variability from dog to dog. Our fast sampling rate revealed a very rapid (approx. 20ms) anterior shift of the tibia occurs as the limb is loaded, which may be responsible for damage to other knee structures often observed in ACL-deficient dogs and humans. The relationship between transverse-plane instability and ACL loss requires further investigation and may depend upon how the animals are actually loading the affected limb, as has been demonstrated with human cadaver studies (Matsumoto, et al., 1993, Reuben, et al., 1989).

We believe this measurement methodology is adequate for a wide range of dynamic, *in-vivo* joint motion studies. Several investigations are now underway to examine the dynamic function of both healthy and injured human and animal joints.

REFERENCES

Selvik, G. *Acta Orthop. Scand. Supp.*, 232, 1-51, 1990.

Karrholm, J. *Acta Orthop. Scand.*, 60, 491-503, 1989.

Flynn, M., et al., *proc. IEEE Medical Imaging Conference*, San Diego, CA, 1994.

Korvick, D.L., et al. *J. Biomech.*, 27, 77-87, 1994.

Matsumoto, H., et al. *Proc. Instn. Mech. Engrs.*, 207, 163-173, 1993.

Reuben, J.D., et al. *Am J Sports Med.* 17, 463-471, 1989.

THE EFFECTS OF REMOVAL AND RECONSTRUCTION OF THE ANTERIOR CRUCIATE LIGAMENT ON PATELLOFEMORAL KINEMATICS

Yeou-Fang Hsieh, Louis F. Draganich, Sherwin Ho, and Bruce Reider

Section of Orthopaedic Surgery and Rehabilitation Medicine
Department of Surgery
The University of Chicago
Chicago, Illinois

ABSTRACT

This study was performed to investigate the effects of removal and intraarticular reconstruction (IAR) of the anterior cruciate ligament (ACL) on the three-dimensional motion of the patella in seven cadaveric knees. A bone-tendon-bone graft from the autogenous central one-third of the patellar tendon was used for the intraarticular reconstruction. Knee loading was produced by extending the knee with quadriceps forces based on one-third of reported maximum voluntary isometric extension moments. The positions of the patellofemoral and tibiofemoral joints were measured between 0° and 90° of knee flexion at 15° increments with a six degree-of-freedom digitizing system. Neither the removal nor the reconstruction of the ACL was found to significantly affect patellar flexion, mediolateral patellar rotation, patellar anteroposterior translation, or patellar proximodistal translation. Excision of the ACL resulted in significant increases in lateral patellar tilt and in lateral patellar shift. The intraarticular reconstruction returned normal patellofemoral and tibiofemoral kinematics to the ACL-excised knee.

INTRODUCTION

Instability of the knee occurring with injury of the anterior cruciate ligament may result in functionally significant disability. Despite the fact that reconstruction of the ACL enhances the stability of the tibiofemoral joint, frequently, even with good stability, patients have complained of pain in the anterior aspect of the knee. The cause of the patellar pain syndrome is still controversial. One possibility is that patellar pain results from a malalignment between the patella and femur which leads to altered patellofemoral pressure. To date, there have been no studies reporting on the effects of ACL-deficiency on patellar tracking. Furthermore, there have been no reports on the effects of ACL reconstruction on the three-dimensional motion of the patella. Therefore, the objectives of this in vitro study were to determine the effects of ACL-deficiency and intraarticular reconstruction of the ACL on the three-dimensional motion of the patella for physiologic levels of quadriceps loads.

MATERIALS AND METHODS

Seven cadaveric knees from seven donors with a mean age of 51.4 years were studied. Testing consisted of applying external flexion moments equivalent to 1/3 of values reported in the literature for maximum isometric quadriceps moments[1], equilibrating the knee with quadriceps forces at a particular flexion angle, and measuring patellofemoral and tibiofemoral joint motions with a six degree-of-freedom digitizer. Tests were performed for three experimental states on each specimen, first on the intact knee, second following the transection of the ACL and IAR of the ACL, and finally following the removal of the intraarticular graft in order to test the knee without the ACL for flexion angles from 0° to 90° at 15° increments. An IAR was performed utilizing the autogenous central one-third of the bone-patellar tendon-bone graft. After the motion data for all experimental states were collected, the knee was disarticulated and bony landmarks of the femur, tibia, and patella were identified and digitized for construction of the anatomical coordinate systems. The three-dimensional motions of the patella and tibia with respect to the femur were each characterized by six kinematics: three rotations and three translations, defined according to the literature[2].

For each knee, we first computed the kinematics of the patellofemoral and tibiofemoral joints as functions of flexion angle for each of the three experimental states. We then normalized these kinematics with respect to those of the intact knee at 0° of knee flexion, according to $Q_m^E = q_m^E - q_0^I$, where Q_m^E was the normalized kinematics at the mth joint position (flexion angle), q_m^E was the kinematics for each of the three experimental states at the mth joint position, and q_0^I was the kinematics of the intact knee at 0° of knee flexion. The kinematics describing the motions of the tibia and patella with respect to the femur were averaged to obtain the results reported. We then performed paired sample t-tests to determine significant differences in patellar motion and in tibial translation between the intact and ACL-excised knees and between the intact and IAR knees. Based on a Bonferroni adjustment for two comparisons at seven flexion angles, an α level of 0.0036 was considered significant.

RESULTS

In the intact knee, the patella flexed from 0° at full extension to 50° at 90° of knee flexion, the patella rotated within a very narrow range, 1.3°, over the range of knee flexion (Figure 1), the patella translated posteriorly from 0

mm at full extension to 18 mm at 90° of knee flexion, and the patella translated distally from 0° at full extension to 40 mm at 90° of knee flexion. Similar results were found for these patellar kinematics for the ACL-excised and reconstructed knees. Excision of the ACL resulted in significant increases ($p<0.001$) in lateral tilt of the patella ranging from 6.3° to 9.0° between 0° and 90° of knee flexion compared to the intact knee (Figure 2). Excision of the ACL also caused significant increases ($p<0.001$) in lateral shift of the patella, compared to the intact knee, ranging from 2.9 mm at 15° and 30° of knee flexion to a maximum of 5.9 mm at 90° (Figure 3). The IAR returned anterior translation of the tibia to levels not significantly different from that of the intact knee. The IAR increased the lateral tilt of the patella by an amount ranging from 2.6° to 4.0°. The IAR also caused the patella to shift laterally by approximately 2.4 mm between 0° and 60° of knee flexion and by 3.7 mm at 75° and 90° compared to the intact knee. However, these differences in patellar motion were not significant.

DISCUSSION

Our results for patellar motion in the intact knee are in agreement with previous studies.[3,4,5,6] Patellar flexion, patellar anteroposterior translation, and patellar proximodistal translation remained almost unchanged with excision of the ACL or with IAR, suggesting that these kinematics are controlled by the complex geometry of the articulating surfaces. We found that the patella rotated within a very narrow range for the intact, ACL-excised, and reconstructed knees. The limited range of patellar rotation is likely to be the result of the high degree of congruity between the patella and femur. The patella was found to shift laterally throughout the range of knee motion studied for the intact, ACL-excised, and reconstructed knees. This characteristic could be attributed to the geometry of the femoral trochlear groove and the lines of action of the quadriceps tendon and the patellar ligament. It was found that excision of the ACL resulted in significant increases in the lateral tilt and lateral shift of the patella. The abnormal changes in patellofemoral kinematics following excision of the ACL might be expected to lead to changes in the patellofemoral contact areas and, thus, lead to excessive lateral pressure syndrome. Although we did not discover patellar motion in the reconstructed knee to be significantly different from that of the intact knee, there were some differences which might become significant with a larger number of samples. It is also important to note that in the present study the IAR returned anterior laxity to the tibia not significantly different from normal. Thus, an IAR that does not return normal laxity to the tibiofemoral joint might be expected not to return normal patellar motion; we are planning studies to investigate this possibility.

Figure 1. Mediolateral patellar rotation

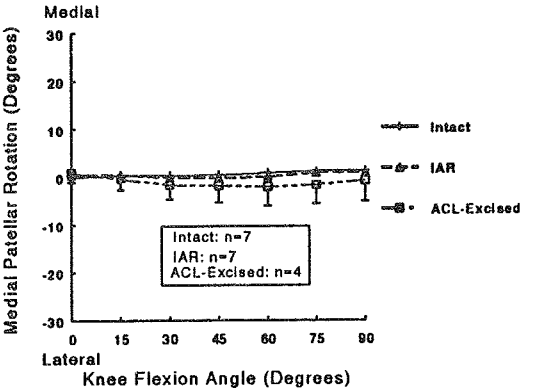

Figure 2. Mediolateral patellar tilt

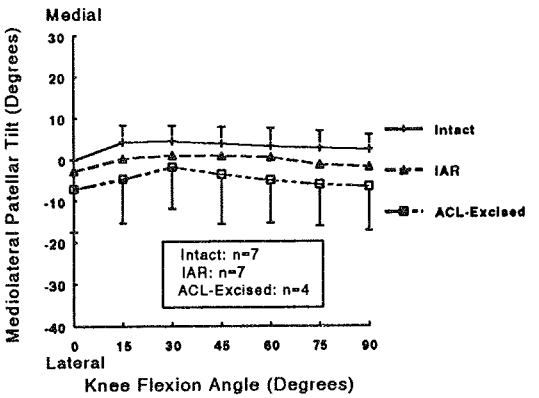

Figure 3. Patellar mediolateral shift

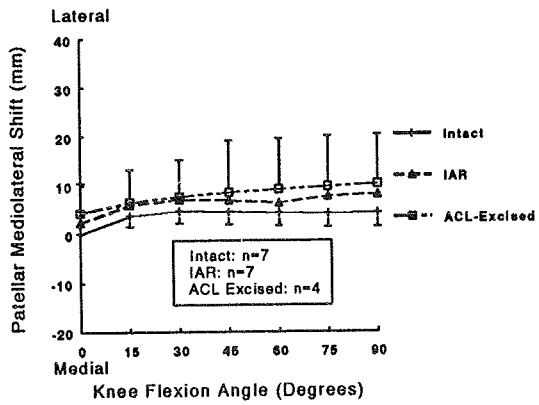

REFERENCES

1. Lieb et al: JBJS, 53A: 749-758, 1971.
2. Grood et al: J Biomech, 105: 136-144, 1983.
3. Van Kampen et al: J Ortho Res, 8: 372-382, 1990.
4. Hefzy et al: J Biomedical Eng, 14: 329-343, 1992.
5. Heegaard et al: Clin Ortho, 299: 235-243, 1994.
6. Koh et al: J Biomech, 25: 637-643, 1992.

JOINT SIMULATION TO DETERMINE EFFECTS OF CO-CONTRACTION

B.A. MacWilliams, B. Chan, E.Y.S. Chao
Orthopaedic Biomechanics, Johns Hopkins University, Baltimore, MD 21239

INTRODUCTION

Proper assessment of lower extremity joint function requires simulation of the natural forces and motions in the intact joint. A joint simulator has been developed to provide precise control of displacements and forces to model physiological conditions for an anatomical specimen. The machine accommodates the degrees of freedom needed for the specimen to be evaluated under loads which approximate *in vivo* conditions. The utility and performance of this mechanism are demonstrated here by examining the effects of various quadriceps and hamstring loads on knee kinematics and joint reaction force. While data from a single preserved specimen is given here, this study is being expanded to include five fresh specimens. Results will be used to assess the effects of certain types of rehabilitation exercises and to validate inverse dynamic computational models.

REVIEW AND THEORY

In vitro investigation of joint biomechanics on anatomical specimens requires a mechanism to produce some type of joint loading so that joint kinematics, pressure distribution, wear, *etc.* can be studied. Such mechanisms have been termed simulators. Early versions (Shaw and Murray, 1974) were designed for wear testing of prostheses. Joint loading was applied through the bones; articulation of the joint was constrained to a specified pattern. Devices still utilizing a single force resultant, but with more flexible controls aimed at biomechanical joint assessment have been recently introduced (Lewis *et al.*, 1988; DiAngelo and Harrington, 1992). Others (Whitside *et al.*, 1985; Haynes *et al.*, 1987) have tested knee mechanics using similar apparatus which apply a vertical load offset by quadriceps force to maneuver the knee through a range of motion. Resulting motions, forces and torques are recorded. Finally, a device designed to simulate level walking using a dual actuator system to simulate forces produced by the quadriceps and hamstring muscle groups has been reported (Szklar and Ahmed, 1987).

A major consideration with joint simulation is the magnitude of the applied forces and how these forces vary with time or joint angle for a given motion. EMG signals from muscles can determine activation and recruitment, but correlations to the actual muscle forces cannot be made. Optimization methods may eventually yield valuable information, but current models have only been applied to simple motions in idealized joints. Without knowing what the physiological forces are in the joint for a given exercise, loading protocols must be developed which will give insight as to how the joint functions.

PROCEDURES

The Johns Hopkins' joint simulator (**Fig. 1**) consists of a loading frame with a long stroke main actuator to apply body weight and vertical displacement, two smaller actuators to apply loads which simulate quadriceps and hamstring forces, and multiple degree of freedom mounting frames which immobilize the femur and tibia and allow simulated hip and ankle movement. An X-Y table is attached to the base of

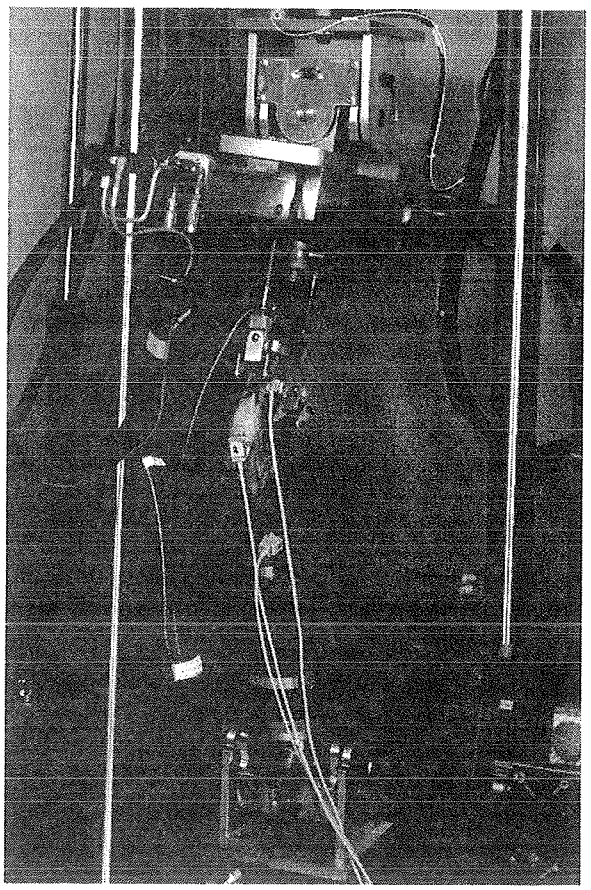

FIGURE 1 - Kinematic knee simulator testing anatomic specimen

the tibial mount for ankle joint alignment and AP and ML translations. Any single degree of freedom or any combination can be fixed.

Four load cells are incorporated in the simulator. Uniaxial load cells are placed in series with each actuator to measure the applied loads, and a six component load cell is positioned below the tibial fixture to measure the reaction forces and moments. Using TestStar® (MTS Systems, Eden Prarie, MN) software, each actuator can be independently controlled in either force or displacement mode with time dependent force or displacement functions. Kinematic measurements are recorded using a three sensor magnetic field position and orientation measurement system (Flock of Birds®, Ascension Technologies, Colchester, VT) to record relative motions of the femur, tibia and patella. Software has been developed to transform raw data into clinically relevant motions using local coordinate systems determined through an alignment procedure.

Specimen preparation involves first removing the skin, exposing approximately 5 *cm* of bone 20 *cm* above and below the knee joint and dissecting free the quadriceps and medial and lateral hamstring tendons. The ends of the bone are potted in woods metal into cups. Knee alignment is achieved using a portable jig which enables the knee to be manipulated into alignment as determined by both AP and ML x-rays. The exposed tendons are sutured about cabled linkages through which the actuated forces are applied.

The knee is then placed in the simulator and run through the specified loading protocols. For the results given here, this consisted of assigning a 0.1 *Hz* sinusoidal displacement function to the main actuator, and applying constant specified loads to the quadriceps and hamstring tendons. Four different load combinations were used.

RESULTS

Tibial kinematic and joint reaction force results from this study are shown in **Figure 2**. Motions are expressed relative to the femur and are plotted *vs.* determined flexion angle. Patella kinematics, measured using the same methods, are not shown. In general, tibial kinematics show only small changes due to altered tendons loadings. The higher quadriceps forces resulted in slightly elevated varus and internal rotations. The highest values of these angles occurred for the maximum Q:H (2:1) ratio, and the lowest for the minumum Q:H ratio (1:2), indicating that the hamstrings act to stabilize knee motions out of the sagittal plane. Joint reaction forces are largely effected, with increased hamstring forces creating greatly increased shears on the tibia, and quadriceps forces having the larger effect on axial force.

REFERENCES

Shaw, J.A. and Murray,D.G. *Clin Orthop Rel Res*, 94:15-23, 1973

Lewis, J.L. *et al. J Biomech Eng*, 110:238-24,. 1988

DiAngelo, D.J. and Harrington, I.J. *Advances in Bioeng*, 22:107-110, 1992

Whiteside, L.A. *et al. Clin Orthop Rel Res*, 219:147-157, 1987

Haynes, D.W. *et al. 13th Ann Meeting Soc Biomat*, p.221, 1987

Szklar, O. and Ahmed, A.M. *J Biomech Eng*, 109:247-251, 1987

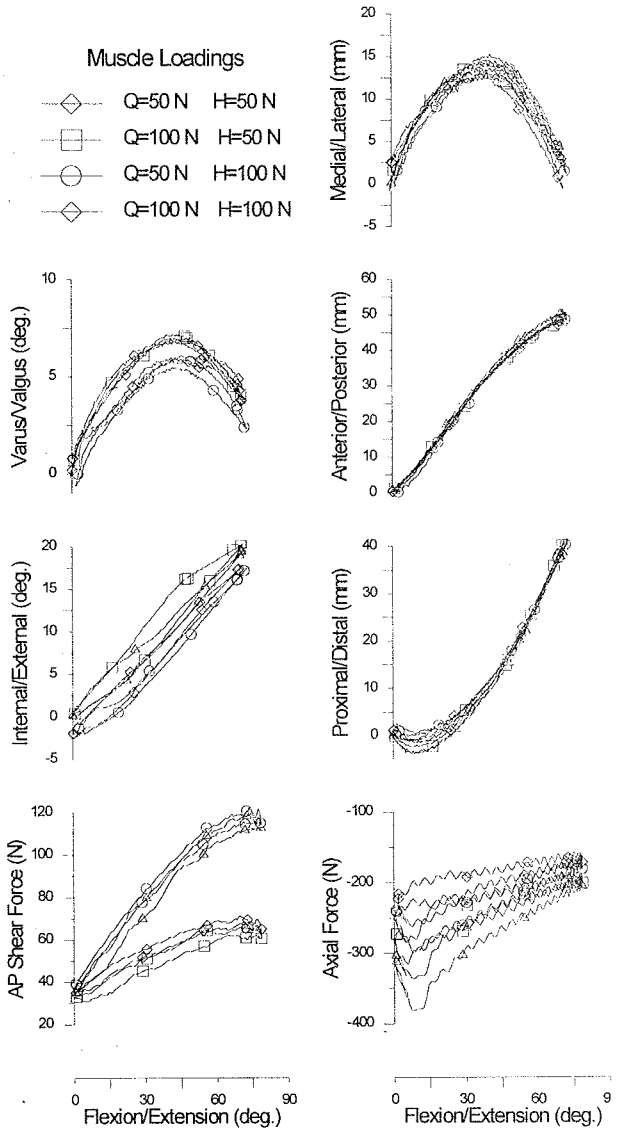

FIGURE 2 - Tibial kinematic and joint reaction forces under various combinations of muscle loads.

KINEMATIC GEOMETRY OF THE KNEE

D.R. Wilson and J.J. O'Connor
Department of Engineering Science and Orthopaedic Engineering Centre
University of Oxford, England

INTRODUCTION

The motion of the knee is governed by the constraints imposed by its anatomical structures. The identification of these constraints and the explanation of their roles in guiding joint motion is an important prerequisite to the understanding of joint mechanics. This abstract describes complementary model and experimental studies whose aim was to quantify the contribution of ligament geometry and articular surface shape to knee kinematics.

REVIEW AND THEORY

The four-bar linkage model demonstrates that the sagittal plane motion of the knee is guided by a mechanism formed by the tibia, femur, anterior cruciate ligament (ACL) and posterior cruciate ligament (PCL). This model has been used to predict the geometry of the anatomical structures in a number of mechanical models of the knee (e.g. Zavatsky et al, 1993). However, because it is restricted to the sagittal plane, this model cannot predict the features of knee motion observed in the transverse and coronal planes. The most significant of these features is the internal rotation of the tibia about its long axis with flexion (the screw-home mechanism). The first aim of this study was to formulate and analyze a three-dimensional analog of the four-bar linkage model: a model that predicts spatial knee motion from the geometry of the anatomical constraints. The second aim was to perform a preliminary validation of this model by comparing its predictions of knee motion to experiment.

PROCEDURES

The geometric model of the knee was formulated by making assumptions about the anatomical structures of the joint in passive flexion (motion from one position of neutral equilibrium to the next). Experimental evidence in the literature suggests that, in passive flexion, there are isometric fascicles in the ACL, PCL and the medial collateral ligament (MCL)(Sidles et al, 1988)(Poliacu Prose et al, 1988). In the model, these isometric fascicles were modelled as inextensible constraints to motion between the tibia and the femur. The articular surfaces of the femoral condyles were assumed to be spherical and the articular surfaces of the tibial condyles were assumed to be planes. In the model, it was assumed that contact was maintained through the range of motion, and the articular constraint in each compartment was modelled as a sphere rolling and sliding on a plane.

The five constraints imposed by the three isometric ligament fascicles and the two sphere-plane contacts were modelled as mechanical connections in a spatial mechanism (Figure 1). A mobility analysis showed that this mechanism has one degree of freedom. A forward kinematic solution procedure was applied to predict the motion of the tibia relative to the femur through the range of flexion (Wilson et al 1994). The position and pitch of the instantaneous screw axis were calculated from the geometry of the constraints (Wilson et al 1994[b]).

The starting configuration of the mechanism is required to determine the kinematics of the model. This is specified at full extension of the knee by the coordinates of the origins of the isometric ligament fascicles on the femur and their insertions on the tibia, the positions of the points of contact between the tibia and femur in the medial and lateral compartments, the positions of the centres of the spheres representing the femoral condyles, and the orientations of the planes representing the tibial condyles.

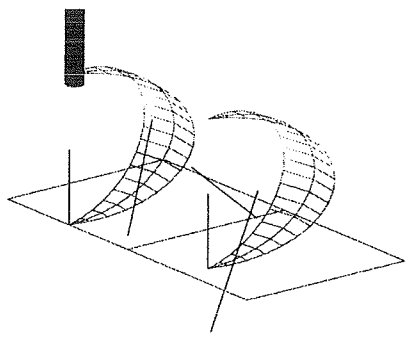

Figure 1: An anteriomedial view of the geometric model

To perform a preliminary validation of the model, experimental measurements of passive knee motion and of the anatomical parameters were made for a cadaver knee specimen. The knee, comprising 20 cm of proximal tibia and 20 cm of distal femur, was removed at autopsy. All tissue except for the bone, ligaments and capsule was removed from the knee. Several small nails were driven into both bones to act as reference markers. The tibial shaft was potted in wax in a plastic tube that was then fixed rigidly to a workbench. An Isotrak-II magnetic tracking system (Polhemus, Vermont, U.S.A.) was used as a three-dimensional tracker and digitizer. At full extension, the positions of the reference markers were digitized. The position of the femur was then tracked as the knee was flexed without applied load through its range of motion. The joint was disarticulated and the shaft of the femur was potted. The proximal tibia and the distal femur were dissected, the menisci were removed and the following positions were digitized: the reference markers, uniformly spaced points on the circumference of the attachment sites of the ACL, PCL and MCL, and uniformly spaced points on the articular surfaces in the medial and lateral condyles.

A computer program was written to analyze the experiments. The transformation between the intact knee and the digitized bones, determined from the relative positions of the reference markers, was used to determine the coordinates of all of the digitized features of the joint at every position. The spheres that best fit the points on

the medial and lateral femoral condyles were calculated, as were the planes that best fit the points measured on the medial and lateral tibial condyles. The isometric fascicles in each of the ligaments were determined by using a search routine to identify, from the group of all possible fascicles joining the points describing the ligament attachments, the fascicle that exhibited the least maximum strain through the range of flexion.

Model predictions of the motion of the tibia relative to the femur were calculated using the anatomical parameters from the specimen. For both experimental and model motion, the orientation of the tibia relative to the femur was represented with Cardan angles (Cole et al, 1993), allowing direct comparison of the results.

RESULTS

The model predicts continuous motion from full extension to 57 degrees of flexion. At this position, the mechanism locks and cannot be flexed further. The experimental specimen flexed from full extension to 130 degrees. In Figure 2, model predictions and experimental measurements of axial tibial rotation are plotted as a function of flexion angle. The model predicts internal rotation of the tibia with flexion from 0 to 38 degrees of flexion, where a maximum of 10.8 degrees of axial rotation is reached. From this position to the extreme of flexion of the mechanism, the tibia exhibits almost no further rotation. In the experiment, the tibia rotated steadily with flexion, reaching 10.3 degrees of internal rotation at 38 degrees of flexion and 14.1 degrees of internal rotation at 57 degrees of flexion.

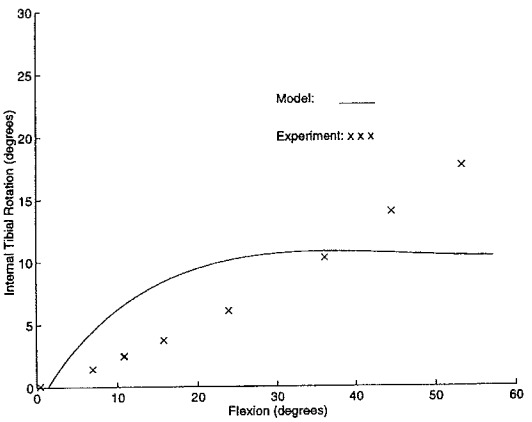

Figure 2: Axial rotation of the tibia with flexion

DISCUSSION

In the range of motion of the mechanism, the model qualitatively predicts the screw-home motion of the knee. The reduced range of motion of the mechanism and the quantitative differences between model predictions and measured motion reflect the simplified geometry of the model. The best fit spheres of the model did not exactly represent the measured geometry of the femoral condyles, and the best fit planes did not exactly represent the measured geometry of the tibial plateaux. The model prediction of locking of the mechanism suggests that the deviation of both the femoral condyle geometry from sphericity and the tibial plateau geometry from planarity is required to allow the full range of motion of the knee while maintaining isometricity in the ACL, PCL and MCL. It also appears that this complex articular geometry is required to maintain steady internal rotation of the knee with flexion.

Experimental and model studies are continuing in order to investigate the role of the articular surfaces in prescribing joint kinematics. Further cadaver specimens are being tested to determine a range of data for the femoral and tibial articular surface geometry, the positions of the isometric fascicles and the passive motion of the knee. In the model, a more accurate representation of the articular surfaces is being studied. Advanced theoretical kinematics methods, including screw theory, are being examined to determine whether they would aid in visualizing and explaining the complex relative kinematic roles of the anatomical structures.

CONCLUSIONS

The preliminary results of the model demonstrate that the ACL, PCL, MCL and contact in the medial and lateral compartments of the knee work together to guide joint motion. While the qualitative patterns of joint motion are explained by the simplified geometry of the model, a more accurate representation of the articular geometry is required to predict the full range of motion of the joint and to predict joint motion quantitatively. This study suggests that disruption of the geometry of any of the constraining structures through surgery or as a result of injury or disease leads to abnormal joint kinematics.

REFERENCES

Cole, G. et al. *J Biomech Eng* 115:344-49, 1993.

Poliacu Prose, L. et al. *Acta Anat* 133:70-78, 1988.

Sidles, J. et al. *J Orth Res* 6:593-610, 1988.

Wilson, D. et al. *Proc 2nd World Cong Biomech* Vol. I p. 62, 1994.

Wilson, D. et al. *CAMARC II Deliverable no. 15: sub goal A.1.* CEC AIM initiative,3-16, 1994.

Zavatsky, A et al. *J Engng Med*, 206:135-146, 1993.

ACKNOWLEDGEMENTS

The authors would like to thank Mr. John Williams and Miss Veronica Conboy for their help in dissecting the specimen, and Prof. Ken Hunt and Dr. Ross MacAree for their advice on theoretical kinematics. This work was supported by the Arthritis and Rheumatism Council (U.K.) and by the Fonds FCAR (Quebec, Canada).

Mapping the Displacement Workspace of the Human Knee

Mingli Zhang, and Michael C. Murphy,
Department of Mechanical Engineering, Louisiana State University, Baton Rouge, LA 70801

Introduction

In the human knee, a combination of parallel passive constraints and redundant, active actuators are used to control the multi-degree-of-freedom joint. The overall understanding of knee kinematics will contribute to the knowledge of mechanical systems with multi-degree-of-freedom joints and parallel passive constraints. This investigation uses mappings of the displacement workspace of the human knee (DWHK) to elucidate the interaction of the different components of the passive constraint system (ligaments and joint surfaces) supporting the joint , and provides significant new insight into the performance of the passive constraint system.

A kinematic model of the ligamentous and articular surface constraints in the knee is used to develop the DWHK. Three-dimensional images and cross-section views of the DWHK are presented. Several performance indices are defined as quantitative measures of the DWHK. The kinematic tolerance of the DWHK resulting from variations in ligament lengths is discussed.

Review and Theory

Early models assumed that the knee was a fixed axis revolute joint, and were embodied in the designs of prosthetics and implants [3]. Crowninshield et. al. [2] developed the first homologue model. A three-dimensional model used in evaluating prosthesis designs was presented by Garg and Walker [4]. Wismans et. al. [6] developed a three-dimensional model of the knee for quasic-static conditions. Blankevoort et.al. [1] revised and extended Wismans'model.

The passive constraint system for the knee was studied by Murphy [5]. Geometric constraints, the articular surfaces, and passive force constraints, including the ligaments and other soft tissues, are both present in the knee. A configuration space with three translational and four rotational (the four components of the unit quaternion) states was defined in the model. The displacement workspace of the human knee was defined as the volume within which every point can be reached by the origin, M, of the moving coordinate frame fixed on the tibia in a reference coordinate frame fixed to the femur.

Procedures

The kinematic model based on DWHK was developed using a parallel manipulator concepts. Four primary ligaments, the anterior cruciate (ACL), the posterior cruciate (PCL),the medial collateral (MCL) and the lateral collateral (LCL), are the principal extensible passive constraints in the human knee. The kinematic equivalent linkages for multiple ligament constraints in the knee comprise a parallel manipulator with several branches (Figure 1). The ligamentous constraint equations for the DWHK can be derived from this parallel manipulator model.

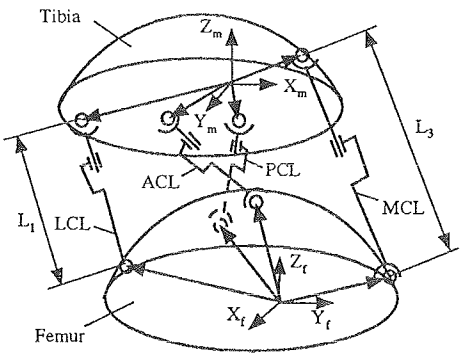

Figure 1 Kinematic equivalent linkages for multiple ligamentous constraints.

Articular surface constraints are the second major type of passive constraint in the knee. The contact surfaces of the femur can be represented approximately by discrete patches. Discrete points are used for the tibia. The surface constraint condition checks whether any point on the tibial surfaces and any patch on the femoral surface are separated, touching, or intersecting. The DWHK is determined by combining the ligament and surface constraint conditions, using Boolean operations.

The DWHK, which is considered as a three-dimensional object, can be represented by an octree.

The object is recursively subdivided into eight suboctrees until suboctrees are reached whose labels are only either FULL or VOID. If a suboctree is entirely inside or outside of the DWHK, the suboctree is given a FULL or VOID label, respectively. Otherwise it is given a MIXED label. The DWHK is composed of all FULL label suboctrees, which are rectangular regions with different sizes.

Ray tracing shading models create more realistic images of three-dimensional objects than other models, such as wireframes. However, significant amounts of computer time are required to generate ray traced models. Removal of hidden surfaces, minimization of the scanning area, and alignment of visible planes were used to reduce the required computer time and generate ray traced models of the DWHK.

Images of the DWHK are informative by themselves, but it is difficult to draw quantitative information directly from 3-D images. A set of performance indices were developed for use as quantitative measures. Measures considered include: volume, centroid, boundary, volume moments, principal volume moments and principal axes of the DWHK.

Results and Discussion

A three-dimensional image of the DWHK and its cross-section views are presented in Figure 2. The volume of the DWHK is 31.15 cm^3 and the boundaries in X, Y, and Z directions are 42.63, 65.22, and 56.53 mm, respectively.

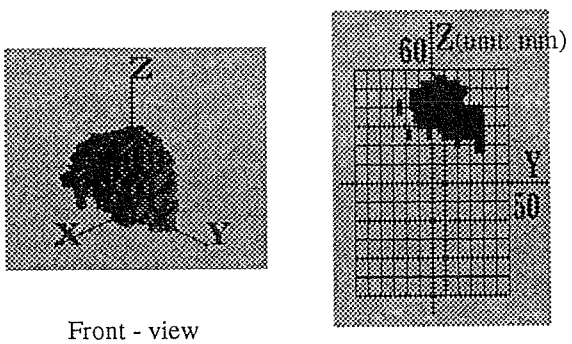

Front - view

(a) (b)

Figure 2. Display of the DWHK: (a) 3-D dimensional image; (b) Cross-section view cut by a plane parallel to the Y-Z plane

Sensitivity of the DWHK to changes in ligament lengths was evaluated using the DWHK volume, volume moment, and principal volume moment as performance measures. The results for volume are shown in Figure 3.

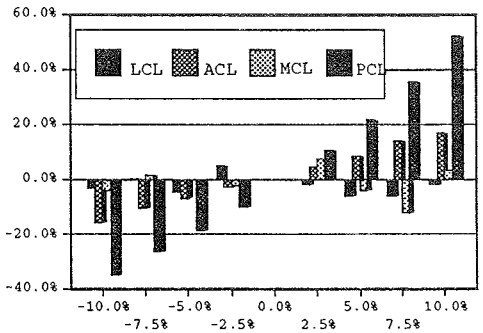

Figure 3. Sensitivity of the DWHK volume to changes in ligament length

The changes in the DWHK volume resulting from variation in ACL and PCL lengths are much larger than those resulting from variation in LCL and MCL lengths. The maximum sensitivity to changes in ±10% of the lengths of ACL and PCL are 17.0% and 52.1%, respectively, but those for LCL and MCL are only 5.5% and 8.2%, respectively.

The kinematic tolerances of the DWHK resulting from variation in ACL and PCL lengths are close to proportional to their lengths, while those for LCL and MCL are smaller.

References

[1] Blankevoort, L. et al. *J. of Biomechanical Eng.* 113: 263-269. 1991.

[2] Crowninshield, R. et al. *J. Biomechanics.* 9:397-405 1976.

[3] Freudenstein, F. et al. *Bulletin of Mathematical Biophysics*, 31,215-232. 1969.

[4] Garg, A. et al. *J. Biomechanics.* 23(1):45-58. 1990.

[5] Murphy, M. C. Ph.D., M.I.T. 1990.

[6] Wismans, J. et al. *J. Biomechanics.* 13:677-685. 1980

Acknowledgments

This work is supported by U.S. National Science Foundation Grant No. BCS-9308948

KNEE KINEMATICS: THE ENVELOPE OF ACCEPTABLE SCREW AXES

C. Mancinelli[1], W. Simons[2], J. D. Blaha[1], V. Kish[1], C. Young[1]
[1]Department of Orthopedics, West Virginia Universtiy, Morgantown, WV 26506
[2]Department of Mathematics, West Virginia University, Morgantown, WV 26506

INTRODUCTION

The purpose of this study was to define the envelope of the knee joint screw axis. Six cadaver specimens were dissected and markers mounted to the femur and tibia. Computerized tomography established marker positions and femur geometry. Each knee was moved by a motor attached to the quadriceps with free weights to the medial and lateral hamstrings. Data were collected from 3 high speed video cameras (VICON). Nonlinear optimization produced an orthogonal matrix that transformed VICON coordinates to CT coordinates without distorting rigid body shape. Marker position vectors were smoothed and differentiated to yield velocity vectors. The screw axis was then calculated. The axes passed through the center of the medial condyle, the notch roof and stretches from the center of the lateral condyle in the direction of the articular surface. The findings of this study do not support the four-bar link model of the knee and can have some total knee design implications.

REVIEW AND THEORY

Normal knee kinematics should provide the standard by which total knee joints are judged. However, there is still considerable question as to what constitutes normal knee motion. The screw axis is a means of describing this three-dimensional motion and the most accurate method of determining the screw axis uses roentgen stereo photogrammetric analysis (RSA).[1,2] Unfortunately, limitations of RSA imaging techniques require stopping joint motion at specific angles to obtain measurements, thus rendering the approach quasi-dynamic. The purpose of this study was to define the envelope of screw axes dynamically in a continuously moving knee.

PROCEDURES

The testing apparatus was a metal frame (0.75m x 0.75m x 0.88m) to which three VICON high speed video cameras (Oxford Metrics, Inc.) were attached. Camera positions were based on the expected position of the specimens to be analyzed within the volume of space to be calibrated. Six right-sided fresh-frozen knee joint specimens were dissected to leave capsule and musculotendinous attachments. Marker blocks were attached to cortical bone of the femur and tibia and specimens scanned in a GE 9800 CT scanner to establish marker positions and geometry of the distal femur. Each femur was rigidly secured to a testing frame in which the knee was extended and flexed by a motor attached to the quadriceps tendon with both symmetric and asymmetric loads on the medial and lateral hamstring tendons. Kinematic data were collected for 2 trials of extension and 2 trials of flexion with symmetric load on the hamstring tendons, with lateral hamstring load, and with medial hamstring load.

Within each video frame, the distances between markers were compared with the distances from CT data. Marker positions were then adjusted using an orthogonal matrix transformation to maintain rigid body shape as defined by the CT data. Markers associated with the most accurate distance calculation were moved the least; markers associated with the least accurate calculation were moved the most. The adjusted positions were compared between successive frames of data by calculating the movement of each marker. Position vectors to markers were smoothed using a method which combines least squares and cubic splines to create differentiable paths from which velocity vectors can be calculated.[3] The screw axis was then calculated using the position and velocity vectors. Position and velocity vectors for each trial were also analyzed statistically using Pearson's Product Moment correlation coefficient.

The CT images were digitized to generate an outline of the distal femur. Femoral contours were converted to 3 sagittal slices by choosing a central contour to represent the intracondylar notch and 2 slices midway between the notch and the epicondyles to represent the lateral and medial condyles. In each of these 3 planes, the screw axis was represented by a point where the axis pierced that plane. A mean reference axis (MRA) was determined for each knee by taking an average of all axes for a given condition. The femoral contours of all 6 knees were then aligned along this MRA so that comparisons could be made between knees.

RESULTS

The Pearson's product moment correlation coefficient showed excellent correlation of the position and velocity vectors for like conditions in the same knee (r=.99). Graphic comparisons can be seen for symmetric, lateral and medial load during extension and flexion (Figs. 1-3). All axes calculated and used in the determination of the MRA are demonstrated in the figures. The axes passed through the center of the medial condyle, stayed in the roof of the intercondylar notch, and passed closer to the articular surface on the lateral side than on the medial side.

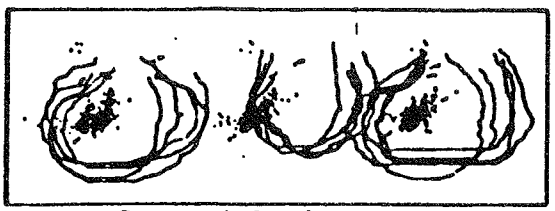

Figure 1 Symmetric Load
(Lateral Condyle, Notch, Medial Condyle)

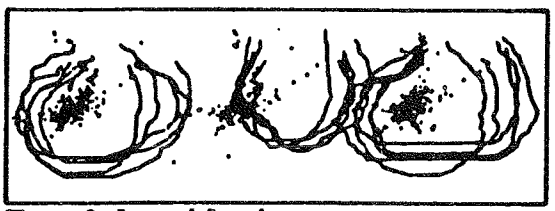

Figure 2 Lateral Load
(Lateral Condyle, Notch, Medial Condyle)

Figure 3 Medial Load
(Lateral Condyle, Notch, Medial Condyle)

DISCUSSION

Consistent screw axis patterns were found similar to those previously reported by van Dijk using RSA[4]. The screw axes were not fixed, rather there was an envelope of axes. However, unlike van Dijk's findings the axes were rarely located at the crossing of the cruciate ligaments. This finding does not support the four-bar link model of the knee. The excursion of the axes (i.e. the envelope of axes) in both symmetric and asymmetric loading conditions was similar except for some decrease in the area of piercing points of the axes with medial load. The axes stretched closer to the articular surface on the lateral side than on the medial side. This finding suggests that the two sides of the joint function kinematically differently and therefore has implications for total knee design.

REFERENCES

(1) Blankevoort, L et al: J Biomech 21: 705-720, 1988.
(2) Van Dijk, R et al: J. Biomech. 12: 727-731, 1979.
(3) Simons, W and Yang, K: J. Biomech Eng. 113: 348-351, 1991.
(4) Van Dijk, R: Thesis, 1983.

SUBMAXIMUM STIMULUS INTENSITY INCREASES MAXIMUM STRENGTH IN ELDERLY

T.M. Owings and M.D. Grabiner
Department of Biomedical Engineering, The Cleveland Clinic Foundation,
Cleveland OH 44195

INTRODUCTION

The normal aging process is associated with decreased muscle mass and strength, the latter of which has been associated with diminished physical capabilities. *High intensity* resistance training has been reported to be an effective countermeasure in very old subjects (Fiaterone et al., 1990; Fiaterone et al., 1994). Interestingly, *low intensity* strength programs have also been demonstrated to result in significant strength gains (Brown & Holloszy, 1991; Agre et al., 1988; Mikesky et al., 1994), but training with submaximum loads do not appear to consistently increase strength (Lundin & Grabiner, unpublished data).

Keen et al. (1994) reported that following a strengthening program, elderly subjects demonstrated significantly improved strength and force control of a hand muscle. Although young subjects demonstrated similar strength gains they did not demonstrate concommitant increases in force control. The above studies suggest that (1) low intensity exercise can significantly increase strength in elderly subjects and (2) increased strength also manifests itself as increased force control in elderly subjects. The aim of the present study was to further investigate the relationship between increased strength and force control. However, we investigated whether training elderly subjects specifically to control force would influence maximum voluntary strength.

PROCEDURES

Ten healthy, elderly subjects (76.6±6.2 years) participated in the training program. The training task involved concentric and eccentric isokinetic knee extensions performed on a KIN COM isokinetic dynamometer at 15°/s. The subjects trained twice a week for a period of 4 weeks. During each training session, the subject attempted to control a submaximal force through a 50° range of motion. Visual feedback was provided at target force values of 15, 30, 45, and 60% of their pre-training maximum voluntary knee extension force. One week prior to the first training session and one week following the last training session, the maximum voluntary knee extension forces and the subject's ability to control submaximal forces at each target force were recorded. Analysis included extraction of the peak moment during the maximum voluntary knee extension trials. For the control trials, the middle third range of motion was extracted and the root mean squared (RMS) error between the exerted force and the target value was determined. The averaged, squared jerk of the force curve was used as a representation of the smoothness of the curve. The control data was subjected to a 4×2×2 repeated measures ANOVA (target level by session by contraction type) and the maximum knee extension force data was analyzed using a 2×2 repeated measures ANOVA (session by contraction type).

RESULTS

The ANOVA revealed a significant effect of testing session (pre vs. post, $p<0.01$) on the peak knee extension moment (Table 1). Not surprisingly, the ANOVA also revealed that the peak eccentric knee extension moments were significantly larger than the concentric values ($p<0.01$). The pre-post by concentric-eccentric interaction term was not significant ($p=0.10$).

Table 1: Mean (std) of maximum voluntary knee extension moments (N∗m)

	Concentric	Eccentric
Pre	80.1(45.8)	136.4(61.3)†
Post	105.5(50.3)‡	150.7(63.4)†‡

† - significantly larger than concentric value ($p<0.01$)
‡ - significantly larger than pre-training value ($p<0.01$)

The ANOVA revealed significant testing session, target force, and concentric-eccentric main effects ($p<0.01$) (Figure 1). Furthermore, the 3-way interaction term was significant ($p<0.01$).

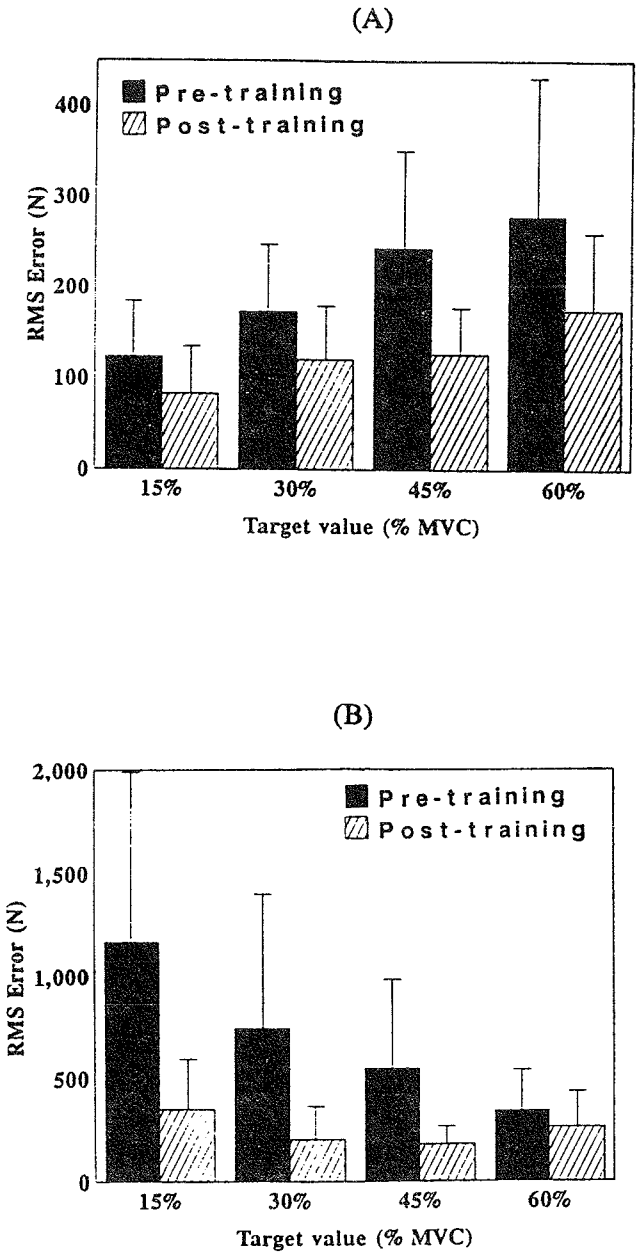

Figure 1: (A) concentric condition. (B) eccentric condition. Mean (std) of the root mean squared error between the subjects exerted force and the target force. Note that the scale for the y-axes are different for the two figures.

DISCUSSION

The results indicate that a short-term training program was sufficient to significantly improve the extent to which elderly subjects could control voluntary, dynamic knee extension force. This was true for both concentric and eccentric contractions. Previous work in our laboratory suggests a substantial age-related difference in the ability to control concentric-eccentric knee extension force. Young subjects demonstrate much smaller differences between measures of concentric and eccentric knee extension force control.

The observed increased ability to control force was associated with significant increases in maximum concentric (31.7%) and eccentric(10.5%) knee extension moment. Correlation analysis revealed the relationships between pre-training maximum concentric and eccentric knee extension moments and force control improvements were generally weak and not significant. However, subjects who had initially lower maximum knee extension moments did tend to demonstrate larger increases in post-training maximum knee extension moments. The results demonstrate that a program of high intensity strength training is not required to significantly improve strength in healthy elderly subjects.

REFERENCES

BROWN & HOLLOSZY *Aging*, 3, 129-139, 1991.
FIATERONE et al. *JAMA*, 263, 3029-3034, 1990.
FIATERONE et al. *NEJM*, 330, 1769-1775, 1994.
KEEN et al. *J. Appl. Physiol*, 77, 2648-2658, 1994.
MIKESKY et al. *Eur J Appl Physiol*, 69, 316-320, 1994.

ACKNOWLEDGMENTS

This work was supported by the Bauerfeind USA, Inc.

A SIMPLE MUSCLE SYNERGY CONTROL FOR DIFFERENT STEADY-STATE PEDALING GOALS

C.C. Raasch, F.E. Zajac

Mechanical Engineering Department, Stanford University, Stanford, California 94305-4021
Rehabilitation R&D Center (153), Veterans Affairs Medical Center, Palo Alto, CA 94304-1200

INTRODUCTION

The kinematics of pedaling impose constraints which define the essential muscle patterns required to pedal the crank steadily. Our analysis suggests that pedaling can be achieved by a phase-locked coordination pattern which excites three agonist/antagonist muscle synergies. This simple controller provides sufficient complexity to adapt to different goals, such as smoothness and energy-efficiency. We are currently exploring how the synergy controller can be adapted to other more novel pedaling tasks such as backward and one-legged pedaling, and pedaling without a seat support.

REVIEW AND THEORY

We have been applying dynamic musculo-skeletal modeling and experiment to understand human bilateral coordination of movement. Currently, we are studying the task of pedaling a stationary bicycle. We have developed a model of pedaling, with controls (18 independent muscle excitations) determined by dynamic optimization, that is compatible with experimentally measured data. In earlier work, we found the optimal controls to produce maximum-speed startup pedaling (Raasch et al., 1995), where the basic goal of the task is to direct as much energy as possible from the muscles to the crank. For steady-state pedaling, where energy transfer to the crank is still a key requirement, we hypothesized that a robust control could be derived by "scaling down" the excitations from maximum-speed pedaling.

In addition, our analysis of the energy flow between muscles and segments indicated that some muscles must work in synergy to propel the crank while avoiding kinematically unfavorable configurations, while others can function independently in certain parts of a cycle. Based on this and measured EMG timings, we generated a simple controller that can produce near-optimal maximum-speed pedaling. This phase-locked controller (Fig. 1) consists of three agonist-antagonist synergy pairs: the uniarticular hip/knee extensors and flexors (E/F pair), the hamstrings and rectus femoris (HAM/RF pair), and the triceps surae and tibialis anterior muscles (TS/TA pair). In normal forward pedaling the HAM/TS and RF/TA controls coincide as shown. Any further reduction in control complexity (e.g., grouping all muscles into Extensor-Flexor synergies only) resulted in large decelerations, free-wheel decoupling, and even reversals at the transitions between downstroke and upstroke. We hypothesize that the simple synergy controller can also produce steady-state pedaling, and can provide a basis for understanding the changes required by the nervous system to coordinate pedaling in different conditions.

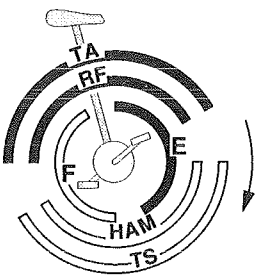

Figure 1: Three agonist-antagonist synergy pairs required for normal pedaling.

PROCEDURES

The linkage model consisted of two legs rigidly connected by cranks to an ergometer inertial and frictional load. Thirteen lower limb muscles, modeled by Hill-type active and passive elements, provide the forces required to move each leg. The thirteen muscles are nominally controlled by nine excitation signals, with muscle groups that act across common joints (hamstrings, uniarticular hip extensors, and uniarticular ankle plantarflexors) receiving common controls. A Hill-based model of muscle heat production (Schutte et al. 1994) was used to calculate muscle metabolic energy consumption.

The excitation signals for steady-state pedaling were derived by averaging on/off times and reducing magnitudes of the first cycle maximum-speed startup controls, for both the nominal 18-signal (complex) control

and the simpler synergy control. With these controls as initial guesses, we used a parameterized optimization algorithm (Pandy 1992) to find controls for steady-state pedaling based on two different cost functions: minimization of velocity variations (maximum smoothness) and minimization of energy consumption. The optimizations included an initial interval of pedaling to allow settling of transients, with only the last cycle subject to steady-state pedaling constraints of fixed time per cycle and equal initial and final velocity.

RESULTS

With equal excitation magnitudes for all muscles, both the complex and the simple controls produced continuous pedaling at 60 rpm, with reasonable energy consumption for the 120 W workload. Assuming aerobic metabolism and similar baseline $\dot{V}O_2$, the resulting total oxygen consumption (1.6 L O_2/min) in the simulation with the complex control agreed well with published data (e.g., Wells et al. 1986). When the simpler E/F-HAM/RF-TS/TA controller was used, the simulation also pedaled steadily, with only slightly higher oxygen consumption (3%). Adaptation to different workloads was accomplished by a simple gain change; that is, an increase or decrease in excitation level for all muscles. For different pedaling cadences, some phase shift in on/off times was also required to account for muscle activation dynamics.

The complex and simple controls demonstrated similar changes when optimized for different task goals (results below are for the simple control). For improved pedaling smoothness, biarticular HAM and RF excitations were increased (47% and 29%, respectively) while the excitation of the uniarticular Extensor group decreased (18%). In the upstroke, uniarticular Flexor excitation was increased (29%). In general, excitation timings did not change much, except for the TS group, which was turned on later in the cycle. When the cost function was set to metabolic energy consumption, however, muscle on/off times changed significantly, resulting in shorter bursts. HAM, RF, TS, and TA excitations were all decreased, while Extensor excitation was higher.

DISCUSSION

The performance of the simple synergy control was found to be very close to that of the more complex control in both the initial and optimized cases. We believe the synergies may represent a central feedforward control for pedaling, which can by modified by sensorimotor feedback.

Increased excitation level in HAM/RF improved smoothness because these muscles are the main energy producers during transitions, as indicated by our mechanical power analysis (Raasch et al. 1995). When muscle excitations are equal, muscle energy input is lowest at transitions, resulting in a drop in crank velocity during this portion of the cycle. Decreased Extensor excitation and later TS on-time served to decrease the velocity peak which occurs during downstroke. Note that during downstroke TS mainly acts to transfer to the crank energy produced by the Extensors, while during transitions it delivers its own muscle energy to the crank. Flexor muscle excitations were increased because they contribute some energy to the latter part of the downstroke-to-upstroke transition. They also allow Extensor excitation level to decrease, reducing the deceleration at transitions caused by their active, lengthening relaxation.

Preliminary analysis indicates that shorter on/off regions reduces metabolic energy consumption because muscle activity is limited to phases where each muscle contributes maximally to crank acceleration. The original maximum-speed control, on the other hand, excites a muscle when any positive contribution to the crank is possible. This shorter-burst strategy also resulted in modified ankle kinematics which allowed use of passive ankle stiffness, rather than active muscle force, to transfer part of the Extensor energy to the crank.

REFERENCES

Pandy, M.G. et al., *J. Biomech. Eng.* 114, 450-60, 1992.

Raasch, C.C. et al., *J. Biomech.*(submitted), 1995.

Schutte, L.M. et al., *IEEE Trans. Rehab. Eng.* 1, 109-25, 1993.

Wells, R. et al., *Eur. J. Appl. Physiol.* 55, 295-301, 1986.

ACKNOWLEDGMENTS

This research was supported by NIH grant NS17662, and the Department of Veterans Affairs Rehabilitation R&D Service. We would like to thank Lena Ting, Steve Kautz, and William Levine for their comments on synergistic control of pedaling.

MUSCLE COORDINATION OF ONE-LEGGED PEDALING

L.H. Ting, C.C. Raasch, F.E. Zajac
Department of Mechanical Engineering, Stanford University, Stanford CA 94305
Rehabilitation R&D Center, Veterans Affairs Medical Center, Palo Alto, CA 94304

INTRODUCTION

Musculoskeletal models can describe the physical constraints of motion; however, because of muscle redundancy, such models cannot uniquely define muscle activation patterns. The body itself may use neural "constraints" such as muscle synergies to reduce the degrees of freedom of a task. Identification of such constraints will increase the usefulness of musculoskeletal models.

With this goal, we studied interlimb sensorimotor control mechanisms of a bipedal task. Subjects pedaled a stationary bicycle ergometer with two legs, and then with only one leg, where the mechanical loads experienced by the leg at the crank were the same in each case. When only one leg pedaled, increased cranking torque was observed during the upstroke, possibly due to an increased flexion synergy. This difference between the control of the two tasks implies that sensorimotor control of one leg affects the control of the contralateral leg.

REVIEW AND THEORY

Studies have revealed interlimb coupling mechanisms which constrain independent bimanual movement in humans (Swinnen, 1991). Interlimb coupling in the legs has not been studied much in humans, though coupling is likely to be even stronger, as the legs have primarily a locomotor function. Furthermore, research in quadrupeds demonstrate interlimb coupling in spinal control mechanisms for locomotor and other tasks (Stein, 1989; Grillner et al., 1988).

In order to study neural mechanisms without directly probing the nervous system, the interaction of the musculoskeletal and nervous systems must be described. By studying mechanically equivalent tasks, changes in EMG timing and amplitude can be isolated from changes in mechanics. The musculoskeletal model is then a valuable tool for interpreting the experimental results.

Analysis of a musculoskeletal model of cycling have suggested simple muscle synergies that are adequate to control steady-state pedaling (Raasch et al, 1995b). We expect such synergies to be disrupted in the absence of contralateral sensorimotor control.

PROCEDURES

Each of 10 subjects was presented with four different pedaling conditions, in the order below. The right and left leg were studied in random order. For all four cases, the subject was asked to pedal at 60 rpm to the beat of a metronome. 1) *Standard Pedaling*: normal, two-legged pedaling; 2) *Aided Pedaling*: subjects pedal with just one leg while a human "motor" pedals on the other crank generating the same cranking torque that the subject did originally in Standard Pedaling 3) *Aided Pedaling with Force Feedback*: subjects use visual force feedback to match the cranking torque that they had generated with the same leg during Standard Pedaling; 4) *Standard Pedaling with Force Feedback*: subjects match the torque trajectory generated during Standard Pedaling.

Crank angle, pedal angle, and normal and fore-aft pedal forces were measured. Surface EMGs were measured from RF, VAS (medialis), HAM (biceps femoris, long head), TA, and GAS (medialis) of each leg. EMGs from 8 subjects were used in the statistical analysis; 2 subject's data were technically corrupted.

EMGs were high-pass filtered (2nd order Butterworth, cutoff =16.5 Hz), demeaned and rectified. EMG onset and offset were recorded with respect to crank position. Mean EMG amplitude was calculated during periods of muscle excitation Averaged quantities were calculated for each trial of each subject,

and used in a two-way ANOVA analysis with subject as a blocking factor. The Student-Neuman-Keuls posthoc test was applied to data rendering significant ANOVA results.

RESULTS

As previously reported (Ting et al., 1994) significant differences between Standard and Aided Pedaling in the average amount of cranking torque generated during upstroke exist. Subjects generated only 12% of the retarding torque of standard pedaling during Aided Pedaling (Fig. 1).

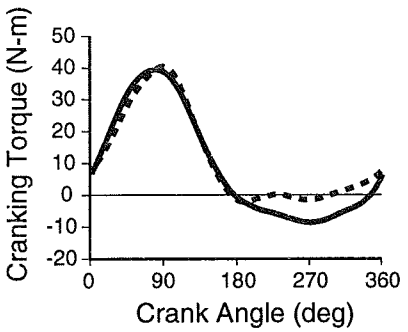

Figure 1: Cranking torque during Standard (solid line), and Aided (dashed line) Pedaling in one subject.

No significant differences in mean EMG ampliitude or EMG offset were found. However, onset of some muscle were significantly different between Standard and Aided Pedaling (Table 1). Both TA and RF have earlier onsets during the upstroke, where increased cranking torque was measured during Aided Pedaling. There were no significant differences between Standard Pedaling and Standard Pedaling with Force Feedback.

Table 1: EMG onset: Differences between Standard and Aided Pedaling (in degrees). Significance: ** 0.01 level, * 0.05 level

TA	MG	VAS	RF	BF
-52.2**	ns	16.4*	-28.8*	ns

DISCUSSION

A dynamic musculoskeletal model with 13 Hill-type muscles per leg (Raasch et al., 1995a) was used to analyze the effects of changes in muscle timing and activation level on pedaling kinetics and kinematics.

A delayed onset in VAS did not significantly alter the cranking torque or angular velocity of the crank in the model. Early excitation of RF can generate only a small amount of cranking torque during upstroke. Early excitation of TA dorsiflexes the ankle, and, in fact, decreases the cranking torque slightly. The short head of biceps femoris, a uniarticular knee flexor, can contribute more cranking torque during upstroke, but not enough to explain the difference in cranking torque observed. However, increasing the gain, or activation level of the uniarticular hip flexors, increases the cranking torque during upstroke to levels comparable to that observed in subjects.

A study of power flow through the limbs during cycling suggests that hip and ankle flexors can theoretically act synergistically to power the crank during upstroke (Fregly, 1993). Thus, the increased duration of TA activity and the increased cranking torque during upstroke in Aided Pedaling are consistent with this hip/ankle synergy.

Since the mechanical task at the crank was the same in all cases, subjects could have performed all tasks in an identical fashion. However, our analysis suggests that with the contralateral leg stationary, an increased flexion synergy is elicited. Thus, sensorimotor control of the contralateral leg may influence the control of a leg. Further study is required to determine what aspects of sensorimotor control of the contralateral leg affect muscle coordination during pedaling.

REFERENCES

Fregly, BJ, PhD thesis, Stanford University (1993).
Grillner, S, et al., *Adv Neurol*, 47, 425-53, 1988.
Raasch, CC, et al., *J Biomech*, (submitted), 1995a.
Raasch, CC, et al., *19th ASB Meeting* (this volume) 1995b.
Stein, PS, *Ann NY Acad Sci*, 563, 1-10, 1989.
Swinnen, SP, et al., *Exp Brain Res*, 85, 163-73, 1991.
Ting, LH, et al., 2nd World Congress Biomech (1994), II-112b.

ACKNOWLEDGMENTS

Supported by NIH Grant NS17662, an NSF Predoctoral Fellowship to LHT, and the DVA Rehabilitation R&D Service.

MUSCLE STRENGTH AND FORCE-TIME CHARACTERISTICS IN MIDDLE-AGED MALE AND FEMALE PATIENTS WITH RECENT-ONSET INFLAMMATORY ARTHRITIS

A. Häkkinen[1], P. Hannonen[1], K. Häkkinen[2]

[1]Department of Physiatry and Medicine, Central Hospital, Jyväskylä
[2]Department of Biology of Physical Activity, University of Jyväskylä, Jyväskylä

INTRODUCTION

Neuromuscular function was compared between twenty middle-aged patients (10 men and 10 women) with relatively recent onset (symptomatic period 17 ± 24 months) rheumatoid arthritis (RA) (experimental group; EG), and twenty age and sex matched heathy people (control group; CG). The measurements in EG were repeated after a six-month period of progressive strength training. At baseline maximal grip strength and maximal dynamic unilateral strength of the knee extensors in EG both in men and women were lower ($p<0.001$ and 0.05) in comparison to CG. The groups did not differ from each other in maximal isometric strength of the trunk flexors and extensors nor the knee extensors but the earlier positions of the average force-time curve were lowered ($p<0.05$) in patients. The 6-month strength training in EG resulted in great increases in maximal dynamic strength of the knee extensors ($p<0.001$), in isometric grip strength ($p<0.001$) and in isometric strength of the trunk flexors ($p<0.05$) and extensors ($p<0.05$) to the level of the healthy controls. ESR ($p<0.001$) and Ritchie's articular index ($p<0.01$) improved during the training period. The results suggest that inflammatory arthritis decreases dynamic and/or isometric maximal muscle strength in selected muscle groups already in the early stages of disease but progressive strength training can rather rapidly increase the neuromuscular performance of the male and female patients even to the level of healthy persons without detrimental effects on disease activity.

REVIEW AND THEORY

It has been reported that patients suffering from rheumatoid arthritis for several years, as compared with heathy people, have greatly decreased isometric and isokinetic muscular strength (Nordesjö et al 1983, Danneskiold-Samsoe et al 1986). This is thought to be inflammation-related processes in the joints, muscles and in periarticular connective tissues, which lead to disuse and thereby also functional and sometimes also structural changes in the neuromuscular system. Consequently, a possible decrease in the voluntary neural activation of the muscles and the degree of muscle atrophy will determine the magnitude of the decrease in muscle strength in various muscle groups. However, much less information is available on muscular strength and neuromuscular performance during the early stages of disease. This type of data on the time course and magnitude of the strength decrease could be useful for optimal preventive and rehabilitational purposes in order to minimize RA-induced negative effects on normal daily functions of the patients. The purpose of this study was to compare maximal strength of various muscle groups and the shape of the force-time curve of the knee extensors in middle-aged patients with recent onset inflammatory arthritis to that of age and sex matched heathy people. Secondly, the measurements were repeated in patients after a six-month period of progressive strength training.

PROCEDURES

Twenty patients (10 women, W; 43 yrs, range 26-51 and 10 men, M; 38, 26-54) with recent onset rheumatoid arthritis (symptomatic period 17±24 months; experimental group, EG) and twenty healthy persons (10 W; 42, 24-57 and 10 M; 39, 27-53) from the hospital staff (control group, CG) volunteered for the study. Sixteen out of the patients (9 W and 7 M) also carried out dynamic strength training for 6 months receiving antirheumatic medication. The study was approved by the Ethics Committee of the hospital. Maximal bilateral and unilateral dynamic strength (1 RM, kg) and maximal bilateral isometric strength of the knee extensor muscles were measured by using the David 200 dynamometer (Häkkinen et al 1987). The force recordings were analyzed for maximal peak force (N), various force-time characteristics and for the maximal rate of rise of force development (Nxs^{-1}). Maximal isometric force of the trunk flexors and extensors was measured by the Digitest-dynamometer and maximal grip strength by the Jamar Standard - dynamometer. Muscle cross-sectional area of the quadriceps femoris was measured by computerized tomography (CT). During the first 2 months of strength training the patients performed exercises (with rubber bands) for all major muscle groups 2 times a week with loads of about 40% of the repetition maximum (RM), from the 3rd month onwards 2-3 times a week with loads of 50-60% and from the 5th month onwards with the loads of 70-80%. The patients performed also other physical activities such as stretching, walking, biking and swimming about 2 times a week. Ritchie's articular index (RI) (Ritchie et al 1968) and erythrocyte sedimentation rate (ESR) were used for the estimation of disease activity.

RESULTS

The unilateral 1 RM values of the knee extensors of 38 kg and 40 kg in MEG for the right and left leg were lower ($p<0.05$) than those 45 kg and 51 kg recorded for MCG. The values of 22 kg and 23 kg in WEG were also lower (ns.) than those of 27 kg and 25 kg recorded for WCG. The 1 RM values per body weight differed ($p<0.05$) in both sexes as well. The maximal bilateral isometric forces of the

knee extensors did not differ significantly between EG and CG. The force-time curves on absolute values differed between the two groups so that the times to produce the two initial force levels were in EG longer ($p<0.05$) than in CG (Fig 1). The maximal rate of rise of force development did not differ significantly between EG and CG. Maximal grip strength values in EG in both sexes were 25% lower ($p<0.001$) than in CG. Maximal isometric trunk flexion and extension values in EG were slightly (3% and 6%) lower than those recorded for CG. The training in EG led to great increases in 1 RM knee extension strength, grip strength, trunk flexion and extension strength (Fig 2). No significant changes occured neither in maximal isometric force nor in the force-time curve of the knee extensors. The individual changes in the shape of the force-time curve correlated negatively ($r=-.55$; $p<0.05$) with age. Muscle CSA increased in men by 6±7% ($p<0.05$) and by 2±6% (ns.) in women. In EG the initial tenderness of the knees correlated ($r=-0.45$; $p<0.05$) with the initial dynamic strength values of the knee extensors. RI (from 12±6 to 5± 5, $p<0.01$) improved and ESR decreased (from 21±17 to 10±9, $p<0.001$) during the 6-month period.

DISCUSSION

The primary findings showed that maximal dynamic strength of the knee extensors was lower in middle-aged patients with RA than in healthy controls. This was true both for men and women. It seems that the loss of dynamic strength of the knee extensors in RA patients may take place already in the early phase of the disease in part due to decreased physical activity. The decrease in strength may also be due to joint tenderness, because the strength values of the knee extensors were the lowest in those patients who demonstrated the highest values for the RI calculated for the knees. Isometric strength of the knee extensors, trunk flexors or trunk extensors did not differ significantly between the two groups. A decrease in isometric strength may therefore require a more prolonged disuse of the muscles accompanied then also by muscle atrophy. The two groups did differ in their isometric grip strength, since the disease usually begins from the small joints of the hands and feet. Although the two groups did not differ in the maximal rate of rise of force development, the average shape of the force-time curve of the knee extensor muscles did differ in its earlier portions. This results probably from the reduced neural activation capacity for explosive performance, muscle fibre type characteristics and/or joint tenderness leading to a avoidness of rapid force production of the muscles. The 6-month gradually progressive strength training in the patients led to great increases in the maximal strength of all examined muscle groups. In general, the magnitude of the training-induced increases in strength was similar between the male and female patients. The increase in strength was probably due to neural adaptations of the trained muscles, although the male patients showed also some hypertrophy of the knee extensors. However, this type of training did not lead to increased explosive strength characteristics of the muscles. Actually, older subjects tended to demonstrate even lowered values in comparison to younger patients. This suggests that special attention needs to be paid to the rehabilitation programs of older patients. Nevertheless, the strength performance capacity of the patients increased during the strength training to the level of the healthy subjects. An individually designed program of proper physical exercises including also explosive type of strength training should therefore be planned and started as soon as possible right after diagnosing RA to courage both male and female patients at all age and prevent/minimize the decreases in their physical and functional capacities.

REFERENCES

Nordesjö, L.O. et al. Scand. J. Rheumatol. 12: 152-156, 1983.

Danneskiold-Samsoe, B. et al. Clin. Rheumatol. 5: 459-467, 1986.

Häkkinen, K. et al. Med. Sport Sci., Kargel, Basel, 224-237, 1987.

Ritchie, D. et al. Q. J. Med. 37: 393-406, 1968

ACKNOWLEDGMENTS

Financially supported by the grants from the Central Hospital of Central Finland and from Yrjö Jahnsson Foundation, Finland.

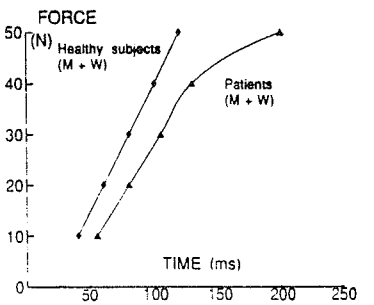

Fig 1 Force-time curves of the knee extensors

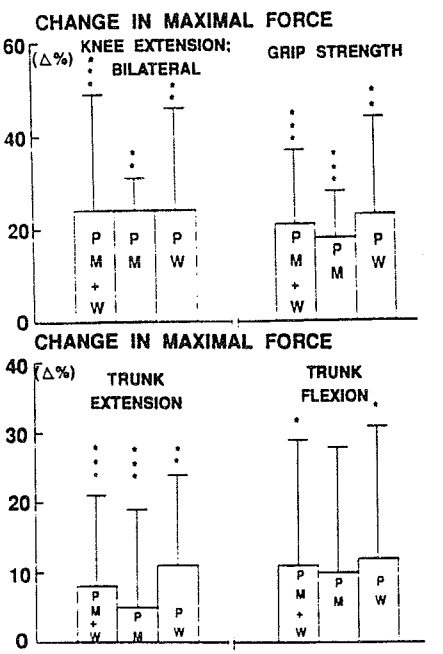

Fig 2 Training-induced increases in stregth in patients (P)

NEUROMUSCULAR FATIGUE AND RECOVERY IN YOUNG VERSUS ELDERLY WOMEN DURING HEAVY RESISTANCE LOADING

K. Häkkinen
Department of Biology of Physical Activity, University of Jyväskylä, Jyväskylä, Finland

INTRODUCTION

To examine neuromuscular fatigue and recovery eight young women (YW) and 8 elderly women (EW) loaded their leg extensor muscles by performing 5 sets in the bilateral leg press exercise on the machine (David 210) with the maximal 10 RM load (5 x 10 RM). Maximal voluntary neural activation (integrated EMG), maximal bilateral isometric force and force-time curves of the leg extensor muscles were measured before and after the loading and after resting for 1 hour, 2 hours, 1 day and 2 days. The loading led to gradual decreases in maximal force in YW by 18.8 ± 7.1% ($p<0.001$) and in EW by 13.7 ± 11.9% ($p<0.01$). Significant ($p<0.05$) decreases also took place in the maximum IEMGs of the exercised muscles in both groups. The earlier positions both in the force-time and IEMG-time curves decreased only in YW ($p<0.001$). Maximal force and maximum IEMG recovered gradually in YW but less systematically in EW. The results suggest that heavy resistance loading both in young and elderly women may result in considerable acute fatigue in the neuromuscular system leading to the decreases not only in the force production but also in the voluntary neural activation of the exercised muscles. However, young women seem to be able to produce greater acute neuromuscular fatigue than elderly women who also may demonstrate less systematic recovery from fatigue.

REVIEW AND THEORY

Human muscle strength decreases with increasing age especially at the onset of the sixth decade both in men and women. The decrease in strength may be related to a great extent to the reduction in muscle mass mediated by a reduction in the size and/or a loss of individual muscle fibres, especially of fast twitch fibres (Lexell et al 1988). A decreased capacity for explosive force production of the muscles may further characterize age-related changes in the neuromuscular system, especially in women (Häkkinen et al 1991).

Heavy resistance loading such as used in strength training in young men and women leads to acute decreases in the maximal voluntary neural activation, maximal strength and in force-time characteristics of the loaded muscles (e.g. Komi et al 1977, Clarke 1986, Häkkinen 1994). However, much less experimental information is available on acute effects of fatigue on the neuromuscular performance in aging people (e.g. Enoka et al 1992), especially in elderly women. Since strength training is nowadays rather commonly utilized also among elderly people, the process of recovery taking place after the termination of heavy resistance loading of the neuromuscular system should also deserve some experimental attention. The purpose of the present study was therefore to examine acute neuromuscular fatigue and short-term recovery from fatigue in young versus elderly women, when the relative loading intensity and the volume of the exercise was kept the same.

PROCEDURES

Eight young women (YW) (25.0 ± 1.4 years) and 8 elderly women (EW) (68.9 ± 3.2 years) volunteered as subjects for the study. Full advise was given to the volunteers regarding possible risk and discomfort that might ensure and all subjects gave their written informed consent to participate. The subjects were healthy and habitually physically active but they had no background in regular strength training. The subjects loaded their leg extensor muscles by performing 5 sets in the bilateral leg extension exercise on the machine (David 210) and performed 10 repetitions in each set with the maximal load possible (10 repetition maximum; 10 RM). The recovery time between the sets was 3 minutes. The loads were adjusted during the course of the exercise due to fatigue so that each subject could perform the required 10 repetitions. The measurements were performed before the loading, after each set, immediately after the loading and after resting for 1 hour, 2 hours, 1 day and 2 days. Maximal voluntary force and force-time curves of the leg extensor muscles were measured during the isometric bilateral contraction on a dynamometer. Electromyographic activity was recorded from the vastus lateralis (VL), vastus medialis (VM) and rectus femoris (RF) muscles by surface electrodes and integrated to obtain maximum averaged voluntary EMG (IEMG) during the maximal force production and during the early phases of explosive force production of the same contraction to obtain the IEMG-time curve (Häkkinen 1994). Blood samples for the determination of blood lactate were also taken during the course of the loading and determined using a lactate analyzer (Roche-640).

RESULTS

The loading in both groups led to decreases in maximal isometric force in YW by 18.8 ± 7.1% ($p<0.001$) (from 2038 ± 413 to 1667 ± 415 N) and in EW by 13.7 ± 11.9% ($p<0.01$) (from 1770 ± 574 to 1511 ± 492 N) (Fig 1.). Significant decreases were observed in the maximum IEMGs of the VL, VM and RF muscles (Fig. 2) so that the averaged IEMG value decreased in YW by 6.3 ± 8.2% ($p<0.05$) and in EW by 11.8 ± 5.6% ($p<0.01$). A great decrease of 25.9 ± 12.0% ($p<0.001$) in the rate of rise of force development in YW was greater ($p<0.05$) than that of 9.8 ± 21.7% (ns.) recorded for EW (Fig.1). Accordingly, significant shifts in the early portions in the force-time curves occured only in YW ($p<0.001$). The maximal rate of rise of EMG development ($p<0.001$) and the averaged IEMG during the first 500 ms in the IEMG-time curve decreased only in YW ($p<0.05$), while EW showed minor changes. The mean blood

lactate concentration increased in YW up to 6.6 ± 1.7 mmol x l^{-1} ($p<0.001$) and in EW up to 5.5 ± 1.6 mmol x l^{-1} ($p<0.01$). Maximal isometric force recovered acutely in both groups but after the second hour of rest the forces were still lower ($p<0.05$) than the preloading values. During the first day of rest maximal force recovered further in YW ($p<0.05$) being on the second day 93.7 ± 17.1% (ns.) from its preloading value. In EW no significant recovery took place in maximal force during the first or second day of rest the force reaching 94.6 ± 17.1% (ns.) from its preloading value. The maximum averaged IEMG recovered ($p<0.05$) in YW primarily during the first and/or second hour of rest. In EW the maximum IEMG recovered ($p<0.05$) during the first and/or second hour of rest but after the first and second day of rest the maximum IEMGs decreased ($p<0.05$) again.

DISCUSSION

The present strenuous heavy resistance loading led to fatigue in the neuromuscular system observable by the great acute decreases in maximal force and by the decreases in the maximal voluntary neural activation of the exercised muscles not only in YW but also in EW. Accumulation of lactic acid inside the muscle with decreased pH level as well as depression in Ca^{2+} transport after exhaustive exercise may have resulted in reduced contractile characteristics of the loaded muscles. The decreases in the maximum IEMG of the loaded muscles, although smaller in magnitude than the decreases in maximal force, suggest in line with previous findings in young men and women (Häkkinen 1994) that high loading strength training stimuli may lead to acute fatigue also in the nervous system in elderly women as well. Whether the decrease in the discharge rate of the motor units was due to the actual decrease in central neural drive and/or how much it was modified by proprioceptive feedback from the muscles is difficult to interpret. Fatigue in YW was observable also by the decrease in explosive force accompanied by the decreases in the voluntary rapid neural activation of the muscles, while EW showed only minor changes. This finding could be related to possible age-related decrease in the fast twitch muscle fibre composition of the exercised muscles (Lexell et al 1988) and/or that the lowered testosterone levels in older women could also imply lowered level of aggressiveness, especially for rapid recruitment during the actual loading. This would contribute to minor fatiguing decreases observed in EW especially in the explosive neuromuscular performance as noted earlier also in older men (Häkkinen 1993). The recovery data in both groups indicate that central recovery from fatigue took place already within the first and/or second hour of rest. The observation that EW showed no systematic recovery in maximal force during the first or second day of rest may in part be a consequence of the delayed muscle soreness. These peripheral factors could also be related to the finding that the maximum voluntary IEMG in EW lowered during the two days of rest rather than it would indicate some kind of delayed decrease in central neural drive. In summary, because the degree of neuromuscular fatigue and the time needed for recovery may differ considerably also between individuals, there is a need to optimize both the contents and the frequency of the training sessions in order to plan proper strength training and/or rehabilitation programmes to match with the individual requirements of women at different ages.

REFERENCES

Clarke, D. Res. Quart. Exc. Sport 57, 144-149, 1986

Enoka, R. et al. II NACOB, 63-64, Chicago 1992

Häkkinen, K. XIVth ISB, 538-539, 1993

Häkkinen, K. et al. Eur. J. Appl. Physiol. 62, 410-414, 1991

Häkkinen, K. Electromyogr. Clin. Neurophysiol. 34, 205-214, 1994

Komi, P.V. et al. Acta Physiol. Scand. 100, 246-254, 1977

Lexell, J. et al. J. Neurol. Sci. 84, 275-294, 1988

ACKNOWLEDGMENTS

Financially supported by the Ministry of Education, Finland.

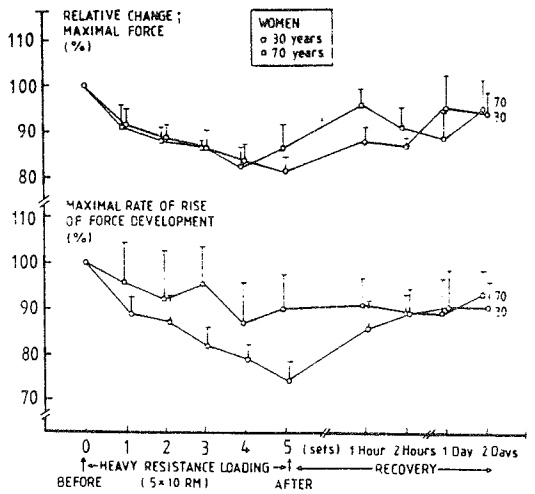

Fig. 1. Changes in maximal force and in explosive strength

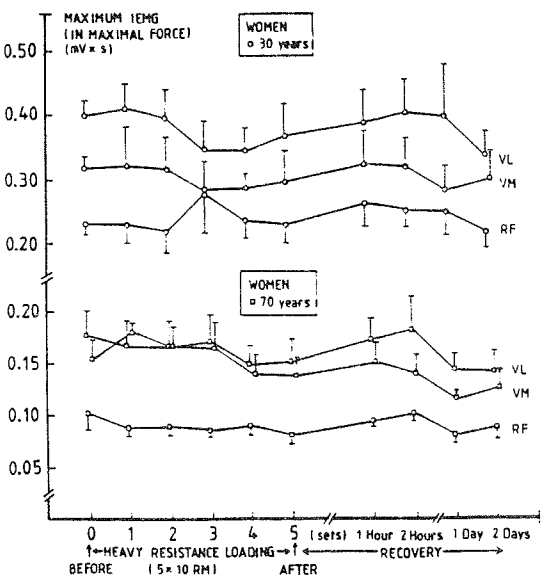

Fig. 2. Changes in maximum IEMGs

MODEL OF MUSCLE TENDON STIFFNESS DURING FIBER RECRUITMENT

T. G. Sandercock and C.J. Heckman
Department of Physiology, Northwestern University School of Medicine, Chicago, IL 60611

INTRODUCTION

The mechanical interaction of individual fibers within a muscle depends on the structure of the muscle's tendon. A key issue is to what degree individual muscle fibers act via a compliance that is independent of that of other fibers versus a compliance that is in common with other fibers. We have developed a distributed parameter model of muscle tendon that allows us to understand the consequences of tendon crosslinks, and to estimate how the stiffness of the tendon varies when different number of muscle fibers have been activated.

BACKGROUND AND THEORY

Our long term goal is to develop a model capable of predicting whole muscle force based on the properties of its constituent muscle fibers. Such a model requires a knowledge of the interaction of fibers through their tendonous links. Muscle fibers terminate in microtendons which run together to form the aponeurosis and external tendon of the whole muscle (Trotter 93). The degree to which the microtendons are crosslinked will influence how the contraction of one fiber will stretch its neighboring fibers or tendons. If their is no crosslinking, activation of a single motor unit would stretch only the microtendons in series with the fibers in the motor unit. The stiffness of the tendon would be proportional to the number of fibers within the motor unit, and, since force from a motor unit is proportional to the number of fibers, the stiffness would also be proportional to the force from the motor unit. Little mechanical interaction between motor units would be observed. On the other hand, if the microtendons are strongly crosslinked, activation of a motor unit will essentially stretch the whole muscle tendon.

Morgan (77) and Proske and Morgan (84) presented a method of separating total muscle compliance into two components, one attributable to the muscle fibers (crossbridges) and one attributable to the series elements (tendon). Muscle stiffness is measured at different levels of muscle activation, transformed to α using the following equation, and plotted as a function of force.

$$\alpha(f) = f/s(f)$$

Assuming the number and stiffness of the crossbridges is proportional to muscle force, and the muscle tendon is linear, the alpha plot is linear

$$\alpha(f) = \alpha_o + fC_t$$

where α_o is the compliance of the muscle fibers and C_t the tendon compliance.

We have previously measured the mechanical interaction between fibers in cat soleus by asynchronously stimulating different parts of the muscle and measuring the degree of nonlinear summation (Sandercock and Heckman 94). The mechanical interaction is remarkably small, suggesting the independent component of tendon compliance is large. In contrast, Proske and Morgan (84) concluded that, if greater than 20% of the muscle was activated the tendon could be considered a single uniform element.

The purpose of this study was to develop a distributed parameter model of muscle tendon enabling us to determine how tendon stiffness varies with different levels of muscle fiber recruitment. A secondary goal was to determine how well a distributed tendon model is fit with Morgan's alpha method.

METHODS

We developed a numerical model of muscle tendon using distributed parameters. The tendon was assumed to consist of individual tendon strands each connected to a single muscle fiber. One to four hundred muscle fibers were used in the model. Each tendon strand was divided into 10 segments, connected in series, with each segment modeled as either a linear or nonlinear spring. The model allowed variable degrees of crosslinking between the strands. The crosslinks were also assumed to be either linear or nonlinear springs.

Tendon stiffness was calculated with different numbers of muscle fibers active. A pseudo-random number generator determined which muscle fibers were active. Active fibers were initially assumed to produce a constant force. Inactive fibers were assumed to move without friction. The set of simultaneous equations was solved to determine the initial tendon stretch. Next, the whole tendon was perturbed with a small increase in length. Tendon stretch was recalculated assuming the active muscle fibers remained fixed at their previous length. The resulting change in force was used to calculate tendon stiffness.

RESULTS

Tendon stretch resulting from two active fibers is shown in figure 1. The tendon segments and crosslinks were linear springs. Similar results were obtained using square or exponential tendon segments and crosslinks. Because individual muscle fibers do not stretch the complete tendon, tendon stiffness is reduced for small numbers of fibers.

Tendon stiffness, plotted as a function of the number of active fibers, is shown in Figure 2. Clearly, as the number of active fibers is increased tendon stiffness increases. Figure 3 shows the same data replotted using the alpha transformation of Proske and Morgan. The distributed parameter model leads to a nonzero y axis

intercept. Proske and Morgan attributed this to the muscle fibers rather than the tendon. Similar results were obtained with nonlinear elements such as square and exponential tendons. The distributed parameter model tended to linearize the overall characteristics of the tendon since parts of the tendon were stretched to different length.

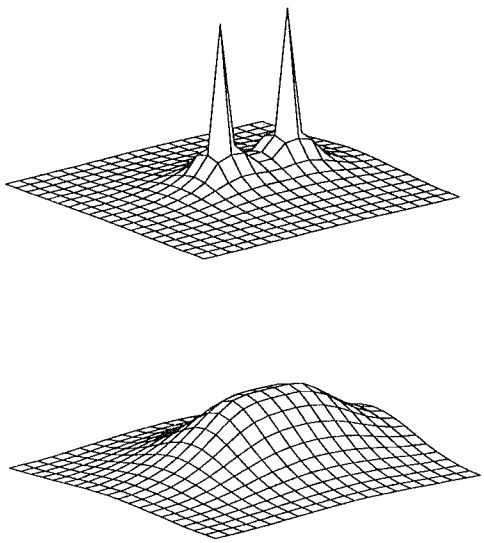

Figure 1: Tendon stretch produced by two active fibers. The cross section of the tendon is square and contains 400 fibers. The vertical axis represents tendon stretch. The upper panel shows the segment nearest muscle fibers. The lower panel shows segment at the distal end of tendon.

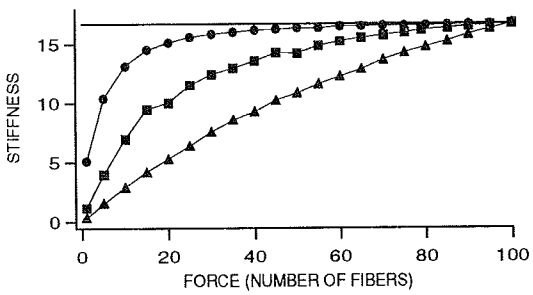

Figure 2: Stiffness of tendon with different number of active fibers. All segment and crosslinks were linear elements.
Solid line: stiffness of 1 element linear tendon.
Circles: distributed model with strong crosslinks (1.0).
Squares: distributed model with moderate crosslinks (0.1).
Triangles: distributed model with weak crosslinks (0.01).

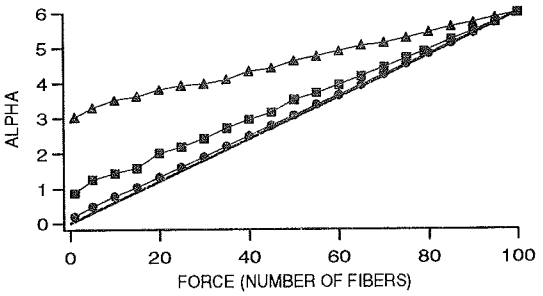

Figure 3: Alpha plot of tendon as a function of muscle force (number of fibers active). All segments and crosslinks were linear elements. Solid line: alpha of 1 element linear tendon.
Circles: distributed model with strong crosslinks (1.0).
Squares: distributed model with moderate crosslinks (0.1).
Triangles: distributed model with weak crosslinks (0.01).

DISCUSSION

Our model predicts that tendon stiffness varies as a function of the number of muscle fibers recruited. Note this result is distinct from the common observation that muscle stiffness varies with force due to the number of attached crossbridges. Variable tendon stiffness may have functional importance during dynamic movements when few muscle fibers are recruited. Our model result is supported by preliminary measurements of the tendon stiffness of single motor units.

The solution of the distributed parameter model showed a linear relationship between alpha and force. This is consistent with the experimental data of Proske and Morgan but suggests a different interpretation. α_0 depends not only on the compliance of crossbridges in the individual fibers, but the degree to which the tendon can stretch independently when different fibers are recruited. The slope C_t depends not on the whole tendon, but rather on the common compliance of the tendon, that is the degree to which the tendon stretches as a whole.

Our present model uses a simplifed tendon geometry. The aponeurosis is generally a thin flat layer. This will limit crosslinking of the tendon and further accentuate the independence of different parts of the muscle.

REFERENCES

Morgan, D.L. *Am. J. Physiol.* 232(1):C45-C49, 1977.

Proske, U. and Morgan, D.L. *J. Neurophysiol.* 52:459-468, 1984.

Sandercock, T.G. and Heckman, C.J. *Conf. Proc. Amer. Soc. Biomech.* :235, 1994.

Trotter, J.A. *Acta. Anat.* 146:205-222, 1993.

IN VIVO MEASUREMENT OF THE MUSCLE DIRECTION OF ROTATION ACROSS THE RANGE OF ELBOW FLEXION

L. Zhang, T. Nishida, J. Butler, G. Nuber, and W. Rymer

Sensory Motor Performance Program, Rehabilitation Institute of Chicago
Departments of Physical Medicine and Rehabilitation, Neurology, and Orthopaedic Surgery
Northwestern University, Chicago, IL 60611

INTRODUCTION

The direction of rotation (DOR) of individual muscles crossing the elbow joint, defined as the direction in which an activated muscle rotated the forearm with respect to the upper arm in 3-D space, was studied across the range of elbow flexion. Electrical stimulation was used to activate an individual muscle crossing the elbow joint selectively. Flexion-extension, supination-pronation and varus-valgus moments generated by the contracting muscle at the elbow joint were measured using a six-axis force sensor and used to determine the muscle DOR.

Muscle DOR is a fundamental property of the musculoskeletal system and it affects the joint moments and motions in 3-D space substantially. Study of the muscle DOR is helpful to extend our understanding of the role of muscles in compensating for joint injuries in 3-D space and of the effects of surgical and therapeutic procedures which alter the anatomical and/or physiological conditions of the musculoskeletal system.

REVIEW AND THEORY

The DOR of an individual muscle is determined by both the multi-axis moment arms (MAs) and the line of action (LOA) of the muscle in 3-D space. Muscle LOAs and MAs are generally determined from cadaveric or radiographic measurements (Pierrynowski 1995). For example, An et al. (1981) measured the centroid, moment arms, volume and fiber length of each muscle of cadaveric elbow joints, and estimated the potential flexion-extension and varus-valgus moment contribution of each muscle at the elbow joint. Muscle LOAs have been modelled as straight or segmented lines from muscle origin to insertion (Pierrynowski 1995). Skeletal, muscle and tendon geometries and anatomical variations, various muscle or joint injuries, and surgical procedures all may affect muscle LOAs and MAs in 3-D space. For biomechanical modeling of musculoskeletal systems, muscle LOAs and MAs affect the predicted joint moments substantially (Nussbaum et al. 1995, An and Morrey 1993).

In an *in vivo* study, Nathan (1992) strapped two rows of electrodes around the forearm and used an electrode from each row to stimulate individual forearm muscles. The direction of the isometric forces generated at the fingertips and the percentage torque generated about the longitudinal axis of the hand segment were measured by a triaxial dynamometer.

The objective of this study was to study the muscle DOR (the combined effect of muscle LOA and MAs in 3-D space) through *in vivo* measurement. The specific problem addressed was: What were the relative amplitudes of the three orthogonal moments at the elbow joint when an individual elbow muscle was activated. In other words, in what direction would the contracting muscle rotate the forearm relative to the upper arm ?

The following directional cosines based on three orthogonal moments generated by an individual muscle were used to quantify the DOR of the muscle:

$$DC_x = \frac{M_x}{\sqrt{M_x^2 + M_y^2 + M_z^2}}$$

$$DC_y = \frac{M_y}{\sqrt{M_x^2 + M_y^2 + M_z^2}} \qquad (1)$$

$$DC_z = \frac{M_z}{\sqrt{M_x^2 + M_y^2 + M_z^2}}$$

where X, Y and Z were the axes of supination-pronation, varus-valgus, and flexion-extension respectively. M_X, M_Y and M_Z were the moments about the X, Y and Z axes respectively. DC_Z=1, for example, meant the muscle functioned as a pure joint flexor and DC_Z=-1 meant it was a pure extensor.

PROCEDURES

Individual muscles crossing the right elbow joint (the lateral, medial and long heads of triceps, anconeus, short and long heads of biceps, brachioradialis and brachialis) were stimulated electrically and the moments and forces generated at the elbow joint were measured by a six-axis force sensor. The signals were low-pass filtered with 8th order Butterworth filters (40 Hz cutoff frequency) and sampled at 125 Hz.

Apparatus: The subject was seated upright in a dental chair. The shoulder was abducted and flexed to 90° and 15° respectively. The right wrist was casted and coupled to an aluminum cylindrical ring in the neutral position. Isometric testing of the elbow at 30° increments was performed in the range of 0° to 120° elbow flexion. The aluminum ring was mounted on one end of an aluminum beam located in parallel and beneath the forearm. The other end of the beam was mounted on the six-axis force sensor which was in turn mounted on a fixed motor shaft. The axis of elbow flexion, the Z-axis of the force sensor, and the motor shaft were aligned with each other, and were vertical to the floor. The aluminum beam, the forearm and upper arm were in the horizontal plane. The position of the ring relative to the beam could be adjusted in three orthogonal directions to make the anatomical axes of the forearm parallel to the mechanical axes of the force sensor.

Anatomical axes: The axis of elbow flexion-extension was defined as passing through the centers of the arc formed by the trochlear sulcus and capitellum (An and Morrey 1993, London 1981). Experimentally, the flexion-extension axis (the Z-axis) was determined as the vertical axis passing through the point which is about 7 mm distal and about 12 mm anterior to the tip of the lateral epicondyle. Supination-pronation was assumed to occur about the line (the X-axis) between the axis of elbow flexion at the level of the groove between the olecranon process and lateral epicondyle and the ring finger in the horizontal plane, with the wrist in the neutral position (palm facing downward). The varus-valgus axis (the Y-axis) was assumed to intersect with the X-axis in the horizontal plane, and the orthogonal XYZ Cartesian axis system of the elbow joint followed the right-hand rule. The positive X and Z were the (forearm) distal and upward directions respectively.

Locating motor point: To activate a targeted muscle without significant stimulation current overflow to surrounding muscles, it was critical to locate the muscle motor points carefully. Bipolar stimulation with small surface electrodes was used to locate the motor points because of its more focused current flow. The stimulation pulse width was 0.3ms and repeated at 1Hz continuously. The current amplitude was adjusted for different muscles and subjects. The location at which a moderate stimulation invoked the strongest contraction of the targeted muscle as compared to the surrounding locations (checked by visual inspection, palpation of the corresponding tendon, and the subject's sensation) was used as the "motor point" in subsequent stimulation.

Stimulation: A Grass Instruments S8800B stimulator with constant current units was used to apply the stimulation. The duration of the square wave pulse train was about 300ms. The pulse width was 0.3ms and was repeated at 50Hz. The current amplitude was adjusted for each muscle so that moderate

contraction of the targeted muscle was invoked without significant current overflow to the surrounding muscles. Of the two current polarities, the one which invoked stronger contraction was used. The stimulation train was applied to the targeted muscle every 3 seconds during a 20s long trial. Each train of stimulation pulses generated a muscle twitch and about seven twitches were recorded during each trial. The stimulation was applied at several current intensity levels. A rest period of 40s was used between two consecutive trials to minimize muscle fatigue. The same procedure was repeated for each of the muscles and each of the elbow flexion angles.

Data Analysis: The six-axis forces and moments were measured with respect to the geometric center of the force sensor. They were transformed from the force sensor coordinates to the anatomical ones. All the six measured force-moment components were used in the transformation. However, only the transformed *moments* in the anatomical coordinate system were analyzed in this study. The offsets of the three moments before the muscle twitches were subtracted and the moment increments or decrements invoked by the stimulation were studied. Interactive editing was done with a computer to determine the time window of the muscle twitch moments. The moments within the window were averaged for the M_X, M_Y and M_Z respectively. If all the three moments generated by the stimulation were too weak to get reliable measurement or if the time-windows were not determined appropriately, the corresponding trial was discarded. The averaged M_X, M_Y and M_Z were used to calculate the muscle DOR described in Eq. (1). Further averaging was done for the DC_X, DC_Y and DC_Z over the several muscle twitches in a trial and across the several contraction levels.

RESULTS AND DISCUSSION

The three orthogonal moments generated by a contracting short head biceps in a trial was shown in Fig. 1. The elbow flexion was 60°. Electrical stimulation trains during the trial invoked moment pulses about the three orthogonal axes every three seconds. As expected, among the three moments, flexion was the strongest. However, the supination and varus moments were also significant.

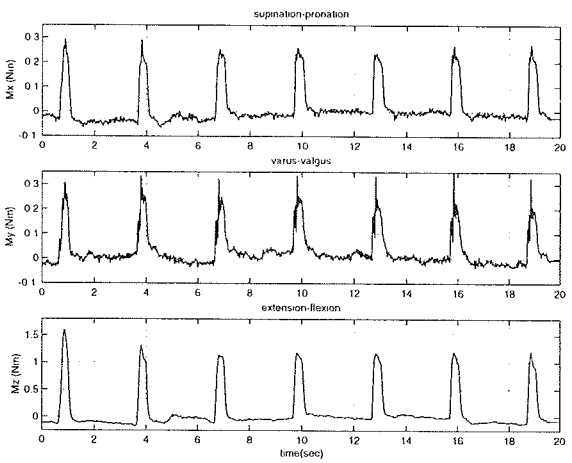

Figure 1: The M_X, M_Y and M_Z twitch moments generated by the short head of the biceps muscle activated electrically during a trial.

Fig. 2 showed the DOR of several elbow muscles from a subject with no joint injuries and neurological disorders. Each data point in the figure was obtained from about 25 muscle twitches recorded over about 4 contraction levels. The star (*), circle (o) and plus (+) symbols represented the averages of the DC_X, DC_Y and DC_Z respectively, and the thick vertical bars gave the corresponding ranges of the mean±σ (standard deviation). As shown in Fig. 2, the measurement was repeatable and σ was minimal for the flexion-extension moment. In comparison, σ was relatively larger for the varus-valgus moment, mainly at the two extreme flexion angles.

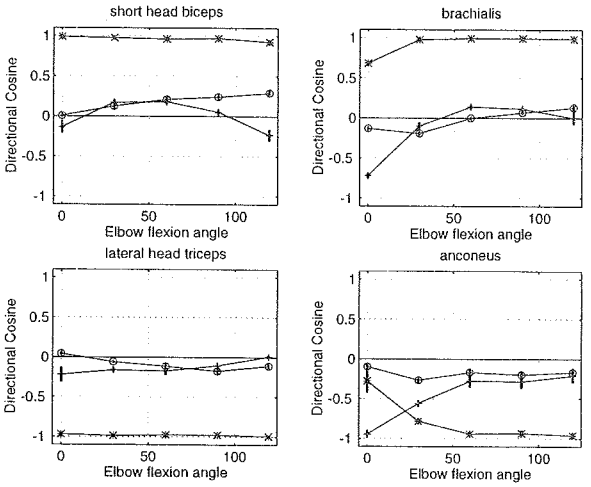

Figure 2: DORs of individual muscles at the elbow joint, described as directional cosines calculated from the three moments—M_X, M_Y, and M_Z, corresponding to the supination-pronation (the o symbol), varus-valgus (+), and flexion-extension (*) moments respectively. The positive directions of them are supination, varus, and flexion respectively. The thick vertical bars at each data point represent the ranges of mean±σ.

With the wrist at the "neutral" position, the biceps muscle acted mainly as a flexor across the range of elbow flexion. Its secondary function was to generate the supination and varus-valgus moments. These functions were not independent of the elbow flexion angle. As the elbow joint moved from full flexion to full extension (0°), the biceps muscle contributed gradually less to the supination. The gradual reduction of the supination moment toward full extension can be felt by palpating the supinating biceps muscle at different flexion angles. In practice, supination activities like using a screw driver are generally performed with the elbow in a flexed position. The biceps generated relatively greater valgus moment at the two extreme joint flexion angles. The brachialis muscle acted predominantly as an elbow flexor. As the elbow was extended near full extension, the brachialis muscle generated relatively more valgus and less flexion moments.

The anconeus muscle generated extension, valgus and pronation moments throughout the range of flexion. The extension and valgus components were generally greater than the pronation component. The σ for DC_Z was relatively large at the full extension. As the elbow was gradually extended, the anconeus muscle contributed gradually relatively less to the elbow extension and more to the valgus moment. The lateral head of the triceps muscle functioned predominantly as an elbow joint extensor.

REFERENCES

An, K. N. et al. *J. Biomech.*, **14**, 659-669, 1981.

An, K. N. and Morrey, B. *The Elbow Joint and Its Disorder.* 53-72. Sauders, 1993.

London, J. T. *J. Bone & Joint Surg.* **63A**, 529-535, 1981.

Nathan, R. H. *ASME J. Biomech. Eng.*, **114**, 162-169, 1992.

Nussbaum, M. A. et al. *J. Biomech.* **28**, 401-409, 1995.

Pierrynowski, M. R. *Three Dimensional Analysis of Human Movement.* 215-256. Human Kinetics, 1995.

ACKNOWLEDGMENT

The authors would like to acknowledge the supports of the Whitaker, Northwestern Memorial and Baxter Foundations, and the NIH.

A SIMPLE METHOD FOR IMPROVING PRECISION OF INVERSE DYNAMICS COMPUTATIONS

A. D. Kuo
Dept. of Mechanical Engineering & Applied Mechanics, University of Michigan, Ann Arbor, MI 48109-2125

INTRODUCTION

Inverse dynamics is used to estimate joint moments (torques) produced by muscles. The standard inverse dynamics technique (Winter, 1990) uses ground reaction forces and accelerations in the Newton-Euler equations of motion to solve for moments and reaction forces at each of the joints. This method has three disadvantages:

1. Results tend to be noisy, because they are usually based on acceleration data found by (twice) numerically differentiating displacement data—a process which amplifies measurement noise.
2. Ground reaction forces are typically more precise, but can only be used when a complete set (e.g., 3 reaction forces and 3 moments for three-dimensional motion) of such data are available, placing high demands on instrumentation.
3. More data are produced than are needed: the method produces ancillary data in the form of resultant joint reaction forces. These data could be separately derived from the moment estimates.

This abstract describes a simple method for improving the precision of inverse dynamics computations. It utilizes a reduced form of the equations of motion to arrive at a redundant set of equations relating accelerations and ground reaction forces to joint moments. Least-squares techniques can be used to find optimal estimates of joint moments.

REVIEW AND THEORY

Equations of motion can be written in terms of generalized coordinates, using the methods of Lagrange, Kane, and others (Greenwood, 1988). In terms of vector of joint or segment angles ϕ:

$$\ddot{\phi} = M^{-1}(\phi,\dot{\phi})\left[t^M + g(\phi) + v(\phi,\dot{\phi}) + \ldots\right] \qquad (1)$$

where t^M, g, and v describe joint torques (moments), gravitational terms, and velocity terms, respectively, and M is the mass matrix. This reduced form takes into account kinematic constraints and eliminates the resultant reaction forces, which do not contribute to motion. The reaction forces may, however, be found by solving for the forces that are necessary to enforce the constraints. The ground reaction forces r_g may then be related to joint moments by an equation of the form

$$r_g = R_t(\phi,\dot{\phi})\cdot t^M + r_{t0}(\phi,\dot{\phi}) \qquad (2)$$

where R_t and r_{t0} are a jacobian matrix and a vector of other forces, respectively.

PROCEDURES AND RESULTS

The proposed method combines the two equations above and views the system of equations as a parameter estimation problem, substituting measured values of angular accelerations and ground reaction forces $\ddot{\phi}_m$ and r_{gm} into the redundant system

$$\begin{bmatrix}\ddot{\phi}_m \\ r_{gm}\end{bmatrix} = \begin{bmatrix}M^{-1} \\ R_t\end{bmatrix}\cdot t^M + \begin{bmatrix}a \\ r_{t0}\end{bmatrix} \qquad (3)$$

where gravity, velocity and additional terms from eqn. (1) have been lumped into vector a. Eqn. (3) may be solved by the pseudo-inverse, which provides a least-squares estimate of t^M (Strang, 1988).

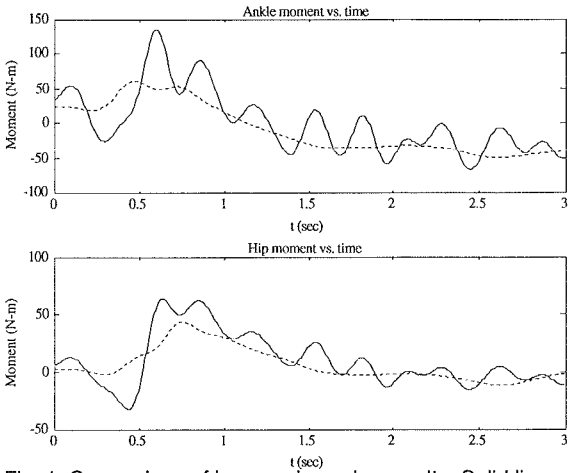

Fig. 1. Comparison of inverse dynamics results. Solid lines: traditional method. Dashed lines: proposed method.

A sample of the ankle and hip moments estimated for human motion in the sagittal plane only is shown in Fig. 1. Note that despite heavy use of filtering, the traditional inverse dynamics results are still noisy.

DISCUSSION

Uncertainty in measurements is generally uncorrelated. The least-squares procedure tends to reject such noise, effectively smoothing the estimated torques. Measurements may also be weighted by the covariance of noise to obtain "optimal" estimates. The proposed method also works when an incomplete set of ground reaction force data is available, and can be used for closed kinematic chains with incomplete force data. It may also be used to smooth estimates of angular accelerations. Finally, the pseudo-inverse method is very fast computationally.

REFERENCES

Greenwood, D. *Principles of Dynamics, Prentice-Hall, 1988.*
Strang, G. *Linear Algebra & Its Applications, Harcourt, 1988.*
Winter, D. A. *Biomechanics & Motor Control of Human Movement, Wiley, 1990.*

ACKNOWLEDGEMENTS

This study was supported by a Whitaker Foundation grant to the author.

The Effect of Muscle Length on Muscle Force Enhancement

D. Hawkins†‡, D. Bosco†
†Department of Exercise Science
‡Biomedical Engineering Graduate Group
University of California, Davis CA 95616

INTRODUCTION

Studies of isolated muscles have indicated that the ability of a muscle to generate greater force during the concentric contraction phase of a stretch-shortening cycle compared to a simple concentric contraction is dependent on the initial length of the muscle (Edman et al. 1982). The objective of this study was to investigate the relationship between muscle force, the occurrence of a stretch-shortening cycle, and the initial length of intact human muscles. This objective was achieved using an elbow extension study. The length of the long head of the triceps muscle was varied by varying the shoulder angle. The triceps muscle extended the elbow both with and without a preceding active stretch. The ratio of the torque developed during the two contraction modes were compared across shoulder angles.

REVIEW AND THEORY

The force generated by a muscle is affected by the muscle's kinematics. It has been shown that a muscle has the potential of generating greater force during a concentric contraction (i.e. an activated muscle that is shortening) when the concentric contraction is preceded by an eccentric contraction (i.e. an activated muscle that is stretched) compared to the concentric contraction occurring without the eccentric contraction (Flitney et al., 1978, Bosco et al., 1981, Edman et al., 1982, Goubel, 1987). In single muscle fibers the magnitude of the force enhancement has been shown to depend on the initial muscle length from which the eccentric contraction is initiated (Edman et al., 1982). This length depends on the position of the joints over which the muscle crosses.

The stretch-shortening cycle (SSC) is of fundamental interest for those interested in human performance. Characterizing the muscle activation sequence and muscle kinematics which will allow a muscle to produce its greatest force or power has direct implications for human performance. The objective of this study was to test the length dependency phenomenon of muscle force enhancement observed for isolated muscle fibers on intact human muscle.

PROCEDURES

Eight volunteers participated in this study. All protocols were approved by a Human Subjects Review Committee. Participants performed a series of elbow extension movements while seated at a LIDO Ergometer. The LIDO is a machine that can control either the resistance imposed upon a limb during movement or the velocity of the limb movement. The LIDO is equipped to monitor and record the torque generated about a given joint during throughout a movement. Maximum elbow extension efforts were performed at 200 ¤/s with the shoulder fixed at angles of 20°, 40°, 60°, 80°, 90°, 100°, and 120° (0° being full extension). For each shoulder angle two conditions were tested (1) concentric elbow extension initiated from an isometric contraction with the elbow angle fixed at 100°, and (2) concentric elbow extension preceded by an eccentric contraction initiated from an initial elbow angle of 95°. Joint torque was evaluated at specific joint angles during the concentric phase of the movement. The torque determined from the eccentric/concentric trials were divided by the torques determined from the concentric trials and the ratio was defined to be the muscle force enhancement (MFE). Force enhancement was said to occur if the MFE value was greater than 1.0. Changes in the shoulder angle were used to change the initial length of the long head of the triceps muscle thus providing a means of assessing the effects of muscle length on MFE. Three repetitions of each trial were performed and the results averaged. Averaged results were then compared across shoulder angles.

RESULTS

Results from this study indicate that muscle force enhancement does occur for intact muscles during a SSC and that the magnitude of the MFE is not dependent of the muscle length over a normal range of motion. For all shoulder angles tested, the average torque generated by the triceps muscle during the initial phase of the concentric contraction was higher for those contractions involving an active stretch prior to the shortening. These results are illustrated in Figure 1 in which the MFE value calculated for elbow flexion angles of 90° is greater than 1.0 for all shoulder angles. The magnitude of the MFE value is fairly consistent for all shoulder angles (~1.1)

indicating very little length dependency for the long head of the triceps muscle over a physiological range of motion.

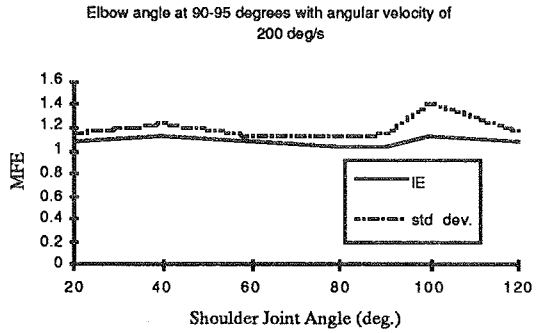

Figure 1: MFE values at 90° of elbow flexion illustrated as a function of the shoulder angle.

MFE values were also determined for elbow joint flexion angles of 65° as illustrated in Figure 2. For the joint angular velocity used in this study the 65° angle was reached approximately 500 ms after the 90° angle. The MFE values at this joint angle and time following the eccentric contraction were all less than 1.0. It is apparent from Figure 2 that MFE is a transient lasting some time less than 500 ms.

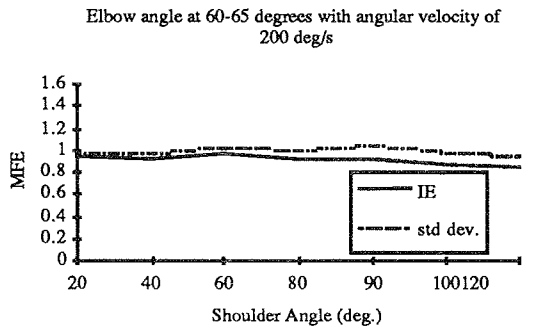

Figure 2: MFE values at 65° of elbow flexion illustrated as a function of the shoulder angle.

DISCUSSION

There are three fundamental findings in this study. The first being that muscle force enhancement can occur in the long head of the triceps, second that the magnitude of the enhancement does not appear to be dependent on the joint position, and third that the muscle force enhancement is transient lasting less than 500 ms. The MFE value of 1.1 immediately following the eccentric contraction is less than observed from other SSCs studies: values ranging from 1.2 to 1.8 (Bosco et al., 1981, Edman et al., 1982). These differences are likely due to differences in the stretch rate, stretch amplitude, and muscle-tendon complex involved.

It was proposed that the MFE would depend on the shoulder joint angle, being greater for small angles in which the long head of the triceps muscle would be in a shortened position. These data suggest that the triceps muscle acts along the plateau region of its force-length curve for a normal physiological range of joint motions.

Edman et al.'s (1982) work on isolated muscles indicated that MFE may last for several seconds for isometric contractions preceded by an eccentric contraction. Results for this study suggest that MFE during dynamic activities is present for a very short time(< 500 ms). These results imply that a SSC may be beneficial for isometric contractions or ballistic-type movements but not for slower and longer lasting movements.

Movements of the elbow involving a stretch-shortening cycle of the triceps muscle have the potential for inducing muscle force enhancement. The potential for force enhancement is independent of the shoulder angle and thus the triceps muscle length. Muscle force enhancement during dynamic activities exists for only a short time implying that only during ballistic-type movements does a SSC have a beneficial effect. Understanding the effects of SSCs is fundamental for modeling human movement and prescribing muscle activation patterns and joint kinematics which will optimize a given movement task.

REFERENCES

Edman, K.A.P., et al., *J. of General Physiol.* **80**(5), 769-784, 1982.

Bosco, C. et al., *Acta. Phsyiol Scand.*, **111**, 135-140, 1981.

Flitney, F.W., and Hirst, D.G. *J. of Physiol.(London)*, **276**, 449-465, 1978.

Goubel, F. *Med.and Sport Sci.* P. Marconnet and P.V. Komi, editors. Karger, Basel, **26**, 24-35, 1987.

Modeling the Metabolic Cost Associated with Muscle Force

D. Hawkins†‡ P. Mole†±,
†Department of Exercise Science
‡Biomedical Engineering Graduate Group
±Nutrition Graduate Group
University of California, Davis CA 95616

INTRODUCTION

This study was designed to quantify the relative effects that muscle shortening velocity have on the metabolic energy expenditure associated with muscle force production. Subjects were required to generate cyclic knee extensor torques (approximately 25 % of maximum isometric) while the knee was either held fixed, allowed to extend, or forced to flex. The exercises caused the quadriceps muscle group to generate either isometric, concentric, or eccentric force respectively. For each test the metabolic energy associated with the force-time interval of the muscle contractions was determined.

REVIEW AND THEORY

An understanding of the relationship between muscle force and metabolic energy expenditure is fundamental for deriving modeling schemes to predict the endurance limit, the efficiency, or the most economical muscle activation profile for a given human movement. The metabolic energy utilized by a muscle to generate a given impulse has been shown to vary as a function of the muscle kinematics (Hill, 1922, Abbot et al., 1953, Curtain, et al. 1975) and the type of fibers comprising the muscle (Suzuki, 1979). Compared to the metabolic energy expended during an isometric muscle contraction initiated from an optimal muscle length, energy expenditure appears to increase as the fiber length is decreased, to increase as the velocity of shortening increases, and to decrease for eccentric contractions. Though numerous studies have been done in this area, very few attempts have been made to quantify these relationships in a manner compatible with gross musculoskeletal modeling and simulation strategies.

The objective of this study was to quantify the relative effects that muscle shortening velocity have on the metabolic energy associated with muscle force production. This objective was achieved using a knee extension protocol and the collection and analysis of data pertaining to joint mechanics and muscle energetics.

PROCEDURES

Isolated knee extension exercises were performed while joint torques and oxygen consumption were monitored. Subjects were seated at a LIDO knee exercise ergometer with an ankle cuff secured around their shank just above the malleoli. The knee joint axis of rotation was aligned with the ergometer lever arm axis. The subjects wore a nose clip and breathed through their mouth into a Sensor Medics 2900 Metabolic System. The subjects were asked to generate a knee extension torque equal to 25 % of their maximum isometric value for joint angular velocities of -150 °/s, -60 °/s, -30 °/s, 0 °/s, 30 °/s, 60°/s, 150°/s, and 250°/s. The knee moved through a range of motion of approximately 90° for the dynamic trials and was set to 55° of flexion for the isometric trials (0° being full knee extension). Subjects performed cyclic contractions for two minutes with roughly 1-1.5 seconds of rest between each contraction. Oxygen consumption was determined during rest prior to each exercise bout, throughout each bout, and until full recovery was obtained after each bout. The total work and impulse were determined for each trial. The total metabolic energy expended for each trial was also determined. The metabolic cost per unit muscle impulse (MCPI) was determined by dividing the energy expenditure resulting from the exercise by the angular joint impulse. These quantities were then used to derive an

expression describing the relative MCPI as a function of the relative muscle shortening velocity.

RESULTS

It was determined that the metabolic cost associated with isometric contractions is less than that for either concentric or eccentric contractions, and that the cost of eccentric contractions is less than that of concentric contractions. Equation (1) was derived based on a regression analysis and describes the relationship between the normalized muscle shortening velocity (V') and the normalized metabolic cost per muscle impulse (MCPI').

$$(MCPI') = (269)(V') + 1.0 \text{ for } V' \geq 0.0 \quad (1)$$
$$= (-112)(V') + 1.0 \text{ for } V' < 0.0$$

Velocities were normalized with respect to a maximum knee extension velocity obtained for an unloaded knee joint. MCPI values were normalized with respect to the MCPI value obtained at zero velocity. The regression analysis yielded R^2 values greater than 0.97. An illustration of the relationship between MCPI' and V' is given in Figure 1.

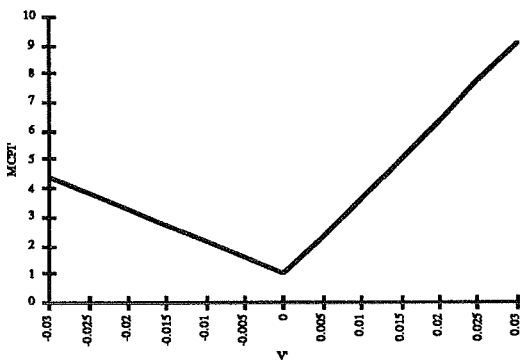

Figure 1: Illustrated is the relationship between normalized muscle shortening velocity (V') and the normalized metabolic cost per unit muscle impulse (MCPI').

DISCUSSION

This study was designed to quantify the relative effects that muscle shortening velocity have on the energy expended per unit of muscle impulse. Initial results from this study indicate that the metabolic cost associated with the impulse developed by a muscle increases as the velocity of shortening or stretch increases. As a function of velocity, the metabolic cost associated with muscle concentric contractions increases at a rate twice that of eccentric contractions. These trends are consistent with those reported by Hill (1922) for shortening muscle but are not consistent with reports by Curtain and Davies (1975) for muscle being stretched. Curtain and Davies (1975) showed the energy demands for eccentric contractions to be much less than that for isometric contractions. The difference in the results obtained in the current study may be due to a greater stretch amplitude employed. Stretch and shortening amplitude are additional factors which may effect the relationship between muscle force and metabolic energy expenditure but factors that were not considered in this study.

A simplistic mathematical model was derived describing the metabolic cost per unit of muscle impulse as a function of muscle shortening velocity. This model was derived to serve as the foundation for the development of more sophisticated models which will include parameters to account for the effects of fiber type, temperature, muscle length, and stretch/shortening amplitude.

REFERENCES

Abbot, B.C., et al. *J. of Physiol,* **117**(3), 380-390, 1952.

Curtain N.A. and Davies, R.E. J. *Mechanochem. Cell Mot.* 147-154, 1975

Hill, A.V., *J. of Physiol..* **56**, 119-41 1922.

Suzuki, Y. *J. Appl. Physiol.: Respirat. Enviorn. Exer. Physiol.* **47**, 263-267, 1979.

ACKNOWLEDGMENTS

The authors are grateful to David Yun for assisting with many of the experiments.

MUSCULAR RESISTANCE TO VARUS AND VALGUS LOADS AT THE ELBOW

Thomas S. Buchanan, Scott L. Delp, and Jason A. Solbeck

Departments of Biomedical Engineering and Physical Medicine & Rebabilitation, Northwestern University, and Sensory Motor Performance Program, Rehabilitation Institute of Chicago, 345 East Superior St., Chicago, IL 60611

INTRODUCTION

The muscular response to varus or valgus loads is not well understood. Although several researchers have reported some electromyographical (EMG) evidence of muscular support of varus loads (Buchanan *et al.*, 1986; Funk *et al.*, 1987; Glousman *et al.*, 1992), no in depth studies have been done to quantify the torque contribution of muscles at the elbow. It is unknown whether any elbow muscle is capable of producing substantial torque in varus or valgus. Furthermore, if a muscle is capable of such torques, it is not known whether that muscle is activated in response to a varus or valgus load.

To address these issues we have performed a set of experiments and computer simulations to examine the extent to which elbow muscles are activated in response to varus or valgus loads. Several subjects performed a variety of isometric tasks that involved a varus or valgus moment at the elbow. During the task, the EMGs of several muscles which span the elbow were recorded. These EMGs were then used as inputs to a computer model of the elbow and surrounding muscles to calculate the joint moments produced by the muscles.

PROCEDURES

A computer graphics model of the elbow muscles was created using the musculoskeletal modeling software described by Delp et al. (1990). The model includes three-dimensional representations of the musculoskeletal geometry to calculate the musculotendon lengths, $\ell^{mt}(\theta)$, and moment arms, $ma_{muscle}(\theta)$, of muscles about the elbow. These moment arms compare well with moment arms we have measured in cadavers (Murray *et al.*, 1995).

The isometric force-generating properties of the muscles were derived by scaling a Hill-type model of muscle. The main parameters of the static muscle-tendon model are optimal muscle fiber length, peak isometric force (F^{peak}_{muscle}), activation (a), and tendon slack length (Zajac, 1989). Optimal muscle fiber length was derived from An et al. (1981) and Lieber et al. (1992). Peak isometric force was derived from measurements of physiological cross-sectional area of muscle (*ibid*). Separate factors were used to scale flexors and extensors. The tendon slack lengths of the elbow muscles were adjusted to match the shapes of the average flexion and extension strength curves determined from our four subjects.

Subjects for this experiment were chosen from a pool of seven males (age 24–37) from which maximum flexion and extension strengths were measured over a range of flexion-extension angles. The four most similar subjects were used to minimize the effects of strength differences among the subjects. Subjects were seated with their shoulders abducted 90°, their elbows flexed 90°, and their forearms in a neutral pronation position. EMGs (surface or intramuscular) were simultaneously collected from eleven muscles while subjects produced static isometric forces at the distal forearm against a load cell as described by Buchanan et al. (1986). The loads corresponded to flexion, valgus, extension, varus and combinations of these at 15° increments in the transverse plane. The load magnitude and direction were displayed on a monitor as a cursor which was driven by output from the load cell. Subjects were instructed to produce a specified load state by matching the cursor with a target on the screen.

Normalized EMG data from the target matching experiments was used as the activation (a) to the elbow model. The model was then used to estimate joint torque (T_{joint}) as defined by the following equations:

$$F_{muscle} = F^{peak}_{muscle} * f\left(\ell^{mt}(\theta), a\right),$$

$$M_{muscle} = F_{muscle} * ma_{muscle}(\theta),$$

$$T_{joint} = \sum_{all\ muscles} M_{muscle}.$$

The results were compared to the moments measured during the experiment and the contributions from individual muscles were evaluated.

RESULTS

The flexion-extension moments calculated with the model correspond closely with the maximum isometric moments measured for the four subjects (Fig. 1). A slight notch in the extension strength curve of the model resulting from the onset of wrapping points in the triceps muscles is the only substantial difference between the model and data.

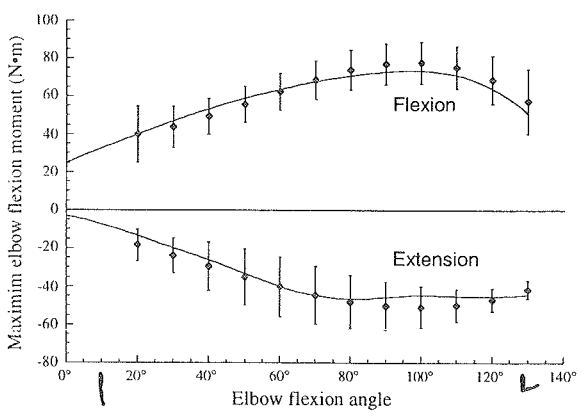

Figure 1. Comparison of maximum isometric moments estimated with the model (curves) to moments measured during maximum voluntary contractions (points). The experimental values are the average of the four subjects. The error bars indicate one standard deviation of the experimental data.

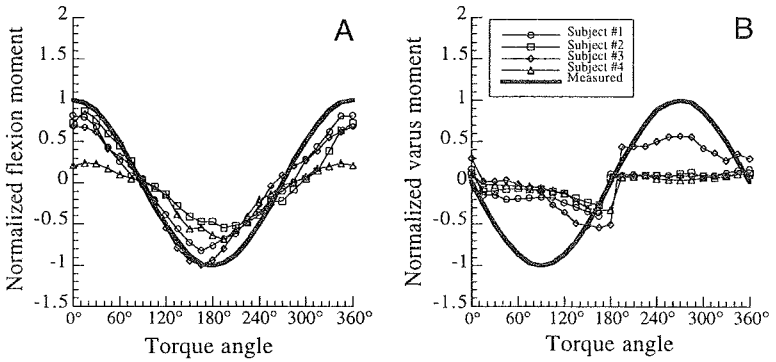

Figure 2: Muscular contributions to flexion-extension (A) and varus-valgus (B) as decomposed from the load cell measurements Note that muscles produce most of the FE moments, but saturate allowing soft tissues (presumably) to take up moments in VV. The torque angles correspond to flexion (0°), valgus (90°), extension (180°), varus (270°) and combinations of these at 15° increments in the transverse plane.

The computer model also reproduced the measured flexion-extension moment when the EMG recordings from the target matching experiment was used as input to the model (Fig. 2A). Here, the flexion-extension (FE) components of the moments were decomposed from the recorded moments. The curves of the model fit the data fairly well, although they tend to be lower in magnitude. For subject #4 the brachialis EMG showed signs of being not well recorded. This probably accounts for the low FE forces estimated for this subject. Overall, however, the model matches the shape of the load rather well for FE. in all subjects.

The varus-valgus (VV) contribution of the muscles varied between subjects, but the general pattern remained constant (Fig. 2B). These patterns demonstrate a saturation of the system. Muscles were only activated in VV loads up to a modest amount and then they were not further employed. None of the subjects matched the VV loads near their peak, but subject #3 produced relatively large varus moments. For all subjects the saturation was prominent.

To determine the relative contribution of each muscle, the torque produced by each muscle at both pure varus and pure valgus was normalized by the magnitude of the total joint torque, averaged across subjects, sorted by level of contribution, and plotted (Fig. 3). In all subjects, anconeus was the largest valgus moment producer and pronator teres was the largest varus moment producer. A large contribution of the pronator teres to varus moment in subject #3 created a high standard deviation for the group mean for that muscle. The order of relative contribution of the secondary muscles varied but stayed close to the same.

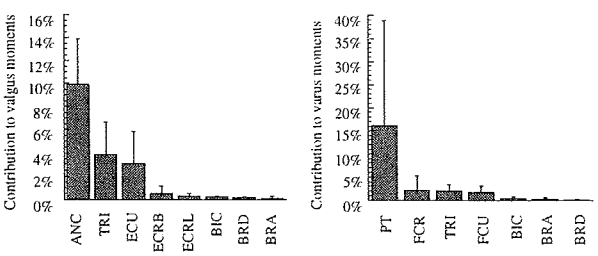

Figure 3: Relative contribution of muscles to varus and valgus, averaged across all subjects (with standard deviations).

DISCUSSION

Although nearly all muscles which cross the elbow are capable of producing torque to stabilize the elbow against varus or valgus loads, only a few are used in this way. Anconeus was found to be the muscle most used for production of valgus moments, and pronator teres for varus moments. The activation patterns of the muscles varied substantially from individual to individual, but several trends were constant across subjects.

All muscles showed some tendency toward activations with varus or valgus loads. Anconeus was active throughout a great deal of the valgus torque angles, and pronator teres was most active in response to pure valgus loads. All other primary elbow muscles had their highest activations at torque angles with slight valgus components.

The wrist muscles were found to play only a small role in the balancing of varus or valgus torques despite their large varus-valgus moment arms at the elbow. The moment generating capacity of the wrist muscles is on the same order of magnitude as anconeus and pronator teres. Clearly, the wrist muscles had the strength to be major contributors, but they were not consistently utilized in this way, as evidenced by the low activations in these muscles. It is difficult to determine whether this was a result of the experimental protocol or is normal physiological behavior.

BIBLIOGRAPHY

An et al. (1981) *J. Biomech.* 14:659-669.
Buchanan T S et al. (1986) *J Neurophysiol* 56:1225-41.
Delp SL et al. (1990) *IEEE Trans Biomed Engng* 37:757-67.
Funk DA et al. (1987) *J Orthop Res* 5, 529-38.
Lieber RL et al. (1992) *J Hand Surg* 17: 787-798.
Glousman RE et al. (1992) *Am J Sport Med*. 20:311-7.
Grierson AE (1994) MS Thesis Northwestern Univ.
Murray WM et al. (1995) *J Biomech* (in press).
Zajac FE (1989) *Crit Rev Biomed Engng* 17:359-411.

ACKNOWLEDGMENTS

This work supported by an NSF Graduate Research Fellowship and NIH R29-AR-40408. We also thank Dr. David Lloyd for his assistance on this project.

Towards Modeling Space Suited Joint Strength

D. Morgan[1], A. Pandya[1], R. Wilmington[1], J. Maida[2], and K. Demel[2]
[1]Lockheed Engineering and Sciences Company, Johnson Space Center, Houston, TX 77058
[2]National Aeronautics and Space Administration, Houston, TX 77058

INTRODUCTION

One of the goals in human modeling at NASA JSC is to create a task-oriented space-suited human model which emulates the physical characteristics of the suited astronaut as closely as possible. While the field of biomechanics is well developed and undergoing continual improvement here on Earth, this field is still in its infancy when concerning space environments. One specific area concerns the physical demands of crew members in the extravehicular (EVA) work environment of space. The varying conditions that exist when performing EVAs create the conditions in which the human capability in a space suit must be better understood in order to maximize productivity through minimizing fatigue, reducing task time, reducing operator discomfort, and ensuring crew safety. At NASA JSC, the Graphics Research and Analysis Facility (GRAF) and the Anthropometry and Biomechanics Laboratory (ABL) have undertaken an effort to model the joint strength capabilities and limitations between shuttle space suited and unsuited individuals. The purpose of this research is to develop a method to easily obtain torque information to be used in a computer model of the suited operator. For this study, elbow and knee torque and angle data were collected from six subjects under unsuited and four different suited conditions. Second order polynomial equations to model each of the conditions were developed and compared against each subject's response. Results show this method can provide a compact and accurate method to determine joint strength given joint angles and the suited condition. This can then be used to extract the maximum torque at a given angle into a computer modeling system to model complex EVA tasks, and to allow mission planners in predicting operator capabilities. This approach may also be used to provide information to suit designers for assessing joint strength limitations.

REVIEW AND THEORY

At NASA JSC, some recent research in the ABL and GRAF has focused on human modeling and strength capabilities. A model by Pandya *et al* (1992a, 1992b) was developed to predict maximum available dynamic strength from isokinetic isolated joint torque functions, as related to the lean body mass. Currently, a more elaborate effort is being undertaken to develop a similar model to include all the major joints of the human body. A pilot study was performed by Wilmington *et al* (1993) measuring and comparing isolated joint strengths for a suited and unsuited subject. This research demonstrated a need to perform a more advanced study to quantify the differences between suited and unsuited subjects as well as between different types of suits. These three previous studies have formed the motivation for this current research. The goal of this study is to describe a method to easily and accurately obtain maximal isokinetic joint strengths for unsuited and EVA suited operators for the purpose of biomechanical modeling of space tasks.

PROCEDURES

Six male subjects were used for this study. The subjects were chosen under the conditions that the subject must fit a large Shuttle Extramobility Unit (EMU) torso. The LIDO Multi-Joint II Isokinetic dynamometer, manufactured by Loredan Biomedical, Inc., was modified and used to collect and record (via a PC data acquisition system) the isolated joint strength measurements. After the subjects were familiarized with the equipment and the muscles warmed up, the subjects performed three repetitions at maximal effort for the knee and elbow joint under the following five randomized conditions: wearing no space suit, wearing a flight ready EVA suit (termed "Class 1"), wearing a control training suit (termed "Class 3") and wearing both suits with a Thermal Meteoroid Garment (TMG) under the suits (termed "Class 1+" and "Class 3+"). The knee and elbow joints were both tested in flexion and extension at a angular velocity of 60° per second. All the data was stored on the Lido's companion PC in ascii text format. These numerous and massive files were transferred to a Silicon Graphics workstation to be processed and analyzed. For each exercise and condition, each subject's three trials were averaged to obtain an averaged torque for each angle, thus representing the entire subject population. A least squares regression was performed on the resulting data to form a second order polynomial function describing the relationships of the angle and torque for each condition and exercise. In addition, each subject's trials were separately averaged to compare against the average population model. A t-test (alpha = 0.05) was performed on the observed population results against the predicted population model and for each individual subject against the predicted population model.

RESULTS

A sample of the results are shown below. Figure 1 shows a plot of the averaged knee flexion and extension torques at each angle. Each of the different lines represents a different EMU condition. Figure 2 shows predicted results for each condition at each angle. Table 1 represents a summary of the squared correlation coefficients, R^2, an indicator of the strength of the mathematical model. Also in Table 1 are the resulting t-test scores used to validate the model. T-tests (alpha=0.05) performed to compare each subject with the corresponding conditional function produced 12 significant scores out of the 60 different tests (5 conditions for 2 joints on 6 subjects). A t-test of average function versus each of the 10 conditional functions suggested 8 out of 10 conditions had statistically different mean torque values.

DISCUSSION

As might be anticipated, the low rate of significance when comparing each individual subject with the predicted average population suggests using the model to predict joint strengths of an individual, taking only the condition of the space suit into account, is not a feasible method. The differences in each condition indicate the need for a separate function for each EVA condition.

However, the high correlation and high rate of significant results from the modeled data indicate that this is an appropriate method of describing maximum joint torques under varying conditions needed for a human simulation program that models an EVA suited operator. This, combined with a method to predict unsuited joint strengths, such as by evaluating lean body mass, can allow biomechanics and human factor engineers to study the many difficult tasks performed by an astronaut during a mission.

REFERENCES

Pandya, A., *et al*, Correlation and Prediction of Dynamic Human Joint Strength from Lean Body Mass, *NASA Technical Report 3207*, June 1992.

Pandya, A., *et al*, The Validation of a Human Force Model to Predict Dynamic Forces Resulting from Multi-joint Motions, *NASA Technical Report 3206*, June 1992.

Wilmington, R., Klute, G.K., and Stoycos, L.E. Comparison of Isolated Joint Strength Measurements for Unsuited and Shuttle Suited Operators: A Pilot Study, *NASA Technical Memorandum*, Unpublished 1993.

ACKNOWLEDGMENTS

The authors would like to thank the subjects for their participation, Crew and Thermal Systems Division at JSC for supplying the EVA suits, and the Graphics Research Analysis Facility and Anthropometry and Biomechanics Laboratory, JSC, Houston, Texas.

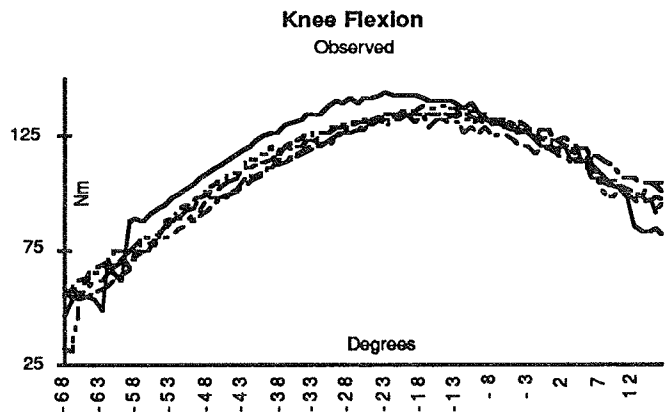

Figure 1 Measured values of knee flexion for all different conditions.

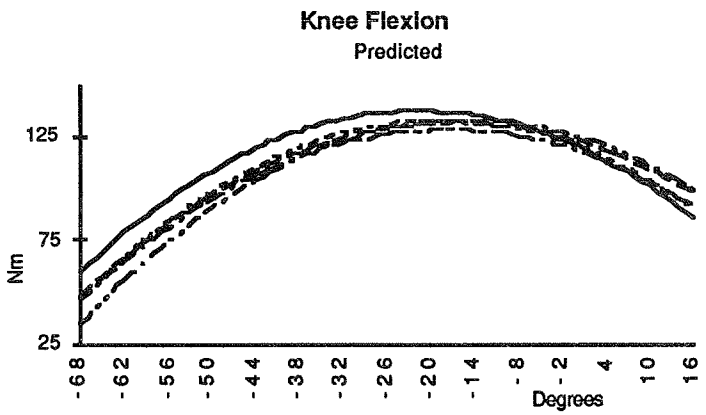

Figure 2 Predicted values of knee flexion for all different conditions.

Table 1. Correlation coefficients and t-scores.

Test	R^2	t-score
Elbow		
Unsuited	.85	.0001
Class 1	.55	.0002
Class 1+	.78	.0002
Class 3	.88	.0001
Class 3+	.69	.0001
Knee		
Unsuited	.98	.0001
Class 1	.96	.0001
Class 1+	.99	.0003
Class 3	.98	.0001
Class 3+	.99	.0001

Author Index